AFFDL-TR-76 141

PRIMARY ADHESIVELY BONDED STRUCTURE TECHNOLOGY (PABST)

PHASE Ib: PRELIMINARY DESIGN

AD A041536

DOUGLAS AIRCRAFT COMPANY
MCDONNELL DOUGLAS CORPORATION
LONG BEACH, CALIFORNIA 90846

DDC
JUL 11 1977
C

DECEMBER 1976

TECHNICAL REPORT AFFDL-TR-76-141
FINAL REPORT FEBRUARY 1975 - OCTOBER 1976

NO INV.
DDC FILE COPY

Approved for public release; distribution unlimited

AIR FORCE FLIGHT DYNAMICS LABORATORY
AIR FORCE WRIGHT AERONAUTICAL LABORATORIES
AIR FORCE SYSTEMS COMMAND
WRIGHT-PATTERSON AIR FORCE BASE, OHIO 45433

NOTICE

When Government drawings, specifications, or other data are used for any purpose other than in connection with a definitely related Government procurement operation, the United States Government thereby incurs no responsibility nor any obligation whatsoever; and the fact that the government may have formulated, furnished, or in any way supplied the said drawings, specifications, or other data, is not to be regarded by implication or otherwise as in any manner licensing the holder or any other person or corporation, or conveying any rights or permission to manufacture, use, or sell any patented invention that may in any way be related thereto.

This report has been reviewed by the Information Office (OI) and is releasable to the National Technical Information Service (NTIS). At NTIS, it will be available to the general public, including foreign nations.

This technical report has been reviewed and is approved for publication.

Jaimie M. Florence
JAIMIE M. FLORENCE
Project Engineer
AFFDL/FBA

Joseph S. Ford
JOSEPH S. FORD, Lt Colonel, USAF
Program Manager AMS Project Office
Structures Division

FOR THE COMMANDER

Howard L. Farmer
HOWARD L. FARMER, Colonel, USAF
Chief, Structural Mechanics Division

Copies of this report should not be returned, unless return is required by security considerations, contractual obligations, or notice on a specific document.

AIR FORCE - 16 MAY 7 - 450

UNCLASSIFIED

SECURITY CLASSIFICATION OF THIS PAGE (When Data Entered)

REPORT DOCUMENTATION PAGE	READ INSTRUCTIONS BEFORE COMPLETING FORM
1. REPORT NUMBER: AFFDL-TR-76-141	2. GOVT ACCESSION NO. / 3. RECIPIENT'S CATALOG NUMBER
4. TITLE (and Subtitle): PRIMARY ADHESIVELY BONDED STRUCTURE TECHNOLOGY (PABST). Phase Ib: Preliminary Design	5. TYPE OF REPORT & PERIOD COVERED: Final rep't. Feb 1975-15 Oct 1976
	6. PERFORMING ORG. REPORT NUMBER
7. AUTHOR(s)	8. CONTRACT OR GRANT NUMBER(s): F33615-75-C-3016
9. PERFORMING ORGANIZATION NAME AND ADDRESS: Douglas Aircraft Company, McDonnell Douglas Corporation, Long Beach, California 90846	10. PROGRAM ELEMENT, PROJECT, TASK AREA & WORK UNIT NUMBERS: 486U0404
11. CONTROLLING OFFICE NAME AND ADDRESS: Air Force Flight Dynamics Laboratory(AFFDL/FBA), Air Force Wright Aeronautical Laboratories, AFSC, Wright-Patterson AFB, OH 45433	12. REPORT DATE: Dec 1976 / 13. NUMBER OF PAGES: 471
14. MONITORING AGENCY NAME & ADDRESS(if different from Controlling Office)	15. SECURITY CLASS. (of this report): Unclassified / 15a. DECLASSIFICATION/DOWNGRADING SCHEDULE

16. DISTRIBUTION STATEMENT (of this Report)

Approved for public release; distribution unlimited

17. DISTRIBUTION STATEMENT (of the abstract entered in Block 20, if different from Report)

DDC PROCESSED JUL 11 1977 C

18. SUPPLEMENTARY NOTES

19. KEY WORDS (Continue on reverse side if necessary and identify by block number)

Adhesive Bonding, Surface Preparation, Adhesives, Bonded Joint Design, Fracture Mechanics, Nondestructive Inspection, Manufacturing Technology, Quality Assurance.

20. ABSTRACT (Continue on reverse side if necessary and identify by block number)

This report covers the design, analysis, and test work conducted during Phase Ib, Preliminary Design of the Primary Adhesively Bonded Structure (PABST) program. The objectives of Phase Ib were two-fold: (1) design definition, (2) surface preparation, adhesive/primer, and coatings/finishes evaluations and screening.

An extensive structural design concept formulation and evaluation effort was conducted culminating in the selection of three concepts which offered the →

DD FORM 1 JAN 73 1473 EDITION OF 1 NOV 65 IS OBSOLETE

UNCLASSIFIED

SECURITY CLASSIFICATION OF THIS PAGE (When Data Entered)

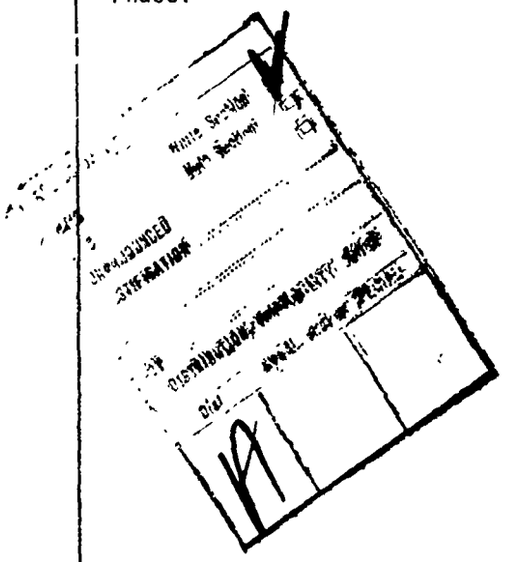
11640

ABSTRACT (BLOCK 20)

greatest potential for acquisition cost, maintenance cost, and weight reduction from the baseline structure. From these three concepts, the design selected for continuation into Phase II, Detailed Design, was a combination close-spaced/wide-spaced, internal/external skin stringer design. Iterative analysis and design support by extensive environmental coupon and component testing constituted the balance of the preliminary design effort of Phase Ib.

Two surface preparations were investigated and resulted in selection of the phosphoric anodize. An immersion tank FPL etch was the reference standard. The adhesive systems considered were the new environmental resistant 250°F cure, modified epoxy adhesives and their respective primers. American Cyanamid's FM-73 adhesive film with a mat carrier used in conjunction with their BR-127 adhesive primer was the selected system for the PABST program.

Coupons and Components fabricated and tested in Phase Ib were subjected to extensive evaluation to ensure adequate quality assurance and to screen candidate state-of-the-art NDI capabilities. The Fabrication and Tooling experience required for the balance of the program was acquired during this Phase.



FOREWORD

This report presents the results of the preliminary design (Phase Ib) of the Primary Adhesively Bonded Structure (PABST) program, Contract F33615-75-C-3016. The effort described herein was performed by the Douglas Aircraft Company, a division of the McDonnell Douglas Aircraft Corporation, with Mr. E. W. Thrall, Jr. as the Program Manager.

This work was sponsored by the Air Force Flight Dynamics Laboratory (AFFDL) under joint management and technical direction of AFFDL and the Air Force Materials Laboratory (AFML), Wright-Patterson Air Force Base, Ohio. This contract is administered as a part of the Advanced Metallic Structures, Advanced Development Programs (AMS ADP), Program Element Number 63211F, Project 486U. Lt. Col Joseph S. Ford is the ADP Manager and Mr. Jamie M. Florence is the Project Engineer for the PABST program.

This work was performed during the period 19 February 1975 to 15 October 1976.

TABLE OF CONTENTS

	Page
SUMMARY	1
INTRODUCTION	5
STRUCTURAL DESIGN	9
Baseline Fuselage	11
Full Scale Demonstration Component	13
Formulation and Evaluation Studies	17
Preliminary Design Studies	21
Weight Analysis	49
STRUCTURAL ANALYSIS	57
Design Criteria	59
External Loads	67
Internal Loads	77
Ultimate Failure Mode - Metal	81
Damage Tolerance	85
Fatigue Analysis	133
Ultimate Mode - Bonded Joints	135
Slow Cycle Fatigue	149
Strength of Flawed Bonded Joints	153
STRUCTURAL TESTS	157
Static Tests	159
Fatigue and Damage Tolerance Tests	165
MATERIALS AND PROCESS	221
Surface Treatment	223
Corrosion Control - Organic Coatings	235
Structural Adhesives	247
Mechanical Fastening Tests	275
Metallic Materials	319
Adhesive Material Properties Obtained from Cast Adhesive Film (Neat Test Specimen)	323

PRECEDING PAGE BLANK-NOT FILMED

TABLE OF CONTENTS (Continued)

	Page
NON-DESTRUCTIVE INSPECTION	325
Evaluation of Built-in Defect Specimens	327
State-of-the-Art Methods Evaluations	333
Bonded Reference Standards	339
Correlation of Non-destructive Testing, NDT Results	341
Cohesive Bond Strength Determination	345
Effect of Bond Flaws	349
Design Review for Production and In-Service Inspectability	353
MANUFACTURING	363
QUALITY ASSURANCE	385
COST EVALUATION	397
Acquisition Cost	399
Description of Concepts	405
Maintenance	407
Results	408
Cost Conclusions	419
APPENDIX A TRADE STUDIES	421
Honeycomb Stiffened Skin Panel Impact Resistance Tests	423
Foreign Object Damage	439
Honeycomb Core Thickness Study	443
External Longeron Evaluation	459
Internal Longeron Shape Study	467
CONCLUSIONS	469
REFERENCES	471

LIST OF FIGURES

Figure		Page
1	PABST Baseline Threeview	7
2	Sideview of Baseline Fuselage	12
3	Full Scale Demonstration Component	14
4	Initial Design Concepts	18
5	Skin Panel - Internal and External Longeron Concept	22
6	Typical Internal Longerons	24
7	Internal and External Longeron - Typical Skin Splices	25
8	Internal Longeron Concept Typical Frame	27
9	Internal Longeron Typical Frames	28
10	Typical Frame and Internal Longeron Intersection	29
11	Typical Internal Longeron and Intermediate Frame Intersection	30
12	Typical Nose Frame and External Longeron Intersection	31
13	Typical Nose Frame and Bonded Skin Splice Intersection	32
14	Internal and External Longeron Wing/Fuselage Interface	33
15	Internal Longeron Front Spar/Fuselage Interface	34
16	Typical External Longerons	36
17	External Longeron Typical Frame	37
18	External Longeron Fuselage to Front Spar Joint	38
19	Sideview - Honeycomb Concept	39
20	Skin Panels - Honeycomb	40
21	Honeycomb - Typical Core Splices and Machined Steps	41
22	Honeycomb - Skin and Panel Splices	43
23	Honeycomb - Frame Tee and Crack Stopper Splice	44
24	Honeycomb Typical Frame	45
25	Honeycomb - Fuselage Cutout Edge Member for Crew Entrance Door	46

Figure	LIST OF FIGURES (Continued)	Page
26	Honeycomb - Wing/Fuselage	47
27	Honeycomb Front Spar to Fuselage Interface	48
28	PABST Center of Gravity Envelope	62
29	Cargo Loading Criteria	63
30	Vehicle Axle Loading Criteria	64
31	Typical Fuselage Load Time History	69
32	Ultimate Fuselage Vertical Shear Envelope	71
33	Ultimate Fuselage Vertical Bending Moment	72
34	Bar Panel and Membrane Elements	76
35	Structural Idealization	79
36	Fuselage Critical Ultimate Conditions	82
37	PABST Fuselage Stresses and Margins of Safety - Ultimate Mode	83
38	Damage Tolerance Analysis Flow Chart for Metal Structure	86
39	Stress Distribution in a Pressurized Stiffened Cylinder	94
40	Non-uniform Stress Distribution Factor	95
41	da/dN versus ΔK-2024-T3 Bare Sheet - T-L Average	97
42	Comparison of da/dN versus ΔK for Two Aluminum Alloys	98
43	PABST Retardation Analysis and Test Data for 2024-T3 T-L Bare	100
44	Critical Points for the Internal Longeron Concept	102
45	Crack Growth Time History for a Circumferential One Bay Crack, Internal Longeron Concept	104
46	Fail-Safe Check for a Two-Bay Circumferential Crack with Center Stiffener Intact	105
47	Fail-Safe Check for a 15-inch Foreign Object Damage Circumferential Crack and Broken Center Stiffener	105
48	Critical Points for the Honeycomb Concept	107

Figure	LIST OF FIGURES (Continued)	Page
49	Model for Honeycomb Structural Damage Tolerance Analysis	109
50	Crack Growth Time History for a Longitudinal Crack Honeycomb Concept	110
51	Fail Safe Check for a Two-Bay Longitudinal Crack with Center Stiffener Intact	110
52	Fail-Safe Check for a 15-inch Foreign Object Damage Longitudinal Crack, in Honeycomb, and Broken Center Stiffener	111
53	Improvement Provided by Bonding	112
54	Damage Tolerance Crack Locations for the Curved Internal Longeron Test Specimen	114
55	Effect of Varying Stress Level on Crack Growth for Skin-Bonded-Stiffener Structure	115
56	Effect of Varying Stress Level on Crack Growth for Honeycomb Structure	116
57	Effect of Varying Stiffener Spacing on Residual Strength	117
58	Effect of Varying Stiffener Area on Residual Strength	118
59	Crack Propagation Data Variation for Sensitivity Study	120
60	Effect of Material Data Variation on Crack Growth Time History	121
61	Crack Propagation Analysis - Test Comparison for an Internal Longeron Stiffened Panel	122
62	Crack Propagation Analysis - Test Comparison for Longitudinal Cracks in an Internal Longeron Specimen	124
63	Crack Propagation Analysis - Test Comparison for a Circumferential Crack in an Internal Longeron Specimen	125
64	Analysis - Test Comparison for the Residual Strength of an Internal Longeron Panel	127
65	Analysis - Test Comparison for the Foreign Object Damage of an Internal Longeron Panel	128
66	Crack Propagation Analysis - Test Comparison for a Stiffened Honeycomb Panel	129

Figure	LIST OF FIGURES (Continued)	Page
67	Analysis - Test Comparison for the Residual Strength of a Stiffened Honeycomb Panel	130
68	Analysis - Test Comparison for the Foreign Object Damage of a Honeycomb Panel	132
69	Double Lap Joints	137
70	Effect of Yielding of Metal	140
71	Adherend Limit Loads for Balanced Single-Lap Joints	142
72	Bonded Circumferential Splice	143
73	Peeling Apart of Skin and Stiffeners	146
74	Frame Bending Failure	147
75	Doublers versus Joints	150
76	Thick Adherend versus Aircraft Configuration Bonded Joints	151
77	Effects of Defects	154
78	Redistribution of Load of Flaws in Bond	155
79	Large, Structural Test Panels	158
80	Frame Bending Test (Specimen 23)	163
81	Cross Section of Frame through Longeron Cutout	164
82	Test Specimen 1 and Flaw Details	168
83	Crack Growth Time Histories of 2 Stringer Riveted and Bonded Panels	170
84	Crack Growth Time Histories of Riveted and Bonded Single Stringer Panels	170
85	Two Stringer Riveted Panel Slow Stable Crack Growth under Static Load	172
86	Two Stringer Bonded Panel Slow Stable Crack Growth under Static Load	173
87	Slow Stable Crack Growth under Static Load for Single Stringer Panels	174

Figure	LIST OF FIGURES (Continued)	Page
88	Bonded Skin Splice Specimen 4A with Metal Flaws	176
89	Bonded Skin Splice Specimen 4B with Adhesive Flaws	179
90	Splice Specimen 4B Photo Stress Data Points	181
91	Stress Distribution in the Bond and Doubler of the Panel 4B Centerline Splice	183
92	Photo Stress Fringe Pattern at Centerline Skin Splice - 20,000 PSI Gross Skin Stress	184
93	Adhesive Bonded, Single Lap, Hoop Splice Specimen	186
94	Crack Origin in Skin Splice	192
95	Stable Crack Region in Skin Splice	192
96	Separated Skin and Splice Showing Depth of Lamination	193
97	Internal Longeron Test - N30A Strain Gage and Failure Locations	194
98	Panel N30 Failure	197
99	Test Specimen N30AB	199
100	Crack Growth Time History - N30AB	200
101	Crack Configuration after Fast Fracture and Arrest	203
102	Residual Strength Diagram-Foreign Object Damage	204
103	Load Cycle Schematic	204
104	Underside View of Test Panel	206
105	Location of Initial Flaws, Residual Strength Sawcuts, and Strain Gages - N21	207
106	Panel Geometry Strain Gage and Initial Flaw Locations-H304	213
107	Panel Geometry, Strain Gage and Initial Flaw Locations-H30B	215
108	H30B Failure	218
109	Panel Geometry Strain Gage and Initial Flaw Location-H30C	219

Figure	LIST OF FIGURES (Continued)	Page
110	Chromic Acid Anodize Sealing Matrix	229
111	Chromic Acid Anodize Matrix	232
112	Surface Treatment Corrosion Resistance	236
113	Comparison of Bonding Primers	240
114	Phosphoric Acid Anodize Protection	241
115	Chromic Acid Anodize Protection	242
116	Comparison of Alloys and Anodic Treatments	243
117	Lap Shear Test	251
118	Test Specimen Configurations	252
119	Metal to Metal T-Peel	253
120	Climbing Drum Peel	255
121	Honeycomb Climbing Drum	256
122	Honeycomb Flatwise Tension Specimen	257
123	Honeycomb Flatwise Tension	258
124	Honeycomb Beam Shear Specimen	259
125	Thick Adherend Lap Shear Specimen	260
126	Double Cantilever Beam	260
127	Crack Extension Data Double Cantilever Beam	261
128	Stressed Lap Shear	263
129	"T" Peel Tests	266
130	Open Faced Climbing Drum Peel	267
131	Wedge Crack Specimens	268
132	Double Cantilever Beam Test Results	270
133	Lap Shear (RAAB) (Two of Seven Test Areas Shown)	271
134	RAAB Sustained Load	272

Figure	LIST OF FIGURES (Continued)	Page
135	Cycled Load/Environmental Test	273
136	Ultrasonic C-scan Record - Bonded Sheet	277
137	Detail Specimen Identification and Traceability to Bonded Parent Sheet	278
138	Adhesive and Delamination Failures	280
139	C-scan Record	280
140	Lap Shear Specimen	281
141	Specimen Separation by Wedging	285
142	Typical Drilled Specimen with Hole Number Orientation	286
143	Drill Configurations	286
144	Controlled Feed and Speed Test Setup	287
145	High Speed Drilling Test Setup	293
146	Bond Interface Adhesive Failure	294
147	Bond Delamination Ultrasonic C-scan Record	294
148	Drill Point Force Test Setup	300
149	Excessive Heat Adhesive Failure	303
150	Photomicrograph Hole No. 18 Adhesive Failure	303
152	Typical Bond Interface of Separated Riveted Specimens	306
153	Photomicrograph of Hole No. 18 Showing Crescent Shaped Metal Sliver	306
154	Photomicrograph of Cross Sectioned Rivet in Bonded Specimen	307
155	Photomicrograph Showing Bond Fracture at Hole Periphery	308
156	Typical Interference Fit Fastener Installation Specimens	309
157	Bond Interface for 0.0045" Interference Fit	311
158	Bond Interface for .0055" and .0065" Interference Fit	312

Figure	LIST OF FIGURES (Continued)	Page
159	Bond Interface for .0075" and .0085" Interference Fit	312
160	Stress Ring - 0.0045" Interference Fit	313
161	Stress Ring - 0.0055" Interference Fit	313
162	Stress Ring - 0.0065" Interference Fit	314
163	Stress Ring - 0.0075" Interference Fit	314
164	Stress Ring - 0.0085" Interference Fit	314
165	Joint Clamp-up 3/16" Nominal Diameter Pin	315
166	Joint Clamp-up 1/4" Nominal Diameter Pin	315
167	Flourescent Penetrant Around Holes in Bottom Sheet	317
168	Cross Section to Show Fastener Installation and Depth of Countersink Cavity	318
169	Fatigue Crack-Growth Data for 0.090-Inch 7475-T761 Sheet (36-Inch)	322
170	Bondtesting Instruments	328
171	Ultrasonic C-scan System and Dry Paper Recorder	329
172	Comparison of Built-In Defect Specimen	333
173	Radiograph of Hysol EA9628 Adhesive with X-ray Opaque Additive	334
174	Fokker Model 67 Bondtester	335
175	Fokker Model 70 Bondtester	336
176	Methods for Fabricating Reference Standards	340
177	Radiographs of Bonded Core Splices	342
178	Correlation of NDT Results	343
179	Typical Fokker Bondtester Quality Diagram	346
180	Positive Reprotudction from X-ray Negative of AF55 Tapered Shim Standard	347
181	Correlation of NDI Test Results with Mode of Failure for Tapered Bonded Splice	350

Figure	LIST OF FIGURES (Continued)	Page
182	Neutron Radiographs of Defect Specimens	351
183	Design Concepts versus Nondestructive Inspectability	354
184	Radiographic (X-ray) of Honeycomb Panels	359
185	Dunegan Acoustic Emission Monitor	361
186	Acoustic Emission Response from Heated Adhesive Bonded Parts	362
187	Typical Structural Integrity Panels	364
188	Curved Panel Bonding Future in Autoclave	365
189	Modified Bond Tool for External Longerons	367
190	Rubber Faced Bond Tool	368
191	DAPCO Cast No. 50 Evaluation	370
192	Shear Panel Assembled with Verifilm	371
193	Schematic of Phosphoric Anodize and Adhesive Prime Operation	373
194	Picture-Frame Fixture used for Anodizing Detail Parts	374
195	Titanium Springs and Clips	375
196	Layout and Sequence of Anodize Operations	376
197	Anodize Tank	377
198	Schematic of Metal Bond Operation	380
199	Typical Bonding Setup for Internal Longeron Concept	381
200	Flow Chart for Overall Quality Assurance Plan	386
201	Flow Chart for Fabrication Quality Assurance Plan	386
202	Control Tests	388
203	Disposition of Major QA Problems	390
204	FPL - Auger Spectra	392
205	FPL - Carbon Depth Profile	392
206	Chromic Acid Anodize - Auger Spectra	393

Figure	LIST OF FIGURES (Continued)	Page
207	Chromic Acid Anodize - Carbon Depth Profile	393
208	Phosphoric Acid Anodize - Auger Spectra	394
209	Phosphoric Acid Anodize - Carbon Depth Profile	394
210	Cost Analysis Estimating Process	400
211	Integrated Measure of Acquisition and Maintenance	418
A1	Impact Resistance Test Panels	424
A2	Gardner Impact Machine Test Setup	425
A3	Photograph of Gardner Impact Machine Test Setup	426
A4	Honeycomb Stiffened Skin Panel after Testing	429
A5	Longeron/Frame Stiffened Skin after Testing	430
A6	Effect of Skin Thickness, Cell Size, and Core Density on Indention of a Honeycomb Panel	432
A7	Effect of Face Sheet Thickness on Idention of a Honeycomb Panel	433
A8	Impact Energy Required to Rupture Honeycomb Face Sheet	434
A9	Honeycomb Stiffened Skin Panel in Support Structure	436
A10	Close-up of Face Sheet Rupture	437
A11	Minimum Core Thickness Required for Fuselage Pressure	447
A12	Honeycomb Panel Compression Load Capability	448
A13	Honeycomb Panel Shear Load Capability	448
A14	Honeycomb Panel Weight for Variations in Core Thickness and Face Sheet Thickness	449
A15	Core Thickness Required for Compression/Shear Interaction	449
A16	Honeycomb Panel Edge Members	452
A17	Evaluated Skin and Doubler Configurations	453
A18	Wind Tunnel Model of YC-15 with External Longerons	461
A19	Longeron Compression Strength	465

LIST OF TABLES

Table		Page
1	PABST Bonded Concept Weights	50
2	Splice and Attach Detailed Weight Summary	51
3	Honeycomb Concept-Inserts and Edge Members Detailed Weight Summary	52
4	Frame and Clips Detailed Weight Summary	53
5	Non-Participating Structure Weight Summary	55
6	Basic Airplane Design Parameters for C-15	60
7	Empty Weight Breakdown	61
8	PABST Payloads	65
9	Summary of Flight Conditions	68
10	Summary of Critical Ground Loads	70
11	PABST Utilization	74
12	PABST Fatigue Payload Summary	75
13	Summary of PABST Critical Fatigue Loads	76
14	Modified Spectra for External Longeron Concept; Check Point B	91
15	Internal Longeron Concept Damage Tolerance Analysis Summary	103
16	External Longeron Concept Damage Tolerance Analysis Summary	106
17	Honeycomb Concept Damage Tolerance Analysis Summary	108
18	Tension Tee Test	159
19	Tension Tee Test - Honeycomb	160
20	Shear - Compression/Tension Interaction Static Test Panel	161
21	Shear Static Test Panel	162
22	Summary of Test Conditions, Specimen 1	169

Table	LIST OF TABLES (Continued)	Page
23	Test Loads for Panel 4A	175
24	Crack Length and Strain Gage Data Specimen 4A	177
25	Test Loads for the Bonded Symmetric Skin Splice Specimen 4B	180
26	Photo Elastic Stress Data at 20,000 PSI	182
27	Specimen 3 Test Loads	185
28	Strain Gage Data Prior to Fatigue Testing	187
29	Change in Strain Gage Data	187
30	Strain Gage Data Prior to Fatigue Testing R.T. (80°F)	188
31	Change in Strain Gage Data at 62.8 KIPS Constant Load	188
32	Strain Gage Data for the 41.9 KIPS Fatigue Test	189
33	Change in Strain Gage Data for 41.9 KIPS Constant Load	189
34	Change in Strain Gage Data at 62.8 KIPS due to Creep at Room Temperature	190
35	Strain Gage Data for the 62.8 KIP Fatigue Cycles at R.T.	190
36	N30A Strain Gage Readings Taken at 12,000 Cycles	195
37	N30A Crack Length vs. Cycles	196
38	Summary of Crack Growth and Strain Gage Data	201
39	Damage Tolerance Flaw Growth Time Histories	208
40	Residual Strength Test RS1 Data	211
41	Residual Strength Test RS2 Data	211
42	Total Cycles vs. Crack Length	214
43	Applied Load, Strain Gage Readings, and Crack Growth Length, H30B	217
44	Strain Gage Readings at Applied Load - H30C	220
45	Phosphoric Acid Anodize Parameters	224

LIST OF TABLES (Continued)

Table		Page
46	Test Matrix	226
47	Chromic Acid Anodize and Sealing Parameters	226
48	Sealing Matrix	228
49	Chromic Acid Anodize Parameters	231
50	Corrosion Resistance - Sealing Matrix	237
51	Corrosion Resistance Chromic Acid Anodize	237
52	Coating System	239
53	Environmental Test Parameters	263
54	Sheet Mechanical Property - Tensile Strength Test Results	276
55	Sheet and Detail Specimen Identification Cross Index	276
56	Lap Shear Test Results	282
57	Controlled Feed and Speed Hole Generation Data	288
58	Controlled Feed and Speed Predrill and 450 RPM Ream Hole Generation Data	291
59	Hand Drilling Hole Generation Data in .087"/.088" Bonded Sheet	294
60	Hand Drilling Hole Generation Data in .1855"/.1875" Bonded Sheet	295
61	High Speed Drilling (20,000 RPM) and High Speed Predrill and Ream Hole Generation Data	297
62	Drill Point Force in Pounds	301
63	Specimen Surface Temperature Data	302
64	Riveted Specimen Configurations	304
65	Interference Fit Test Variables	310
66	Joint Clamp-up Test Variables	316
67	Smooth Fatigue 7475-T761 Sheet	317
68	Fracture Toughness 7475-T761 Sheet	321

Table	LIST OF TABLES (Continued)	Page
69	Correlation of NDT Results for Built-in Defects in Laminate Panels	330
70	Correlation of NDT Results for Built-in Defects in Honeycomb	331
71	PABST In-Service Inspectability (Design Concepts)	355
72	PABST In-Service Accessibility-General All Concepts	356
73	Cost Estimating Factors	402
74	Parts Breakdown and Quantity Comparison	409
75	Tool Type and Quantity Comparison	410
76	Types of Tools Estimated	411
77	Cost Summary by Major Resources Element	413
78	Damage Repair Cost Summary	414
79	Basic Cost Measure Data	416
A1	Depth of Indentation for Honeycomb Panels	428
A2	Impact Energy Required for Honeycomb Face Sheet Rupture	428
A3	Honeycomb Panel Required for Minimum Weight	447
A4	Fastener Installation in High Density Honeycomb Core (.080 inch thick)	454
A5	Weight Comparison Between Edge Member Concepts	454
A6	Labor and Material Costs for Given Configurations of Honeycomb Panel Edges	456
A7	Concept Evaluation and Ranking	458
A8	Longeron Cross Sectional Shape Evaluation	460
A9	Cruise Drag and Configuration Penalty	464

LIST OF SYMBOLS

a	- half crack length - inch
ADP	- Advance Development Program
c.g.	- center of gravity
CRT	- cathode ray tube
da/dN	- crack propagation rate - inches/cycle
DT	- damage tolerance
E	- metal modulus of elasticity
G	- adhesive shear modulus
Hz	- cycles/second
K	- crack tip stress intensity factor - ksi$\sqrt{in.}$
MAC	- mean aerodynamic chord
MEK	- methyl-ethyl-ketone
M.S.	- margin of safety
N	- cycles
NDI	- non-destructive inspection
Nx	- lateral load factor
Ny	- longitudinal load factor
Nz	- vertical load factor
P	- pressure
pcf	- pounds per cubic foot
psf	- pounds per square foot
psi	- pounds per square inch
R	- max stress/min stress
RAAB	- Reduced Area Adhesive Bond
RS	- residual strength
t	- thickness
T-L	- transverse-longitudinal
γ	- adhesive strain
η	- bond thickness
σ	- stress in pounds per square inch
τ	- adhesive stress in pounds per square inch

Subscripts

e	- elastic
p	- plastic

SUMMARY

The purpose of the PABST Program is to determine the economic and technical feasibility of adhesively bonded primary aircraft structure. The program consists of four Phases. Phase Ib was the preliminary design phase, Phase II consists of the detail design of the selected concept, Phase III consists of the fabrication and assembly of the component and Phase IV performs the fatigue, damage tolerance, residual strength and ultimate test of the selected component. This report summarizes the results of Phase Ib of this program.

External loads were generated based on the C-15 design speeds, gross weights, cargo loading capability and payloads. Internal loads using idealizations based on the skin and stringer concepts and the honeycomb concept were generated.

Initially five concepts were designed and evaluated consisting of (A) wide spaced longeron (B) close spaced longeron (C) honeycomb (D) corrugations (E) beads and (F) external longeron employing fairings. Concept (D) was eliminated early in Phase Ib and the remaining design effort was expanded on (1) a concept combining concepts (A) and (B), (2) concept (C) and (3) a variation of concept (F) without the complete aerodynamic fairing, i.e., external longeron only and local fairings at each longeron.

The three concepts were analysed for damage tolerance requirements with the critical points on the fuselage selected on the basis of the internal loads generated. Four critical points were selected for the internal and external longeron concept and two points for the honeycomb concept. The critical points were checked for slow crack growth with a one bay crack and fail safe conditions with (A) a two bay crack with center stiffener intact and (B) 15" foreign object damage - center stiffener out. A sensitivity analysis was made for variation in stress level, bonded strap spacing, bonded strap area and da/dn vs ΔK material data. Verification of the analysis methods was made with tests of longeron and honeycomb panels.

Analyses were made for intact adhesively bonded joints for the double-strap joints used in longitudinal splices, the flush single-strap joints used in circumferential splices and the peeling apart of the skin and stiffening elements under internal cabin pressure. Tests were performed and the test results confirmed the predictions for the bonded joints for the ultimate mode.

An extensive slow cycle testing program at ambient and in hot ($140^{o}F$) humid (100% RH) environments was performed to demonstrate that the new adhesive bonding technology selected had adequate environmental durability. The test specimens consisted of double strap splices in thin sheet using a 30 minute cycle and a small number of thick adherend specimens using a one hour cycle.

Slow cycle testing will be done and analyses procedures developed to demonstrate the strength of flawed bonded joints. These flaws include porosity, voids, fractured bondline, surface contamination, low bonding temperature, excessive out time and short cure.

Various structural and environmental tests were performed in the selection of the bonding system. Surface treatments, primers and protective coatings were extensively evaluated to find an optimum combination. Tests were performed to obtain material property data on the candidate adhesives. The effects of mechanical fasteners through bonded joints were evaluated. Hole preparation, riveting methods, and interference-fit fastener installation were areas of investigation. A newer aluminum alloy 7475-T761 was being considered for some primary structure applications. Data was obtained for fatigue, fracture toughness and crack growth for this alloy.

Non-destructive inspection methods for adhesive bonds in primary structure were extensively evaluated. Each non-destructive inspection method was tested for its ability to detect defects in adhesively bonded assemblies and its application and limitations. Types of bonded joints were assessed as to their degree of difficulty for inspection. Studies were begun to select a non-destructive inspection method for production inspection, in-service inspection and the acceptable flaw sizes.

Approximately 600 bonded test specimens and 94 mechanical assemblies have been fabricated up to this time. The specimens fabricated range from small coupons used for adhesive system testing to large fuselage panels used for structural concept verification. Bonding fixtures have been fabricated to facilitate the manufacture of both curved and flat bonded assemblies.

A production type quality assurance plan was used for the PABST program. This plan involved a total approach to product quality with an overall goal to prove structural integrity and durability of fuselage structure when manufactured in a production environment. This plan encompassed the elements of (1) design engineering and release, (2) material procurement, (3) planning, (4) tooling, (5) fabrication, (6) receiving and inspection, and (7) engineering test and evaluation. Failure and Rejection Reports (FRRs) were made on all discrepancies encountered during the fabrication of Phase Ib components.

To determine the economic viability of bonded structure various cost aspects were taken into consideration. The acquisition, maintenance and repair costs were all considered for each configuration. The costing was an on-going study which was used in the overall process of evaluating and selecting both design and manufacturing concepts.

INTRODUCTION

The use of adhesive bonding in components of aircraft structure has increased dramatically over the last 15 years to the point where most aircraft delivered today utilize some degree of adhesive bonding. However, these applications have been confined primarily to secondary structure where the adhesive bond stress is a low percentage of the adhesive shear strength. This experience with secondary structure has led to the recognition that problems with adhesive bond durability, inspection and the effects of defects must be solved prior to the extensive use of adhesive bonding on primary structure.

Extensive government and industry exploratory development programs over the past few years have resulted in improved adhesives, primers and surface preparation, as well as improved laboratory test techniques that can closely simulate the type and nature of service experience. In addition, nondestructive inspection techniques for adhesive bonds have been vastly improved. These developments have provided confidence that a final validation program should be pursued to prove the adequacy of adhesive bonding for primary structure.

A series of interrlated Air Force sponsored programs have been constructed to obtain additional bond durability data on coupons and components, provide data on sonic fatigue resistance of bonded structure and develop the necessary manufacturing, field and depot repair methods, and the verification of bondline defects.

In February of 1975 the Douglas Aircraft Company, under contract to the Air Force, initiated a technology validation program for primary adhesive bonded structures (PABST). This program was to perform a preliminary design, perform detail design, fabricate test articles and perform coupon, component and full scale fatigue, static and damage tolerance testing. The baseline configuration was fifty-two (52) foot section of the fuselage of the YC-15 airplane. See Figure 1. The objective of PABST was to validate that application of adhesive bonding could result in substantial cost and weight

PRECEDING PAGE BLANK-NOT FILMED

savings when compared to conventional fabrication techniques, while providing significant improvements in structural safety and durability. This report documents the results of the Phase Ib Preliminary Design effort.

CHARACTERISTICS DATA

ITEM	WING (BASIC)	HORIZONTAL TAIL	VERTICAL TAIL
AREA SQ FT	2107.2	643	462.76
ASPECT RATIO	8 342	5.0	0.8947
TAPER RATIO	0 242	0.45	1 0
SWEEP C/4	5°13'32"	4°46'12"	41°
ANHEDRAL	0°	3° AT TE	~
THICKNESS % CHORD	13.68% AVERAGE	11%	12%
VOLUME RATIO	~	1.069	0 0857

CARGO COMPARTMENT SIZE
- 544-IN LENGTH (EXCLUDES WALKWAY)
- 140-IN WIDTH
- 136-IN HEIGHT (MIN)
- 146-IN HEIGHT (MAX)

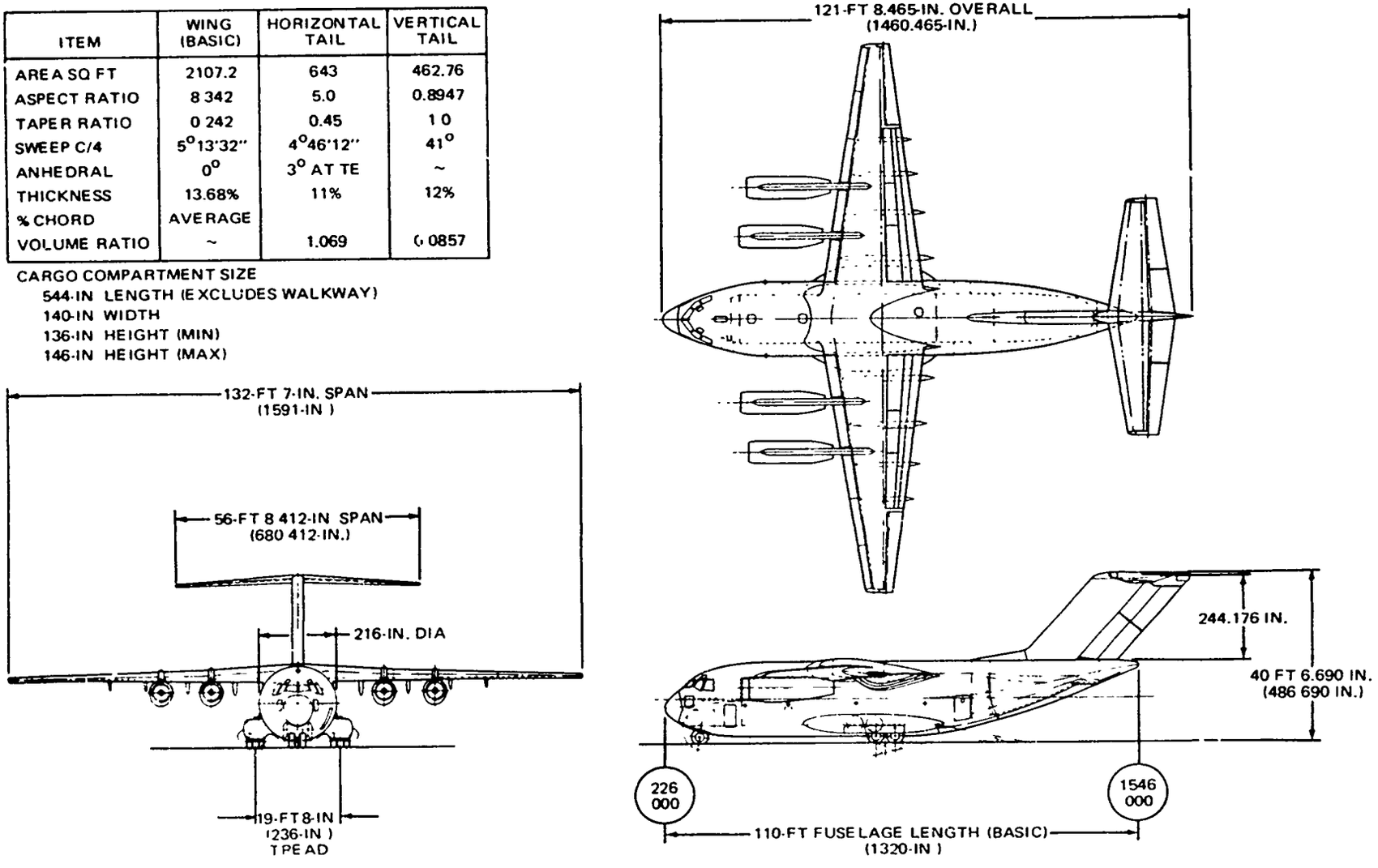


FIGURE 1. PABST BASELINE THREE VIEW

STRUCTURAL DESIGN

The design effort for Phase Ib consisted of three tasks. First a formulation and evaluation activity determined those structural concepts with a significant pay-off potential for an AMST class of fuselage. This task concluded with the selection of three (3) concepts which were to be continued through preliminary design. Concurrently, a baseline airplane was defined that made maximum utilization of the YC-15 program as the baseline data source. At the conclusion of these tasks, a design activity was conducted which led to the generation of three preliminary design layouts of the ADP component based on selected and approved concepts. These three preliminary designs were developed to equivalent levels of detail.

PRECEDING PAGE BLANK-NOT FILMED

Baseline Fuselage

A side view of the baseline fuselage is shown in Figure 2 . This baseline fuselage consists of a nose section, forward of station 439, and a cargo compartment section, aft of station 439. Most of the fuselage shell is cylindrical with a constant 108 inch radius circular cross section starting from station 516 and running to station 992.5 aft. Forward of station 516 to station 330, the shell is conical (out of round) in cross sectional shape. In the cargo compartment section, a trapezoidal wing box mounts to the upper portion of the fuselage between stations 703 and 847. The cargo compartment floor extends aft from station 439 to station 987 at a constant height, $z = -75.70$. This floor continues forward to intersect a vertical pressure bulkhead in the nose section at station 366. This vertical pressure bulkhead seals off the lower half of the fuselage shell up to $z = -26$ where it then runs horizontally forward to station 330. A crew entrance door is located at the cargo compartment floor level in the nose section between stations 394 and 430. An emergency evacuation door is located in the cargo compartment section about 18 - 22 inches above the floor between stations 559 and 583. Two escape hatches are located on the upper fuselage centerline between stations 607 and 631 and stations 943 and 967. Keels are located under the floor of the cargo compartment at $x = \pm 21$. Access to the area under the floor is provided by a hell hole door located between keels on the lower centerline of the fuselage between station 799 and 823. Two (2) windows on each side are provided between stations 559 and 583 and stations 943 and 967. In the nose area, a pilots floor is provided at $z = -3.075$ which runs from station 330 aft to station 439.

The semimonocoque baseline fuselage is structurally similar to the internal longeron concept, except that mechanical fasteners are used instead of bonding. Because of this difference, the baseline longerons are Z-sections and fuselage frames are attached to the shell by means of angle-section shear clips. Titanium tear stoppers are provided under each fuselage frame shear clip. Two 7075-T6 longitudinal tear stopper straps are provided externally on the side of the shell where the longerons are wide spaced.

PRECEDING PAGE BLANK-NOT FILMED

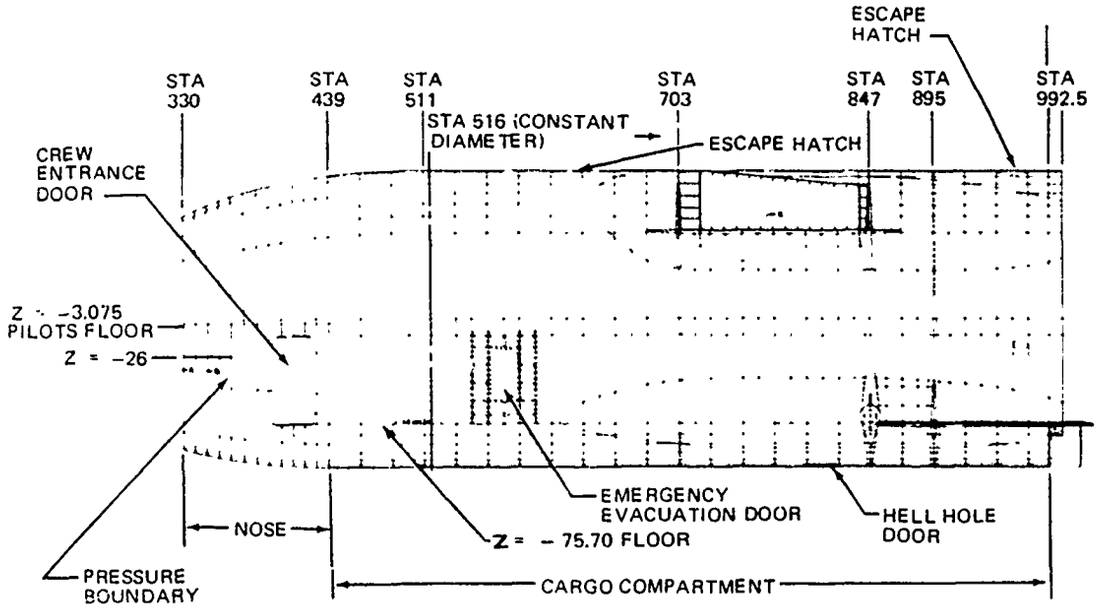


FIGURE 2. SIDE VIEW OF BASELINE FUSELAGE

Full Scale Demonstration Component

A view of the component is shown in Figure 3. This component consists of a nose section, forward of station 439, and a cargo compartment section, aft of station 439. Most of the fuselage shell is cylindrical with a constant 108 inch radius circular cross section starting from station 516 and extending aft to station 871. Forward of station 516 to station 367 the shell is circular in cross sectional shape, while the lofted shape from station 367 to station 516 is a circular arc. In the cargo compartment section, a rectangular wing box mounts to the upper portion of the fuselage between stations 703 and 847. The cargo compartment floor extends aft from station 367 to station 875 at a constant height, Z = -75.7.

The extruded floor planks extend from X = $\pm$ 25 to the side of the fuselage; i.e., the center approximately four feet of fuselage width has no floor planks. The open area located at the fuselage centerline has several advantageous features.

- The amount of planking installed is sufficient to provide the necessary load paths and stiffness requirements for the component while minimizing fabrication and installation costs.
- Installed planking will provide sufficient data for cost analysis purposes.
- The open center section provides easy access to the under floor area for manufacturing, inspection, engineering, and test personnel.

A crew entrance door is located at the cargo compartment floor level in the nose section between stations 391 and 427. Keel members (extruded channels) are located below the cargo floor and mechanically fastened to the top of the inner flange of the frame members at X = $\pm$ 25.

One window is provided on the left side of the fuselage just below longeron 9 between stations 559 and 571. The "window" is a cutout (8.50 inch dia.) in the skin with an aluminum sheet simulating the clear plexiglas window. This approach provides the desired anomaly (a cutout in the exterior

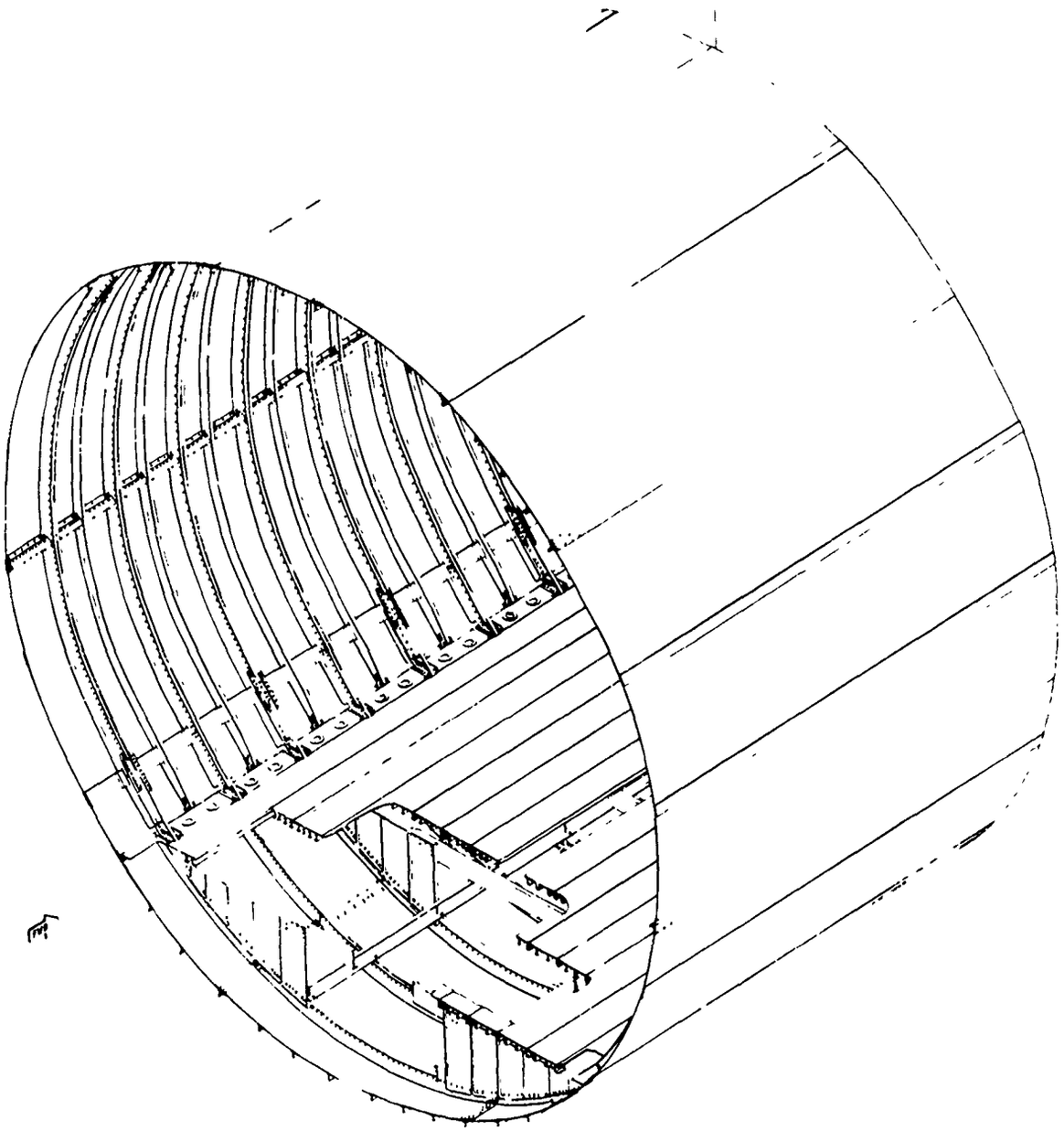


FIGURE 3. FULL-SCALE DEMONSTRATION COMPONENT

skin) while minimizing the cost impact on the program.

The semimoncoque fuselage component is structurally similar to the internal longeron concept above the floor including longeron 10 and to the external longeron concept below the floor. Three 7475-T761 longitudinal tear stoppers are provided externally on the fuselage side where the longerons are wide spaced. Two tear stoppers are located between longerons 8 and 9. The panel assembly between longerons 9 and 10 has one tear stopper below longeron 9 and a bonded longitudinal splice which functions as a tear stopper located close to longeron 10.

Formulation and Evaluation Studies

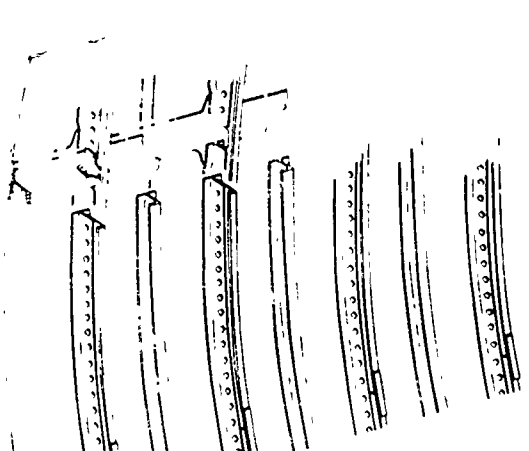
Five concepts were initially formulated and evaluated. These concepts, shown in Figure 4, were (A) wide spaced longeron (B) close spaced longeron, (C) honeycomb (D)corrugations (E) beads and (F) external longeron employing fairings. Evaluation of these concepts was sufficient to determine those concepts with a significant pay-off potential for the AMST class of fuselage.

Of the five concepts formulated, beads and corrugations were determined to have the least pay-off potential. Their advantages over conventional structure were the higher shear allowables for a panel of equal skin gage, fewer parts, and more uniform axial load distribution. The bead height was restricted due to material stretch forming limitations. Weight advantage of the beaded section under axial load was lost at the frame where the beads were flattened and produced eccentric loading. The transition from beads to corrugation required a frame. Corrugation end fittings caused problems in installation. Corrugation splices were difficult to make because of alignment and nesting problems. Joggles in the corrugations were impractical. The shear tie between the fuselage frames and the skin was difficult with corrugations. Both beads and corrugations are closed sections which are difficult to inspect and repair and which present moisture traps that can lead to corrosion.

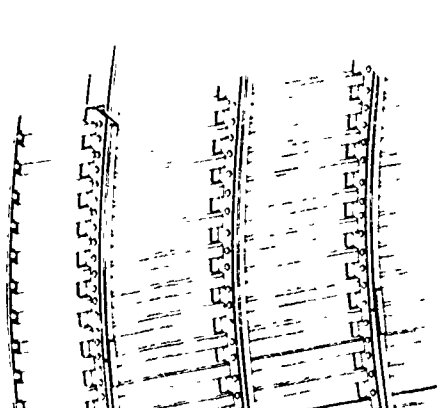
The honeycomb concept was competitive with conventional structure because of reduced number of parts, better failsafe capability, and doublers could be buried in between the face sheets to provide a more uniform bonding surface. In addition, the minimal number of frames simplified placement of unique items within the structure. The primary disadvantage of honeycomb was its susceptability to foreign object damage. Other possible problems were splice areas, edge members, and repair problems. However, due to the potential reduced cost payoff, honeycomb was selected as one of the three concepts for continued evaluation.

The external longeron concept had many structural disadvantages when external fairings were considered to reduce the aerodynamic penalty. Thus,

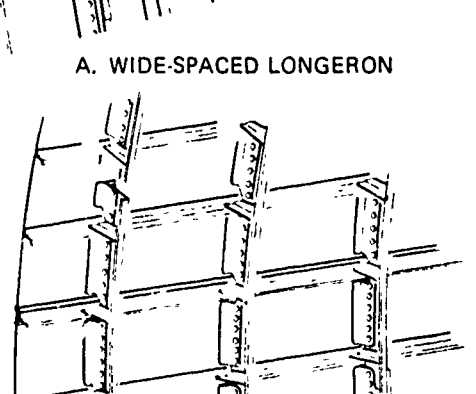
PRECEDING PAGE BLANK-NOT FILMED



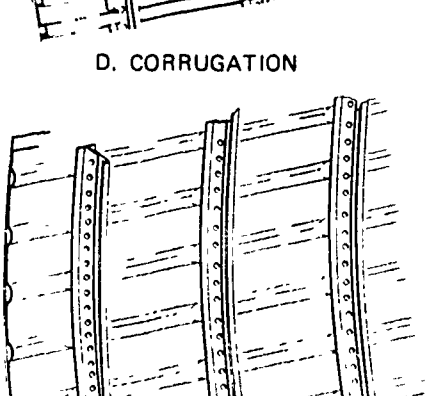
A. WIDE-SPACED LONGERON



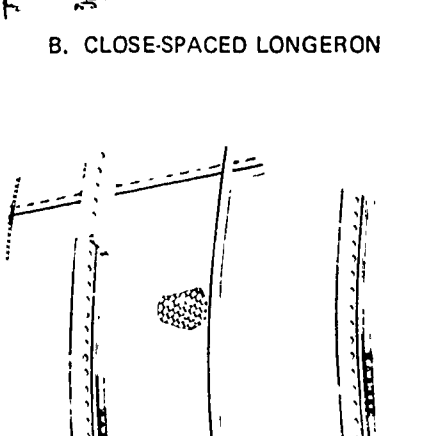
D. CORRUGATION



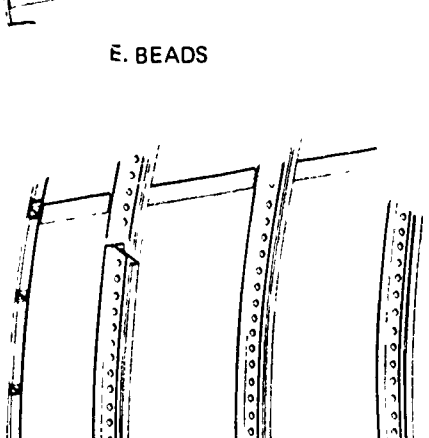
B. CLOSE-SPACED LONGERON



E. BEADS



C. HONEYCOMB



F EXTERNAL LONGERON

FIGURE 4. INITIAL DESIGN CONCEPTS

visual inspection and NDI were more difficult; close out areas were more complex; light fairings were more susceptible to field damage; tooling and manufacturing costs were increased. Without fairings, the concept of external longerons was competitive with the other concepts. Frames, pressure bulkhead caps and floor support bulkhead would attach directly to the skin. Continuous frames without longeron cutouts would delete the need for circumferential tear stoppers. An evaluation was made to quantify the aerodynamic penalty for external longerons with and without fairings, See Appendix A. Because of the structural potential of external longerons without fairings and with knowledge of the aerodynamic penalty, this concept was selected and approved as one of the final concepts for continuation through preliminary design.

Close and wide spaced bonded longeron concepts were about equal in their potential payoff for an AMST class of fuselage. The close spaced longeron concept was similar to conventional structure except bonding replaced mechanical attachments. This similarity gave a high degree of confidence in the structural arrangement and structural integration for close spaced longerons. Wide spaced longerons required fewer cutouts in the frames. Thus, the frame-to-skin shear tee could function as a crack-stopper and simple tooling would be required for bonding. Each of these concepts were continued through preliminary design. They were combined so the best advantages of each would be utilized. Thus, close spaced longerons were used for the upper and lower shell where longitudinal loads were highest. Wide spaced longerons were used for the side of the shell where the shear loads were high.

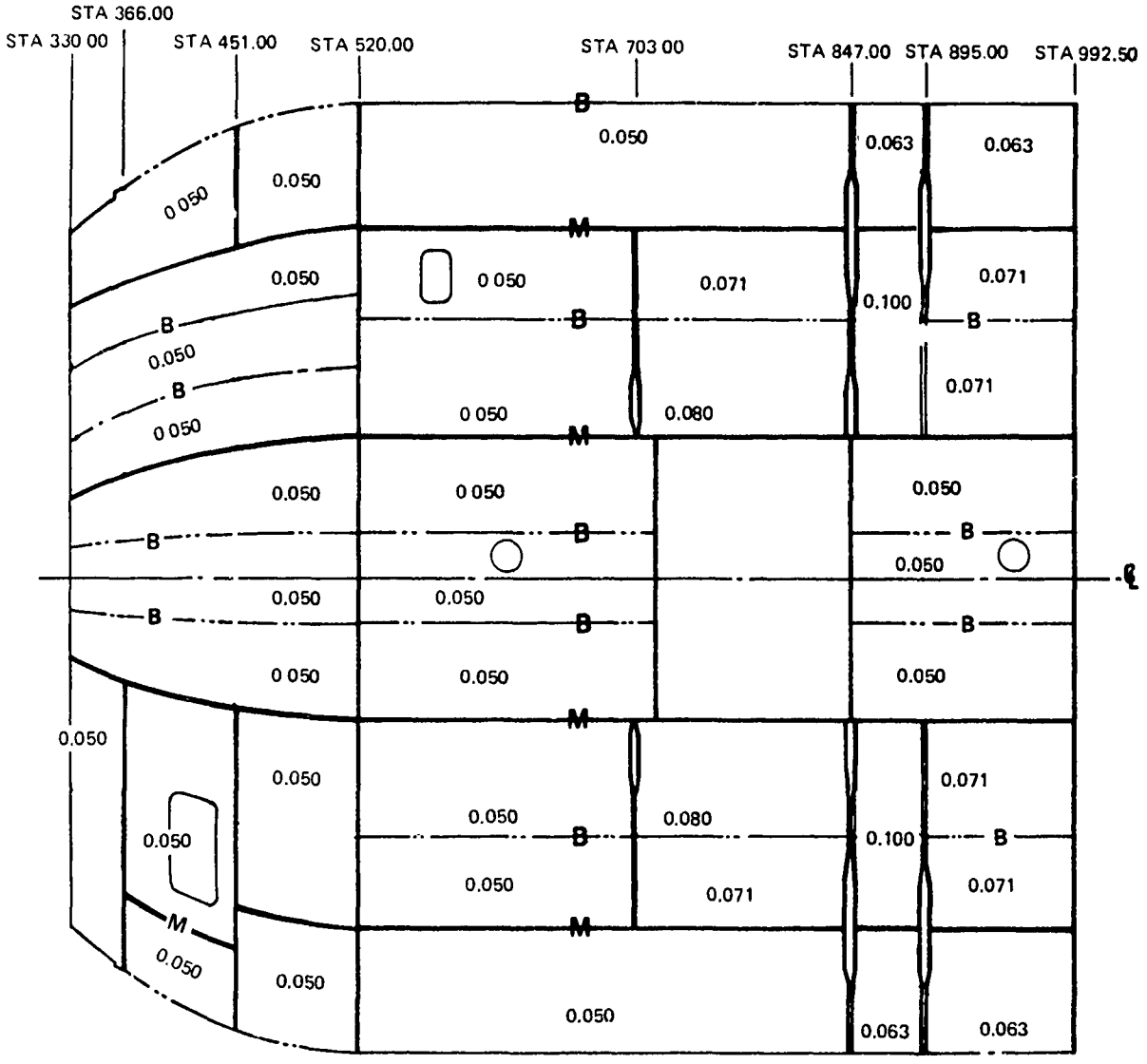
Preliminary Design Studies

Based on the formulation and evaluation studies, concepts selected and approved for preliminary design were (1) the internal longeron concept, (2) the external longeron concept, and (3) the honeycomb concept. Preliminary design layouts for these three concepts were generated to an equivalent level of detail which included general structural arrangement, structural sizing, splices, intersections, cutouts, and interface problems. Supporting trade studies for these preliminary design layouts are included in Appendix A. It was assumed, for all concepts, that floors, floor bulkheads, keels, pressure bulkheads and wing box structures were common items which would be made similar to the baseline structure.

Internal Longeron Concept. - The internal longeron concept general arrangement is similar to the baseline, shown in Figure 2 . Basic frame spacing in the cargo compartment (stations 439-987) is 24 inches. Floor support bulkheads are at stations 439, 463, and every 48 inches thereafter to station 987; i.e., every other frame station. Aluminum 7475-T761 tear stoppers are provided under each longeron for fail-safe requirements. Two longitudinal straps are also provided on the side of the fuselage to give added fail-safe capability where the longerons are wide spaced. Light frames are provided between the 24 inch spaced frames on the side of the fuselage where the longerons are wide spaced in order to increase the initial buckling stress of the thin skins. In the nose area between stations 330 and 439, frames are spaced at 9 inch intervals to resist bending moments induced by cabin pressure in the out-of-round section. These frames are not cut-out for longeron continuity as in the cargo compartment.

Skin Panels: - Skin panels for the internal longeron concept are shown in Figure 5. Mechanical splices are denoted by M and bonded splices are denoted by B. Longitudinal mechanical splices were set at maximum distances based on a manufacturing constraint for handling that limited the bonded panel sizes to a maximum arc segment of 96 degrees. Longitudinal bonded skin splices within the boundaries of the longitudinal mechanical skin splices were determined by a vendor manufacturing constraint on the skin width of 94 inches for 0.050 inch thick skin. A transverse mechanical splice is provided at the boundary between the fuselage constant section and double contoured section

PRECEDING PAGE BLANK-NOT FILMED



NOTE

1 ALL SKINS ARE 7475-T761

FIGURE 5. SKIN PANEL – INTERNAL AND EXTERNAL LONGERON CONCEPT

to accomodate the separate tooling required for the nose section. Transverse mechanical splices are also provided at the front spar, rear spar, and drag link frame so the external loads from the wing and main landing gear will have a direct path into the frames. In the nose section, transverse mechanical splices are provided so the door panel can be made as one piece to simplify manufacturing.

Minimum skin thickness over the entire fuselage was set at C.050 inch based on foreign object impact considerations. All skin material is 7475-T761 bare aluminum alloy. Skin thickness ranges from a minimum of 0.050 inch in the area forward of the wing to a maximum of 0.10 inch between the rear spar and drag link frames where shears are high due to landing loads induced by the main landing gear and flight loads induced by the wing.

Fuselage skins are stiffened longitudinally by extruded J-section longerons. These sections are 7075-T6 aluminum extrusion material. They are spaced about 13 inches on center for the upper and lower shell. One longeron breaks up the side shell at 75 inch spacing. Typical dimensions for the internal J-section longerons are shown in Figure 6 for a longeron at a bonded splice and a basic longeron. Overall longeron height is 1.25 inch for the basic longeron and 1.35 inch for the splice longeron. A J-section longeron was chosen in preference to the more efficient Z-section longeron since it was better suited for the bonding process adopted for the PABST Program. Thus, bonding pressure applied in the autoclave to the outstanding flange of the J-section will produce more uniform bonding surface pressure if the flange against the skin is symmetrical with respect to the longeron web.

Typical skin splices required for the internal longeron skin panels are shown in Figure 7. They consist of longitudinal and transverse skin splices for both mechanical and bonded joints. Longitudinal bonded skin splices are double lapped joints that consist of an inner and outer bonded splice plate with a longeron bonded along the centerline of the splice. The longitudinal mechanical splice is also a double lapped splice. For this splice the splice plates are cold bonded to the skin and also mechanically attached with two rows of 0.188 inch diameter lockbolts spaced about 1.25 inches on center.

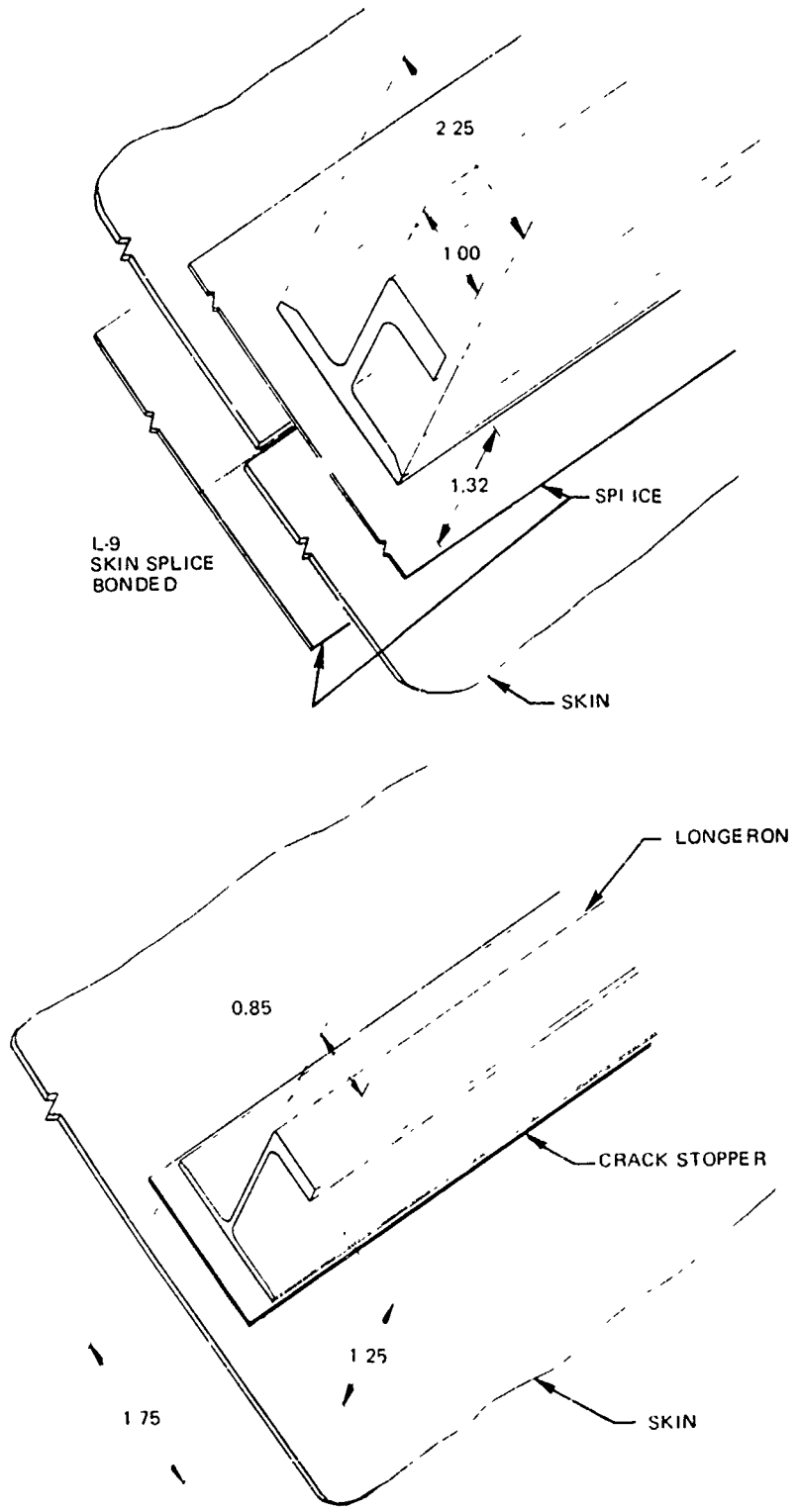


FIGURE 6. TYPICAL INTERNAL LONGERONS

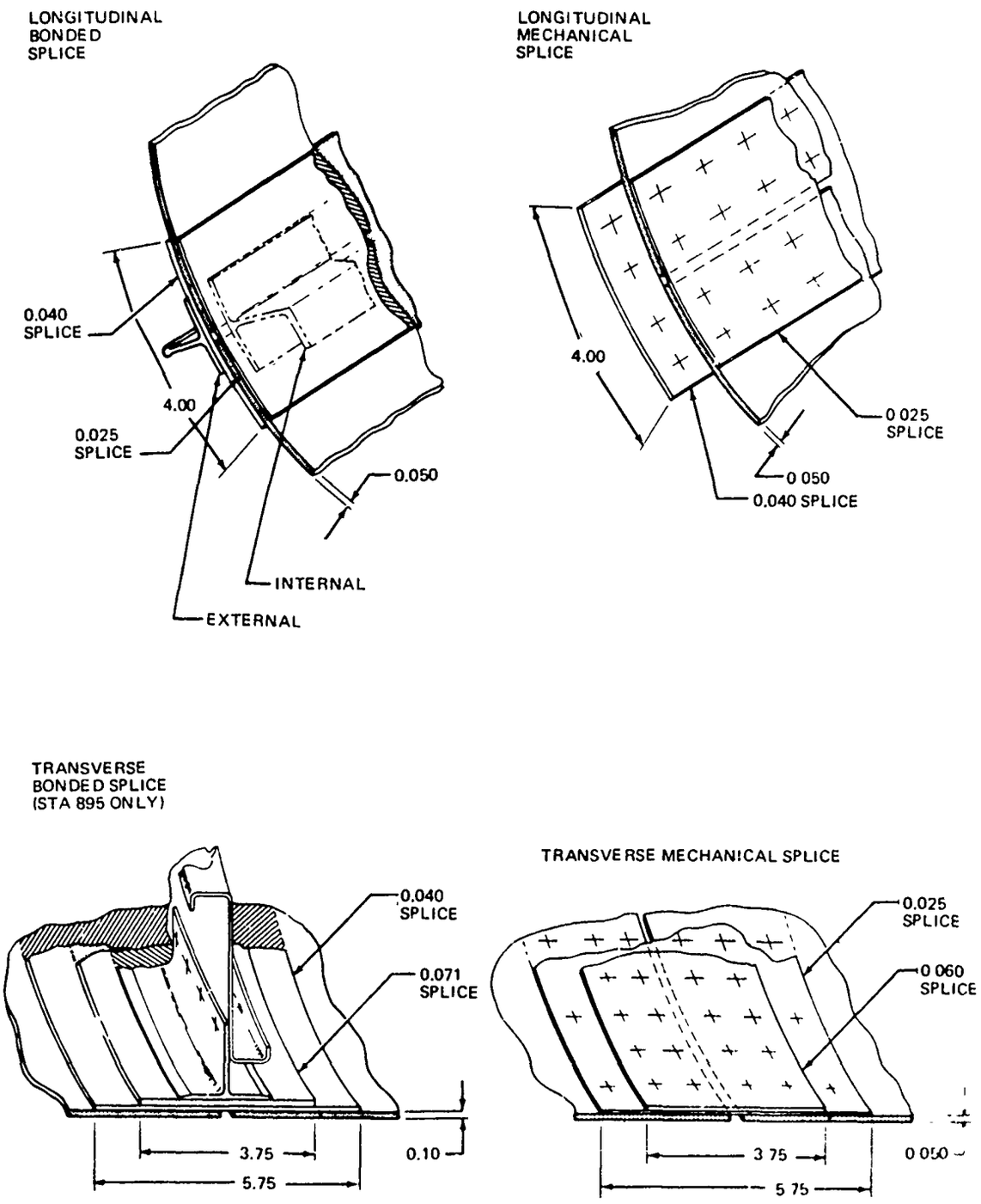


FIGURE 7. INTERNAL AND EXTERNAL LONGERON – TYPICAL SKIN SPLICES

The transverse bonded and mechanical splices are flush with respect to the outside surface because of aerodynamic considerations. Two inner doublers, one thick and one thin, join the skins together. These doublers are stepped in order to produce a more uniform load transfer. For the transverse mechanical splice, doublers and skin are cold bonded together. Two rows of 0.188 inch diameter lockbolts spaced at 1.25 inch on center tie the thick and thin doublers to the skin. A lead row of 0.188 inch diameter lockbolts spaced 2.5 inch on center tie the thin doubler to the skin.

Frames:- Transverse stiffening for the fuselage shell is provided by frames. A typical fuselage frame in the cargo compartment is shown in Figure 8 for the internal longeron concept. A frame tee with cutouts to provide longeron continuity is bonded to the skin. A Z-section frame is attached to this shear clip by means of 0.188 inch diameter rivets spaced about 1.0 inches on center. Mechanical splices for the frames are staggered with respect to skin splices as shown. Frame-shear clip height is 4.75 inch in the nose section and 4.95 inch in the cargo compartment section as shown in Figure 9. Frame thickness is 0.050 inch in the nose section and 0.063 inch in the cargo compartment except under the wing where it is 0.080 inch. Frames are rolled 7075-T6 material. The floor support bulkhead frames are extruded 7075-T6 channel sections. The frame shear clips are 7075-T6 extruded T-sections.

Intersections:- A typical intersection, in the cargo compartment, for frames and longerons, is shown in Figure 10. A 7475-T761 aluminum tear stopper is bonded under the longeron. This tear stopper is tabbed where it intersects the frame tee. The frame tee, is cutout at this intersection to allow a continuous longeron. It is joggled to fit on top of the tear stopper so that load path continuity is provided through the cutout. A mechanically fastened shear clip ties the longeron to the frame to provide rolling stability.

On the sides of the fuselage shell where the longerons are wide spaced, intermediate frames are provided between the 24 inch spaced frames. These intermediate frames run from longeron 8 to longeron 10 at the cargo floor. A typical intersection for an intermediate frame at longeron 8 is shown in Figure 11. The internal mechanical splice plate at longeron 8 is cutout so that it will fit over the intermediate frame tee when the skin panels are

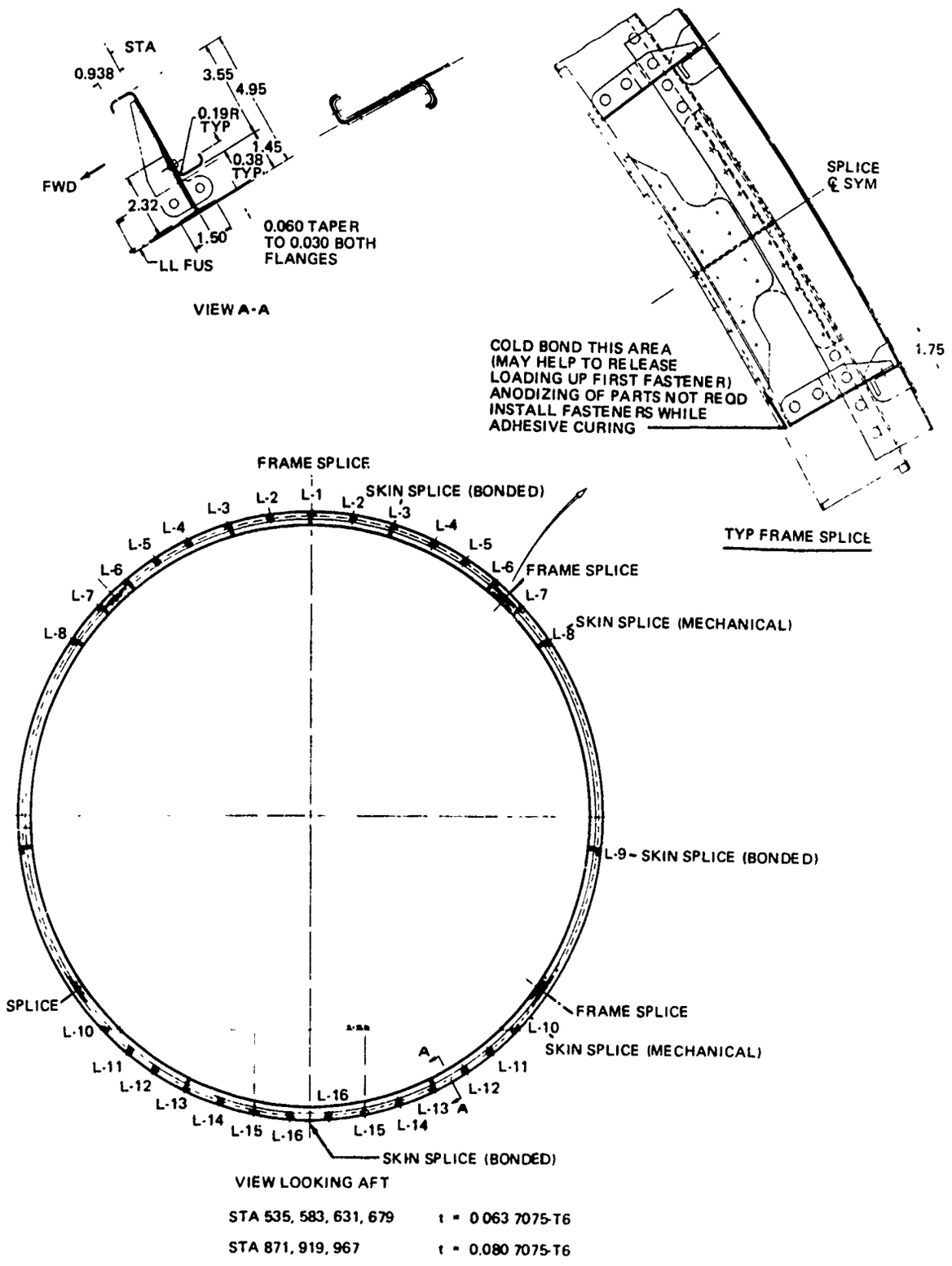
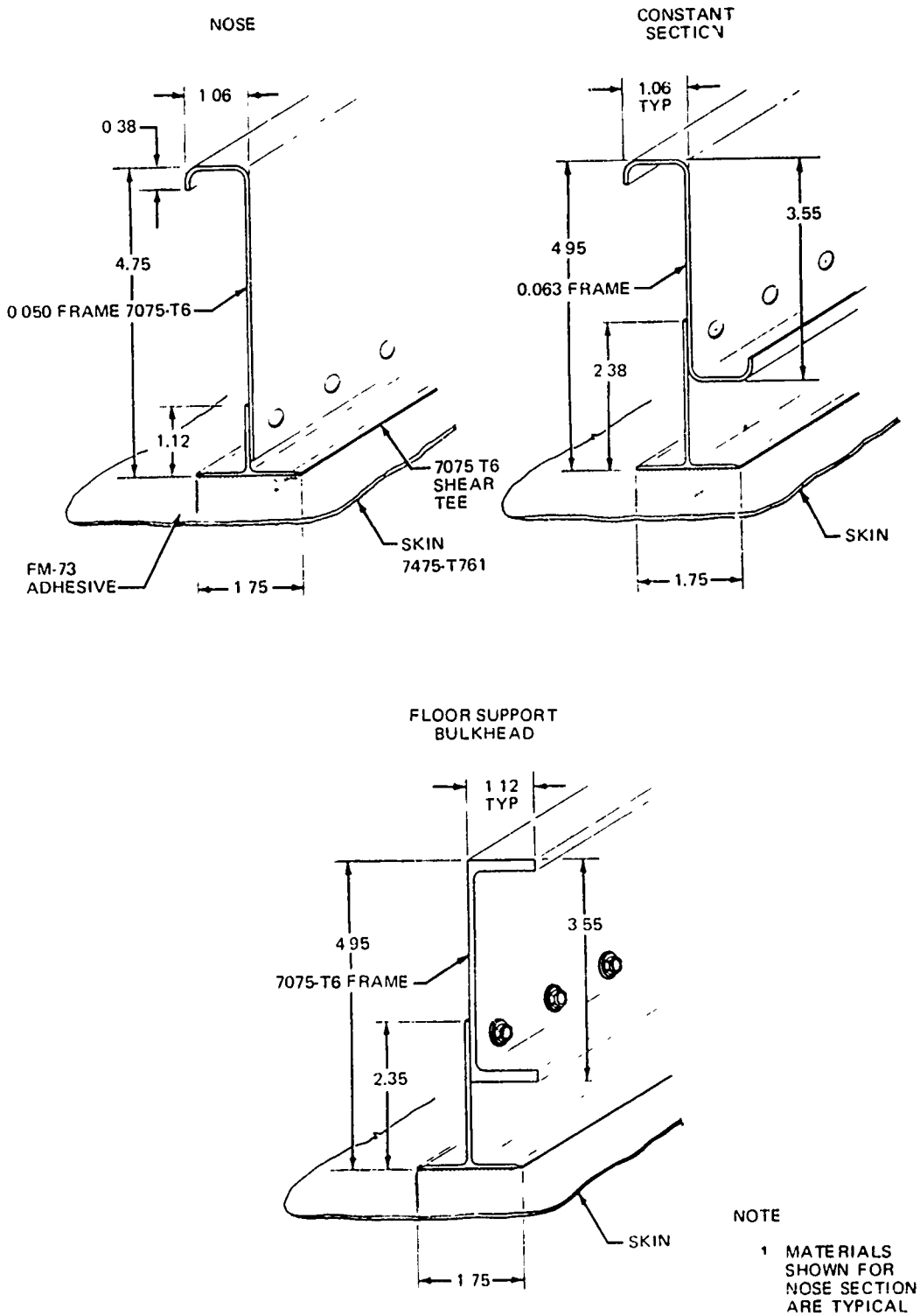


FIGURE 8. INTERNAL LONGERON CONCEPT TYPICAL FRAME



NOTE

1 MATERIALS SHOWN FOR NOSE SECTION ARE TYPICAL

FIGURE 9. INTERNAL LONGERON TYPICAL FRAMES

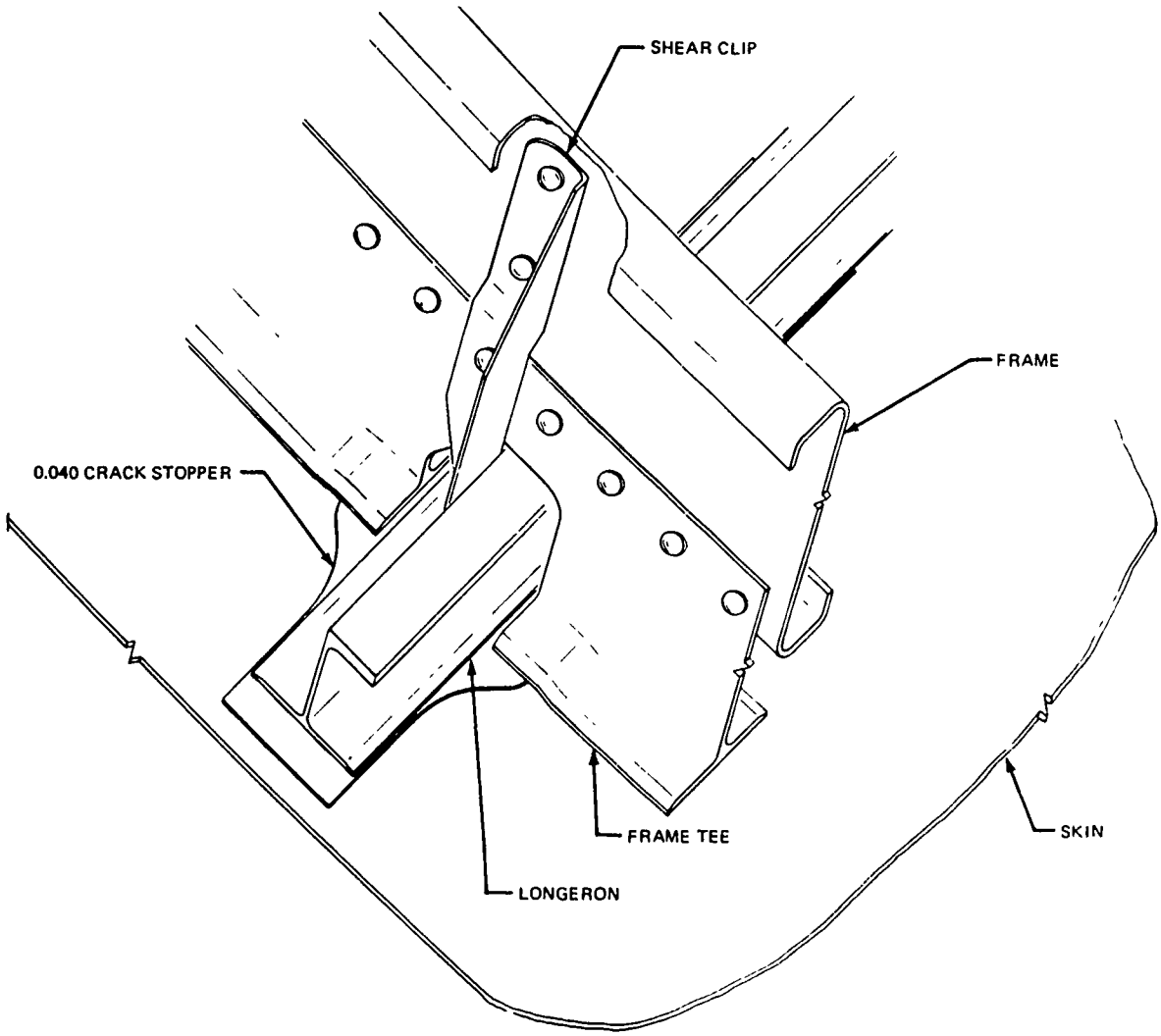


FIGURE 10. TYPICAL FRAME AND INTERNAL LONGERON INTERSECTION

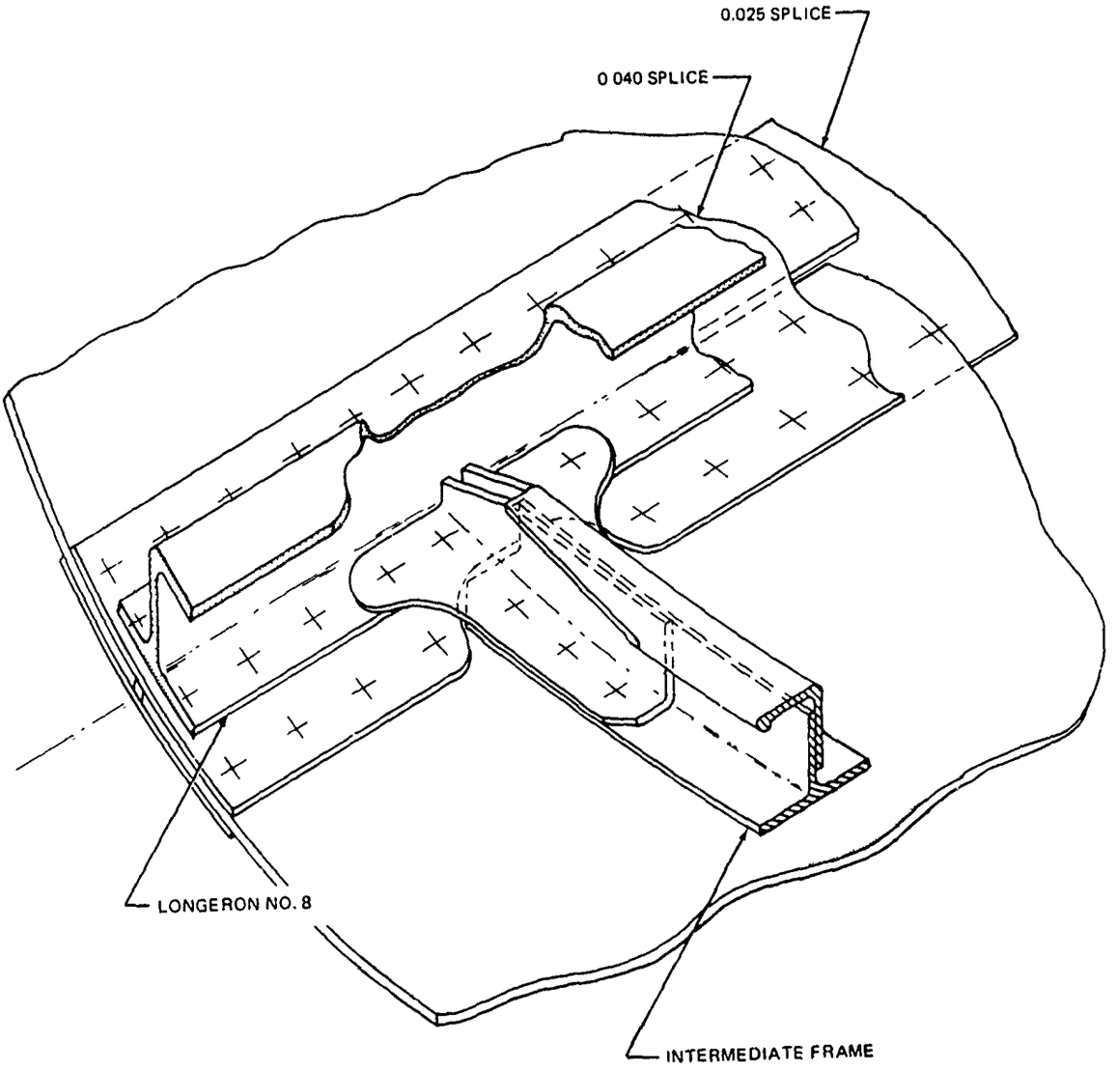


FIGURE 11. TYPICAL INTERNAL LONGERON AND INTERMEDIATE FRAME INTERSECTION

mechanically joined together. Two back-to-back splice angles tie the intermediate frame and the flange of longeron 8 together with 0.188 inch diameter lockbolts.

A typical intersection for the nose frame and longeron is shown in Figure 12. The longeron stops short of the frame tee flange against the skin. This assembly is hot bonded. The frame is then mechanically fastened to the frame tee with aluminum rivets. Two back-to-back angles mechanically fasten the flange of the longeron against the skin and the vertical web of the longeron to the flange of the frame tee.

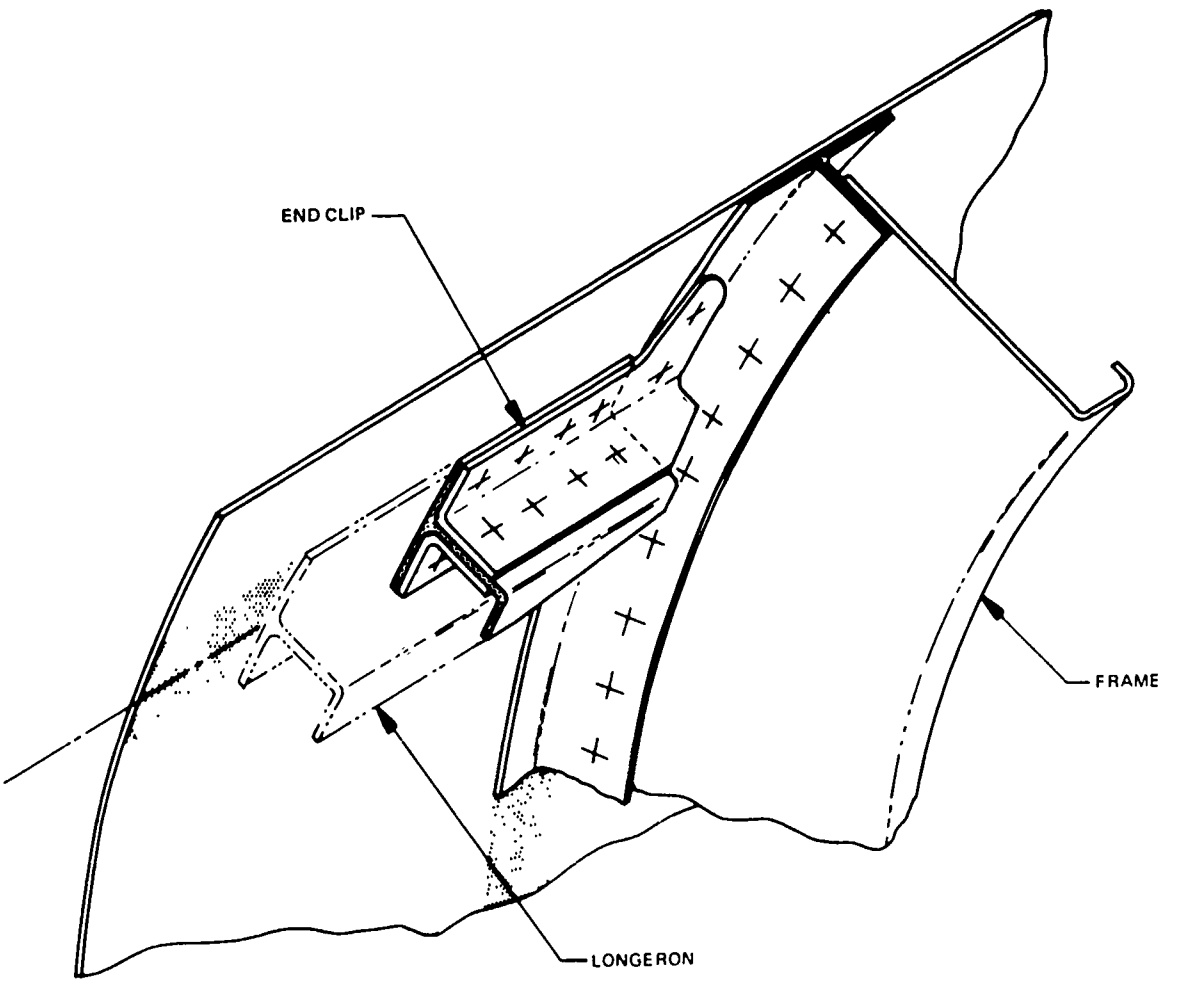


FIGURE 12. TYPICAL NOSE FRAME AND EXTERNAL LONGERON INTERSECTION

A typical intersection for the nose frame and bonded skin splice is shown in Figure 13. The nose frame tee stops short of the skin doublers. The skin, skin doublers, and frame tee are hot bonded together. After bonding, the frame is installed with aluminum rivets. Two back-to-back angles and a filler plate are used to splice the frame tee across the bonded skin splice. Flush 0.188 inch diameter lockbolts tie the angles to the frame tee, skin, and skin doublers. Aluminum rivets tie the angles and filler plate to the vertical frame tee and frame web.

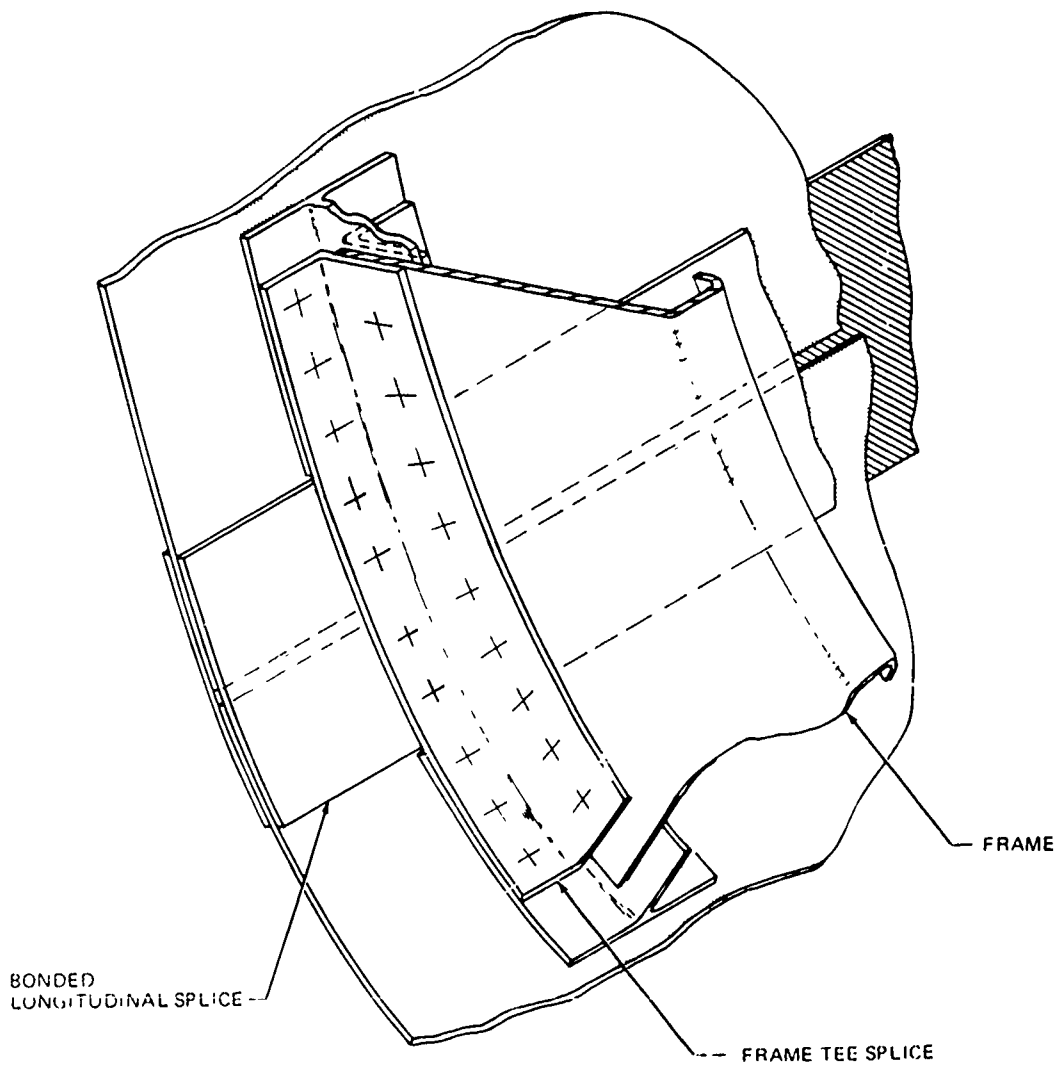


FIGURE 13. TYPICAL NOSE FRAME AND BONDED SKIN SPLICE INTERSECTION

Wing-Fuselage Interface:- The fuselage attaches to the lower wing surface between station 703 and 847 by means of a titanium T-section flex joint shown in Figure 14. The fuselage skin bolts directly to this T-section as shown. Machined posts extend from the front and rear spar frame to pick up trapezoidal panels that bolt to the wing spars. Wing vertical shear and torque are reacted through these machined posts to the fuselage. Fuselage longitudinal loads are transmitted through the wing box at the intersection of the wing ribs and fuselage. Typical fuselage hardpoints for these ties are shown in Figure 15, for the front spar.

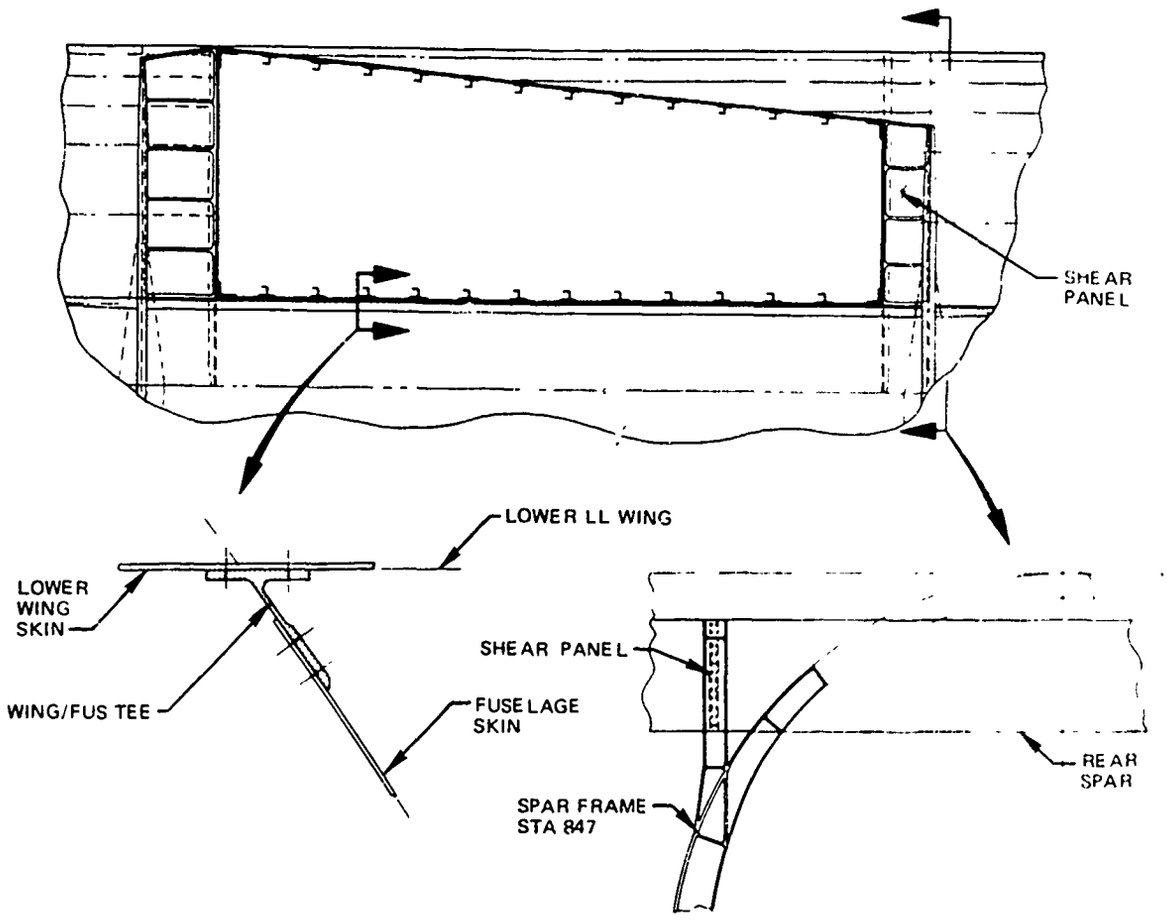


FIGURE 14. INTERNAL AND EXTERNAL LONGERON WING/FUSELAGE INTERFACE

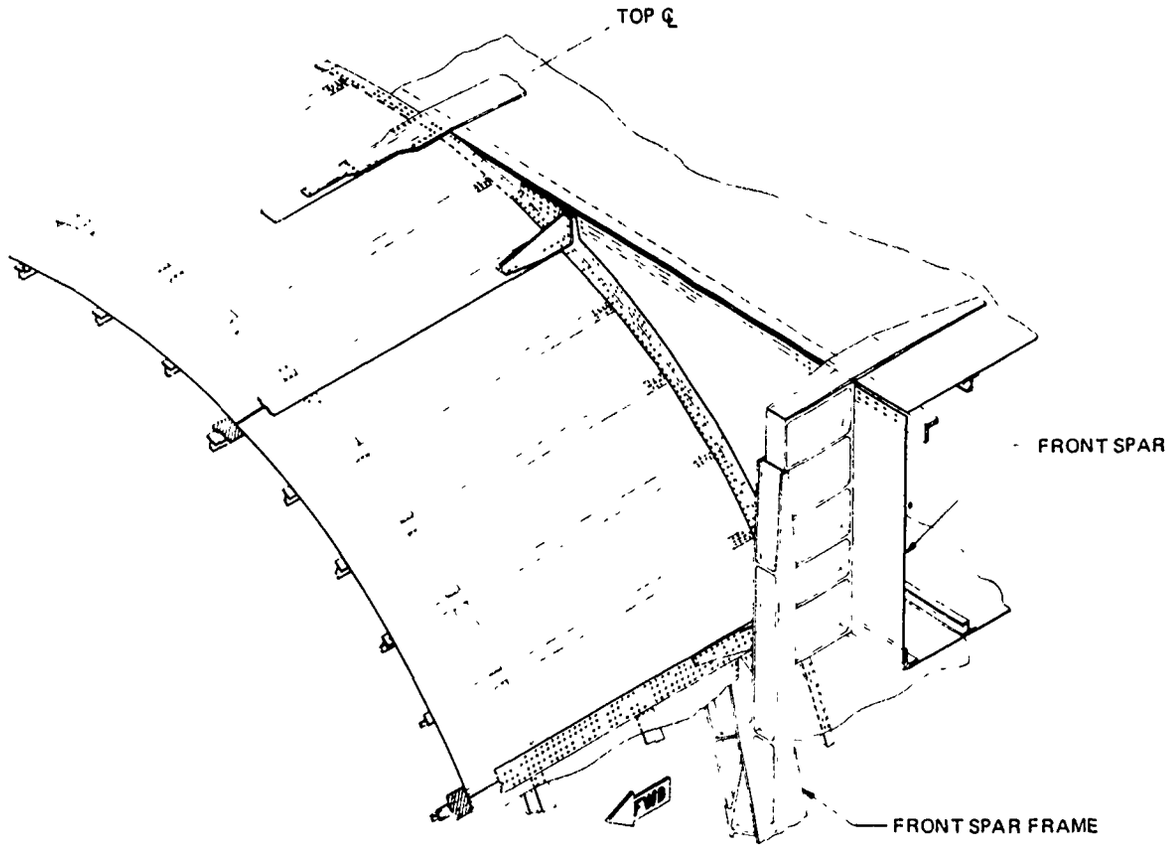


FIGURE 15. INTERNAL LONGERON FRONT SPAR/FUSELAGE INTERFACE

External Longeron Concept - This concept is identical to the internal longeron concept with respect to general arrangement (Figure 2), skin panel sizes and skin gages (Figure 5), skin splices (Figure 7), and wing fuselage interface (Figure 14). The basic difference is that the longerons are on the outside surface of the fuselage shell which permits simpler design particularly of the frame-to-longeron intersections. The longerons are

bulbed T-sections which were selected in preference to a plain T-section because of the increased compression allowable strength. Typical dimensions are shown in Figure 16 for a basic external longeron and a longeron at a bonded splice. Overall longeron height is 1.205 inch for the basic longeron and 1.708 inch for the splice longeron. The longerons are 7075-T6 aluminum extrusion material. They are spaced exactly the same as the internal longerons. Thus, about 13 inches on center for the upper and lower shell and 75 inches on the side of the shell.

Frames:- Figure 17 shows a fuselage frame that is typical for both the nose section and the cargo compartment. The frame consists of a continuous extruded T-section outer cap which is bonded to the skin panel and a rolled section which is mechanically fastened to the extruded T-section by means of 0.188 inch diameter rivets spaced about 1.0 inch on center. Overall frame height is 4.75 inches. Frame thickness is 0.050 inch in the nose section and 0.063 inch in the cargo compartment section. Frame material is 7075-T6 aluminum alloy.

Wing-To-Fuselage Interface:- Fuselage load continuity through the wing cutout area is provided at the wing ribs. Typical hardpoints for the external longeron concept are shown in Figure 18 at the intersection of the fuselage with the wing front spar. The centerline hardpoint consists of a machine tapered T-section which splices to the external centerline longeron and shears the load directly into the wing skin at the centerline wing rib. Off the centerline, the wing skin is higher than the fuselage skin at the wing and fuselage intersection. In this area, the fuselage load is transferred to the wing by a machined tension T-section spliced to the external longeron.

Honeycomb Concept.- The honeycomb fuselage design concept is shown in Figure 19. Basic frame spacing in the cargo compartment is 48 inches. This spacing corresponds with the spacing of the floor support bulkheads. Tear stoppers are provided on the internal honeycomb face sheet between cargo compartment frames for fail-safe requirements except under the wing where frame spacing is 24 inches as a result of the bending moments induced by vertical loads on the wing. In the nose area frames are spaced at 18 inch intervals to resist bending moments induced by cabin pressure in the out-of-

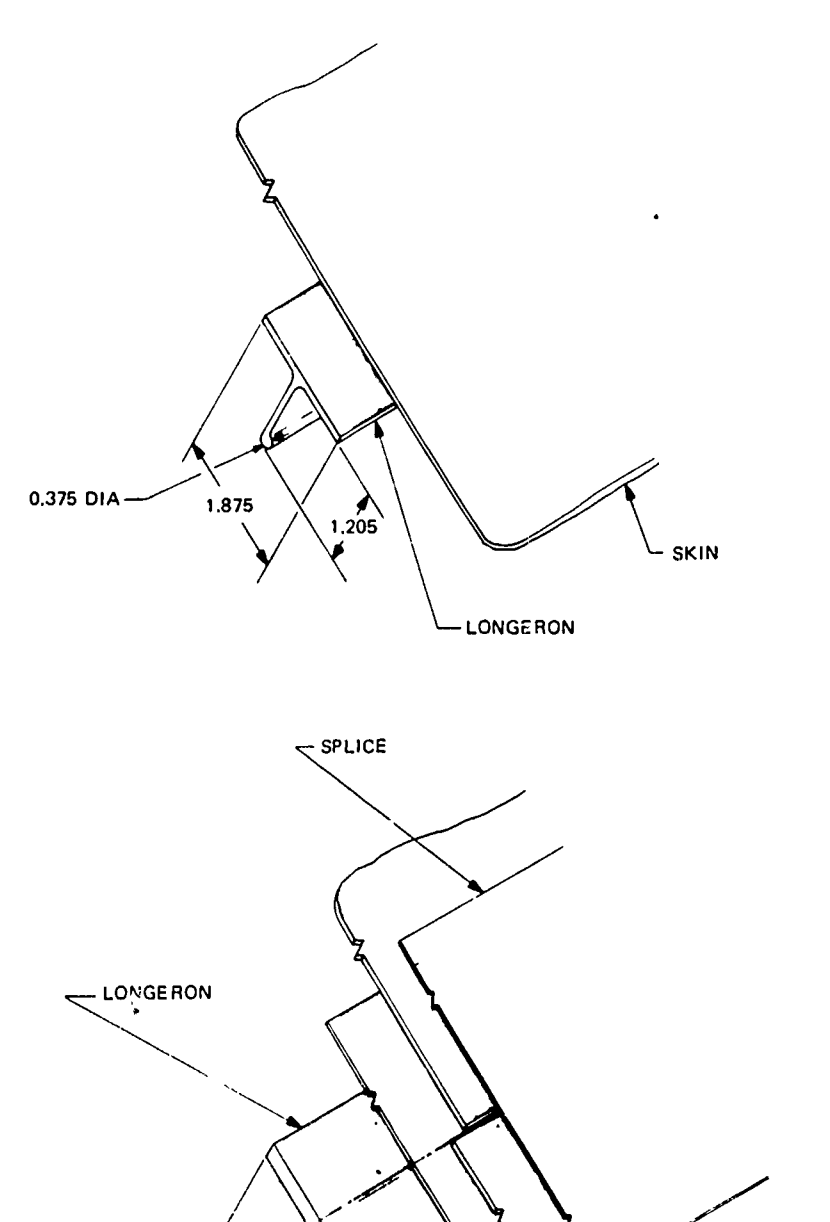


FIGURE 16. TYPICAL EXTERNAL LONGERONS

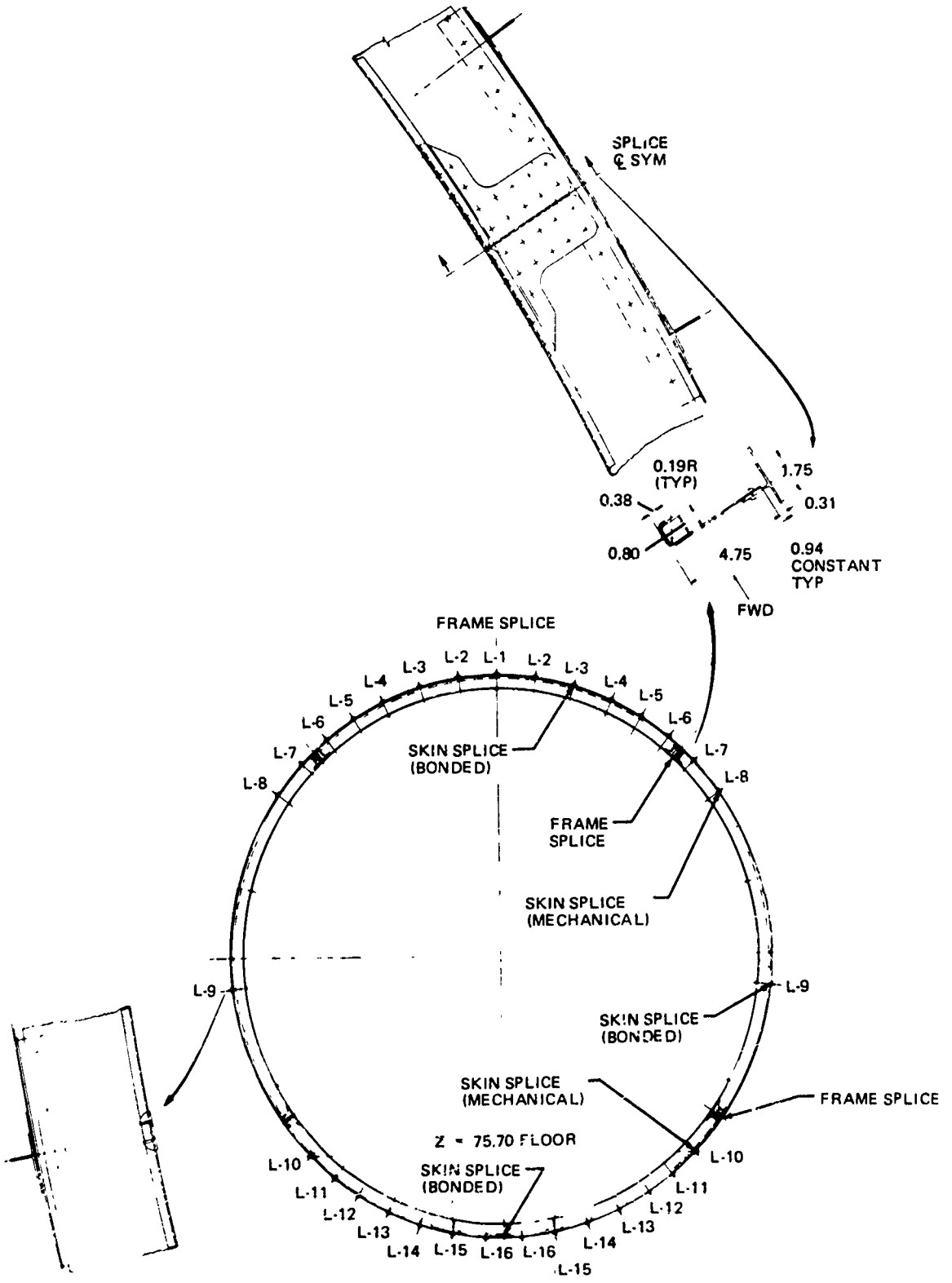


FIGURE 17. EXTERNAL LONGERON TYPICAL FRAME

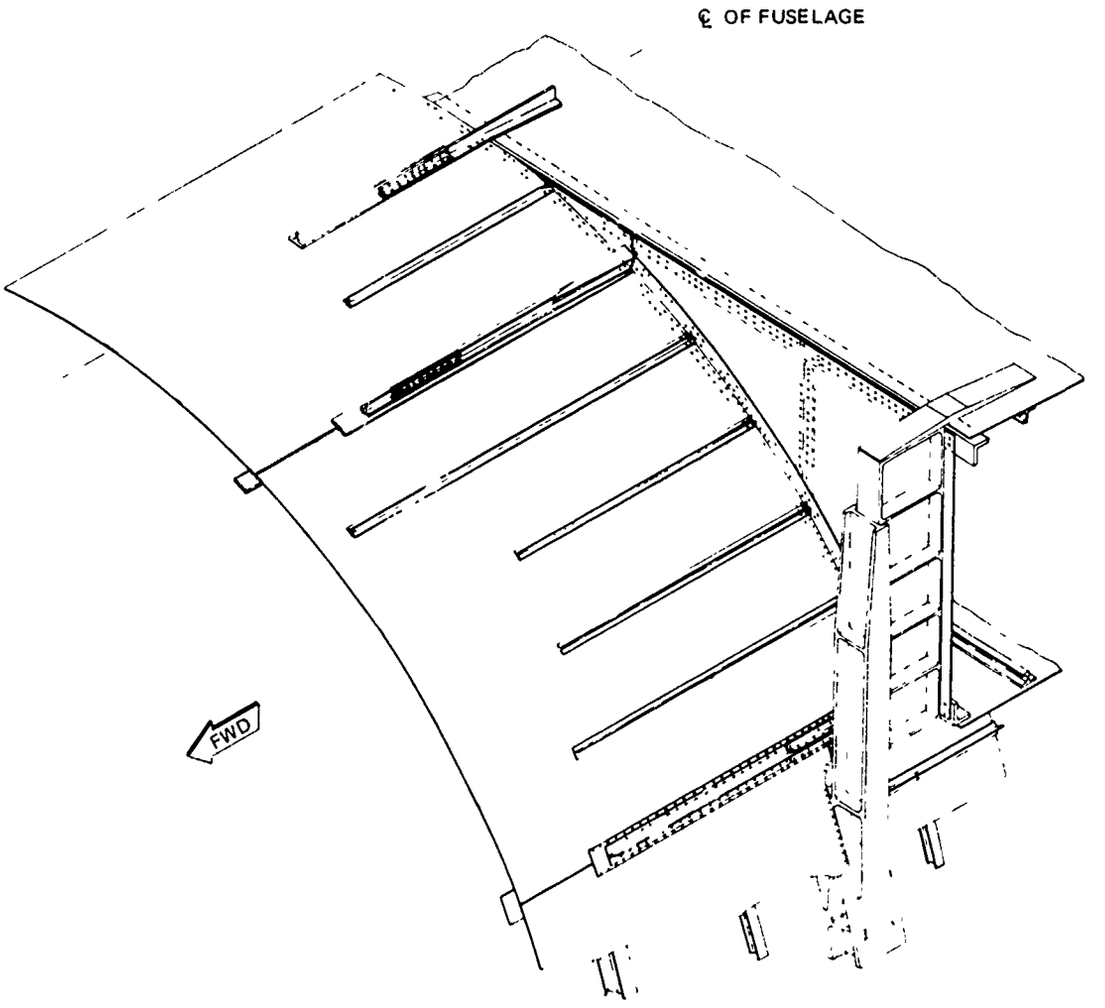


FIGURE 18. EXTERNAL LONGERON FUSELAGE TO FRONT SPAR JOINT

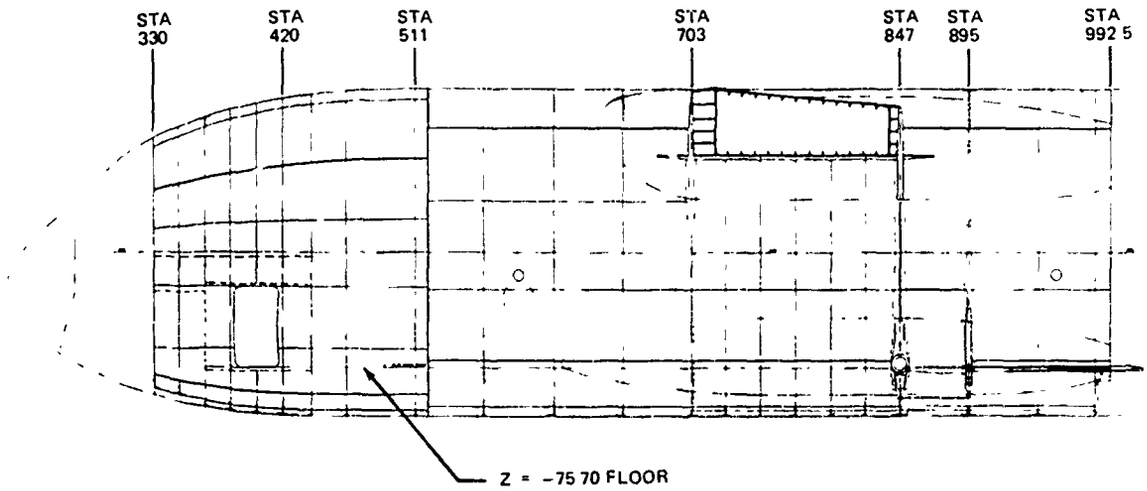


FIGURE 19. SIDE VIEW – HONEYCOMB CONCEPT

round section.

Skin Panels:- Honeycomb skin panels and skin gages are shown in Figure 20. Longitudinal mechanical splices were set at maximum distance based on a manufacturing constraint which limited the bonded panel sizes to an arc segment of about 96 degrees. Longitudinal bonded skin splices within the boundaries of the longitudinal mechanical splices were determined by a vendor manufacturing constraint on the skin width of 60 to 62 inches for 0.020 inch thick aluminum sheet. A transverse mechanical splice is provided at the boundary between the fuselage constant section and double contoured section to accomodate the separate tooling required for the nose section. Transverse mechanical splices are also provided at the front spar, rear spar, and drag link frames so that the external loads from the wing and main landing gear can be introduced directly into these frames.

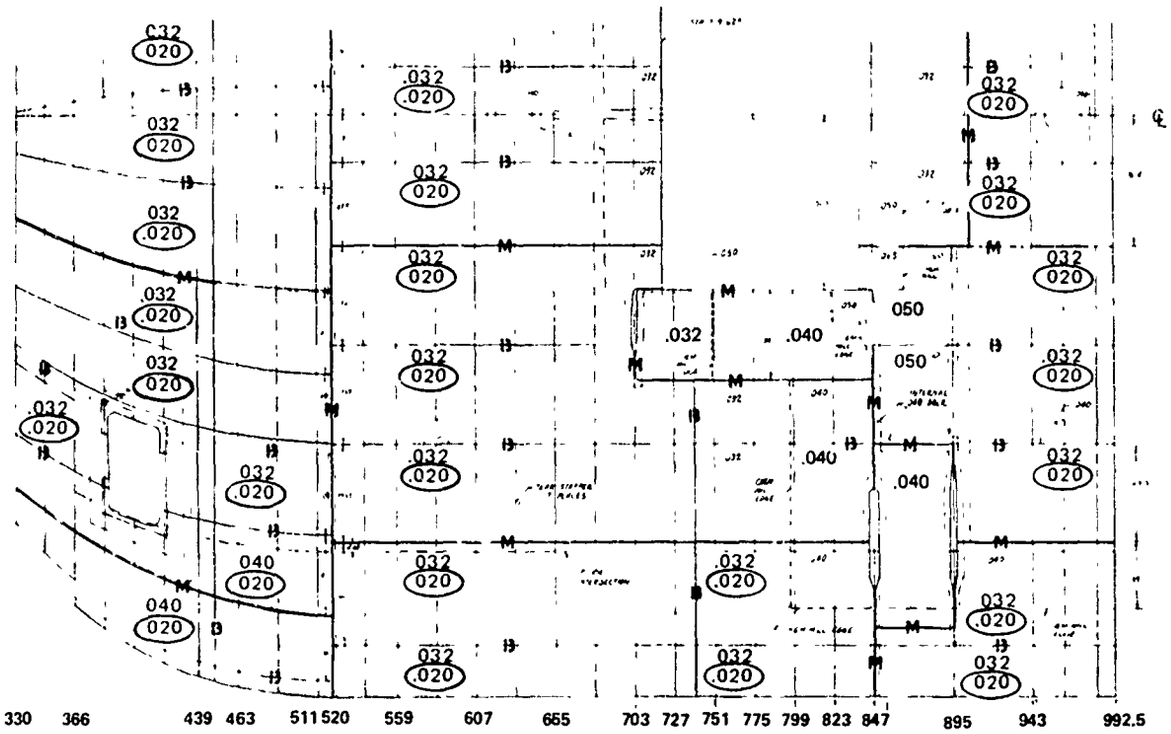


FIGURE 20. SKIN PANELS – HONEYCOMB

The basic minimum face sheet thickness over the entire fuselage is 0.032 inch for the outer face sheet and 0.020 inch for the inner face sheet. All skin material is 2024-T3 bare aluminum alloy. The 0.032 inch outer face sheet thickness was set to minimize foreign object damage. The 0.020 inch inner face sheet thickness was determined as minimum based on handling considerations. In the nose belly area, outer face sheet thickness was increased to 0.040 inch because of the higher likelihood of foreign object impact due to particles impelled by the nose landing gear. In the area of the wing and aft, the 0.040 inch thick material shown in Figure 20 was required for both inner and outer face sheets because of strength and cra. . propagation require ments.

The honeycomb core is basically 0.80 inch thick hexagonal cell. Core material is 5056 non-perforated, corrosion resistant aluminum, having a density of 3.4 pcf corresponding to a cell diameter of 0.250 inch and a cell wall thickness of 0.0015 inch. Typical core splices and core machine cuts are shown in Figure 21. At machined cut areas the core is machined on both sides so all doublers required for the face sheets can be buried between the outer and inner face sheets. This provides a smooth internal surface to facilitate the bonding of required intercostals and frames. Core splices were determined primarily because of handling requirements.

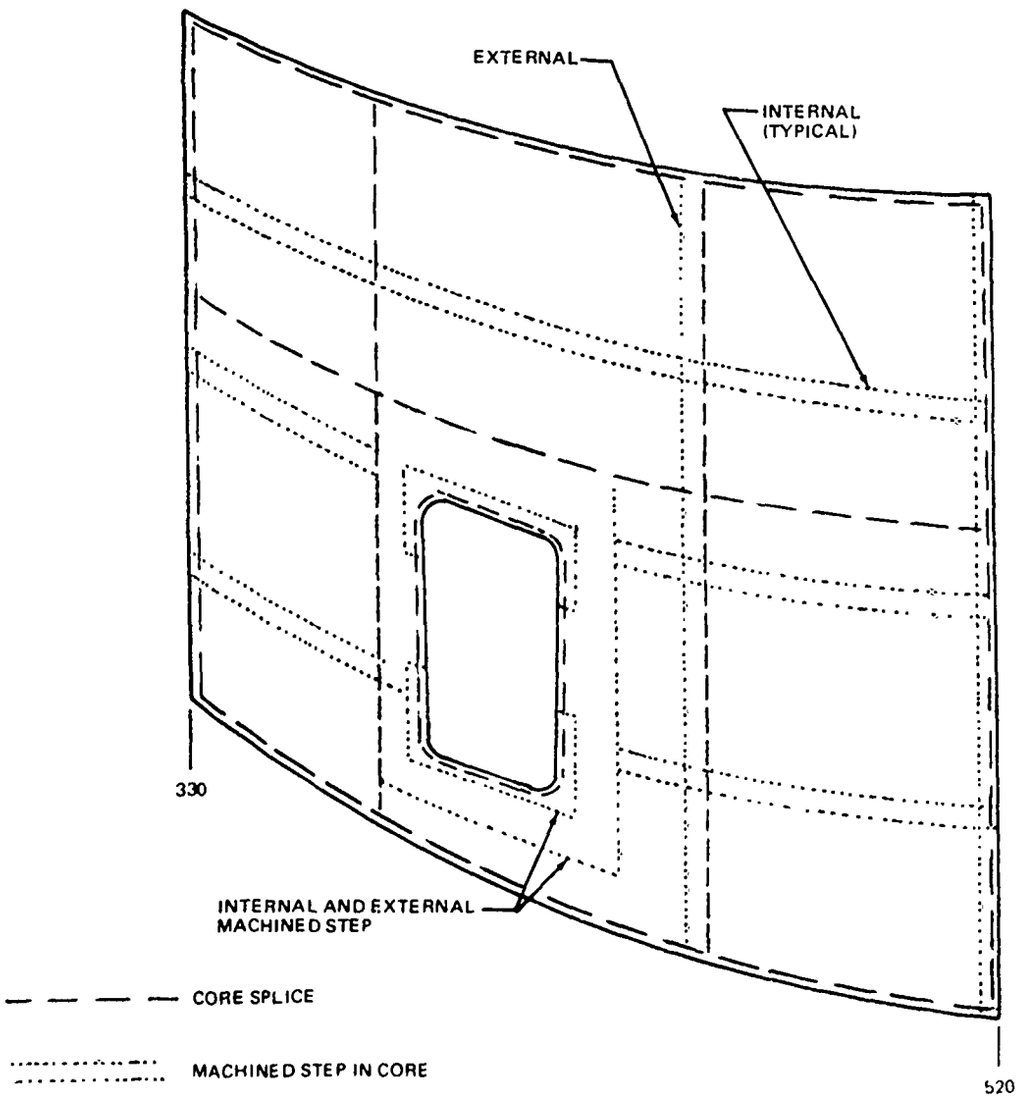


FIGURE 21. HONEYCOMB – TYPICAL CORE SPLICES AND MACHINED STEPS

Typical splices required for the honeycomb skin panels are shown in Figure 21 & 33. They consist of (1) transverse and longitudinal bonded skin splices, (2) transverse and longitudinal mechanical panel splices, (3) a frame T-section splice and (4) a crack stopper splice. For transverse bonded or mechanical splices, the outside surface skin splice is required to be flush to minimize drag. This requires an undercut in the outside surface of the core. Longitudinal splices are not required to be flush on the outside surface. Therefore, the mechanical splice is a simple inner and outer splice doubler. The bonded longitudinal splice is flush on the inner skin panel surface so a smooth surface can be maintained for bonding of the frame T-section to the inner face sheet of the honeycomb skin panel. This requires an undercut in the inside surface of the honeycomb core. At the direction of the USAF, in all cases when mechanical fasteners are used to join honeycomb skin panels, solid aluminum blocks are provided to prevent the entrapment of moisture and resulting corrosion in the honeycomb core. All splice fasteners are titanium 0.188 inch diameter lockbolts. All mechanically spliced doublers are cold bonded. The faying surface seal for the mechanically spliced doublers of the full scale demonstration components will be applied per MIL-S-81733 Type IV-12.

Frames: - A typical frame/bulkhead cross-section for the honeycomb concept is shown in Figure 23. The frame material is 7075-T6 aluminum with a depth of 4.75 inches and a thickness of 0.050 inches. The frame is attached to the honeycomb skin panels by means of a T-section hot bonded to the inner face sheet of the panel. The formed frame is mechanically fastened to the T-section with 0.188 inch diameter rivets spaced about 1.0 inches on center. Mechanical splices for the frames and skin panels are staggered as shown in Figure 24.

Fuselage Cutouts: - Fuselage cutouts are reinforced by a machine edge member shown in Figure 25 for the crew entrance door. This edge member is bonded directly into the honeycomb skin panel. Two inner and two outer face sheet doublers are provided around the cutout in addition to the edge member. One set of doublers distribures the concentrated corner stresses into the skin panel. The other set of doublers distributes the overall shear stresses around the cutout.

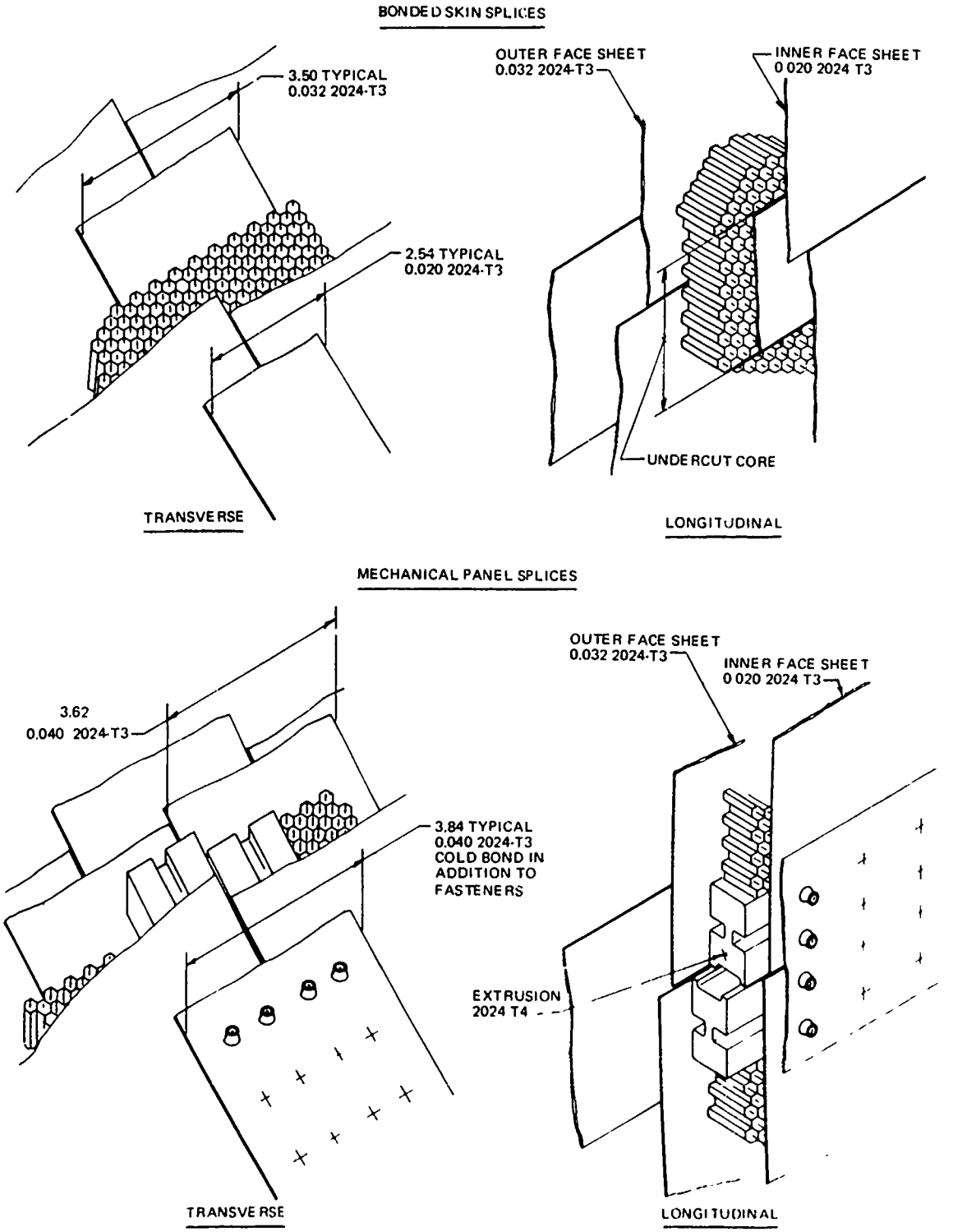


FIGURE 22. HONEYCOMB – SKIN AND PANEL SPLICES

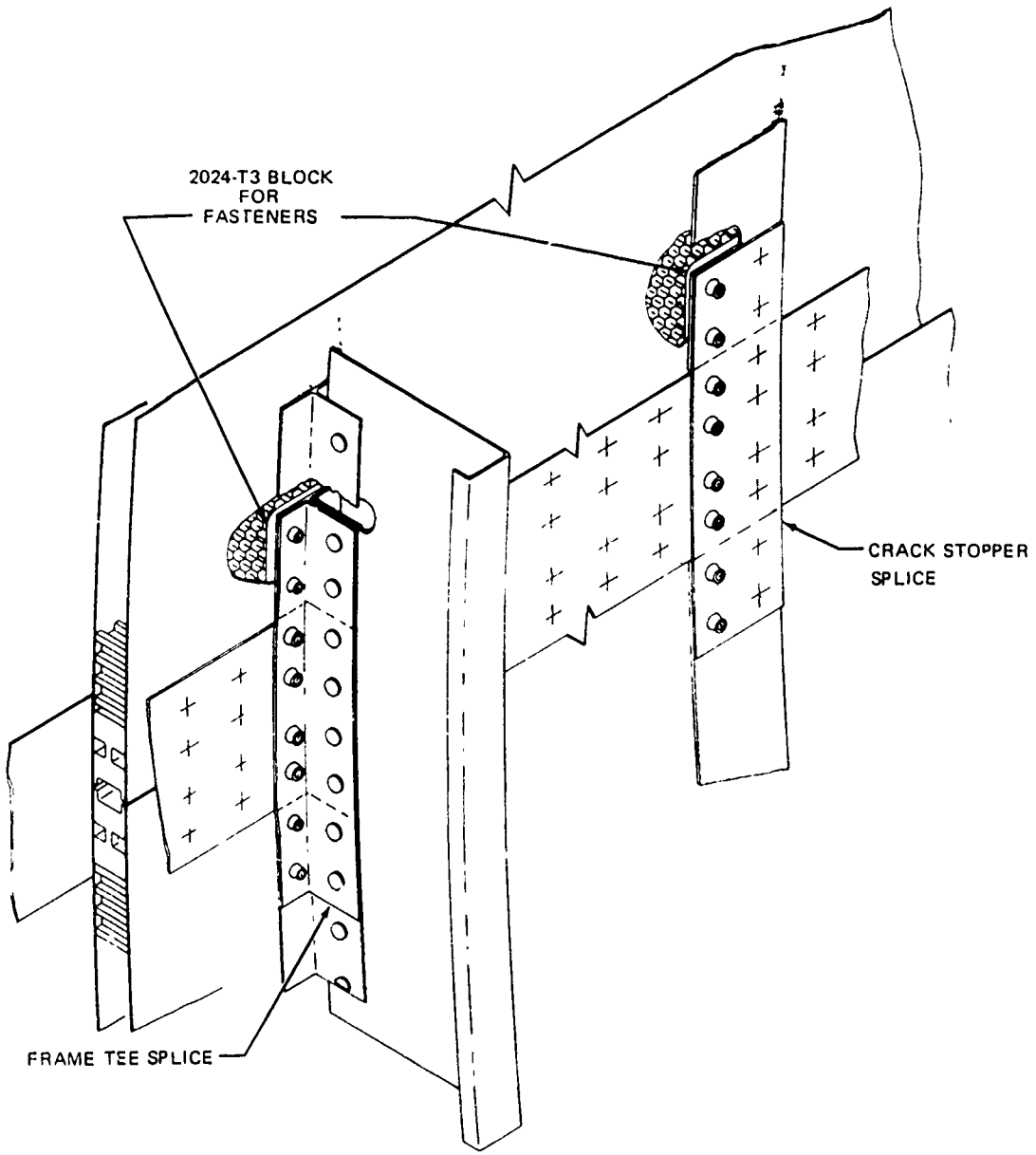


FIGURE 23. HONEYCOMB – FRAME TEE AND CRACK STOPPER SPLICE

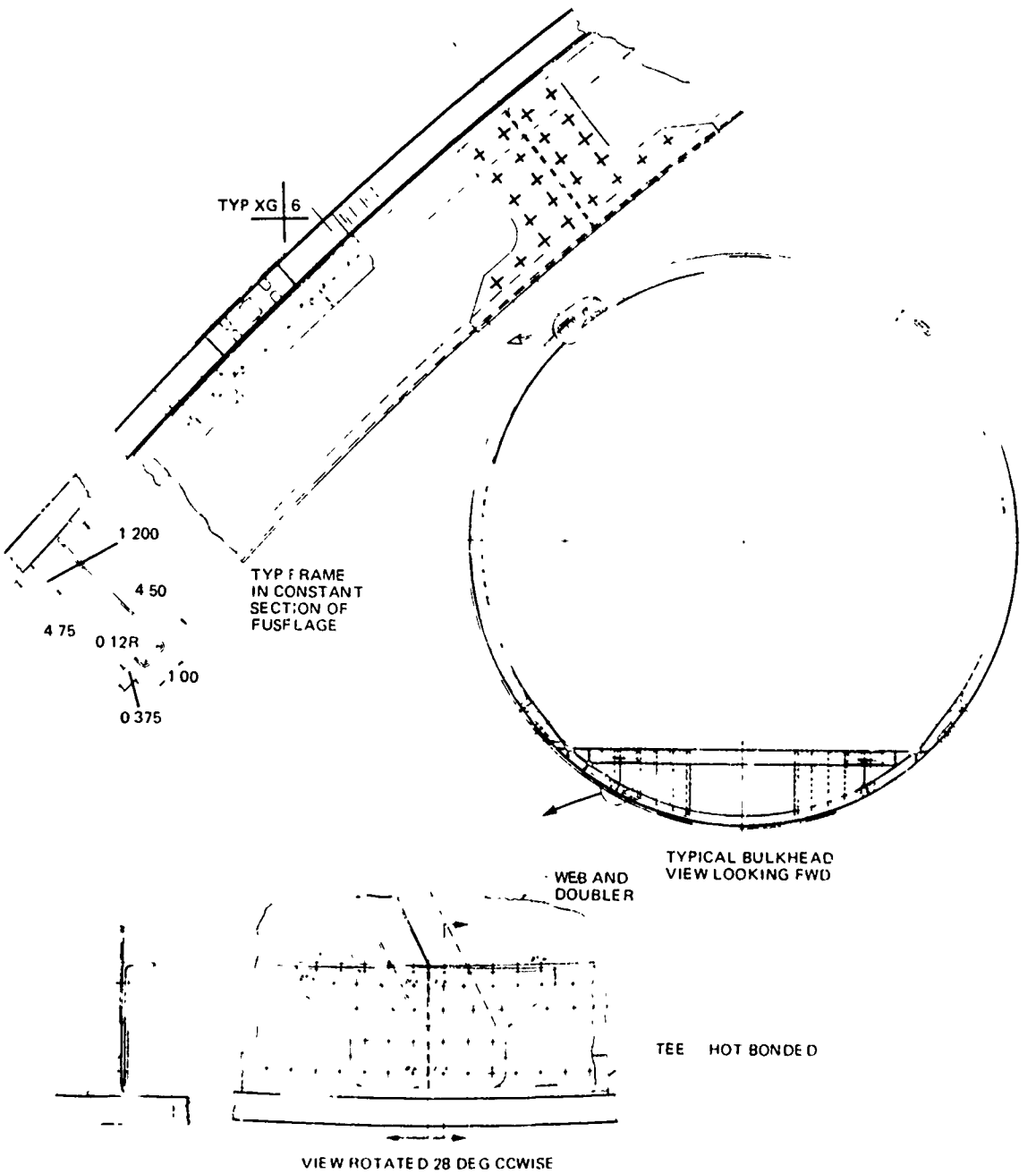


FIGURE 24. HONEYCOMB TYPICAL FRAME

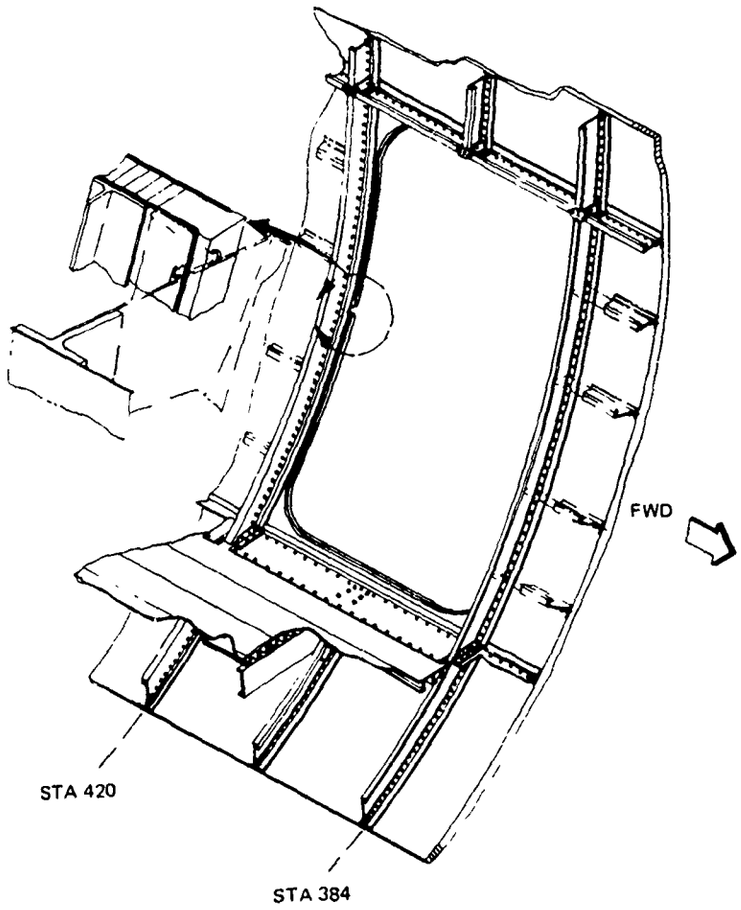


FIGURE 25. HONEYCOMB – FUSELAGE CUTOUT EDGE MEMBER FOR CREW ENTRANCE DOOR

Wing-Fuselage Interface:- The fuselage attaches to the lower wing surface between stations 703 and 847 by means of a titanium T-section flex joint shown in Figure 26. The honeycomb fuselage skin is bolted directly to this T-section as shown. Machined posts extend from the front and rear spar frames to pick up trapezoidal panels from the wing spars. Wing vertical shear and torque are reacted through these machined posts to the fuselage. Fuselage longitudinal loads are transmitted through the wing box at the intersection of the wing ribs and fuselage. A typical fuselage hardpoint is shown in Figure 27, at the center-line of the fuselage. Two machine tapered plates are bonded inside the honeycomb skin panel along with an inner and outer skin doubler. Wing splice plates and fittings are bolted directly through the fuselage skin at hardpoints such as this.

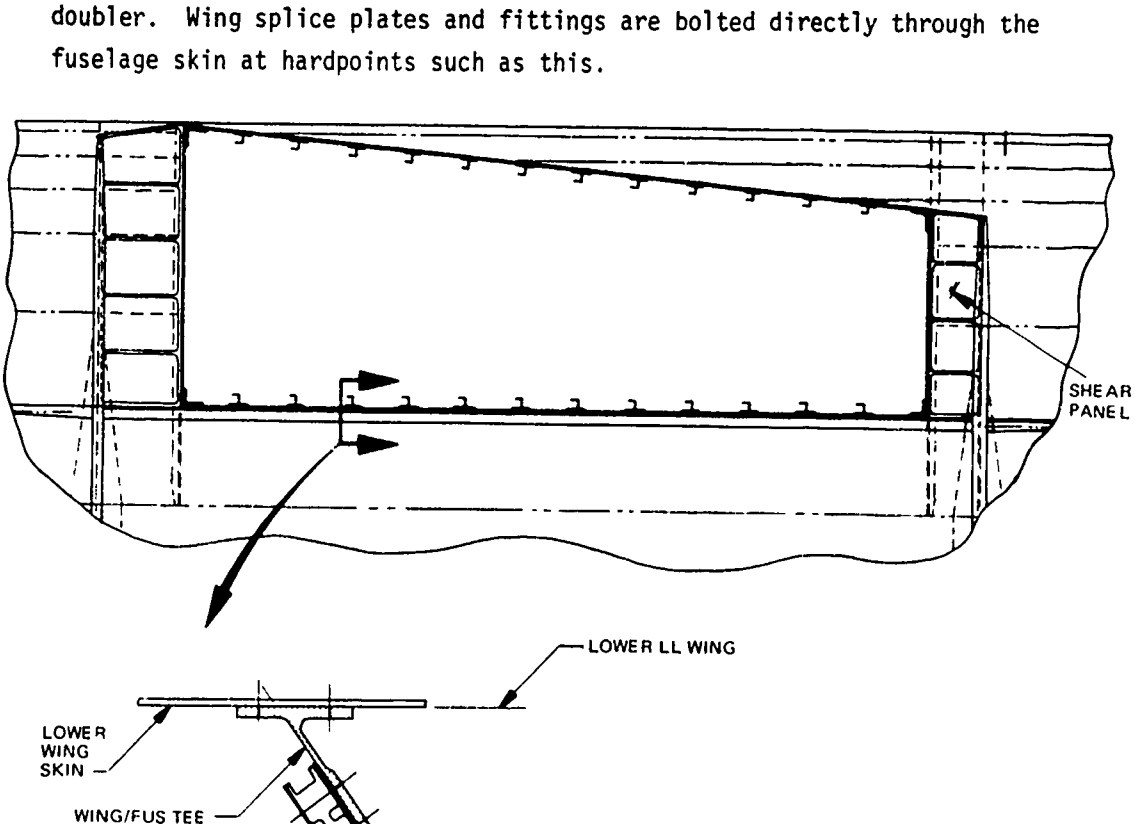


FIGURE 26. HONEYCOMB – WING/FUSELAGE

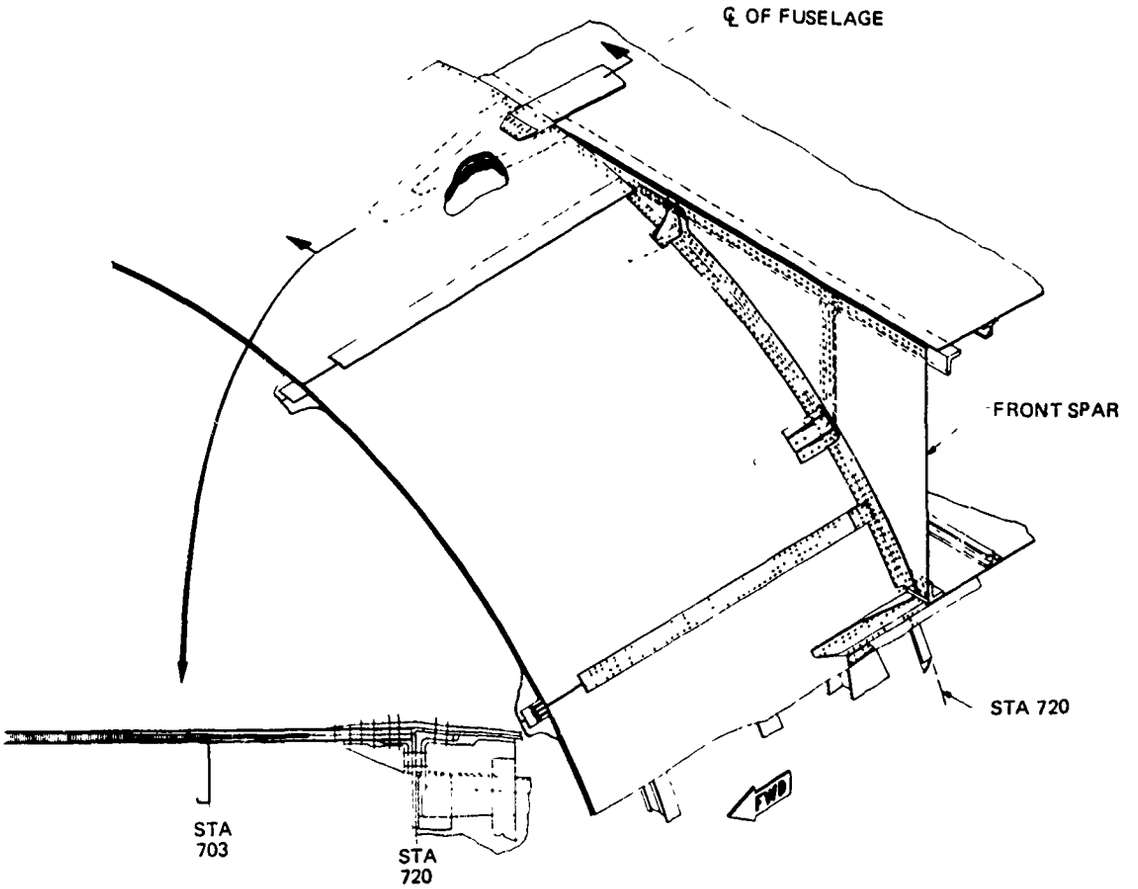


FIGURE 27. HONEYCOMB FRONT SPAR TO FUSELAGE INTERFACE

Weight Analysis

Concept weights were determined on a consistent basis in order to provide a valid weight comparison. All items that varied significantly between concepts were identified and provided with an accurate weight variance. These items and those varying relative to a mechanically fastened Baseline were called "participating structure." "Non-participating structure" was typical aircraft structure which was essentially unchanged between concepts. Dummy structure was non-typical aircraft structure.

For the weight cost comparisons, the ADP component was assumed to run from fuselage station 366 to 992.5. This section of fuselage has a lateral surface area of 2708 ft^2 not including 27 ft^2 of doors and windows and the cutout for the wing.

Weight Comparison of the Bonded Concepts. - The weight breakdown for the internal, external, and honeycomb concepts are shown in Table 1. The breakdown includes both participating and non-participating structure.

Participating Structure: - The skin and doubler weight for the Honeycomb concept is 12 percent lighter than that of the bonded longeron concepts, Table 1. Table 2 shows a detailed weight summary of the items which are included in the splice and attach weight. The honeycomb concept splices are over four times heavier than the internal or external longeron concept splices. Total adhesive weights for the ADP component are presented in Table 2 also.

The weight of the inserts and edge members required by the honeycomb concept are listed in Table 3, and Table 4 presents the detail weight breakdown for the frames and clips. The honeycomb frame weight is significantly lighter than the other concepts because it only has fifteen frames versus twenty-seven for the internal and external longeron concepts since all frames aft of Sta 439 are omitted that are not floor support bulkheads or under the wing.

TABLE 1

PABST BONDED CONCEPT WEIGHTS

ITEM	INTERNAL LONGERON	EXTERNAL LONGERON	HONEYCOMB
TOTAL PARTICIPATING STR WEIGHT (L3)	((6,503))	((6,486))	((6,724))
SKIN AND LONGERONS	(4,272)	(4,227)	(5,079)
SKIN	2,317	2,311	2,188
DOUBLERS	420	422	217
LONGERONS AND INTERCOSTALS	522	549	0
INTERMED. CIRCUMFERENTIAL STIFF.	240	240	0
HONEYCOMB CORE	0	0	597
FAIL-SAFE PROVISIONS	119	47	51
SPLICE AND ATTACH	394	398	1,564
MISC STIFF./INSERTS AND EDGE MEMBERS	26	26	228
MISC COMMON STRUCTURE	234	234	234
FRAME INST (EXCL MLG AND F SPAR FORGINGS*)	(2,231)	(2,193)	(1,579)
FRAMES AND CLIPS	1,210	1,209	595
BULKHEADS	881	844	844
MISC FRAME STRUCTURE	140	140	140
KEEL AND FLOOR ATTACH TEES	(0)	(66)	(66)
NON-PARTICIPATING STRUCTURE	((5,846))	((5,846))	((5,846))
*MAIN LANDING GEAR AND FRONT SPAR FORGINGS	1,478	1,478	1,478
FLOOR AND KEEL	2,799	2,799	2,799
OTHER NON-PARTICIPATING STR	1,569	1,569	1,569
TOTAL PARTICIPATING AND NON PART. STR. WEIGHT (LB)	12,349	12,332**	12,570

** PLUS DRAG PENALTY

NOTE: ADP COMPONENT FROM FUSELAGE STATION 366 TO 992.5

TABLE 2

SPLICE AND ATTACH DETAILED WEIGHT SUMMARY

ITEM	ILC	ELC	HCC
LONGITUDINAL MECHANICAL SKIN SPLICES	108	108	688
TRANSVERSE MECHANICAL SKIN SPLICES	94	94	421
LONGITUDINAL BONDED SKIN SPLICES	83	83	110
TRANSVERSE BONDED SKIN SPLICES	0	0	21
LONGERON SPLICES	43	49	0
GENERAL DOUBLERS TO SKIN BOND	25	22	12
CARGO FLOOR DOUBLERS TO SKIN BOND	10	10	0
LONGERON TO SKIN BOND	12	13	0
FRAME TO SKIN BOND	15	15	7
INT. CIRC. STIFFENER TO SKIN BOND	4	4	0
HONEYCOMB CORE & FITTINGS TO SKIN BOND	0	0	325
TOTAL SPLICE & ATTACH WEIGHT (LB)	394	398	1564
TOTAL ADHESIVE WEIGHT IN ADP COMPONENT (LB)	95	84	409

TABLE 3

HONEYCOMB CONCEPT

INSERTS AND EDGE MEMBERS DETAILED WEIGHT SUMMARY

	WEIGHT (LB)
FORWARD ENTRY DOOR FITTINGS	21
EMERGENCY EXIT DOOR FITTINGS	9
HELL HOLE DOOR FITTINGS	7
DITCHING HATCH FITTINGS (2)	14
MAIN LANDING GEAR POD PROVISIONS	35
WING FAIRING PROVISIONS	35
MAIN LANDING GEAR DRAG LINK PROVISIONS	40
UNDERWING EDGE MEMBERS	33
STA. 703 & 847 WING CUTOUT EDGE MEMBERS	34
TOTAL INSERT & EDGE MEMBER WEIGHT	228

TABLE 4

FRAME AND CLIPS DETAILED WEIGHT SUMMARY

	INTERNAL LONGERON		EXTERNAL LONGERON		HONEYCOMB	
	FWD OF STA 439	STA 439 AND AFT	FWD OF STA 439	STA 439 AND AFT	FWD OF STA 439	STA 439 AND AFT
FRAME	124	612	124	572	54	286
FRAME TEE	75	0	75	348	34	190
SHEAR CLIP	0	352	0	0	0	0
BUTTERFLY CLIP	0	47	0	0	0	0
FRAME SUPT. INTERCOSTALS	0*	0	17	73	5	26
TOTAL	199	1011	216	993	93	502
WEIGHT(LB)	1210		1209		595	

* intercostals are charged to longerons since they carry axial load.

Non-Participating Structure: - A weight summary of the items comprising the non-participating structure is presented in Table 5 based on the forward pressure bulkhead being located at Station 366. Most of these weights are YC-15 values, changed where practical, to reflect PABST modifications.

Dummy Structure: - Final dummy structure weights are not available at this time. However, the dummy wing structure (including the over wing barrel) and the transition structure aft of Station 992.5 are roughly estimated to weigh 6,000 lb and 2,000 lb, respectively. Addition of the dummy structure to the participating and non-participating structure brings the total ADP component weight to over 20,000 lb.

Weight Summary: - As shown in Table 1, the honeycomb concept, relative to the bonded longeron concepts, was approximately 300 lb lighter in skin and doubler structure and 800 lb lighter in longitudinal and circumferential stiffening. However, the honeycomb concept required over 1,000 lb of edge members and inserts and about 300 lb of adhesive at the two face sheet bondlines. Thus, the honeycomb concept was over 200 lb heavier than either the internal or external concepts.

Baseline Weight. - The final Phase Ib Baseline was defined as the internal longeron concept with mechanical fasteners rather than adhesives as the primary means of attachment.

As presently designed, the internal longeron concept skin and doublers would not appear to offer any weight saving relative to the Baseline and the weight difference between the longerons appears to be small. It was estimated that the Baseline fail-safe provisions and frames would be 119 lbs. lighter than the corresponding internal longeron concept items.

The present weight estimate shows that the Baseline was approximately 100 lb lighter than the internal longeron concept.

TABLE 5

NON-PARTICIPATING STRUCTURE WEIGHT SUMMARY

	WEIGHT (LB)
WING/FUSELAGE ATTACH STRUCTURE	252.5
PAINT & MARKINGS	113.4
SEALANT-NOSE	13.5
FLIGHT DECK FLOOR SUPPORT	100.5
FORWARD ENTRANCE DOOR	135.1
STA 366 PRESSURE BULKHEAD	384.3
FWD ENTRANCE DOOR JAMB	52.7
STA 366 FLOOR BEAM	38.0
MISC. DOORS, SEALANT & DITCHING HATCHES	216.6
EXIT DOOR, HELL HOLE DOOR, MLG FITTINGS & INTERCOSTALS	189.1
CARGO FLOOR	2411.1
WINDOWS	45.0
FLIGHT DECK FLOOR PANEL	28.3
MAIN LANDING GEAR (STA 847 & 895) AND FRONT SPAR (STA 703) FORGINGS	1478.0
KEEL	387.8
TOTAL NON-PARTICIPATING STRUCTURE WEIGHT	5845.9

STRUCTURAL ANALYSES

In Phase Ib,structural analyses were conducted of the PABST fuselage for fatigue, fail safe, damage tolerance and static strength conditions. The external loads were developed to reflect the design weights, payloads and center of gravity envelopes of the production YC-15. The internal loads were generated using structural idealizations of the internal/external skin-longeron concept and the honeycomb concept.

PRECEDING PAGE BLANK-NOT FILMED

Design Criteria

A summary of C-15 design weights and basic design parameters applicable to PABST are shown on Table 6 with the empty weight breakdown on Table 7. For purposes of external loads the PABST incremental fuselage weight changes do not significantly effect the overall aircraft weights.

The airplane center of gravity envelope is shown on Figure 28 with the Operating Weight Empty (OWE).

Maximum Fuel capacity is 77,714 lbs. with 47,097 lbs. in the exposed wing tanks and 30,617 lbs. in the center wing tank. The maximum STOL landing fuel weight is 20,000 lbs.

The basic design payloads consist of all vehicles and bulk and palletized cargo within the aircraft center of gravity envelope up to the design payloads. The maximum payload for CTOL is 62,100 lbs. and the maximum payload for STOL is 27,000 lbs.

The C-15 cargo floor loading criteria are shown on Figure 29 with an explanation of the derivation of each loading.

Figure 30 contains vehicle axle load diagrams which were established from a survey of military vehicles within the STOL and CTOL design envelopes.

The most critical payloads for the C-15 ultimate strength criteria are tabulated in Table 8.

PRECEDING PAGE BLANK-NOT FILMED

TABLE 6

BASIC AIRPLANE DESIGN PARAMETERS FOR C-15

	GROSS WEIGHT (LB)	PAYLOAD (LB)	(4) FUEL (LB)	LIMIT MANEUVER LOAD FACTOR n_z	FLAP LIMIT SPEED δ_F (DEG)/V_{L_F} (KEAS)(2)			SLOW DOWN FOR GUST V_G/M_G (KEAS)	LEVEL FLIGHT V_H/M_H (KEAS)	LIMIT V_L/M_L (KEAS)	(4) SINK RATE (FT/SEC)	RUNWAY ROUGHNESS(3) (MIL-A-008862A)
					TAKEOFF CONFIGURATION	APPROACH CONFIGURATION	LANDING CONFIGURATION					
EMPTY WEIGHT	109,504	—	—	—	—	—	—	—	—	—	—	—
MINIMUM FLYING WEIGHT	113,504	0	4,000	−1 0 TO 3 0	(0 20)/200	(20 35)/150	(35 50)/100	270/0 76	350/0 76	400/0 82	16 0	UNPREPARED
BASIC FLIGHT DESIGN WEIGHT AT MIDPOINT OF 400 N MI	153,422	27,000	16,918	−1 0 TO 3 0	(0 20)/200	(20 35)/150	(35 50)/100	270/0 76	350/0 76	400/0 82	16 0	UNPREPARED
MAXIMUM DESIGN WEIGHT WITH MAXIMUM PAYLOAD	219 180	62,100	47,576	0 TO 2 25	(0 20)/200	(0 20)/200	(0 20)/200	270/0 70	325/0 70	400/0 82	6 0	PAVED
LANDPLANE LANDING DESIGN WEIGHT	190,965	62,100	19,361	0 TO 2 25	(0 20)/200	(0 20)/200	(0 20)/200	270/0 70	325/0 70	400/0 82	10 0	PAVED
STOL TAKEOFF AND LANDING DESIGN WEIGHT	153,422	27,000	16,918	−1 0 TO 3 0	(0 20)/200	(20 35)/150	(35-50)/100	270/0 76	350/0.76	400/0.82	16.0	UNPREPARED

(1) INCLUDES M109 OR M110 HOWITZER (COMBAT LOADED)
(2) 0 TO 100 PERCENT TAKEOFF THRUST
(3) CBR = 6 USED FOR UNPREPARED RUNWAYS
(4) MAXIMUM FUEL WEIGHT - 77,714 LB

COMPLIANCE WITH
- MIL A 008860 SERIES, AIRPLANE STRENGTH AND RIGIDITY
- MIL-A 83444, DAMAGE TOLERANCE REQUIREMENTS
- DC 10 FAIL-SAFE REQUIREMENTS

PR6-PAB-564

TABLE 7

Empty Weight Breakdown

	WEIGHT (LB)
Wing	20,747
Horizontal Tail	3,110
Vertical Tail	3,345
Fuselage	26,999
Landing Gear	8,832
Flight Controls	3,427
Propulsion System	21,075
Fuel System	1,242
Auxiliary Power Unit	976
Instruments	1,588
Hydraulics	1,720
Pneumatics	583
Electrical System	1,807
Avionics	2,182
Furnishings	3,986*
Air Conditioning	883
Ice Protection	286
Handling Gear	2,214
Test Instrumentation	XX
MANUFACTURER'S EMPTY WEIGHT (MEW)	105,000
OPERATIONAL ITEMS	4,505
OPERATORS EMPTY WEIGHT (OEW)	109,505

*Includes cargo loading system (rollers, channel, restraint fittings, et

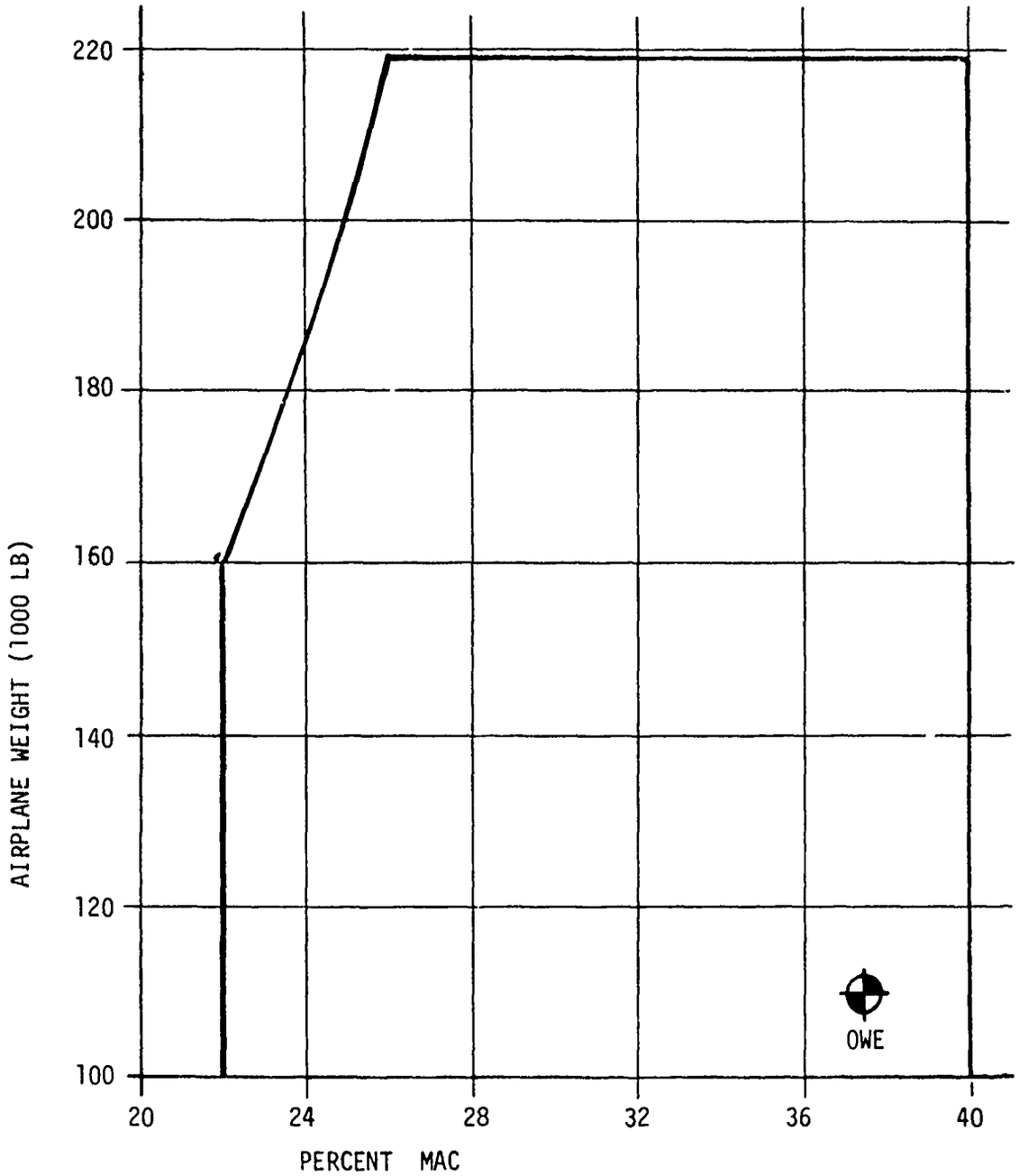
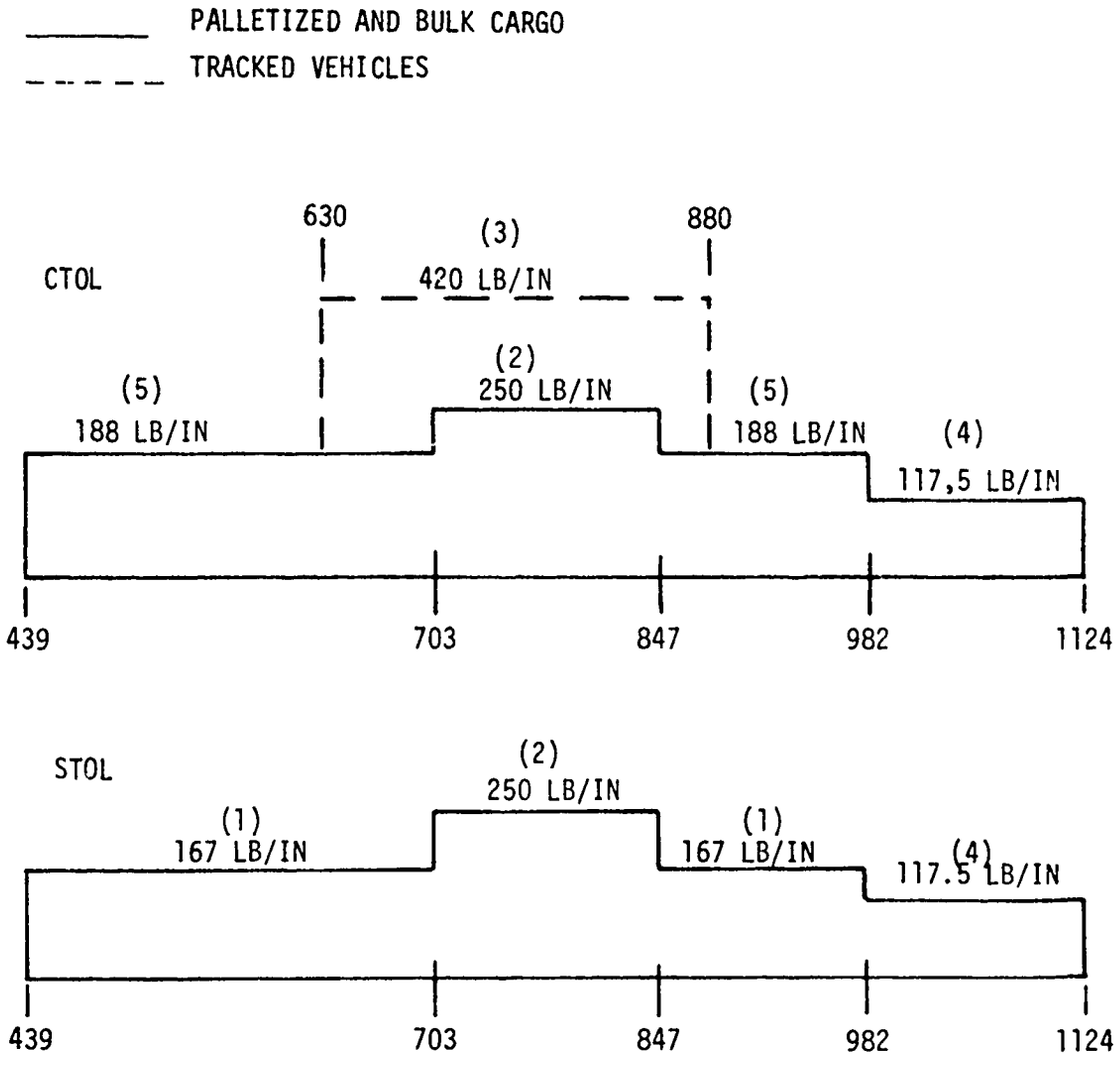


FIGURE 28. PABST CENTER OF GRAVITY ENVELOPE



(1)	MIL-A-008865A	(2,000 LBS/FT = 167. LBS/IN)
(2)	MIL-A-008865A	(3,000 LBS/FT = 250 LBS/IN)
(3)	M110E2 HOWITZER	(62,100. LBS ÷ 148. IN = 420. LBS/IN)
(4)	MILITARY PALLET	(10,350 LBS ÷ 88 IN. = 117.5 LBS/IN)
(5)	MIL VAN	(45,000 LBS ÷ 240 IN = 188 LBS/IN)

FIGURE 29. CARGO LOADING CRITERIA

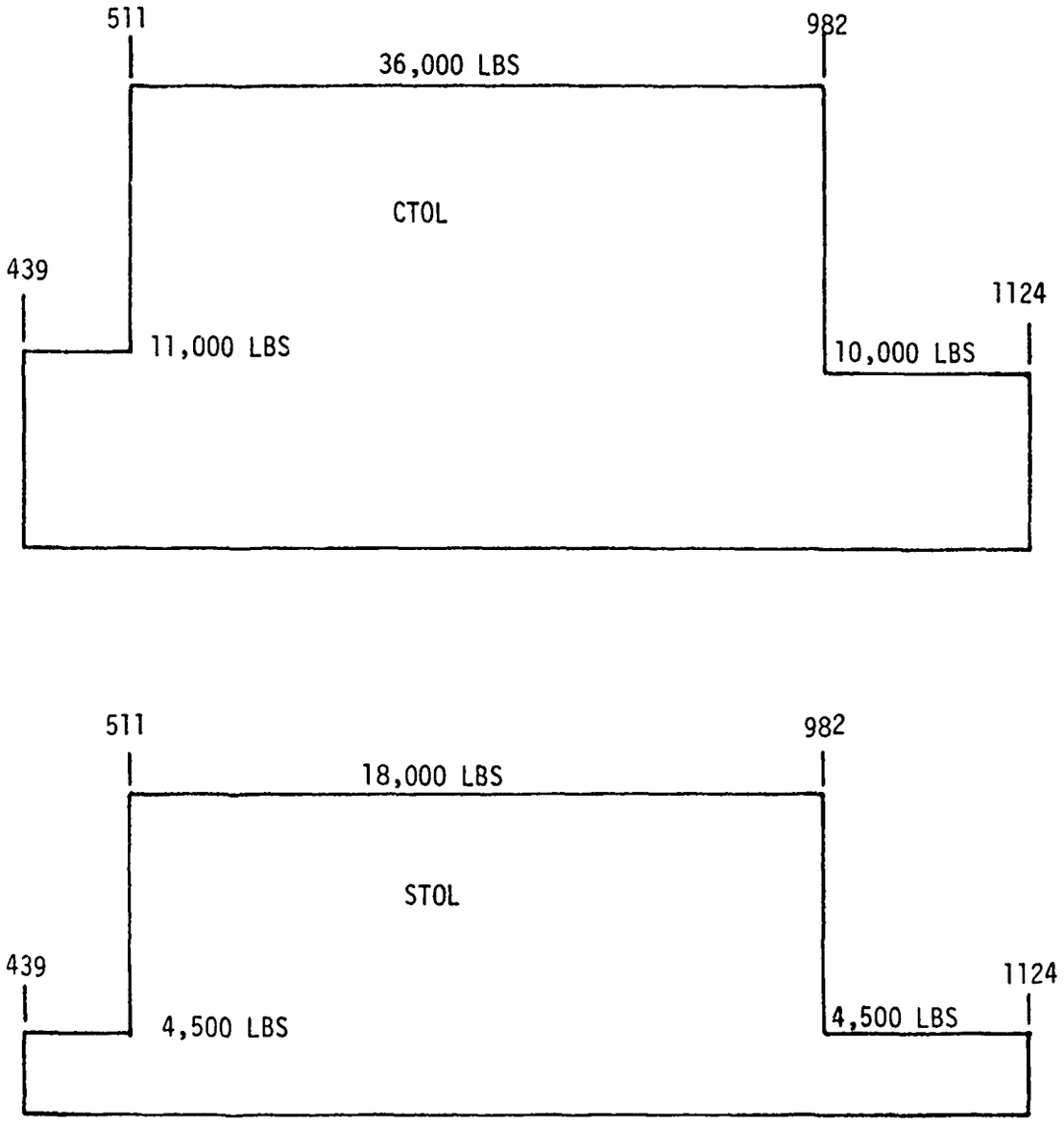


FIGURE 30. VEHICLE AXLE LOADING CRITERIA

TABLE 8

PABST PAYLOADS

	DESCRIPTION	PAYLOAD NUMBER	
		FWD C.G.	AFT C.G.
BULK AND PALLETIZED CARGO	MINIMUM WEIGHT FOR FWD. & AFT C.G.	1	
	MAXIMUM PAYLOAD (62,100 LBS.)		
	DUMBELLED	2	3
	MAX. SHEAR @ FRONT SPAR	4	
	PAYLOAD FOR MAXIMUM FUEL (31,155 LBS.)		
	LUMPED	5	6
	MAXIMUM STOL PAYLOAD (27,000 LBS.)		
	DUMBELLED	7	8
	MAX. SHEAR @ FRONT SPAR	9	
CTOL VEHICLES	62,100 LB. HOWITZER	10	
	15K FORKLIFT + 2-1/2T TRUCK (62,000 LBS.)	11 (26,000 LB. AXLE FWD.)	
	8T GOER + 2-1/2T TRUCK (61,370 LBS.)	12 (22,450 LB. AXLE FWD.)	
STOL VEHICLES	27,000 LBS. GOER	13	
	27,000 LBS. CARGO CARRIER	14	

External Loads

Flight Loads. - Flight Loads were developed for the PABST C-15 fuselage in conformance with the MIL-A-008860A series specifications for the basic aircraft design parameters listed in Table 6.

For conditions in which the airframe flexibility is negligible, the fuselage shears, moments and torques were generated by the Fuselage Loads program which sums the applied loads at each fuselage check station. In addition, the Fuselage Loads program was used to investigate each of the payloads in Table 8 for discrete gust loading as a function of speed and altitude. The conditions selected for internal loads analysis are shown in Table 9.

The Continuous Turbulence Analysis program was used to investigate power spectral density gust loads, but these were not critical for the fuselage.

The limit pressure differential between the pressurized portions of the fuselage and the ambient atmosphere are

(a) 7 psi + .15 psi valve tolerance + local aerodynamic loads

(b) -1.0 psi collapsing pressure + maximum flight loads

(c) 1.33 x 7.15 psi + 1g ground loads

The local aerodynamic loads were derived from wind tunnel pressure distributions from previous aircraft models. All flight conditions are checked for full pressurization and zero pressurization.

Fuselage internal loads were developed for Aerial Delivery conditions during the original YC-15 design. These were not found to be critical forward of the Station 982 frame. Consequently these have not been included in the present ADP analysis.

Ground Loads. - The ground loads consist of the landing, taxi, towing and jacking conditions of MIL-A-008862A for the aircraft design parameters listed in Table 6 . The Dynamic Landing Program was used for all landing conditions except for the lateral drift landing which contains the gear loads specified in MIL-A-008862A Para. 3.2.9. The Dynamic Landing Program incorporates the flexible airframe dynamic response and provides time histories of selected fuselage loads including shears, moments and torques plus the gear loads. These time histories were reviewed and the critical time points selected for internal loads analysis. A typical fuselage load time history is shown on Figure 31.

PRECEDING PAGE BLANK-NOT FILMED

TABLE 9

SUMMARY OF FLIGHT CONDITIONS

COND. NO.		DESCRIPTION	PAYLOAD GROSS WEIGHT				LOAD FACTOR			ACCEL (RAD/SEC)		
NO PRESS	7.15 psi PRESS		NO.	KIPS	KIPS	% MAC	N_x	N_y	N_z	ROLL	PITCH	YAW
	1	2 P INTERNAL PRESSURE (14.3 psi)										
2	102	VL_F GUST	2	62.1	175.6	23.3	0	0	2.131	0	-.45	0
3	103	2nd PEAK PULL UP	14	27.	150.	23.4	0	0	3.00	0	-1.18	0
4	104	1st PEAK PULL UP	7	27.	150.	23.4	0	0	1.026	0	.775	0
5	105	3G BAL MAN	7	27.	140.5	22.4	0	0	3.00	0	0	0
6	106	2G BAL MAN	2	62.1	175.6	23.3	0	0	2.00	0	0	0
7	107	3G BAL MAN & MISTRIM	7	27.	150.	23.4	0	0	3.00	0	0	0
8	108	V_H GUST		11.9	125.4	22.4	0	0	3.666	0	-.29	0
9	109	V_H GUST	2	62.1	175.6	23.3	0	0	2.729	0	-.169	0
10	110		4						2.729		-.176	
11	111		10						2.730		-.214	
12	112		11						2.730		-.156	
13	113	V_H GUST	12	62.1	175.6	23.3	0	0	2.735	0	-.032	0
14	114	V_H LATERAL GUST	13	27.	140.5	22.7	.213	-.57	1.00	2.22	0	-.376
15	115	OPPOSITE COND 14										
16	116	UNCOORDINATED ROLL	0	0	113.5	37.3	0	.985	1.00	1.42	0	.654
17	117	OPPOSITE COND 16										
18	118	ENGINE FAILURE	3	62.1	216.7	39.3	-.09	.342	1.00	0	0	.091
19	119	OPPOSITE COND 18										
20	120	3G BAL MAN & MISTRIM	7	27.	150.	23.4	0	0	3.00	0	0	0
21	121	CHECKED ROLL	8	27.	150.	39.8	.007	-.638	2.40	3.20	0	.077
22	122	OPPOSITE COND 21										

THIS
PAGE
IS
MISSING
IN
ORIGINAL
DOCUMENT

TABLE 10

SUMMARY OF CRITICAL GROUND LOADS

COND. NO.		PAYLOAD		GROSS WEIGHT		LOAD FACTOR			ACCEL (RAD/SEC)		
NO PRESS	DESCRIPTION	NO	KIPS	KIPS	% MAC	N_x	N_y	N_z	ROLL	PITCH	YAW
23	BRAKED ROLL	5	31.1	98.5	25.9	.440	0	1.117	0	.600	0
24											
25	TURN + BRAKING	5	31.1	193.5	25.9	.461	.052	1.388	-.047	.150	-.250
26	OPPOSITE COND 25										
27	DRIFT LANDING	0	0	150.	37.4	0.	.665	1.95	.791	-.278	.113
28	OPPOSITE COND 27										
29	DRIFT LANDING	9	27.	150.	23.4	0.	.665	1.95	.961	-.336	.187
30	OPPOSITE COND 29										
31	2G TAXI	6	31.1	219.2	36.3	0	0	2.00	0	0	0
32	2G TAXI	4	62.1	219.2	26.1	0	0	2.00	0	0	0
33	BRAKED ROLL	3	62.1	193.3	39.8	.96	0	1.20	0	-1.0	0
34	.5G TURN	3	62.1	219.2	39.2	0	.5	1.00	0	0	0
35	OPPOSITE COND 34										
36	REVERSE BRAKE	3	62.1	219.2	39.2	-.80	0	1.00	0	0	0
37	2 PT 3.8° TAIL DN LANDING	7	27.	140.5	22.4	-1.00	0	VARIES	0	VARIES	0
38	2 PT 3.7° TAIL DN LANDING	8	27.	140.5	39.9	1.66					
39	2 PT 3.8° TAIL DN LANDING	7	27.	140.5	22.4	1.21	0	VARIES	0	VARIES	0
40											
41	4.3° PITCH 6.9° YAW LAND.	8	27.	153.4	36.8	.59	VARIES	VARIES	.375	VARIES	VARIES
42	OPPOSITE COND 41										

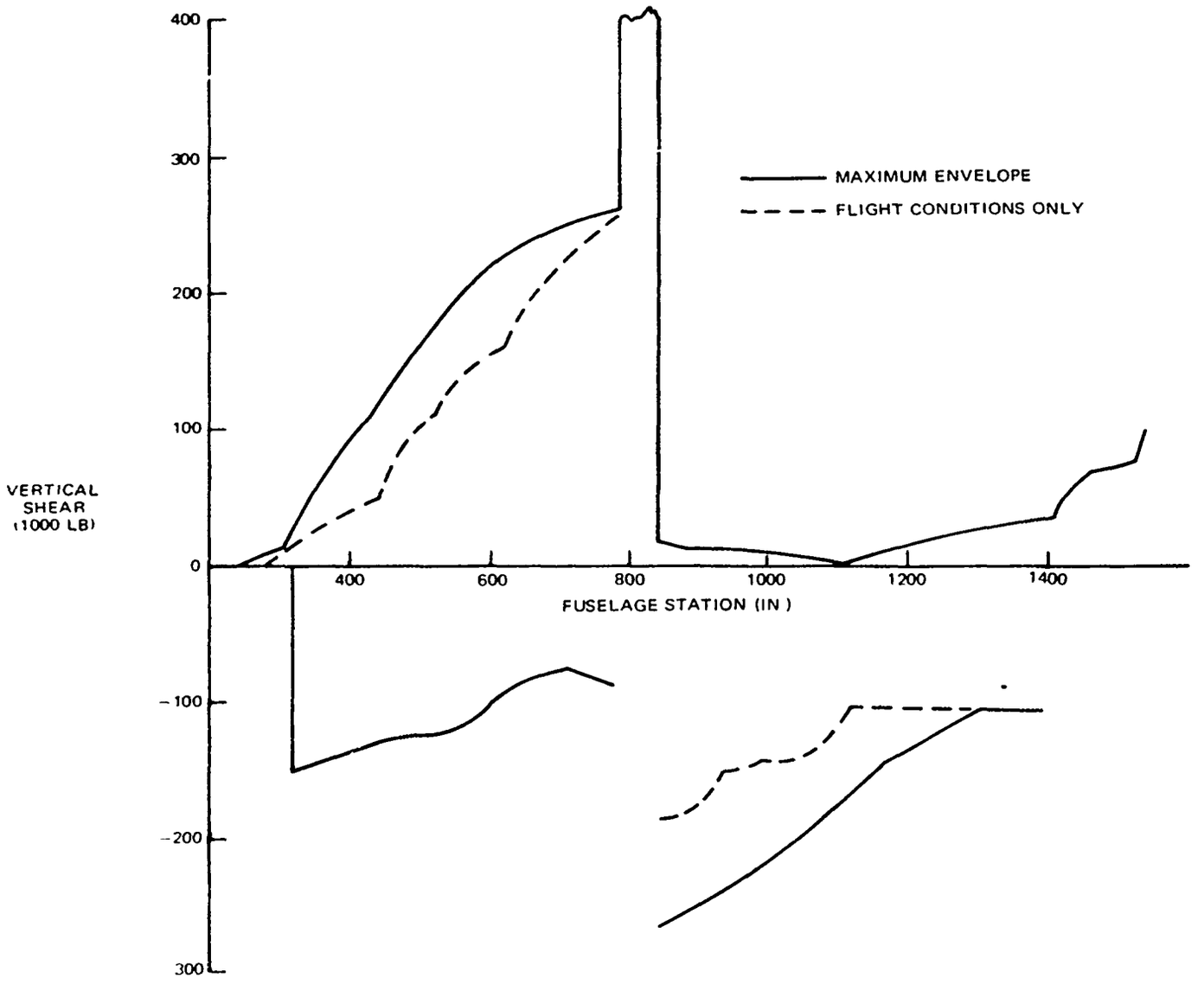


FIGURE 32. ULTIMATE FUSELAGE VERTICAL SHEAR ENVELOPE

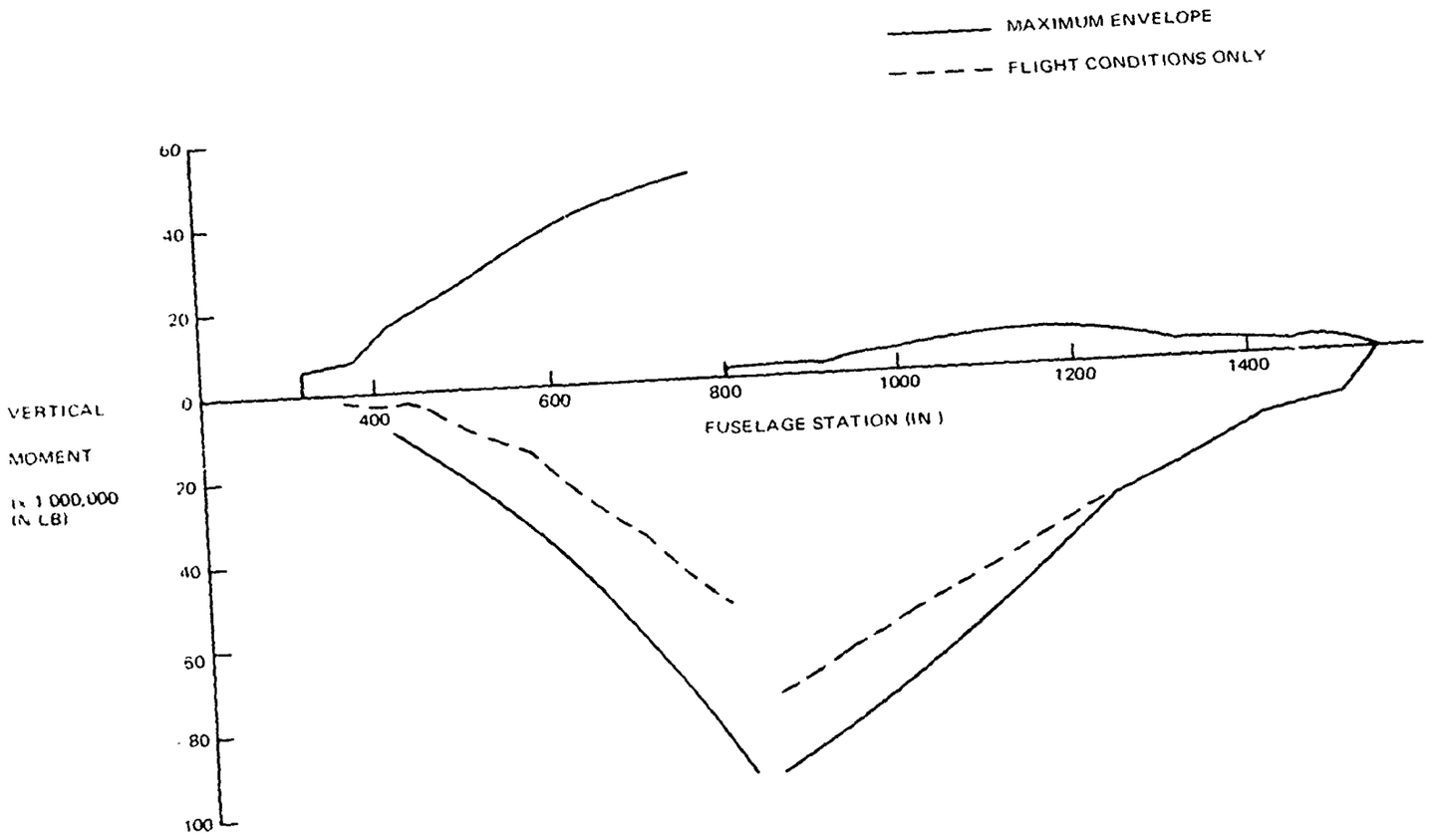


FIGURE 33. ULTIMATE FUSELAGE VERTICAL BENDING MOMENT

Fatigue Loads. - A set of fuselage fatigue conditions was established for internal loads analysis in the following manner. The projected PABST utilization consists of 8 missions; however, for fatigue analysis purposes, this was simplified to the 6 mission "Modified Utilization" in Table 11. A segment-by-segment mission profile was performed on each flight and the initial taxi and cruise segments were selected for FORMAT internal loads analysis. For the cruise segment, the 1G and 2G (or stall) maneuver loads were obtained from which fatigue spectrum stresses can be obtained. For taxi, only the 1G loads are derived; the stresses due to incremental load factors are assumed to be proportional to the 1G stresses

A representative set of payloads was established for each mission. These payloads are defined in Table 12. Particular attention is paid to axle load distribution with frame station 559 selected for detailed frame analysis.

Since the payloads for Basic Training Missions 2-1 and 2-2 payloads are also included in the Typical Cruise Missions 1-1 and 1-2, separate internal loads were not run for the Training Missions. The major difference between the cruise segments for the Training and Typical Missions is the pressurization.

FLIGHT PROFILE	DESCRIPTION	FUSELAGE CRUISE P (psi)
1-1A 1-2A	Typical A Typical B	7.15
2-1A 2-2A	Training A Training B	4.35 Outb'd. 3.2 Return
3-1A 3-2A	Low Alt. Resupply A Low Alt. Resupply B	0

A summary of the fatigue conditions selected for internal load analysis is on Table 13 .

The pressurization internal loads are obtained separately (condition 87 Table 13) to facilitate the incorporation of different pressurization spectrums in the fatigue analysis.

Additional conditions 85 and 86 contain 1G and 2G maneuver loads for a typical flight condition with zero payload to permit superposition studies.

TABLE 11 PABST UTILIZATION

MISSION SYMBOL	DESCRIPTION	MISSION LENGTH FLIGHT HOURS	MISSION LENGTH N MI	LANDINGS PER MISSION STOL	LANDINGS PER MISSION CTOL	LANDINGS PER MISSION TOUCH & GO	HOURS PER LANDING	SERVICE LIFE FLIGHT HOURS	SERVICE LIFE % TOTAL FLIGHT HOURS	SERVICE LIFE LANDINGS STOL	SERVICE LIFE LANDINGS CTOL	SERVICE LIFE LANDINGS TOUCH & GO	SERVICE LIFE LANDINGS TOTAL	SERVICE LIFE LANDINGS % TOTAL	SERVICE LIFE NUMBER OF MISSIONS	PAYLOAD LBS.	
1-1	BASIC	2.76	989	*	1	1	0.92	20007	66.7	7236	7236	7236	21708	47.1	7236	20250	OPT CRUISE
2		2.0	715		1	1	1.0	1894	6.3		947	947	1894	4.0	947	54250	OMIT FROM FLIGHT 1-2
								21901	73.0	7236	8183	8183	23602	51.1	8183	
4-1	BASIC TRAINING	1.6	394	1	1	6	0.2	1974	6.6	1234	1234	7404	9872	21.4	1234	20250	15000 FT 10000 FT
4-2		1.4	370	1	1	6	0.2	126	0.4	90	90	540	720	1.5	90	54250	
								2100	7.0	1324	1324	7944	10592	22.9	1324		
5-1	LOW ALTITUDE RESUPPLY	2.0	582	3	1		0.5	3000	10.0	4500	1500		6000	13.0	1500	27000	500 FT.
3-2		2.0	573		4		0.5	3000	10.0		6000		6000	13.0	1500	62000	2 HOURS
								6000	20.0	4500	7500		12000	26.0	3000		
								30001	100.0	13060	17007	16127	46194	100.0	12507		

2(8183) = 16366 FULL PRESSURE CYCLES
2(1324) = 2648 PARTIAL PRESSURE CYCLES
19014 PRESSURE CYCLES (ACTUAL UTILIZATION HAS 17150 PRESSURE CYCLES).

TABLE 12

PABST FATIGUE PAYLOAD SUMMARY

MISSION PROFILE	MISSION MISSIONS/LIFE	PAYLOAD (LBS.)	PAYLOAD DESCRIPTION	MISSIONS / LIFE	MAX. AXLE LOAD (LBS)	PABST C-15 FATIGUE PAYLOAD NO.
1-1	TYPICAL A (7236)	20250.	DISTRIBUTED	5789.	NONE	F1
			MIXED JEEPS & TRUCKS	1447.	4380.	F5
1-2	TYPICAL B (947)	54250.	DISTRIBUTED	758.	NONE	F3
			TWO 5T TRUCKS	142	9800.	F6
			8T GOER + 2 1/2T TRUCK	28	18220.	F7
			47^k FORKLIFT + 3/4T TRUCK	19	26000	F8
2-1	TRAINING A (1234)	20250	DISTRIBUTED	987	NONE	F1
			MIXED JEEPS & TRUCKS	247	4380	F5
2-2	TRAINING B (90)	54250	8T GOER + 2 1/2T TRUCK	63	18220	F7
			47^k FORKLIFT + 3/4T TRUCK	27	26000	F8
3-1	LOW ALT. RESUPPLY A (1500)	27000	DISTRIBUTED	750	NONE	F2
			MIXED JEEPS & TRUCKS	300	4380	F9
			5T TRUCK	75	9820	F10
			8T GOER	375	18220	F11
3-2	LOW ALT RESUPPLY B (1500)		DISTRIBUTED	750	NONE	F4
			M110E HOWITZER	150	TRACKED	F12
			ONE M114 & TWO M113	300		F13
			ONE M578 + JEEP & TRAILER	300	TRACKED	F14

TABLE 13
SUMMARY OF PABST CRITICAL FATIGUE CONDITIONS

FORMAT COND NO.	Δp (PSI)	FLT PROFILE	DESCRIPTION	P.L. WT (LB)	P.L. NO.	n_z
43	0	1-1	STOL	20,250	F1	1
44	0	1-1	STOL	20,250	F5	1.
45	0	1-2	CTOL	54,250	F3	1
46	0	1-2	CTOL	54,250	F6	1
47	0	1-2	CTOL	54,250	F7	1.
48	0	1-2	CTOL	54,250	F8	1.
49	0	3-1	STOL	27,000	F2	1.
50	0	3-1	STOL	27,000	F9	1
51	0	3-1	STOL	27,000	F10	1
52	0	3-1	STOL	27,000	F11	1.
53	0	3-2	CTOL	62,000	F4	1.
54	0	3-2	CTOL	62,000	F12	1.
55	0	3-2	CTOL	62,000	F13	1.
56	0	3-2	CTOL	62,000	F14	1
57	7 15	1-1	STOL	20,250	F1	1.
58	7 15	1-1	STOL	20,250	F1	1.771
59	7 15	1-1	STOL	20,250	F5	1.
60	7.15	1-1	STOL	20,250	F5	1 771
61	7 15	1-2	CTOL	54,250	F3	1.
62	7 15	1 2	CTOL	54,250	F3	1 75
63	7 15	1-2	CTOL	54,250	F6	1
64	7 15	1-2	CTOL	54,250	F6	1 75
65	7 15	1-2	CTOL	54,250	F7	1.
66	7 15	1-2	CTOL	54,250	F7	1.75
67	7 15	1-2	CTOL	54,250	F8	1.
68	7 15	1 2	CTOL	54,250	F8	1.75
69	0	3-1	STOL	27,000	F2	1.
70	0	3-1	STOL	27,000	F2	1 996
71	0	3-1	STOL	27,000	F9	1
72	0	3 1	STOL	27,000	F9	1 996
73	0	3-1	STOL	27,000	F10	1
74	0	3-1	STOL	27,000	F10	1 996
75	0	3-1	STOL	27,000	F11	1.
76	0	3 1	STOL	27,000	F11	1 996
77	0	3 2	CTOL	62,000	F4	1
78	0	3-2	CTOL	62,000	F4	1 99
79	0	3-2	CTOL	62,000	F12	1.
80	0	3-2	CTOL	62,000	F12	1 99
81	0	3-2	CTOL	62,000	F13	1
82	0	3 2	CTOL	62,000	F13	1 99
83	0	3 2	CTOL	62,000	F14	1
84	0	3 2	CTOL	62,000	F14	1 99
85	7 15	1 2	CTOL	0	0	1
86	7 15	1 2	CTOL	0	0	2
87	7 15		1 P			0

Internal Loads

The PABST ADP was analyzed in the same manner as a conventional aircraft fuselage. Internal loads were generated using the standard McDonnell Douglas FORMAT computer program. The basic approach was to replace the actual structure with a series of bars, panels and membrane elements with the load capabilities shown in Figure 34.

The external loads were applied at the nodes and equilibrium and compatibility equations were generated for each node and element in terms of the unknown internal forces. These forces are solved by matrix inversion. The program also used the FORMAT capability to generate the margins of safety for input allowable stresses including the interaction effects of biaxial and shear stresses.

A computer generated diagram of the overall idealization is included in Figure 35. As shown, typical shell structure was idealized by a series of bars for the longerons and frames and shear panels for the skin. For the wing attachment and landing gear frames, both inner and outer caps were included along with all major structural connections. The floor, wing box and bulkheads were all included in a similar manner.

Two idealizations were created

(1) Internal and External Longerons Concepts

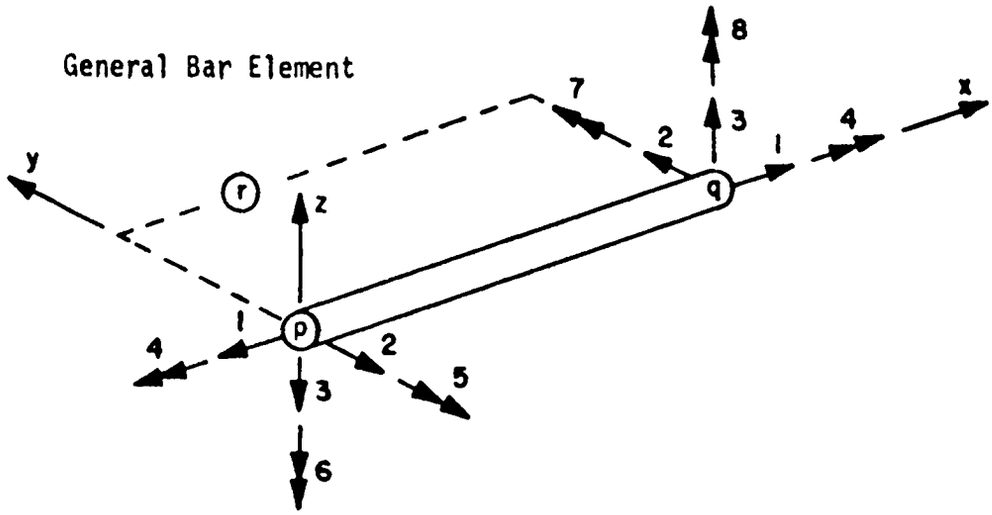
(2) Honeycomb Sandwich Concept

Both idealizations had identical geometries; the only difference was the section properties for the longeron and sandwich shells. The longerons carry no bending or transverse shear whereas the sandwich elements include transverse bending and shear stiffness. For the two longeron concepts, identical section properties were assumed allowing the use of a single idealization.

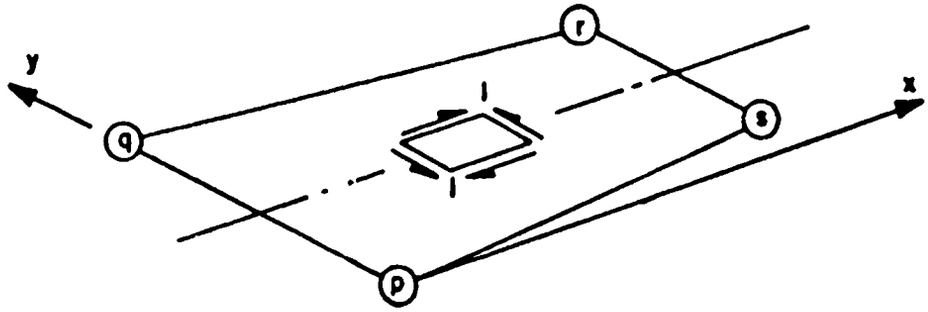
A list of the ultimate flight, ground and fatigue load conditions are included on Tables 9,10 and 13. Loads were applied at the node points to duplicate the airloads, inertias, wing and landing gear loads.

The internal loads were generated directly onto microfilm for all ultimate and fatigue conditions. A set of output on standard computer forms is also available for reference.

General Bar Element



Shear Panel



Triangular Membrane

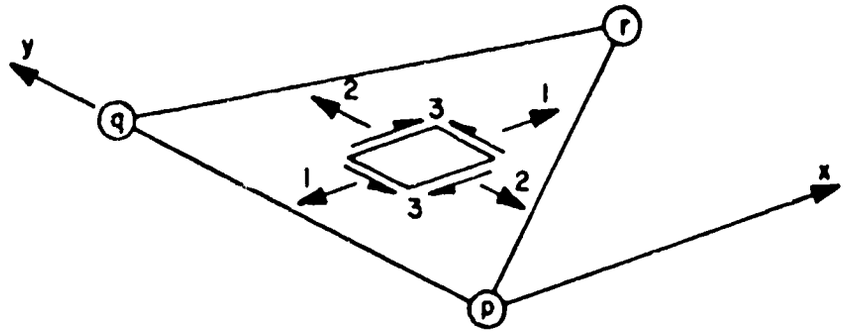


FIGURE 34. - BAR, PANEL AND MEMBRANE ELEMENTS

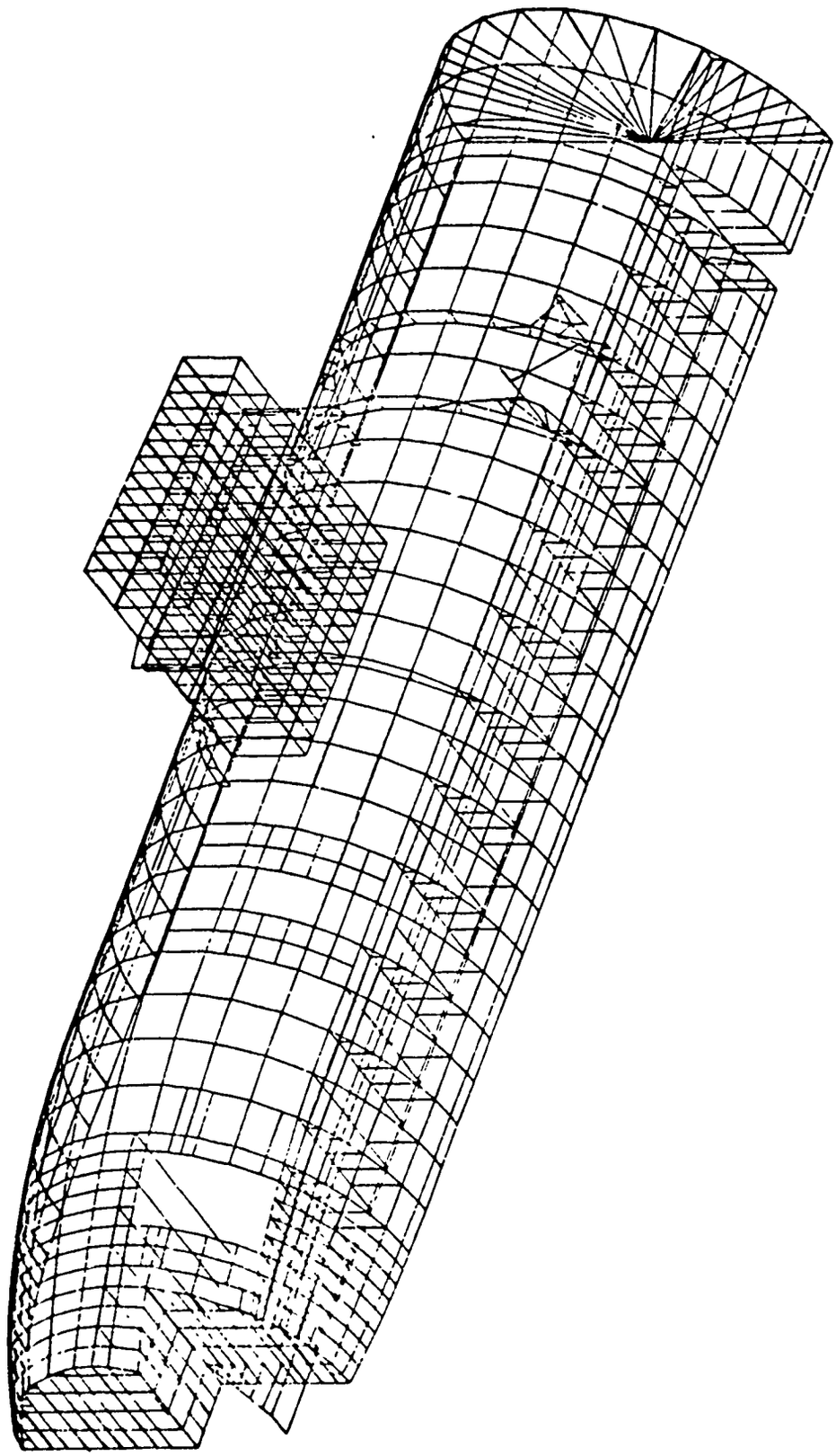


FIGURE 35. STRUCTURAL IDEALIZATION

Ultimate Failure Mode - Metal

An auxiliary to the FORMAT internal load program has been used to derive the ultimate stresses and margins of safety in the metal. This stress program uses the loads and section properties from the internal load program to determine the three most critical margins of safety for axial, shear and principal stress in each bar and panel member and additionally for interaction between longeron axial load and skin shear. The results of this program output are summarized by loading condition type in Figure 36 and the stress and margin of safety values for selected locations are shown in Figure 37. A set of the complete program output is also available for reference.

PRECEDING PAGE BLANK-NOT FILMED

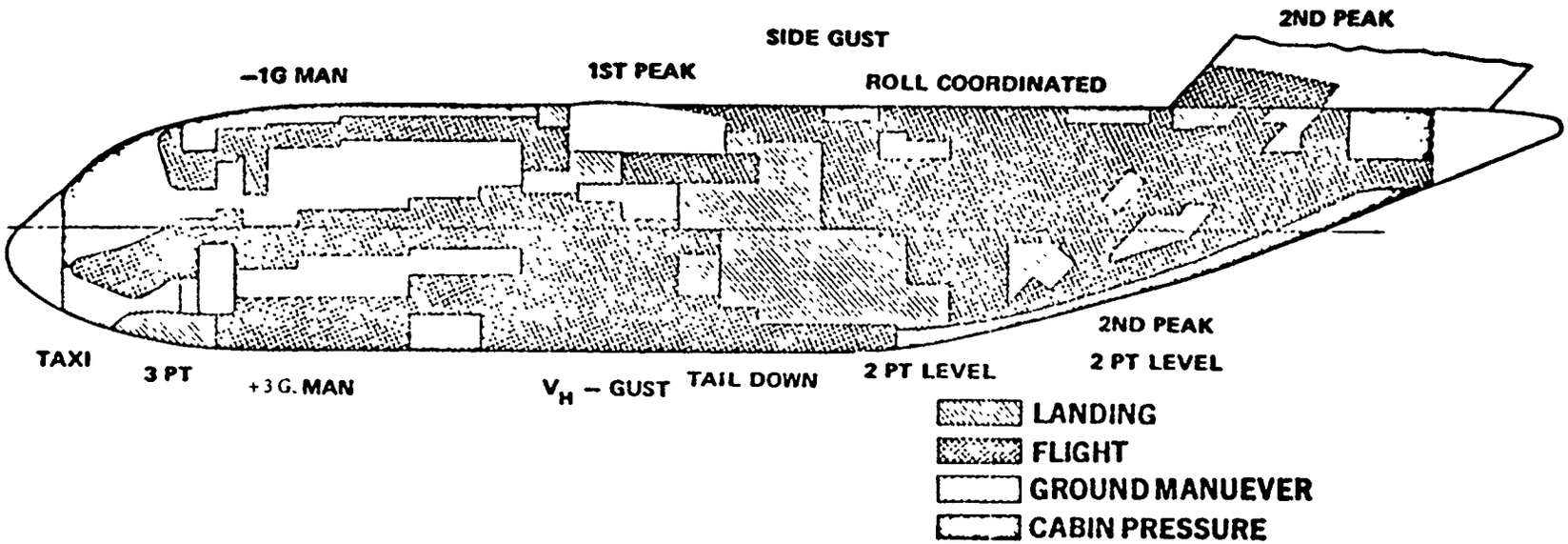


FIGURE 36. FUSELAGE CRITICAL ULTIMATE CONDITIONS

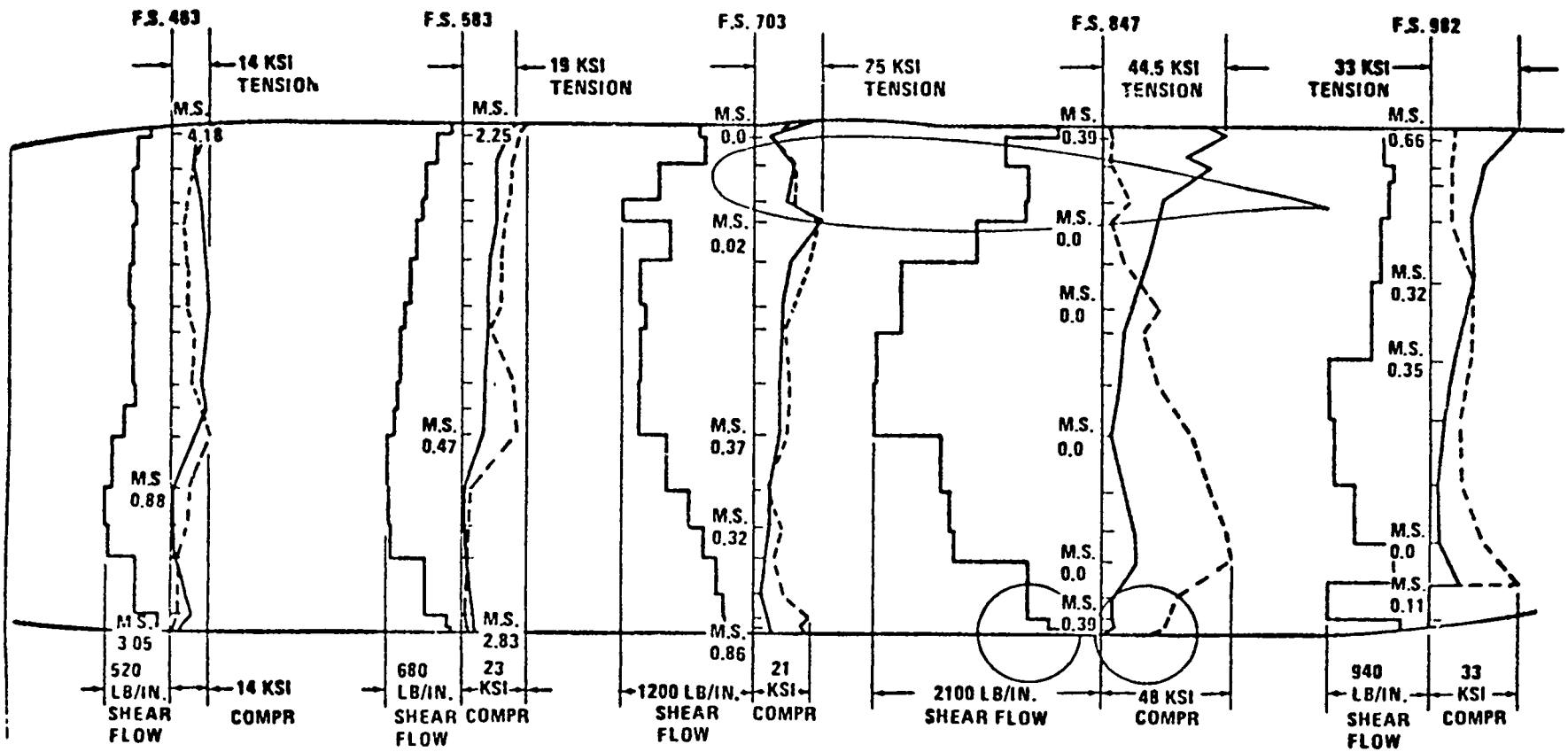


FIGURE 37. PABST FUSELAGE STRESSES AND MARGINS OF SAFETY-ULTIMATE MODE

Damage Tolerance

This section includes the damage tolerance requirements, analysis methods, material property data, PABST structural concept analyses and analysis-test correlation. Information applicable only to adhesives is presented separately within each subsection from the information on the assembled bonded metallic structure, called "metal" in this section for convenience.

A flow chart of the damage tolerance analysis procedure for the metal structure is shown in Figure 38.

The criteria for the metal structure and for the adhesive bonds for the Phase Ib of the PABST study are presented. The additions to the criteria that will be made for Phase II are briefly listed at the end of the subsection.

Applicable Documents. - The following documents apply to the extent specified: MIL-STD-1530(USAF) "Aircraft Structural Integrity Program, Airplane Requirements" (1 September 1972) except for sections: 4.2d, 4.2e, 5.1.1, 5.2.3, 5.2.7, 5.2.8, 5.2.9, 5.2.10, 5.2.11, 5.3.1.2, 5.3.4, 5.3.4.1, 5.3.4.2, 5.3.5, 5.3.5.1, 5.3.5.2, 5.3.5.3, 5.3.5.4, 5.3.6, 5.3.6.1, 5.3.6.3, 5.3.7, 5.3.8, 5.3.8.1, 5.3.8.2, 5.4 and its subsections and 5.5 and its subsections. Temperature and sonic fatigue criteria for PABST, to be used in lieu of these MIL-STD-1530 exceptions, are to be defined and will be implemented during Phase II.

MIL-A-83444 "Airplane Damage Tolerance Requirements" except for Sections 3.1.1.1b, 3.1.1.3 and its subsections, 3.1.3 paragraph on fail safe structure, 3.2.2 and its subsections, and 3.2.3 and its subsections.

MIL-A-008866A "Airplane Strength and Rigidity, Ground Tests" except for Sections: 3.6 (except as modified for STOL by McDonnell Douglas Report MDC J6066), 3.10, 3.11, 3.12, 3.13, 3.13, 4.3

MIL-A-008867A "Airplane Strength and Rigidity, Reliability Requirements, Repeated Loads and Fatigue" except for Sections: 3.2.3f, 3.2.3g, 3.3.4.1c except for environment, 3.3.4.2 environmental effects, 3.4.1.1, 3.4.4.2, 3.4.5.2, 3.4.5.3, 3.4.5.5 except real time and environment, 3.4.5.6, 3.4.5.9, 3.5.3, 3.7, 3.7.1, and 3.8.

PRECEDING PAGE BLANK-NOT FILMED

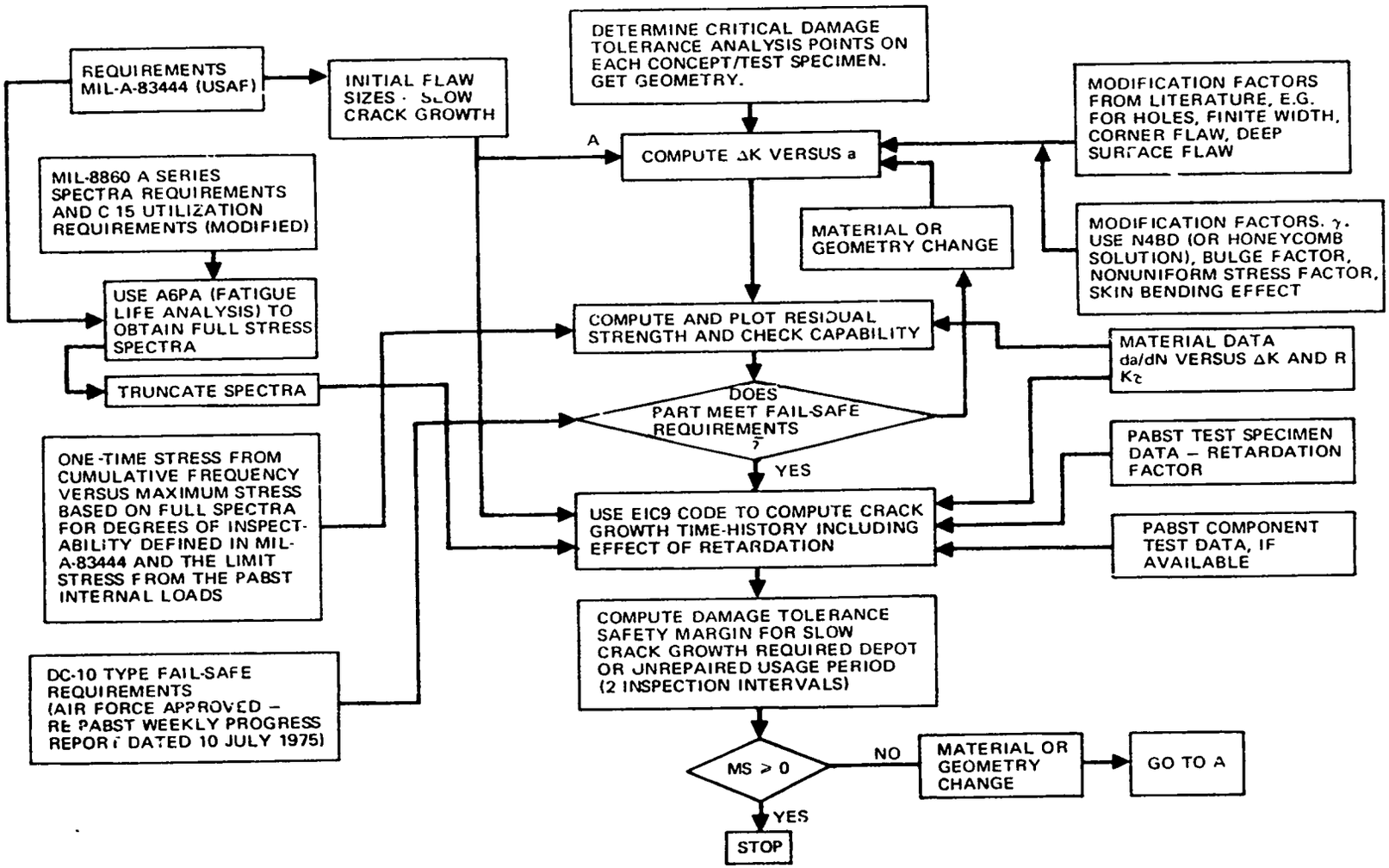


FIGURE 38. DAMAGE TOLERANCE ANALYSIS FLOW CHART FOR METAL STRUCTURE

Fatigue Criteria. - The PABST fatigue criteria shall incorporate a utilization model considering all pertinent loadings arising from preflight taxi, post-flight taxi including effects of reverse thrust, landing impact, vertical and horizontal gusts, flight maneuvers, pressurization, thermal loads, ground handling loads and the influence of the environment on the strengths of the various materials.

Service Life. - The design service life and design usage of PABST are shown exclusive of scatter factor.

Flight Service Life	30,000 Hours and 12,507 Flights
Pressurizations	19,014
Landings, Full Stop	29,977
Touch and Go's	16,127

The projected equivalent utilization for fatigue analysis of the PABST ADP Component is given in Table 11.

Design Fatigue Life. - The design fatigue life is the service life defined above multiplied by a scatter factor of 4.0.

Service Loads and Environment Spectra. - The basic inputs to define the cyclic loads spectra shall be as defined in MIL-A-008861A and MIL-A-008866A modified to incorporate the higher sink rates associated with STOL type aircraft. For the metal structure in Phase Ib, the environment used was room temperature and laboratory air. See the adhesives subsection for the adhesives environment. In addition, refer to the Phase II list at the end of the subsection.

Slow Crack Growth Damage Tolerance Criteria - Metallic Structure. - PABST safety of flight structure shall be qualified as slow crack growth under the appropriate sections of MIL-A-83444 and shall be designed so the possibility of catastrophic failure will be extremely remote. Compliance with these criteria shall involve residual strength and crack growth analysis and/or tests. In addition, the structural design and analysis shall account for the fail safe criteria in the following paragraph.

Fail Safe Criteria - Metallic Structure. - The PABST fuselage shall have a fail safe capability equivalent to that of the DC-10 commercial airplane. The fail safe requirements of MIL-A-83444 Section 3.1.1.1b, 3.1.1.3, 3.1.3, 3.2.2, 3.2.3 and their subsections will not be met since slow crack growth was used.

The structure shall be capable of withstanding (1) limit load with a two bay crack and (2) the maximum average internal member load occurring in 20 lifetimes, or limit load which ever is less, for foreign object damage as specified in the following subsections.

Longitudinal Cracks: - The structure with a longitudinal crack shall be able to withstand (1) a two-bay skin crack or a skin-to-longeron disbond and the center frame (or splice) intact, and (2) a 15 inch long foreign object damage skin crack with both the center frame (or splice) and crack arrest member (if present) failed. For the first requirement, at least the skin crack adjacent to a frame (or splice), where high stresses are induced from frame bending and pressure, shall be considered. All cracks considered shall be assumed to propagate in both directions.

For honeycomb structure, the longitudinal skin crack shall be in the face sheet on the side opposite the stiffening members. For foreign object damage, both face sheets and the core are cracked through a common plane.

Circumferential Cracks: - The structure with a circumferential crack shall be able to withstand (1) a two-bay crack with the center longeron (or splice) intact, and (2) a 15 inch long foreign object damage crack with the longeron or splice and crack arrest member (if present) failed. All flaws shall propagate in both directions.

For honeycomb, the damage shall be as specified in the longitudinal cracks subsection.

Damage Tolerance Criteria - Adhesive Bond Areas. - The requirements of MIL-A-83444, for metal and mechanically joined elements shall be supplemented with the following requirements for the design of adhesive bonds joining two or more elements of the structure. Compliance with these criteria shall be developed by analysis and/or test. The analytical damage tolerance assessment shall be confined to residual strength estimates. The analyses shall assume the presence of flaws in the bond placed in the most unfavorable location and orientation with respect to applied stress and material properties. The experimental investigation shall be limited to distinguishing between flaws which grow and those which do not. Thermal and humidity effects shall be accounted for.

Entire panels or parts which are improperly processed, i.e. parts with global damage, shall be rejected. Parts with local contamination or flaws shall be reworked to a quality in which the flaws shall not grow to unacceptable sizes within two airframe lifetimes.

Initial Flaw Sizes: - An initial flaw shall be assumed to exist in each and every bond in its most critical location including those highly stressed areas resulting from variable bondline thickness. The size of the flaw shall be the greater of (1) the minimum detectable size for the NDI technique used on the bond, or (2) the smallest flaw remaining after a larger flaw has been repaired. Each flaw shall be analyzed for residual strength independently of all other flaws, either in the bond or metal. Initial flaws shall be located so there is no interaction between them.

Bond Inspectability: - The detail design shall minimize the use of uninspectable bonds and, wherever practical, shall be such as to force the first evidence of failure into a visible or easily inspectable area. Techniques, such as staggering the ends of the overlaps, shall be used to facilitate inspection of the bonds. Each uninspectable bond shall be limited in extent to a subcritical size.

Flaw Growth in Bonds: - Flaws in bonds induced in service shall not grow from initial sizes defined above to critical size within two airframe lifetimes. All flaws large enough to grow in service shall be repaired prior to delivery of the aircraft to preclude corrosion. In addition, bonds which contain subcritical flaws in areas subject to corrosion shall be sealed to provide environmental resistance.

Fail Safe Capability: - The fail safe capability of the bonded structure shall be demonstrated by test and/or analysis. The structure shall be capable of withstanding (1) limit load with each of the following two-bay disbond configurations:

(a) a two bay disbond in only one side of a double lap splice,

(b) a two bay disbond in a single sided bonded splice,

(c) a two bay longeron-to-skin disbond, and

(d) a two bay shear-clip-to-skin or crack-arrest-member-to-skin disbond;

and (2) the maximum average internal member load occurring in 20 lifetimes, but less than limit load, for impact or the foreign object damage specified as:

(a) a 15" disbond on both sides of a splice, and

(b) a 15" long foreign object damage skin crack with both the center frame (or splice) and the crack arrest member failed or with both the longeron (or splice) and crack arrest member failed as applicable.

Additional Criteria for Phase II. - The following criteria areas will be added in the Phase II portion of the PABST program: (a) the effect of thermal and chemical environments on metallic structure (note: the the effect on adhesives is included in Phase Ib), (b) the effect of sonic fatigue, (c) the effect of sustained load flaw growth in the metallic structure.

Stress Spectra Generation. - The internal load (stress) spectra for the design concept check points were generated for airplane usage as defined by the PABST flight profiles. The profiles were based on expected C-15 missions. These flight profiles were the basis of a series of load conditions applied to an internal loads mathematical model which gave stresses for each load condition.

These stresses, at critical fuselage locations, were used to develop the applied stress spectra. The stresses at these locations were used to generate tables of stresses and $\Delta\sigma/g$ for each segment of the flight profiles. The tables were input to the Douglas A6PB spectra computer program which outputs tables of stresses and cycles. The stress and cycles tables were then used to generate the stress spectra input to the Douglas crack growth time history computer program E1C9. An example of the E1C9 spectrum for the external concept check point B is shown in Table 14.

Damage Tolerance Analysis Methods (Metals). - The crack growth and residual strength analyses of the metallic structure were based on classical linear elastic fracture mechanics in which the model consists of a symmetric crack growing from a through-the-thickness flaw in an infinite sheet. A basic assumption made is that the local stress conditions at the crack tip are defined by the local stress intensity K, where:

$$K = \sigma\sqrt{\pi a}$$

σ = gross area stress remote from the crack tip, psi

a = half crack length, inches

The general equation for stiffened thin-walled structure of finite size is:

$$k = \sigma\sqrt{\pi a}\ \beta_1\beta_2\cdots\beta_N$$

where the β_N terms are modification factors including the following,

TABLE 14

Modified Spectra for External Longeron Concept, Check Point B

	LOAD BLOCK	NUMBER OF CYCLES PER LOAD CYCLE	NUMBER OF CYCLES AT END OF BLOCK	SIGMA MAX	SIGMA MIN
GAG	1	241.	241.	18759.00	-2217.00
FLT	2	478.	719.	4500.00	3150.00
FLT	3	639.	1358.	6500.00	5850.00
FLT	4	5417.	6775.	9500.00	8550.00
FLT	5	440.	7215.	10500.00	9450.00
FLT	6	3545.	10760.	15500.00	13950.00
FLT	7	859.	11619.	16500.00	14850.00
FLT	8	3435.	15054.	19500.00	17550.00
GAG	9	32.	15086.	19912.00	-2313.00
FLT	10	6.	15092.	4500.00	3150.00
FLT	11	110.	15202.	5500.00	3850.00
FLT	12	14.	15216.	6500.00	4550.00
FLT	13	91.	15307.	7500.00	6750.00
FLT	14	11.	15318.	8500.00	5950.00
FLT	15	961.	16279.	10500.00	9450.00
FLT	16	276.	16555.	11500.00	10350.00
FLT	17	24.	16579.	12500.00	11250.00
FLT	18	3.	16582.	13500.00	9450.00
FLT	19	91.	16673.	17500.00	15750.00
FLT	20	240.	16913.	20500.00	18450.00
FLT	21	56.	16969.	21500.00	19350.00
FLT	22	5.	16974.	22500.00	20250.00
GAG	23	241.	17215.	19758.00	-2217.00
FLT	24	108.	17323.	3500.00	2450.00
FLT	25	808.	18131.	4500.00	3150.00
FLT	26	21.	18152.	550.00	2750.00
FLT	27	1681.	19833.	6500.00	5850.00
FLT	28	6.	19839.	7500.00	3750.00
FLT	29	5871.	25710.	9500.00	8550.00
FLT	30	487.	26197.	10500.00	9450.00
FLT	31	19.	26216.	11500.00	8050.00
FLT	32	1.	26217.	12500.00	8750.00
FLT	33	3262.	29479.	15500.00	13950.00
FLT	34	817.	30296.	16500.00	14850.00
FLT	35	17.	30313.	17500.00	15750.00
FLT	36	3946.	34259.	19500.00	17550.00
FLT	37	62.	34321.	20500.00	18450.00
FLT	38	8.	34329.	21500.00	19350.00
GAG	39	32.	34361.	19912.00	-2312.00
FLT	40	10.	34371.	4500.00	3150.00
FLT	41	87.	34458.	5500.00	3850.00
FLT	42	12.	34470.	6500.00	4550.00
FLT	43	88.	34558.	7500.00	6750.00
FLT	44	11.	34569.	8500.00	5950.00
FLT	45	661.	35230.	10500.00	9450.00
FLT	46	172.	35402.	11500.00	10350.00
FLT	47	13.	35415.	12500.00	11250.00
FLT	48	1.	35416.	13500.00	9450.00
FLT	49	79.	35495.	17500.00	15750.00
FLT	50	265.	35760.	20500.00	18450.00
FLT	51	57.	35817.	21500.00	19350.00
FLT	52	4.	35821.	22500.00	20250.00
GAG	53	41.	35862.	15325.00	-2217.00
FLT	54	7.	35869.	3500.00	2450.00
FLT	55	100.	35969.	4500.00	3150.00
FLT	56	2.	35971.	5500.00	2750.00
FLT	57	121.	36092.	6500.00	5850.00
FLT	58	1283.	37375.	9500.00	8550.00
FLT	59	93.	37468.	10500.00	9450.00
FLT	60	5.	37473.	11500.00	8050.00
FLT	61	38.	37511.	13500.00	12150.00
FLT	62	4.	37515.	14500.00	13050.00
FLT	63	1333.	38848.	15500.00	13950.00
FLT	64	546.	39394.	16500.00	14850.00
FLT	65	15.	39409.	17500.00	15750.00

TABLE 14 (CONTINUED)

Modified Spectra for External Longeron Concept, Check Point B

	LOAD BLOCK	NUMBER OF CYCLES PER LOAD CYCLE	NUMBER OF CYCLES AT END OF BLOCK	SIGMA MAX	SIGMA MIN
GAG	66	3.	39412.	16479.00	-2313.00
FLT	67	46.	39458.	5500.00	4950.00
FLT	68	12.	39470.	6500.00	5850.00
FLT	69	9.	39479.	7500.00	6750.00
FLT	70	1.	39480.	8500.00	7650.00
FLT	71	49.	39529.	10500.00	9450.00
FLT	72	15.	39544.	11500.00	10350.00
FLT	73	1.	39545.	12500.00	11250.00
FLT	74	3.	39548.	15500.00	13950.00
FLT	75	87.	39635.	17500.00	15750.00
FLT	76	8.	39643.	18500.00	16650.00
FLT	77	1.	39644.	19500.00	17550.00
GAG	78	41.	39685.	11551.00	-2217.00
FLT	79	148.	39833.	500.00	450.00
FLT	80	1002.	40835.	3500.00	3150.00
FLT	81	154.	40989.	8500.00	7650.00
FLT	82	4.	40993.	9500.00	6650.00
FLT	83	2149.	43142.	12500.00	11250.00
FLT	84	54.	43196.	13500.00	12150.00
FLT	85	5.	43201.	14500.00	13050.00
GAG	86	3.	43204.	12226.00	-2313.00
FLT	87	1.	43205.	4500.00	3150.00
FLT	88	43.	43248.	5500.00	4950.00
FLT	89	11.	43259.	6500.00	5850.00
FLT	90	31.	43290.	7500.00	6750.00
FLT	91	9.	43299.	8500.00	7650.00
FLT	92	1.	43300.	9500.00	6650.00
FLT	93	10.	43310.	10500.00	9450.00
FLT	94	1.	43311.	11500.00	8050.00
FLT	95	96.	43407.	12500.00	11250.00
FLT	96	37.	43444.	13500.00	12150.00
FLT	97	3.	43447.	14500.00	13050.00
GAG	98	241.	43688.	2500.00	-2217.00
FLT	99	30102.	73790.	3500.00	2450.00
FLT	100	1187.	74977.	4500.00	1350.00
GAG	101	41.	75018.	2500.00	-2217.00
FLT	102	184904.	259922.	3500.00	2450.00
FLT	103	7286.	267208.	4500.00	1350.00
GAG	104	3.	267111.	-2432.00	-2313.00
GAG	105	50.	267161.	1764.00	-2397.00
FLT	106	88010.	355161.	2500.00	750.00
FLT	107	26010.	381161.	3500.00	350.00
GAG	108	50.	381211.	3404.00	-3150.00
FLT	109	114057.	495268.	4500.00	3150.00
GLT	110	14307.	509575.	5500.00	1650.00
FLT	111	1301.	510876.	6500.00	650.00

as applicable:

$F\ (^{a}/r)$ = Bowie correction for symmetric or asymmetric cracks at holes

λ_1 = Finite width correction for eccentric cracks (Reference 1)

λ_2 = Finite width correction for single edge cracks (Reference 1)

a_b = Liu back surface correction factor for corner flaws (Reference 2)

M_k = Kobayashi factor for deep surface discontinuities (Reference 3)

γ = Swift factor accounting for the effect of stiffening on a cracking sheet (Reference 4)

B = Correction factor accounting for the effect of bulging on a cracking curved sheet due to pressure. (Reference 5)

ξ = Effect of non-uniform stress distribution, from the pressurized uncracked stiffened cylinder, on a longitudinal skin crack. See Figures 39 and 40.

F = Knock down factor for the effect of the skin bending stress on a circumferential crack near a frame in a pressurized shell.

The damage tolerance analyses were based on the Hart-Smith method of predicting the stress distribution in a pressurized stiffened cylinder, Figure 39. This method is more accurate than the classical solution since:

(a) the distortion under load included in shell buckling theory is accounted for,

(b) the deflected shape is defined by non-oscillatory exponential decay functions,

(b) the correct frame stresses are obtained by using the junction stresses between the skin and frame determined by the skin bending moments, and

(d) the axial stiffener influence on the skin stresses is accounted for (through Poisson effects).

The crack growth time histories of the cracked structural members analyzed were calculated using a Douglas computer program that is an expanded version of the Air Force CRACKS program, and da/dn vs ΔK material data. Residual strength was calculated using critical stress intensity, i.e. k_c, data. These material data are discussed in a subsequent subsection.

It should be noted that in the Phase Ib analysis, all of the metallic structural components and the bond were assumed to be elastic for the damage tolerance analysis of the metal structure. An on-going research (IRAD)

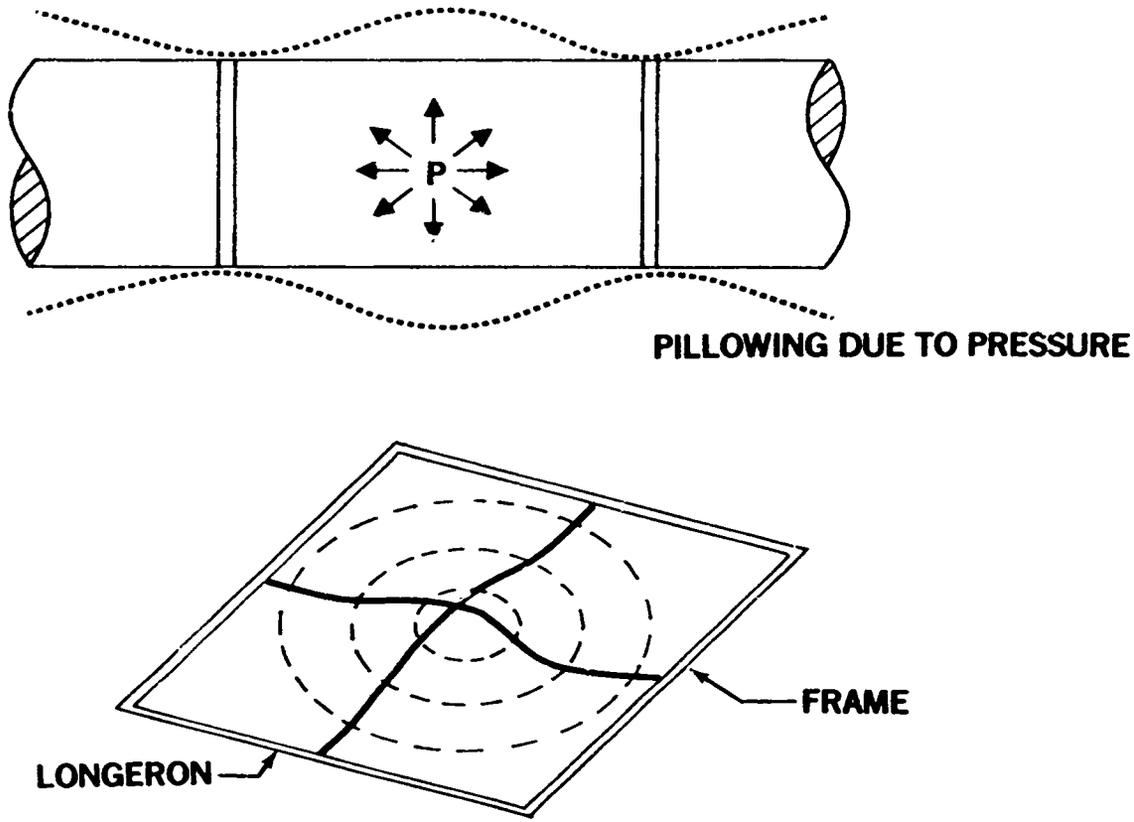
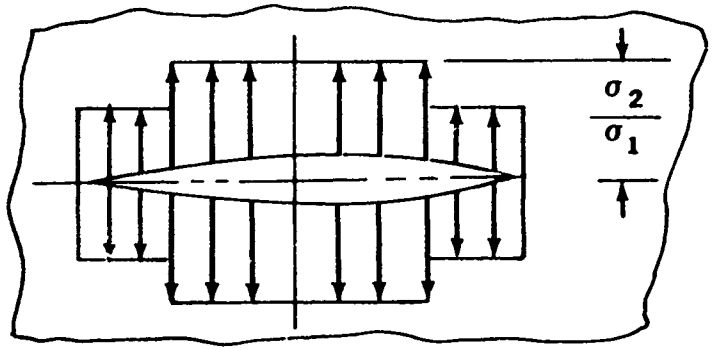


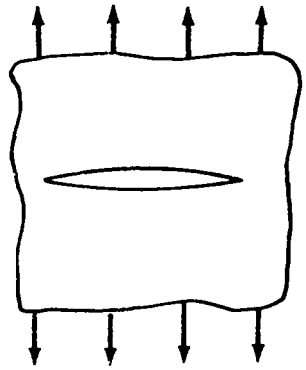
FIGURE 39. STRESS DISTRIBUTION IN A PRESSURIZED STIFFENED CYLINDER

- NON-UNIFORM STRESS DUE TO PRESSURIZATION

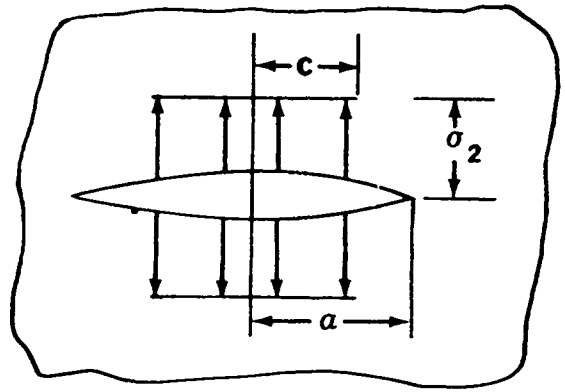


- GREEN'S FUNCTION APPROACH

- SUPERPOSITION



+



- $K - f(\sigma_1, \sigma_2, a, c) = \sigma\sqrt{\pi a}\ \xi$

FIGURE 40. NONUNIFORM STRESS DISTRIBUTION FACTOR

effort on metallic structure and PABST analysis of adhesives indicate that the use of linear elastic fracture mechanics for the cracking member with an elastic-plastic capability for the adhesive and the attached structure would improve the accuracy of the analysis. This recommendation was corroborated by a PABST flat stiffened panel test.

Material Data-Metals. - The da/dn vs ΔK curves for Phase Ib were taken from data available in the literature, primarily Battelle data. Both average and upper bound curves were prepared for the following aluminum alloys:

1) 2024-T3 both bare and clad sheet,
2) 7075-T6 clad sheet,
3) 7075-T73 extrusion, and
4) 7475-T761 bare sheet.

A decision was made that the curves for all aluminum alloys and R values would pass through 10^{-8} at $\Delta K = 2$ ksi $\sqrt{in.}$ This decision was based on available NASA data for 2219 aluminum and had customer concurrence.

An example plot of da/dn vs ΔK data is shown in Figure 41 for 2024-T3 bare sheet. A da/dn vs ΔK plot for 2024-T3 and 7075-T6 alloys for R = 0 is shown in Figure 42 to indicate the shift in the curves that occurs for a change in alloy.

It should be noted that because of the log-log scale of the plots, small ΔK displacements of the curves can lead to significant changes in da/dn magnitude which can greatly affect the analytical determination of crack growth time history. For this reason, current da/dn vs ΔK data will be reviewed for Phase II to incorporate any recent data from Douglas (IRAD) tests and from the literature.

K_c Values: - The following K_c values were used in the analysis of the test specimens and design concepts.

Aluminum Alloy	Applicable Analysis	Temp °F	* K_c	* (Obtained from Douglas IRAD tests)
2024-T3 Bare	Test	RT	130	
	Concept	-65	130	
7075-T6 Clad	Concept	-65	40	
7475-T761 Bare	Test	RT	120	
	Concept	-65	109	

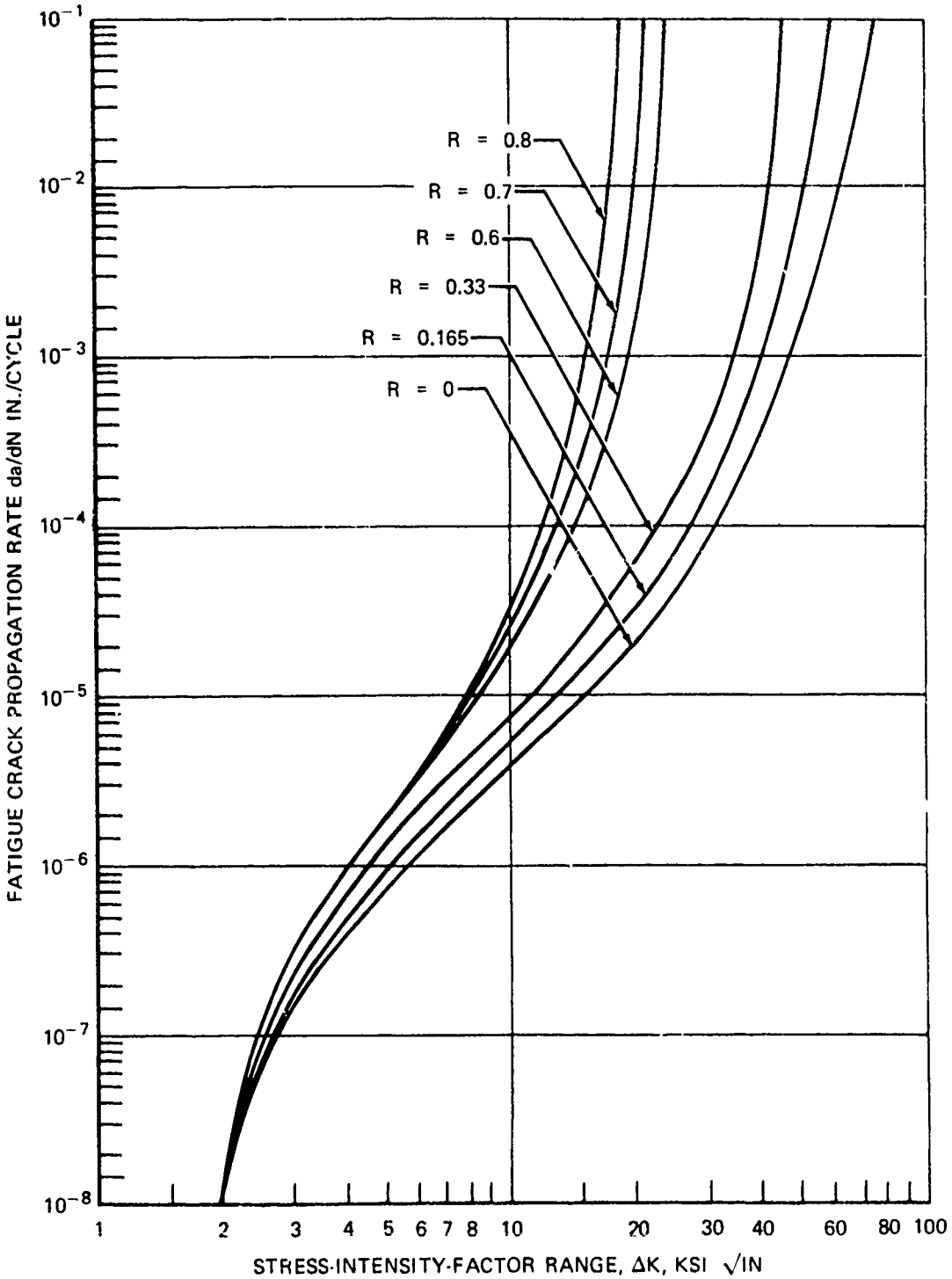


FIGURE 41. da/dN VERSUS ΔK –2024-T3 BARE SHEET T – L AVERAGE

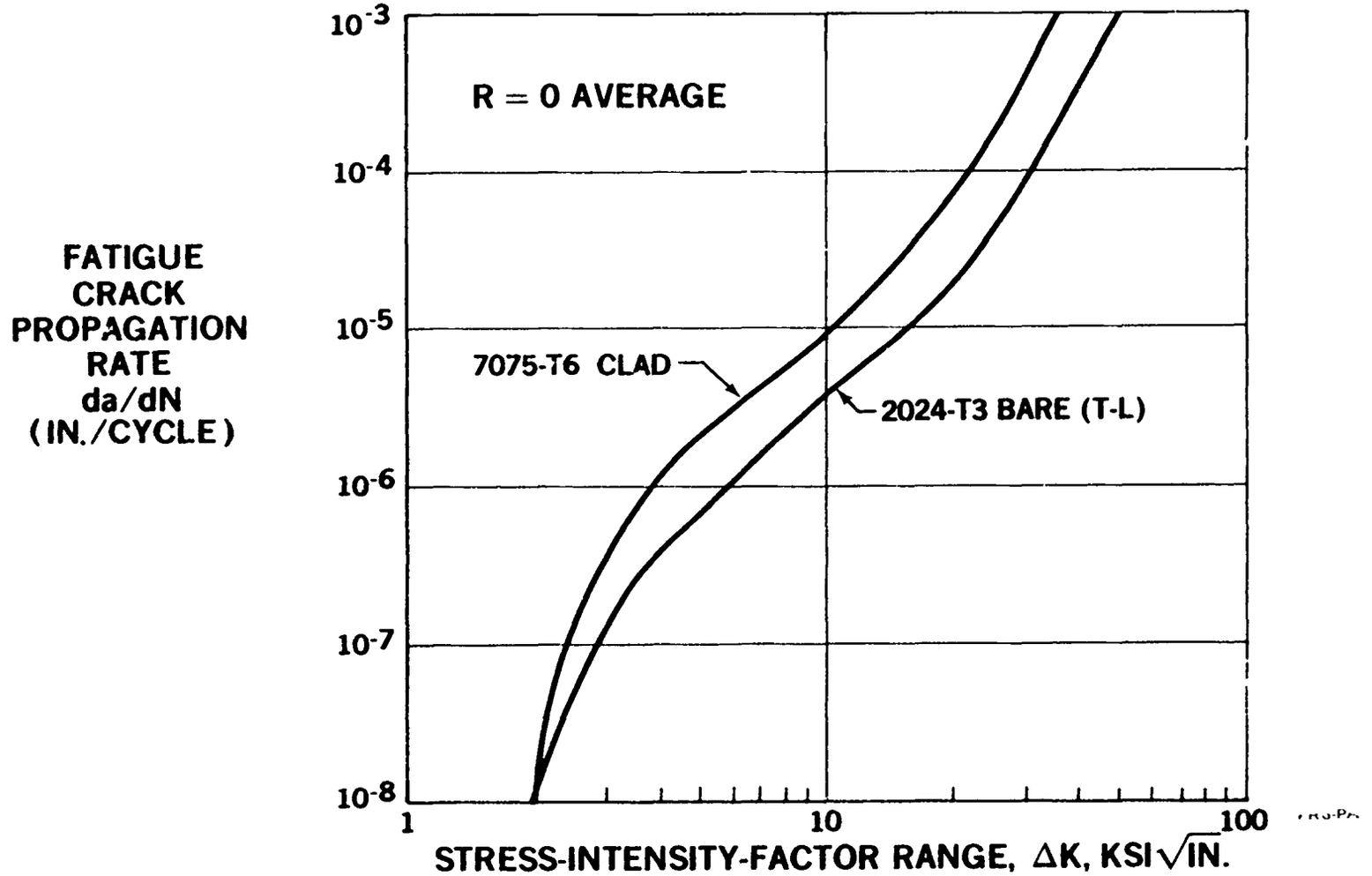


FIGURE 42. COMPARISON OF da/dN VERSUS ΔK FOR TWO ALUMINUM ALLOYS

Retardation: - Four flat unstiffened center-cracked panels were tested to measure retardation in crack growth due to infrequent high loads under spectrum loading and to establish a retardation model for crack growth analysis. The specimens were:

Number of Specimens	Specimen Thickness	Specimen Material	Test Temperature
1	0.05	2024-T3 Bare	Room Temperature
1	0.05	7475-T761 Bare	Room Temperature
1	0.05	7475-T761 Bare	-65°F
1	0.05	7075-T6 Clad	Room Temperature

The spectra for the 2024 and 7475 specimens is shown in Figure 43. The spectra for the 7075-T6 specimen was:

σ_{max}	R	Cycles Spectrum	$\Delta\sigma$
13500	0.1	1	12150
10750	0.3	168	7525
8062	0.7	584	2419
13500	0.1	1	12150
8062	0.7	584	2419
10750	0.3	168	7525

The results for the 2024-T3 specimen test are shown in Figure 43 with analysis based on the Willenborg retardation model with the factors shown. The test data fell to the right of the Willenborg curve for R = 1.0 for all room temperature tests. For the cold temperature test, the test data fell to the left of the Willenborg curve for R = 0.6. Chemical analysis of the 7075-T6 specimen showed it to be close to the specification for 7475 alloy and analysis based on 7475 da/dn vs ΔK data showed better agreement with test data than the 7075 material data did.

Attempts to correlate the data with existing retardation models was not successful. A retardation factor of 0.8 to 0.9 and a Willenborg model based on previous Douglas experience was therefore used for PABST.

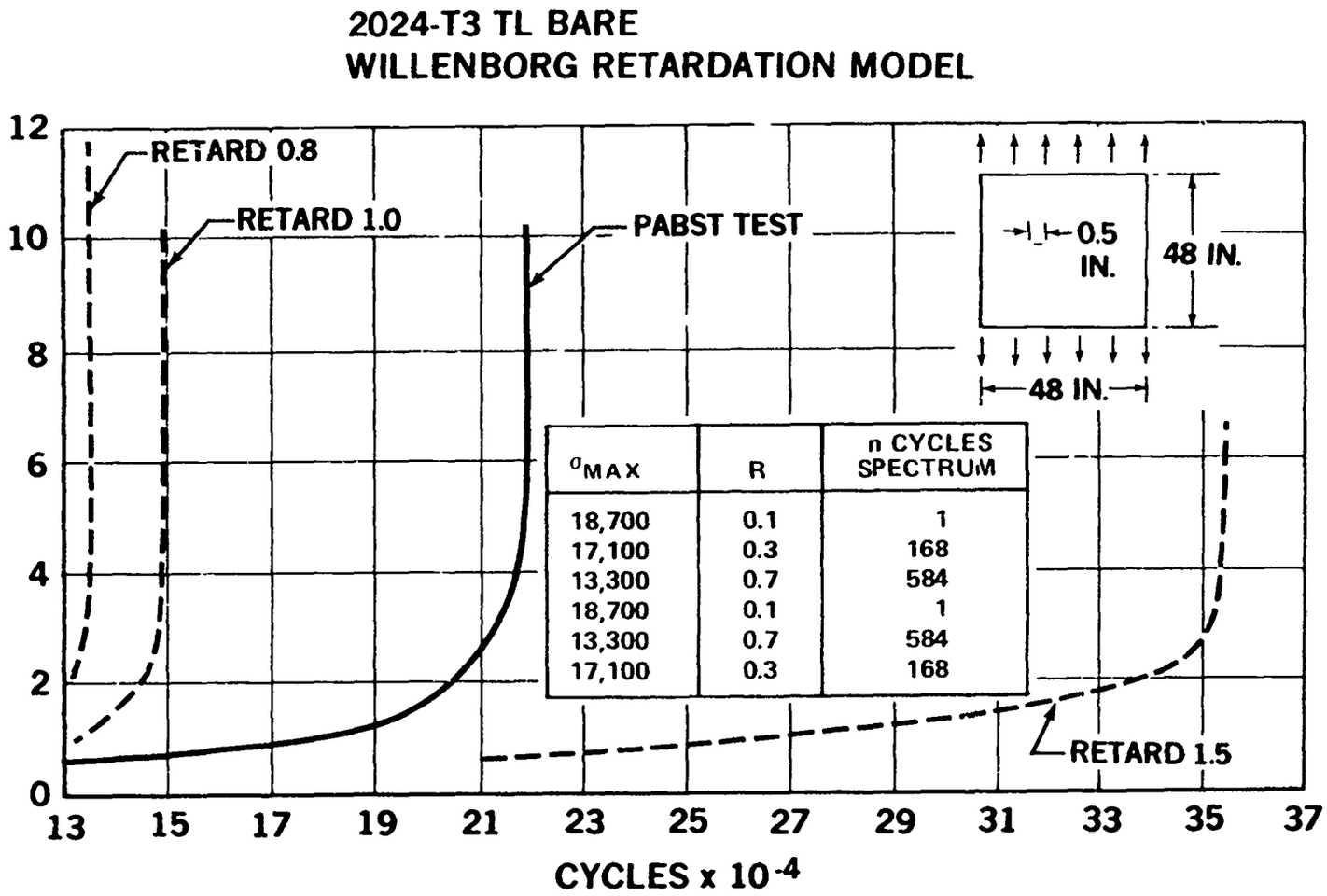


FIGURE 43. PABST RETARDATION ANALYSIS AND TEST DATA FOR 2024-T3 TL BARE

Concept Analysis (Metals). - The three concepts described in the Design Concepts Section were analyzed for the damage tolerance requirements using the analysis methods and material data described in the previous subsections. The critical points on the fuselage used for analysis were selected on the basis of the internal loads as described in the following paragraphs. Margins on life were obtained for structure analyzed for slow crack growth based on the Forman equation for the da/dn vs ΔK curve,

$$\frac{da}{dn} = \frac{C\,(\Delta K)^n}{(1-R)K_c - \Delta K}$$

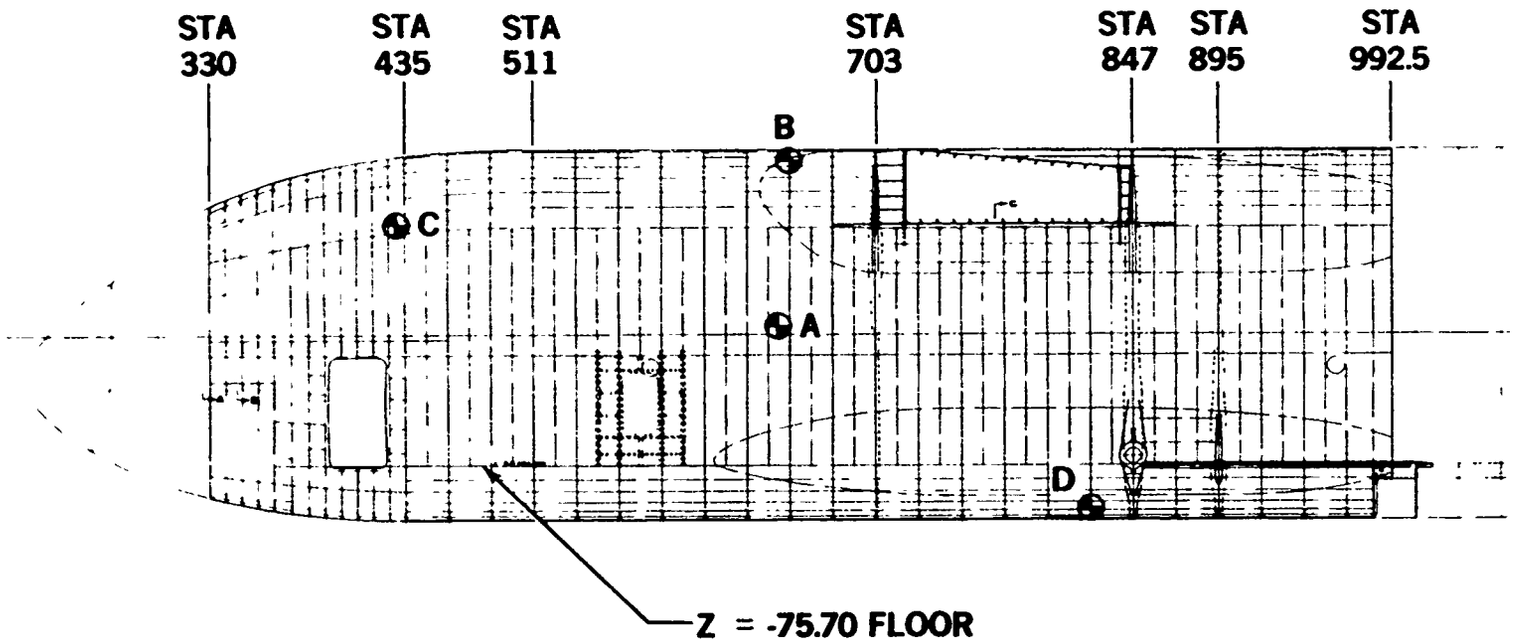
where: a = half crack length
N = cycles
R = Stress Ratio
K_c = Critical stress intensity
K = Difference in stress intensity
n,C = Material constants

In the region of the initial crack where the contribution to the total lifetime is greatest, ΔK is much less than K_c. For efficiently designed structure, the margin is low and the $[(1-R)K_c - \Delta K]/C$ term can be assumed to be relatively constant in the applicable da/dn vs ΔK region since the region is small enough to permit a linear approximation. A relationship between life and stress can then be obtained which is:

$$\sigma_1 = \sigma_2 \left(\frac{N_2}{N_1}\right)^{1/n} \quad \text{or} \quad \sigma_{allowable} = \sigma_{failure} \left[\frac{N_{failure}}{N_{criteria}}\right]^{1/n}$$

$$\text{margin on Life} = \left[\frac{N_{failure}}{N_{criteria}}\right]^{1/n} - 1.$$

Internal Longeron Concept: - The critical points for the analysis of the internal longeron concept are shown in Figure 43. All of the points were in the 0.05" thin skin region. Critical point A was selected as a high axial and pressure tensile stress area in the wide spaced longeron region. Critical point B was in the highest axial and pressure tensile stress area. Critical



● CRITICAL POINTS

FIGURE 44. CRITICAL POINTS FOR THE INTERNAL LONGERON CONCEPT

point C was in an area subjected mainly to pressure stress but was needed to check the adequacy of the close spaced frame/wide spaced longeron geometry in the nose. Critical point D was under the floor in the region with highest axial compression as well as the pressure tensile stress. The axial compression tends to open a longitudinal crack increasing the effective crack tip stress intensity.

The results of the analysis are shown in Table 15. For the original design of the wide spaced longerons Figure 44 at critical point A, the fail safe criteria for a circumferential crack was not met. One fail safe strap was added between each pair of longerons as shown in the Design Concepts section. The method of determining the strap stiffening and area is discussed in the sensitivity analysis subsection.

TABLE 15

INTERNAL LONGERON CONCEPT DAMAGE TOLERANCE ANALYSIS SUMMARY

Critical Point	Slow Crack Growth	Fail Safe	
	One Bay Crack	Two Bay Crack-Center Stiffener Intact	15" Foreign Object Damage-Center Stiffening Broken
Point A Circumferential Crack	3% Margin on Life, Original Design	Original design did not meet Criteria. Fail Safe Strap added	Original Design did not meet Criteria. Fail safe Strap added.
Point B Longitudinal Crack	9% Margin on Life	Criteria met	Criteria met
Point B Circumferential Crack	0% Margin on Life	Criteria met	Criteria met
Point C Circumferential Crack	13% Margin on Life	Criteria met	Criteria met
Point D Longitudinal Crack	8% Margin on Life	Criteria met	Criteria met

With the addition of the straps, critical point B becomes the area of lowest margin on life, for the circumferential crack. The slow crack growth

criteria is critical for a one bay crack. The associated skin crack growth time is shown in Figure 45. The applicable stress spectra is shown in Table 14 and was used with a Willenborg retardation model and 0.9 factor. The fail safe checks are shown in Figures 46 and 47. It can be seen that (1) The two bay-center stiffener intact criteria was met since the panel did not fail until a half crack of 19.2 inches was reached, and (2) the 15" foreign object damage crack fast fractured then arrested at a half crack of 14.9 inches. The panel failed when a half crack of 15.6 inches was reached.

External Longeron Concept: - The internal loads for this concept were the same as for the internal longeron concept. The critical points for analysis were at the same locations, see Figure 43 . The results of the analysis are

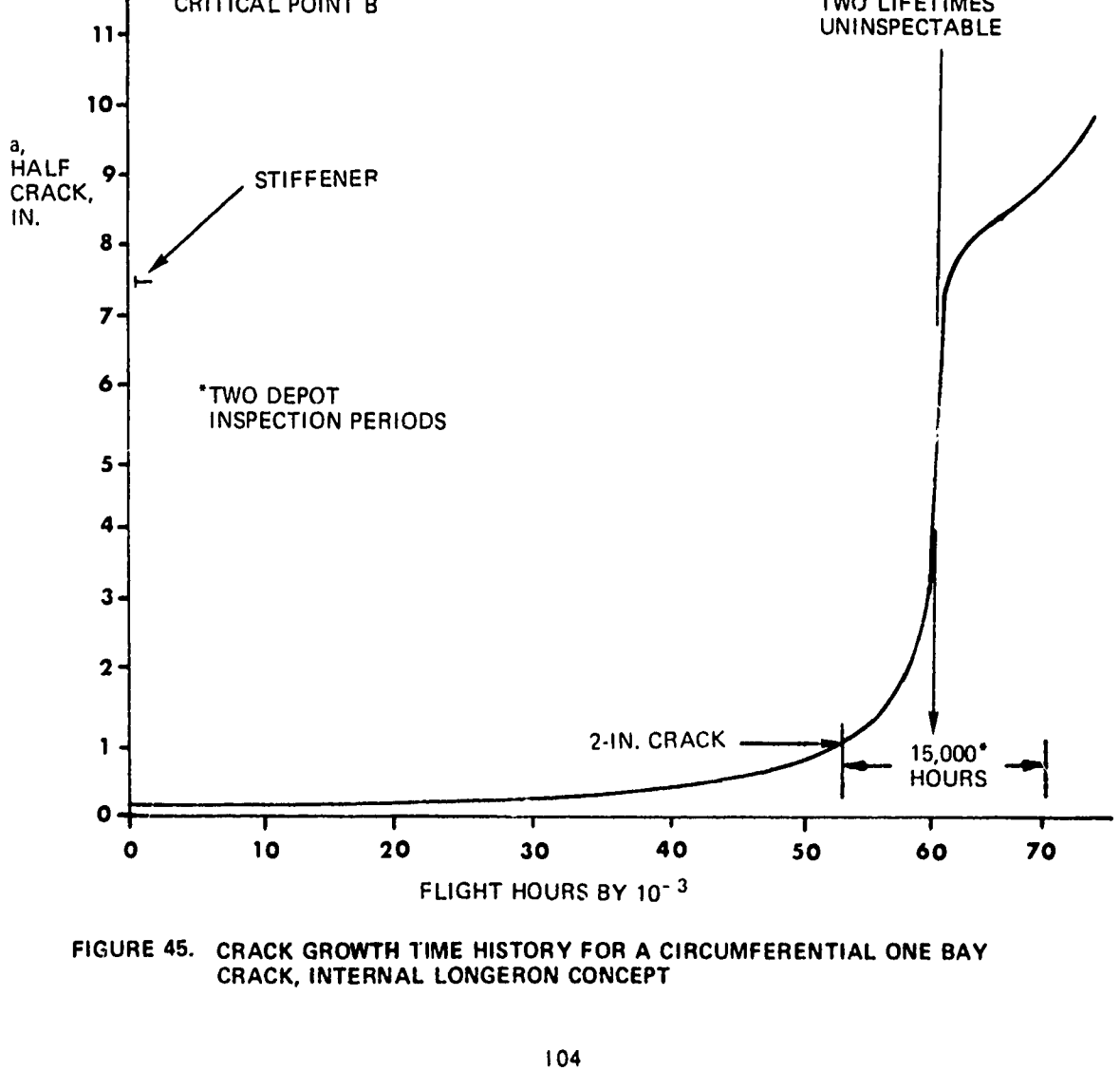


FIGURE 45. CRACK GROWTH TIME HISTORY FOR A CIRCUMFERENTIAL ONE BAY CRACK, INTERNAL LONGERON CONCEPT

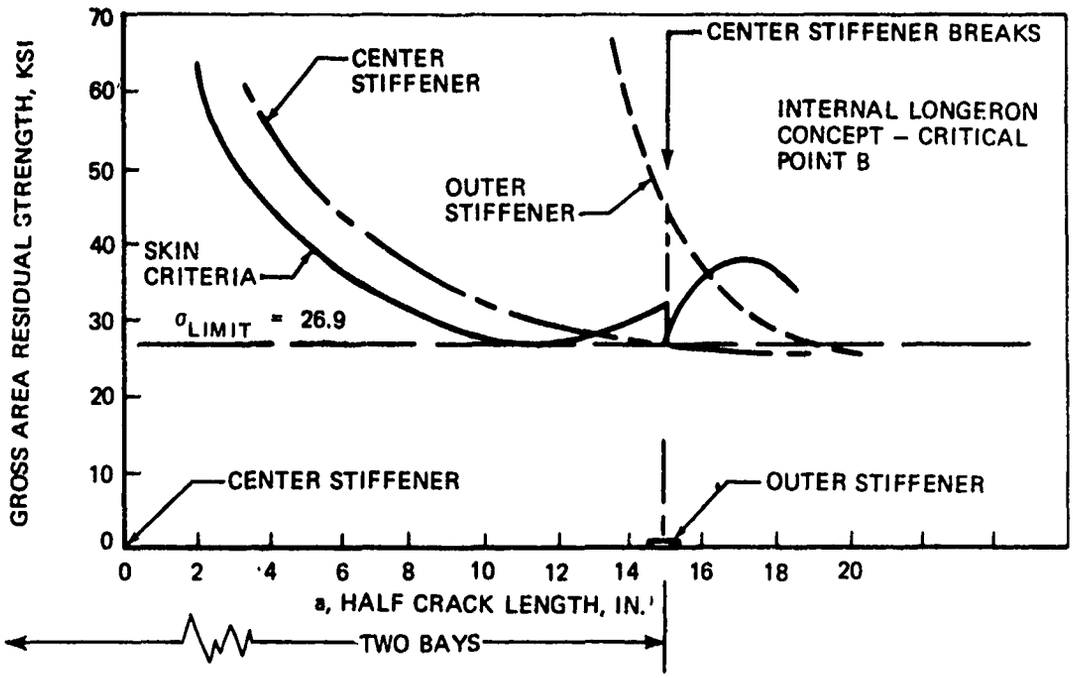


FIGURE 46. FAIL-SAFE CHECK FOR A TWO-BAY CIRCUMFERENTIAL CRACK WITH CENTER STIFFENER INTACT

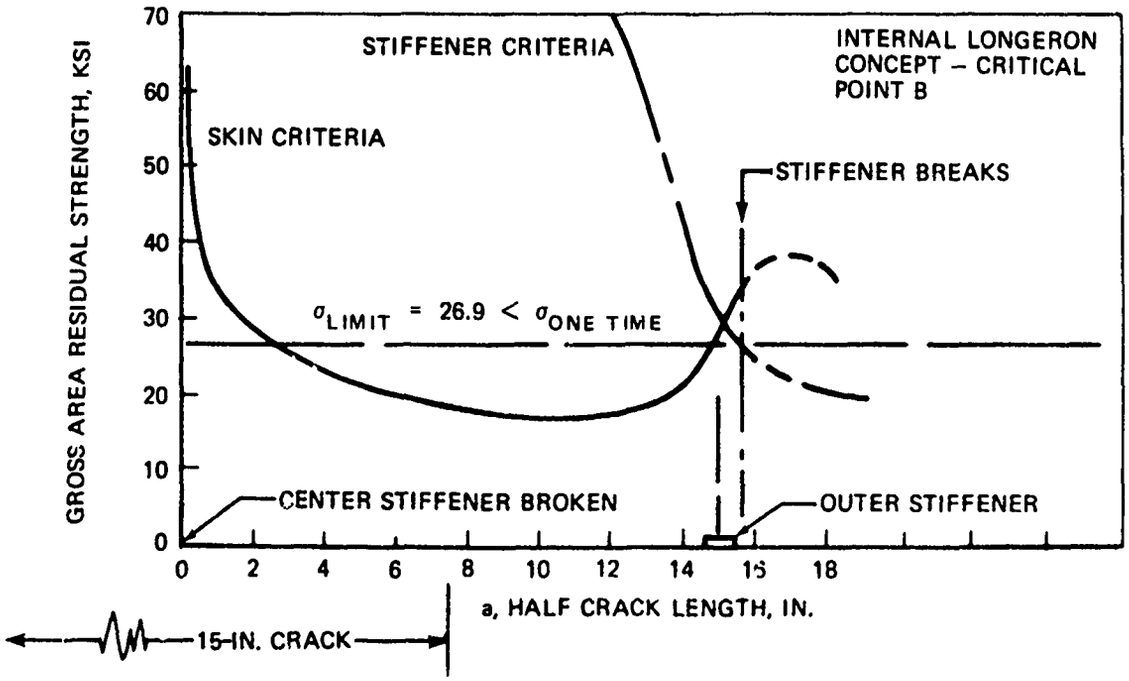


FIGURE 47. FAIL-SAFE CHECK FOR A 15-INCH FOREIGN OBJECT DAMAGE CIRCUMFERENTIAL CRACK AND BROKEN CENTER STIFFENER

shown in Table 16 . An analysis of an initial crack in the frame at critical point B showed the case of the initial crack in the skin was more critical. This result confirmed the same conclusion for frame analyses performed during the initial screening of concepts early in Phase Ib. The longerons were also less critical than the skin in the screening analyses.

TABLE 16

EXTERNAL LONGERON CONCEPT DAMAGE TOLERANCE ANALYSIS SUMMARY

Critical Point	Slow Crack Growth	Fail Safe	
	One Bay Crack	Two Bay Crack-Center Stiffener Intact	15" Foreign Object Damage-Center Stiffening Broken
Point A	3% Margin on Life, Original Design	Original design Marginal. Fail Safe Strap Added.	Original design Marginal. Fail Safe Strap Added.
Point B Longitudinal Crack	10% Margin On Life	Criteria met	Criteria met
Point B Circumferential Crack	0% Margin On Life	Criteria met	Criteria met
Point C Circumferential Crack	12% Margin On Life	Criteria met	Criteria met
Point D Longitudinal Crack	8% Margin	Criteria met	Criteria met

Honeycomb Concept: - The critical points for the analysis of the honeycomb concept are shown in Figure 48. As shown in the Design Concept section, almost the entire honeycomb fuselage has an 0.032 inch face sheet on the outside and an 0.020 inch face sheet on the side with the frames and fail safe straps. Critical point A was in the highest axial and pressure tensile stress area. Critical point B was under the floor in the region with highest axial compression as well as the pressure tensile stress. Since the geometry is constant throughout most of the honeycomb fuselage, these are the only

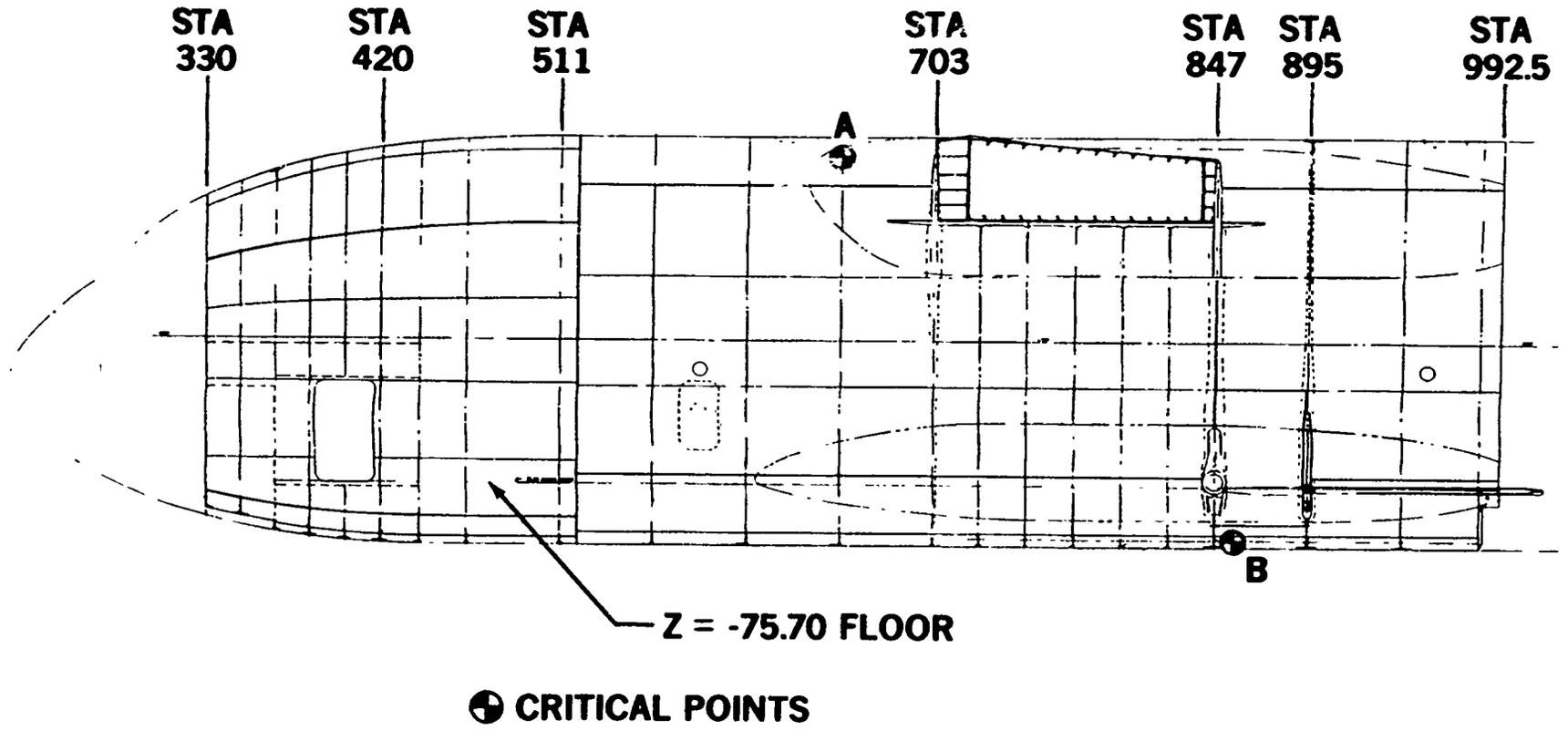


FIGURE 48. CRITICAL POINTS FOR THE HONEYCOMB CONCEPT

critical points needed.

The results of the analysis are shown in Table 17. The model for the slow crack growth analysis and the fail safe analysis of a two bay crack with center stiffener intact is shown in Figure 49. For both of these analyses, the panel was assumed to act like an unstiffened honeycomb sandwich; i.e.,with no frames or straps. A flat honeycomb panel fail safe test in Phase Ib showed good agreement with this analysis, see the analysis test correlation subsection. The model for the 15 inch foreign object damage, (in which the center frame, core, and both face sheets are cut) was: (1) an unstiffened center cracked face sheet, (2) a cracked fact sheet stiffened by frames and straps, and (3) no contribution by the core.

TABLE 17

HONEYCOMB CONCEPT DAMAGE TOLERANCE ANALYSIS SUMMARY

Critical Point	Slow Crack Growth	Fail Safe	
	One Bay Crack[1]	Two Bay Crack-Center Stiffener Intact	15" Foreign Object Damage - Center Stiffening Broken[2]
Point A Longitudinal Crack[3]	52% Margin On Life	Criteria met	Criteria met
Point B Longitudinal Crack[3]	Criteria met	Criteria met	Criteria met

Notes: 1. Crack in face sheet on side opposite to stiffening. Analyzed as unstiffened honeycomb panel with one cracked face sheet

2. Both face sheets, core and center stiffener cut.

3. Circumferential crack less critical than longitudinal crack.

The longitudinal crack at point A was critical for slow crack growth. The associated crack growth time history is shown in Figure 50. The spectra was constant amplitude from zero to full pressure which is conservative. The fail safe checks are shown in Figures 51 and 52. The criteria was met for both cases.

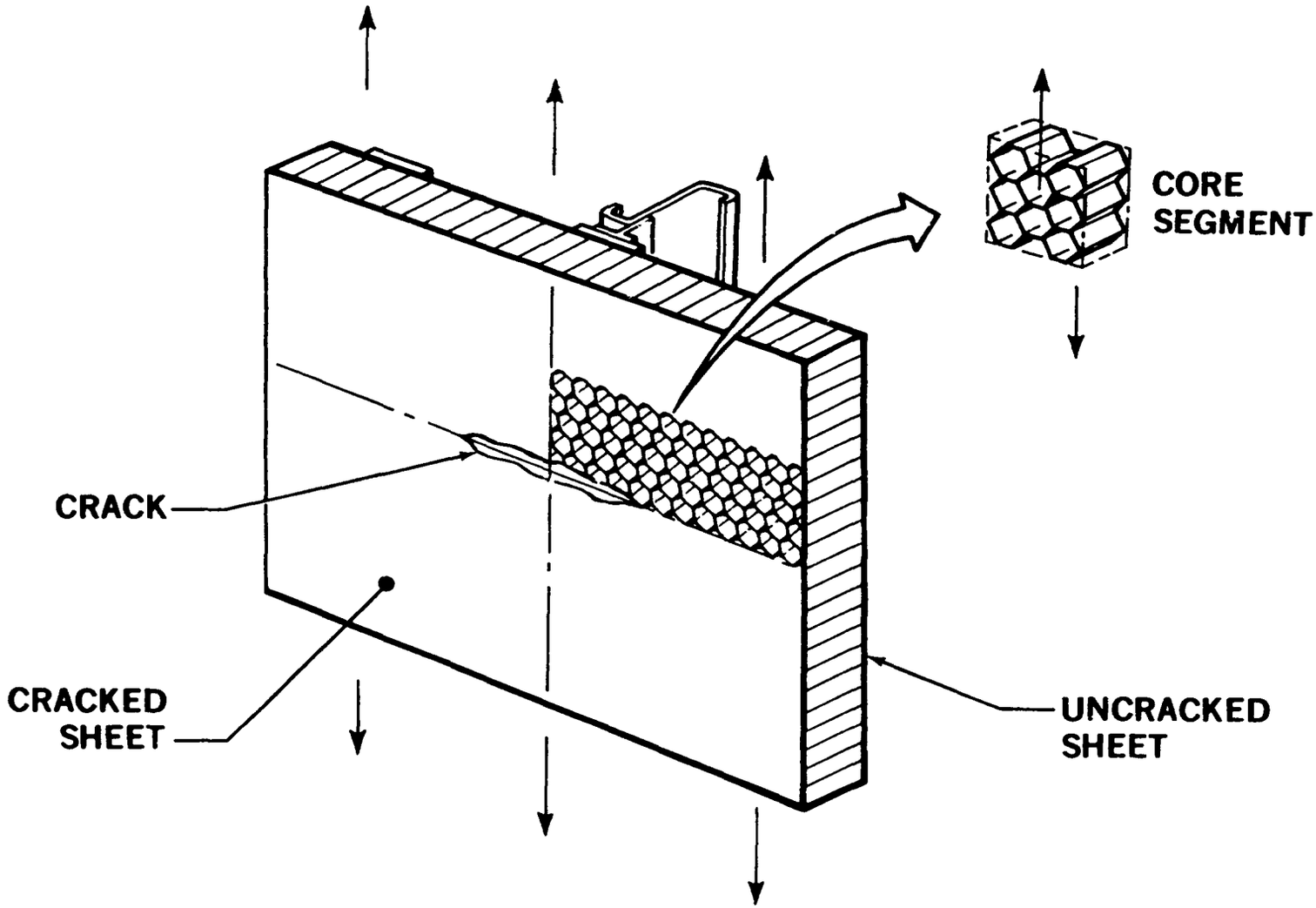


FIGURE 49. MODEL FOR HONEYCOMB STRUCTURE DAMAGE TOLERANCE ANALYSIS

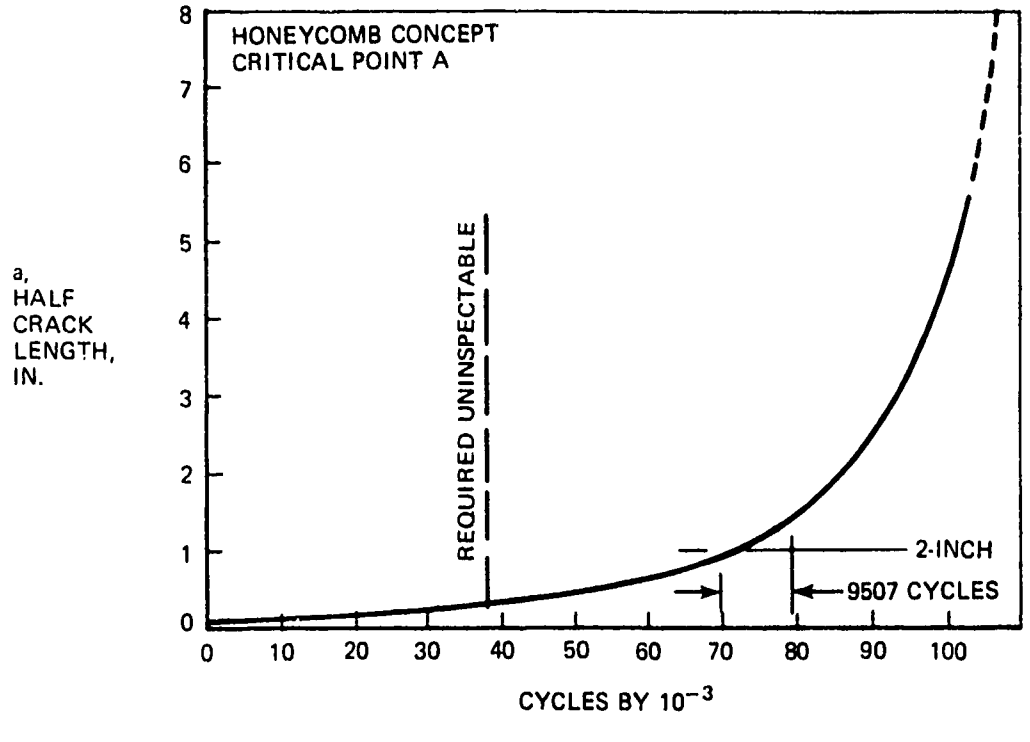


FIGURE 50. CRACK GROWTH TIME HISTORY FOR A LONGITUDINAL CRACK, HONEYCOMB CONCEPT

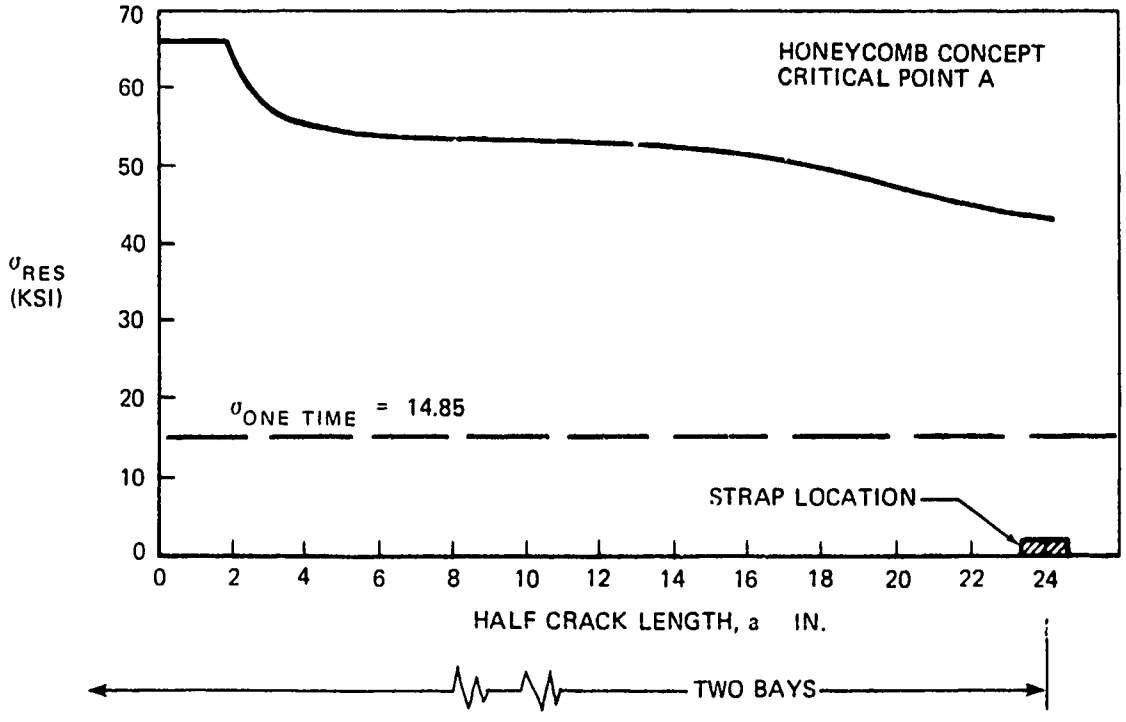


FIGURE 51. FAIL-SAFE CHECK FOR A TWO-BAY LONGITUDINAL CRACK WITH CENTER STIFFENER INTACT

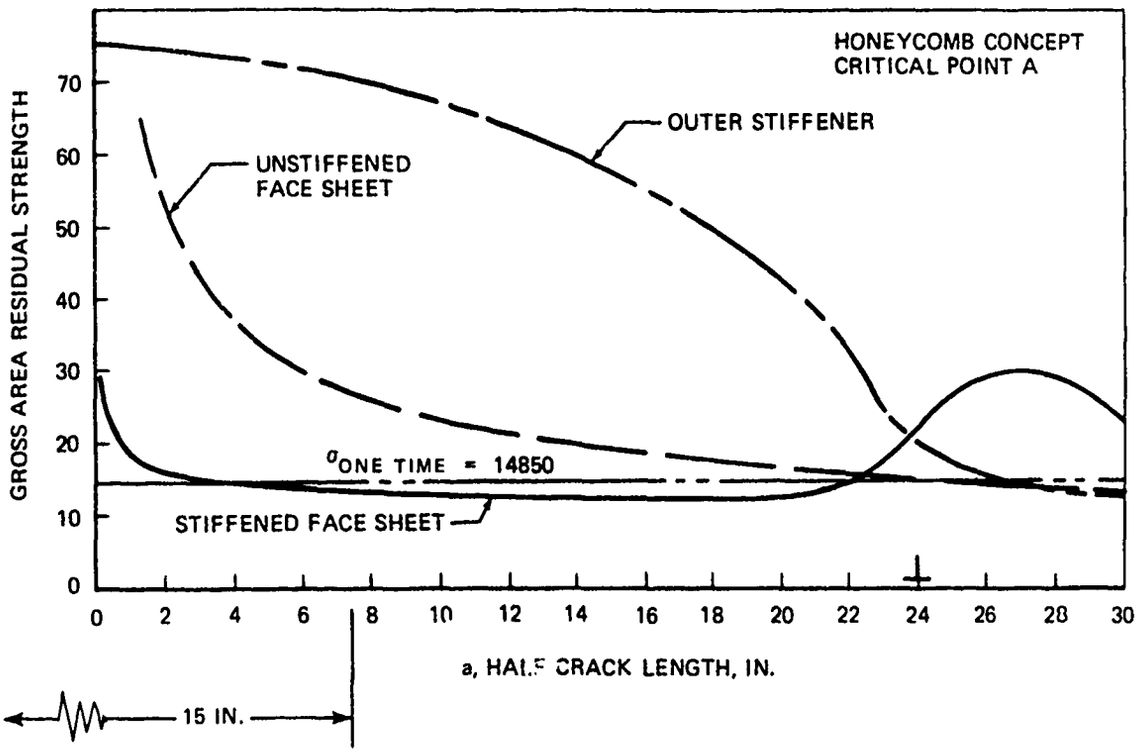


FIGURE 52. FAIL-SAFE CHECK FOR A 15-IN. FOREIGN OBJECT DAMAGE LONGITUDINAL CRACK, IN HONEYCOMB, AND BROKEN CENTER STIFFENER

Sensitivity Analysis (Metals). - A sensitivity analysis was made for each of four parameters to guide the design of various PABST concepts and to evaluate the impact of a change in basic material data. The four parameters were: stress level, bonded strap spacing, bonded strap area, and da/dn vs ΔK material data. The methods described in the Damage Tolerance Analysis Methods Section were used in the analyses.

It should be noted that the effect of bonding itself, compared to riveting, was determined early in Phase Ib. The associated modification factors accounting for the effect of stiffening on cracked sheet for elastic structure were compared. The result is shown in Figure 53. Since the factor is related directly to the stress intensity k, see Damage Tolerance Analysis Methods Section, the improvement in residual strength provided by bonding the stiffening is clearly evident.

MODIFICATION FACTOR (γ) ACCOUNTS FOR THE EFFECT OF STIFFENING ON A CRACKED SHEET

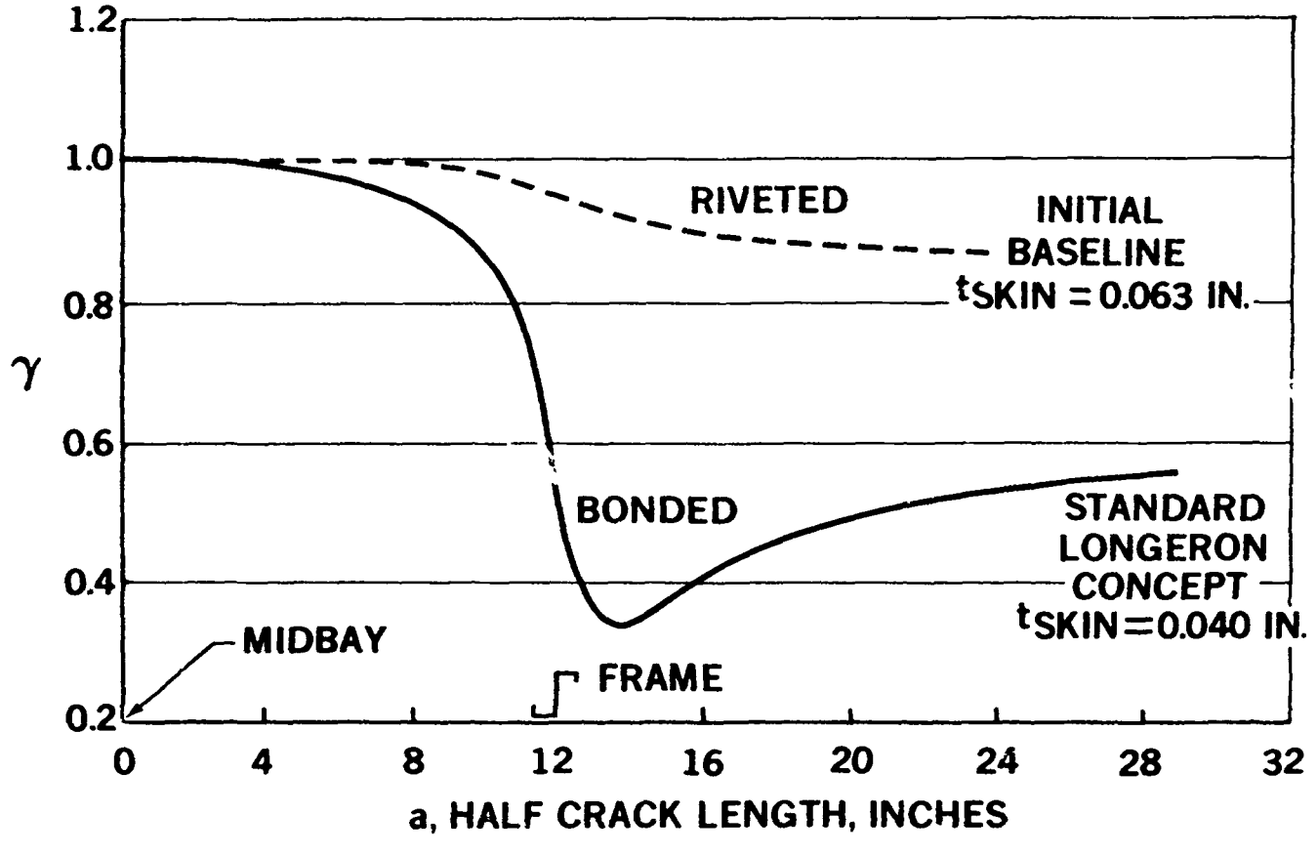


FIGURE 53. IMPROVEMENT PROVIDED BY BONDING

Effect of Varying Stress Level: - The sensitivity of stress intensity (K) to stress level was determined for both the skin-bonded stiffener design concepts and the honeycomb concept.

The internal and external longeron concepts were considered to be represented sufficiently for this analysis by the geometry of test specimen N21 and the crack DT4, as shown in Figure 54. Three stress levels were selected: (a) the longitudinal stress due to pressure only, 11,180 psi, (b) the longitudinal stress due to pressure added to the full skin bending stress, 24,347 psi, and (c) the average of the two. The first and second stress levels represent the lower and upper bound values. The results, see Figure 55, show that the structure is very sensitive to high stress levels. In this example, a 50% increase in stress from the lower bound decreased the life by 84%.

Honeycomb is similarly affected, Figure 56. The analysis performed was for test specimen 30A, which has the same geometry as the honeycomb concept. As stated previously, honeycomb crack growth analysis considers that the structure acts like an unstiffened honeycomb panel unaffected by the frames and straps.

Effect of Varying Bonded Strap Spacing: - The effect of varying strap spacing on residual strength was determined for the skin-bonded stiffener concepts. A circumferential crack parallel to and close to the frame at critical point A for the external longeron concept, Figure 44 was analyzed with one, two, and three crack arrest straps between the wide spaced longerons. The result of decreasing strap spacing is to increase residual strength as shown in Figure 57. It should be noted that in the analysis for all three cases, the strap area was not sufficient to keep the strap from breaking before the two bay-center stiffener intact fail safe criteria was met. However, it is clear that a further increase to four straps would result in the criteria being satisfied with no increase in area.

Effect of Varying Bonded Strap Area: - The effect of varying strap area only on residual strength was also determined for the critical point A case discussed above with the strap spacing fixed (one strap). The results are shown in Figure 58. An increase in area to 0.213 square inches provided sufficient residual strength to meet the fail safe criteria. Additional

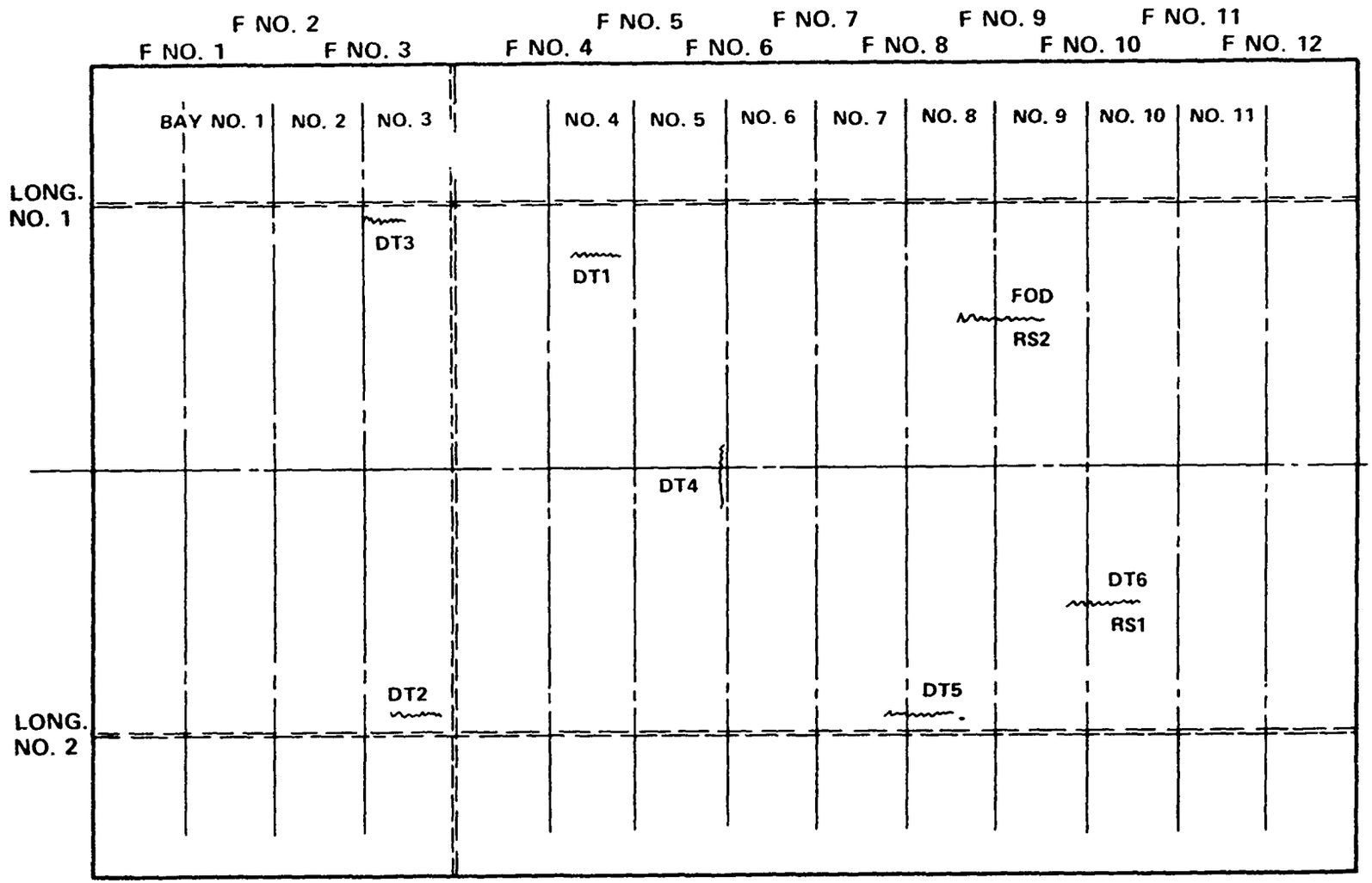


FIGURE 54. DAMAGE TOLERANCE CRACK LOCATIONS FOR THE CURVED INTERNAL LONGERON TEST SPECIMEN

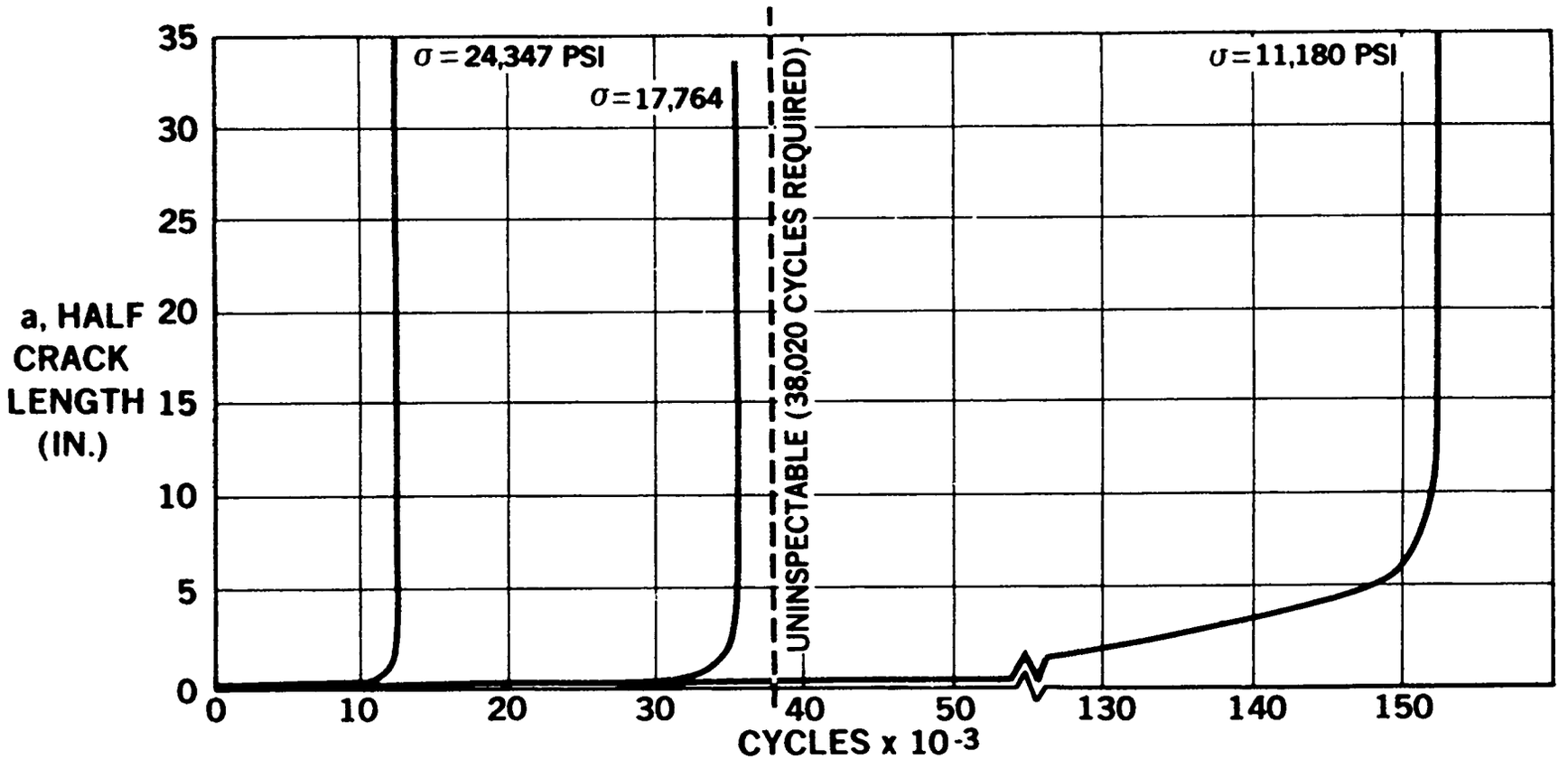


FIGURE 55. EFFECT OF VARYING STRESS LEVEL ON CRACK GROWTH FOR SKIN-BONDED-STIFFENER STRUCTURE

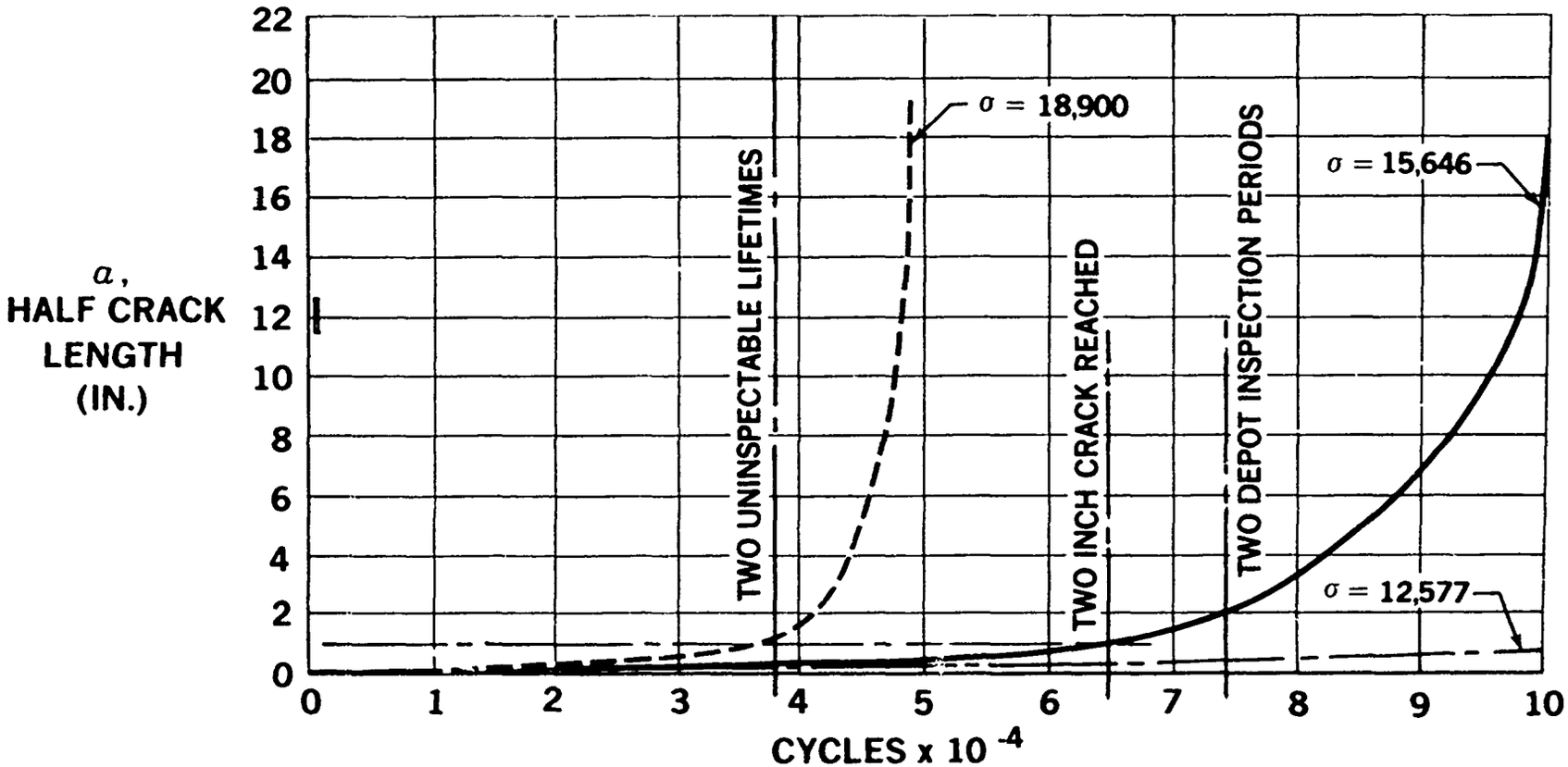
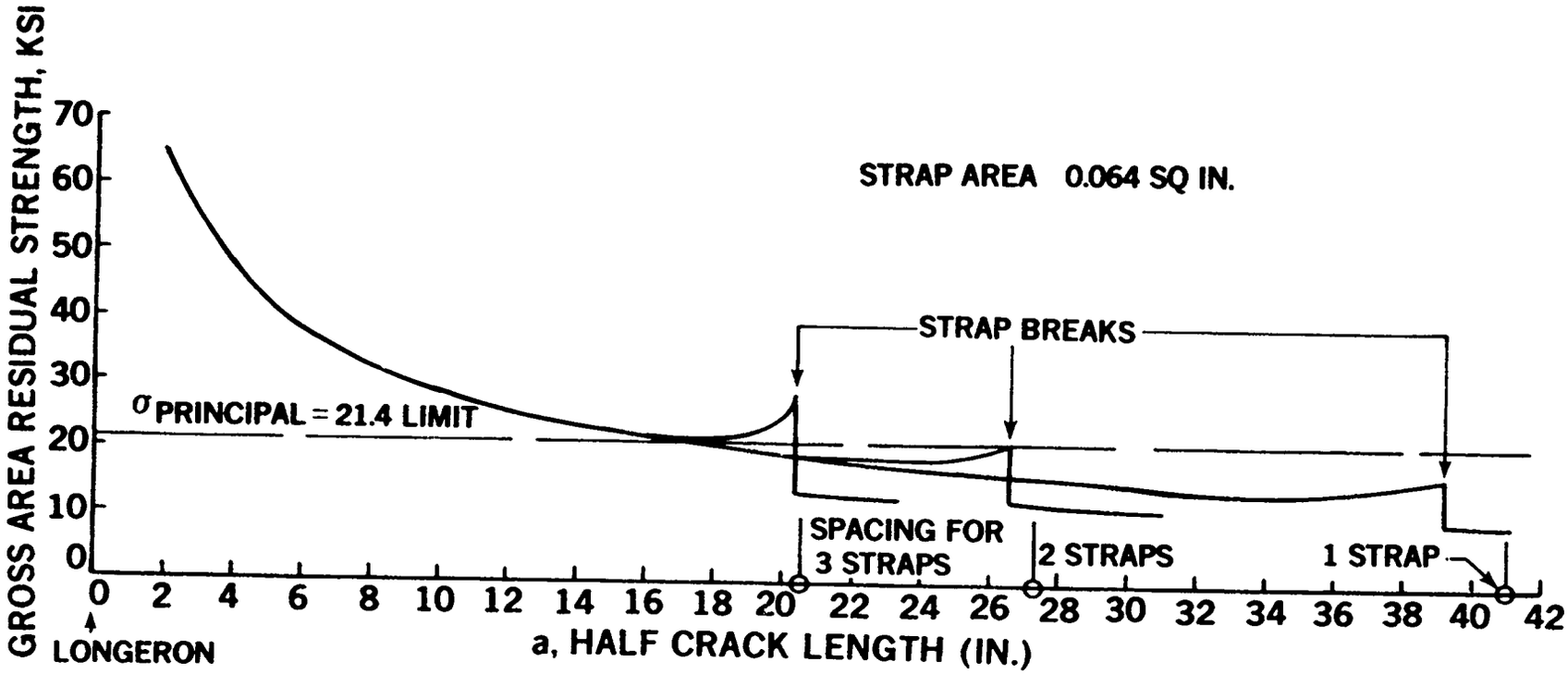


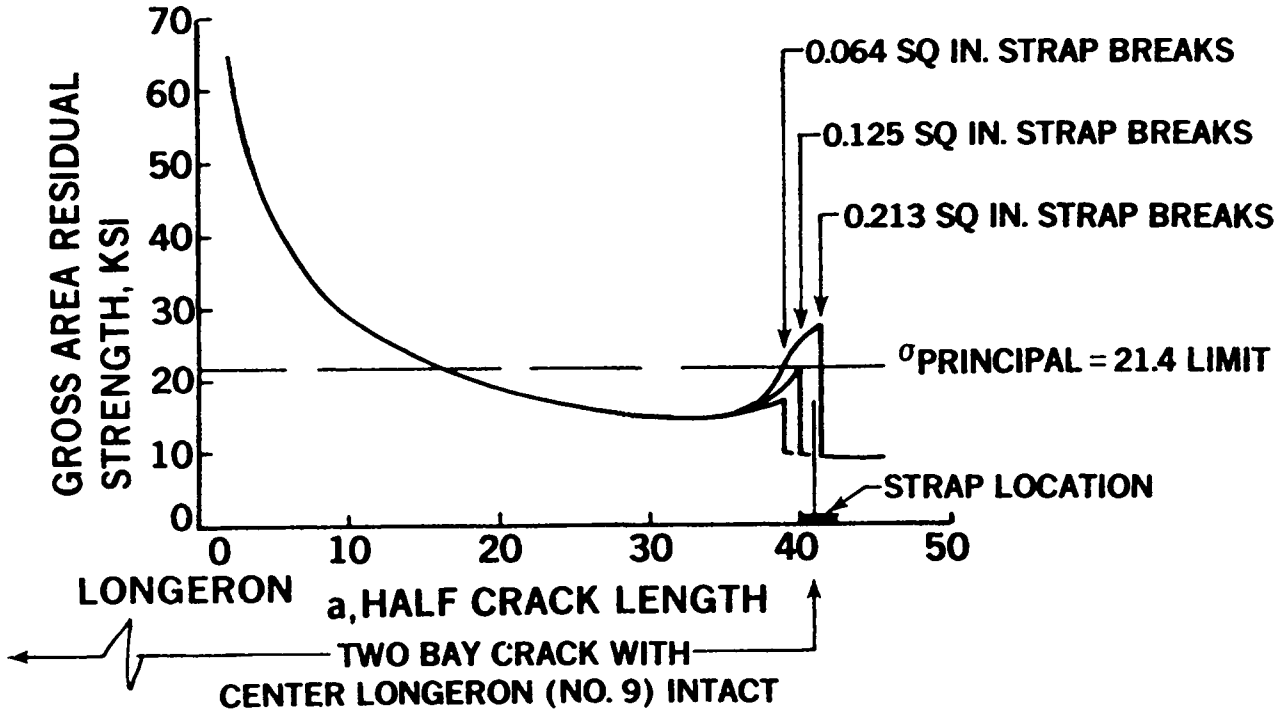
FIGURE 56. EFFECT OF VARYING STRESS LEVEL ON CRACK GROWTH FOR HONEYCOMB STRUCTURE



NOTE: STIFFENER CRITERIA NOT SHOWN

EXTERNAL LONGERON CONCEPT — WIDE SPACED LONGERON REGION
TWO BAY CIRCUMFERENTIAL CRACK

FIGURE 57. EFFECT OF VARYING STIFFENER SPACING ON RESIDUAL STRENGTH



NOTE: STIFFENER CRITERIA NOT SHOWN

EXTERNAL LONGERON CONCEPT — WIDE SPACED LONGERON REGION
TWO BAY CIRCUMFERENTIAL CRACK

FIGURE 58. EFFECT OF VARYING STIFFENER AREA ON RESIDUAL STRENGTH

analysis would be required to determine the best geometry for cost and weight by varying both spacing and area.

Effect of Varying da/dn vs ΔK: - The sensitivity of crack growth time history analysis to da/dn vs ΔK material data noted in the Material Data Section was studied. An analysis was made of a flat unstiffened center-cracked 7075-T6 sheet which was 48" wide and 0.05" thick. The initial 0.50" crack was grown analytically by spectrum load. The PABST curves and a set of curves displaced at the lower end from PABST data were used. Figure 59 shows the placement of the curves for R = 0 only. The resulting crack growth time histories are shown in Figure 60. It should be noted that the ΔK value associated with maximum growth from the initial crack size was 6686 at R = 0.3. (The life depends primarily on the growth period associated with the starting crack). For this geometry and material, the decrease of initial da/dn from 1.5×10^{-5} to 6.0×10^{-6} for the initial ΔK value decreased the life by a factor of 3, Figure 59. This sensitivity study is especially significant since there is little data below $\Delta K = 5 \times 10^{-7}$ for aluminum alloys. This is an important region for PABST since the small MIL-A-83444 crack sizes and low fuselage stresses place much of the structure in this region.

Analysis-Test Correlation (Metals). - A comparison was made between test panel analysis and the test data from the design verification tests of the internal longeron and honeycomb concepts to check the analysis methods. The panels were analyzed using the methods described in the Damage Tolerance Analysis Methods section, including the appropriate modification factors.

Internal Longeron Concept: - Two large stiffened panels with the internal longeron configuration were tested.

The first, a flat panel loaded by uniaxial tension, is described in Structural Test Section specimen N30A. The test panel failed prematurely from fatigue in the longeron cutout region. Only about two inches of growth from the 0.25 inch initial damage tolerance cracks cut into the panel was obtained. The experimental crack growth time history for the one bay damage tolerance crack is shown in Figure 61 along with the analytical data. The agreement is fairly good. The unconservatism can be corrected by adjusting the da/dn vs ΔK material data a small amount in the low ΔK region as was discussed previously.

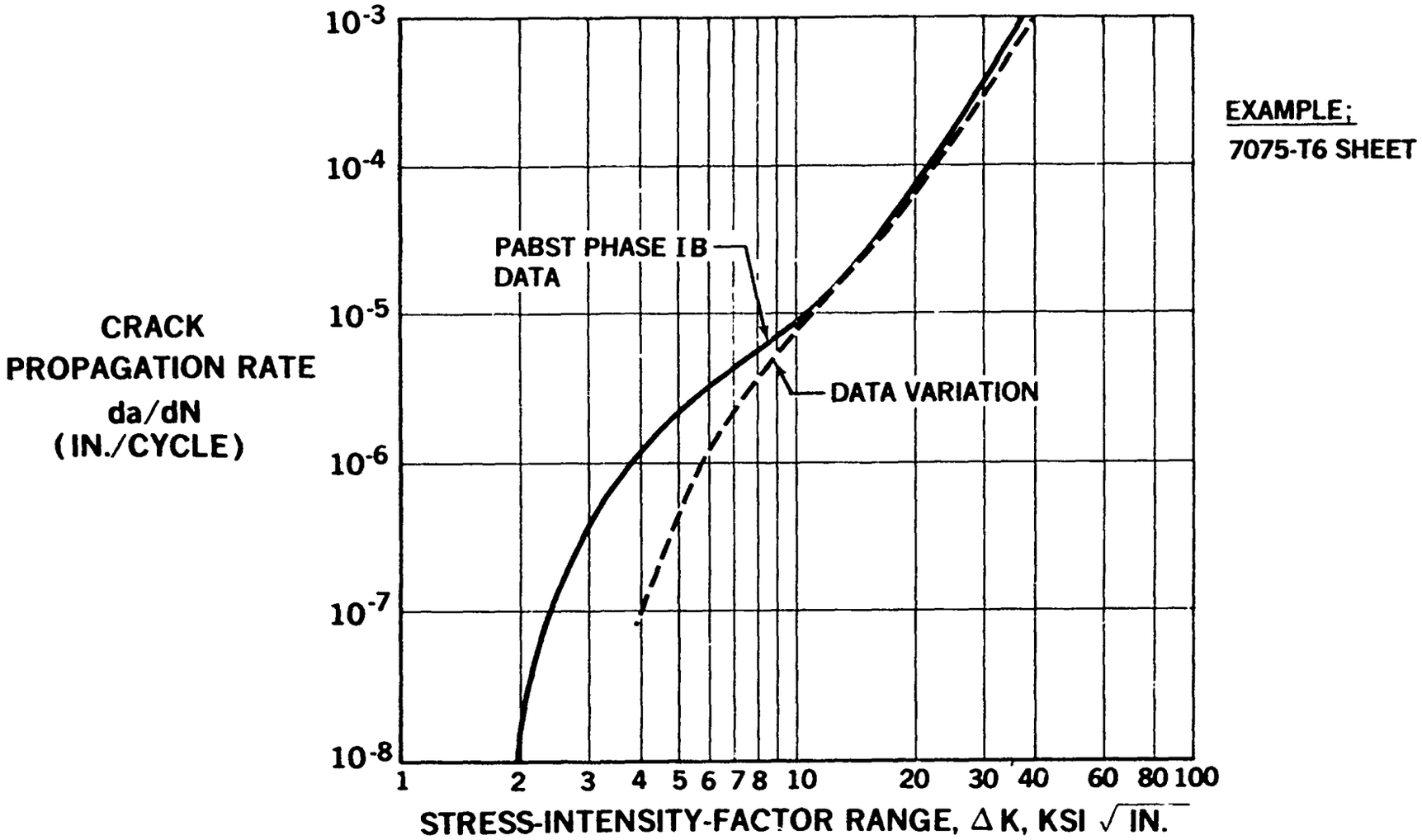


FIGURE 59. CRACK PROPAGATION DATA VARIATION FOR SENSITIVITY STUDY

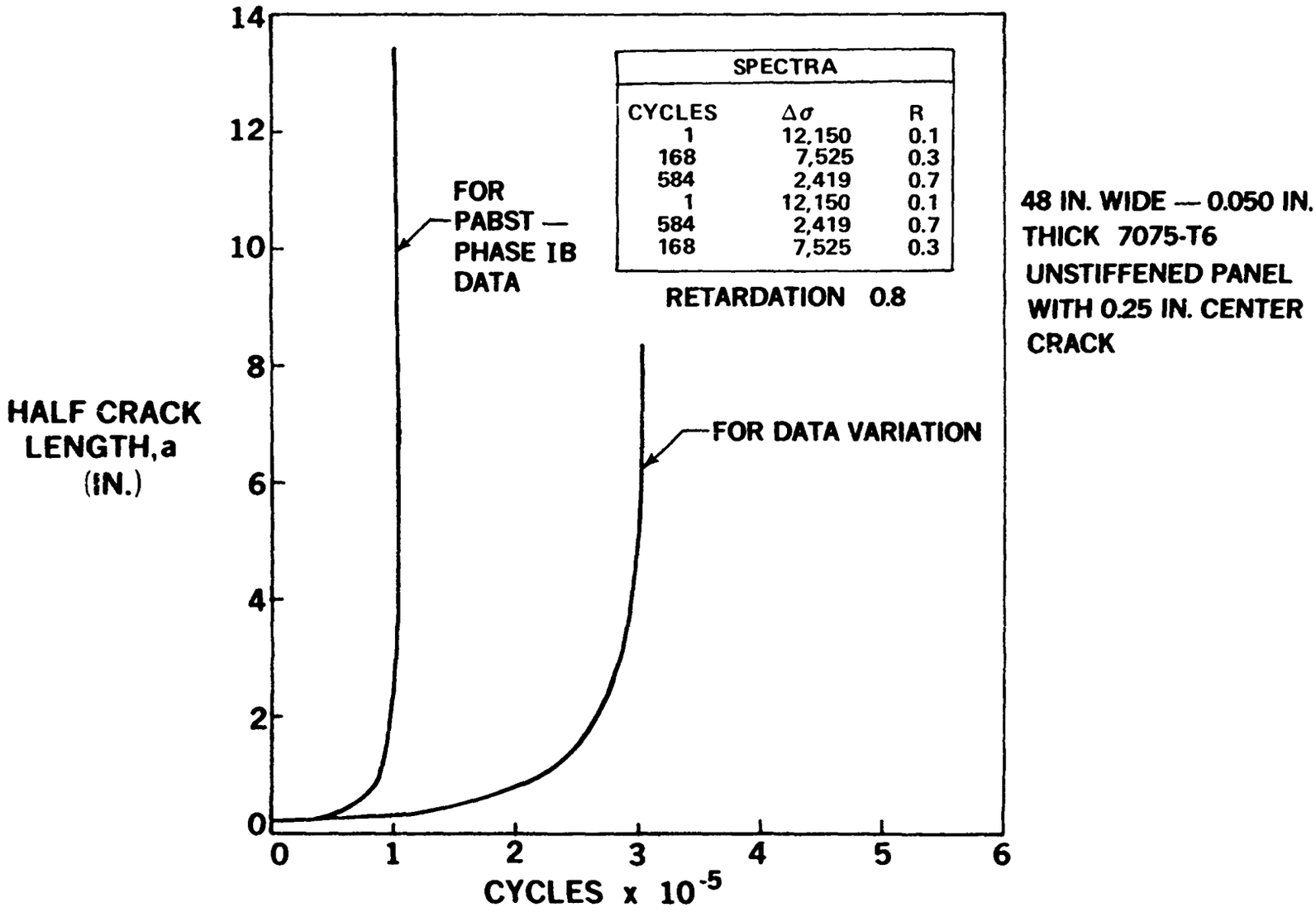


FIGURE 60. EFFECT OF MATERIAL DATA VARIATION ON CRACK GROWTH TIME HISTORY

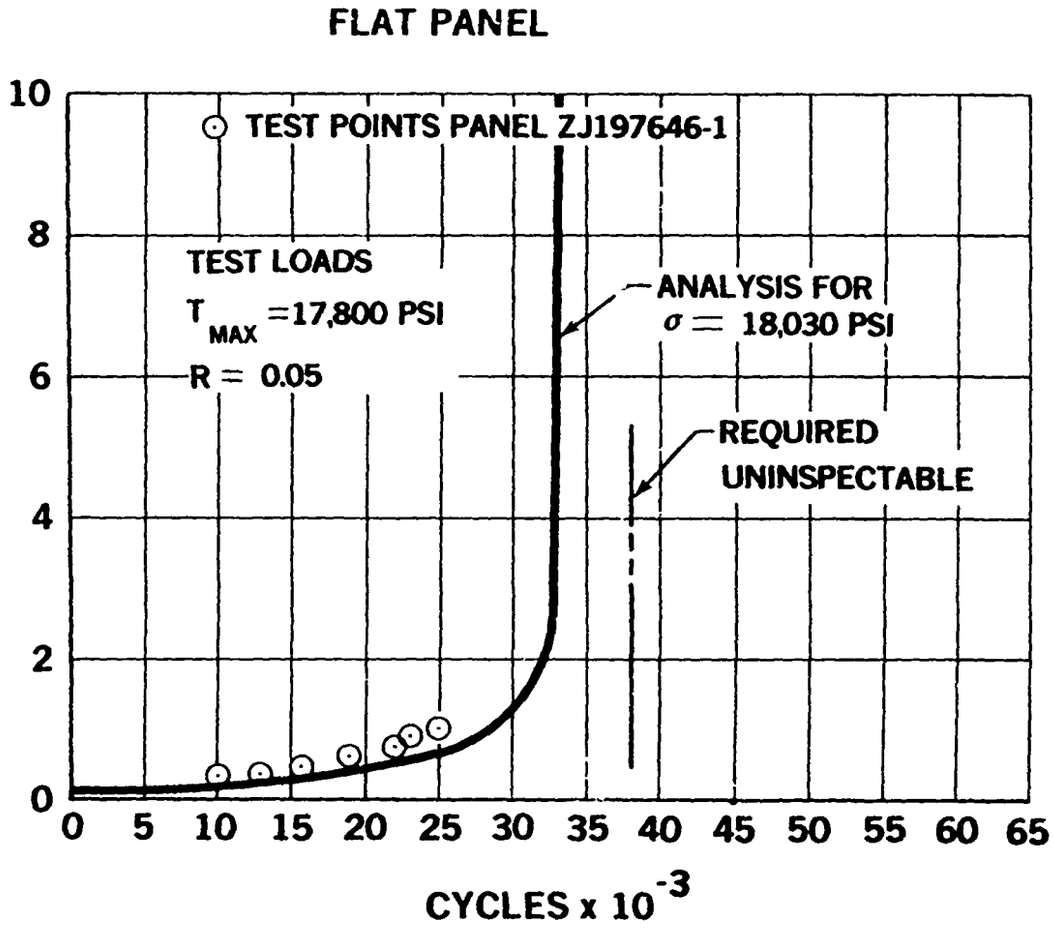


FIGURE 61. CRACK PROPAGATION ANALYSIS-TEST COMPARISON FOR AN INTERNAL LONGERON STIFFENED PANEL

The second panel was a curved specimen tested under pressure to verify the effects of biaxial stress on the design. The location of the damage tolerance cracks and the residual strength cuts in the 110" X 168" panel are shown in Figure 54. The test is described in Structural Test Section specimen N21. The comparison between analysis and test for the longitudinal one bay cracks DT1 and DT2 is shown in Figure 62. The analysis of both cracks was identical, i.e. no skin bending at the longeron assumed. Reasonable agreement for crack DT1 was obtained except in the knee of the curve. An adjustment in the da/dn vs ΔK curve will be studied in Phase II for this case also since the effect of the stiffener is still four to five inches away. Agreement for the DT2 crack was poor. The knee of the experimental curve had not been reached by the time the crack was patched to allow other testing. It had been thought that DT2 would grow more rapidly than DT1 due to the bending of the skin from the pressure "pillowing" of the skin at the longeron, Figure 39, and from the more severe bulge condition wherein the longeron holds one side of the skin while the other side bends outward thus increasing the crack tip stress intensity more than for DT1, where the bulging is symmetrical. The test results, however, indicate a decrease in stress intensity from that of DT1. Current thinking is that the longitudinal stress in the skin is higher at the longeron than in the center of the bay. The problem will be studied further in Phase II.

It should be noted that it does not appear to be necessary to make corrections to the method of analyzing the hoop stress distribution in a pressurized stiffened shell. The hoop stress at the center of a bay was recorded by the strain gages as 14,287 psi versus 14,113 psi by analysis. The hoop stress in the skin at the frame was recorded by the strain gages as 9558 psi versus 9898 psi. This is good agreement considering manufacturing tolerances, etc.

The comparison between test and analysis for crack DT4 is shown in Figure 63. The shift in da/dn vs ΔK curve mentioned above will be used to adjust some of the unconservatism in the analysis at the beginning of crack growth. The crack was patched at 31,290 cycles so that fail safe tests could be run. The patch was not sufficient to prevent the crack from opening during the fail safe loading. The change in the curve in Figure 63 from the patching to about 45,000 cycles appears to be from retardation. The fail safe

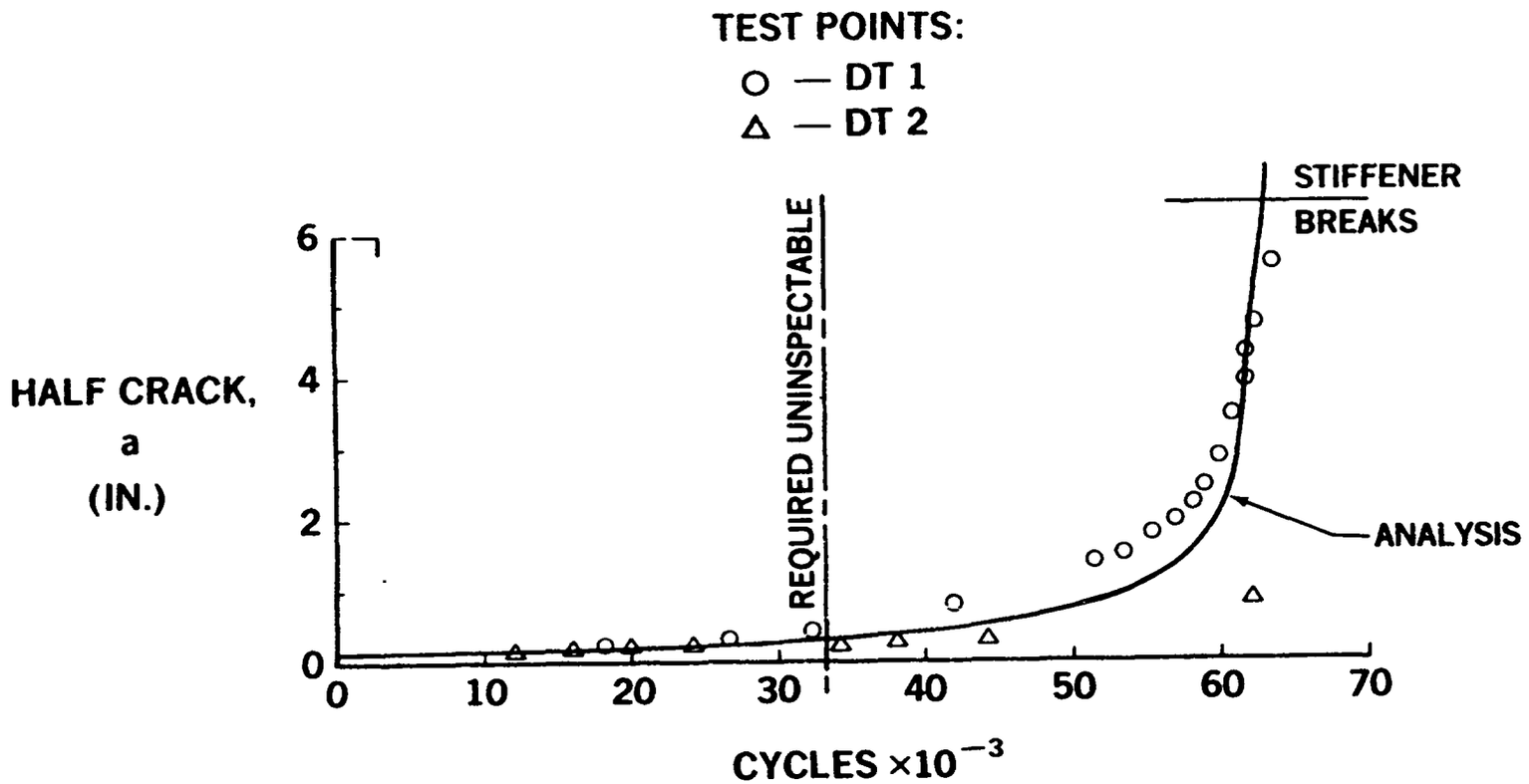


FIGURE 62. CRACK PROPAGATION ANALYSIS-TEST COMPARISON FOR LONGITUDINAL CRACKS IN AN INTERNAL LONGERON SPECIMEN

TEST SPECIMEN N21
CRACK: DT4

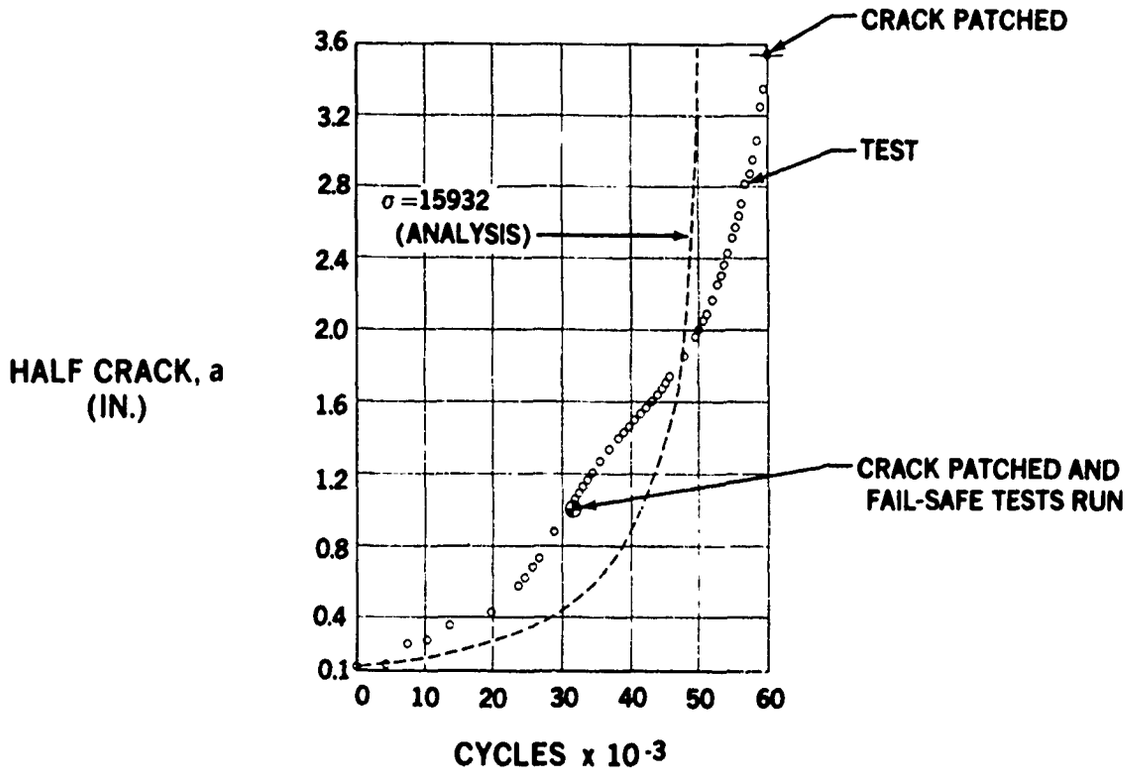


FIGURE 63. CRACK PROJECTION ANALYSIS – TEST COMPARISON FOR A CIRCUMFERENTIAL CRACK IN AN INTERNAL LONGERON SPECIMEN

load with retardation will be added to the analysis in Phase II to check correlation.

The residual strength test results for the two bay crack with center stiffener intact are shown in Figure 64. The skin progressively saw cut to nine, ten, and eleven inches did not fail at the limit stress of 14,100 psi, as predicted by analysis. However, the actual residual strength was not checked by test since the specimen was to be used for further testing.

The results of the foreign object damage, i.e. a fifteen inch skin crack with the center stiffener broken, are shown in Figure 65. In the test, this crack fast fractured to the frame at a stress of 13,600 psi, and arrested. This is 9% below the stress for fast cracking predicted by analysis. The panel with the two bay crack was subsequently tested to the required one-time stress of 14,100 psi. There was no crack growth and the outer stiffener remained intact. The analysis predicted that the outer stiffener would fail at the one-time stress for a 23.4 inch crack. The analysis appears to load the stiffener too much and the skin too little.

Honeycomb Concept: - Two large flat stiffened honeycomb panels were tested in uniaxial tension. The tests are described in Structural Tests.

The first panel was used to demonstrate both crack growth and fail safe capability. The test results are shown in Figures 66 and 67 respectively along with the analytical results. As stated previously, unstiffened honeycomb analysis methods were used. The experimental crack propagation data showed good agreement with analysis for approximately 60,000 cycles. The analysis and test curves then deviated with the analysis becoming conservative until the curves crossed at approximately 92,500 cycles. For the residual strength test, the case of a two bay crack with center frame intact was checked by sawing a 38 inch crack (rather than 48" full two bay crack) and the panel pulled to failure with a rising load. The panel failed at 298,000 pounds. The analysis predicted that failure would occur at 296,000 pounds. This agreement is excellent. Since the analysis for ΔK versus half crack length (a) for both tests is identical, the disagreement between analysis and test for the crack growth test is apparently due to the da/dn versus ΔK material data used for the 2024-T3 face sheets.

- INTERNAL LONGERON — N21 — CURVED PANEL
- TWO-BAY — CENTER FRAME INTACT — CRACK RS1
- TEST STRESS OF 14.1 KSI — NO FAILURE

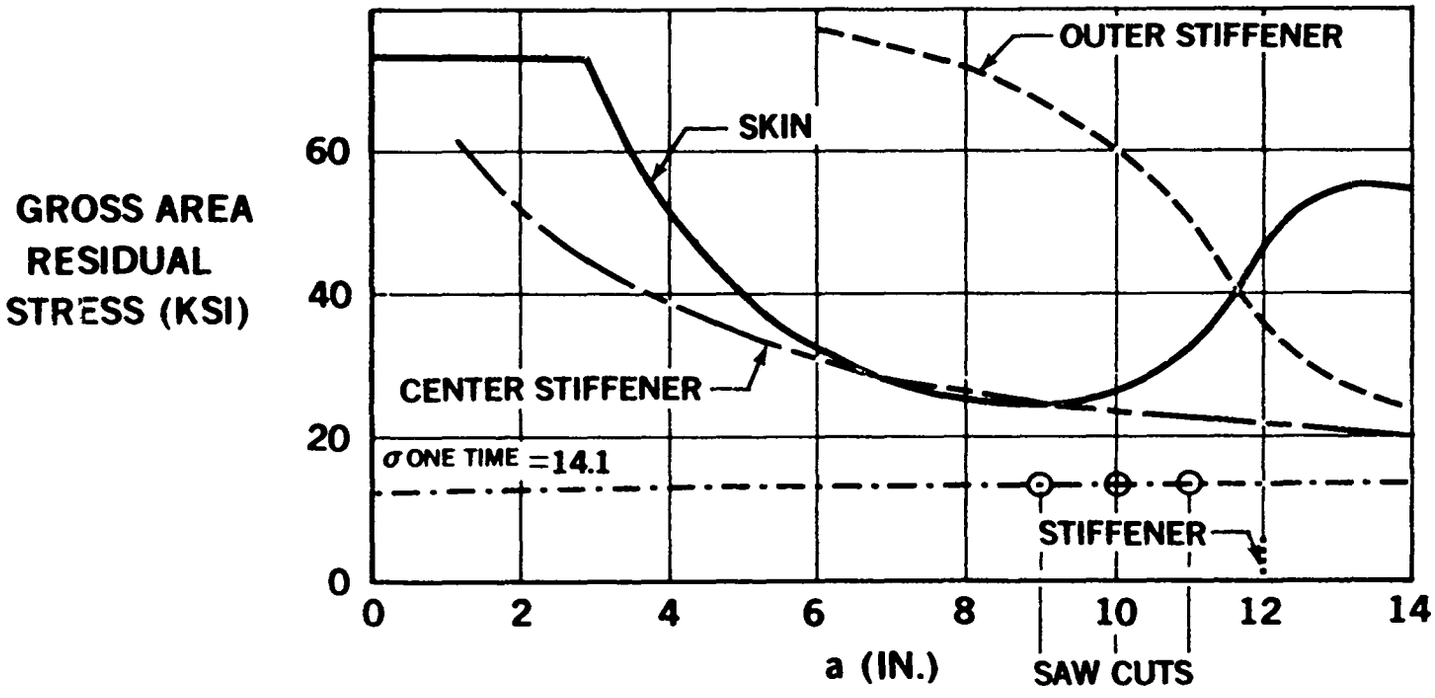


FIGURE 64. ANALYSIS-TEST COMPARISON FOR THE RESIDUAL STRENGTH OF AN INTERNAL LONGERON PANEL

- INTERNAL LONGERON — N21 — CURVED PANEL
- FOREIGN OBJECT DAMAGE — CRACK RS2
- TEST STRESS OF 14.1 KSI — NO FAILURE

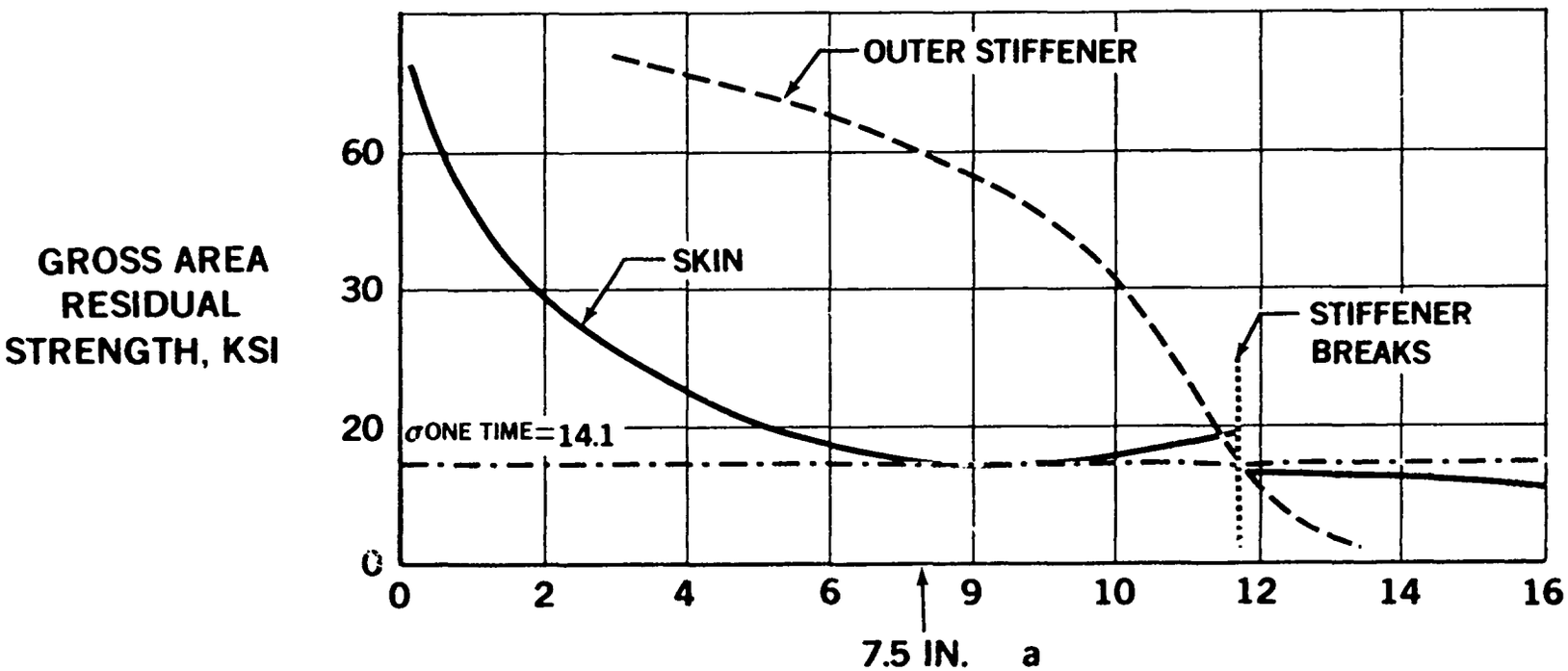


FIGURE 65. ANALYSIS-TEST COMPARISON FOR THE FOREIGN OBJECT DAMAGE OF AN INTERNAL LONGERON PANEL

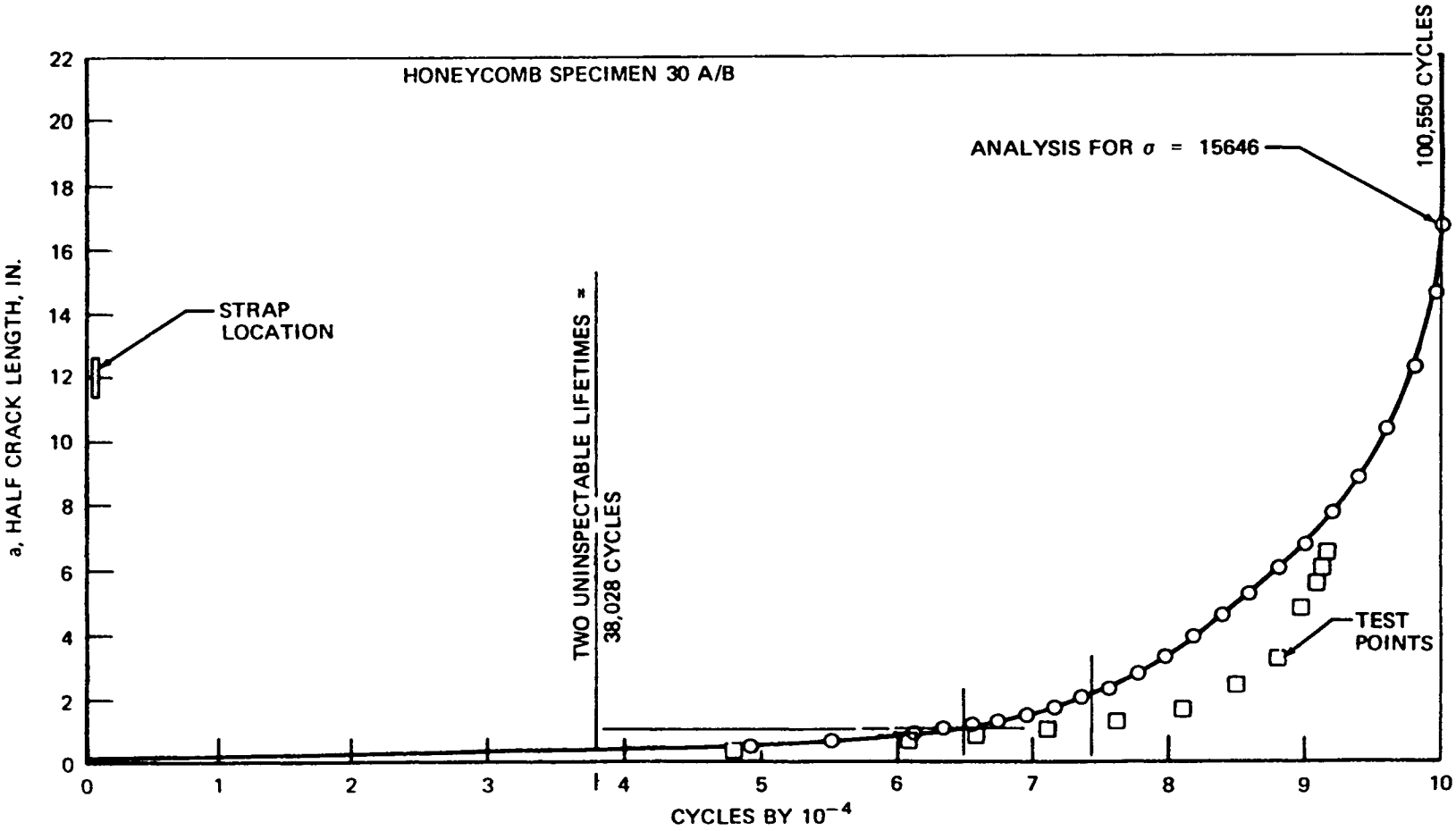
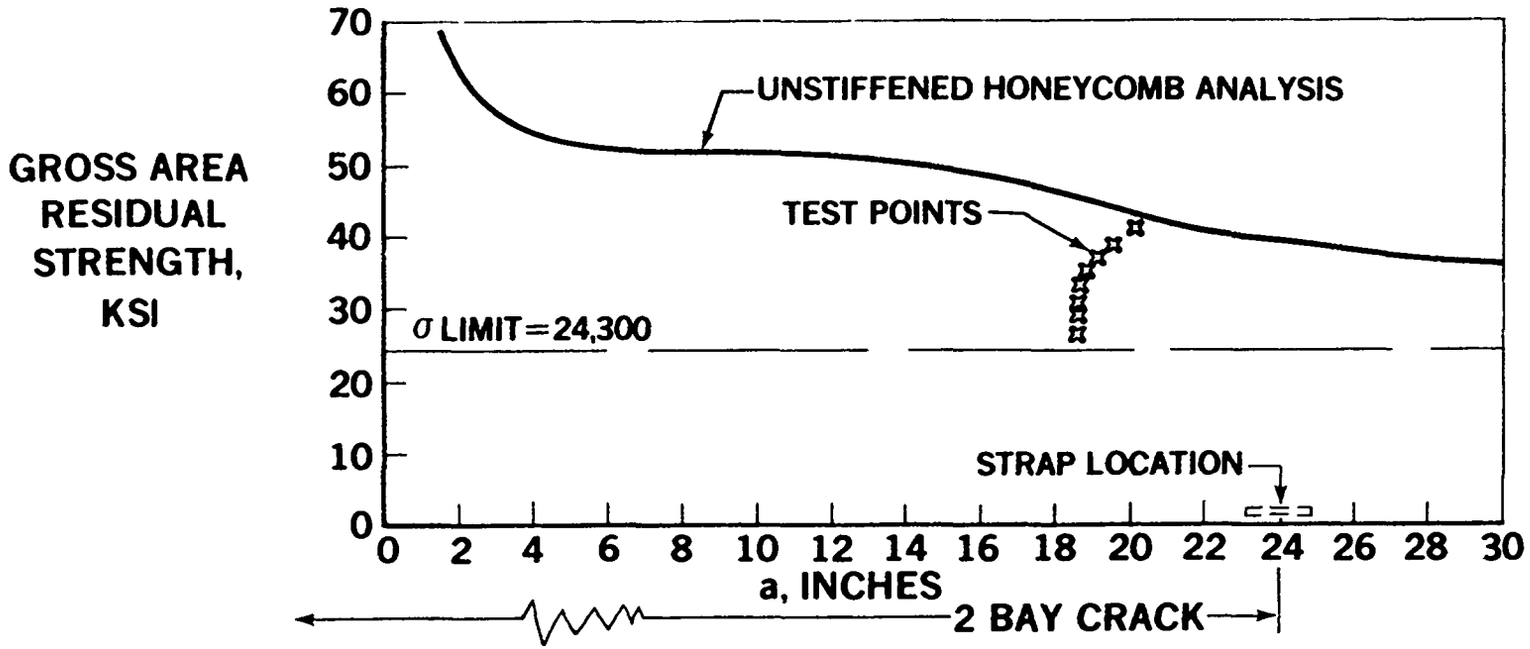


FIGURE 66. CRACK PROPAGATION ANALYSIS – TEST COMPARISON FOR A STIFFENED HONEYCOMB PANEL



TEST SPECIMEN 30B — HONEYCOMB

TWO BAY CRACK WITH CENTER FRAME INTACT

FIGURE 67. ANALYSIS-TEST COMPARISON FOR THE RESIDUAL STRENGTH OF A STIFFENED HONEYCOMB PANEL

The second panel was tested for foreign object damage by pulling the damaged panel to failure under rising load. The test and analysis results are shown in Figure 68. The analysis considered that the panel acted like a cracked unstiffened face sheet and a stiffened cracked face sheet with no influence from the core as stated previously. Failure occurred at the 25,000 psi stress predicted by analysis. However, the predicted fast fracture of the stiffened skin prior to panel failure could not be verified. Failure of the parts of the panel appeared to be a single occurrence.

- HONEYCOMB SPECIMEN 30C
- FOREIGN OBJECT DAMAGE — RESIDUAL STRENGTH
- FAILURE STRESS = 25 KSI

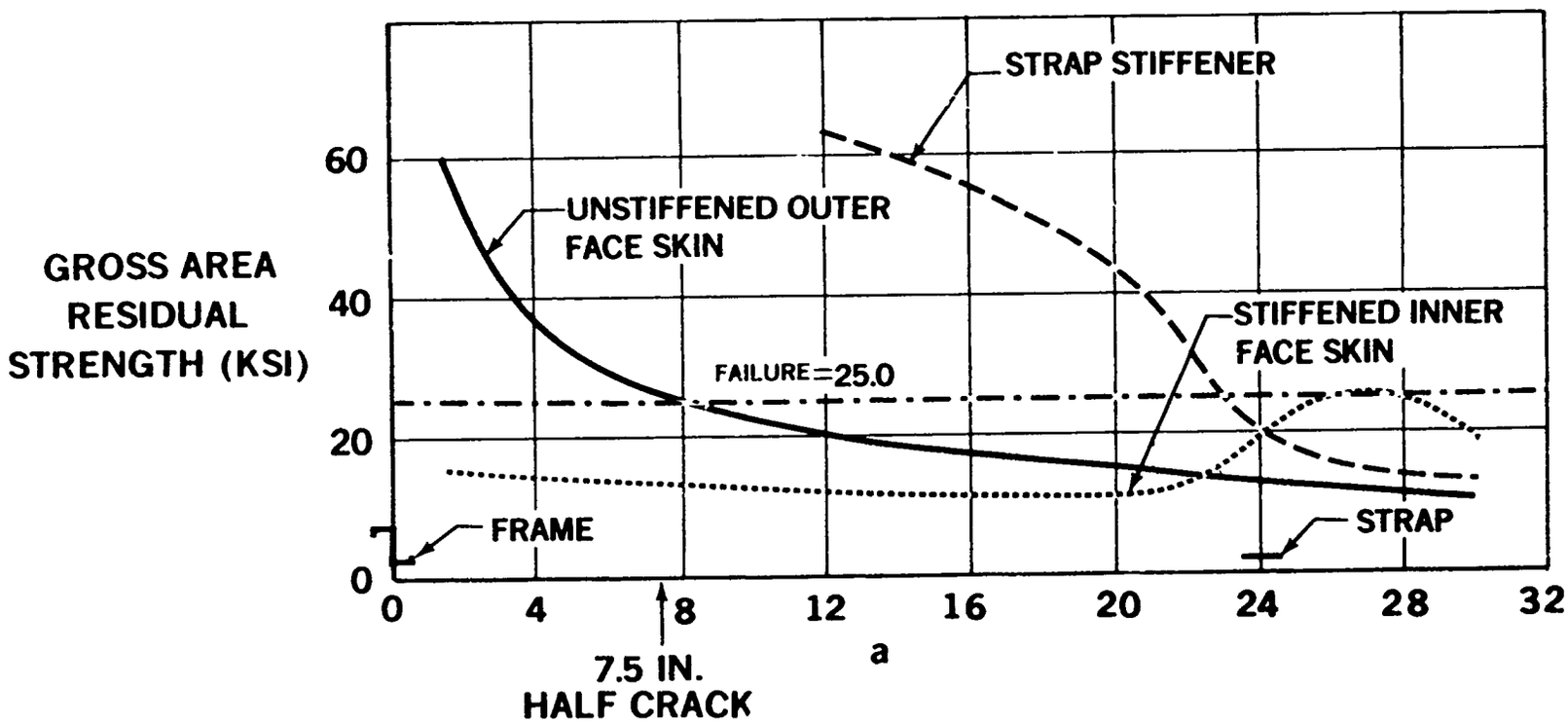


FIGURE 68. ANALYSIS-TEST COMPARISON FOR THE FOREIGN OBJECT DAMAGE OF A HONEYCOMB PANEL

Fatigue Analysis

The fatigue criteria, service life and design fatigue life are presented in Damage Tolerance - Requirements. The PABST utilization is given in Table 11.

Fatigue Analysis Methods. - Conventional fatigue analysis based on Miner's Cumulative Damage Rule and a scatter factor of 4.0 was used with appropriate S-N material data.

Concept Analysis. - The three concepts described in the Design Concepts Section were analyzed for the fatigue requirements. The critical points checked on the fuselage were the same as the points used for damage tolerance, Figures 44 and 48.

Internal and External Longeron Concepts: - Fatigue analysis based on DC-10 riveted structure S-N data showed no fatigue damage, i.e. "Infinite" life.

The pressure panel cyclic test N21, described in the Structural Test Section, showed no fatigue cracking in participating structure in over four lifetimes.

Honeycomb Concept: - Based on test data for a honeycomb splice, the fatigue response of the honeycomb structure was the same as for an unnotched sheet. The splice test was for σ_{max} = 20,000 at R = 0.05 and over 10^6 cycles. The analysis of the honeycomb concept based on this material data showed no fatigue damage, i.e. "infinite" life.

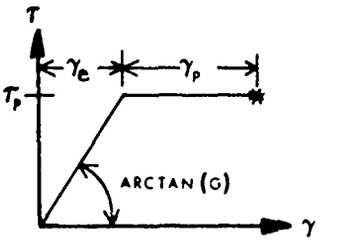
The pressure panel cyclic test H25, in progress, has shown no fatigue cracking in participating structure in over three lifetimes.

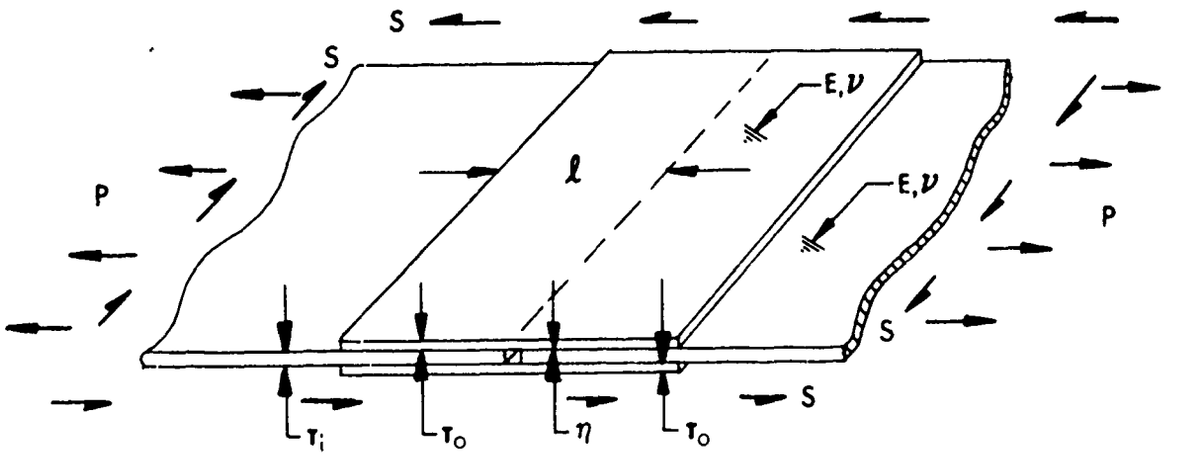
Ultimate Mode - Bonded Joints

Analyses of intact adhesive bonded joints have been performed for three situations: (1) the double-strap joints used in longitudinal splices, (2) the flush single-strap joints used on circumferential splices, and (3) the peeling apart of the skin and stiffening elements under internal cabin pressure. Tests have been performed for each of these categories. The test results have confirmed the predictions and established the adequacy of the bonded joints for the ultimate mode for the thin and only moderately thick components required for PABST. The conclusions for the bonded joints in intact structure may be summarized as follows. The metal elements are more critical than the adhesive for loads less than sufficient to yield the metal. Once yielding occurs, the adhesive fails progressively, as long as the associated loads are maintained, until complete failure occurs.

Double-Lap and Double-Strap (Longitudinal) Splices. - The analysis method for the double-strap joints are summarized as follows.

Temperature	$\tau_{p\,(psi)}$	G psi	γ_e	γ_p
R.T. (70°F)	5,000	50,000	0.1	1.0
-50°F	7,000	60,000	0.12	0.5
+160°F	2,500	40,000	0.063	1.5





Typical Characteristics for 250°F Curing Ductile Adhesives

PRECEDING PAGE BLANK-NOT FILMED

FM-73 was found to be slightly stiffer and less ductile at room temperature, but the effect is not large - these preliminary values were used to size the bond overlaps reported below. Those for FM-73 can be reduced by 0.06 inch in the range 0.040 to 0.080 in. central adherend thicknesses.

For tensile or compressive lap shear, the bond load capacity per unit width is given as:

$$P = \text{Lesser of } \sqrt{2\tau_p\eta\left(\frac{\gamma_\varepsilon}{2}+\gamma_p\right)2E_it_i\left(1+\frac{E_it_i}{2E_ot_o}\right)} \quad \text{AND} \quad \sqrt{2\tau_p\eta\left(\frac{\gamma_\varepsilon}{2}+\gamma_p\right)4E_ot_o\left(1+\frac{2E_ot_o}{E_it_i}\right)}$$

The bond strength for in-plane shear loading, likewise, is

$$S = \text{Lesser of } \sqrt{2\tau_p\eta\left(\frac{\gamma_\varepsilon}{2}+\gamma_p\right)\frac{E_it_i}{(1+\nu)}\left(1+\frac{E_it_i}{2E_ot_o}\right)} \quad \text{AND} \quad \sqrt{2\tau_r\eta\left(\frac{\gamma_\varepsilon}{2}+\gamma_r\right)\frac{2E_ot_o}{(1+\nu)}\left(1+\frac{2E_ot_o}{E_it_i}\right)}$$

Note that both P and S are <u>independent</u> of the overlap ℓ, except for very small values of ℓ for which P or S is given by $2\tau_p\ell$. For good design practice, P and S should exceed nominal requirements by 50% to provide for unknowns such as local flaws and variable thickness bondlines. The required minimum lengths to develop the strengths are:

$$\ell = \frac{P\,(\text{or } S)}{2\tau_p} + \frac{2}{\lambda\,(\text{or } \lambda_s)} \quad \text{where} \quad \lambda = \sqrt{\frac{G}{\eta}\left(\frac{1}{E_ot_o}+\frac{2}{E_it_i}\right)}$$

Greater overlaps, of

$$\ell = \frac{P\,(\text{or } S)}{2\tau_p} + \frac{6}{\lambda\,(\text{or } \lambda_s)} \qquad \lambda_s = \sqrt{\frac{2(1+\nu)G}{\eta}\left(\frac{1}{E_ot_o}+\frac{2}{E_it_i}\right)}$$

are recommended for design purposes to provide a reserve of strength for fatigue resistance and damage tolerance and to ensure that the adhesive stresses in the middle of the overlap are sufficiently low so that the adhesive there can never creep (See Figure 69). This area of very low stressed adhesive is intended to provide a resistance to environmental degradation. It acts as an anchor, or memory, permitting the differential stresses in the adherends to push the adhesive back to its initial state each time the joint is unloaded. Short overlap joints, in which all of the adhesive is strained significantly do not have this characterisitc. This is probably the reason for the poorer environmental resistance of test coupons such as the RAAB specimen than have been demonstrated by good adhesive bonds in service.

- USED ON LONGITUDINAL SKIN SPLICES
- HIGH STATIC MARGINS FOR INTACT SPLICES
- OVERLAP SET TO PREVENT CREEP TO PROVIDE ENVIRONMENTAL RESISTANCE

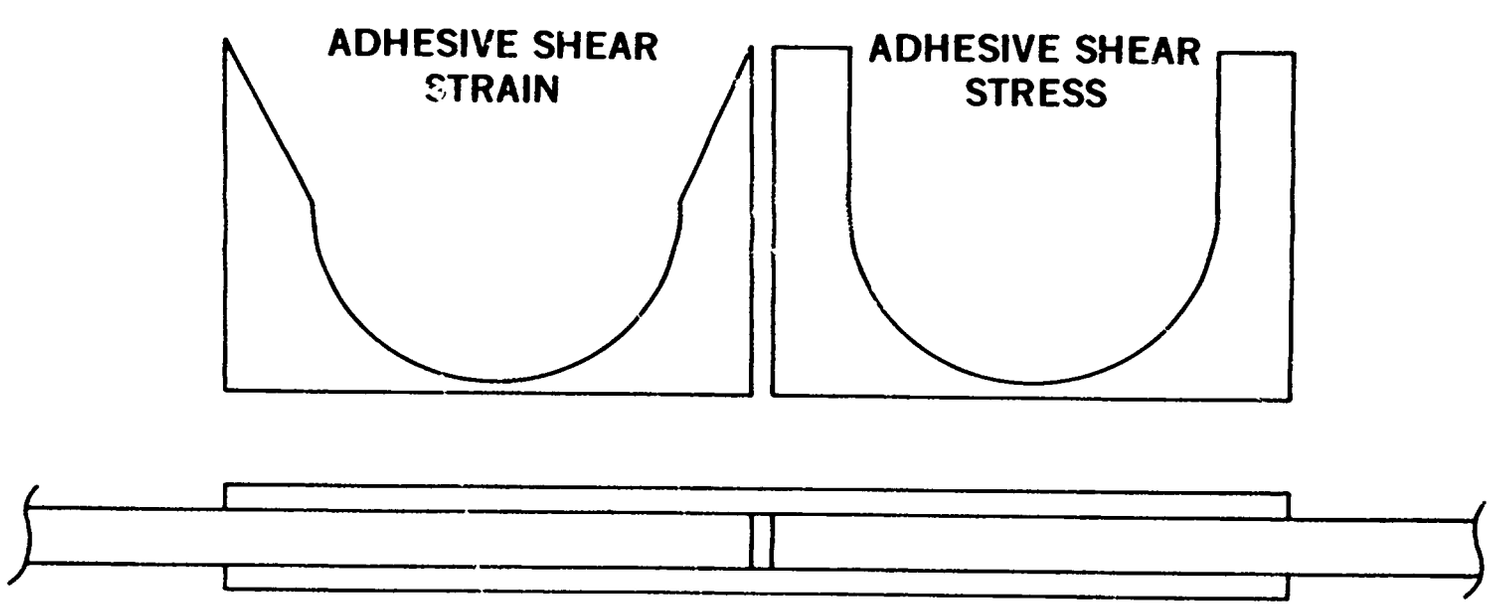


FIGURE 69. DOUBLE-LAP JOINTS

The following table gives the nominal recommended overlaps for balanced double-lap and double-strap joints used in the PABST designs.

Central Sheet Thickness t_o (inch)	0.040	0.050	0.063	0.071	0.080	0.090	0.100	0.125
Recommended Overlap ℓ (inch)†	1.21	1.42	1.68	1.84	2.01	2.20	2.39	2.84
Strength of 2024-T3 Aluminum (lb/in.)	2600	3250	4095	4615	5200	5850	6500	8125
Potential Ultimate Bond Strength (lb/in.) * ‡	8115	9073	10184	10812	11477	12173	12831	14346

† Based on 160°F properties giving lowest value of λ.

* Based on -50°F properties giving lowest joint strength. (The thicker adherends, say 0.100 and 0.125, would need peel stress relief by feathering the outer edges of the splices.)

‡ For nominal adhesive thickness η = 0.005 in.

The lengths calculated are for balanced joints - slightly different overlaps would be used if $E_i t_i \neq 2E_o t_o$. These overlaps are sufficient to permit riveted repairs if necessary. The potential bond shear strengths can be multiplied by the following sequential modification factors as necessary.

For thin bonds - reduce strengths in ratio $\sqrt{\eta/0.005}$

For in-plane shear - reduce in ratio 0.62:1

For fatigue with γ_{max} restricted to 0.05 - reduce in ratio 0.138:1

For stiffness imbalance, see table below

$2E_o t_o/E_i t_i$	0.2	0.4	0.6	0.8	1.0	1.2	1.4	1.6	1.8	2.0
Ratio of Strengths of Unbalanced and Balanced Joints	0.35	0.53	0.69	0.85	1.0	0.96	0.93	0.90	0.88	0.87

In the case of combined tension (or compression) and in-plane shear loads, the effective maximum adhesive shear strain derives from the condition

$$(\gamma_{MAX})^2 \not> (\gamma)^2_{P\ LOAD} + (\gamma)^2_{S\ LOAD}$$

It should be noted that the recommended overlaps above are less than half as great as would have been required by the arbitrary design rule of a uniform bond stress of 500 psi over the entire bond area. Thus, the improved understanding of the actual load transfer and non-uniform stresses in bonded joints has permitted a considerable weight savings in splices with respect to previous bonded joint technology.

Results. - The typical joint strength values calculated above give no cause for concern about a properly processed bond being weaker in ultimate mode than the metal elements of the structure.

Static testing of such double-lap and double-strap bonded joints in 0.040 and 0.080 inch thick central adherends demonstrated consistent failures in the metal, usually in the splice members. Therefore, for the 0.040 to 0.071 inch central sheets, the splice plates were made one gage thicker than a balanced joint. The small decrease in potential bond strength can be afforded because the nominal bond strength is so much in excess of the adherend strength. Balanced joints (t_o = 1/2 t_i) were retained for 0.08 inch sheets and above. (For the combined mechanically-fastened cold-bonded splices, the outer splices were made thick enough to accept a flush rivet head.) A series of static tests performed at a very slow load rate (5 to 10 minutes to reach ultimate strength) demonstrated how the adhesive fails if the metal stress is held at the yield value or above. The failure mechanism is illustrated in Figure 70.

Single-Lap (Longitudinal) Splices. - The PABST design does not currently call for any single-lap skin splices. However, they can have certain potential advantages over double-lap splices, provided that they are proportioned properly. Therefore the pros and cons of such splices are outlined briefly here. The key advantage is a lower cost from fewer pieces to be bonded together, easier bond inspection, and only half as many fasteners. The disadvantages are a reduced fatigue life and increased crack growth rate because of the eccentricity in the load path at the ends of the overlap. These disadvantages can be minimized, at the expense of a small weight penalty, by increasing the overlap. An overlap of 50 times the sheet thickness has about the same weight as a double-lap bonded splice between such sheets, and represents a 1.5:1 stress concentration factor with respect to a nominal skin stress of about 20 ksi.

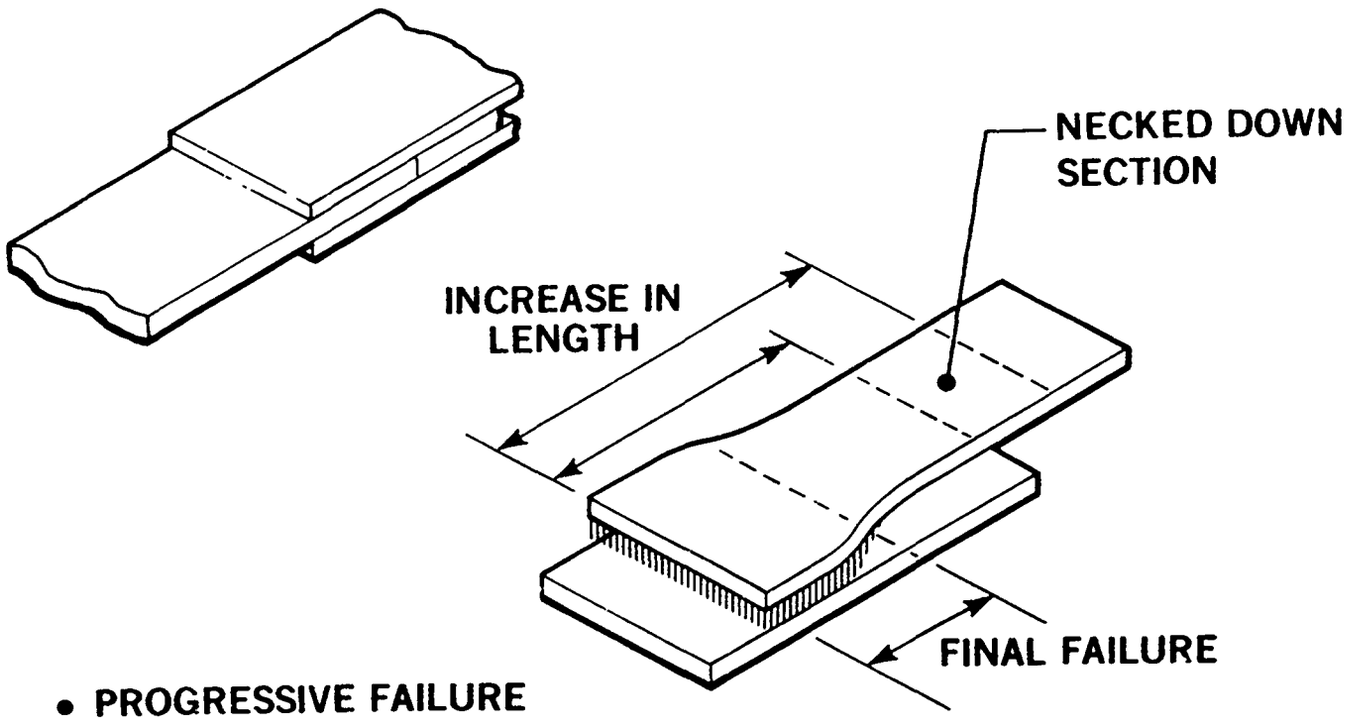


FIGURE 70. EFFECT OF YIELDING OF METAL

Single-lap skin splices are particularly inefficient if the overlap is too short; for example, with an ℓ/t ratio of 20:1, an average sheet stress of 20 ksi is increased locally to 55 ksi by the bending moment at the eccentricity whereas, if ℓ/t equals 100, the same 20 ksi average stress induces a maximum of only 25 ksi. Figure 71 depicts the relationship between maximum and average stresses for different ℓ/t ratios. Note that the abscissa reads nearly directly as ℓ/t for aluminum adherends. For the skin gages typical of transport aircraft fuselages, good structural adhesives have more than adequate shear capability if the overlap is adequate. The two potential weak links are adherend bending and adhesive peel at the ends of the overlap. Both problems can be alleviated by increasing the overlap and the second can be minimized by a shallow chamfer at the end of each sheet.

Single-Strap, Flush (Circumferential) Splices. - The circumferential splices in the PABST ADP are combined mechanically fastened/room-temperature bonded joints. The sheet sizes available, and the location of such necessary manufacturing breaks as the compound-curved to cylindrical shape, the major wing and landing gear frames and the cargo door cut-out are such that intermediate bonded circumferential splices are not needed.

Analyses and testing of such a purely bonded splice have been conducted. The test panel was 24 inches wide and 48 inches long, with a central transverse splice 6.5 inch wide. Two longitudinal stiffeners, spaced 12 inches apart were bonded to the same side of the skin as the splice plate, having a flush exterior surface. The joint geometry is shown in Figure 72. This panel was tested at high frequency and demonstrated a more than adequate fatigue life under such circumstances of 100,000 cycles at the nominal 16 ksi stress followed by 33,400 cycles before failure at 24 ksi nominal load. However, the failure was catastrophic and without warning. A short fatigue crack grew in the splice plate, at the skin junction, and was only 0.7 inch long on the invisible faying surface side and 0.3 inch on the visible interior surface where it was held shut by the compression on that side of the splice. This small flaw fast fractured over the entire 24 inch width and the bonded stiffeners unzipped instead of acting as crack stoppers. Analysis of this bonded joint indicated severe bending moments in the splice at the skin junction and in the skins at the edge of the overlap (see Figure 72). The strain gages recorded a compressive stress on the inner face of the splice. The presence of the longerons

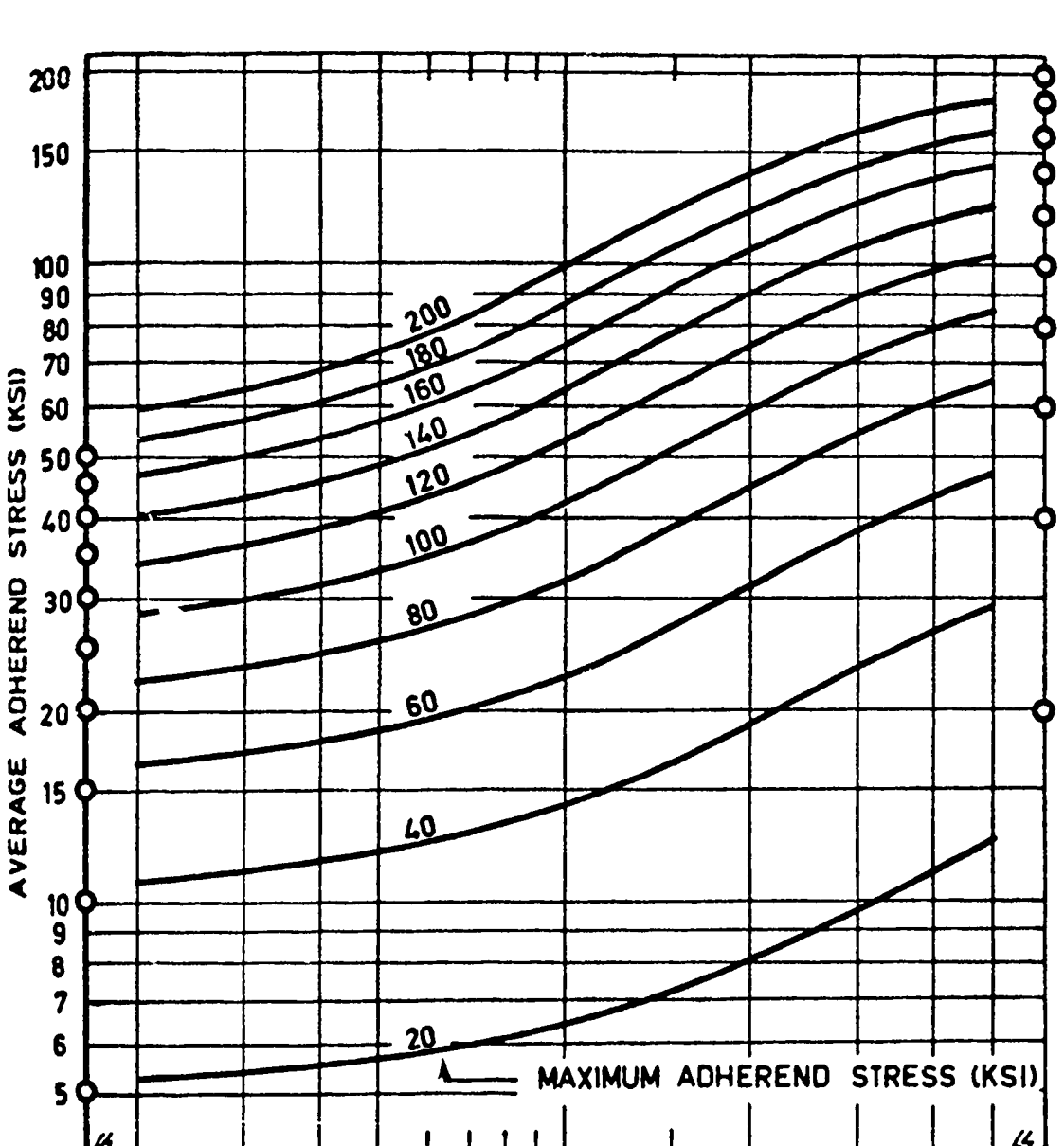


FIGURE 71. ADHEREND LIMIT LOADS FOR BALANCED SINGLE-LAP JOINTS

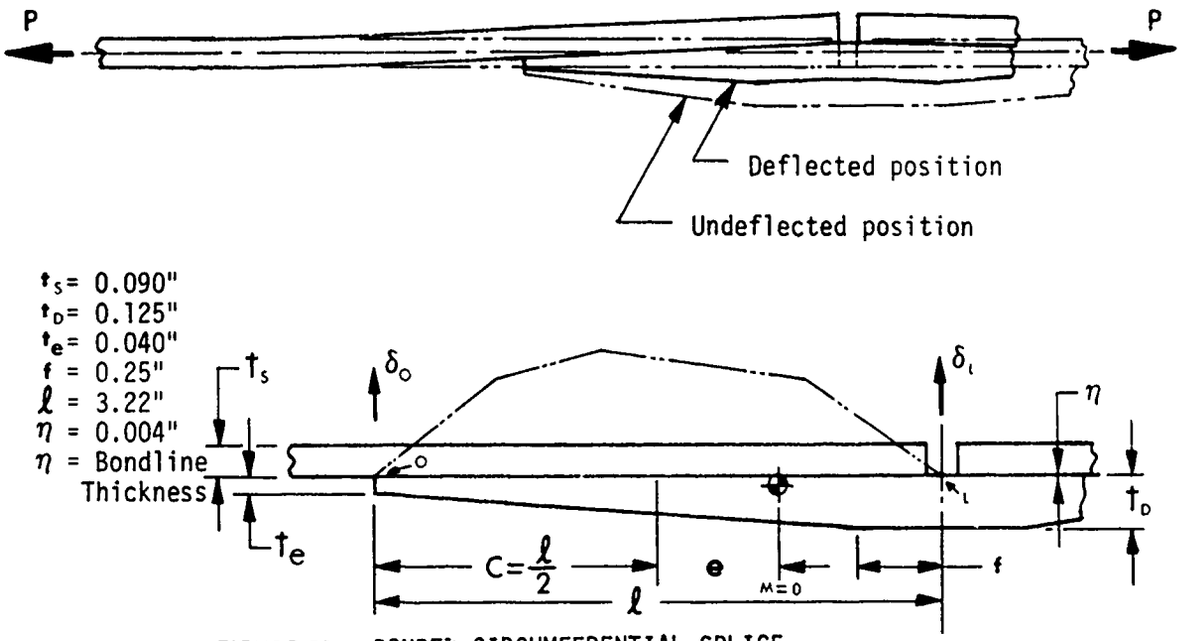


FIGURE 72. BONDED CIRCUMFERENTIAL SPLICE

The table below gives the results of a non linear iterative solution of the stress and deflection of the splice subjected to various skin stress levels.

σ_{avg} psi skin	σ_{max} psi o	σ_{max} psi L	σ_{peel} psi o	σ_{peel} psi L	σ_o"	δ_L" **	e/c
10,000	19,060	25,602	1,312	5,765	0.014	0.054	-0.19
12,000	22,155	29,743	1,471	6,612	0.013	0.057	-0.20
14,000	25,155	33,637	1,616	7,380	0.012	0.059	-0.21
16,000	28,074	37,318	1,749	8,082	0.011	0.061	-0.21
18,000	30,924	40,814	1,872	8,726	0.011	0.063	-0.22
20,000	33,718	44,145	1,987	9,319	0.010	0.064	-0.22
22,000	36,459	47,336	2,095	9,867*	0.010	0.066	-0.22
24,000	39,154	50,402	2,195	10,377*	0.009	0.068	-0.22

* σ_{peel} = 10,000 psi is failure

** moment is reduced to zero when δ_L = 0.11 in.

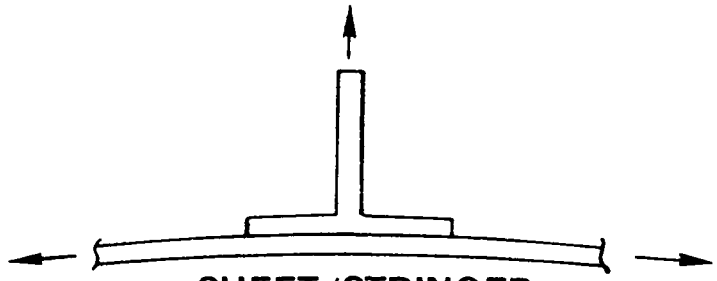
restrained the panel from deflecting quite as much as in the unstiffened sheet analyzed, but the agreement was still good. For example, at 24 ksi, the combined bending and stretching stresses away from the longerons were measured as 37 ksi in the skin vs 39 predicted, and 44.5 ksi in the splice vs 50.5 predicted. High peel stresses were predicted in the adhesive at the skin junction and delaminations of up to 0.3 inch were detected by dye penetrant.

The circumferential splice joint has been redesigned as a conventional mechanically fastened joint with room-temperature curing adhesive to enhance the fatigue life. The overlaps for mechanically-fastened splices are significantly less than those which are desirable for bonded splices, so the latter are heavier. A length-to-overlap ratio of 100 is desirable for bonded single-lap and single-strap joints, with a minimum acceptable ratio of about 50. In the present case, the mechanically-fastened joint has a major advantage over the bonded splice - in the former, the splice plate can bend smoothly over the distance between the two inner rows of fasteners while, in the latter case, the bending is sharper because it is confined to the immediate vicinity of the skin junction.

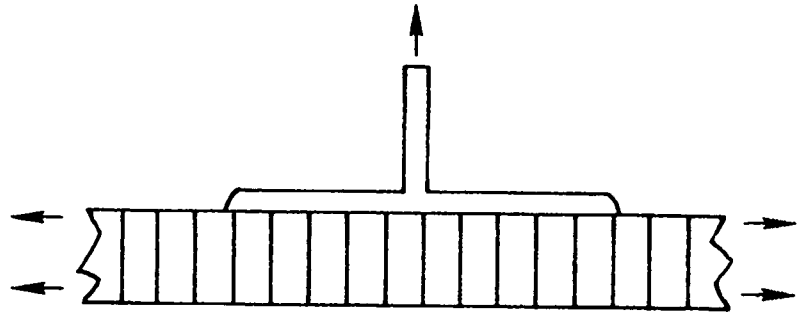
Skin-to-Stiffener Joint. - The bending to separate the skin from the bonded stiffeners, both longerons and frame shear tees, arises from two basic load conditions. The first is the pillowing due to internal pressurization, while the second is the wrinkling of the skin under shear loading. Analyses and tests have been performed for the skin to stiffener junction stress. Both the coupon and panel testing confirm there is no problem in this area wherever the stiffener is continuous. In many instances, the stiffener web was ripped off the bonded flanges that remained attached to the wrinkled skin. There is often a real or potential problem where the stiffener is cut, as at the shear T cutout at the frame/longeron intersection. The only successful analyses that have been and can be conducted show high margins but these are all for the non-critical continuous stiffener cases. The analyses performed are for the onset of buckling in shear and for the pillowing of the pressurized skin between the frames. No analyses are available for the skin-to-stiffener forces associated with fully developed shear wrinkles or for discrete stiffener lengths. Preliminary analysis and past experience indicated that the stiffeners should be of T or J cross section rather than L or Z, otherwise, the skin could easily peel away from under the hard web of the stiffener.

Figure 73 indicates qualitatively the nature of the distribution of the contact stresses between stiffener and skin under peeling loads for both sheet skin and honeycomb skin. The distributions are distinct, with the honeycomb panel being much stronger. The core failed every time for the honeycomb tests while the bond failed every time for the sheet metal tests (See Test Section). The reason for this is that the sheet metal is so flexible the analytical bond stress distribution shows some 49 percent of the bond pushing the other 51 percent apart. Even so, the test results (See Test Section) are very much greater than the requirements to resist the pressure loads.

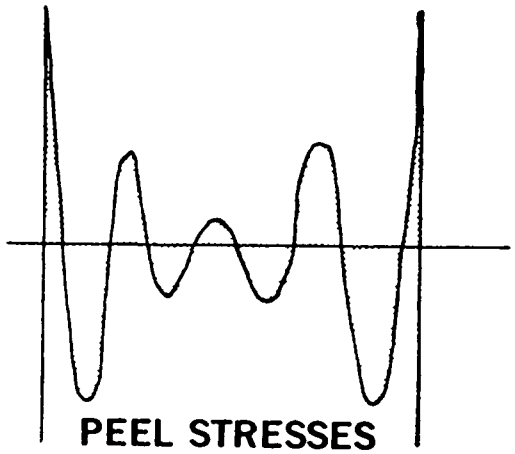
In the frame-bending test, Figure 74, it was definitely observed that the first failure was a break in the skin to a shear tee bond locally at the abrupt discontinuity in the shear tee where it was notched to permit the longeron to pass through. Once this happened, the skin over the shear tee cutout was free to buckle, thereby reducing the effective frame bending strength and stiffness at that location. The frame bent sharply and the bond between the skin and shear tee unzipped at two of the three frames in the panel. The load developed was sufficient to meet the design requirements but the mode of failure was so undesirable that the shear tee cutout area details will be improved for subsequent work. There was also some indication in the testing of some of the stiffened shear panels that the abrupt discontinuity in the shear tee triggered the failure. While all of the shear panels tested developed adequate strength, those with external longerons or honeycomb skin had uniform uninterrupted frames and attained consistently the highest strengths. It is now evident that the nature of the stiffening of shear panels can be more important even than the basic skin gage. If, as is often the case, the frame cripples locally at the frame/longeron intersection, local reinforcement of the frame outer cap or improved detailing of the intersection is a more expeditious approach to increasing the panel strength than raising the skin gage.



• SHEET/STRINGER

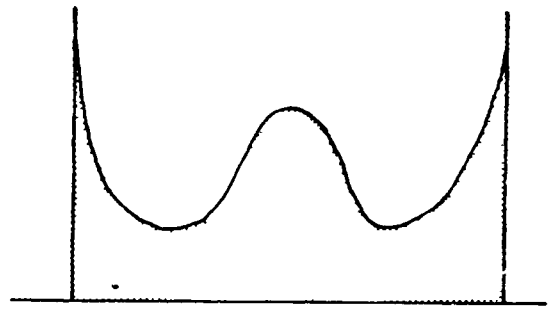


• HONEYCOMB/STRINGER



PEEL STRESSES

• PROBLEM ALLEVIATED BY HIGH b/t RATIOS



PEEL STRESSES

• NONLINEAR ANALYSIS (GEOMETRIC DISTORTIONS UNDER LOAD)
• WORK IN PROGRESS

FIGURE 73. PEELING APART OF SKIN AND STIFFENERS

FAILURE LOAD 56,742 IN-LB
DESIGN LOAD 50,000 IN-LB

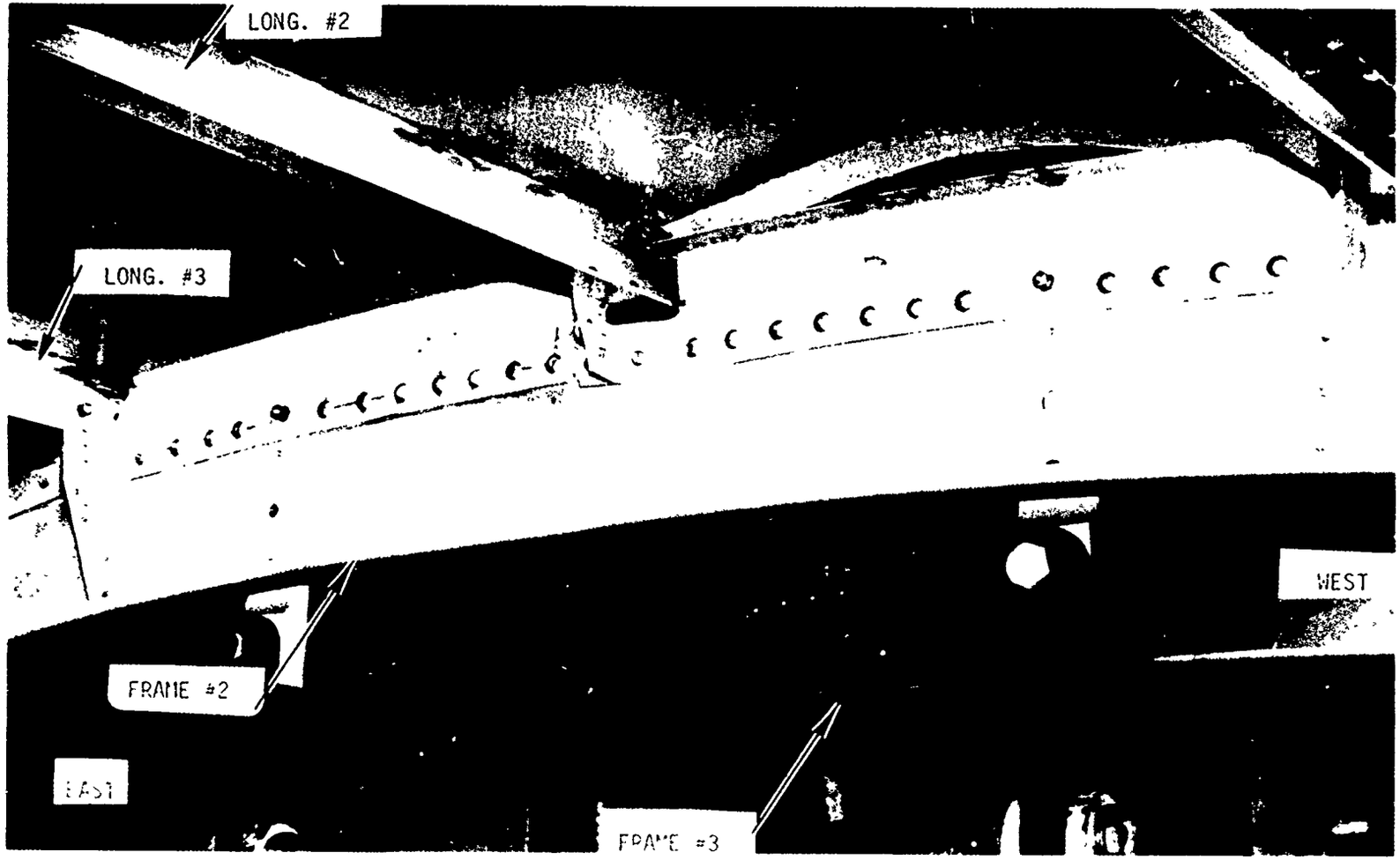


FIGURE 74. FRAME BENDING FAILURE

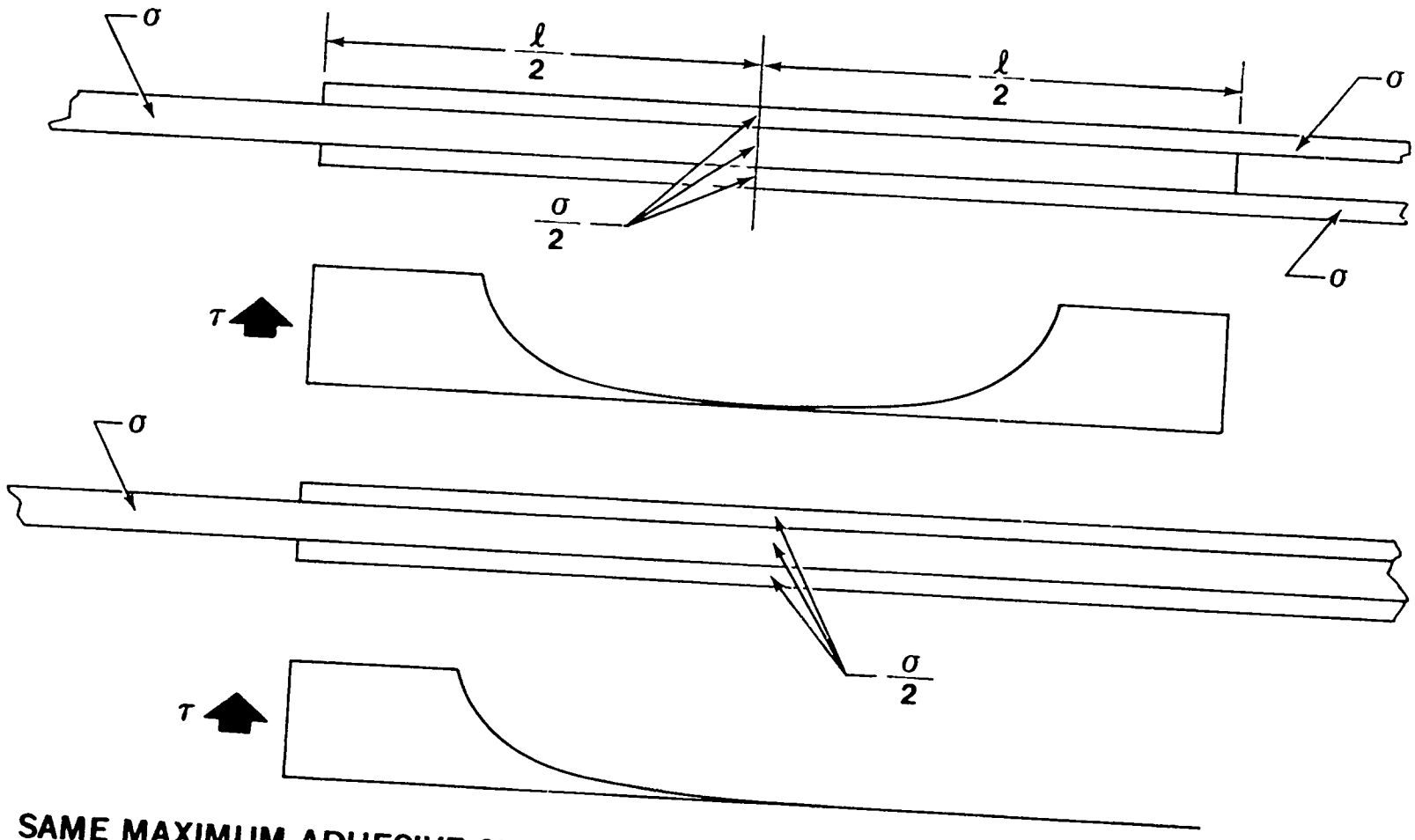
Slow Cycle Fatigue

The service experience with adhesive-bonded joints falls into two categories - those which last apparently forever, and those which have fallen apart completely under environmental attack. The service failures have been attributed to inadequate or improper surface preparation in conjunction with adhesives which absorb much moisture. The use of phosphoric acid anodize surface preparation in combination with an environmentally resistant primer should eliminate problems associated with the use of FPL etch under inadequate control. Therefore, there should be no reason to anticipate further environmental or durability problems for the adhesive. Prior bonding experience has been mainly with doublers rather than structural joints. (As far as the adhesive is concerned, however, it is worked equally hard in both cases, as explained in Figure 75.) Therefore, those satisfactory service experiences from past applications indicate that adhesives can be strong enough and durable enough for the primary structural applications in PABST.

Boeing fatigue tests at slow cycle rates of the new-generation 250°F-cure modified epoxy adhesives indicated the probability of inadequate life when the adhesive was tested in a hot (140°F) humid (100 percent RH) environment at load rates and durations more representative of service conditions than the customary 30Hz used in prior testing. The differences between testing such a joint and one more akin to real geometry are not well understood. This is explained in Figure 76. So, to the original task of demonstrating that more extensive use of adhesive bonding should be made in fuselage construction, the program had to prove also that the new adhesive selected had adequate environmental durability. This has led to an extensive slow cycle testing program in which the cycle consists of five minute load-up, 15 minutes hold, five minutes unload, and five minutes hold. The test environment is nominally 140°F, 100 percent RH. The joints tested include double-strap splices for 0.04 inch and 0.08 inch skin using aircraft geometry overlaps, 1.15 and 1.94 inch, respectively. A small number of thick adherend short overlap specimens (half inch single overlap in 0.25 inch plate) has been included. It is planned to add tension tee testing as well.

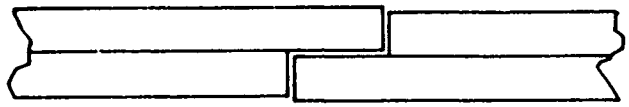
PRECEDING PAGE BLANK-NOT FILMED

- SAME ADHESIVE STRESSES IN EACH CASE

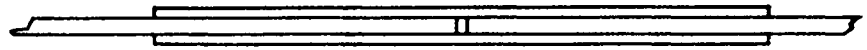


- SAME MAXIMUM ADHESIVE SHEAR STRAIN FOR SAME ADHERENDS AND METAL STRESSES

FIGURE 75. DOUBLERS VERSUS JOINTS



- UNIFORM SHEAR STRAIN IN ADHESIVE
- ADHESIVE CREEP OCCURS EVERYWHERE
- ONLY WEAK ADHESIVE LOCKED-IN STRESSES TO RESTORE TO ORIGINAL STATE
- JOINT CANNOT RECOVER DURING UNLOAD PERIODS, SHORT OR LONG
- ENVIRONMENTALLY DEGRADED
- USEFUL TEST TO INVESTIGATE ADHESIVES
- RESULTS NOT NECESSARILY INDICATIVE OF CONFIGURED JOINTS



- NONUNIFORM ADHESIVE SHEAR STRAIN
- ADHESIVE CREEP OCCURS ONLY AT ENDS OF OVERLAP – NONE IN ELASTIC TROUGH
- HIGH LOCKED-IN METAL STRESSES TO RESTORE TO ORIGINAL CONFIGURATION
- JOINT RECOVERS DURING LONG UNLOAD PERIODS
- NO EVIDENCE OF IN-SERVICE DEGRADATION, EXCEPT AT INTERFACE WITH POOR SURFACE TREATMENT
- MOST FAILURES IN METAL
- NOT SUITABLE FOR COMPARING ADHESIVES
- NECESSARY TO VERIFY ENVIRONMENTAL DURABILITY

FIGURE 76. THICK ADHEREND VERSUS AIRCRAFT CONFIGURATION BONDED JOINTS

A successful conclusion to this phase of the testing would be no failures in specimens other than the thick adherend short overlaps. The slow cycle testing will continue through later phases of the program. It is anticipated that the fatigue failures at bonded joints in the structure will be in the metal, not the adhesive.

Some exploratory tests were run to assess the influence of local creep in the adhesive, at the ends of the overlap, on the overall response of adhesive bonded joints under repeated loading. Two double-lap joints were butted back-to-back to magrify the signal and strain gages were glued across the gap. Repeated tests were run for 30 min. (DAC) cycles and 85 min.(Boeing) cycles. Specimens of two widths were run, with 0.080 inch central adherends.

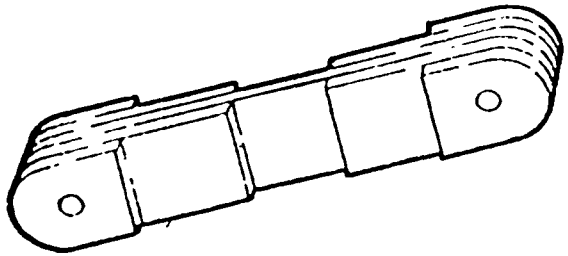
The same loads were applied to all specimens in every cycle. The adhesives does not affect the fatigue life of bonded joints when those joints are of real structural configurations. The load versus strain gage signals were not identical for the first few cycles but became so by about the fifth cycle. Most importantly, even though recovery was not complete during the unloaded portions of the cycles, by the end of each loaded segment the strain gage readings were identical - that is, what creep there was at the extremities of the overlap was shown not to be cumulative. This is because, for a given load, the joint deflections are dominated by the strains in the metal. The adhesive strain is zero in the middle of the overlap, so the relative motion at the ends of the overlap, across the glue line, is always the same for a given load. This is not the case for the short overlap joints, such as the thick-adherend and RAAB specimens, in which the progressively accumulated adhesive creep leads to failure of the adhesive under slowly repeated loads. This factor is very important in projecting from the behavior of joint coupons, specially configured to enforce bond failures, to joints of real structural proportions, designed to develop the full strength of the metal. The tests reported above verified the adequacy of the test technique which, so far at least, is the only one shown to have given consistent readings from such small signals - adhesive strains are small enough to be difficult to measure but the perturbations on these due to creep are sub-microscopic. The result lend confidence to the belief that structural adhesive joints will not fail in service due to fatigue of the bond.

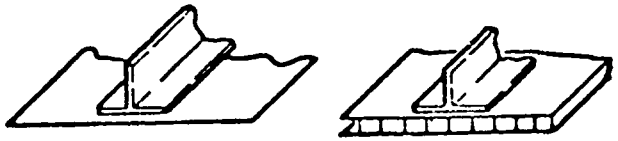
Strength of Flawed Bonded Joints

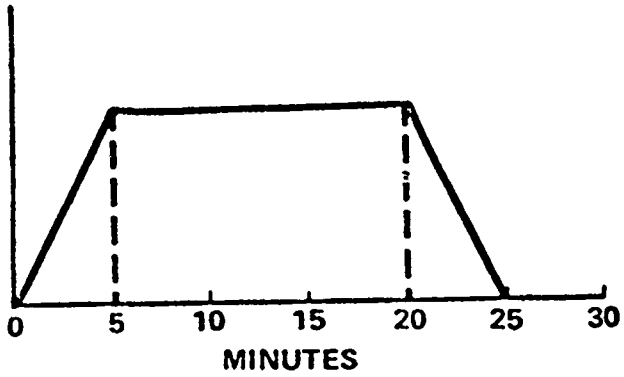
Future testing planned for the PABST program includes an extensive investigation into the effect of defects in the bonds. These tests are to be conducted at the DAC slow cycle rate (5 minutes loadup, 15 minutes hold, 5 minutes unload, 5 minutes dwell) in a 140°F, 100 percent RH environment. The scope of the program is outlined in Figure 77. The specimens are double-lap splices, sheet-metal tee skin/stiffener combinations and honeycomb/tee joints. The flaws considered include both processing variables which are likely to lead to incompletely cured adhesive that could react adversely with the environment and a variety of mechanical defects. The latter include porosity, voids, and a bondline which has been fractured at the edges. Experience at Douglas with the new 250°F curing epoxy adhesives indicates these adhesives flow so much that it has been difficult to deliberately create such a flaw. Anticipated improvements in the manufacturing methods for bonded assemblies will make the detail parts fit together better for bonding so that the incidence of natural flaws will be negligible. Preliminary testing of bonded coupons at MCAIR for the PABST support program "Definition and Non-Destructive Detection of Critical Adhesive Bond-Line Flaws" has established that bond flaws do not grow under high frequency testing - the metal fatigues away just as for unflawed bonds. Therefore, any such investigation must be conducted at load rates and durations close to those experienced in service. The adhesives to be employed in this investigation include: (1) FM-73, the selected 250°F adhesive for PABST, (2) the selected room-temperature curing adhesive for enhancing the fatigue life of the mechanical splices at the manufacturing breaks, AF-55. AF-55 is radio-opaque permitting inspection by X-Ray, and (3) PL729 which is a higher temperature curing epoxy used on the B-1 and is less likely to be sensitive to the environment.

Those flaws which would permit corrosion of the structure will naturally be repaired prior to delivery. For other local flaws it is likely that the effect of the flaw will be nullified by transferring load into the otherwise lightly-loaded elastic trough in the adhesive. If the global, as opposed to local, problems due to out-of-tolerance processing prove to be a problem during test it will be necessary to tighten up the processing and inspection

OBJECTIVE: JOINT PERFORMANCE WITH DEFECTS







EXCESSIVE OUT TIME
CONTAMINATION
LOW BONDING TEMPERATURE

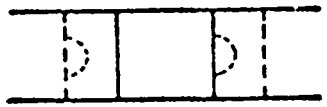
EA9309
FM73
PL729
AF55

SHORT CURE

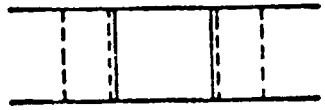
POROSITY



VOIDS



FRACTURED BONDLINE



LOCAL SURFACE DING
CRUSHED CORE



FIGURE 77. EFFECTS OF DEFECTS

techniques to remove faulty parts for re-treatment prior to assembly. Otherwise, the bonded structures are anticipated to be very tolerant of local bond flaws during manufacture and service.

Analysis into bonded defects is proceeding along two paths. The one-dimensional stepped-lap joint analysis program A4EG has been modified to permit variable adhesive properties and thickness along the length of the overlap. This program also can account for partial or complete local voids in the adhesive which redistribute the load transfer along the load direction. This program is being debugged. A two-dimensional analysis program has been prepared for flaws large enough to affect a gross redistribution of load transfer, as explained in Figure 78. The latter program has been modified to account also for the adjacent parallel stiff and soft load paths associated with variable thickness adhesive bonds. This work will be reported separately when completed.

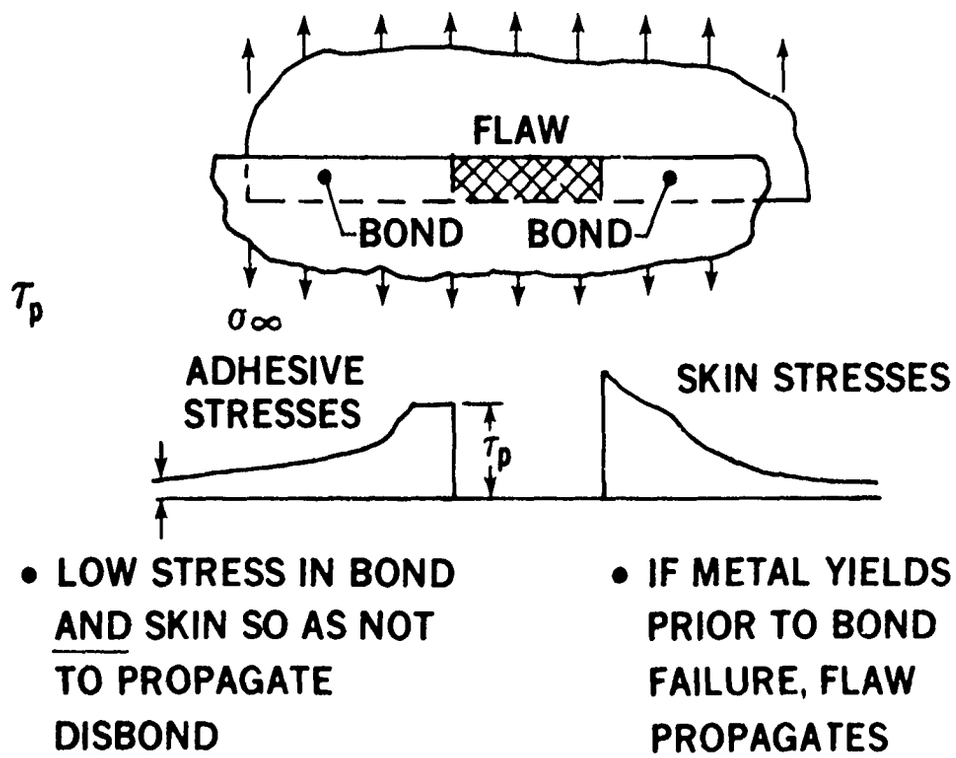


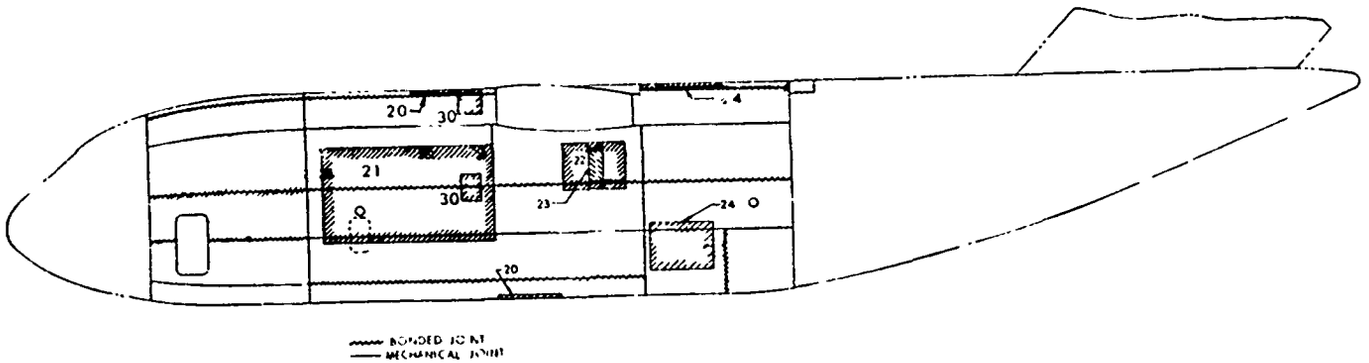
FIGURE 78. REDISTRIBUTION OF LOAD AT FLAWS IN BOND

STRUCTURAL TESTS

Structural tests on small specimens and on large flat and curved panels were conducted in Phase Ib to obtain allowable strength data and to verify that the fatigue and damage tolerance criteria could be met. The large static and cyclic load panels are identified and the panel sizes and loading methods tabulated in Figure 79 .

The following subsections describe: (1) the tension tee tests, (2) the shear, tension-shear interaction, and compression-shear interaction tests, (3) the frame bending test, and (4) the fatigue and damage tolerance uniaxial and biaxial tests.

PRECEDING PAGE BLANK-NOT FILMED



SPECIMEN IDENTIFICATION	20 CURVED PANEL - MEDIUM	21 CURVED PANEL - LARGE	22 CURVED PANEL MEDIUM	23 FRAME REFERENCE	24 CURVED PANEL MEDIUM	30 METALLIC DAMAGE TOLERANT
SPECIMEN SIZE	49 x 615	110 x 148	48 x 615	52 x 62	48 x 615	84" x 144" or 108" x 144"
LOADING *	CBS	P	S	B	BES	T
TESTS: STATIC	6	—	3	1	6	—
TESTS: FATIGUE	—	—	—	—	—	—
TESTS: DAMAGE TOLERANCE	—	2	—	—	—	4
TESTS: CRITICAL MODE TBD	—	—	—	—	—	—
TOTAL SPECIMENS	6	2	3	1	6	4

FIGURE 79. LARGE, STRUCTURAL TEST PANELS

Static Tests

Tension Tee Static Tests. - These tests were made to determine the joint static strength between the frame tee shear clip and the skin under the simulated cabin pressure (14.3 psi ult) load. The test results are summarized in Table 18 and 19. All failures in Table 18 were in the bond and generally of the cohesive type failure. All failures in Table 19 were in the honeycomb core except as noted.

TABLE 18
TENSION TEE TEST

SKIN	ADHESIVE	PRIMER	FAILURE LOAD TEST TEMP			DESIGN LOAD
			-50 ± 5°F	R.T.	140 ± 5°F	-50°F
0.090 7075-T6	FM 73	BR 127	1740 LB			249 LB
0.040 7075-T6	FM 73	BR 127	1595 LB			389 LB
0.090 7075-T6	AF 55	XA 3950			4000 LB	249 LB
0.090 7075-T6	M 1133	BR 127	2170 LB			249 LB
0.090 7075-T6	AF 55	XA 3950	5910 LB	5050 LB	5075 LB	249 LB
0.090 7075-T6	M 1133	BR 127	2640 LB	4650 LB		249 LB
0.040 7075-T6	AF 55	XA 3950	1670 LB	3700 LB	4220 LB	389 LB
0.040 7075-T6	M 1133	BR 127	2105 LB	3275 LB	3358 LB	389 LB

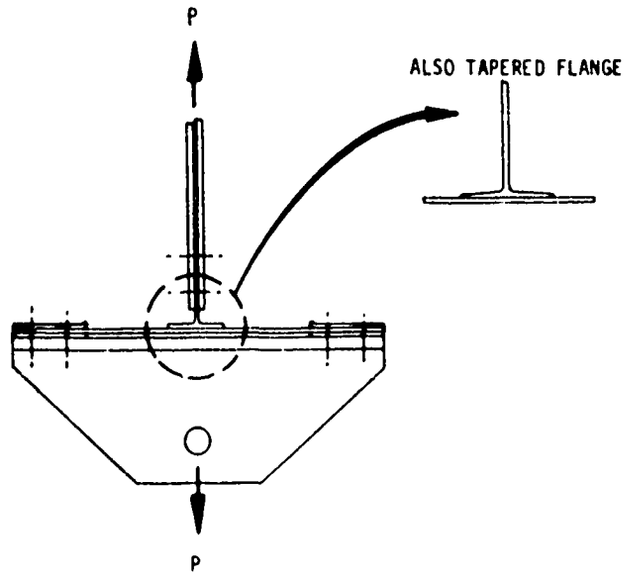
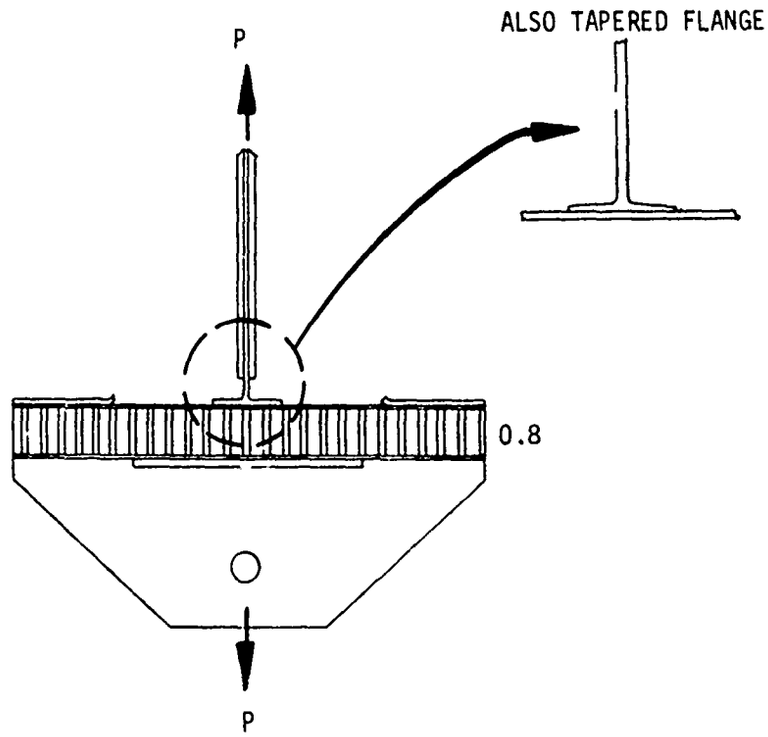


TABLE 19

TENSION TEE TEST - HONEYCOMB

FACESHEET THICKNESS	CORE DENSITY	TEE THICKNESS	TEST TEMPERATURE	FAILING LOAD (LB)	TYPE OF FAILURE*	DESIGN LOAD (LB)
0.020 7075-T6	3.4PSF	0.050	-50	2580	(1)	462
			AMBIENT	2530	(1)	
			+140	2460	(1)	
0.020 7075-T6	5.2	0.050	-50	3720	(1)	462
			+140	3830		
0.020 7075-T6	7.9	0.050	-50	5210	(2)	462
			+140	3340	(2)	
0.020 7075-T6	5.2	TAPERED	-50	3580	(1)	462
0.040 7075-T6	5.2	0.094	-50	4100	(1)	392
0.040 7075-T6	7.9	0.094	-50	6975	(1)	392

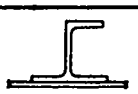
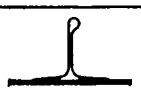
*(1) CORE SHEAR (2) FACESHEET TO CORE BOND DELAMINATION (TENSION)



Shear Static Test Panels. - These tests were to determine the static shear and the combined shear plus tension or compression strength of the fuselage shell concepts, Figure 79. The test results are shown in Tables 20 and 21. All visible evidence of the test specimens indicated that failures initiated in the metal with occasional secondary adhesive disbond. A significant observation is that, in those specimens having shear tee cutouts at the frame/longeron intersections, failure was initiated by crippling of the Z frame flange closest to the skin. It should be noted also that, in the absence of such cutouts, the shear tee was often ripped along the web/flange intersection, with the flange still bonded securely to the sharply wrinkled skin.

TABLE 20
SHEAR – COMPRESSION/TENSION INTERACTION STATIC TEST PANEL

ADHESIVE FM73, PRIMER BR127, TEST TEMP = 140°F

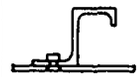
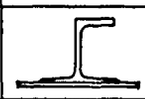
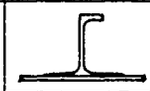
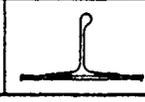
SPEC NO.*	SKIN 7075T6	LONGERON	TEST		DESIGN	
			SHEAR (KSI)	AXIAL (KSI)	SHEAR (KSI)	AXIAL (KSI)
20	0.05		18.1	−29.2	17.8	−14.0
24	0.05		23.0	56.5	13.4	55.4
20	0.09	NONE	16.9	−8.7	16.3	−8 4
24	0.05		30.6	67.9	13.4	55.4
20	0.05		18.0	−18.2	17.8	- 14 0

AXIAL STRESS - = COMPRESSION, + = TENSION

*SEE FIGURE 79

TABLE 21
SHEAR STATIC TEST PANEL NO. 22***

PRIMER BR127

SKIN 7075T6	LONGERON	ADHESIVE	TEST TEMP	TEST SHEAR (KSI)	DESIGN SHEAR (KSI)	ANALYSIS FAILURE PREDICTION (KSI)
0.04		FM73	−50°F	19.8	13.0	18.3
0.09		RIVETED	R.T.	24.6	20.0	21.8
0.09		FM73	R.T.	26.5	20.0	21.8
0.04		M1133	−50°F	27.5	13.0	18.3
0.04		M1133	140°F	25.3	13.0	18.3
0.09	NONE	FM73	140°F	19.6	20.0	10.6
0.09*	NONE	FM73	140°F	23.8	20.0	12.6
t_o (2024T3) = 0.02, t_i = 0.020**	NONE	FM73	R.T.	42.6	13.0	23.5
t_o = 0.04, t = 0.04**	NONE	FM73	140°F	48 0	39.0	23.5
0.0434		FM73	140°F	30.7	13.0	23.3

*12 IN. FRAME SPACING **48 IN. FRAME SPACING ***SEE FIGURE 79

Frame Bending Test. - These tests determine the static strength of a typical frame-longeron-skin combination, Specimen 23 on Figure 79, under pure bending in the frame. The test setup and frame section properties are shown in Figures 80 and 81 respectively. The test results are shown in Figure 73. Initial failure occurred for a one-inch length in the bond between the skin and frame tie shear clip, starting at the edge of the shear clip cutout for the longeron, followed by complete disbond between longerons and subsequent frame crippling.

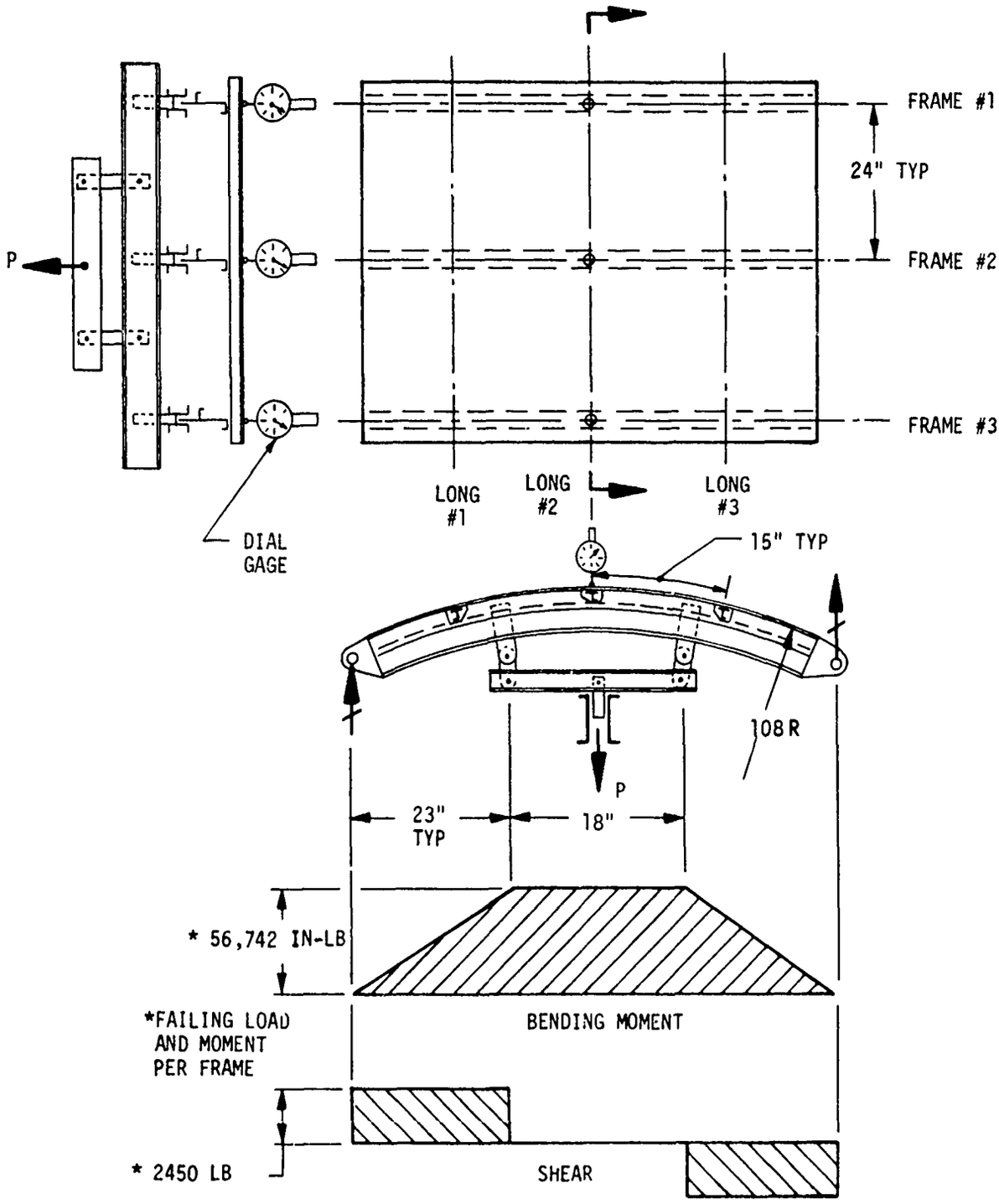
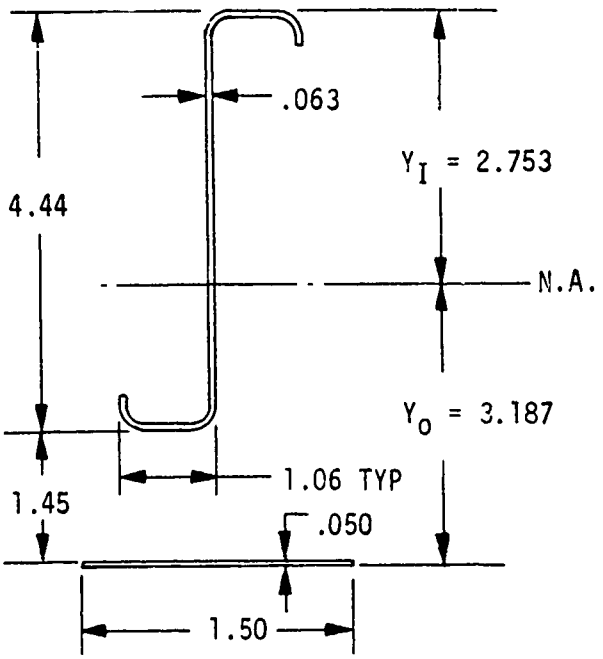


FIGURE 80. FRAME BENDING TEST (SPECIMEN 23)



FRAME MAT'L 7075-T6 CLAD
SKIN MAT'L 7475-T61 BARE

AREA = .520 IN^2

$I_{N.A.}$ = 2.097 IN^4

FIGURE 81. CROSS SECTION OF FRAME THROUGH LONGERON CUTOUT

Fatigue and Damage Tolerance Tests

The fatigue and damage tolerance tests in Phase Ib of the PABST program were designed to:

(1) Evaluate bonded structure to determine if there are significant improvements in fatigue life and damage tolerance when compared to equivalent riveted structure,

(2) Demonstrate that the internal longeron, external longeron, and honeycomb design concepts meet the fatigue and damage tolerance criteria of MIL-A-008866, MIL-A-83444 and the additional DC-10 residual strength criteria,

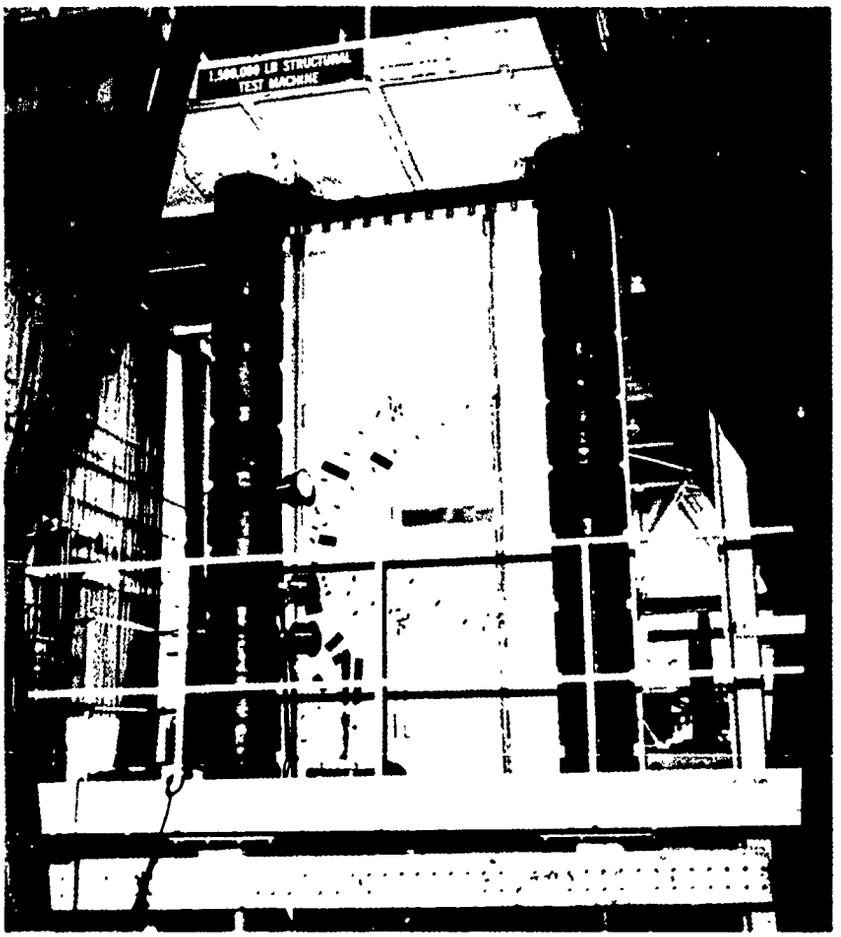
(3) Demonstrate correlation with analysis procedures.

The first series of tests (Specimens 1, 3 and 4) using panels with Z sections attached to skins by bonding and riveting did show that bonding reduced the rate of flaw growth particularly in the region of the stiffener. This was due to the greater stiffness of the adhesive which resulted in the stiffener picking up the skin load much more rapidly than would be the case with the more flexible rivets. The residual strength showed a marginal improvement over the equivalent mechanically fastened panels. The absence of fastener holes naturally resulted in improvement of fatigue life.

Later tests (Specimens 21 and 30 on Figure 79) showed that each of the three concepts could and did meet the damage tolerance, fatigue and residual strength criteria. The analysis/test correlation was also good. At least one problem area was uncovered during the internal longeron flaw growth time history test. It was found that, at the frame longeron intersection in the shear tee cutout area, a severe fatigue stress concentration existed. This was due to the discontinuity of the frame shear clip at the longeron transferring a shear clip load into the skin. Due to the high stiffness of the bond, the load was transferred locally into the skin in the region of the shear clip cutout with the result that fatigue cracks were developed in four of the eight cutouts in the panel. The remaining four cutouts had the longerons joggled over a skin splice so there was much better continuity of load path. Though this cutout condition does exist in mechanically fastened structure, the greater flexibility of the fasteners permits the load to be

transferred over a greater length of the frame and thus shear into a greater width of the skin. The modification to correct this situation was to bridge the shear tee cutouts with straps extending from the tee flanges to the longeron flange. This modification was incorporated in the subsequent residual strength panel. This panel attained the required life. The cutout area remained highly stressed and demands continued attention. No cracks developed in or near these bonded straps in the absence of initial flaws. However, where the skin was pre-cut at one of the cutouts in the shear tee, the splice strap cracked completely through on one side and debonded on the other side.

During this entire series of tests, great care was taken to monitor the bondlines, and the growth of known bondline flaws. There was no instance of disbonding or bondline flaw propagation during any of these tests. There were cases of disbonding but these were all initiated and propagated by metal yielding. A typical test installation is shown below.



Riveted vs Bonded Damage Tolerance Tests. - This series of tests compared the crack growth and residual strength characteristics of riveted and bonded reinforced aluminum panels.

Test specimen configuration, Specimen 1, and details are shown in Figure 82 and Table 22 toether with a summary of the test conditions. All the panels were tested at room temperature except one of the bonded panels which was tested at 140°F. Each of the bonded panels was inspected ultrasonically and some voids were found along the free edge of the Z section stiffener. There was no evidence of these voids propagating during the test, nor did they significantly influence the test results.

The panels were all subjected to a constant amplitude stress cycle

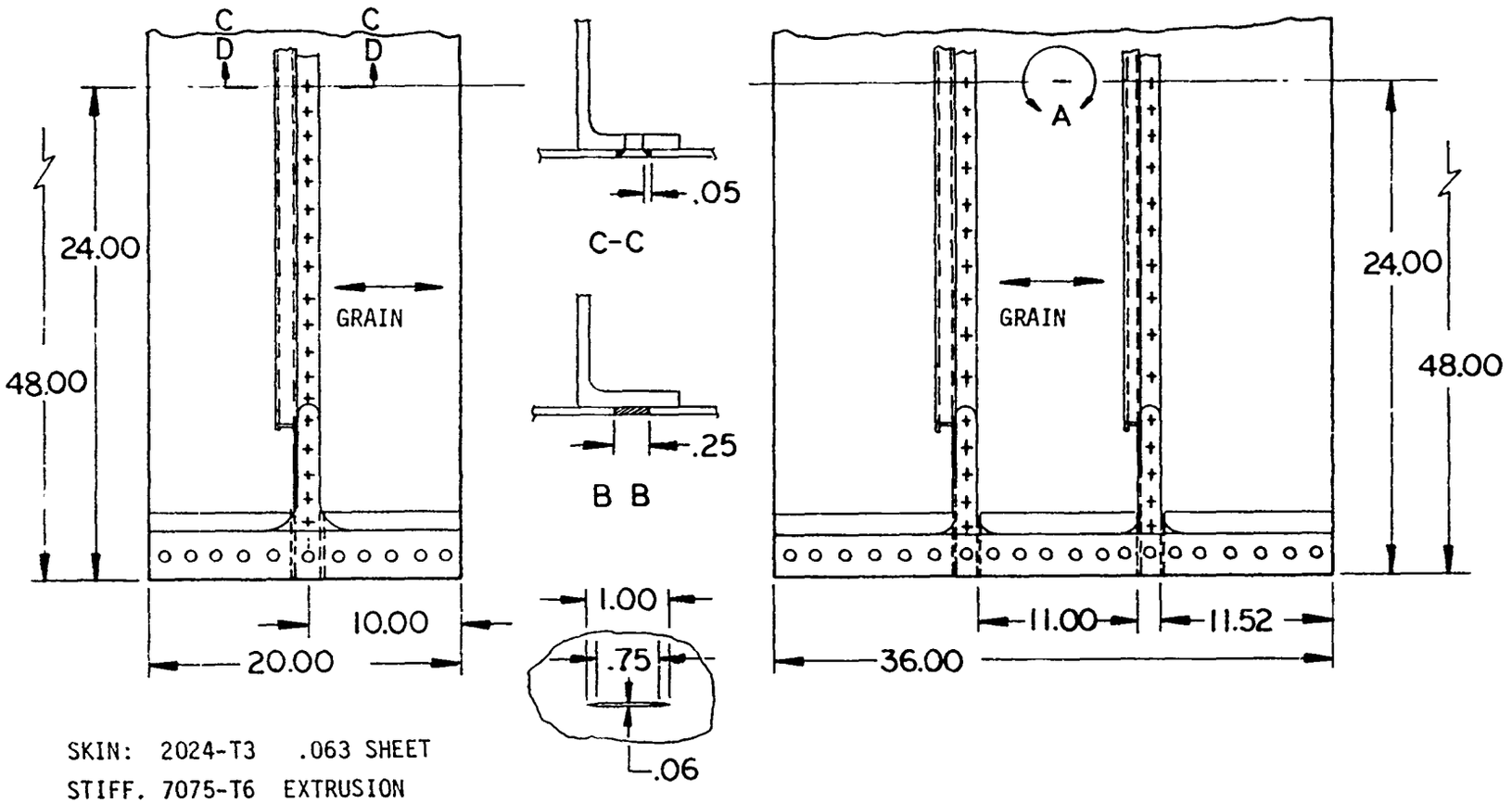
$$\sigma max = 14{,}000 \text{ psi} \qquad R = 0.05.$$

The rate of cycling was approximately 3Hz on the Schenk Machine.

Each panel was cycled until the cracks were grown from the initial 0.25 in. sawcuts to predetermined lengths. When these crack lengths were achieved, the panels were loaded statically to failure to determine the residual strength.

The crack growth time history data for the two-stringer panels are shown in Figure 83 . The interesting feature is that as the crack approaches the stiffener, the retardation in the bonded panel was significantly greater than in the corresponding riveted panel. This is due to the higher stiffness of the adhesive which permits faster transfer of load out of the skin and into the stiffener; i.e., more effective in retarding crack growth.

For the single stringer panels with the initial flaw in the skin under the stiffener flange, see Figure 84, the adhesive showed a higher crack retardation than the riveted panel. It should be noted that the bonded panel which was tested at 140°F showed an even greater crack growth life than the bonded room temperature specimen. It would appear that decreased bond stiffness with temperature should result in faster crack growth. Though there is no data to substantiate this, it is thought that the basic material da/dN characteristics improve with temperature, at least in the lower Δk ranges.



SKIN: 2024-T3 .063 SHEET

STIFF. 7075-T6 EXTRUSION

NOTE: Only riveted specimens are shown. In the case of bonded specimens, the Z section longerons were bonded to the skin. Everything else is the same.

FIGURE 82. TEST SPECIMEN 1 AND FLAW DETAILS

TABLE 22

SUMMARY OF TEST CONDITIONS, SPECIMEN 1

STIFFENER TO SKIN ATTACHMENT	NUMBER OF STIFFENERS	INITIAL FLAW SIZE AND LOCATION	GROSS AREA IN^2	FINAL CRACK SIZE	TEST CONDITION
Riveted	2	1.0 in. mid bay at sym. center line	2.742	13.80	R.T. Lab Air
Bonded	2	1.0 in. mid bay at sym. center line	2.742	14.03	R.T. Lab Air
Riveted	1	.100 in. flaw on one side of the countersink	1.497	6.00	R.T. Lab Air
Bonded	1	.25 in. flaw at panel center line in the skin under stiffener flange	1.497	5.99	R.T. Lab Air
Bonded	1	" "	1.497	6.04	140^{o} F Dry Air

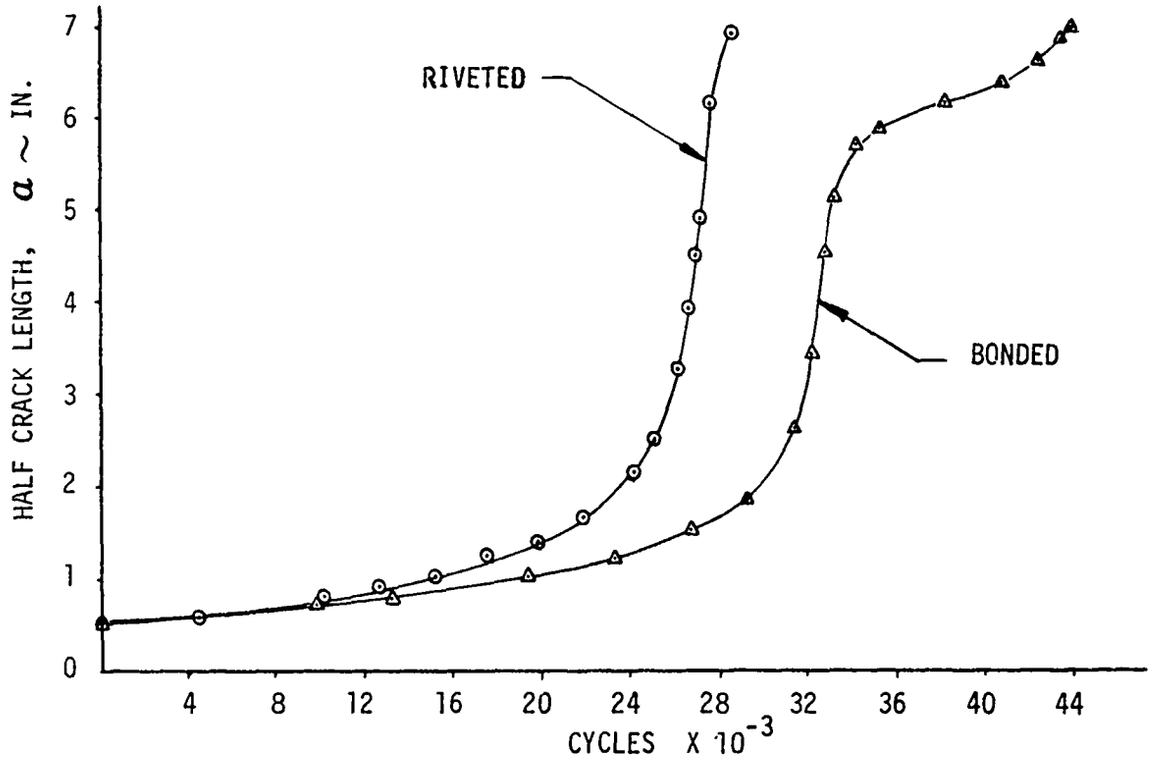


FIGURE 83. CRACK GROWTH TIME HISTORIES OF 2 STRINGER RIVETED AND BONDED PANELS

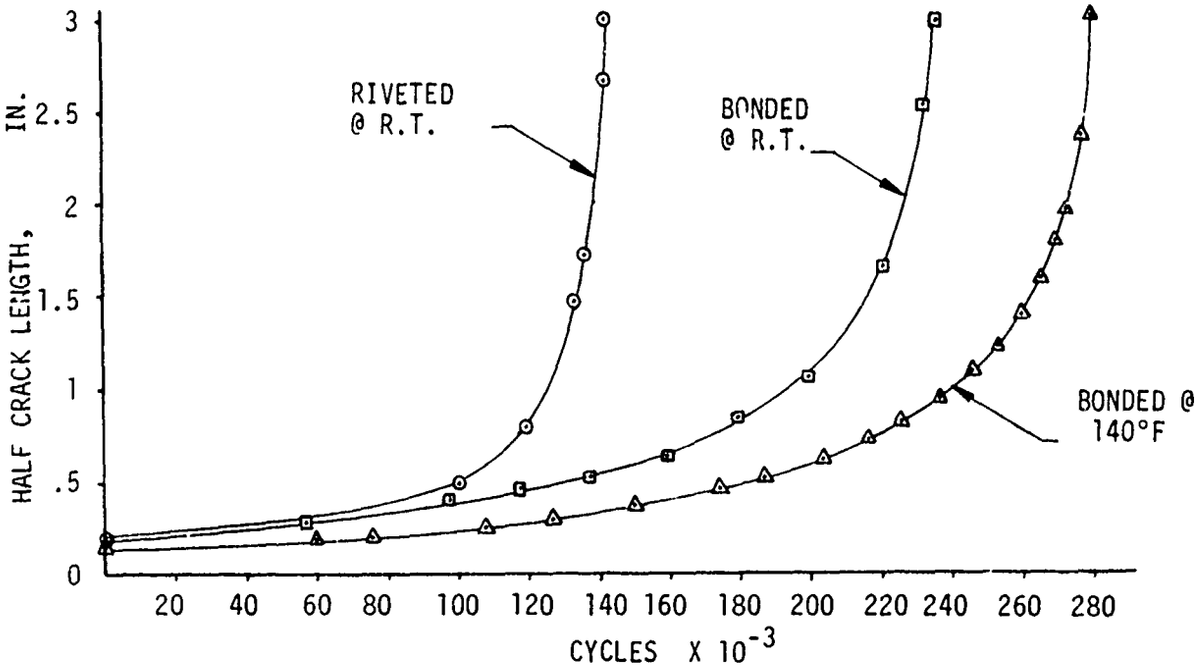


FIGURE 84. CRACK GROWTH TIME HISTORIES OF RIVETED AND BONDED SINGLE STRINGER PANELS

Also, this improvement in da/dN could dominate the loss of stiffness of the adhesive. Perhaps an increase in strain energy of the adhesive, because of its greater ductility at 140°F, is capable of explaining the improved life.

From the above, it is apparent that significant improvements in crack growth time histories can be anticipated in bonded skin-stiffener structure.

A characteristic of 2024-T3 material is slow stable crack growth under static load. Each of the five panels exhibited this phenomenon as shown in Figures 85 through 87. The failure loads of each panel were:

Panel Configuration	Crack Length at Failure-In.	Failure Load-Lb.
Two Stringer Riveted	16.5	73,887
Two Stringer Bonded	15.45	83,903
Single Stringer Riveted	6.79	44,418
Single Stringer Bonded (R.T.)	6.72	47,042
Single Stringer Bonded (140°F)	6.58	46,128

Though the bonded panels show a higher residual strength than the corresponding riveted panels, the differences are not great and could be explained by the variations in the total crack length at failure. Analysis of the failure indicated the following sequence:

(i) Stiffener yielding at a gross area stress of 23,000 psi;

(ii) Stiffener to skin disbond for approximately 2.8 in. on each side of the crack;

(iii) Stiffener to skin disbond increasing to 3.5 in. with increasing load to 30,600 psi remote stress;

(iv) At the remote stress of 30,600 psi, the skin crack tip stress intensity reaches critical value and results in fast fracture of the skin;

(v) Next, the stiffeners disbond from the skin and fail at the ends.

The stiffeners had permanent set on examination after the test.

Significant improvements can be expected in the damage tolerance characteristics in using adhesive bonding to join skin and stiffeners.

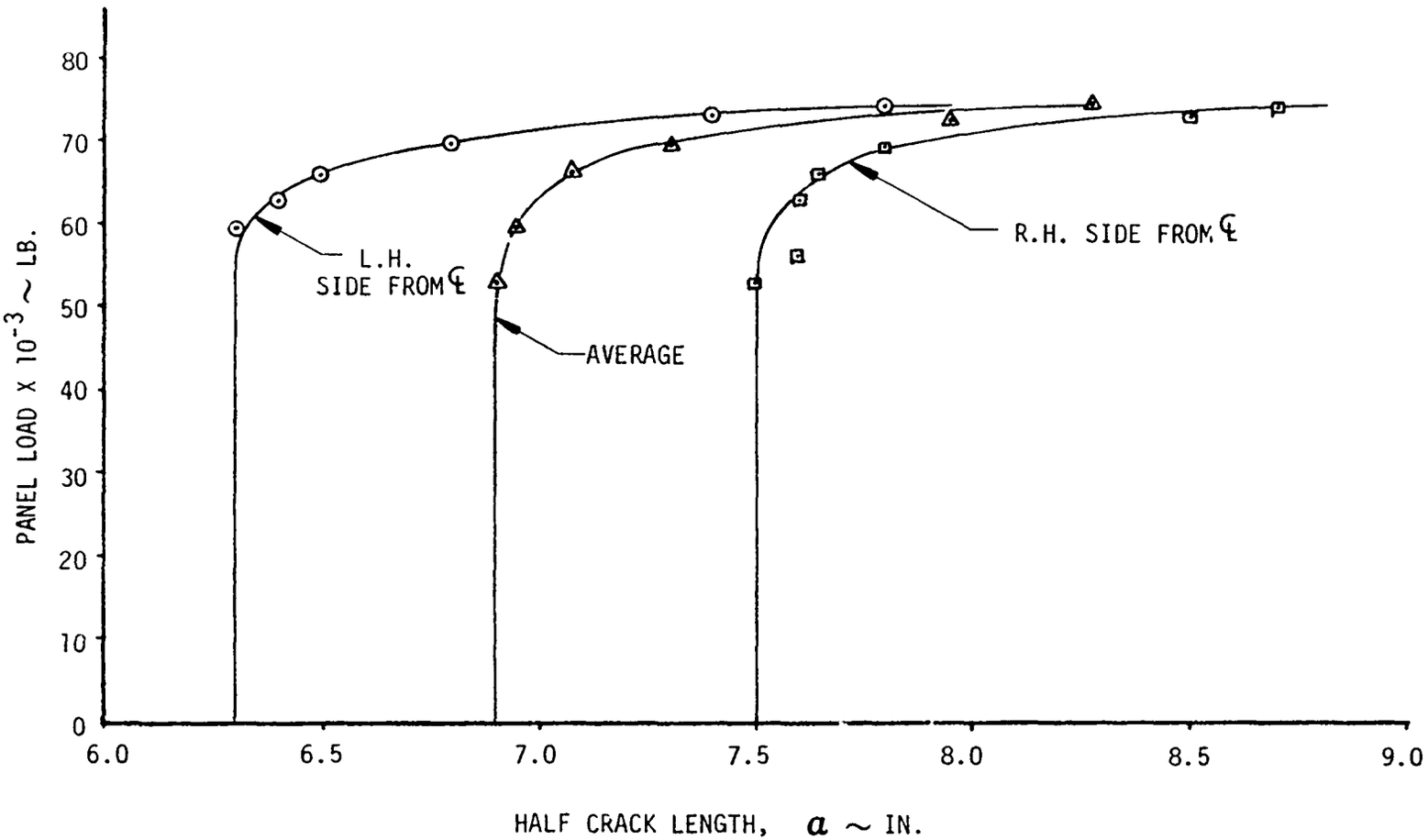


FIGURE 85. TWO STRINGER RIVETED PANEL SLOW STABLE CRACK GROWTH UNDER STATIC LOAD

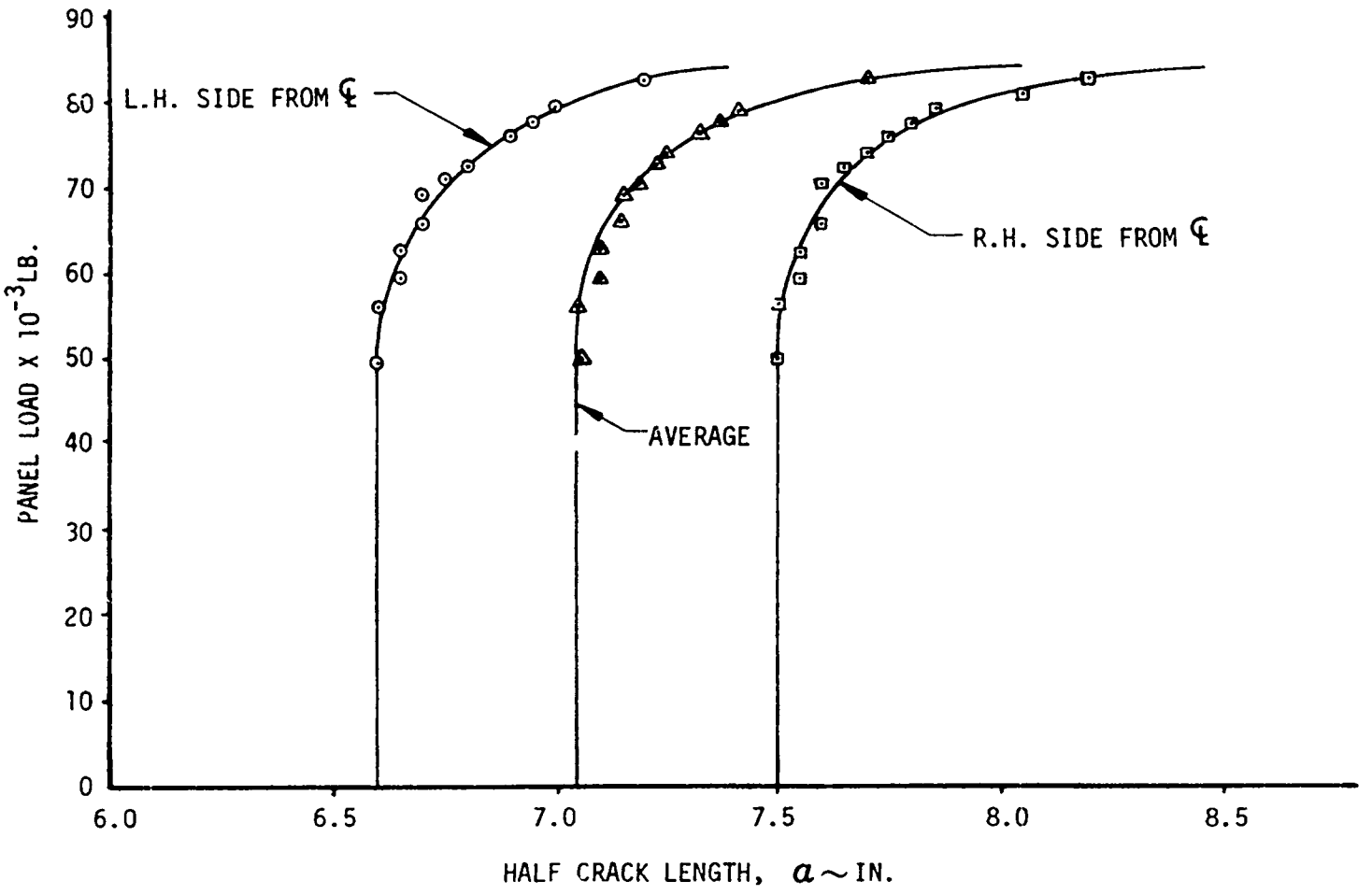


FIGURE 86. TWO-STRINGER BONDED PANEL SLOW STABLE CRACK GROWTH UNDER STATIC LOAD

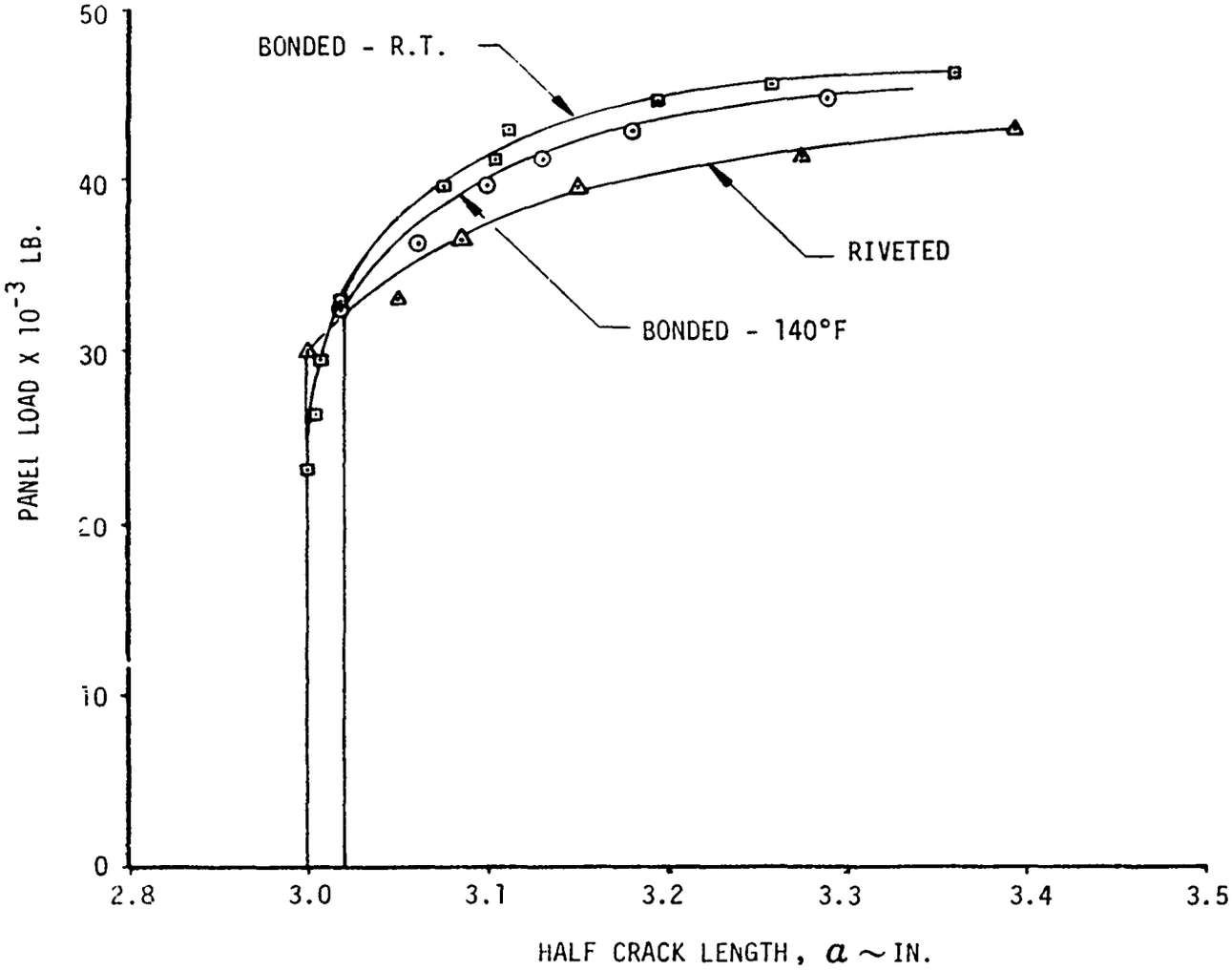


FIGURE 87. SLOW STABLE CRACK GROWTH UNDER STATIC LOAD FOR SINGLE STRINGER PANELS

Fatigue Test of Bonded Splice with Metal Flaws. - A full scale panel, with a typical bonded symmetric skin splice, was fatigue tested with metal flaws in the skin and doubler. This test was conducted to determine the number of cycles necessary to initiate a crack in the adjacent element for cases where a primary crack terminates due to an element failure.

The details of the specimen, 4A, are shown in Figure 88. The significant features of the panel design are the .090 thick skins and .050 doublers made from 2024-T3 bare sheet. The elements were bonded using phosphoric acid anodize, BR127 primer and FM73 adhesive.

The flaws were eloxed in the skin and doubler before bonding as shown in Figure 88. Test loads and environment planned for this specimen are given in Table 23.

TABLE 23

TEST LOADS FOR PANEL 4A

No.	σ Max PSI	R	Max Load Pounds	Min Load Pounds	Cycles	Test Temp. °F
1	14,000	.05	31,400	1,600	100,000	140°F
2	16,000	.05	35,900	1,800	85,000	140°F
3	20,000	.05	44,900	2,200	100,000	140°F
4	24,000	.05	53,900	2,700	26,040*	140°F

* Panel failed after 26,040 cycles at σmax = 24,000 psi.

Two strain gages were installed on the panel. One on the doubler over the elox slot in the skin and the second on the doubler opposite and over the elox slot in the doubler. The crack growth in the skin was monitored by X-rays until the crack grew past the splice doubler. Table 24 gives the crack length and associated strain gage data as functions of cumulative fatigue cycles.

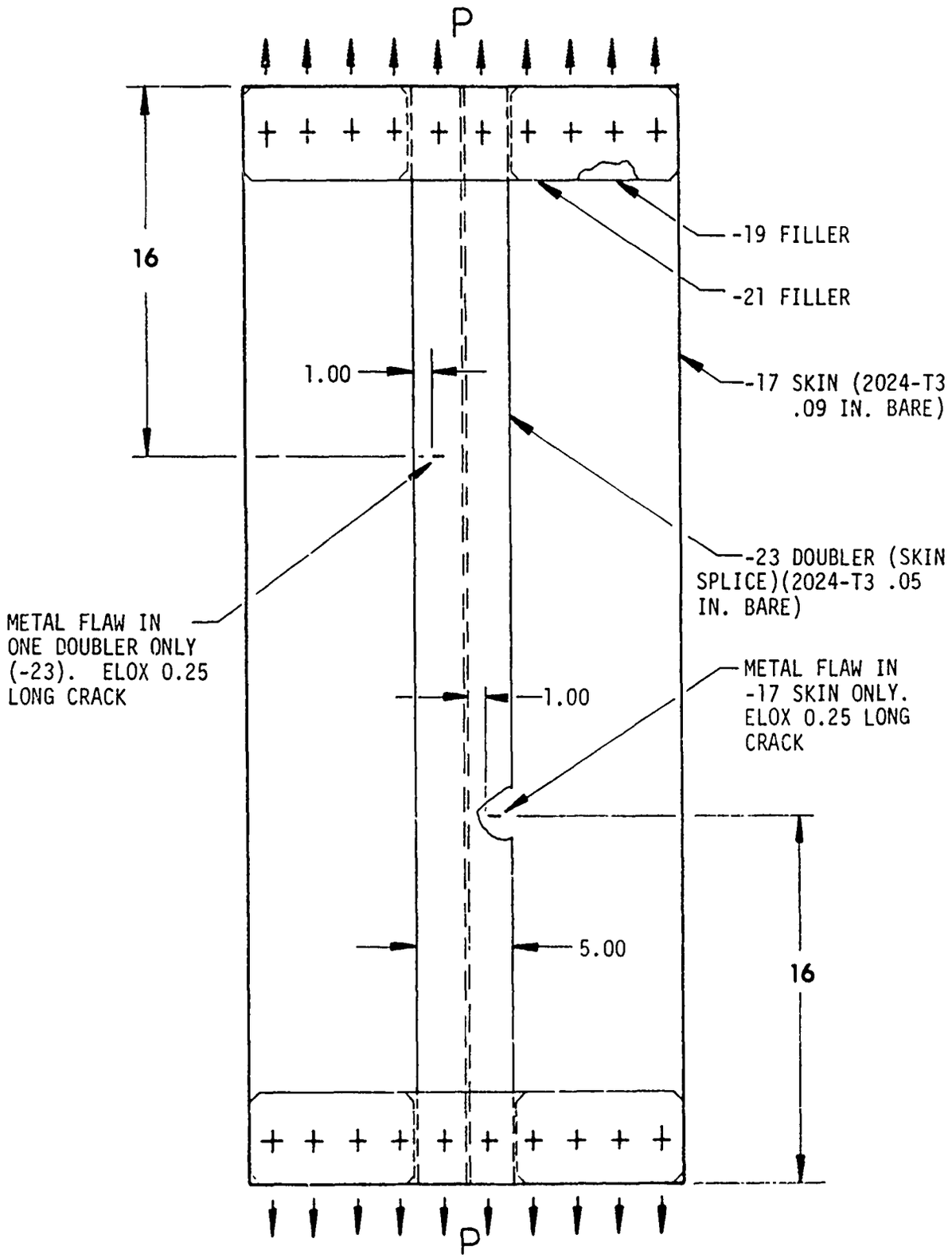


FIGURE 88. BONDED SKIN SPLICE SPECIMEN 4A WITH METAL FLAWS

TABLE 24

CRACK LENGTH AND STRAIN GAGE DATA SPECIMEN 4A

LOAD - LBS. (STRESS-PSI)	No. OF CYCLES	DOUBLER CRACK LENGTH	CRACK DOUBLER STRESS PSI	SKIN CRACK LENGTH	CRACK DOUBLER STRESS PSI
31,400	0	0.25 in.	STRAIN	0.22 in.	STRAIN
	40,000	.27	GAGE		GAGE
	60,000	.32	NOT		NOT
(14,000)	80,000	.37	INSTALLED		INSTALLED
	100,000	.44			
	100,000	.44	14,730		16,770
	120,000	.55	14,150		16,830
35,900	140,000	.70	13,600		16,420
	160,000	.83	12,100		17,100
(16,000)	180,000	.92	11,640		17,380
	185,000**	.96	11,630	0.65	17,490
	185,000	.96	15,610		21,750
	195,000	1.14	-		-
	205,000	1.29	14,670		22,940
	215,000	1.43	-		-
44,900	225,000	1.62	14,170		23,840
	232,000	1.70	14,110		24,170
	245,000	1.82	13,740		24,320
(20,000)	249,620*	1.92	13,300		24,400
	265,000	1.92	13,480		24,880
	279,380	2.42	13,840		25,200
	285,000	2.43	14,060		24,980
	285,000	2.43	17,630		30,320
	295,000	2.64	18,700	2.45	32,020
	302,010	2.80	19,460	2.58	33,050
53,900	305,000	2.82	-	2.63	
	308,000	2.90	-	3.00	GAGE
(24,000)	309,630**	2.92	19,830	3.60	OUT
	310,470	2.92	-	4.25	
	310,800	2.93	-	4.50	
	311,040	-	-	FAILED	-

* Double crack propogated to R/H edge of doubler.

** Crack length measured by X-ray.

The following observations were made on examination of the specimen after the test:

(1) There was no evidence of any disbonding as the flaws propagated through both the skin and doubler,

(2) The final failure occurred through the skin flaw. Though approximately 15,000 cycles at σmax = 24,000 psi were applied to the panel after the crack reached the edge of the first skin under the doubler, no evidence of a fatigue nucleus was found in the second skin adjacent to the crack,

(3) The flaw in the doubler propagated on both sides of the elox slot until it reached the near side edge at 249,620 cycles. It then continued to propagate on the other side until panel failure through the skin flaw. There was no evidence of a fatigue crack developing in the skin or in the opposite doubler.

Fatigue Test of Bonded Splice with Adhesive Flaws. - A full scale panel, Specimen 4B, with a typical bonded symmetric skin splice, was fatigue tested with built-in adhesive flaws in the bond area. The growth of these flaws was to be monitored by periodic non-destructive inspection and by photo stress methods. After completion of the test, the specimen was to be cut up and peeled apart to study bondline flaw growth, if any.

The test specimen details are shown in Figure 89 showing the intended size and locations of the bondline flaws. The skin and doublers were made from 7075-T6 bare material. The specimens consisted of three skin splices:

(1) Constant doubler thickness splice at the upper grip end,
(2) Symmetric centerline splice with flaws,
(3) Tapered symmetric splice at the lower grip end.

The bondline flaws were to have been achieved by cutting out the adhesive to the size and locations of the desired flaws. However, during the curing process, adhesive flowed in to fill the void and only a small irregular flaw was achieved at the centerline. The test loads planned for this specimen were as shown in Table 25.

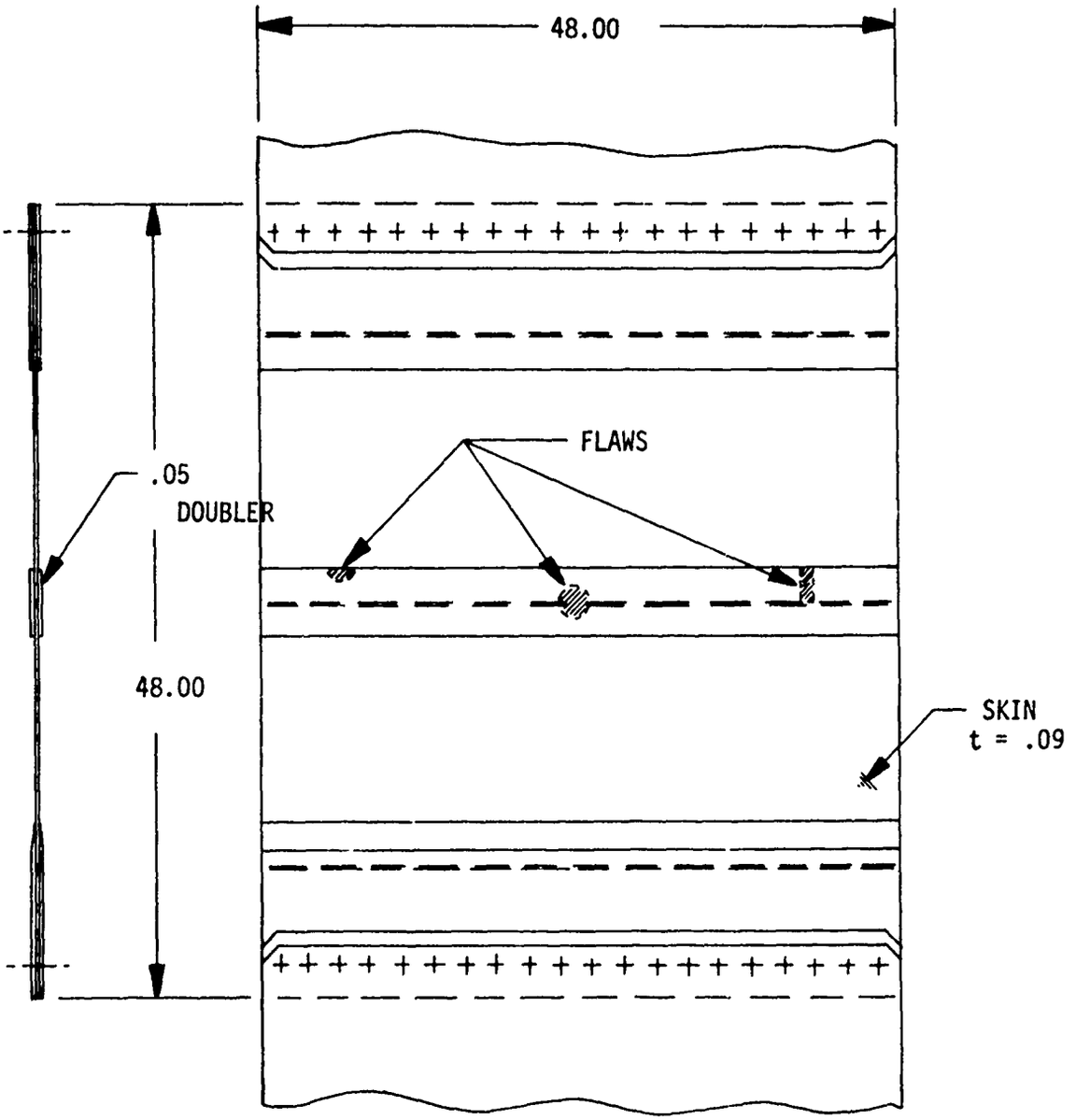


FIGURE 89. BONDED SKIN SPLICE SPECIMEN 4B WITH ADHESIVE FLAWS

TABLE 25

TEST LOADS FOR THE BONDED SYMMETRIC SKIN SPLICE SPECIMEN 4B

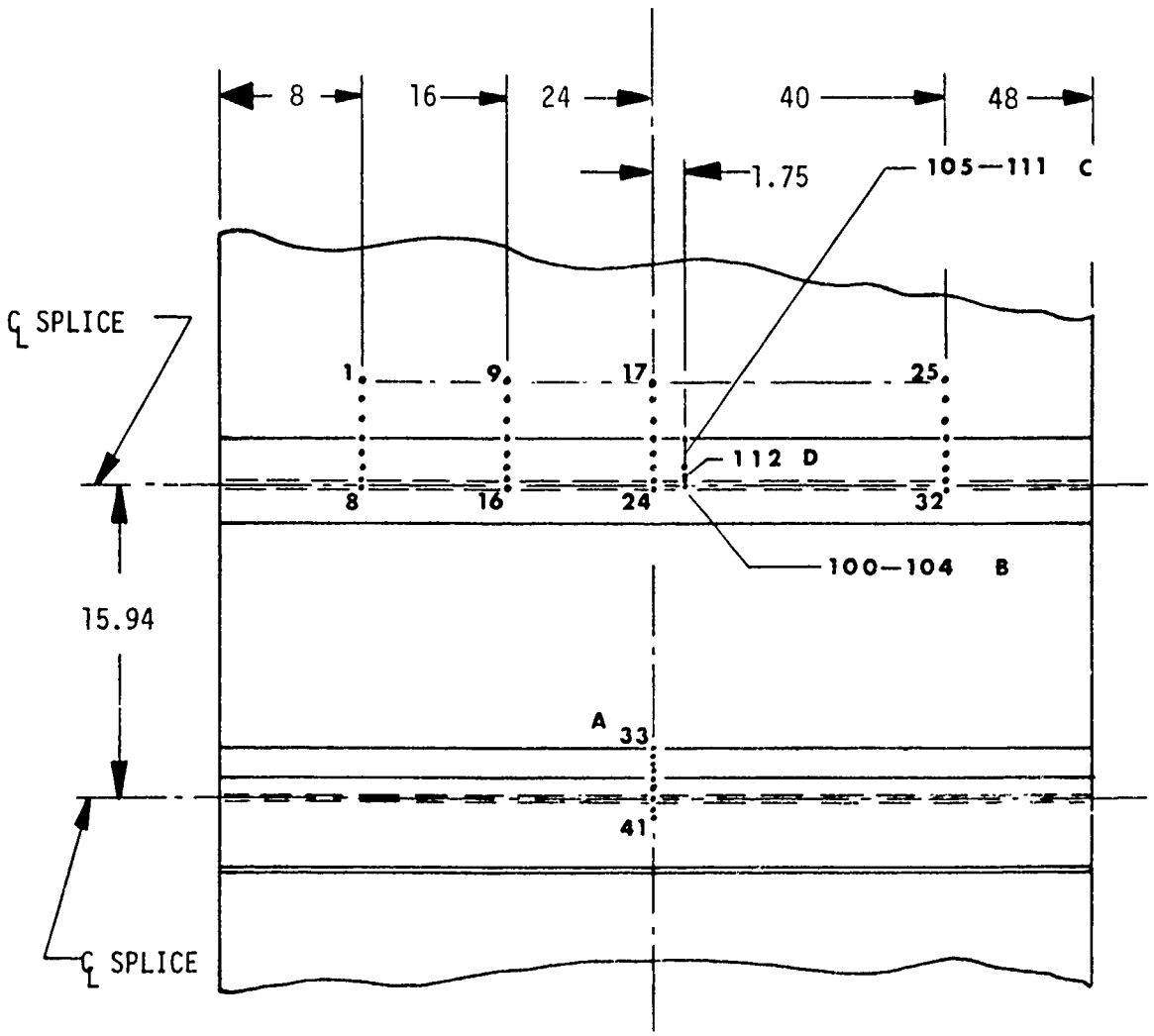
NO.	σ_{max} psi	R	P_{max} Pounds	P_{max} Pounds	NO. OF CYCLES	PHOTO STRESS DATA RECORDED AT , CYCLES
1	14,000	.05	60,500	3,000	100,000	0; 20,000, 40,000; 60,000 80,000
2	16,000	.05	69,000	3,500	100,000	0; 20,000, 60,000
3	18,000	.05	77,800	4,000	100,000	0; 40,000, 80,000
4	20,000	.05	86,500	4,300	100,000	0; 40,000, 80,000*
5	24,000	.05	103,700	5,200	100,000	0; 40,000

* Oblique angle incidence photo stress fringe data at this point.

The above schedule was followed until failure of the test panel at 452,340 cycles; i.e., 52,340 cycles into loading at 24,000 psi.

The instrumentation consisted of photo elastic plastic bonded over both sides and full width of the centerline splice and the skin ahead of the splice. A short length (10 inches) of the photo stress plastic was applied to one side of the lower grip end tapered splice. The locations of the points at which photo elastic data was taken are shown in Figure 90. A set of photo elastic stress data taken at 20,000 psi and 80,000 cycles is given in Table

Photo elastic stress data taken at the intervals indicated in Table 26 showed little or no variation. This demonstrates that the adhesive flaws did not propagate during the test. This was later confirmed by a teardown inspection of the panel. The stresses measured by photo elastic method at points 100 through 112 are plotted in Figure 91. This stress distribution in the splice doubler could only result from a shear stress distribution as shown in the second curve of Figure 91 . A color photograph of the fringes in the photo elastic plastic at 24,000 psi are shown in Figure 92 . These indicate a variation from nominal stress at the middle of the splice by up to 25 percent, which is attributed to the different stiffnesses of variable thickness bondlines.



A - Points 33-41 spaced 0.40 in. apart
B - Points 100-104 spaced 0.05 in. apart
C - Points 105-111 spaced 0.10 in. apart
D - Point 112 0.70 in. from splice center line

FIGURE 90. SPLICE SPECIMEN 4B PHOTO STRESS DATA POINTS

TABLE 26

PHOTO ELASTIC STRESS DATA AT 20,000 PSI

POINT NO.	P psi	Q psi	POINT NO.	P psi	Q psi
9	19,741	363	100	15,224	288
10	19,069	-738	101	15,888	1,179
11	19,083	271	102	16,867	1,408
12	915	-4,559	103	14,550	-507
13	7,634	-3,425	104	13,907	-614
14	11,281	-1,180	105	11,961	279
15	14,715	438	106	10,794	-754
16	12,088	-1,805	107	10,446	-351
17	21,120	2,012	108	9,039	-1,276
18	22,681	2,681	109	5,752	-3,599
19	19,113	407	110	5,569	-1,343
20	-736	-5,961	111	3,787	-982
21	9,146	-1,571	112	11,365	-1,416
22	11,393	-1,789			
23	15,220	1,101			
24	13,552	-78			

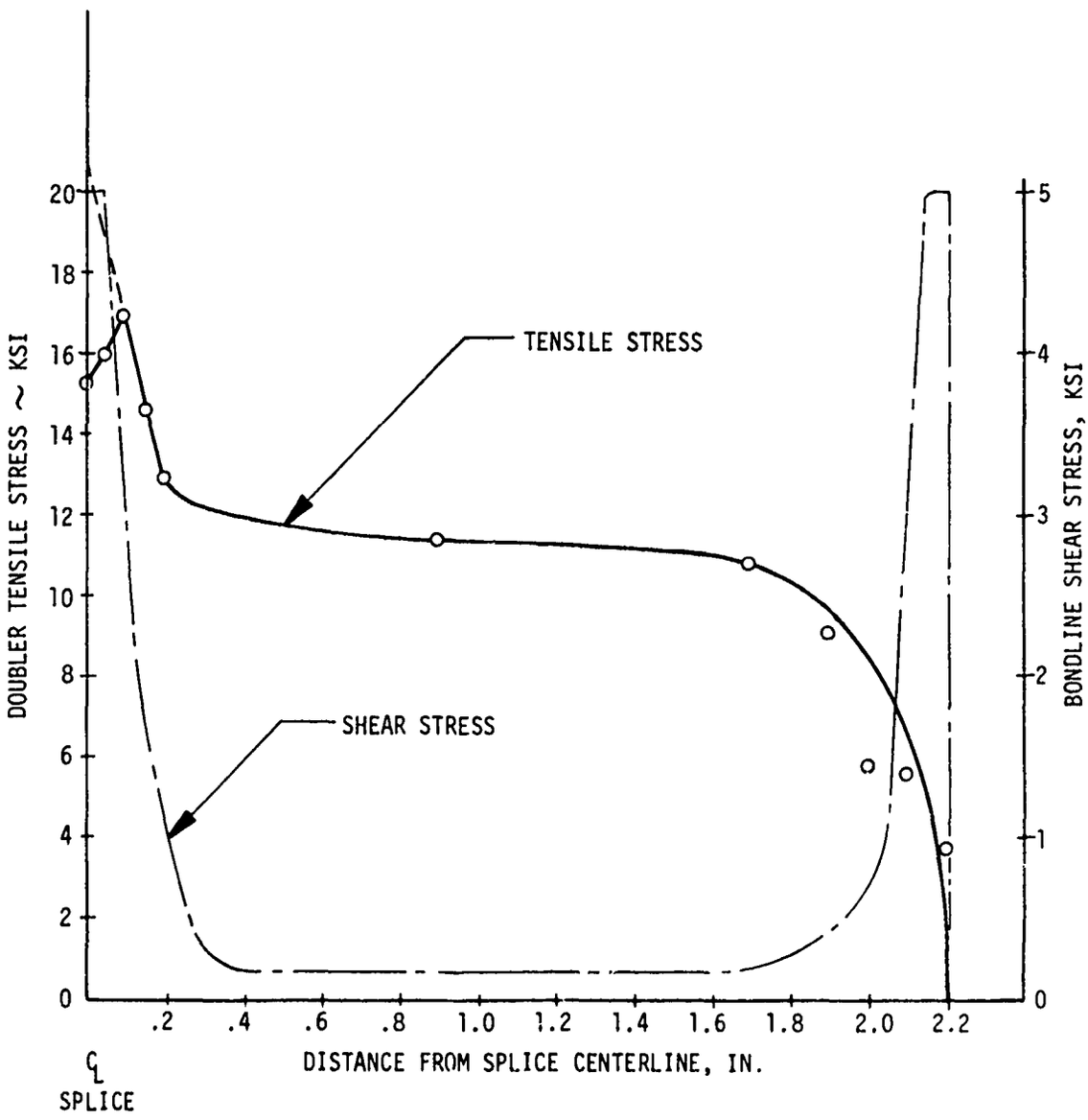


FIGURE 91. STRESS DISTRIBUTION IN THE BOND AND DOUBLER OF THE PANEL 4B CENTERLINE SPLICE

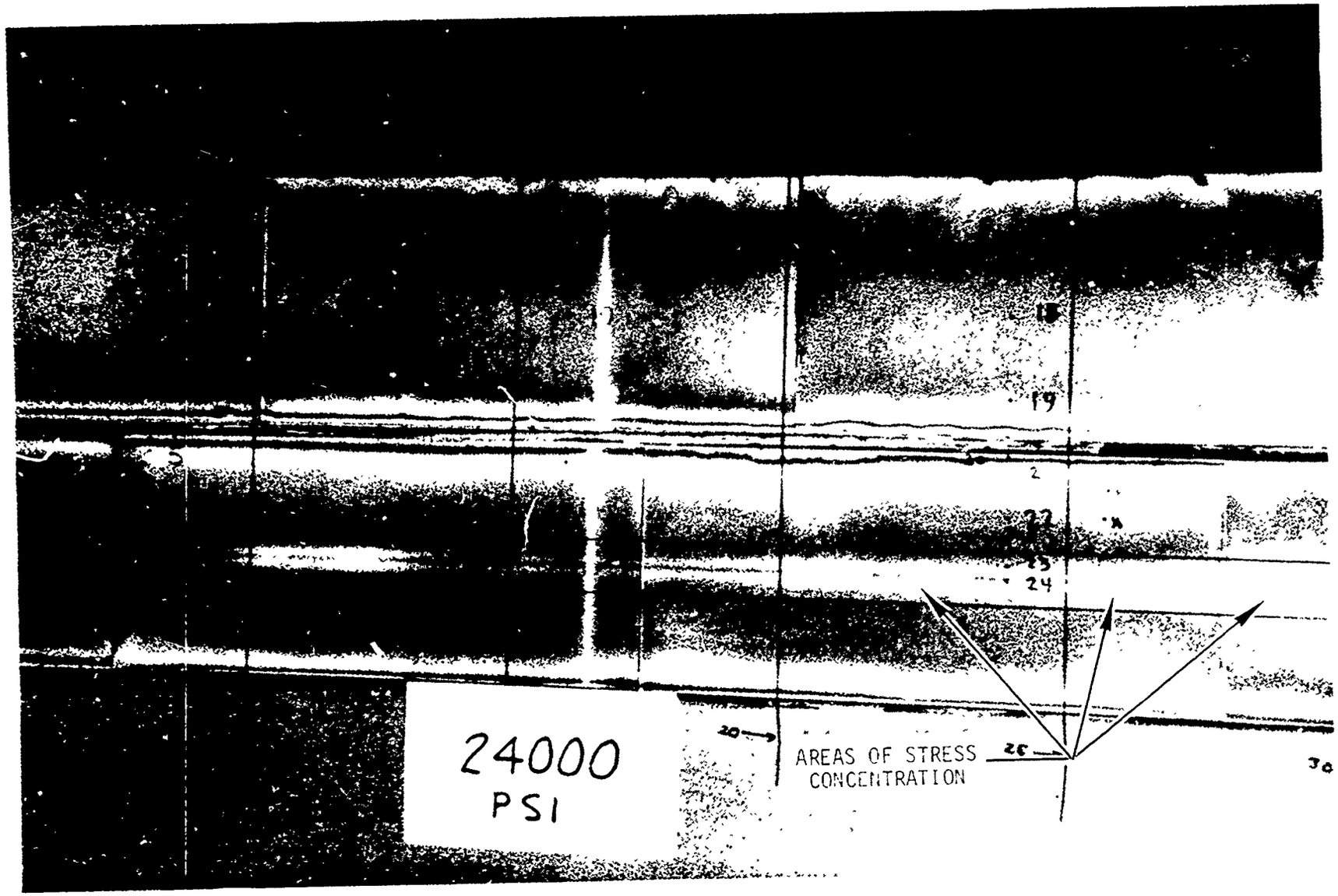


FIGURE 92 PHOTO STRESS FRINGE PATTERN AT CENTERLINE SKIN SPLICE - 24,000 PSI GROSS SKIN STRESS

The panel failed after 452,340 cycles; i.e., 52,340 cycles into the 24,000 psi load level. The failure originated at the corner of the lower tapered splice. There was evidence of fatigue crack for approximately 0.8 in. from the edge. The rest was static failure. This was confirmed by electron microscope fractographic examination.

Fatigue Test of Bonded Single Lap Splice. - This test was conducted to determine the fatigue life of a bonded, single lap, hoop splice under varying fatigue cycle loads at both elevated (140°F) and room temperatures, Specimen 3. The location and mode of failure, crack propagation, and the load redistribution in the panel due to metal or adhesive creep were also test objectives.

The test specimen details are shown in Figure 93. The significant features of the design are:

(1) 7075-T6, .09 in. bare sheet skins,
(2) 7075-T6, .125 in. bare sheet doublers,
(3) 7075-T6, bare sheet skin splice tapered from .125 in. to .040 in. at the edges,
(4) 7075-T6 extrusion longerons.

The skins, doublers, longerons and splice were bonded using BR 127 adhesive primer and FM-73 adhesive. The assembly was ultrasonically inspected prior to testing.

The test loads are shown in Table 27.

TABLE 27

SPECIMEN 3 TEST LOADS

LOAD NO.	MAX LOAD KIPS	MIN LOAD KIPS	MAX STRESS KIPS	SPECIMEN TEMP. °F	CYCLE RATE	NUMBER OF CYCLES
1	41.9	2.13	16.0	144	3 Hz	100,000
2	62.8	3.20	24.0	R.T.	3 Hz	33,400*

* Panel failure occurred at 33,400 cycles at maximum load.

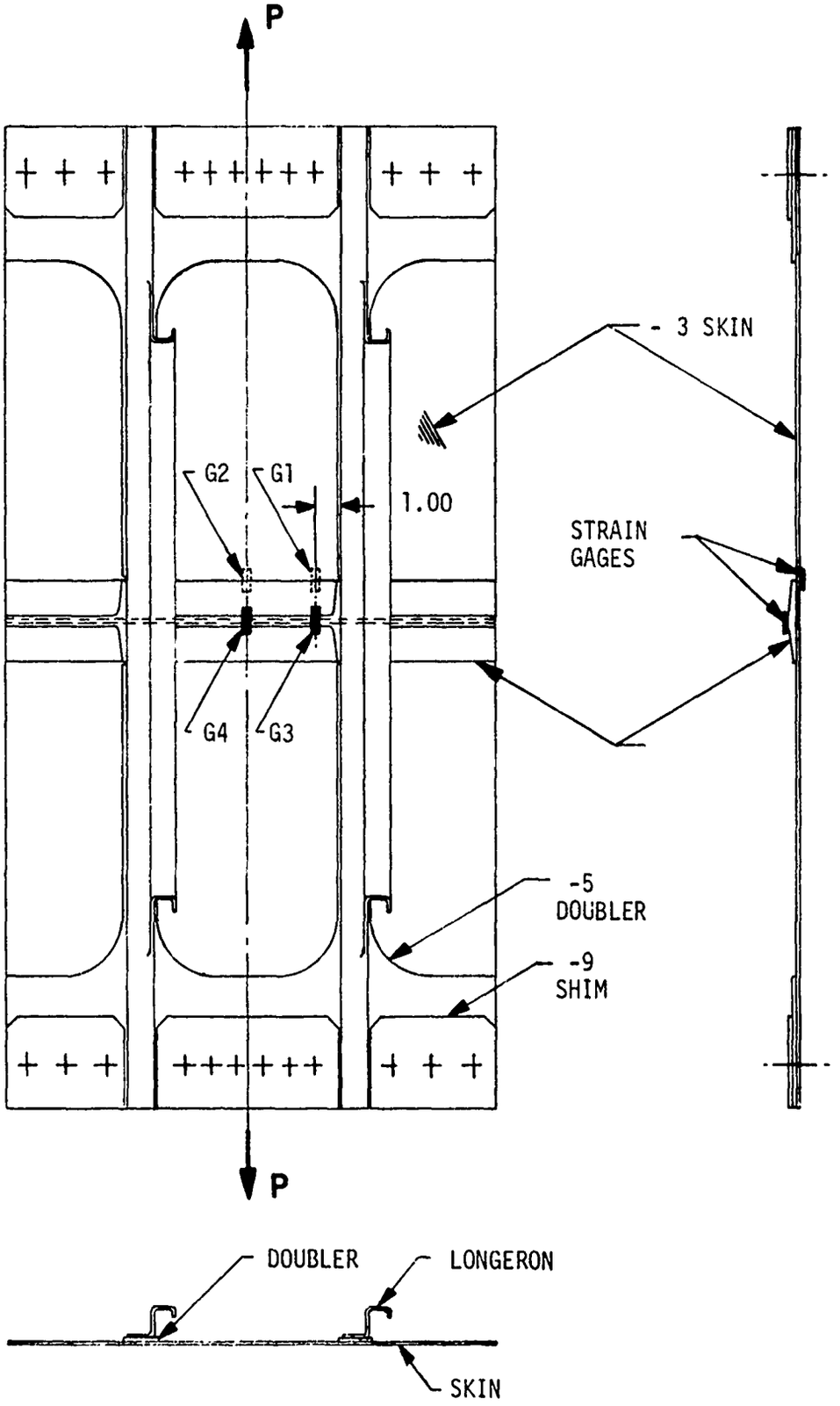


FIGURE 93. ADHESIVE BONDED,SINGLE LAP, HOOP SPLICE SPECIMEN

Static loads of 41,900 lbs. and 62,800 lbs. were applied and held for as long as 4 hours and 140°F to determine stress redistribution due to adhesive creep. Four strain gages were installed on the panel as shown in Figure 93. Not shown are seven thermocouples used to monitor the temperature. Creep data was recorded prior to fatigue testing. Table 28 shows the stresses at each gage location as a function of load at 140°F.

TABLE 28

STRAIN GAGE DATA PRIOR TO FATIGUE TESTING

LOAD ~KIPS	GAGE-G1 STRESS-KSI	GAGE-G2 STRESS-KSI	GAGE-G3 STRESS-KSI	GAGE-G4 STRESS-KSI
0	0	0	0	0
10.5	2.62	2.20	-0.77	-2.71
20.9	5.19	4.04	-1.32	-4.85
31.4	7.75	5.81	-1.71	-6.56
41.9	10.33	7.60	-1.94	-7.90
0	0.00	0.00	0.01	0.00

Temperature +140°F

The load was held at 41,900 lbs. for one hour, the strain gage data being recorded at 10 min. intervals. The load redistribution in the panel is shown in Table 29.

TABLE 29

CHANGE IN STRAIN GAGE DATA

TIME MIN.	GAGE-G1 ΔSTRESS-KSI	GAGE-G2 ΔSTRESS-KSI	GAGE-G3 ΔSTRESS-KSI	GAGE-G4 ΔSTRESS-KSI
0	0	0	0	0
10	-0.06	-0.11	-0.24	-0.43
20	-0.08	-0.13	-0.33	-0.58
30	-0.08	-0.16	-0.39	-0.68
40	-0.10	-0.17	-0.43	-0.75
50	-0.10	-0.19	-0.47	-0.80
60	-0.10	-0.20	-0.48	-0.84

Load held at 41.9 KIPS (16 KSI Stress) and at 140°F. (Load held at 41.9K to determine load redistribution in panel due to creep).

It should be noted that the Z stiffeners are bonded to the panel for their entire length with no mechanical fasteners used. However, the important point is that strain gages are sensitive to load redistribution because of bondline creep. Table 30 shows the strain gage data taken at room temperature up to a load of 62,800 lbs.

TABLE 30

STRAIN GAGE DATA PRIOR TO FATIGUE TESTING - R.T. (80°F)

LOAD -KIPS	GAGE-G1 STRESS-KSI	GAGE-G2 STRESS-KSI	GAGE-G3 STRESS-KSI	GAGE-G4 STRESS-KSI
0	0	0	0	0
10.5	2.54	2.00	-0.60	-2.29
20.9	5.08	3.81	-0.97	-4.03
31.4	7.63	5.59	-1.19	-5.43
41.9	10.19	7.41	-1.28	-6.51
52.3	12.70	9.16	-1.39	-7.57
62.8	15.25	11.01	-1.52	-8.46

This maximum load was held and changes in the four gages recorded as shown in Table 31, indicating bondline creep even at room temperature.

TABLE 31

CHANGE IN STRAIN GAGE DATA AT 62.8 KIPS CONSTANT LOAD

TIME MIN.	GAGE-G1 ΔSTRESS-KSI	GAGE-G2 ΔSTRESS-KSI	GAGE-G3 ΔSTRESS-KSI	GAGE-G4 ΔSTRESS-KSI
0	0	0	0	0
10	-0.02	-0.06	-0.05	-0.30
20	-0.03	-0.09	-0.13	-0.45
30	-0.04	-0.10	-0.17	-0.53
40	-0.06	-0.13	-0.21	-0.60
50	-0.04	-0.11	-0.21	-0.63
60	-0.03	-0.11	-0.23	-0.66

24.0 KSI stress at R.T. before start of fatigue cycling. Load held at 62.8 KIPS to determine load redistribution due to creep.

During the 41,900 lb. maximum fatigue load (16 KSI stress) cycle testing strain gage readings were taken before the cycling began, after 42,600 cycles, and after 100,000 cycles. This data is shown in Table 32.

TABLE 32

STRAIN GAGE DATA FOR THE 41.9 KIPS FATIGUE TEST

LOAD KIPS	GAGE-G1 KSI	GAGE-G2 KSI	GAGE-G3 KSI	GAGE-G4 KSI	REMARKS
0	0	0	0	0	
10.5	2.71	2.71	-0.88	-2.99	Readings taken just
20.9	5.30	4.10	-1.46	-5.26	prior to start of
31.4	7.88	5.89	-1.87	-7.09	fatigue cycling at 140°F
41.9	10.46	7.67	-2.13	-8.48	
41.9	10.21	6.82	-2.92	-10.28	Readings taken after
1.4	7.76	5.13	-2.52	-8.53	42,600 fatigue cycles
20.9	5.16	3.47	-1.90	-6.18	at 140°F
10.5	2.56	1.83	-0.98	-3.04	
0	-0.17	-0.22	0.17	0.58	
0	0	0	0	0	
10.5	2.67	1.95	-1.21	-3.62	Readings taken after
20.9	5.18	3.47	-1.99	-6.38	100,000 fatigue cycles
31.4	7.72	5.01	-2.45	-8.33	at 140°F
41.9	10.24	6.64	-2.65	-9.67	
0	-0.01	-0.02	-0.01	0.00	

Table 33 shows the change in strain gage readings, with the load held at 41,900 lbs (16 KSI) and the temperature at 140°F, to determine load redistribution due to adhesive creep after 100,000 fatigue load cycles.

TABLE 33

CHANGE IN STRAIN GAGE DATA FOR 41.9 KIPS CONSTANT LOAD

TIME MIN.	GAGE-G1 STRESS-KSI	GAGE-G2 STRESS-KSI	GAGE-G3 STRESS-KSI	GAGE-G4 STRESS-KSI
0	0	0	0	0
20	-0.04	-0.07	-0.02	-0.06
40	-0.02	-0.06	-0.05	-0.10
60	-0.15	-0.19	+0.07	+0.02
80	-0.39	-0.46	+0.32	+0.27

Table 34 then indicates the change in strain gage readings recorded, with the load held at 62,800 lbs. (24 KSI) and ambient temperature, to determine load redistribution due to creep at the higher load.

TABLE 34

CHANGE IN STRAIN GAGE DATA AT 62.8 KIPS DUE TO CREEP AT ROOM TEMPERATURE

TIME HOURS	LOAD KIPS	GAGE-G1 ΔSTRESS-KSI	GAGE-G2 ΔSTRESS-KSI	GAGE-G3 ΔSTRESS-KSI	GAGE-G4 ΔSTRESS-KSI
0	62.8	0	0	0	0
1/2	62.8	-0.04	-0.07	0.00	0.05
1	62.8	-0.06	-0.10	0.01	0.05
1-1/2	62.8	-0.07	-0.11	0.02	0.06
2	62.8	-0.09	-0.13	0.03	0.05
2-1/2	62.8	-0.12	-0.17	0.06	0.03
3	62.8	-0.14	-0.18	0.07	0.02
3-1/2	62.8	-0.19	-0.24	0.08	0.01
4	62.8	-0.22	-0.27	0.11	0.01

Table 35 shows the strain gage data recorded during the 62.8KIPS (24 KSI) fatigue cycle testing. Readings were taken at zero cycles, 10,000, 20,000 and 30,000 cycles. Panel failure occurred at 33,400 cycles.

TABLE 35

STRAIN GAGE DATA FOR THE 62.8 KIP FATIGUE CYCLES AT R.T.

LOAD KIPS	GAGE-G1 KSI	GAGE-G2 KSI	GAGE-G3 KSI	GAGE-G4 KSI	REMARKS
62.8	15.23	9.91	-2.05	-10.92	Readings taken before start of fatigue cycling
62.8	15.33	9.86	-1.41	-9.81	Readings taken after 10,000 fatigue cycles
62.8	15.23	9.72	-0.70	-9.09	Readings taken after 20,000 fatigue cycles
62.8	15.22	9.67	-0.10	-8.48	Readings taken after 30,000 fatigue cycles

Panel failure occurred at 33,400 cycles.

The panel failed after experiencing 100,000 cycles at σmax = 16,000 psi and 140°F and 33,400 cycles at σmax = 24,000 psi and room temperature. The failure initiated on the faying surface side of the .125 in. thick splice doubler approximately 4 in. from the edge of the panel. The location of the failure in the splice doubler is shown in Figure 94 and the fracture face at the fatigue origin is shown in Figure 95. Analysis of this panel predicted both the high peel stresses and the high bending stresses in the splice plate because of the eccentricity in load path.

A striation count of the fatigue origin indicated approximately 35,500 cycles of crack growth prior to failure. This number corresponds to the number of cycles at σmax = 24,000 psi. It is therefore conjectured that the fatigue crack initiated during cycling at σmax = 24,000 psi.

There was some evidence of bond delamination, adjacent to the skin junction, by visual observation during the test. The extent of this delamination was measured with the aid of dye penetrant and then prying the skin and splice doubler apart. The extent of the disbond can be seen in the dark areas in Figure 96.

One Bay Crack Growth Time History Specimen N30A . - This internal longeron concept test was conducted to obtain crack propagation data and verify that the initial flaw does not attain critical length in two lifetimes (38,028 cycles) or that a two inch crack does not attain critical length in two depot inspection periods (9,807 cycles); and verify analysis methods.

Figure 97 shows the panel geometry and strain gage and failure locations. The panel and splice doublers were of 7475-T761 bare aluminum sheet. The frames and longerons were of 7075-T6 aluminum. The panel was installed in the 1.5 million pound testing towers and cycled at approximately 1 Hz. The applied stress was 17,800 psi with a R ratio of 0.05.

Table 36 records the strain gage readings at the maximum applied stress. Failures 3-10 were skin cracks at the ends of the shear tee cutouts for the longeron as shown in Figure 97. At 36,803 cycles, cracks 6, 8 and 10 joined to precipitate failure of the panel.

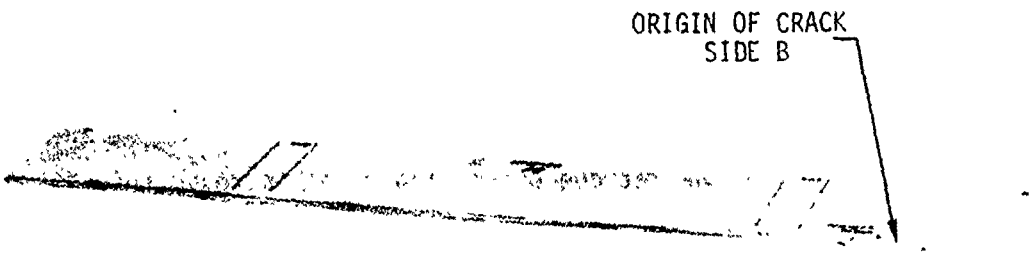


FIGURE 94. CRACK ORIGIN IN SKIN SPLICE

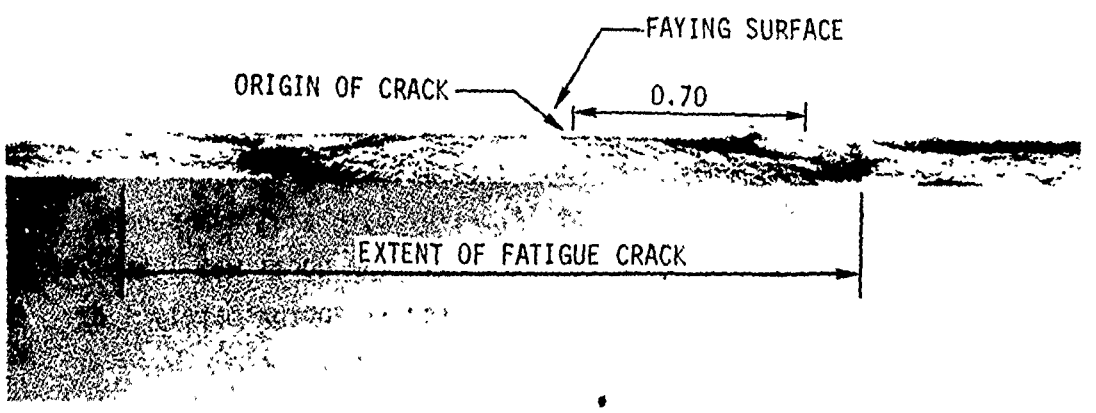


FIGURE 95. STABLE CRACK REGION IN SKIN SPLICE



FIGURE 96. SEPARATED SKIN AND SPLICE SHOWING DEPTH OF DELAMINATION

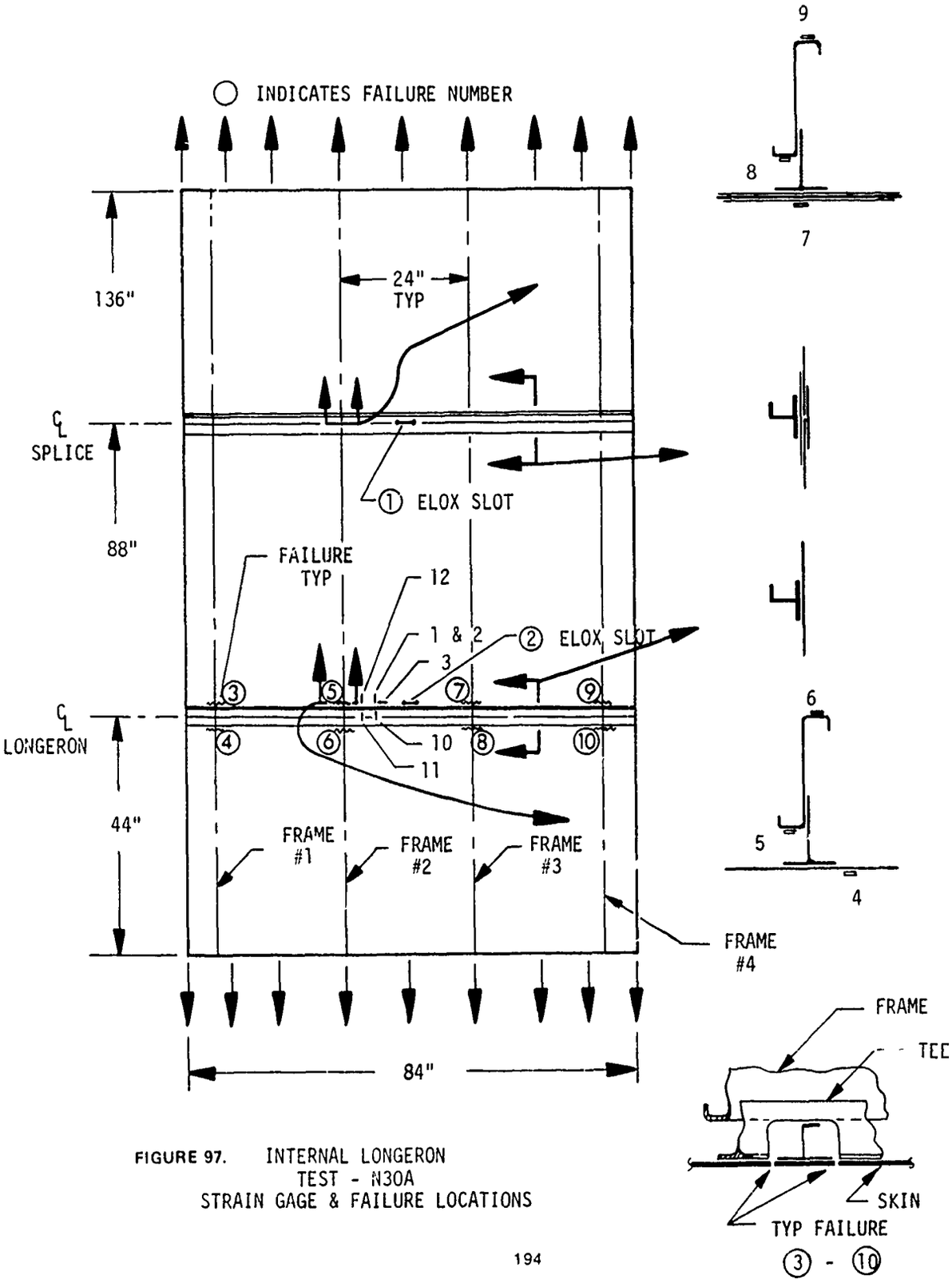


FIGURE 97. INTERNAL LONGERON
TEST - N30A
STRAIN GAGE & FAILURE LOCATIONS

TABLE 36

N30A STRAIN GAGE READINGS TAKEN AT 12,000 CYCLES

STRAIN GAGE NUMBER	STRESS PSI
1	23,500
2	11,250
3	4,250
4	13,375
5	16,000
6	21,000
7	16,750
8	17,750
9	21,500
10	18,250
11	19,000
12	12,000

As a result of this type of failure, engineering design changes were incorporated in the remaining internal longeron concept flat panel specimens to bridge the gaps in the shear tees at the longeron cutout. Crack lengths for the failures noted in Figure 97 are tabled vs cycles in Table 37. Figure 98 is a sketch of the failure of the panel.

TABLE 37

N30A Crack Length vs Cycles

Total Crack Length - Inches

	FAILURE NUMBER									
CYCLES	1	2	3	4	5	6	7	8	9	10
0	.2	.2								
3,000	.2	.2								
6,000	.2	.2								
9,000	.2	.2								
12,000	.2	.2								
15,000	.2	.405								
18,000	.2	.530								
21,000	.2	.660								
24,001	.2	.779								
27,000	.2	1.005								
30,000	.2	1.240								
31,370	.2					4.25				
32,370	.2					4.97				
33,191	.2	1.580								
33,370	.2					6.10				
34,100	.2	1.750								
34,370	.2					7.70				
35,070	.2	1.870					2.29	2.51	1.23	2.00
35,370	.2	2.050				10.20				
36,016	.2	2.050					2.50	2.75	1.32	2.31
36,370	.2					14.10				
36,800	.2					21.80				
36,803	.2	2.78*	1.12*	2.50*	**	28.50*	2.63*	3.18*	1.13*	1.46*

Cracks 6, 8, and 10 joined to precipitate failure of the panel.

* Readings taken after failure

** Undetected visually after failure

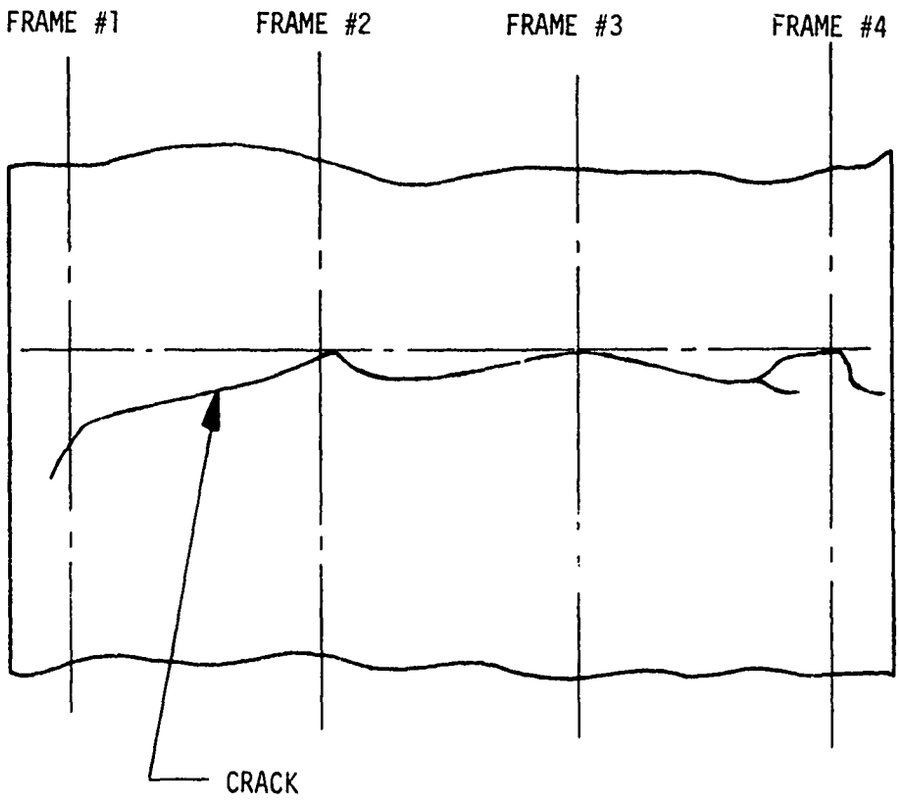


FIGURE 98. PANEL N30A FAILURE

Crack Propagation and Residual Strength Test N30AB-1 - Two tests were conducted on the N30AB panel which represented the internal longeron concept. The purpose of the first test was to establish the adequacy of the modification to the frame-longeron intersection area to retard crack growth in the skin. The N30A panel previously discussed developed fatigue cracks in the skin at the frame-tee discontinuity which ultimately led to failure. In addition, the N30AB panel was tested to demonstrate fail safety for foreign object damage.

The test panel consisted of 108 in. wide skin panel stiffened by 5 equally spaced frames 24 in. apart. The panel was 144 in. long. At its midpoint there was a longeron which intersected the frames creating 10 frame-tee discontinuity areas. The panel is shown in Figure 99. Each of the frame-tee discontinuities was reinforced by a cold bonded strap which bridged the gap in the skin between the frame-tee flange and the longeron flange. This is also illustrated in Figure 99. A 0.29 in. slot was sawcut in the skin between two adjacent reinforcing straps. This slot lies in the narrow piece of skin bounded by the longeron and frame tee-flanges in the vertical direction and the two reinforcing straps in the lateral direction. The slot was centered at the frame tee centerline of the middle frame.

The test loads were:

σ_{max} = 17,795 PSI , P_{max} = 148,944 Lbs

R = 0.05 P_{min} = 7,449 Lbs

The cycling rate was approximately 1 Hz.

The specimen was cycled at the above loads for 37,208 cycles. The crack length was measured and strain gage data recorded periodically. At 37,208 cycles, the crack length had reached the objective of 15 inches, approximately 7 1/2 inches on each side of the frame. The crack growth time history data is plotted in Figure 100, and summarized in Table 38. The strain gage data shows that there was little or no change in the value of the skin stress until the crack tip grew to within 5 inches of the strain gages. This completed the crack growth phase of the test.

Note: Strain gages 1 through 6 are located as shown. Strain gages 1 and 2 are back to back.

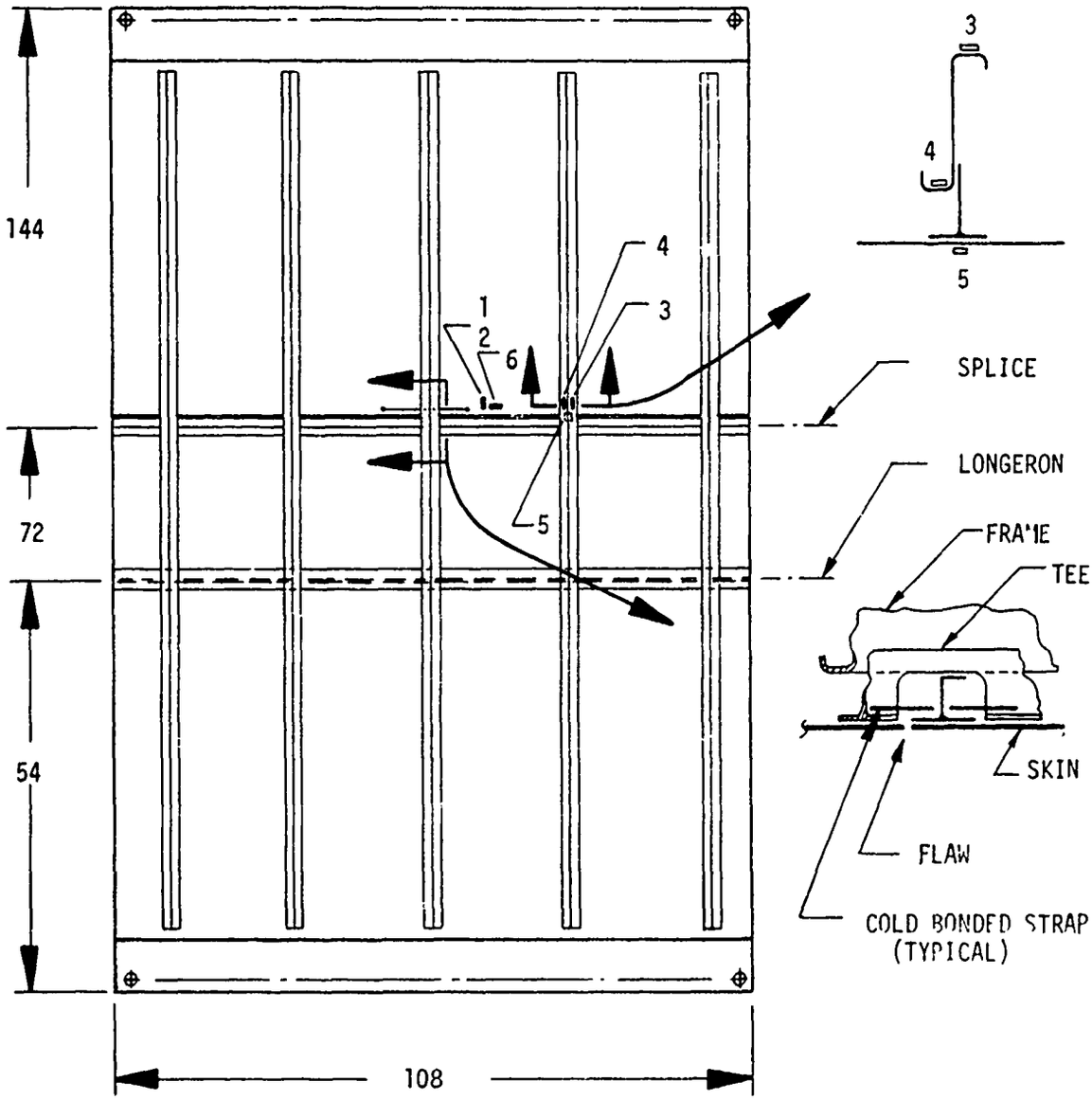


FIGURE 99. TEST SPECIMEN N30AB

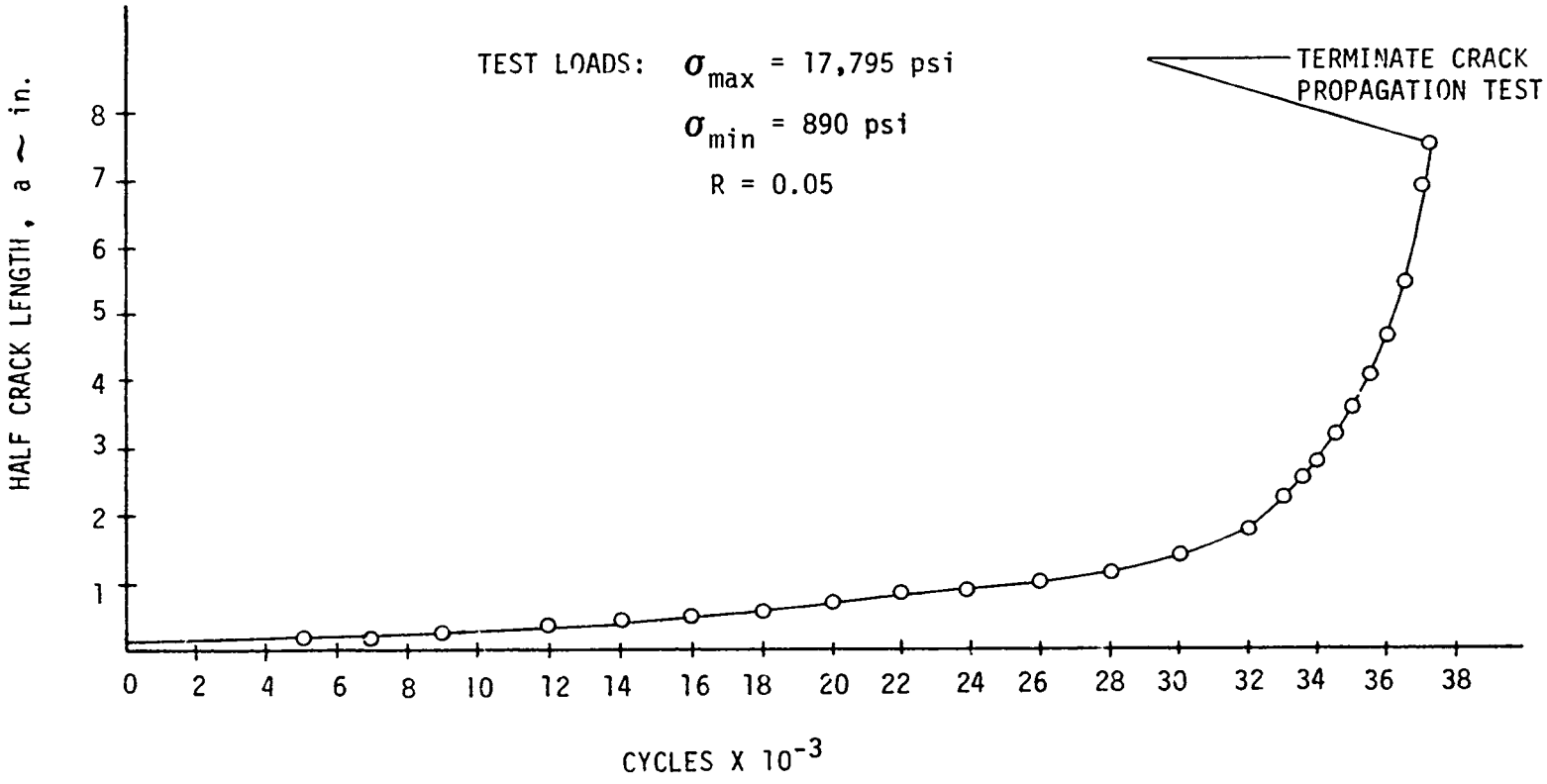


FIGURE 100. CRACK GROWTH TIME HISTORY - N30AB

TABLE 38

Summary of Crack Growth and Strain Gage Data

Cycle No.	Flaw Length In.	STRAIN GAGE DATA @ MAX. LOAD ~ PSI					
		1	2	3	4	5	6
0	.290	24,000	11,100	17,700	17,600	24,800	-5,100
4,000	Crack Growth Starts	24,400	11,450	18,500	18,400	25,500	-5,400
6,000	.36	24,500	12,000	18,650	18,600	25,000	-5,250
12,000	.71	24,600	12,500	18,400	18,500	23,400	-5,000
16,000	.98	24,600	10,900	17,500	18,000	25,000	-5,100
20,000	1.39	24,000	10,600	17,500	18,200	25,200	-5,100
24,000	1.85	23,700	10,600	17,900	17,750	25,000	-5,350
28,000	2.36	24,800	10,900	17,000	18,000	24,800	-5,000
32,000	3.60	24,000	11,000	17,000	18,100	24,800	-4,800
34,000	5.53	24,000	11,000	17,000	18,500	25,000	-4,650
36,000	9.28	25,200	11,000	17,000	17,900	25,000	-4,400
37,000	13.66	29,800	11,900	17,900	18,400	26,200	-2,250
37,208	15.06	30,000	11,800	18,000	19,000	26,200	-1,000

The second phase of the test was residual strength for foreign object penetration. This damage consisted of a 15-inch skin crack with the center frame broken. The skin crack size had been achieved during the crack propagation phase. The frame was sawcut, at the longeron-frame intersection, above the skin crack to simulate the foreign object penetration. The fail safe load was applied and sustained. This load was:

$$\sigma_{max} = 18{,}400 \text{ PSI} \quad \text{or} \quad P_{max} = 153{,}770 \text{ Lbs.}$$

The load was applied in 10% increments with a loading rate of 15,000 Lb/Min. At 100% fail safe load the panel fast fractured and arrested at the two adjacent frames. The load was dumped automatically. On reapplication of the fail safe load, the panel failed at 154,000 Lbs.

The crack configuration at arrest is shown in Figure 101. The residual strength diagram with the test points is shown in Figure 102.

Curved Panel Biaxial Fatigue and Damage Tolerance Test, Specimen N21.
This test of the internal longeron concept was conducted to determine the effect of biaxial stress on fatigue and damage tolerance. Testing was accomplished in the following order:

(1) Fatigue test for two lifetimes (38,028 pressure cycles),
(2) Crack propagation tests for two additional lifetimes. The flaws to be created at the specified locations by saw cutting,
(3) Residual strength tests under the following conditions:
    (i) Two bay longitudinal crack with the center frame intact,
    (ii) Foreign object damage (15" sawcut) with outer frame broken.

The load cycle was as shown in Figure 103 with the hoop and longitudinal loads being applied symmetrically.

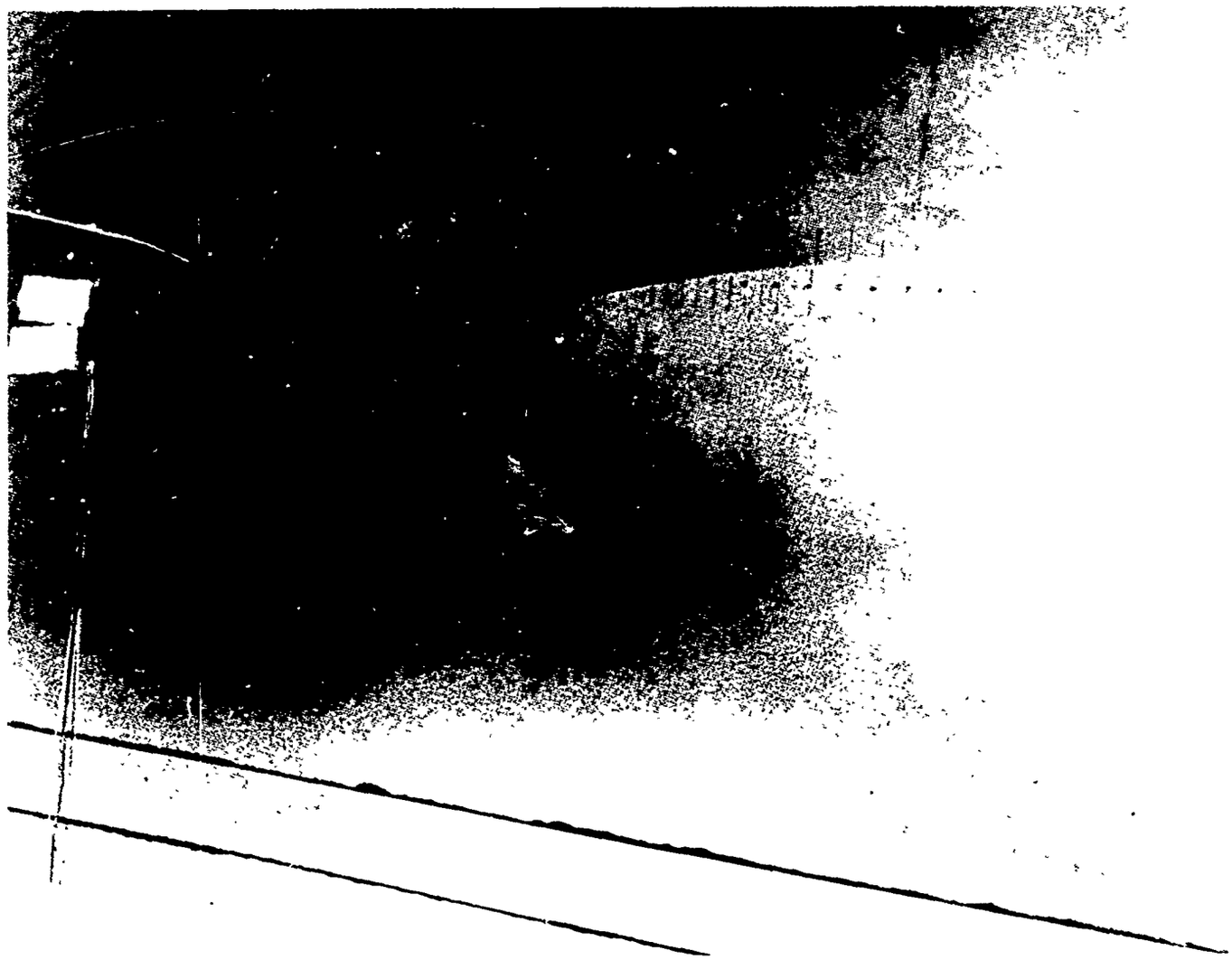


FIGURE 101. CRACK CONFIGURATION AFTER FAST FRACTURE AND ARREST

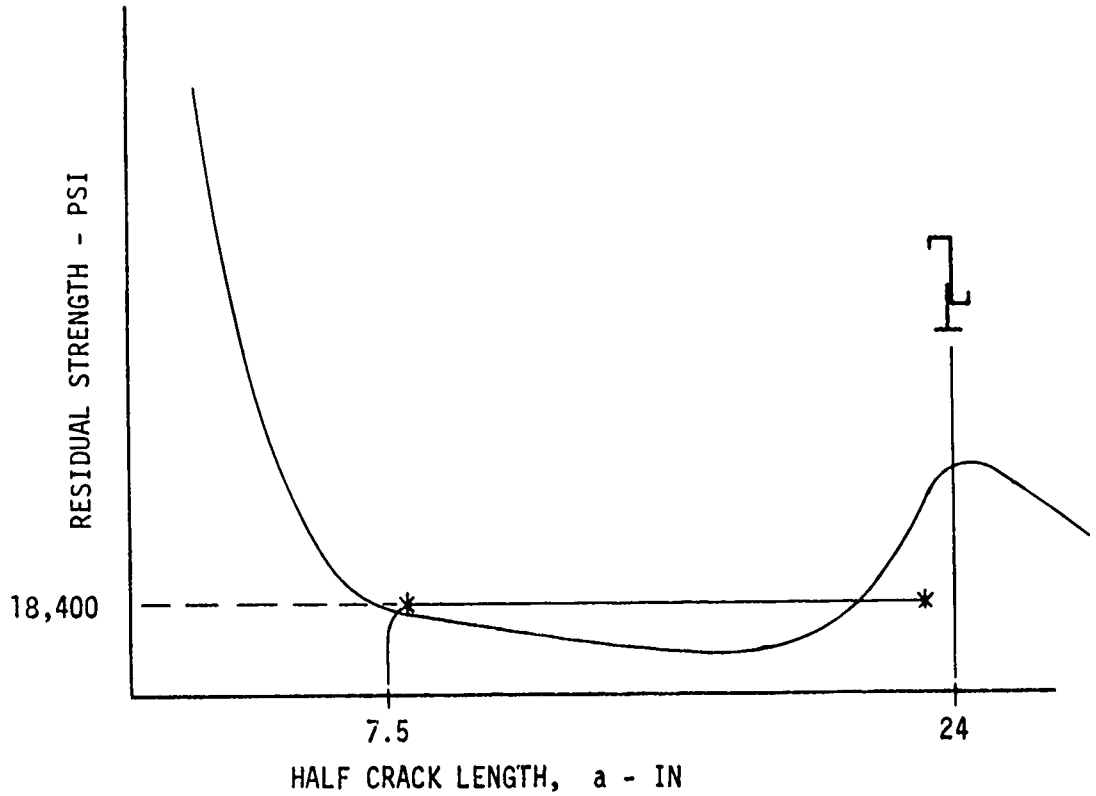
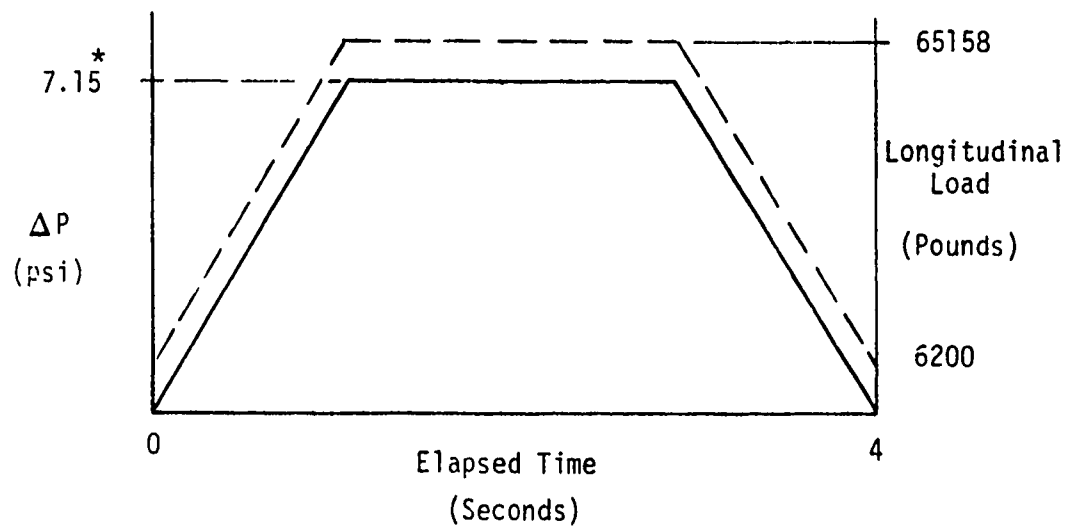


FIGURE 102. RESIDUAL STRENGTH DIAGRAM - FOREIGN OBJECT DAMAGE



*NOTE: 8.6 psi was required in the test to achieve the correct load.

FIGURE 103. LOAD CYCLE SCHEMATIC

The internal pressure loads were applied by suction on the upper surface such that atmospheric pressure on the inside surface created the required ΔP across the panel. The longitudinal loads were applied by servo controlled hydraulic actuators. The two systems were synchronized such that they achieved their peak values and decay simultaneously.

The pressure loads were reacted through a system of whiffle trees, the reactions being measured by load cells. On application of $\Delta P = 7.15$ psi it was found that the total reaction load was well below the 116,000 Lbs. desired. The ΔP value was increased to 8.6 psi at which the 116,000 Lbs. reaction load was achieved. This was then the load at which the panel was cycled.

Figure 104 shows the underside of the panel installed in the test fixture. The longitudinal and transverse whiffle-trees are shown. It should be noted that the frame loads are whiffled directly to the frames. A sketch of the panel, Figure 98, shows the locations of the damage tolerance (DT) flaws, the residual strength (RS) saw cuts, and the strain gages.

The fatigue test consisted of 38,028 load cycles. During this test there were no fatigue cracks generated in the participating structure. Subsequent to this, after the damage tolerance flaws were introduced, an additional 38,028 cycles were applied. Other than the propagation of the damage tolerance flaws, again no fatigue cracks were encountered in the participating structure. After the residual strength tests, an additional 37,000 cycles, almost two lifetimes, were imposed on the specimen and still no fatigue failures. The specimen was therefore subjected to a total of almost six lifetimes without experiencing any fatigue failures.

The damage tolerance flaws were introduced by sawcutting as shown in Figure 105. The damage tolerance flaws are shown circled as DT1 through DT6. Strain gage locations are shown with circled numbers from 1 through 16. Flaws DT5 and DT6 did not grow at all during the entire test. The flaw at the edge of the fastener hole indicated in Figure 105, also did

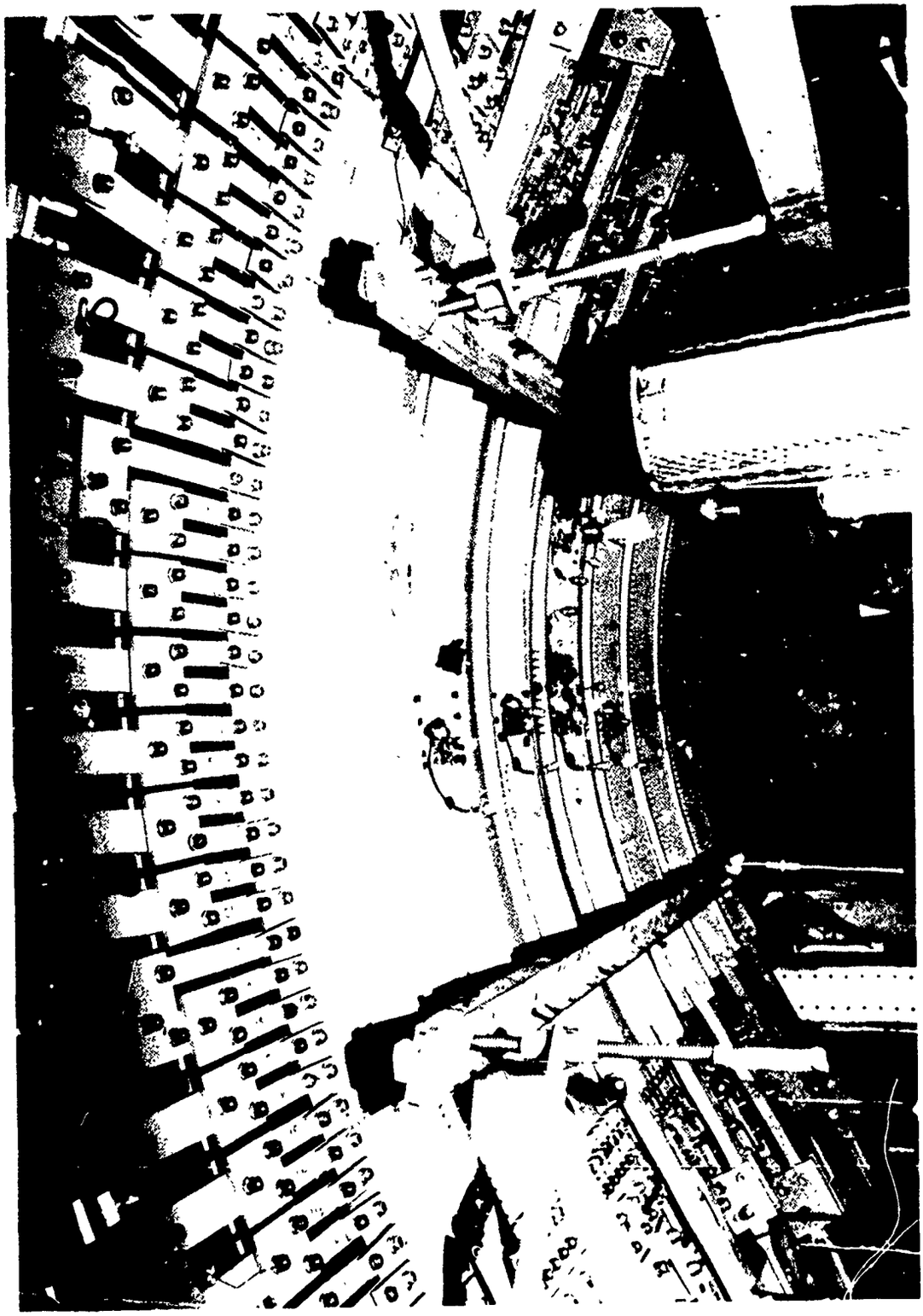
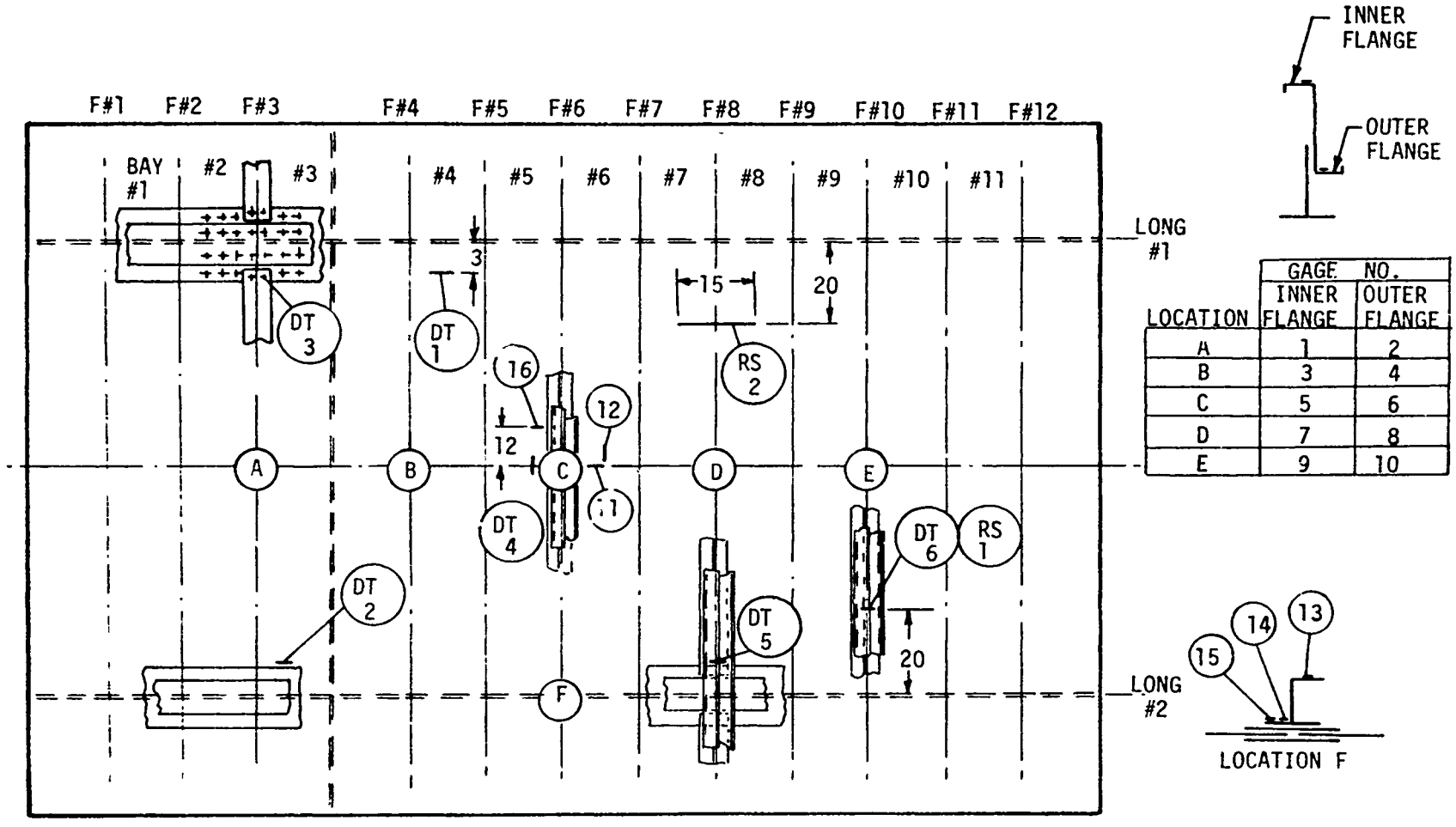


FIGURE 104. UNDERSIDE VIEW OF TEST PANEL N21



LOCATION	GAGE NO. INNER FLANGE	GAGE NO. OUTER FLANGE
A	1	2
B	3	4
C	5	6
D	7	8
E	9	10

FIGURE 105. LOCATION OF INITIAL FLAWS, RESIDUAL STRENGTH SAWCUTS, AND STRAIN GAGES - N21

not grow. This flaw was monitored periodically by X-rays during the test with no evidence of growth. The other three flaws DT1, DT2 and DT3 evidenced rates of growth as detailed in Table 39 .

TABLE 39

Damage Tolerance Flaw Growth Time Histories

NO. OF CYCLES	TOTAL CRACK LENGTH			STRAIN GAGE READINGS			ΔP PSI
	DT1	DT2	DT4	STR.GAGE # 11	STR.GAGE # 12	STR.GAGE # 16	
0	.221	.250	.250				
9,000	.221	.270	.250	12,483	9,739	17,390	8.894
12,000	.328	.270	.500	11,805	8,938	17,081	8.679
14,825	.328	.270	.540	11,990	9,061	16,895	8.679
18,000	.410	.280	.720	12,298	9,493	16,957	8.691
24,000	.450	.280	.850	11,681	8,692	16,895	8.631
28,000	.510	.280	1.15	11,866	8,815	16,772	8.571
29,000	.560	.330	1.25				
32,000	.660	.330	1.61				
34,000	.670	.430	1.93	12,914	8,912	17,673	8.667
38,030	.91	.50	1.95				
42,030			2.56				
44,530		.65	2.80	11,281	9,031	16,957	8.613
47,530			3.05	10,849	9,697	16,338	8.649
49,530	1.58		3.20				
51,530			3.43	11,897	8,987	17,081	8.517
54,030	1.75		3.72				
57,465			4.21				
59,530	2.82	1.12*	4.63				

*C

Crack from west end of initial sawcut entered skin splice bondline

TABLE 39 (CONTINUED)

Damage Tolerance Flaw Growth Time Histories

NO. OF CYCLES	TOTAL CRACK LENGTH			STRAIN GAGE READINGS, PSI		
	DT1	DT2	DT4	STR.GAGE # 11	STR.GAGE # 12	STR.GAGE # 16
60,570	2.97		4.88			
62,405	3.17	1.22	5.44			
64,030	3.75	1.30	5.94	12,575	9,123	17,270 8,565
64,530	3.88	1.55	6.15			
66,030	4.41	1.55	7.1**			
70,130			8.6			
70,000			8.95			
70,530			9.43			
70,780			9.91			
71,030			10.40			
71,200			10.80	11,897	9,000	17,019 8,514
71,590			11.10			
74,480		2.30				
74,805		2.45		11,959	9,431	16,833 8,433

** Crack had stopped at a rivet hole on the North side of the original sawcut.

The residual strength testing was accomplished in the following manner: (1) The flaw DT6, skin was sawcut beyond the frame tee flange for a total length of 18 in. This flaw was renamed RS1. Approximately 40 cycles at ΔP = 5 psi were applied to sharpen the sawcut tip with a small but visible fatigue crack at each tip. Fail safe load was then applied. The fail safe load is ΔP = 7.15 psi (hoop reaction load = 116,000 Lb.)***
Longitudinal load = 114,500 Lb.

*** NOTE: An 8.6 PSI test pressure was required to obtain this load.

The loading sequence was to pressurize to full ΔP and then increase the longitudinal load from zero to 114,500 lb. Note that the sequence of load application was to achieve full ΔP first and then apply the longitudinal load in increments. No flaw growth was noted on application of the pressure loading. However, on application of the longitudinal load, the crack tip turned 90° and grew in the circumferential direction to a total length of 0.65 in. The crack was approximately evenly centered about the original crack. This phenomenon was observed only on the west side crack tip. No failure was encountered for flaw length of 18 in.

The next step was to sawcut an additional one inch at each tip, to a total length of 20 in. The crack was sharpened by cycling at ΔP = 5 PSI and then the fail safe load was applied. On application of the longitudinal load in the fail safe load sequence, the crack grew circumferentially .52 in. at the west tip only. This was at the newly establish crack tip. Again, no failure was encountered. The sawcut was finally extended to 22 in. to the edge of both frame tee flanges. On application of the longitudinal load of the fail-safe loading sequence, both the crack tips propagated into the frame shear tee bondlines and turned circumferentially, in opposite directions. Again, no failure was encountered on application of the fail safe load. The data for this test is shown in Table 40 . A patch repair was installed to permit continued testing.

(2) The next step was the residual strength test RS2, simulating foreign object damage. The location of this damage is shown in Figure 105 . It consisted of a 15 in. sawcut, both through the skin and frame. It was intended that the fail safe load be applied in the same sequence as for RS1. However, at ΔP = 6.9 PSI and zero longitudinal load, the flaw propagated to the adjacent frames and disappeared into the frame tee flange glue lines. The loading sequence was changed to applying the pressure and longitudinal load simultaneously to the peak value and holding the ΔP and relaxing the longitudinal loads in steps. No further failure was encountered. The data is given in Table 41 .

TABLE 40

Residual Strength Test RS1 Data

FLAW LENGTH IN.	ΔP PSI	LONGITUDINAL LOAD POUNDS	STRAIN GAGE DATA - PSI		
			STRAIN GAGE #		
			11	12	16
18.0	8.601	27,000	4,469	11,774	13,058
		68,800	11,928	9,370	17,452
		95,700	16,490	8,075	20,671
		111,000	18,894	7,459	22,527
20.0	8.385	0	0	13,192	11,078
		27,000	4,715	11,466	12,996
		69,500	12,298	9,061	17,514
		97,600	17,044	7,767	20,856
		111,400	19,325	7,089	22,527
22.0	8.433	0	0	12,205	11,635
		24,900	3,945	10,849	13,553
		63,700	10,356	8,876	17,762
		90,000	14,548	7,890	21,042
		117,500	18,516	6,904	24,570

TABLE 41

RESIDUAL STRENGTH TEST RS2 DATA

ΔP PSI	Longitudinal Load Pounds	Strain Gage Data - PSI		
		Strain Gage #		
		11	12	16
0	0	0	0	0
	31,280	5,229	-1,356	4,177
	60,404	10,089	-2,404	8,695
	89,705	14,704	-3,452	13,213
	113,500	18,457	-4,253	16,926
2.260	113,867	19,072	-1,417	20,145
5.036	114,138	18,518	2,465	22,744
7.393	113,957	17,841	5.979	24,848
8.469	114,048	17,411	7,582	25,746
8.230	98,449	15,011	7,767	23,858
8.230	74,738	11,135	8,753	21,320
8.326	46,882	6,152	10,356	18,721
8.326	16,223	- 184	12,205	16,122

One Bay Crack Growth Time History - Specimen H30A - This honeycomb concept test was conducted to:

(1) Obtain crack propagation data and verify that the initial flaw does not attain critical length in two lifetimes (38,028 cycles) or that a two inch crack does not attain critical length in two depot inspection periods (9,507 cycles); and

(2) Verify analysis methods.

Figure 106 shows the panel geometry with strain gage and initial flaw locations. Significant features are that it was made of 2024-T3 bare sheet aluminum honeycomb sandwich panels. The splice doublers were also of bare 2024-T3 sheet. The longitudinal straps were of 7475-T761 aluminum sheet while the frames were made of 7075-T6 aluminum.

The panel was installed in the 1.5 million pound testing towers and cycled at approximately 1 Hz. The applied stress was 15,646 psi with a R ratio of 0.05.

Table 42 records the total crack length versus cycles.

At a total crack length of 13.160 inches with a total of 92,102 cycles, the test was stopped and the panel repaired for further testing.

Residual Strength - Two Bay Crack, Center Stiffener Intact-H30B. - The purpose of this honeycomb concept test was to verify the residual strength of the honeycomb concept for failsafe criteria with a two bay crack in the outer skin, and verify analysis methods.

Figure 107 shows the panel geometry with strain gage and initial flaw locations. The panel was made of 2024-T3 bare sheet aluminum honeycomb sandwich panels. The panel splice doublers were also of bare 2024-T3 sheet. The longitudinal straps were of 7475-T761 bare aluminum sheet and the frames of 7075-T6 aluminum. The panel was loaded to 100,000 pounds in 20,000 pound increments. From 100,000 pounds to failure, the load was increased in 10,000 pound increments.

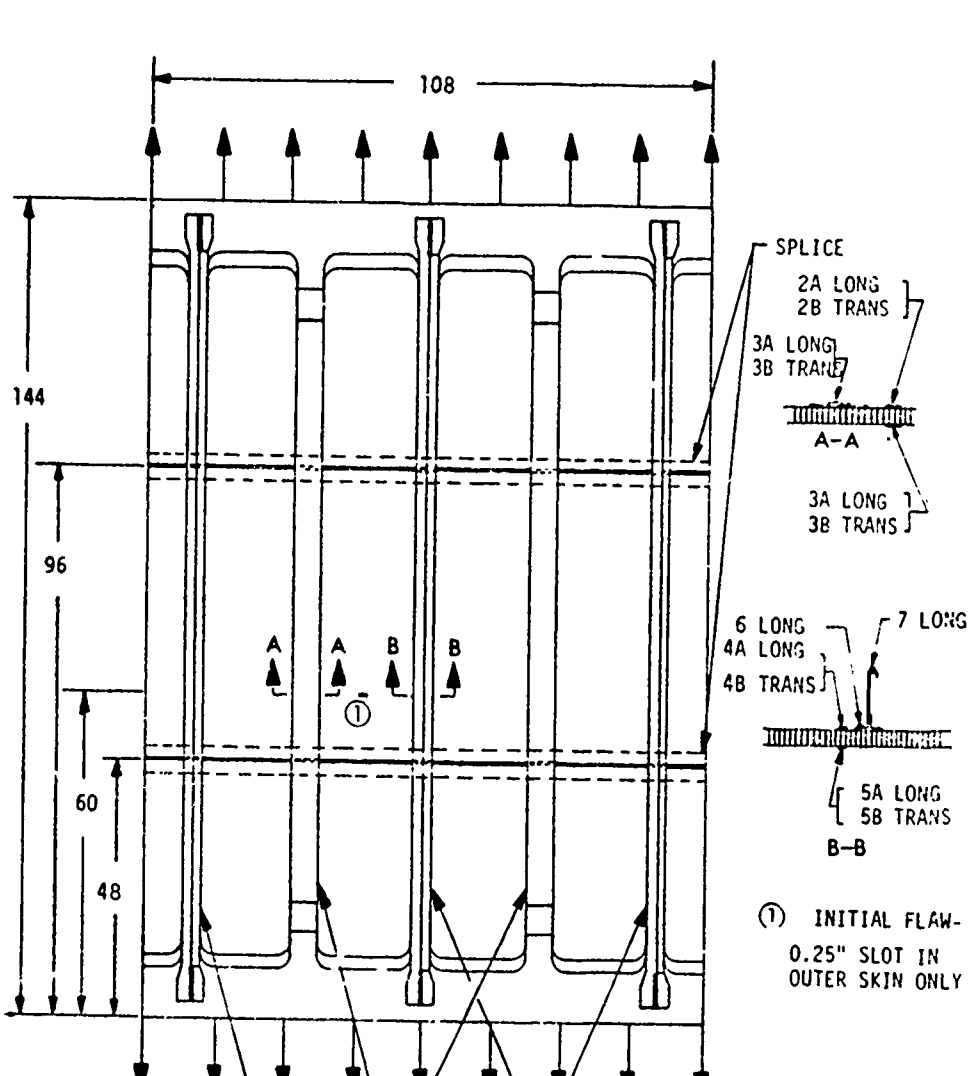
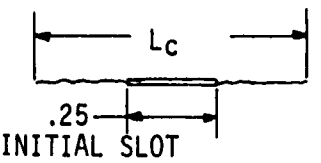


FIGURE 106. PANEL GEOMETRY, STRAIN GAGE, AND INITIAL FLAW LOCATIONS-H30A

TABLE 42

Total Cycles vs. Crack Length

CYCLES	L_c
33,195	.530
35,305	.570
38,027	.575
40,560	.610
43,000	.650
43,357	.680
45,501	.720
48,001	.760
50,500	.830
54,698	.920
55,906	1.020
61,000	1,130
66,000	1.400
71,000	1.770
76,000	2.380
81,000	3.070
85,010	4.380
88,010	6.520
90,010	9.250
90,977	10.560
91,501	11.800
92,002	12.890
92,102	13.160



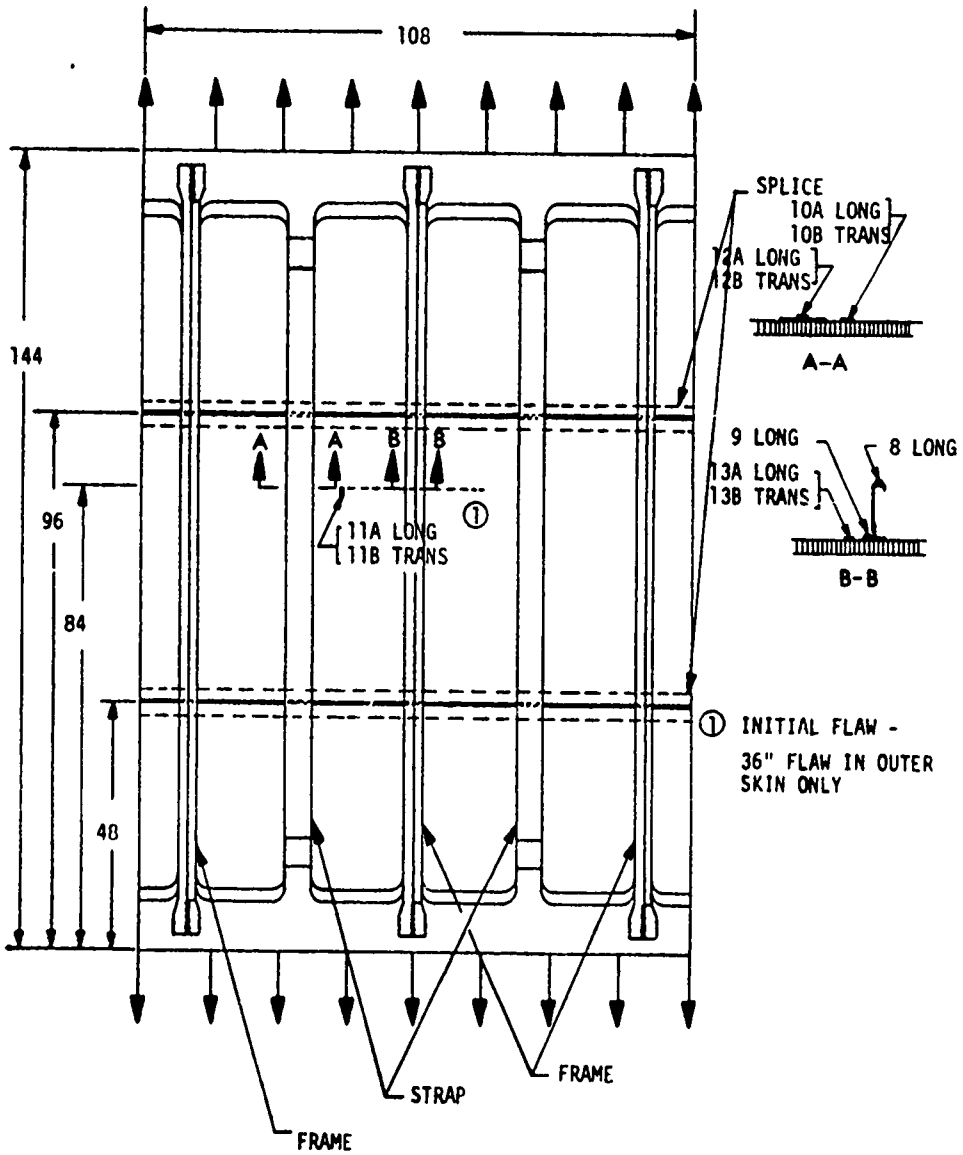


FIGURE 107. PANEL GEOMETRY, STRAIN GAGE AND INITIAL FLAW LOCATIONS-H30B

Table 43 lists the panel applied loads, strain gage readings, and crack lengths. The panel failed at an applied load of 298,000 pounds as shown in Figure 108.

Residual Strength-Foreign Object Damage-H30C. This honeycomb concept test was conducted to show the structure has adequate residual strength in the presence of a 15 inch flaw through the center frame and honeycomb sandwich panel, and determine the ultimate strength of the panel.

The geometry, initial flaw, and strain gage locations for this panel are shown in Figure 109. Significant features are that it was made of 2024-T3 bare sheet aluminum honeycomb sandwich. The splice straps were also made of 2024-T3 bare sheet. The frames were of 7075-T6 with the longitudinal straps of 7475-T761 bare sheet. The panel was installed in the 1.5 million pound testing towers, and loaded at a rate of approximately 13,000 pounds/minute to failure.

Table 44 lists the strain gage readings at several applied load levels. The panel failed at an applied load of 180,617 pounds when the panel separated in line with the original flaw.

TABLE 43

Applied Load, Strain Gage Readings, and Crack Length, H30B

APPLIED LOAD	SG 8	SG 9	SG 10A	SG 10B	SG 11A	SG 11B	SG 12A	SG 12B	SG 13A	SG 13B	TOT CRACK LENGTH
LBS	PSI	PSI	PSI	PSI	PSI	PSI	PSI	PSI	PSI	PSI	IN
0	0	0	0	0	0	0	0	0	0	0	36.00
100,000	5,700	23,000	13,200	- 100	17,800	- 4,700	13,200	- 3,300	19,600	- 2,000	36.00
120,000	7,000	28,200	15,900	- 100	21,200	- 5,500	15,900	- 3,900	24,800	- 4,000	36.00
140,000	8,200	34,800	19,000	100	25,400	- 6,600	18,900	- 4,500	32,800	- 5,900	36.06
160,000	9,700	38,800	22,000	300	29,700	- 7,500	21,800	- 5,200	43,000	- 5,700	36.20
180,000	11,000	39,200	25,200	1,100	34,200	- 8,200	24,800	- 5,700	55,500	- 2,500	36.34
200,000	12,400	39,200	28,800	2,300	39,200	- 8,700	27,900	- 6,300	69,500	- 1,000	36.39
220,000	14,200	39,500	33,500	4,100	46,500	- 9.300	32,000	- 6,700	89,500	- 1,000	36.61
240,000	16,000	39,600	38,000	6,300	55,000	-10,000	36,800	- 7,400	120,000	- 200	37.30
260,000	17,500	43,400	42,200	9,200	65,500	-10,300	40,800	- 7,600	160,000	1,300	38.67
270,000	18,100	43,600	45,600	12,000	75,500	-10,600	44,600	- 8,100	186,000	3,100	39.14
280,000	19,000	43,700	46,000*	15,600	91,800	-10,300	49,500	- 8,800	236,000 175,000	11,000	39.81
290,000	20,000	43,700	46,000*	19,000	113,500	- 9,800	55,500	- 9,800	155,000	14,800 7,000	41.00
298,000	20,800	43,700	46,000*	19,500	132,500	- 8,300	58,800	-10,000	149,000	8,000	FAILURE
0	48,000*	36,000	38,500	- 2,600	15,000	10,900	22,500	- 2,300	60,000	- 5,300	

* Recording pen reached mechanical stop

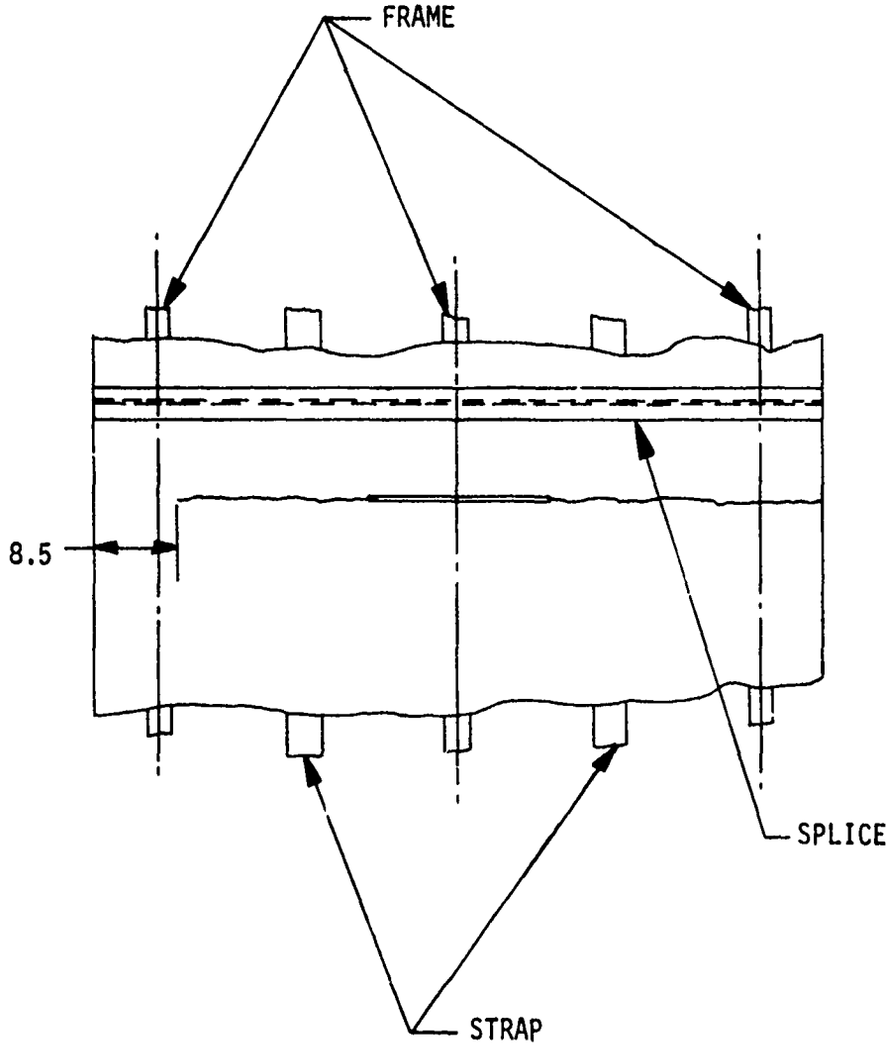


FIGURE 108. H30B FAILURE

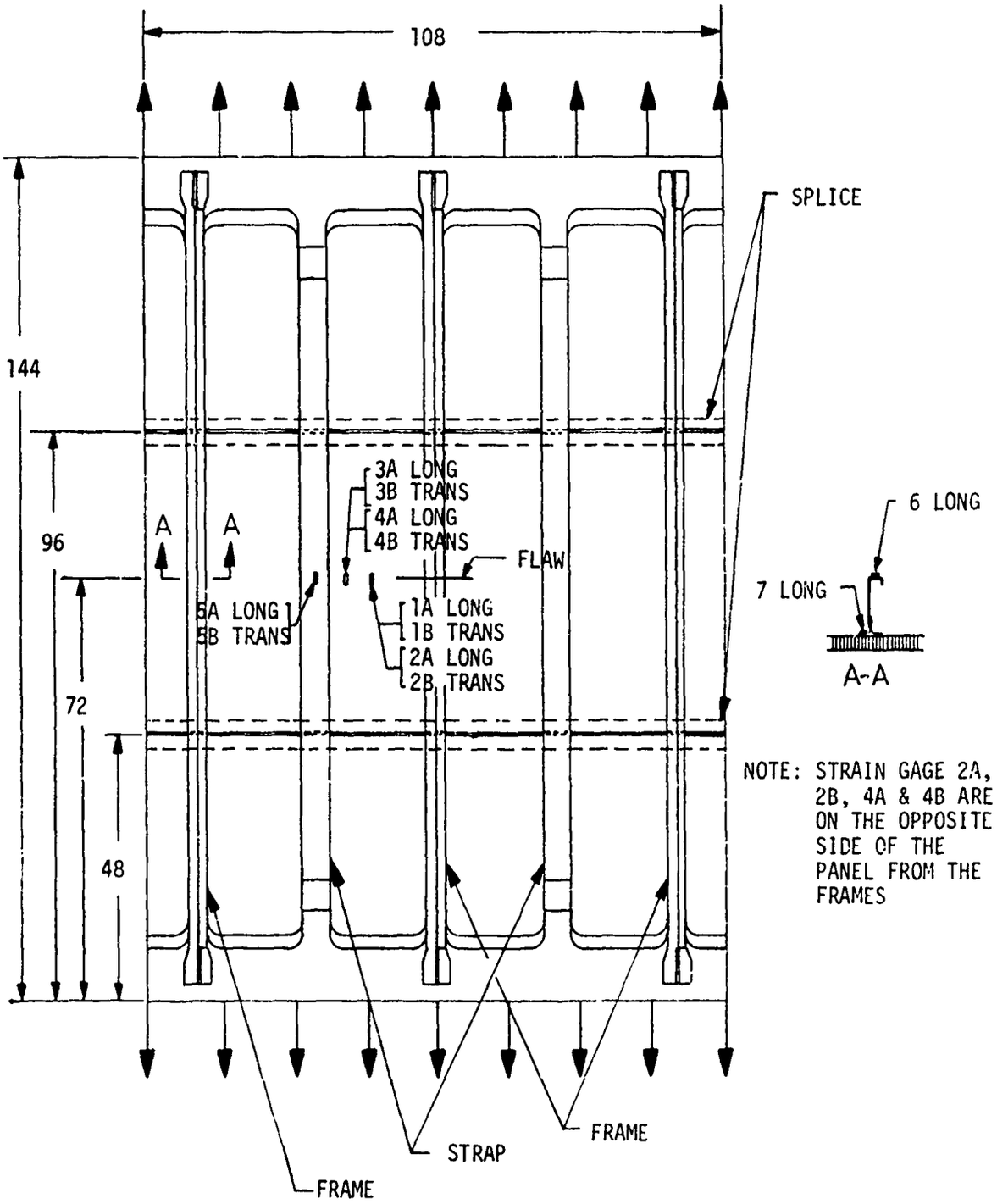


FIGURE 109. PANEL GEOMETRY STRAIN GAGE & INITIAL FLAW LOCATION-H30C

TABLE 44

Strain Gage Readings at Applied Load-H30C

TOTAL LOAD	SG 1A	SG 1B	SG 2A	SG 2B	SG 3A	SG 3B	SG 4A	SG 4B	SG 5A	SG 5B	6	7
LBS	PSI	PSI	PSI	PSI	PSI	PSI	PSI	PSI	PSI	PSI	PSI	PSI
145	33	0	33	0	33	0	0	- 33	- 64	32	32	32
60,792	15,162	-1,873	8,882	- 997	12,297	-2,809	8,580	-2,073	11,019	-3,435	9,124	7,825
98,213	24,793	-2,642	15,486	- 665	19,635	-4,415	14,656	-2,876	17,695	-5,509	14,092	12,696
151,164	48,848	-2,675	30,180	2,661	31,866	-6,421	24,371	-2,441	27,645	-8,880	21,101	19,937
160,313	58,619	-1,505	35,694	4,091	35,083	-6,689	26,775	-1,806	29,914	-9,560	22,437	21,235
168,573	68,183	401	42,926	6,187	38,869	-6,823	29,613	-1,036	32,215	-9,820	23,606	22,534
178,594	68,183	17,392	67,393	10,511	48,754	-5,886	36,624	1,806	37,400	-10,954	25,424	24,353
180,617	68,183	68,500	67,393	9,713	68,591	10,970	68,341	15,218	66,180	-11,473	27,892	27,048

MATERIALS and PROCESS

This section contains a summary of the effort during Phase Ib for the selection of the anodize and primer surface treatment, the corrosion control and the various structural and environmental tests leading to the selection of the adhesive. Additional tests of cast adhesives, or neat specimens, were performed to obtain material property data on the candidate adhesives.

Mechanical fastening tests were made to determine the effect on the bond line of chips and high speed drills. Fatigue, fracture toughness and crack growth data was also obtained for 7475-T6 aluminum.

Surface Treatment

Process Selection. - Three surface treatment processes for structural bonding were selected for study. These processes included two different procedures for chromic acid anodizing and a system of phosphoric acid anodizing. They were as follows: (1) Phosphoric Acid Anodize, Spec. BAC-5555, Boeing Co. (2) Chromic Acid Anodize, Spec. BPS FW4352, Rev. G, Bell Helicopter Co., (3) Chromic Acid Anodize, Spec. PS-13201, McDonnell Douglas Corp. The sulfuric acid, sodium dichromate etch (FPL), Spec. BAC-5514, Boeing Co., was used as the baseline control treatment.

Adhesion Evaluation Test Methods. - The primary evaluation criteria for bond durability of the surface treatments was the wedge crack propagation test. The test specimen configuration and dimensions are shown in the section on Adhesive Environmental Properties. All surface treatment processes were evaluated by processing 6 x 6 x .125 inches panels. These panels, after bonding, were cut into five (5) one inch wide wedge crack test specimens. The wedge was driven into one end of the specimen, and after a stabilizing period of one hour, the crack in the specimens were measured and then exposed to 100% relative humidity at 140°F (temperature and humidity studies). The crack growth was measured after one (1) hour exposure and then measured again after three (3) hours exposure.

The adhesive that was used in all the surface treatment evaluation test was Bloomingdale FM73 and BR127 adhesive primer.

Chemical Analysis & Solution Control. -

Alkaline Cleaner: - The phosphoric acid anodizing process per BAC-5555 required the use of alkaline cleaner as specified in specification BAC-5749. Turco's 4215S (which is listed), a nonsilicated alkaline cleaner, was used for all surface treatment processes evaluated. Control limits of the active ingredient in 4215S alkaline cleaner, as submitted by the Turco Division of Purex, is on file in the Douglas Aircraft Company laboratory.

PRECEDING PAGE BLANK-NOT FILMED

Deoxidizing Solutions: - (a) There are two (2) deoxidizers allowed by BAC-5555 to be used to prepare parts for phosphoric acid anodizing. The Amchem #6-16 deoxidizer was chosen instead of the $Na_2Cr_2O_7$-H_2SO_4 solution for the following reasons: (1) it can be used to remove heavy oxides, (2) it can be used in existing laboratory and production tanks without installation of new liners, and (3) it is operated at ambient temperature. The Amchem 6-16 deoxidizer as used for specimens and parts processed by phosphoric acid anodizing. The list of active ingredients in the #6 and the #16 deoxidizer as submitted by Amchem Products is on file in the Douglas Aircraft Company laboratory. (b) Douglas developed deoxidizer #1051 was used for all specimens processed with chromic acid anodize per McDonnell Douglas PS 13201. (c) A sulfuric acid-sodium dichromate solution at 140° - 160°F was used to deoxidize all specimens processed with the Bell Helicopter chromic acid anodize per BPS FW4352, Rev. G.

Temperature and Humidity Study. - To establish the optimum temperature to conduct the wedge crack propagation test, 2024-T3 and 7075-T6 panels were alkaline cleaned, deoxidized and phosphoric acid anodized. The concentration of the anodize solution was maintained in the middle of the concentration range as shown in Table 45.

TABLE 45

PHOSPHORIC ACID ANODIZE PARAMETERS

VARIABLES	PROCESSING LIMITS		
	LOWER	MEDIAN	UPPER
Acid Concentration (op2)	11	13.5	16
Voltage	8	10	12
Solution Temp °F	65	77.5	90
Anodizing Time (minutes)	20	22.5	25

The anodized panels were bonded using the FM73/BR127 adhesive and primer. The temperature evaluation was conducted in 100% relative humidity at temperatures of 100°F, 140°F and 160°F. The test results for the FPL etched specimens were very erratic. However, the 140°F temperature seemed to be adequate for the phosphoric acid anodized specimens. The 140°F temperature at 100% relative humidity was chosen to be the test condition for all future wedge crack tests.

Phosphoric Acid Anodizing Process Parameters Confirmation. - The processing parameters for the phosphoric acid anodizing process were confirmed by the use of the matrix as shown in Table 46. In accordance with the test matrix of this Table 46, the effects of such variables as solution concentration (C_1C_2), applied voltage (V_1V_2), solution temperature (T_1T_2), and the anodizing time (t_1t_2), were evaluated. Five (5) wedge crack test specimens for each of the two alloys (2024-T3 and 7075-T6) were prepared for each of the test grids indicated in the matrix diagram. Sixteen data points or 80 wedge crack test specimens per data point were tested in the matrix per alloy. The variables investigated were the highs and lows of the anodizing parameter shown in Table 45. After anodizing, the specimens were primed with BR127 adhesive primer. FM73 adhesive film was applied and the test specimens bonded in an autoclave at 250°F for 90 minutes under 40 psi pressure. All test specimens were NDI C-scan inspected. No voids were noted in the bonded test specimens. The specimens were then cut into one inch wide test specimens, and wedge crack tested at 100% RH and 140°F. The crack growth was measured after one (1) hour and after three (3) hours. In addition to the shorter periods, some specimens were also exposed for periods of 18 and 168 hours. It appeared that the primary crack growth took place within the first hour and this time was used for data points in the matrix. The wedge crack growth test results for each condition showed the adhesive failure to be cohesive and that the processing limits specified per BAC 5555 provided a satisfactory surface treatment for good bond durability.

Chromic Acid Anodize Trade-Off Study-McDonnell Douglas Versus Bell. - A comparison of two chromic acid anodizing processes, McDonnell Douglas PS 13201 and Bell Helicopter Co. BPS FW4352, Rev. G, was conducted using their respective medium processing range. Both the Bell and McDonnell Douglas chromic acid anodizing and sealing parameters are shown in Table 47. This test was made to decide which system would be used for further evaluation. One set (2 panels) each of nonclad 2024-T3 and 7075-T6 for the McDonnell Douglas anodizing were processed using the median processing range shown in Table 47. The bonded specimens were cut into five (5) wedge crack

TABLE 46

TEST MATRIX

		C_1		C_2	
		V_1	V_2	V_1	V_2
T_1	t_1	X	X	X	X
	t_2	X	X	X	X
T_2	t_1	X	X	X	X
	t_2	X	X	X	X

TABLE 47

. CHROMIC ACID ANODIZE & SEALING PARAMETERS

	VARIABLES	PROCESSING LIMITS					
		MDC			BELL HELICOPTER		
		LOWER	MEDIAN	UPPER	LOWER	MEDIAN	UPPER
ANODIZE	Chromic Acid Conc. (% free acid)	4.5	5.25	6	3	-	-
	Voltage	17	20	23	38	40	42
	Solution Temperature °F	85	95	100	92	93.5	95
	Anodizing Time - Mins	25	35	40	30	32.5	35
SEALING	Additive Chemical	Potassium Dichromate			Chromic Acid		
	Concentration MDC-% bw Bell-ppm	2.5	5	6	75	102.5	120
	Temperature °F	185	195	205	180	182.5	185
	Time - Mins	8	12.5	17	7	8	9
	pH	4.2	5.5	6	2.5	3.15	3.8

test specimens and the crack growth was measured after one (1) hour and after three (3) hours. The above test was repeated for the Bell chromic acid anodizing process.

The Bell anodize wedge crack test results on the 2024-T3 specimens showed considerable adhesive failures associated with large crack growths. The Bell system on 7075-T6 and the McDonnell Douglas anodize on both 2024-T3 and 7075-T6 did not show any adhesive failure. Because of the adhesive failures of the Bell anodized 2024-T3 specimen, the McDonnell Douglas chromic acid anodize was chosen for further evaluation.

Chromic Acid Anodize - Sealing Parameters Confirmation. - The processing range for the sealing operation of the McDonnell Douglas chromic acid anodizing process was studied by using the matrix as shown in Table 48. All the anodizing was done at the median processing range as shown in Table 47. In accordance with the test matrix of Table 48, the effects of such variables as the concentration of potassium dichromate (C_1C_2), type of water (W_1W_2), solution temperature (T_1T_2), and the sealing time (t_1t_2), were evaluated. Wedge crack test specimens of each of the two alloys, 2024-T3 and 7075-T6 nonclad, were anodized and sealed for each of the test grids indicated in the matrix diagram. The results of the sealing evaluation are presented in Figure 110 and show the failure mode of each specimen. A cohesive failure mode (C) indicates that the adhesive strength of the adhesive system to the treated aluminum is greater than the cohesive strength of the FM73 adhesive. The cohesive failure is considered to be the ultimate in adhesion as a result of surface treatment. An adhesive failure, mode (A), is considered to be worst type of adhesion as a result of surface treatment.

Specimens having the failure identified as "AE" indicate a minor adhesive failure at the edge of the specimen in the crack zone. Though these failures are minor, they are considered important since this edge area of the specimen are the points where the anodize/adhesive faying surface are immediately exposed to the test environment. It also is an indication of the method of specimen preparation and the effects of cutting glue lines in manufacturing. Brittle anodizes that fracture during machining can be sources of included areas for the start of corrosion. The complete sealing matrix was repeated using the deionized water seal solution at a pH of 4.0.

TABLE 48

SEALING MATRIX

		C_1		C_2	
		W_1	W_2	W_1	W_2
T_1	t_1	10	10	10	10
	t_2	10	10	10	10
T_2	t_1	10	10	10	10
	t_2	10	10	10	10

		$K_2 Cr_2 0_7$ CONCENTRATION													
		2.5%								6.0%					
TEMP	TIME	3.8 pH		4.0 pH		4.2 pH		4.8 pH		3.8 pH		4.0 pH		6.0 pH	
185°	8	–	–	C	C	AE	AE C	–	–	–	–	C	C	A AE	A AE
	17	–	–	C	C	AE	AE	–	–	–	–	C	C	AE	A
205°	8	–	C	C	C	C	C	A	A	–	C	C	C	A AE	A
	17	–	C AE	A AE	C	AE	AE	A	A	–	C	C	C	AE	AE
ALLOY		24	75	24	75	24	75	24	75	24	75	24	75	24	75

ACCEPTABLE SEALING RANGE

- $K_2 Cr_2 0_7$ CONC 4.0 – 6.0 % bW
- TEMP 185 – 195°F
- TIME 8 – 12 MINUTES
- pH 3.8 – 4.2
- WATER – DEIONIZED

ANODIZING PARAMETERS FOR SEALING MATRIX STUDY

- $Cr0_3$ CONC 7 OZ/GAL
- VOLTAGE 20
- TEMP 95°F
- TIME 35 MINUTES

A ADHESIVE
AE ADHESIVE EDGE
C COHESIVE
– NO TEST
LIMIT

PR6-PAB-0130

FIGURE 110. CHROMIC ACID ANODIZE SEALING MATRIX

All these tests have shown that the pH of the dichromate seal solution is of greater importance than originally believed. The data indicates that poor resistance to moisture is a product of high pH (4.8 and above) and to a lesser degree to concentration of the solution and the temperature.

The optimum processing range for the sealing operation for the McDonnell Douglas chromic acid anodize is shown in Figure 110.

Chromic Acid Anodizing Process Parameters Confirmation. - The processing parameters for the McDonnell Douglas chromic acid anodizing process were evaluated by the use of the matrix as shown in Table 46 for phosphoric acid anodize. In accordance with the test matrix of Table 46, the effects of such variables as solution concentration (C_1C_2), applied voltage (V_1V_2), solution temperature (T_1T_2) and the anodizing time (t_1t_2) were evaluated.

Wedge crack test specimens for each of the two alloys, 2024-T3 and 7075-T6 nonclad, were prepared for each of the test grids indicated in the matrix diagrams. The variables investigated were the highs and lows of the anodizing parameter shown in Table 49. Panels for each alloy were anodized at the low concentration and low temperature and all specimens had an iridescent appearance which indicated a thin anodic film. Another set of panels for each alloy was processed at low concentration, low temperature, low voltage and time. The thickness of the specimens were measured using a Permascope tester type EC. The film thickness of the panels ranged between 0.00001 to 0.00005 inches on the 7075-T6 alloy. The coating thickness on the 2024-T3 alloy could not be measured.

Because the anodic coating of these tests caused sufficient iridescence to suggest inadequate or thin anodic coating, it was decided to raise the temperature of the bath from 85°F to 90°F for the confirmation tests involving the higher acid concentrations.

The wedge crack results shown in Figure 111 indicated that the best results as far as adhesion, was obtained at high temperature (100°F), longer time (40 minutes), high concentration (8 oz/gal), and high voltage

TABLE 49

CHROMIC ACID ANODIZE PARAMETERS

VARIABLES	PROCESSING LIMITS		
	LOWER	MEDIAN	UPPER
Acid Conc. oz/gal	6.0	7.0	8.0
Voltage	17	20	23
Solution Temperature °F	85	92.5	100
Anodizing Time (minutes)	25	35	40

		CONCENTRATION									
		6 OZ/GAL				7 OZ/GAL		8 OZ/GAL			
TEMP	TIME	17V		23V		20V		17V		23V	
85°	25	A	A	A	AE	–	–	–	–	–	–
	40	AE	AE	AE	AE	–	–	–	–	–	–
90°	25	–	–	–	–	–	–	A	AE	A	AE
	40	–	–	–	–	–	–	AE	AE	AE	AE
95°	35	–	–	–	–	C	C	–	–	–	–
100°	25	AE	AE	AE	AE	–	–	C	AE	C	C
	40	C	AE	AE	C	–	–	C	C	C	C
105°	25	–	–	–	–	–	–	AE	–	C	–
	40	–	–	–	–	–	–	AE	–	C	–
	ALLOY	24	75	24	75	24	75	25	75	24	75

ACCEPTABLE ANODIZE RANGE

95-100°F

7-8 OZ/GAL CONC

20-23 VOLTS

35-40 MIN

SEALING PARAMETERS FOR ANODIZE MATRIX STUDY

$K_2CR_2O_7$ CONC 5.0% BY WT

TEMP 190°F

pH 3.8-4.0

WATER DEIONIZED

A ADHESIVE

AE ADHESIVE EDGE

C COHESIVE

– NO TEST

LIMITS

PR6-PAB-0102

FIGURE 111. CHROMIC ACID ANODIZE MATRIX

(23 volts). Specimens were also tested to determine if the range could be extended by increasing the temperature to 105°F at high voltage and high concentration. The results of those tests are also shown in Figure 111. A review of the data, including tests from the sealing matrix showed that a workable range existed. The shaded blocks of Figure 111 show the proposed limits. The proposed range is narrow, but for use as a back-up system, it is possible to use it both in the laboratory and in production. Further testing should be conducted at a later date to expand the processing limits.

Effects of Anodizing on Different Alloy and Temper. - The following nonclad aluminum alloys were anodized using the median processing range (Table 45) of the phosphoric acid anodized process:

Alloy	Tempers
7075	T73 and T76
7475	T6, T61, T76, T731 and T761

A set of specimens for each alloy and temper were bonded using the FM73/BR127 adhesive system. The bonded specimens were C-scan inspected and no voids were noted. The panels were then cut into wedge crack specimen and tested. The results indicated that the choice of alloy and temper did not effect the bond strength produced by phosphoric acid anodize.

Cathodic Protection of Lead in Phosphoric Acid. - During the early phosphoric acid anodizing runs, a dark deposit was found on the sides and bottom of the anodizing tank. Sometimes portions of this loose spongy deposit could be seen suspended in the solution or floating on the surface. Analysis of the deposit showed it consisted primarily of lead with small amounts of copper and phosphorous. A deposit containing heavy metals should not float in the phosphoric acid electrolyte but this deposit was spongy and probably contained appreciable quantities of trapped hydrogen.

After more use of the solution, white pearlescent needles were also found in the tank. Analysis of the needles showed them to be lead phosphates. Obviously, the lead lining in the anodizing tank was being dissolved by the phosphoric acid electrolyte. Since the lead lining is the

cathode during anodizing, it was suspected that the attack was occurring when the tank was at rest. If this were true, then cathodic protection should stop the attack of the tank lining and prevent the formation of both the dark, spongy deposit and the white needles. A series of electro-chemical measurements was made to determine critical potentials and to compare the electro-chemical behavior of pure lead with lead antimony (Pb 94%, Sb 6%). The electrodes used were: (1) Chemically pure lead (Pb), (2) Lead antimony alloy (Pb-Sb), (3) Platinized titanium (Pt-Ti), (4) Carbon (C), and (5) Saturated calomel electrode (SCE). Results indicated that, depending upon the anode-cathode couple, the current potential necessary to prevent the lead from dissolving into the solution ranged from 1.3 to 2.1 volts. Even though a satisfactory anode material has not been found, the use of cathodic protection for the lead alloy tank lining has been effective to prevent attack and formation of deposits.

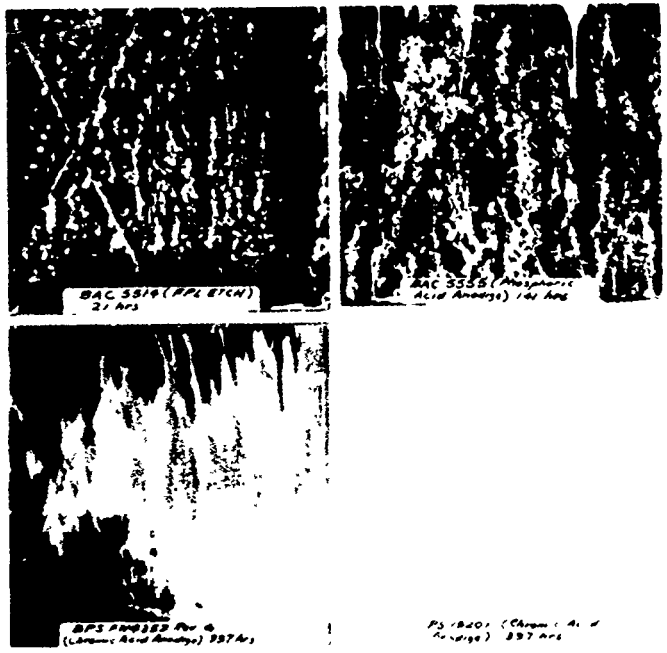
Dissolution Rate of Lead and Lead-Antimony Alloy in Phosphoric Acid. - The tank lining material for the principal laboratory phosphoric acid anodizing tank is pure lead with a lead 6% antimony alloy for the secondary tank. The production tank lining is constructed with this same alloy. The following test was initiated to gauge the rate of this dissolution in phosphoric acid solution. One inch specimens of the pure lead and the lead-6% antimony alloy materials were cleaned, oven dried and weighed. Specimens were suspended in their respective beakers of anodizing solution for specified periods, removed, re-weighed and re-measured. The dissolution rates were computed as inches of material lost per 1000 hours. Results indicated that although the loss of material was insignificant over a one-year period, the dissolution rate of lead antimony was twice that of pure lead.

Corrosion Control-Organic Coatings

Surface Treatment Corrosion Resistance. - Four surface treatments (see Process Selection) were subjected to 5% salt spray to determine their relative corrosion resistance. Treatments were tested with and without being coated with BR127 bond primer. The unprimed panels were exposed for a maximum period of 336 hours per MIL-A-8625. The primed panels were exposed for 3000 hours. The results are shown in Figure 112 and indicate the following: (1) Chromic acid anodize has better corrosion resistance than phosphoric acid anodize, and (2) When coated with a corrosion resistant adhesive bonding primer, phosphoric acid anodize is equivalent to or better than chromic acid anodize.

Corrosion Resistance-McDonnell Douglas Chromic Acid Anodize Sealing Matrix. - Tests were conducted to determine the sealing parameters that provided the best corrosion resistance to the chromic acid anodize. Nonclad 2024-T3 and 7075-T6 panels were processed per the matrix and parameter of Figure 110, and exposed to 1000 hours of 5% salt spray. Results are shown in Table 50. The sealing that provided the best corrosion resistance for both alloys was obtained at the upper limits of the dichromate concentration, temperature and time and using deionized water. In addition, these panels exhibited minimal or no staining of the anodized surface.

Corrosion Resistance-Chromic Acid Anodize. - Specimens representing the four corners of the McDonnell Douglas chromic acid anodize matrix and sealed per the limits determined in Figure 110 were exposed to 5% salt spray for 1000 hours. Results, as shown Table 51, indicated the following: (1) Best corrosion resistance was obtained at the upper limits of the anodizing parameters, and (2) Panels anodized in excess of 100°F produced a powdery film and have lower salt spray corrosion resistance.



EXPOSURE TEST 5-PERCENT SALT SPRAY

SUBSTRATE 7075-T6 BARE

SURFACE TREATMENT:

BAC 5514 (FPL) EXPOSURE TIME 21 HOURS

BAC 5555 EXPOSURE TIME 141 HOURS

BELL CHROMIC ANODIZE EXPOSURE TIME 337 HOURS

MCAIR CHROMIC ANODIZE EXPOSURE TIME 337 HOURS

CORROSION RESISTANCE OF SURFACE TREATMENTS

SURFACE TREATMENT	BR127 (MILS)	SALT SPRAY TIME (HRS.)	OBSERVATIONS
Boeing BAC5514 (FPL Etch)	Unprimed	21	Heavy corrosion and pits over entire panel.
	0.13	336	Scattered blisters with corrosion underneath. No corrosion extending out from scribe.
		3000	No additional corrosion or enlargement of the blisters and corrosion.
Boeing BAC5555 (Phosphoric Acid Anodize)	Unprimed	141	Same as the unprimed FPL etch.
	0.15	3000	No corrosion extending out from the scribe mark or on the face.
MDC PS13201 (Chromic Acid Anodize)	Unprimed	336	Scattered minute corrosion pits.
	0.18	3000	Same as the primed BAC5555.
Bell Helicopter BPS FW4352 Rev. G. (Chromic Acid Anodize)	Unprimed	336	Same as the unprimed PS13201.
	0.35	3000	Same as the primed BAC5555.

PR6-PAB-0088

FIGURE 112. SURFACE TREATMENT CORROSION RESISTANCE

TABLE 50

. CORROSION RESISTANCE - SEALING MATRIX*

WATER		DEIONIZED				TAP			
CONC. (%, BW)		2.5%		6.0%		2.5%		6.0%	
TIME (MIN)		8	17	8	17	8	17	8	17
TEMP. (°F) / ALLOY									
2024	185°	288	288	168	168	168	168	168	168
	205°	288	336	840	▶	168	384	288	288
7075	185°	840	840	384	648	384	336	648	648
	205°	840	1000	▶	▶	384	▶	840	840

* Failure is as defined per MIL-A-8625. All specimens were examined at 168, 288, 336, 384, 648, 840 and 1000 hours. Hours to failure data is intended to be comparative at these periods.

▶ No failure at 1000 hours.

TABLE 51

. CORROSION RESISTANCE CHROMIC ACID ANODIZE*

CONC.		6 OZ/GAL				8 OZ/GAL			
VOLTAGE		17V		23V		17V		23V	
TIME (MIN)									
TEMP.									
85°	25	168	696	---	---	---	---	---	---
90°	25	---	---	---	---	338	▶	---	---
100°	40	---	---	696	▶	---	---	500	▶
105°	40	---	---	---	---	---	---	384	---
ALLOY		2024	7075	2024	7075	2024	7075	2024	7075

* Failure is as defined per MIL-A-8625. Specimens were examined at 48, 120, 168, 336, 384, 500, 696, 540 and 1000 hours. Hours to failure is intended to be comparative at these periods.

--- = Not tested ▶ No failure at 1000 hours

Comparison of Bonding Primers. - Four adhesive/bond primer systems were evaluated: (1) American Cyanamid - FM73/BR127, (2) Hysol - EA9628/EA9202, (3) 3M - AF55/XA3950, and (4) NARMCO - M133/6740. Tests were conducted to compare the performance of each primer and to determine their compatibility with the coating systems of Table 52. The substrate used was nonclad 7075-T6 alloy treated with phosphoric acid anodize. Environmental tests included wet adhesion, humidity, 5% salt spray, immersion corrosion, exfoliation corrosion, bilge fluid and beach exposure. Exfoliation corrosion tests are shown in Figure 113. Results showed the following: (1) The optimum primer is BR127, (2) The decreasing order of corrosion resistance is BR127-XA3950-EA9202-NARMCO 6470, (3) All primers are compatible with any of the coating systems tested, and (4) BR127, used under the coating systems reduces the degree of coating failure in dissimilar metal areas.

Surface Treatment Protection. - Tests were conducted to determine the ability of the various coating systems to protect the different anodic surfaces. Test specimens were prepared using the following surface treatments and materials: (1) 2024-T3, 7075-T6, 7075-T73 and 7075-T76 nonclad aluminum alloys and tempers, (2) Chromic acid anodize and phosphoric acid anodize, (3) American Cyanamid BR127 and FM73 bonding primer and adhesive, (4) Coating systems, See Table 52. Environmental tests included: wet adhesion, humidity, 5% salt spray, immersion corrosion, exfoliation corrosion, bilge fluid and beach exposure. In addition, coated lap shear specimens were scribed through the bond joint and exposed to the same environment prior to determining their mechanical properties. Shear strength values were not affected and all adhesive failures were cohesive. Corrosion fatigue tests were conducted for 10 million cycles with no failures. Results showed that all of the coating systems provided adequate protection in all the tests except in the acidified salt spray exfoliation environment.

The conclusions drawn from Figures 113 through 116 are:

(1) The optimum surface treatment is phosphoric acid anodize. The primed panels of phosphoric and chromic acid anodize performed equally well in all test except in the exfoliation corrosion test. In this test the phosphoric acid anodized panels exhibited greater resistance to general and exfoliation corrosion than the chromic acid anodized panels on all the alloys and tempers

TABLE 52

COATING SYSTEM

CODE	COATING SYSTEM
C-1	MIL-P-23377
C-2	MIL-P-23377 + MIL-C-83286
C-3	MIL-P-23777 + PR1432GP + MIL-C-83019
C-4	PR1432GP + MIL-C-83019
C-5	MIL-C-8514 + MIL-P-8585 + EC 843S

EXFOLIATION CORROSION (672 HR) OF COATED PHOSPHORIC ACID ANODIZED ALUMINUM

BONDING PRIMERS		NARMCO 6740		3M XA3950		HYSOL EA9202		AM. CYAN. BR127	
FASTENER INSTALLATION		WET MIL S 18733 (PR 1436 G)	DRY	WET MIL-S-18733 (PR 1436 G)	DRY	WET MIL-S-18733 (PR 1436 G)	DRY	WET MIL-S 18733 (PR 1436 G)	DRY
COATING SYSTEMS OVER BONDING PRIMER	BONDING PRIMER ONLY (CONTROL)								
	MIL P 23377								
	MIL P 23377 + MIL C 33286								
	MIL P 23377 + PR 1432 GP + MIL C 83019								
	PR 1432 GP + MIL C 83019								
	MIL C 8514 + MIL P 8585 + EC 843								

NOTE FASTENERS – CD PLATED STEEL (NAS 1202)
PANELS – 7075 T6 NONCLAD

PR6-PAB-0105 1

FIGURE 113. COMPARISON OF BONDING PRIMERS

EXFOLIATION CORROSION (672 HR) OF COATED PHOSPHORIC ACID ANODIZED ALUMINUM

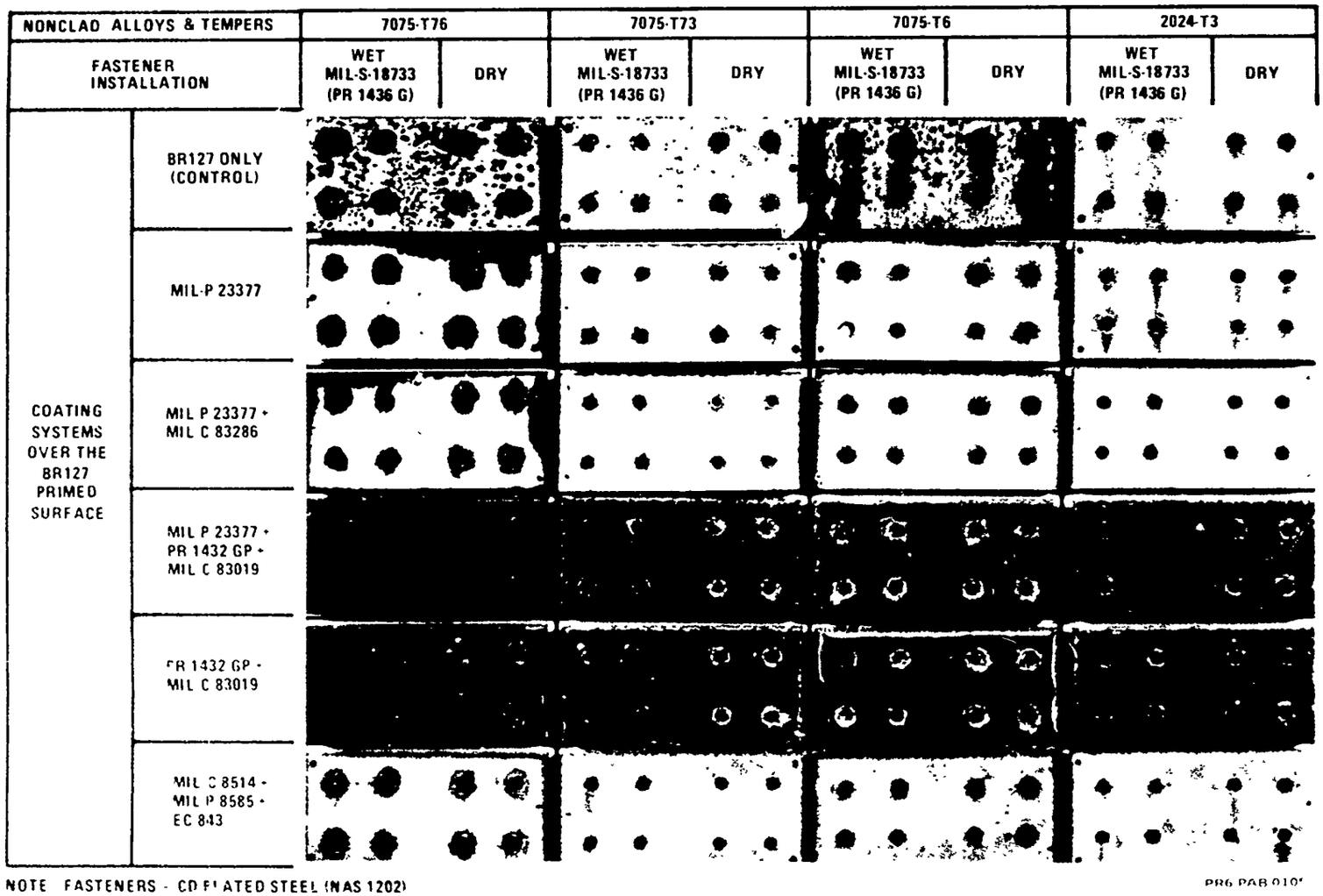
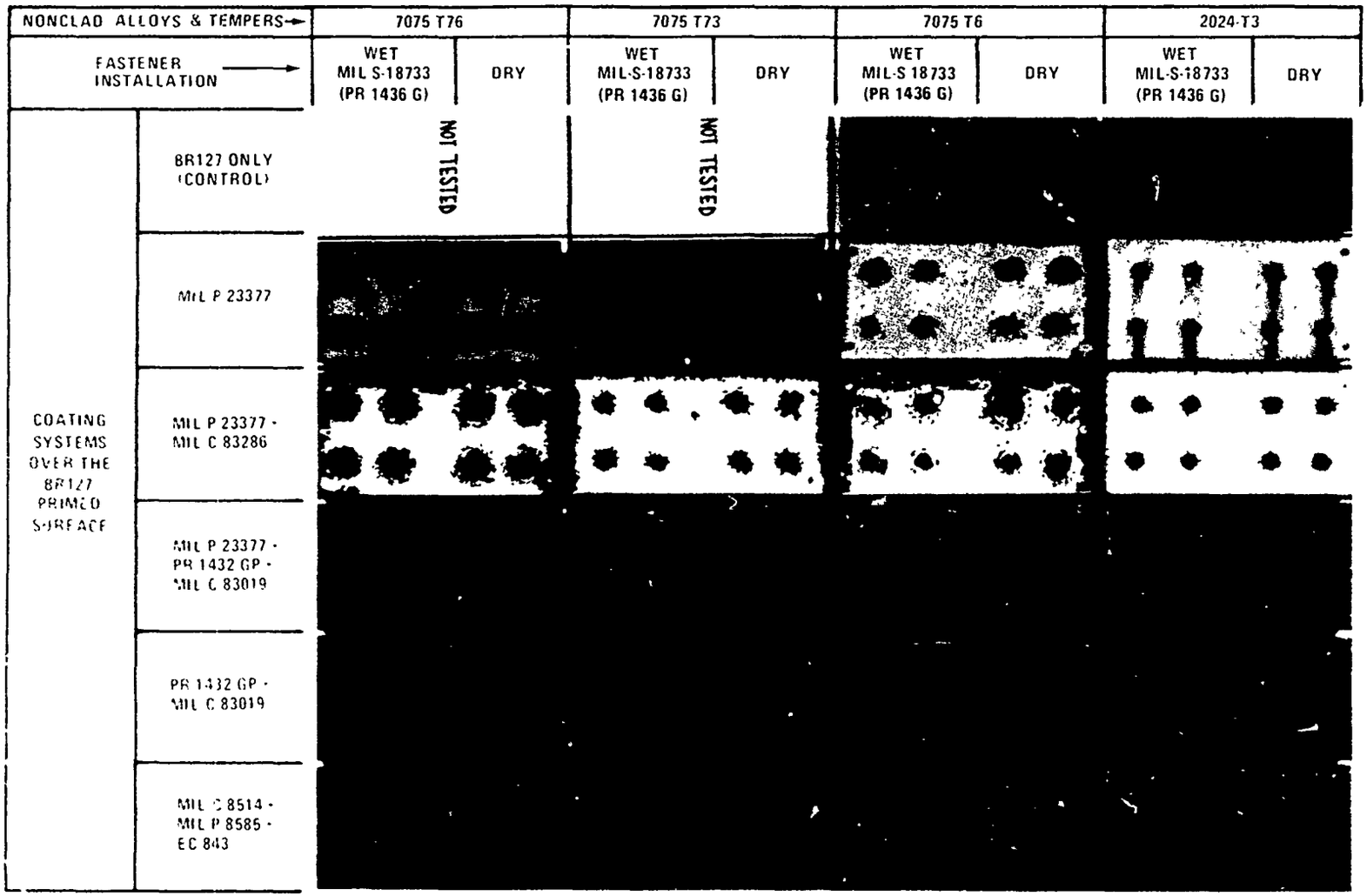


FIGURE 114 PHOSPHORIC ACID ANODIZE PROTECTION

EXFOLIATION CORROSION (672 HR) OF COATED CHROMIC ACID ANODIZED ALUMINUM



NOTE FASTENERS CD PLATED STEEL (NAS 1202)

FIGURE 115 CHROMIC ACID ANODIZE PROTECTION

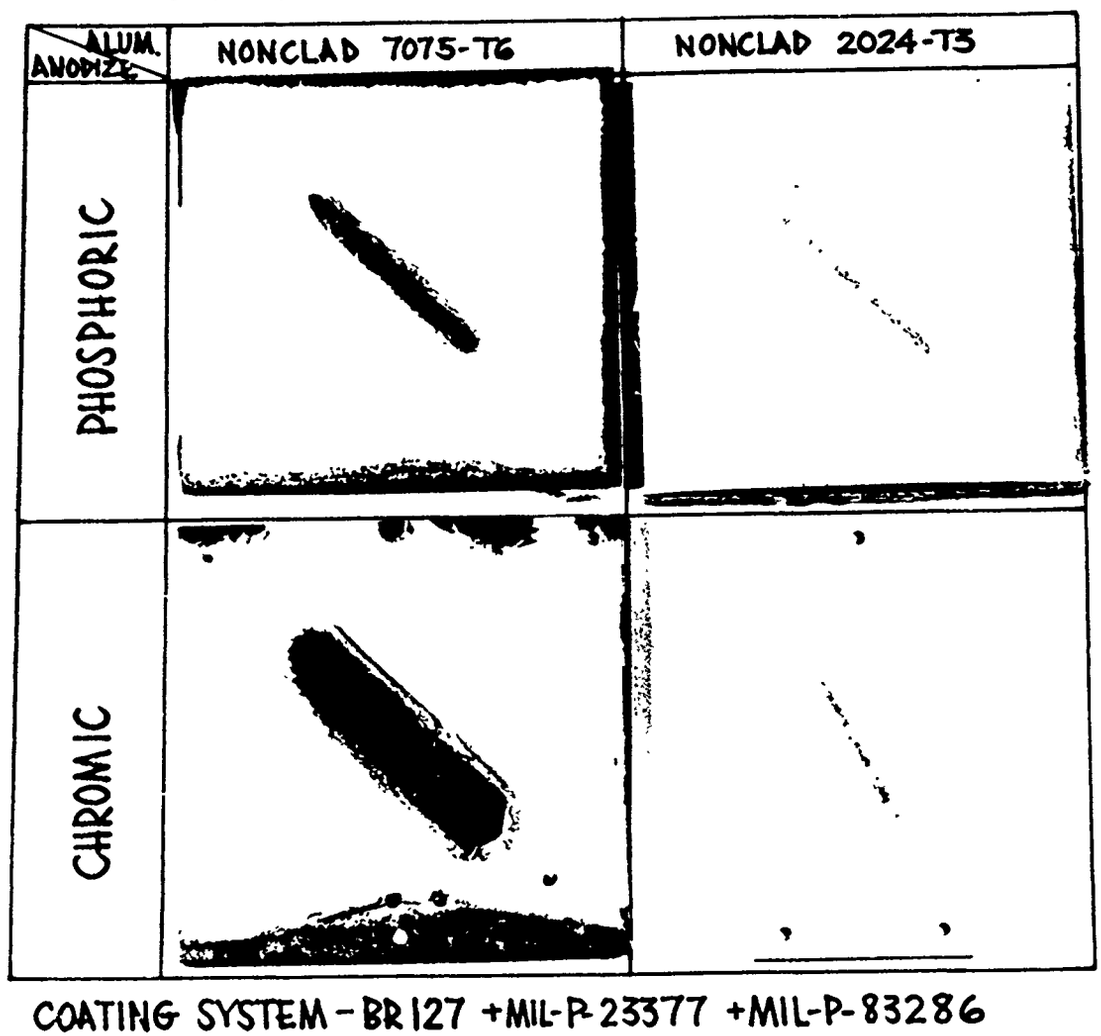


FIGURE 116. COMPARISON OF ALLOYS AND ANODIC TREATMENTS

tested. It also reduced the degree of coating failures.

(2) The corrosion resistance in decreasing order of the various alloys and tempers tested is as follows:

ACIDIFIED SALT SPRAY			5% SALT SPRAY
General Surface Corrosion	Exfoliation Corrosion		General Surface Corrosion
2024-T3	7075-T73	Equal	7075-T6
7075-T73	7075-T6		2024-T3
7075-T6	2024-T3		
7075-T76	7075-T6		

Decreasing Corr Resist. ↓

(3) The optimum exterior coating system over the BR127 primer is MIL-P-23377 primer plus MIL-C-83286 topcoat (system C-2). This system appears to inhibit exfoliation as well as or better than Corogard (system C-5).

(4) The optimum interior coating systems over BR127 are as follows: (a) Above the floor line is MIL-P-23377 primer (system C-1). (b) Below the floor line is MIL-P-23377 primer plus MIL-C-83286 topcoat (system C-2). This is in preference over the MIL-P-23377 primer plus PR1432GP sealant primer plus the MIL-C-83019 clear overcoat (system C-3). The reasons are: (a) any bond failure or corrosion initiating under system C-3 cannot be easily detected visually, (b) ease of stripping may be a problem, (c) coating failure in dissimilar metal areas are more gross, and (d) adhesion of the MIL-C-83019 clear to the PR1432GP is marginal to poor.

Rework of Coatings in Bond Line Areas. - The following items relative to rework of damaged coatings were investigated:

Mechanical Properties of Bond Line: - The bond line of different lap shear specimens were exposed to organic stripper and to grit blasting to determine if these methods of coating removal affected the mechanical properties of the bond. Lap shear specimens were made of nonclad 7075-T6, phosphoric anodize, BR 127 primer and overcoated with the MIL-P-23377 primer and MIL-C-83286 topcoat system. The bond line of different specimens were

exposed to Turco 5351 brush-on stripper for 2 hours and to grit blasting with aluminum oxide grit for 3 minutes and with walnut shell for 10 minutes. Grit blasting time was dependent on removal of the coating system down to the metal substrate. Results showed that the shear strength values were not affected by any of the removal methods.

Stripping of Coating Systems: - Stripping tests using a MIL-R-25134 stripper (Turco 5351 brushable) were conducted on the different coating systems applied over BR127 bond primer. Test period was 90 minutes. Coating systems are as noted in Table 52. Removal of BR127 was also attempted with acid strippers. Results of the stripping tests are as follows: (1) All systems using MIL-P-23377 primer over the BR127 were removed down to the MIL-P-23377 primer. The MIL-P-23377 primer softened only slightly. (2) All systems without the MIL-P-23377 primer were strippable down to the BR127 primer. (3) The PR1432 GP sealant softened slightly and required repeated scraping and stripper reapplication for removal. (4) No brush on stripper has been found that would readily remove properly applied and cured BR127 primer from a phosphoric acid anodized surface. Brush on acid strippers, such as Turco 6017 and Fiber Resin ES-1, were as ineffective as the phenolic type, Turco 5351.

Adhesion of Reworked Exterior Coat System: - Nonclad 7075-T6 panels were phosphoric anodized, BR127 primed and overcoated with the MIL-P-23377 primer and MIL-C-83286 topcoat. One panel each was grit blasted down to the bare metal with aluminum oxide and walnut shell. Panels were solvent cleaned with MEK, treated with Alodine 1200 and recoated with the exterior coating system. Wet adhesion tests were conducted after 7 days air dry. Both panels exhibited cohesive failure in the MIL-P-23377 primer. Another set of panels was prepared and retested with the same results.

BR127 Versus BR127A. - BR127A has been formulated as a bonding primer to improve the peel strength at subzero temperature. Douglas test data verified the low temperature properties. The formulations of BR127 and BR127A differ in resin ratio and solvent composition. The comparison of these two primers was made to determine if differences exist in their

corrosion resistance. Primers were applied to phosphoric acid anodized non-clad 7075-T6 alloys and tested. (1) Immersion in an acidified salt solution initiates minute filament type corrosion tracks extending out from the scribe line for both primers. (2) Exposure to acidified salt spray shows corrosion pits appearing earlier on the BR127A specimens than on the BR127 specimens. BR127A provides less corrosion protection to the phosphoric acid anodize surface than BR127.

Structural Adhesives

Adhesive Selection for Test. - At the beginning of the program, the flight parameters of the baseline aircraft indicates that a typical 250°F cure modified epoxy adhesive system would produce all the mechanical properties required. The goal was to select an adhesive system that would have the required environmental resistance and durability when used with the phosphoric acid anodize and a suitable corrosion inhibiting adhesive primer.

Several of these adhesive systems were available Based on test work performed by Boeing, McDonnell Douglas, Bell Helicopter and several other companies, the systems, called "new generation," indicated a superiority in moisture resistance and were very durable. Most of these adhesive systems came into existence during the last six years due to the on-going efforts of the adhesive manufacturers to produce a more durable and moisture resistant class of adhesives.

In addition, more sophisticated methods for testing the durability of the adhesive became available. The importance of cycle stressed testing of adhesives in an elevated temperature and humid environment was recognized. This type of testing emphasized the inherent weaknesses of some adhesives and of some surface treatments.

The purpose of this task was to select and test the best available state-of-the-art alloys, surface treatments, adhesive primers and adhesives for use in the manufacture of the final article.

The ground rules of the test program also included the requirements of nonclad adherends in the fabrication of all details. This requirement is compatible with MIL-A-83377. It is also compatible with Air Force criteria that includes painting of all surfaces of the aircraft, both interior and exterior. Subsequent testing of wedge crack specimens in a beach atmosphere which included both clad and nonclad adherends indicates that the nonclad specimens have better environment resistance, the clad 7075-T6 specimens failing very rapidly even with the phosphoric acid anodize and the corrosion inhibiting primers.

Final Adhesive Selection for Large Scale Test Article:- FM73 was selected based on a series of mechanical, and environmental tests on both the primer and the adhesive in conjunction with the optimized phosphoric anodize system.

In each case, the adhesive system showing the best environment and corrosion resistance in the tests was FM73. These tests included the effects of the carrier used in the adhesive. The mat carrier always gave lower T-peel properties, however the effect of this mechanical property could be minimized by proper panel design. The primary criteria was the basic overall durability of the systems especially in the tests that included stressed and cycle stressed environment exposure.

Adhesive Systems: - The following adhesive systems and batch numbers were used for material evaluation:

Material	Type	Batch No.	Mfg.
FM73 Nonwoven Carrier	Adhesive Film .045 psf	Batch 86 Roll 326	American Cyanamid
BR127	Primer	Batch 560	" "
EA9628 Woven Carrier	Adhesive Film .045 psf	Batch 076-134 Roll D	Hysol Div. of the Dexter Corp.
EA9202	Primer	Batch 103-186	"
AF55 Woven Carrier	Adhesive Film .045 psf	Batch 1D5P	Minn. Mining & Mfg. (3M)
XA3950	Primer	Batch 3B5P	"
M1133 Woven Carrier	Adhesive Film .045 psf	Batch 30 Roll 1	Namco Materials Inc.
M6740	Primer	Batch 17	"

These four adhesive systems were the primary considerations for the program. They are 250°F cure and all had corrosion inhibiting primer systems. Other adhesive systems such as Plastilock 729-3 and Redux 775 were used in some tests for comparison but were not considered primary candidates in this program. Most of the data gathered on these two other systems will be in the Slow Cycle Fatigue tests which are still in test.

Surface Preparation: - All test specimen surfaces were prepared for adhesive bonding using the phosphoric acid anodize process except where the tests were for surface treatment comparison. All precautions for processing,

as determined by the surface treatment investigation, were observed.

Primer Application: - The procedures for application and cure of the adhesive primers were provided by the individual manufacturers of the systems. All primers were corrosion inhibiting. They all also were intended to be used at a thickness range of 0.0001 to 0.0003 inches for maximum mechanical properties and corrosion resistance. The primers were fully cured systems prior to adhesive application. The cure cycle was 255°F for 60 minutes. The primers were applied to the adherends while the adherends were still on the anodize racks to eliminate the handling of the anodized surfaces.

One of the Tasks of the program was to verify the processing tolerances of the primer system. Since the adhesive was considered "state-of-the-art," the tests were conducted on the maximum and minimum tolerance provided by the adhesive supplier for thickness and cure. Satisfactory mechanical and durability results were obtained when varying the primer thickness between .0001 inch and .0003 inch and when curing the primer at a temperature of plus and minus 25°F from the average cure temperature mentioned above. Primed panels were exposed to the clean room environment for periods up to 20 days. There was no effect from that length of exposure to the clean room environment. To keep possible contamination to a minimum, the normal processing requirements for the test panels and final article, bonding is to take place within 96 hours of primer dry.

Adhesive Application and Cure: - The adhesives for all new systems were stored at 0°F and allowed to reach room temperature prior to the application to the primed adherends. The time between curing of the primer and the final cure of the assembled details was held to less than eight hours on the laboratory test specimens. All specimens were cured in the autoclave at 250°F for 60 to 90 minutes at a pressure of 40 psi. Some test programs altered these parameters to determine the effects of the processing variables.

Tests for processing parameters were conducted on the adhesive as well as the adhesive primer. These tests included: heat-up rate to the cure temperature varying from 1.5°F per minute to 12°F per minute, and adhesive out time in the clean room up to two months. The specimens exhibited satisfactory lap shear and wedge crack failures, however the fresh FM73 had a porous glueline when exposed to a rapid heat-up rate.

Slow cycle fatigue tests with processing variables for the adhesives are

also under test. The slow cycle specimen configuration is more representative of the final article bond joint than the lab specimens and will therefore be a valuable confirmation of the lab tests.

Adhesive Mechanical Properties: - Prior to the start of preliminary design, a series of tests were performed to provide the required allowables. The following test descriptions indicate the many variables and properties of the adhesive systems that were classified:

Tensile Lap Shear. Tensile overlap shear specimens, 0.50 inch overlap by 1.0 inch wide, were standard for determining the basic shear strength of the adhesives at room temperature, at -70°F and +180°F. The adherend alloy was bare 7075-T6, 0.063 inch thick. All four adhesives with their primer systems were tested. Figure 117 contains the results of the lap shear tests. See Figure 118 for the test specimen configuration.

Double Overlap Shear Tests. An investigation was made to determine if the large amount of eccentricity normally found in standard lap shear specimens had an adverse effect on the shear strength of the adhesive. Double overlap shear specimens were fabricated with two adherends bonded at one end of another adherend, overlapping the one adherend 0.50 inch. See Figure 118 for the specimen configuration. In these tests, all the specimens broke the metal except in the +180°F tests. The relative shear strengths of the adhesive specimens, when bonded in the single overlap or double overlap configurations, were very close. The single lap shear had a lightly higher shear strength than the double lap shear at 180°F.

"T" Peel Tests. Metal to metal T-peel tests were made on the four adhesive systems. The specimen configuration (Figure 118) was a typical specimen used at Douglas Aircraft for determining the peel strength of adhesives. The bare 2024-T3 specimen was one inch wide, 12 inches long and 0.032 inch thick. The results are shown in Figure 119. It should be noted that the peel strength for the three adhesive systems with the woven carrier are generally higher than for the system with the mat or nonwoven carrier. Initially, it was considered that the woven carrier was a very desirable feature for the adhesive systems. However, further testint of double cantilever beam specimens and cycle stressed environmental

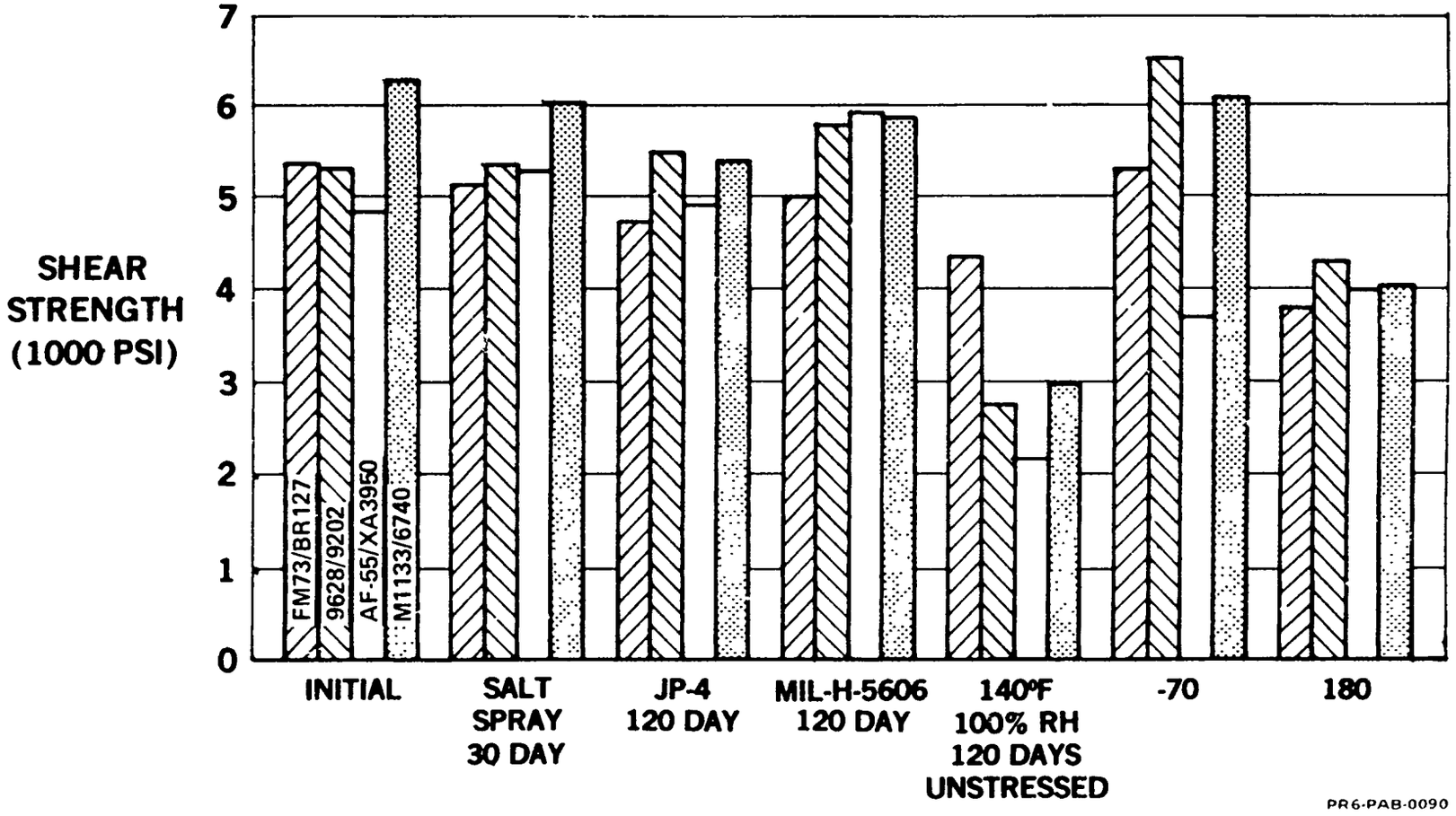
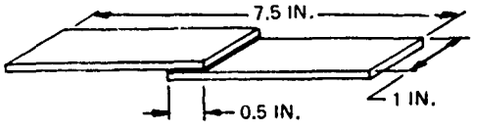
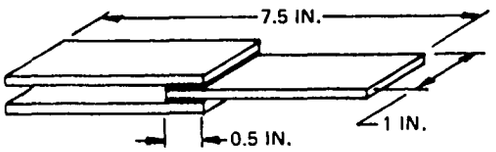


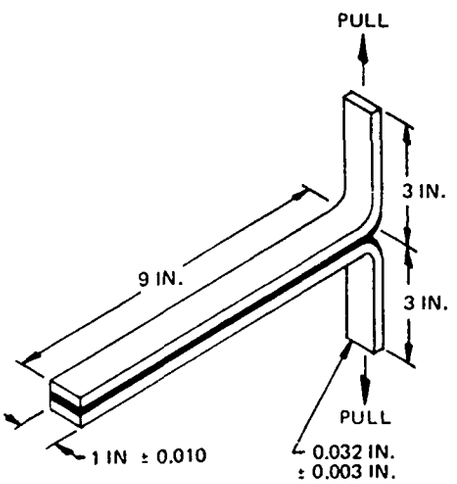
FIGURE 117. LAP SHEAR TEST



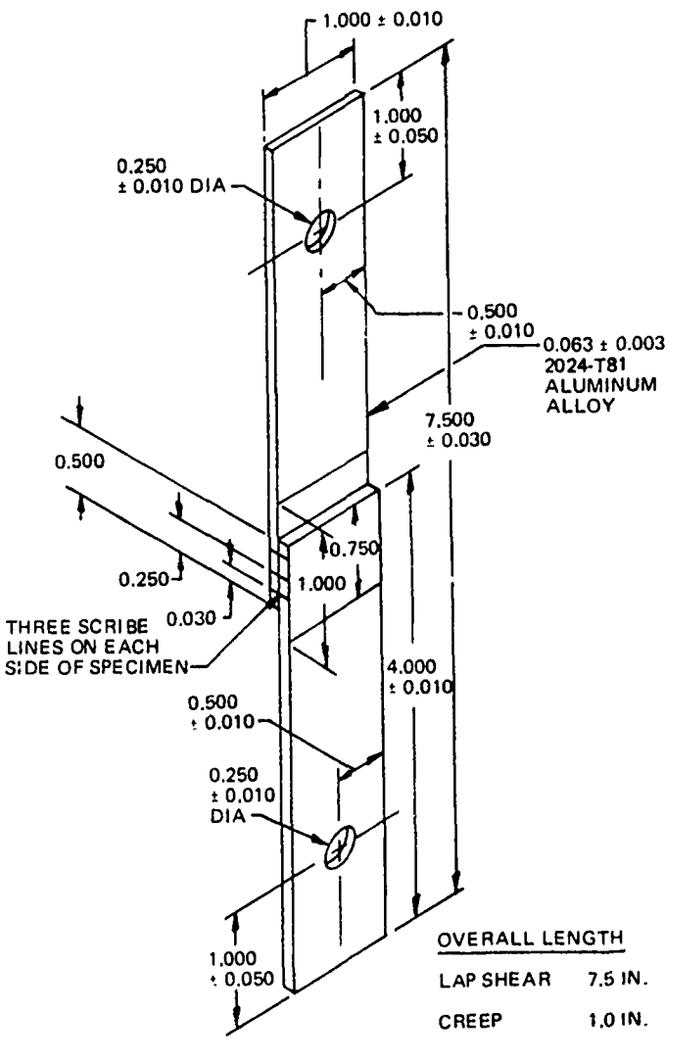
LAP SHEAR



DOUBLE LAP SHEAR



PEEL SPECIMEN



CREEP AND LAP SHEAR SPECIMEN

FIGURE 118. TEST SPECIMEN CONFIGURATIONS

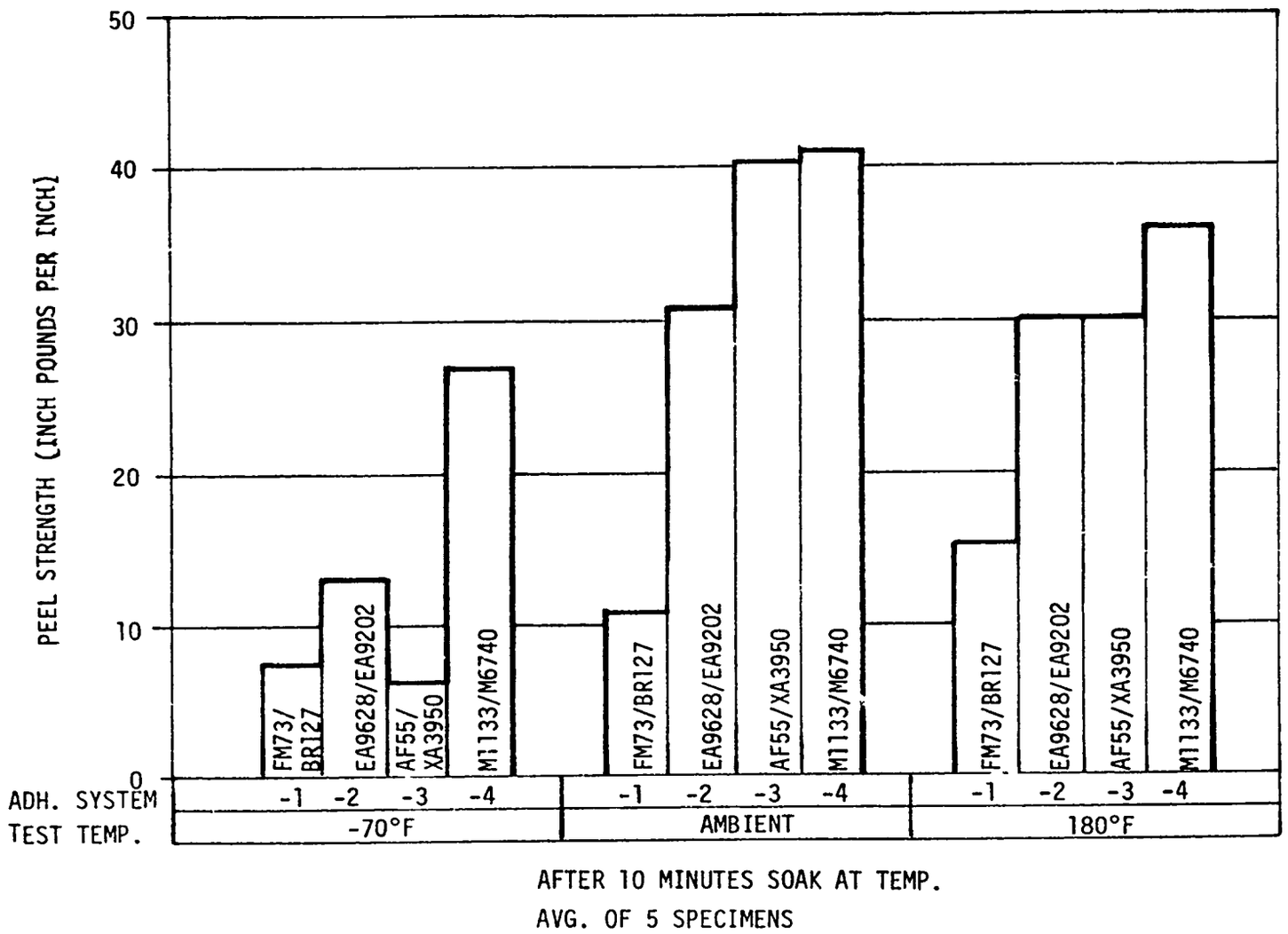


FIGURE 119. METAL TO METAL T-PEEL

specimens reversed this conclusion.

Metal to metal creep. The creep test used a modified single overlap shear specimen fabricated from bare 7075-T6 alloy, Figure 118. After fabrication, the specimens were scribed on the edge and loaded to 250 psi. They were then exposed to room temperature and to 180°F for 200 hours. Measurement of the displacement of the scribe lines was made after the exposure period. None of the adhesives indicated measurable creep.

Climbing Drum Peel. The possibility of using honeycomb for the final design required the testing of the adhesive systems used in the fabrication of honeycomb structure to determine their properties. One of the basic tests was the honeycomb climbing drum peel. The specimen configuration was a 12 inch by 3 inch,.020 inch thick 7075-T6 skin bonded into a sandwich configuration with a 2 mil foil 3/16 inch hex honeycomb core approximately .625 inch thick. The 2 mil foil honeycomb was intended to force the failure into the adhesive. In the test, the specimen was rolled on a drum as shown in Figure 120. Test results were based on the averages over a test length of about seven inches expressed in inch pounds per inch of width, see Figure 121. Again, the adhesive with the non woven carrier had generally lower average peel strengths than the woven carried adhesives at the temperatures tested.

Honeycomb Flatwise Tension. Honeycomb flatwise tension was determined on 2 by 2 inch specimens fabricated from the materials used for the climbing drum peel specimens. When bonded to aluminum blocks as shown in Figure 122 and stressed in a direction perpendicular to the face of the skin adherend, the tension strength of the skin to the honeycomb was determined, see Figure 123. All of the adhesives had comparable strength when tested at the two temperatures +180°F and room temperature.

Honeycomb Sandwich Beam Shear. This test determined adhesive honeycomb properties using test configuration shown in Figure 124. The test specimen was similar to the drum peel specimen. When stressed under single point load, the core sheared in every case. The honeycomb core used in the test had a shear strength equal to or higher than any core expected to be used in a honeycomb design.

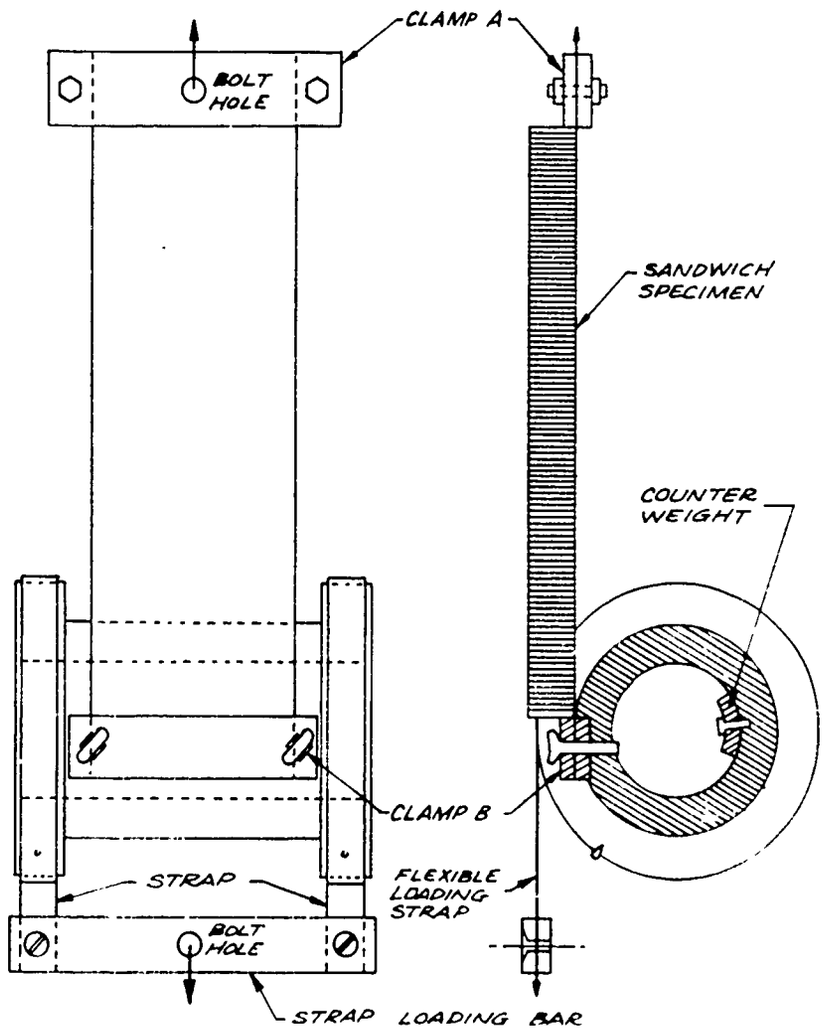


FIGURE 120. CLIMBING DRUM PEEL

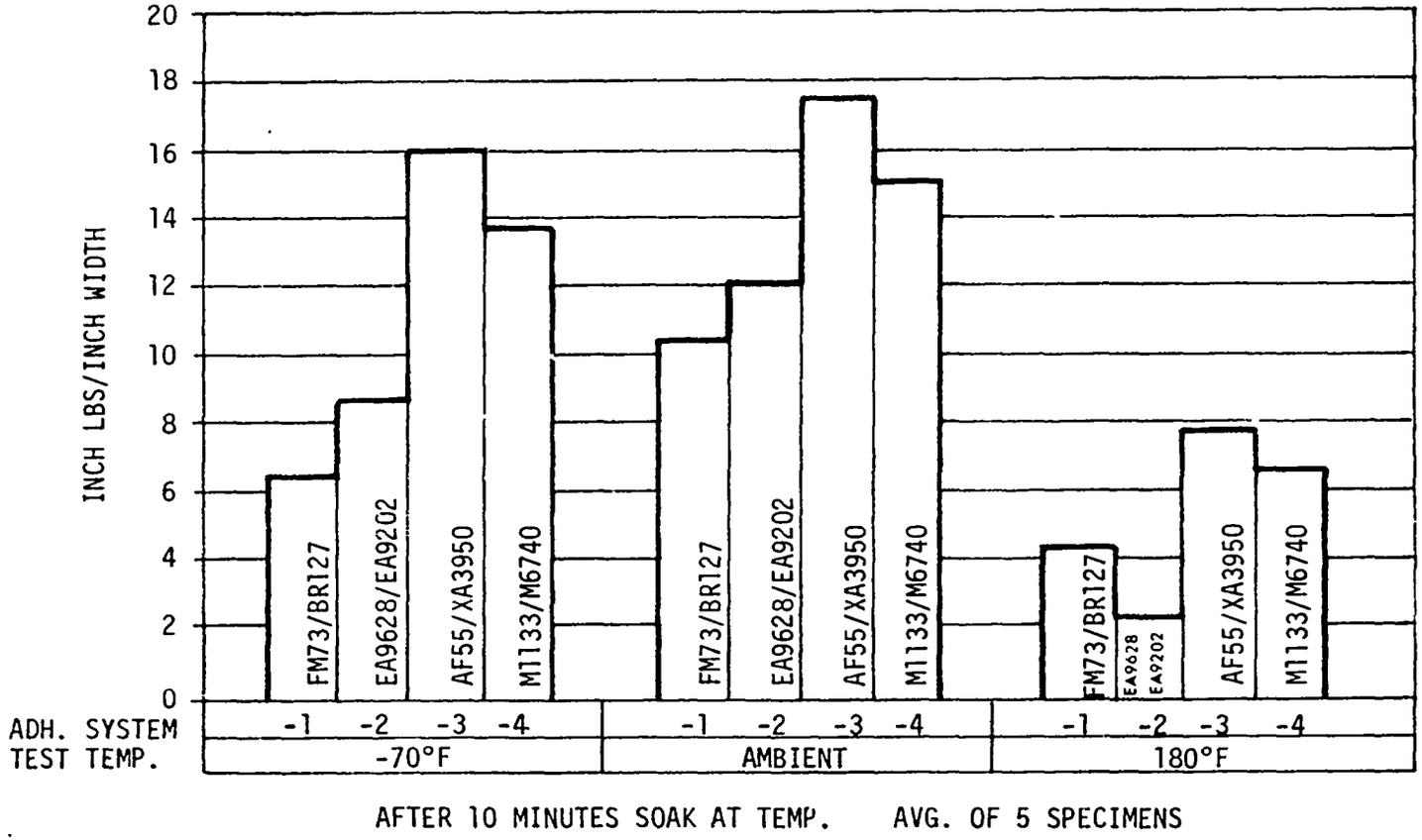


FIGURE 121. HONEYCOMB CLIMBING DRUM

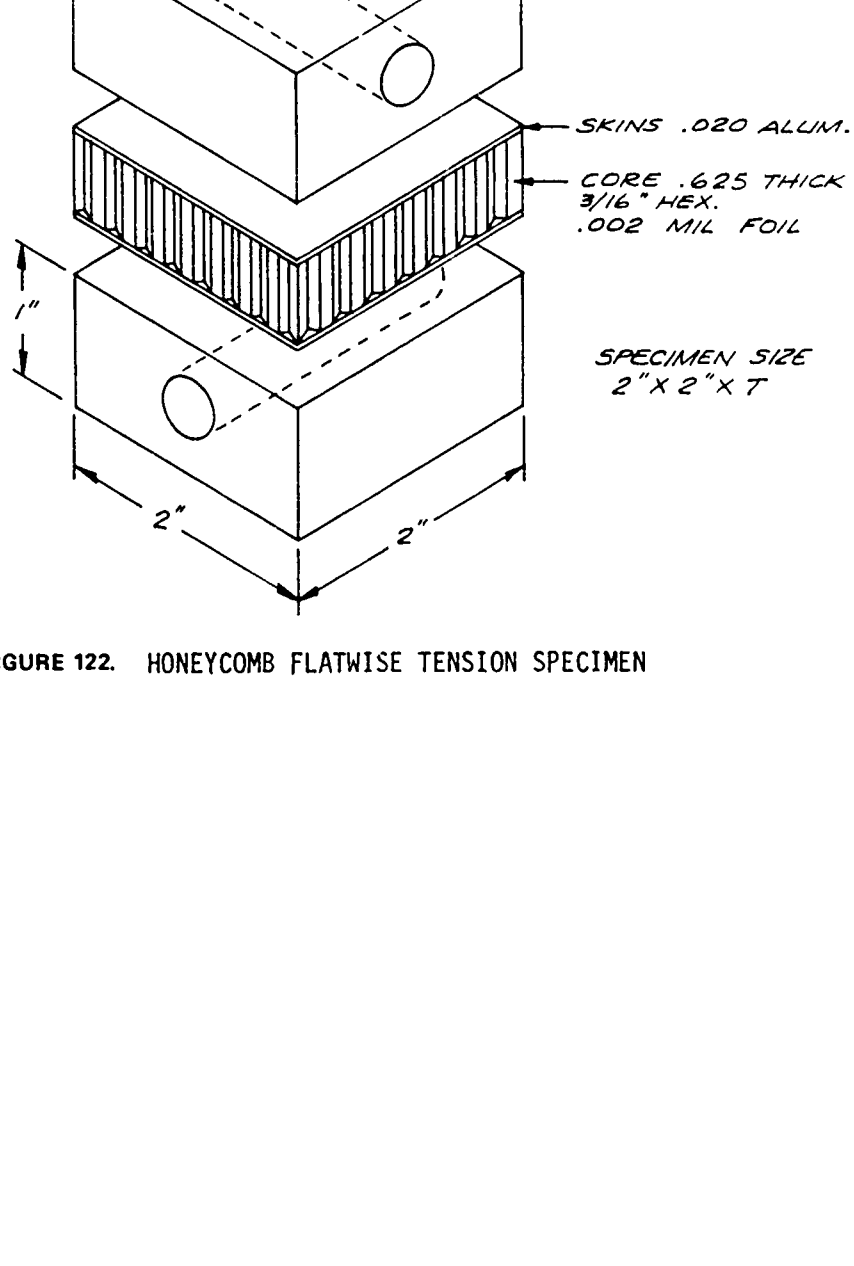


FIGURE 122. HONEYCOMB FLATWISE TENSION SPECIMEN

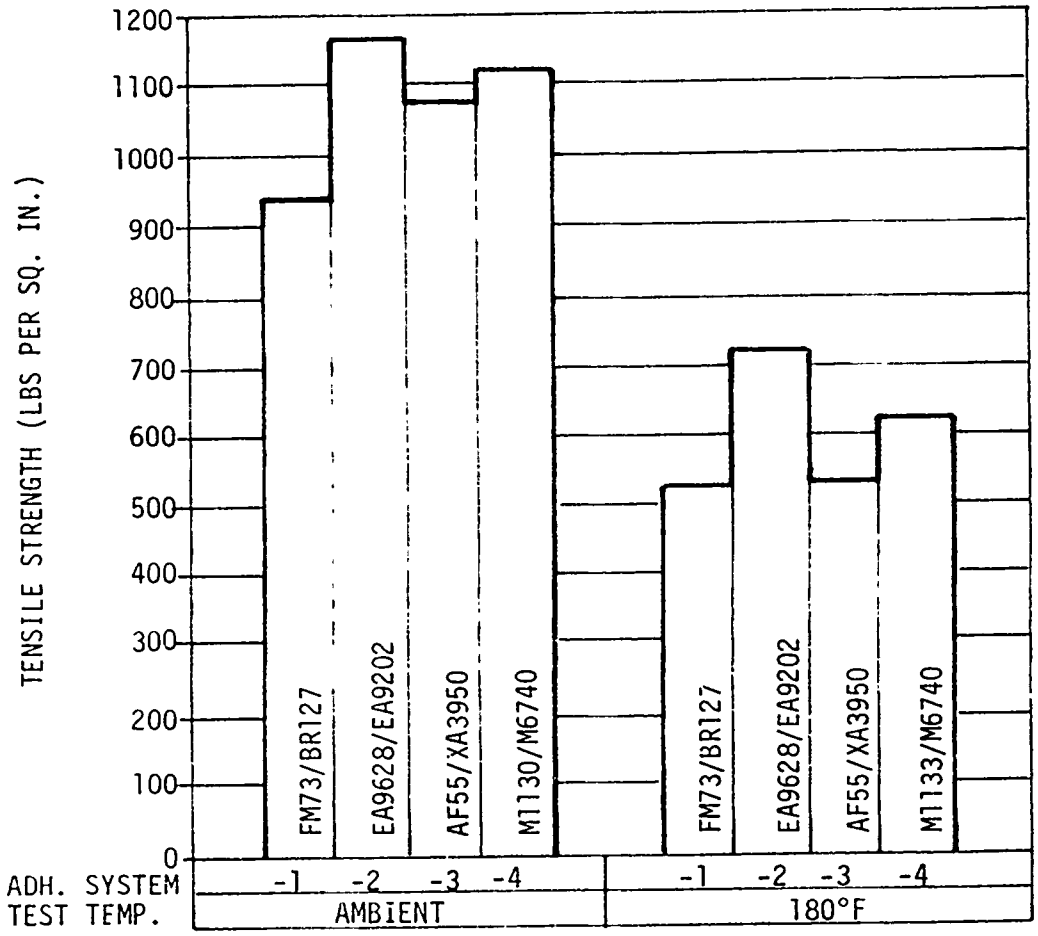


FIGURE 123. HONEYCOMB FLATWISE TENSION

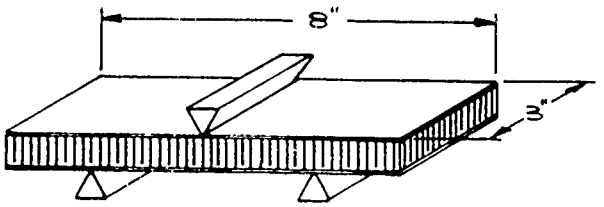


FIGURE 124. HONEYCOMB BEAM SHEAR SPECIMEN

Shear Modulus. Two bonded specimen types were used to determine shear modulus. The first method used the thick adherend lap shear specimen, see Figure 125. The adherends were .500 inch thick and the test area was .5 square inch, as in the lap shear specimen. A zero guage length extensometer was used to record the movement in the bond joint as the specimen was stressed.

The second method was the Napkin Ring shear test. The specimens consisted of relatively thin walled tubes bonded together end to end. They were loaded by rotating one adherend relative to the other about an axis coincident with the longitudinal axis of the specimen. These tests were conducted by The Singer Company, Kearfott Division in Little Falls, New Jersey.

The shear modulus determined from both test procedures compared very closely for each adhesive system tested. The average shear modulus for FM73 was 83,000 psi, EA9628 was 70,000 psi and AF55 was 93,000 psi as tested.

Double Cantilever Beam. Crack propagation characteristics of the adhesives were investigated using the double cantilever beam specimen, see Figure 126. The end of the specimen was wedged open, using the two screws, to approximately .10 inches. Measurements of the crack extension were made periodically during the test period. A calculation for G_1, crack extension force in inch pounds per square inch, was made using the formula in Figure 126. The specimens exposed to only ambient laboratory conditions showed very slow crack growth, see Figure 127. Subsequent to this test, the specimens have been placed at the Sea Atmosphere test station for long term beach exposure.

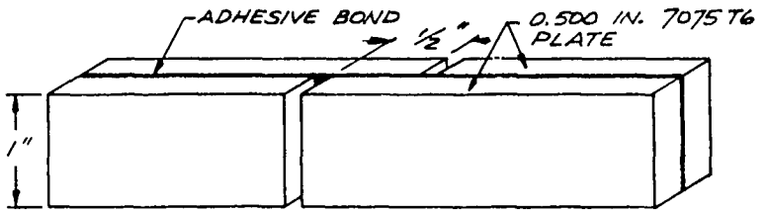
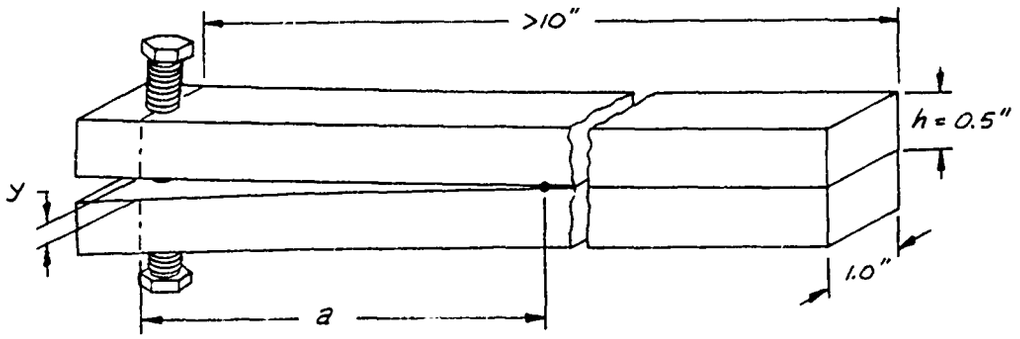


FIGURE 125. THICK ADHEREND LAP SHEAR SPECIMEN



$$G_I = \frac{y^2 M h^3 [3(a+.6h)^2 + h^2]}{16[(a+.6h)^3 + ah^2]^2}$$

WHERE:

G_I = CRACK EXTENSION FORCE, IN LBS/IN^2

y = DISPLACEMENT AT LOAD POINT, INCHES

a = DISTANCE FROM LOAD POINT TO CRACK TIP, INCHES

h = HEIGHT OF ONE BEAM, INCHES

M = MODULUS OF ADHEREND, LBS/IN^2

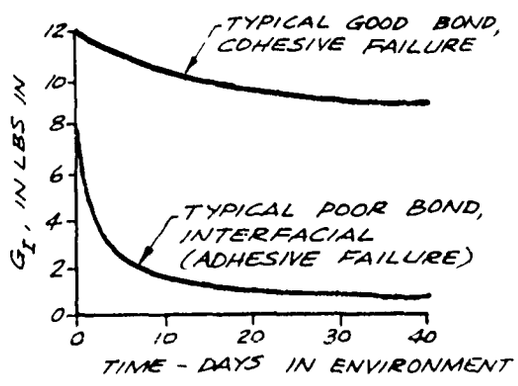


FIGURE 126. DOUBLE CANTILEVER BEAM

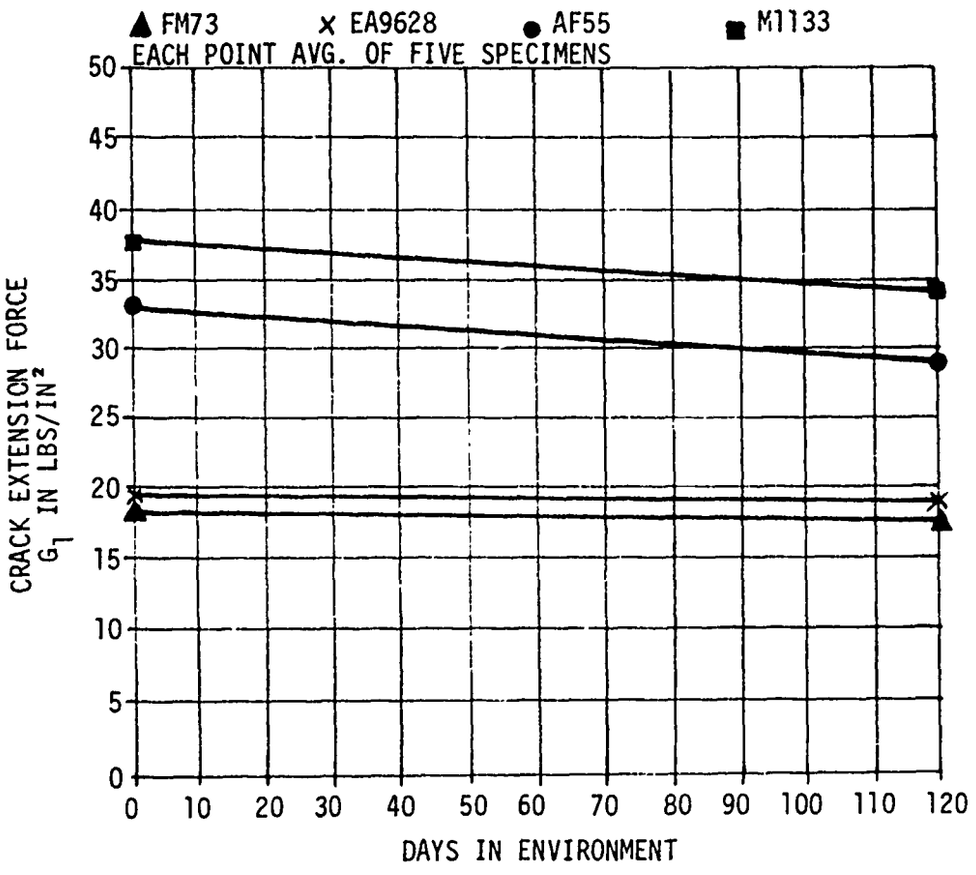


FIGURE 127. CRACK EXTENSION DATA DOUBLE CANTILEVER BEAM

Adhesive Environmental Properties: - After the mechanical testing had been started, each adhesive system was tested in various environments, see Table 53, to determine the respective environmental resistance of each adhesive system. Additional types of test specimen configurations were used to help determine this resistance.

Lap Shear Specimen Tests. Unstressed lap shear specimens, Figure 118, were exposed to environments of: salt spray, JP-4 jet fuel, MIL-H-5606 hydraulic fluid, and 140°F and 95-100% relative humidity. The exposure requirements are expressed in the Table and results are in Figure 128. The first indication of an effect from a 140°F and high humidity environment was evident. The three adhesives having the woven carrier had the largest strength loss.

Stressed lap shear specimens were also exposed to hydraulic fluid, TT-S-735 reference fluid and JP-4. The exposures were the same as shown in Table 53. The stress level was 900 psi on a .50 inch overlap shear specimen. The specimens indicated little or no effect from the exposure, see Figure 128.

"T" Peel Tests. T-peel specimens were subjected to the same types of environments as the non-stressed lap shear specimens. The effect of the woven carrier versus the non-woven carrier was very evident in the results, see Figure 129. Those adhesives with the woven carrier were more affected by exposure to JP-4, percent wise, than the mat or non-woven carrier. In all cases, the non-woven carrier adhesives had lower peel strength but were unaffected by the environment exposure.

Open Faced Climbing Drum Peel Test. This test was similar to the standard honeycomb peel test except that the specimen was fabricated with only one skin. The specimen was then exposed to the selected environment which allowed full exposure of the honeycomb-skin bond to the environment. The specimens were then removed from the environment, after the test period, and the second (opposite) face or skin was bonded with a fast cure cold bond adhesive. The specimen was then tested on the standard climbing drum fixture, see Figure 120. The results, in Figure 130 , show very little effect from the environments but do show that the non-woven carrier in the FM73 produced lower peel strengths.

TABLE 53

ENVIRONMENT TEST PARAMETERS

TEST ENVIRONMENT	EXPOSURE TEMPERATURE	EXPOSURE TIME SPAN	REMARKS
TT-S-735	AMBIENT	120 DAYS	IMMERSION
JP-4	AMBIENT	120 DAYS	IMMERSION
MIL-H-5606	AMBIENT	120 DAYS	IMMERSION
RELATIVE HUMIDITY 95-100%	140°F	120 DAYS 30 DAYS (APPROX) ONE HR	METAL TO METAL HONEYCOMB WEDGE CRACK
SALT SPRAY 5%	95°F	30 DAYS	
CHEM MILL ETCH	185° – 200°F	15 MINUTES DROP APPLICATION	PRIMER IMMERSION WEDGE CRACK
BILGE FLUID	AMBIENT	7 DAYS	WEDGE CRACK
ALKALINE CLEAN MIL-C-25769	AMBIENT	7 DAYS	WEDGE CRACK
IMMERSION CORROSION 5% NACL pH3 WITH ACETIC ACID	AMBIENT	30 DAYS	LAP SHEAR T-PEEL

PR6-PAB-451

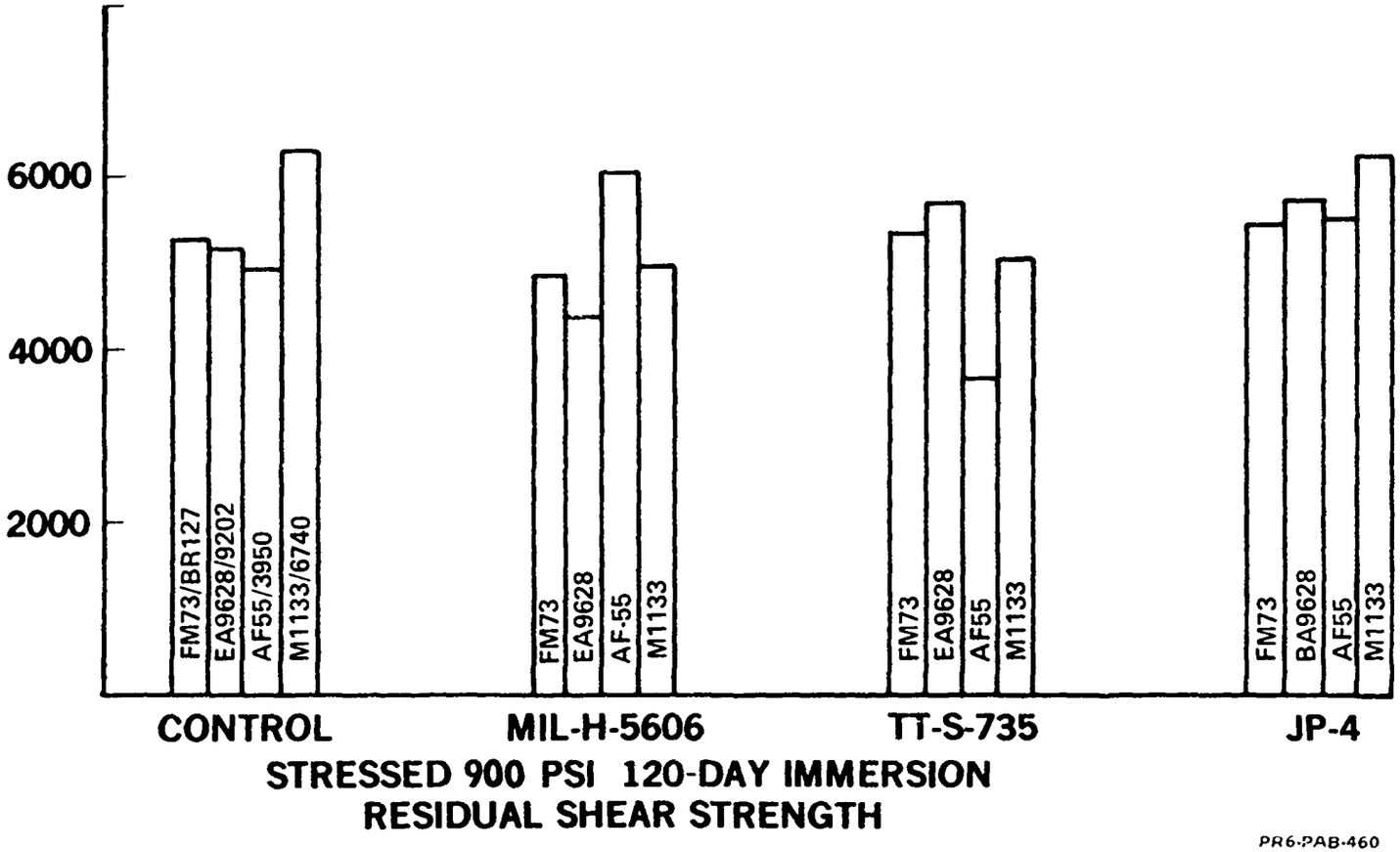


FIGURE 128. STRESSED LAP SHEAR

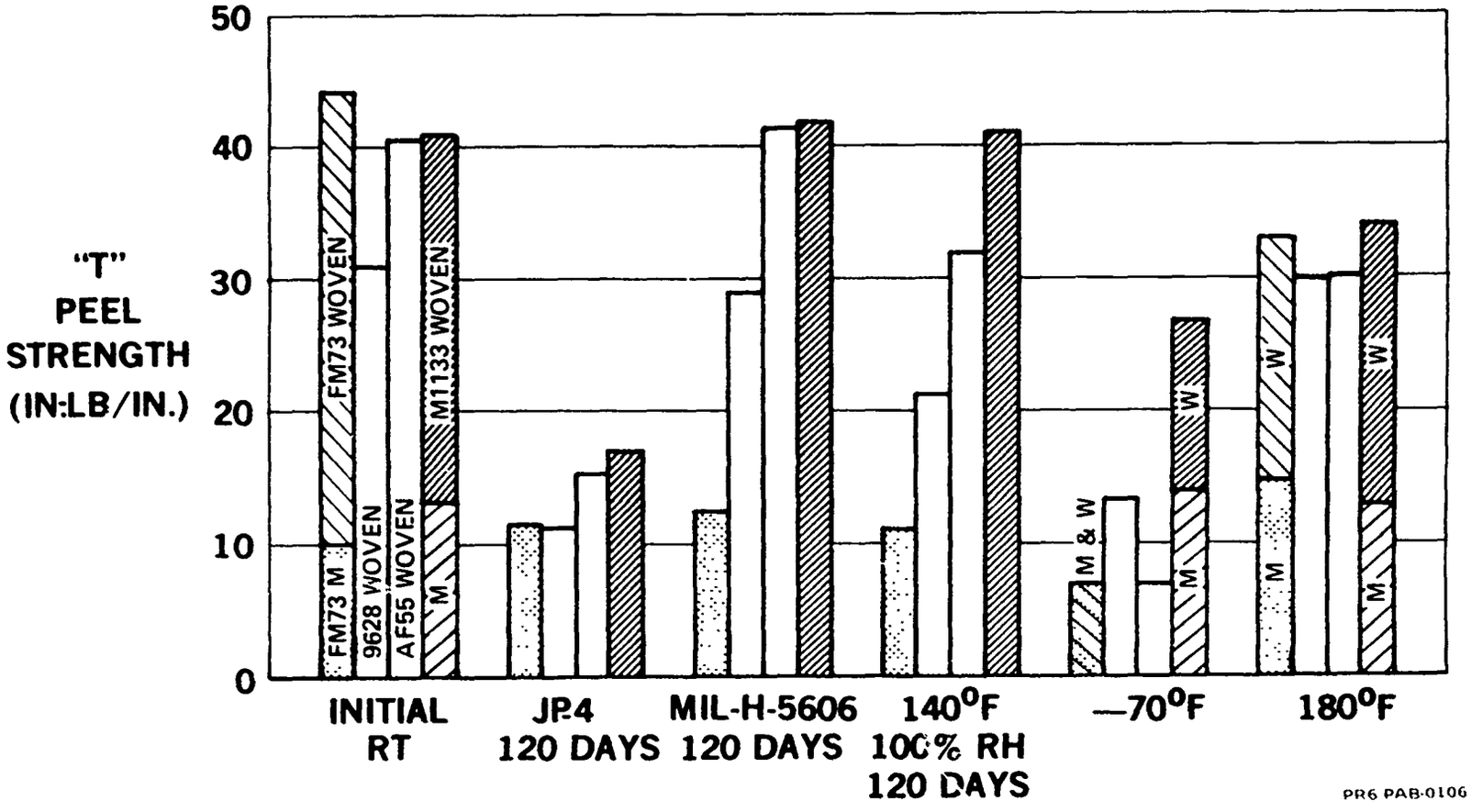


FIGURE 129. "T" PEEL TESTS

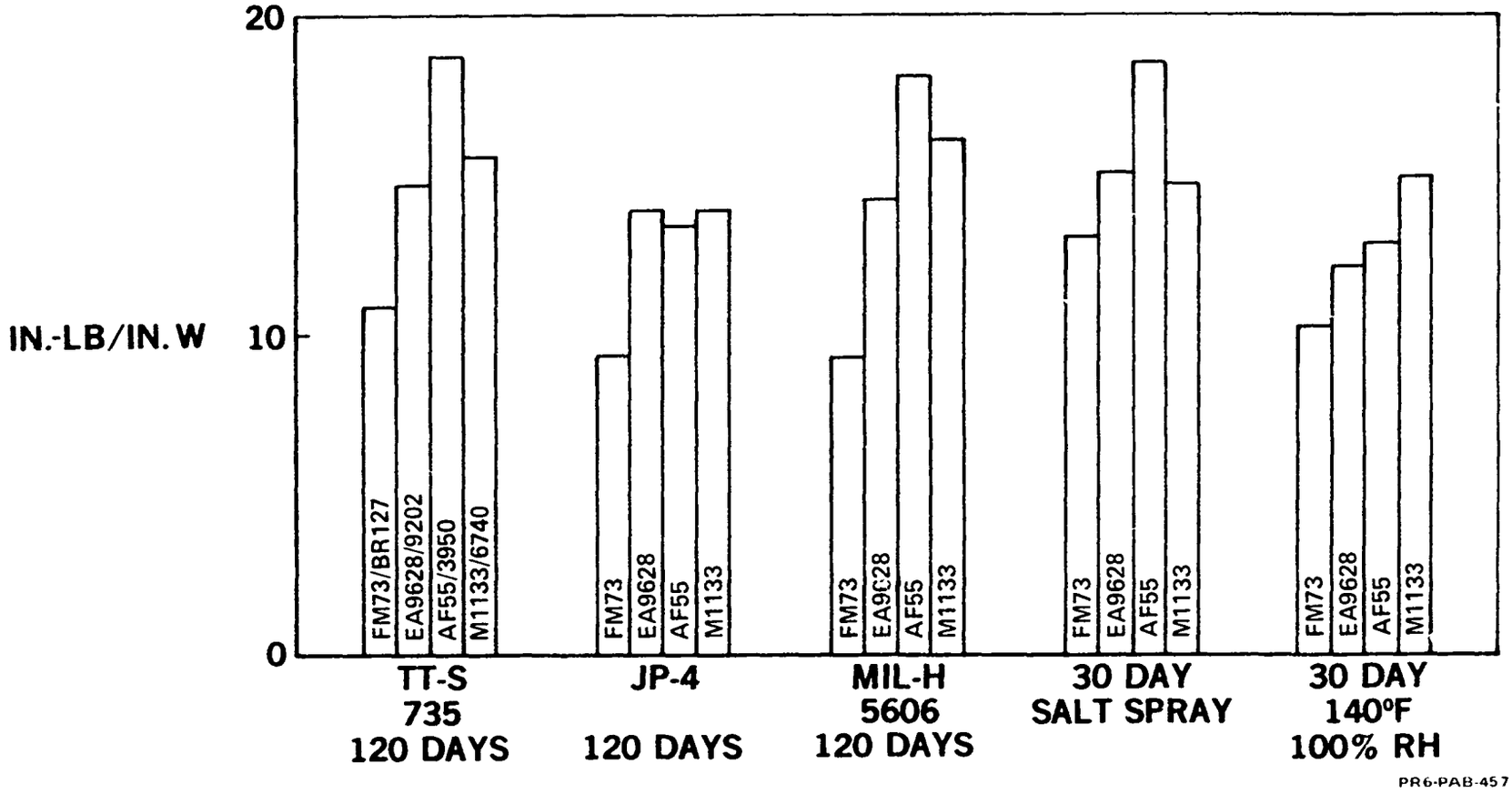


FIGURE 130. OPEN FACED CLIMBING DRUM PEEL

Wedge Crack Tests. Wedge crack specimens were used extensively in the program for environmental testing and for process control of all detail parts and test specimens processed through the surface treatment system. Well over 4000 individual specimens have been made and tested. The procedure was to bond two .125 inch thick bare 7075-T6 aluminum plates 6 inches by 6 inches together. The plate was then cut into one inch wide specimens and a .125 inch thick wedge driven into one end of the specimen to a depth of approximately one inch. A measurement was made of the extent that the adhesive was fractured down the specimen, see Figure 131. The specimen was then exposed to one of the various environments in the test program. For process control, this environment was a one hour exposure to 140°F and 100% relative humidity. The specimen was then measured for crack growth after exposure and the mode of failure determined. An acceptable cohesive mode of failure was experienced on all the specimens tested in all environments. The environments included: TT-S-735, JP-4, MIL-H-5606, 140°F and 100% RH, salt spray, chem mill etch applied to the crack tip, bilge fluid, and MIL-C-25769 cleaner. The bilge fluid test was a solution of 0.46% sodium sulfate, 0.82% sodium chloride at a pH of 7.8. The specimens were positioned so the fluid-air interface was at the crack tip. The specimen was vibrated at 70 Hz for 7 days. Specimens were also immersed in a 6% solution of Air-O-Foam fire extinguisher chemicals. In addition to the cohesive mode of failure which is a basic requirement, all crack growths were below 0.2 inch.

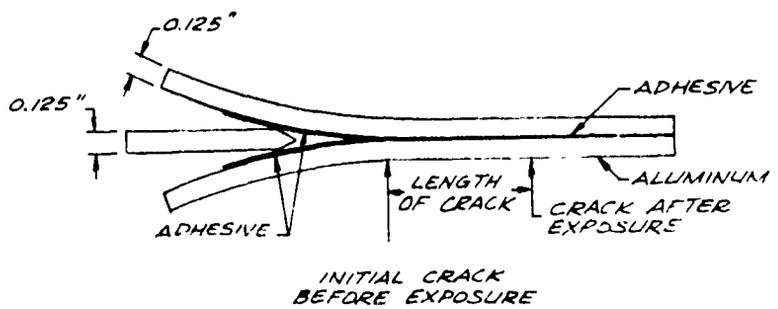


FIGURE 131. WEDGE CRACK SPECIMEN

Double Cantilever Beam. These environmental tests used the specimen described in Figure 126. After being wedged open, the specimens were exposed for 120 days to 100% relative humidity at 140°F. This test indicated that the woven carrier might be more susceptible to moisture intrusion than the non-woven carrier. Beside having larger crack extensions than the FM73, the three materials with woven carriers had some corrosion in the bond line in the uncracked edges of the specimens. The non-woven FM73 had no corrosion in that area. The results of the test are found in Figure 132.

RAAB Sustained Load. The RAAB test specimens, which are difficult to manufacture, were used for comparison tests only. Their main advantage is, that for 0.2 inch overlap area, they have 2.75 inches of exposed bond-line edge. The tests are normally conducted at 140°F and 100% relative humidity. Tests are currently in progress at -70°F and cycled environment tests are proposed. In the 140°F and 95 to 100% RH environment, RAAB specimens, see Figure 133, were stressed at three different load levels, 1450 psi, 1750 psi and 2050 psi. The results are shown in Figure 134. Here, again, the non-woven carrier adhesive system sustained the stress for the longest period of time.

RAAB Cycled Load. Tests run at the Boeing Commercial Aircraft Company and at Bell Helicopter Company indicated that cycle stressed lap shear specimens in the same environment would fail in a shorter load time period than sustained load specimens. RAAB tests were started at three load levels; 1500 psi, 900 psi and 300 psi. The cycle rate is one hour loaded and 15 minutes unloaded. Comparing the number of cycles, which in turn is the number of hours under load, it can be seen that the cycled specimens stressed to 1500 psi failed after only an average of 200 hours at load. The sustained loaded panels in the same environment and loaded at 1450 psi failed at a much higher time of exposure. Additional tests are in progress to determine the effects of different primers and carriers for each of the adhesives. The results of the cycled specimen tests are shown in Figure 135.

Additional RAAB cycled tests will be made during Phase II in the 600 series Tasks. These tests will include cycling of several types of adhesives in the RAAB configuration. These tests will compare adhesive systems in service with the PABST system using identical specimens and environment conditions. Also included will be a cycled environment with the cycled load which should be more representative of the actual conditions expected to exist in an adhesive bonded fuselage. Other types of specimens such as shear, bonded tees to skins, T-peel and configurated specimens should allow a very good comparison of a large spectra of adhesives when tested as the PABST adhesives are. Tests will also be run on determining the optimum cycle including ramp to load and unload rates which will help set a standard for future cycle testing. Tests on "neat" adhesive specimens will continue to develope parameters for the characterization of the FM73 adhesive.

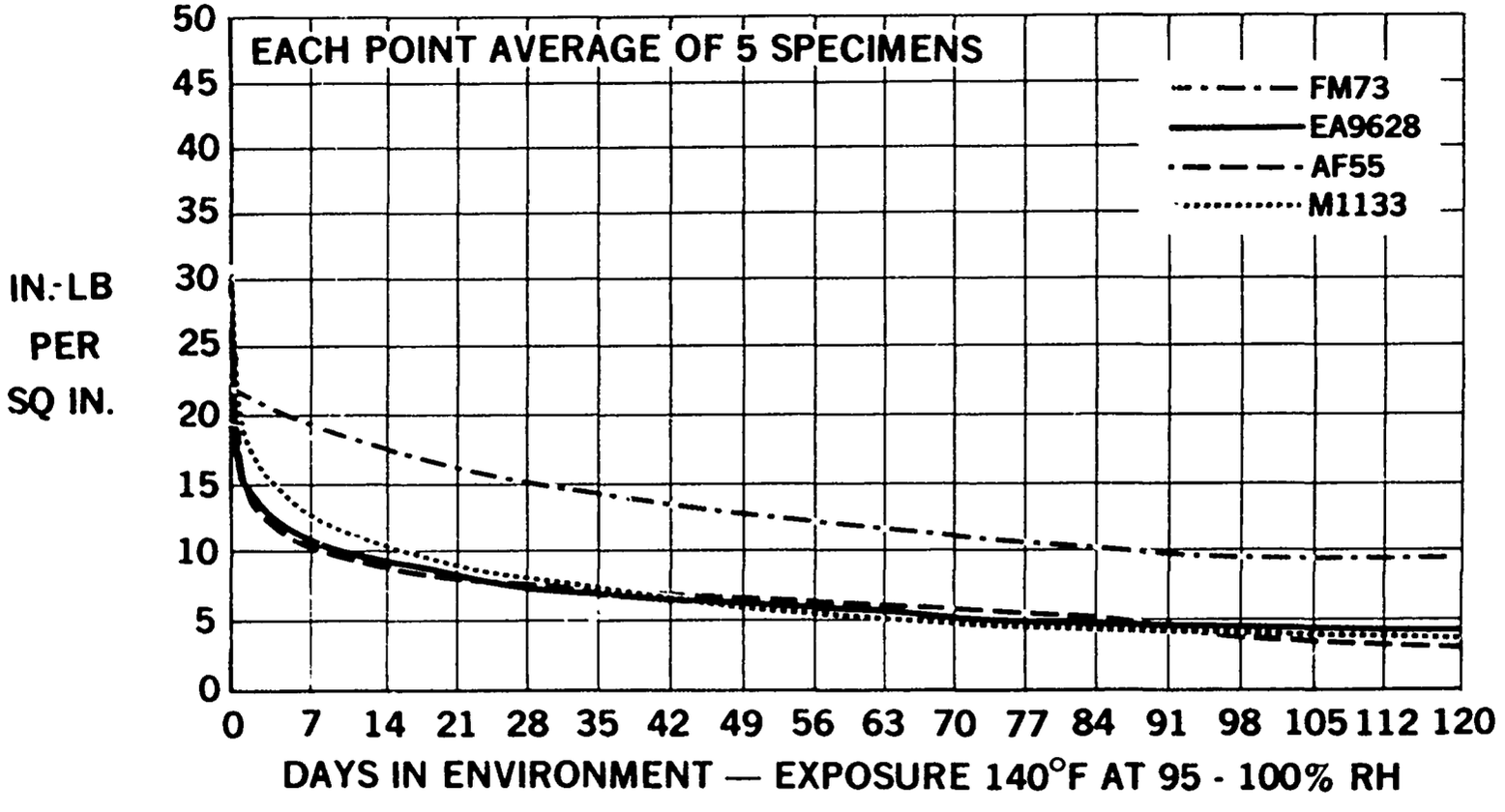


FIGURE 132. DOUBLE CANTILEVER BEAM TEST RESULTS

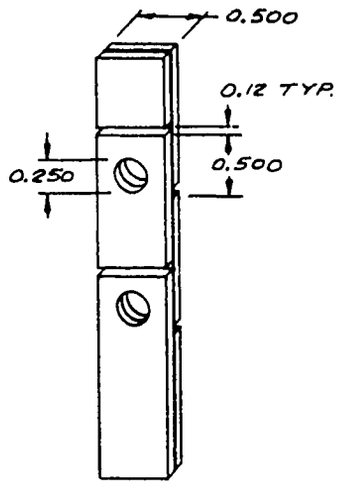


FIGURE 133. LAP SHEAR (RAAB) (TWO OF SEVEN TEST AREAS SHOWN)

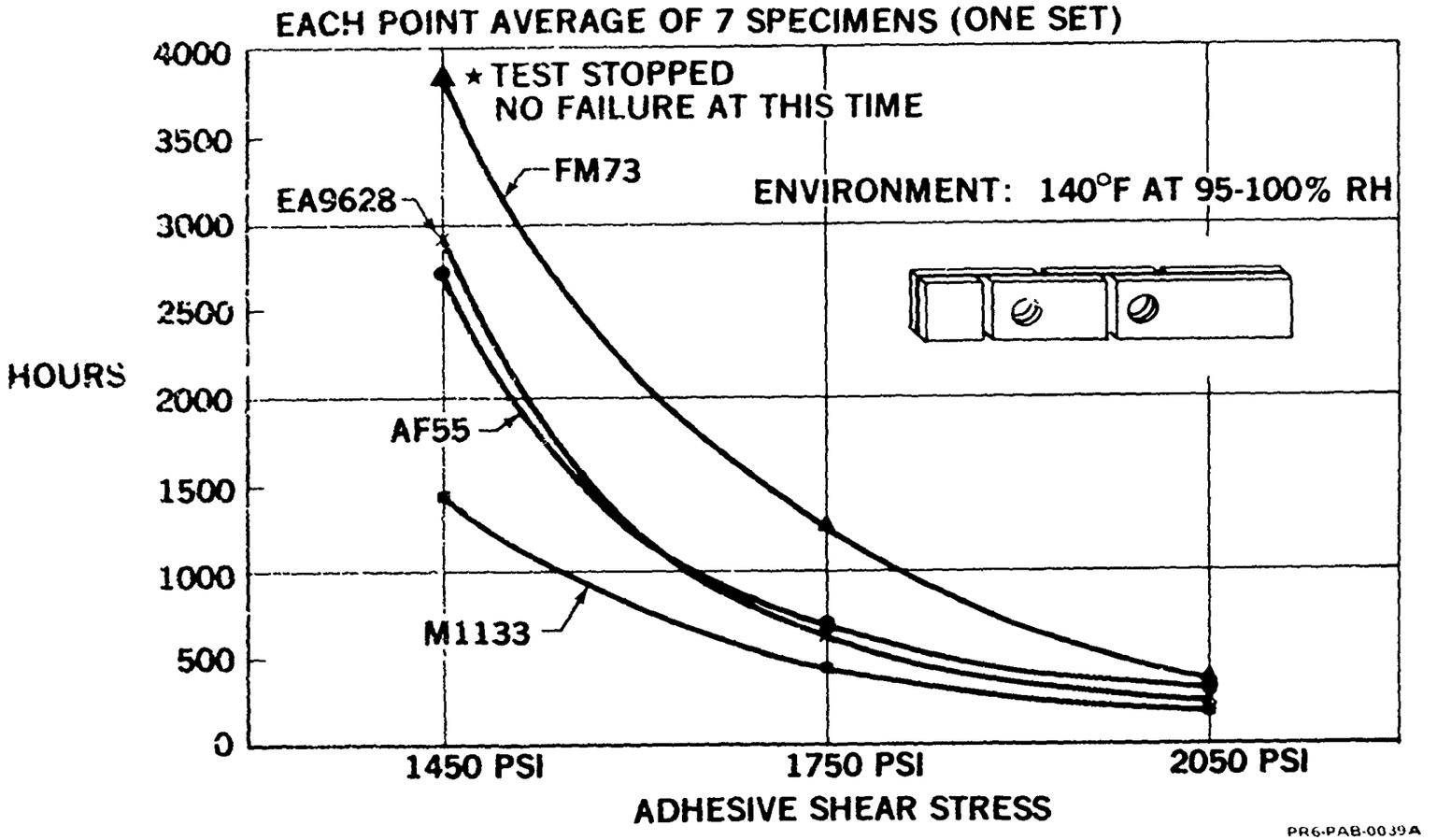


FIGURE 134. RAAB SUSTAINED LOAD

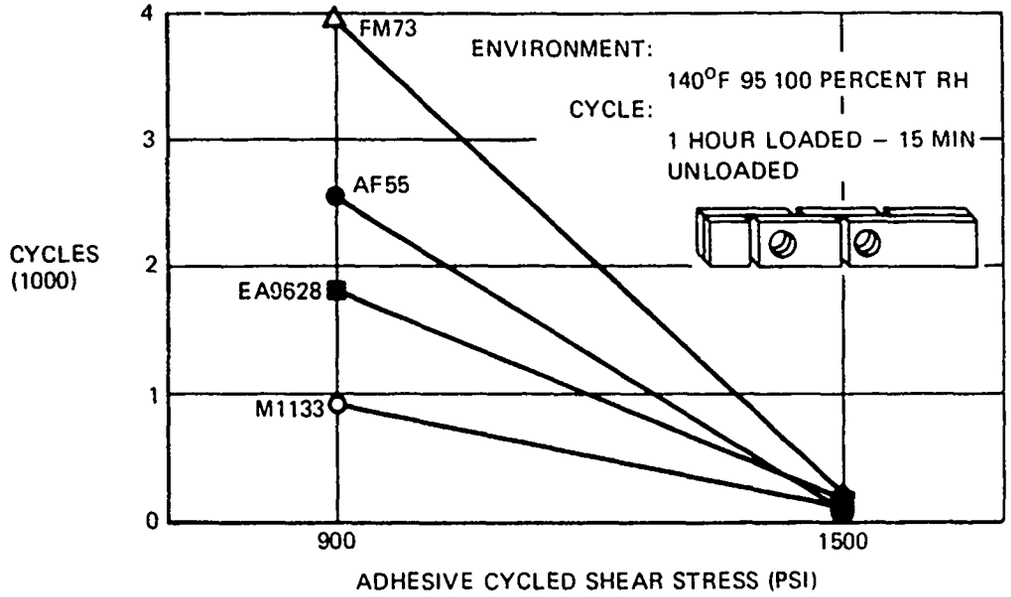


FIGURE 135. CYCLED LOAD/ENVIRONMENT TEST

Mechanical Fastening Tests

Mechanical fastening of Primary Adhesively Bonded Structural Components is primarily limited to major longitudinal and circumferential joints. The objective of this program is to establish manufacturing procedures, requirements and limitations associated with hole preparation and mechanical fastening of bonded joints. The areas of investigation cover hole generation, riveting methods and interference-fit fastener installations. Drill lubricants, coolants and solvents used for this program were also evaluated to determine the effect on FM73 adhesive system.

Test Procedures and Results.-

Test Specimen Fabrication for Hole Generation, Riveting Methods and Interference Fit Fastener Installations: -Coupons were taken from each parent sheet of 7075-T6 unclad aluminum alloy material used in this program. A minimum of three coupons per parent sheet were tested in compliance with Federal Test Method Std. No. 151B to determine sheet mechanical properties. Test results are recorded in Table 54.

Parent sheets (48" x 144") of .040" and .090" gages were sized into 48" x 72" sheets for subsequent mating. Sheets were phosphoric acid anodized and BR127 primed using production processing. The FM73 adhesive film was applied by materials and process engineering metal bond personnel. Bagging and autoclave cure was conducted. Autoclave temperature was 255°F, pressure application was 40 psi, and sheet temperature ranged from 250°F to 255°F for 95 minute cure cycle. Bonded sheets were sized into 36" x 48" sheets, assigned an identification number and ultrasonic C-scan inspected. The C-scan recordings indicated neither bond delamination nor bond voids for all parent sheets. Each detail specimen was identified prior to shearing (.040-.040") or sawing (.090-.090") to 4" x 5" size for traceability to the parent sheet. A cross-index of sheet identification to detail specimen numbers with material and bond data is recorded in Table 55. Figure 136 shows the C-scan record for bonded sheet No. A1-1. Figure 137 shows the method used for traceability of detail specimen to bonded sheet.

Bond delamination at specimen edges was observed as the various detail specimens (.090" - .090") were subjected to ultrasonic C-scan inspection and visual examination of the bond interface. This condition was attributed to

PRECEDING PAGE BLANK-NOT FILMED

TABLE 54

SHEET MECHANICAL PROPERTY – TENSILE STRENGTH TEST RESULTS

LABORATORY TEST DATA

TEST NO 10204

SHEET 1 OF 1

TEST DESCRIPTION TENSILE STRENGTH MATERIAL 7075-T6 BARE

DATE 9 JULY 1975 SALES ORDER DJ19A2E0 T2-1 E W O NO

REQUESTED BY W. D. GAST PHONE QUANTITY OF COUPONS 9

TEST PROCEDURE TY&E AT ROOM TEMPERATURE

2-INCH GAGE LENGTH

LOAD RATE 95 KSI/MIN STRAIN RATE E.S.T PSI ULT

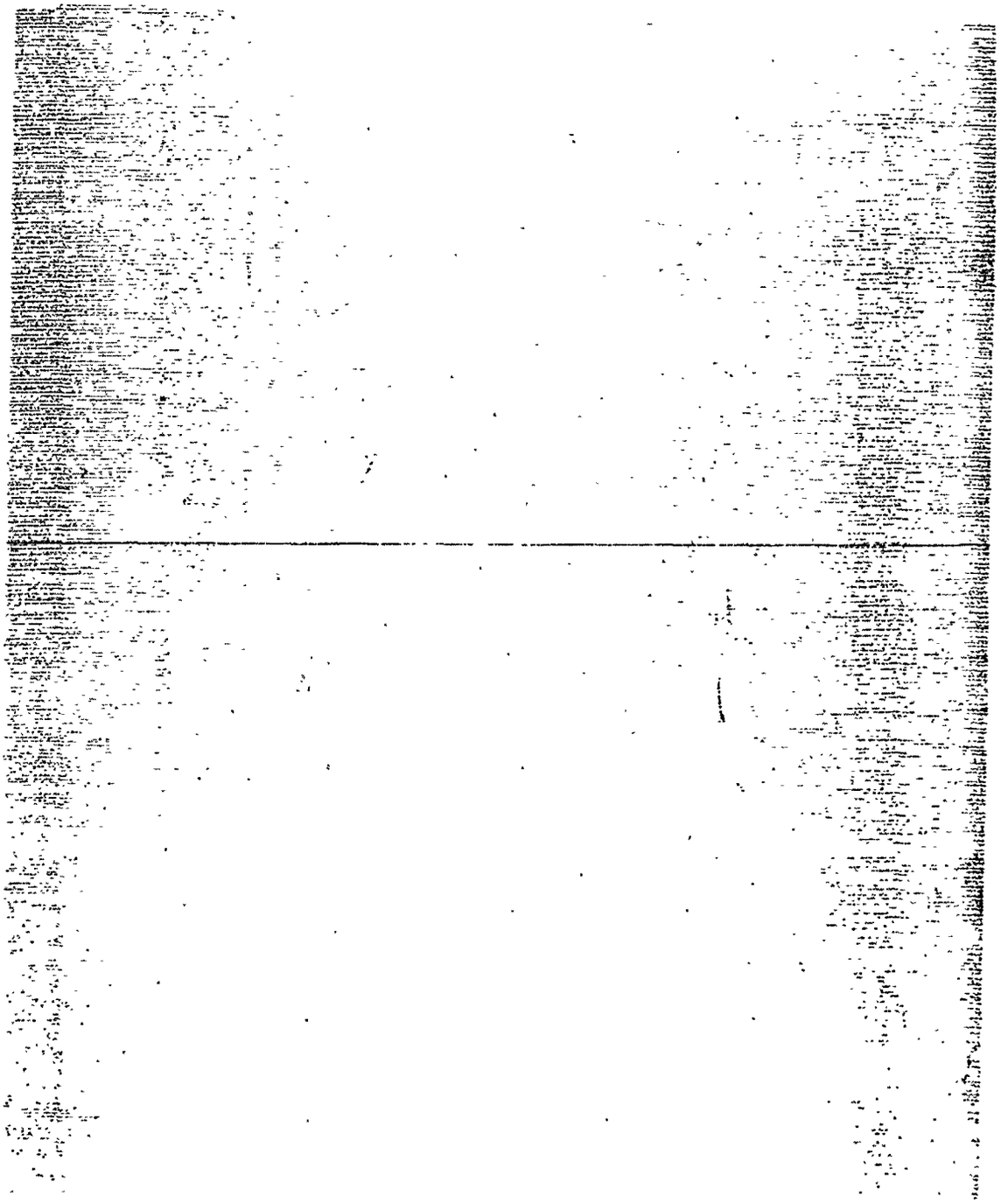
ASSIGNED TO R. F PHILLIPS WITNESS

SPECIMEN CODE	SIZE (IN) W	T	AREA (SQ IN)	ELONGATION (%)	ULT TENS STR LOAD	PSI	ULT YLD STR LOAD	PSI
MP-1-A1	0 5470	0 0390	0 0213	11.8	1830	85,915	1650	77,464
MP-2-A1	0 5471	0.0396	0 0217	11 7	1860	85,714	1671	77,000
MP-3-A1	0 5472	0 0393	0 0215	11.0	1867	86,837	1686	78,418
MP-1 A2	0 5483	0.0391	0 0214	11.7	1848	86,355	1674	78,224
MP-2 A2	0.5476	0.0395	0 0216	11 4	1867	86,435	1689	78,194
MP-3-A2	0 5474	0 0392	0 0214	11 3	1854	86,635	1680	78,504
MP-1-A3	0 5470	0 0907	0 0496	11.5	4170	84,072	3942	79,475
MP-1-A3	0 5478	0 0910	0 0498	11 6	4189	84 116	3960	79,518
MP-1-A3	0 5480	0 0902	0 0494	11 8	4167	84,352	3930	79,554

TABLE 55

SHEET AND DETAIL SPECIMEN IDENTIFICATION CROSS INDEX

SHEET IDENTIFICATION NO	SHEET MATERIAL	FM73 BOND FILM	BOND THICKNESS RANGE	DETAIL SPEC NO
A1 1	7075-T6 (0 040-0 040 IN)	1 PLY	0 007 0 008 IN	S1 S78 INCL
A2 1	7075-T6 (0 040-0 040 IN)	2 PLY	0 012 0 014 IN	S141 S178 INCL
A3 1	7075 T6 (0 090-0 090 IN)	1 PLY	0 0055 0 0075 IN	S79 S140 INCL
A3 2	7075-T6 (0 090-0 090 IN)	2 PLY	0 0120 0 0135 IN	S179 S216 INCL



41-1

FIGURE 136. ULTRASONIC C-SCAN RECORD - BONDED SHEET

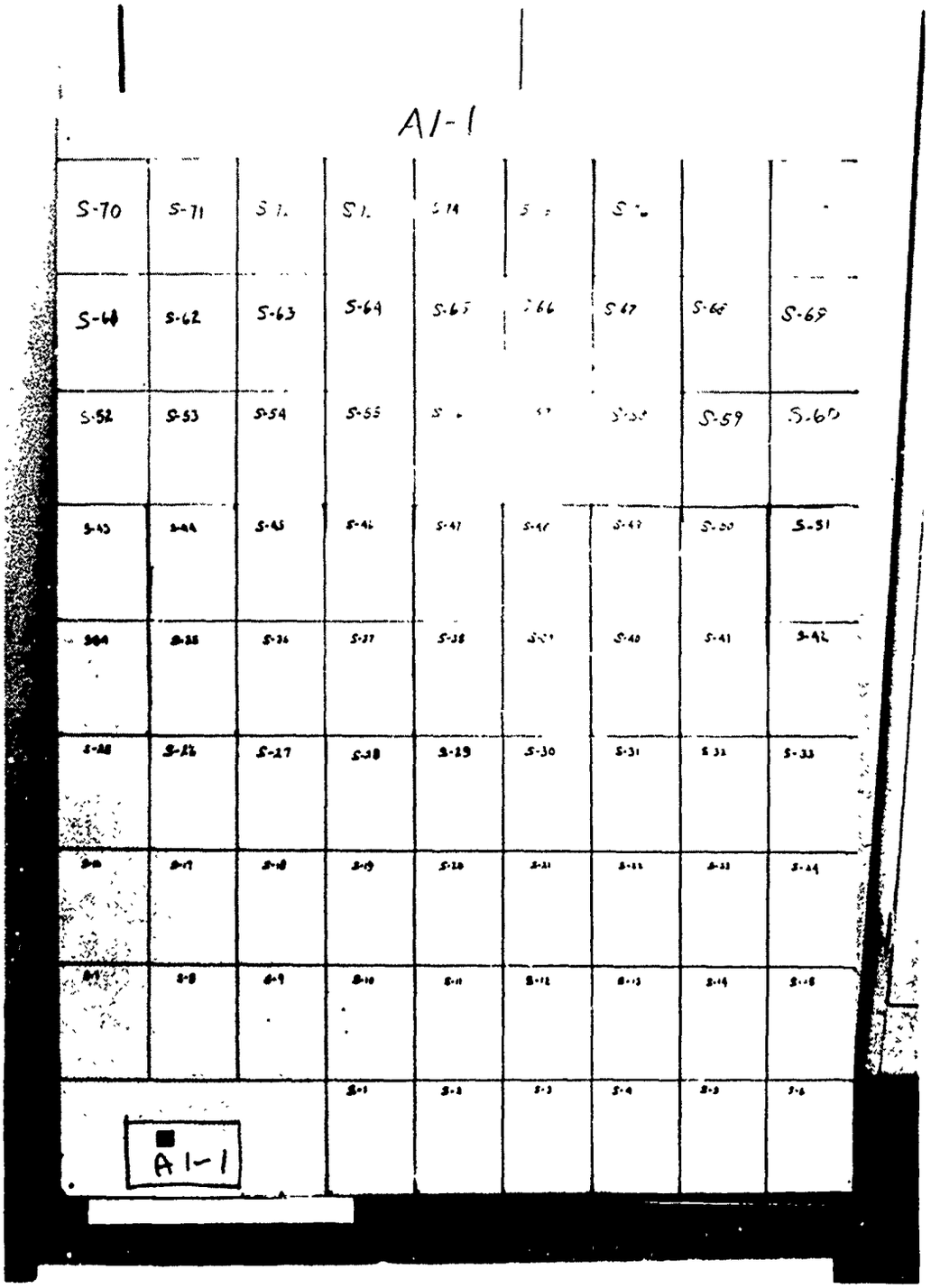


FIGURE 137. DETAIL SPECIMEN IDENTIFICATION AND TRACEABILITY TO BONDED PARENT SHEET

heat generated from the sawing operation when detail specimens were sawed to size from the parent sheet. Penetration of fluorescent penetrant occurred on less than one-half of the total area showing bond delamination by ultrasonic C-scan or by visual examination. This condition had no affect upon the outcome or results of the planned mechanical fastening tests but it is being reported to high-light a potential problem associated with sawing of bonded members. See Figures 138 and 139 for typical bond delamination by visual examination and C-scan record.

Lap Shear Specimen Fabrication and Test Procedure: - A sheet of 7075-T6 .125" unclad aluminum alloy was sawed to size for lap bonding with FM73 adhesive after phosphoric acid anodize and BR127 prime. The bonded sheets were identified as A4-1 and A4-3. A total of 28 lap shear specimens were sawed to size from the bonded sheets per ZC008242-511 configurated drawing. The 28 specimens were identified and checked with a Fokker bond tester prior to drilling of .250" diameter holes. See Figure 140 for illustration of typical lap shear specimen.

Specimens (seven per variable) were submerged in type A drill lubricant (DAC Proprietary), type B drill lubricant (DAC Proprietary), and solvent (1-1-1 Trichloroethane). Seven specimens were retained as control (no-soak).

Five specimens of each variable were removed from the solutions after 138 days of submersion. These specimens in addition to five control specimens were subjected to lap shear test.

The remaining specimens were removed from the solutions after 139 days of submersion and were visually examined with the remaining control specimens for bond line porosity. Examination showed an absence of porosity in specimens from A4-1 sheet, but specimens from A4-3 sheet displayed porosity in the bond line. Specimens were then subjected to lap shear test.

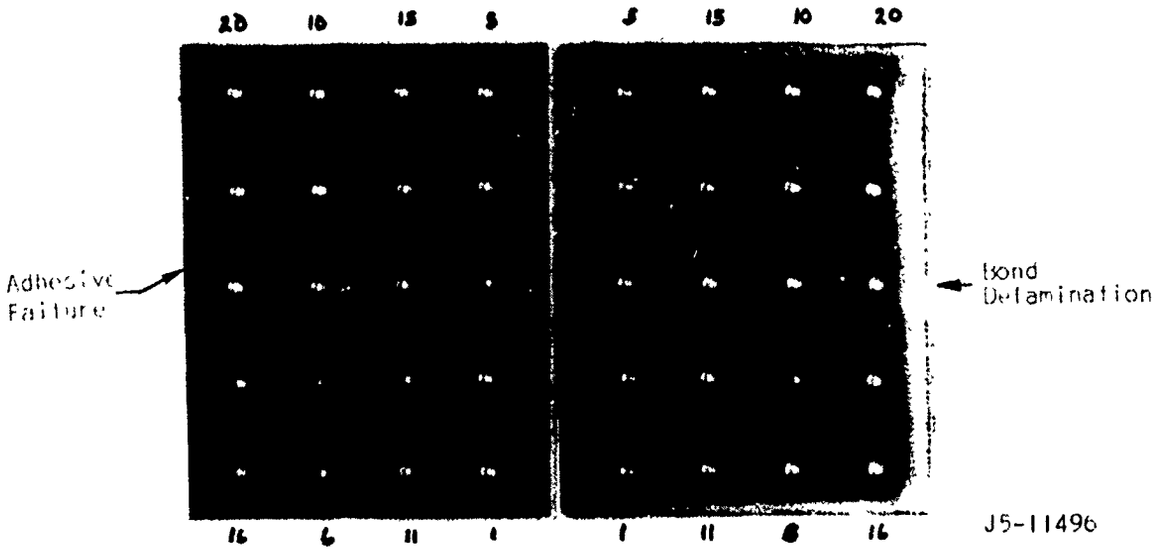


FIGURE 138. ADHESIVE AND DELAMINATION FAILURES

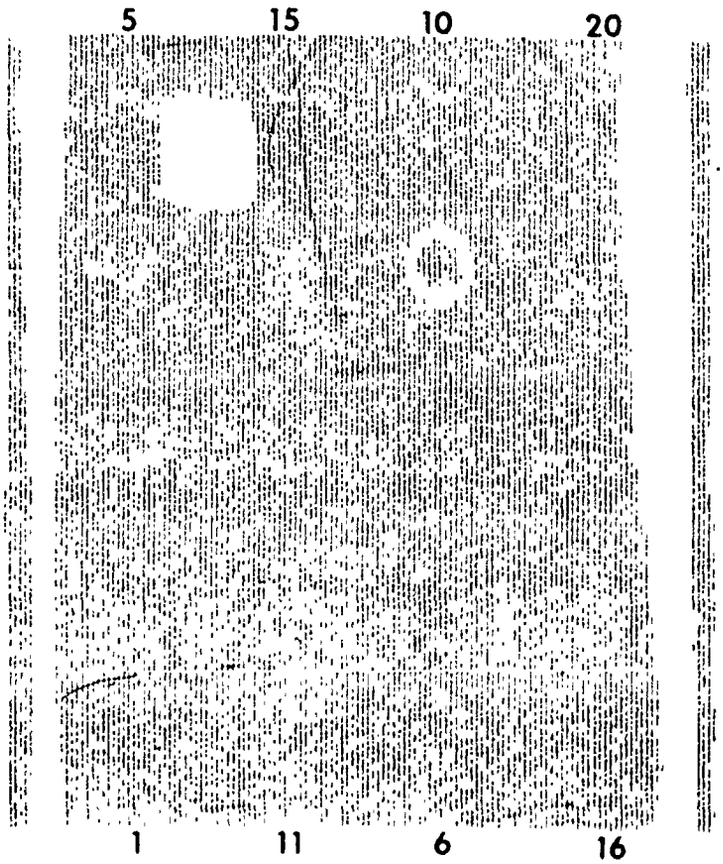
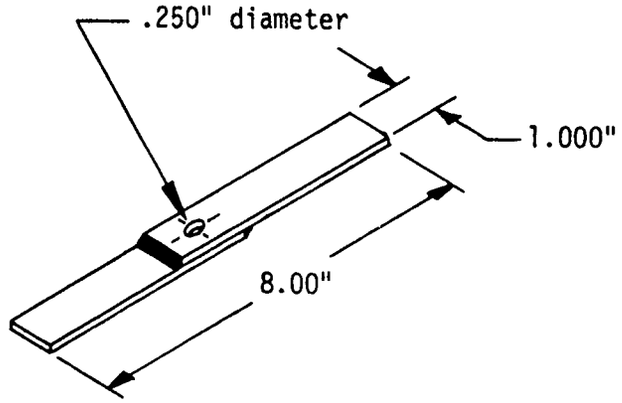


FIGURE 139. C-SCAN RECORD



.125" - 7075-T6 Bare Aluminum Alloy/FM73-1 Ply Adhesive (Wt. .045/ft^2)

FIGURE 140. LAP SHEAR SPECIMEN

The failure mode for the initial 20 tested specimens was of a cohesive type. All 20 specimens exceeded the minimum psi lap shear strength requirement of 4000 psi as specified per DAC Specification DPS 1.950 SPEO 001 "D." However, comparison of test results revealed that specimens from the A4-1 sheet provided higher shear strengths (4,885 psi average) than those from the A4-3 sheet (4,143 psi average), see Table 56.

TABLE 56

LAP SHEAR TEST RESULTS

Spec. No.	Parent Sheet No.	Test Variable	Fokker Quality Units	Ultimate Shear Load	Shear Psi (Net Area)
1	A4-1	Control	21R	4662	4846
2	A4-1	↓	20R	4620	4838
3	A4-1	↓	20R	4340	4618
4	A4-1	↓	20R	4875	5121
5	A4-1	↓	21R	4590	4889
* 27	A4-1	↓	17R	4641	4990
* 28	A4-1	Control	17R	5051	5056
6	A4-1	Type A -Drill Lube	14R	4180	4442
7	A4-1	↓	12R	4640	4911
8	A4-1	↓	12R	4470	4802
9	A4-1	↓	22R	4972	5098
10	A4-1	↓	22R	4912	5058
* 21	A4-3	↓	20R	4215	4282
* 22	A4-3	Type A -Drill Lube	20R	4365	4421
11	A4-1	Type B -Drill Lube	20R	4650	4900
12	A4-1	↓	20R	4870	5110
13	A4-3	↓	20R	3990	4094
14	A4-3	↓	20R	4080	4117
15	A4-3	↓	20R	4200	4256
* 23	A4-3	↓	20R	4502	4669
* 24	A4-3	Type B -Drill Lube	20R	4360	4508
16	A4-3	Solvent	20R	4042	4167
17	A4-3	↓	20R	4200	4301
18	A4-3	↓	20R	4003	4036
19	A4-3	↓	20R	4070	4165
20	A4-3	↓	20R	3940	4006
* 25	A4-3	↓	20R	4390	4437
* 26	A4-3	Solvent	20R	4427	4493

NOTE: Initial testing of 20 specimens was conducted on 3 December 1975.

*Follow-up testing of 8 specimens was conducted on 8 December 1975.

The remaining 8 specimens failure modes were also cohesive. The minimum psi lap shear strength exceeded 4000 psi, and the strength values were once again lower on specimens from the A4-3 parent sheet.

A review of test results indicates that drill lubricants and solvents used for this specific test do not affect the shear strength of FM73 adhesive. However, presence of porosity from the bonding process does reduce the bond shear strength. A comparison of Fokker Bondtest quality units showed no direct correlation to shear strength values. However, Fokker values indicated that shear values were within 60 to 80 percent of the maximum rated shear strength. Refer to Table 56 for recorded results.

Detail Specimen Bondline Inspection and Examination Procedures: - Detail specimens were inspected and examined upon completion of the various test variables. The procedural sequence follows: ultrasonic C-scan, dye penetrant application, separation of specimens bond line and examination of bond interface. Any deviation of this procedure shall be stated wherever applicable.

Ultrasonic C-scan inspection was conducted by nondestructive test (NDT) laboratory personnel. A C-scan record of each specimen is on file for future reference.

Three materials were used for the penetration check; Hy-Rez type SKL-H Magnaflux dye penetrant, Sandoz aluminum blue "A" dye penetrant and ZL60 high sensitivity flourescent penetrant. The latter material is preferred and was adopted after initial use of the two dye penetrants was deleted.

Hy-Rez dye penetrant was applied to holes with a brush and allowed to air dry prior to separation of specimen by wedging apart.

Sandoz aluminum blue "A" dye was applied by submerging detail specimens in a bell jar. A vacuum was applied to evacuate all air from the chamber. The vacuum was removed to allow atmospheric pressure to enter. Specimens were water rinsed and oven dried at 125°F for a period of 4 hours before wedging apart.

The procedure for application of ZL60 flourescent penetrant was the same as for Sandoz aluminum blue "A" dye except that specimens were air dried in place of furnace dried.

A full width wedge (see Figure 141) was adopted for use after one specimen (S-42) was separated with one inch wide wedges. The full width wedge is driven in one direction providing ease of specimen separation and elimination of sheet distortion. The wedging stress lines are in one plane whereas wavy stress patterns develop when small wedges are inserted in multi-directions.

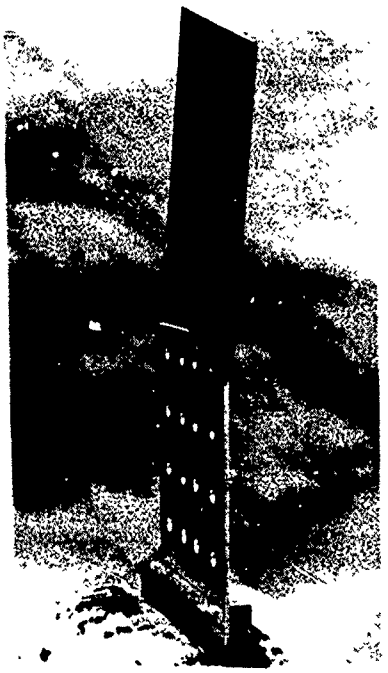
Specimen bond interfaces were visually examined using incandescent light and ultraviolet black light where fluorescent penetrant was applied.

Hole Generation: - This investigation utilized three methods of hole generation; controlled feeds and speeds hand drilling (2700 rpm) and high speed drilling (20,000 rpm). In addition, the effects of excessive drill point force and excessive heat from dull drills were investigated.

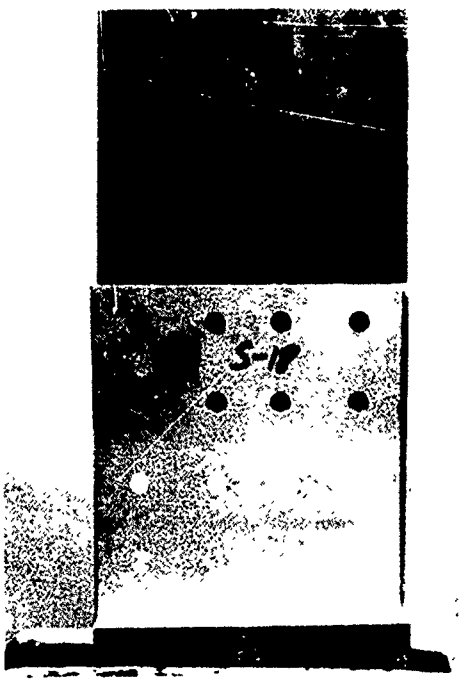
All specimens prepared by the three hole generation methods were positioned in a drill fixture or to a drill plate. A new unused drill was used to drill a total of 20 holes in each specimen as shown in Figure 142 with drill configurations as shown in Figure 143. The first, tenth and twentieth holes drilled were visually examined for microinch finish. A ball-gage and a micrometer were used to determine hole diameter, elongation and taper. Exit burr heights were measured with a micrometer. Specimens were subjected to bond line inspection and examination.

A QDA-10 Quackenbush pneumatic power unit was used in conjunction with No. 20, 3/16" and .2344" x 6" extension standard jobbers drills to drill holes. Gears were interchanged in the power unit to provide the desired feed and speed variables. The feed variables were .002 and .006 inch per revolution (IPR). The speed variables were 400, 1400 and 3000 rpm (spindle speed). Drill lube (Type A) was applied to drills in a mist from spray applicator. Jobbers drills are shown in Figure 143. The .2344" holes were finish sized with a piloted machine reamer (.2340 pilot x .2450" body) and a 450 rpm (spindle speed) hand motor. A typical controlled feed and speed test set-up is shown in Figure 144.

The measured hole data results are recorded in Tables 57 and 58. The C-scan records and visual examination revealed no delamination around the drilled holes. Examination under ultraviolet black light showed penetration of fluorescent penetrant from a trace to .032" at the hole periphery as

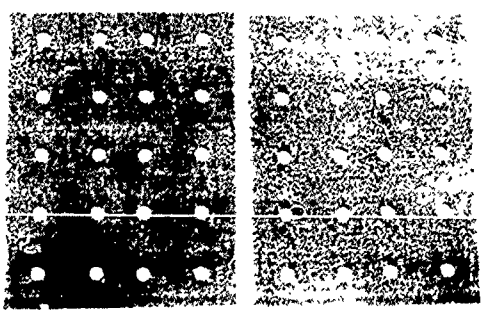


Step 1 - Insertion of Wedge



Step 2 - Wedge Inserted Approximately 1/2 Length of Specimen





Specimen Completely Wedged Apart

FIGURE 141. SPECIMEN SEPARATION BY WEDGING

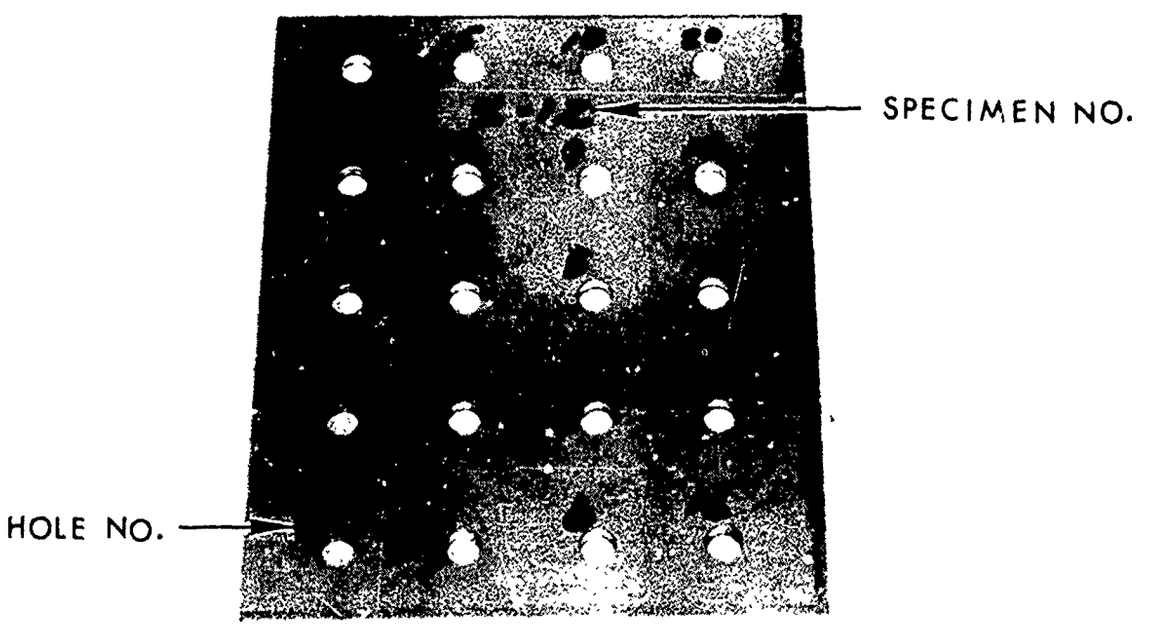


FIGURE 142. TYPICAL DRILLED SPECIMEN WITH HOLE NUMBER ORIENTATION

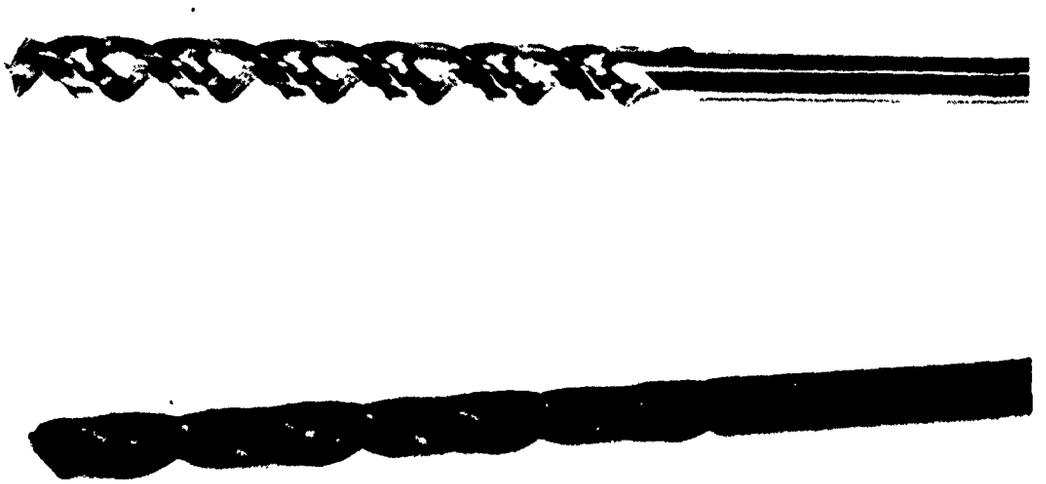


FIGURE 143. DRILL CONFIGURATIONS

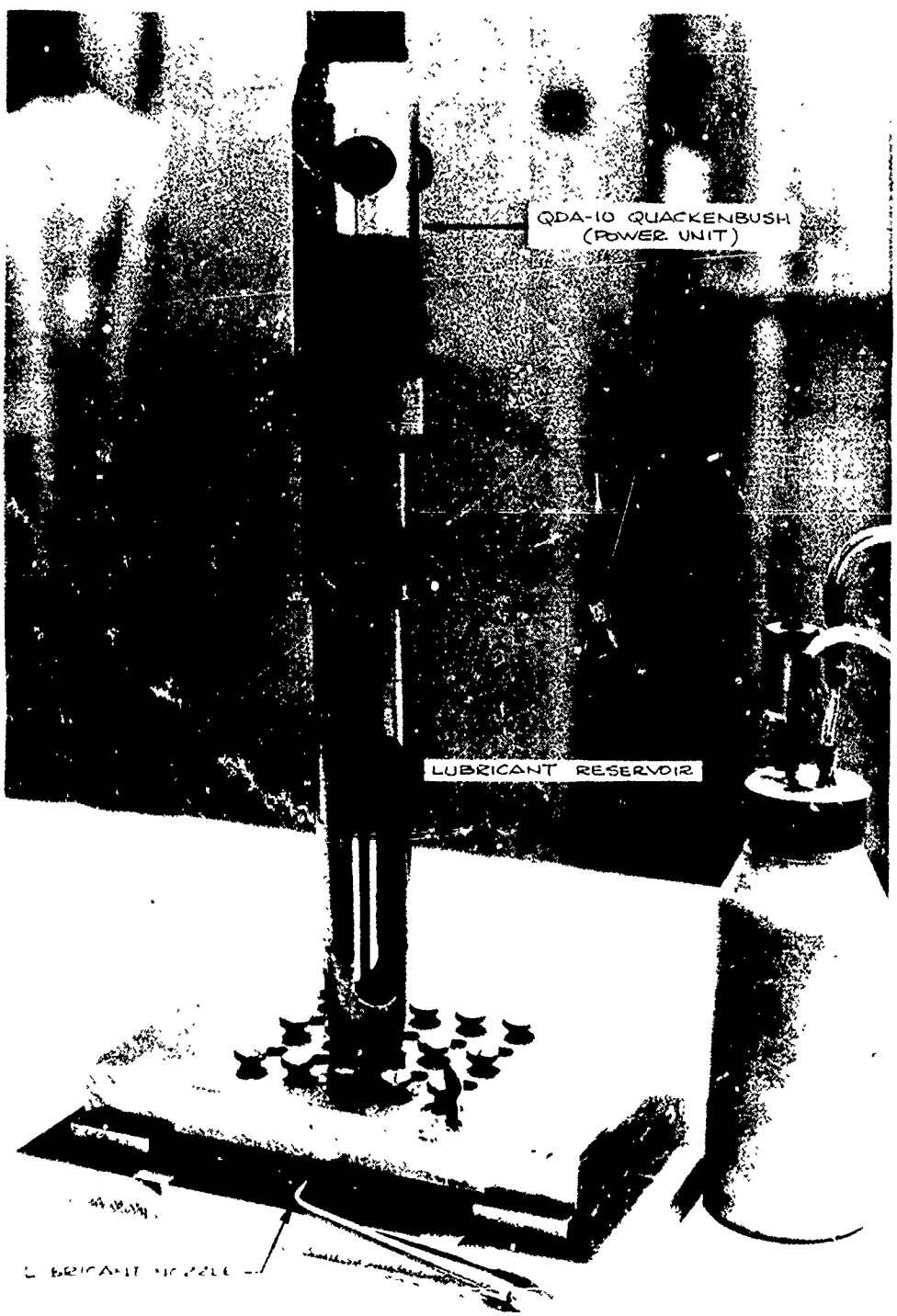


FIGURE 144. CONTROLLED FEED AND SPEED TEST SETUP

TABLE 57

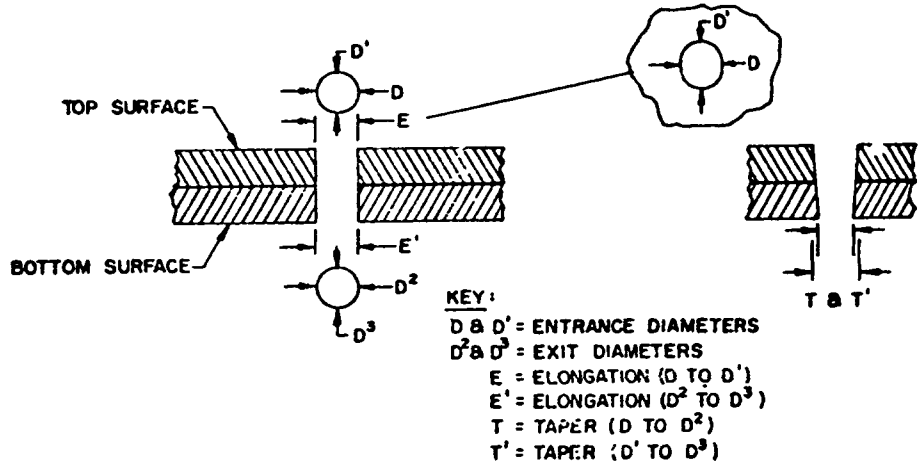
CONTROLLED FEED & SPEED HOLE GENERATION DATA

(#20 Drill In .087"/.088" Bonded Sheet)

SPEC. NO.	DRILL SIZE	SPEED rpm	FEED ipr	LUBRICANT	HOLE NO.	HOLE GENERATION DATA POINTS (INCHES)								MICROINCH HOLE FINISH	EXIT BURR HEIGHT	FLUORESCENT PENETRATION
						D	D'	E	D^2	D^3	E'	T	T'			
S-1	#20	400	.002	Type A	1st	.1622	.1624	.0002	.1621	.1621	none	.0001	.0003	32-63	Zero	Trace at 2 holes
					10th	.1624	.1622	.0002	.1619	.1615	.0004	.0005	.0007			
					20th	.1629	.1638	.0009	.1629	.1610	.0019	None	.0028			
S-4	#20	400	.006	Type A	1	.1615	.1612	.0003	.1613	.1613	None	.0002	.0001	32-63	Zero	.032" at hole #16
					10	.1612	.1611	.0001	.1618	.1614	.0004	.0006	.0003			
					20	.1613	.1612	.0001	.1614	.1612	.0002	.0001	None			
S-7	#20	1400	.002	Type A	1	.1620	.1628	.0008	.1613	.1616	.0003	.0007	.0012	32-63	Zero	.032" at hole #5
					10	.1618	.1613	.0005	.1612	.1618	.0006	.0006	.0005			
					20	.1613	.1612	.0001	.1612	.1611	.0001	.0001	.0001			
S-10	#20	1400	.006	Type A	1	.1643	.1637	.0006	.1621	.1617	.0005	.0022	.0020	63-125	Zero	Trace at 10 holes
					10	.1630	.1628	.0002	.1616	.1616	None	.0014	.0012			
					20	.1629	.1630	.0001	.1610	.1612	.0002	.0019	.0018			
S-13	#20	3000	.002	Type A	1	.1628	.1633	.0005	.1630	.1623	.0007	.0002	.0010	32-63	Zero	.032" at hole #5
					10	.1637	.1636	.0001	.1625	.1620	.0005	.0012	.0016			
					20	.1636	.1636	None	.1632	.1624	.0008	.0004	.0012			
S-16	#20	3000	.006	Type A	1	.1614	.1618	.0004	.1610	.1610	None	.0004	.0008	32-63	.000/.005"	.032" at hole #15
					10	.1616	.1615	.0001	.1611	.1612	.0001	.0005	.0003			
					20	.1612	.1619	.0007	.1616	.1608	.0008	.0004	.0011			

Specimen material - 7075-T6 X .040" bonded to .040"
Bond line thickness .007"/.008"
Equipment - QDA-10 Quackenbush
Drills - DAC No. 04520-206-020

HOLE GENERATION DATA POINTS



KEY:
D & D' = ENTRANCE DIAMETERS
D^2 & D^3 = EXIT DIAMETERS
E = ELONGATION (D TO D')
E' = ELONGATION (D^2 TO D^3)
T = TAPER (D TO D^2)
T' = TAPER (D' TO D^3)

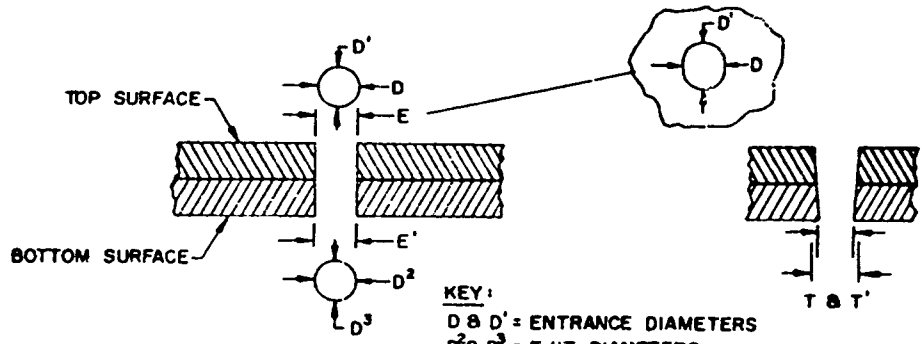
TABLE 57. (CONTINUED)

CONTROLLED FEED & SPEED HOLE GENERATION DATA
(#3/16 Drill in .087"/.088" Bonded Sheet)

SPEC. NO.	DRILL SIZE	SPEED rpm	FEED ipr	LUBRICANT	HOLE NO.	HOLE GENERATION DATA POINTS (INCHES)								MICROINCH HOLE FINISH	EXIT BURR HEIGHT	FLUORESCENT PENETRATION
						D	D^1	E	D^2	D^3	E^1	T	T^1			
S-2	3/16	400	.002	Type A	1st	.1877	.1883	.0006	.1877	.1873	.0004	None	.0010	32-63	Zero	None
					10th	.1884	.1879	.0005	.1870	.1873	.0003	.0014	.0006			
					20th	.1883	.1880	.0003	.1875	.187-	None	.0008	.0011			
S-5	3/16	400	.006	Type A	1	.1872	.1877	.0005	.1873	.1876	.0003	.0001	.0001	32-63	Zero	None
					10	.1872	.1875	.0003	.1872	.1874	.0002	None	.0001			
					20	.1874	.1871	.0003	.1870	.1871	.0001	.0004	None			
S-8	3/16	1400	.002	Type A	1	.1872	.1873	.0001	.1876	.1875	.0001	.0004	.0002	32-63	Zero	None
					10	.1870	.1872	.0002	.1871	.1874	.0003	.0001	.0002			
					20	.1874	.1878	.0004	.1873	.187e	.0003	.0001	.0002			
S-11	3/16	1400	.006	Type A	1	.1876	.1875	.0001	.1871	.1867	.0004	.0005	.0008	63-125	Zero	None
					10	.1676	.1875	.0001	.1871	.1871	None	.0005	.0004			
					20	.1875	.1877	.0002	.1870	.1872	.0002	.0005	.0005			
S-17	3/16	3000	.002	Type A	1	.1900	.1900	None	.1892	.1891	.0001	.0008	.0009	32-63	Zero	None
					10	.1895	.1894	.0001	.1892	.1893	.0001	.0003	.0001			
					20	.1896	.1894	.0002	.1896	.1890	.0006	None	.0004			
S-14	3/16	3000	.006	Type A	1	.1872	.1870	.0002	.1872	.1873	.0001	None	.0003	63-125	.000/.005"	None
					10	.1878	.1881	.0003	.1878	.1877	.0001	None	.0004			
					20	.1885	.1884	.0001	.1876	.1884	.0008	.0009	None			

Specimen material - 7075-T6 X .040" bonded to .040"
Bond line thickness .007"/.008"
Equipment - QDA-10 Quackenbush
Drills - DAC No. 04520-206-137

HOLE GENERATION DATA POINTS



KEY:
D & D' = ENTRANCE DIAMETERS
D^2 & D^3 = EXIT DIAMETERS
E = ELONGATION (D TO D')
E' = ELONGATION (D^2 TO D^3)
T = TAPER (D TO D^2)
T' = TAPER (D' TO D^3)

TABLE 57. (CONTINUED)

CONTROLLED FEED & SPEED HOLE GENERATION DATA
(#3/16 Drill In .1855"/.1875" Bonded Sheet)

SPEC. NO.	DRILL SIZE	SPEED rpm	FEED ipr	LUBRICANT	HOLE NO.	HOLE GENERATION DATA POINTS (INCHES) D	D'	E	D^2	D^3	E'	T	T'	MICROINCH HOLE FINISH	EXIT BURR HEIGHT	FLUORESCENT PENETRATION
S-79	3/16	400	.002	Type A	1st	.1871	.1872	.0001	.1866	.1871	.0005	.0005	.0001	32-63	.005/.010"	None
					10th	.1868	.1870	.0002	.1872	.1870	.0002	.0004	None			
					20th	.1865	.1870	.0005	.1870	.1870	None	.0005	None			
S-81	3/16	400	.006	Type A	1	.1878	.1878	None	.1880	.1875	.0005	.0002	.0003	32-63	.005/.010"	Trace at 15 holes
					10	.1883	.1883	None	.1872	.1875	.0003	.0011	.0008			
					20	.1882	.1882	None	.1875	.1880	.0005	.0007	.0002			
S-83	3/16	1400	.002	Type A	1	.1879	.1880	.0001	.1875	.1880	.0005	.0004	None	32-63	.000/.005"	Trace at 3 holes
					10	.1884	.1883	.0001	.1880	.1885	.0005	.0004	.0002			
					20	.1883	.1887	.0004	.1883	.1875	.0008	None	.0012			
S-85	3/16	1400	.006	Type A	1	.1878	.1876	.0002	.1874	.1871	.0003	.0004	.0005	63-125	.000/.005"	Trace at 2 holes
					10	.1878	.1875	.0003	.1874	.1873	.0001	.0004	.0002			
					20	.1876	.1879	.0003	.1875	.1875	None	.0001	.0004			
S-89	3/16	3000	.002	Type A	1	.1885	.1879	.0006	.1884	.1883	.0001	.0001	.0004	32-63	.000/.005"	Trace at 9 holes
					10	.1884	.1885	.0001	.1880	.1880	None	.0004	.0005			
					20	.1886	.1885	.0001	.1883	.1882	.0001	.0003	.0003			
S-87	3/16	3000	.006	Type A	1	.1877	.1881	.0004	.1873	.1872	.0001	.0004	.0009	32-63	.000/.007"	Trace at 5 holes
					10	.1879	.1884	.0005	.1877	.1878	.0001	.0002	.0006			
					20	.1877	.1876	.0001	.1880	.1878	.0002	.0003	.0002			

Specimen material - 7075-T6 X .090" Bonded to .090"
Bond line thickness .0055"/.0075"
Equipment - QDA-10 Quackenbush
Drills - DAC No. 04520-206-137

HOLE GENERATION DATA POINTS

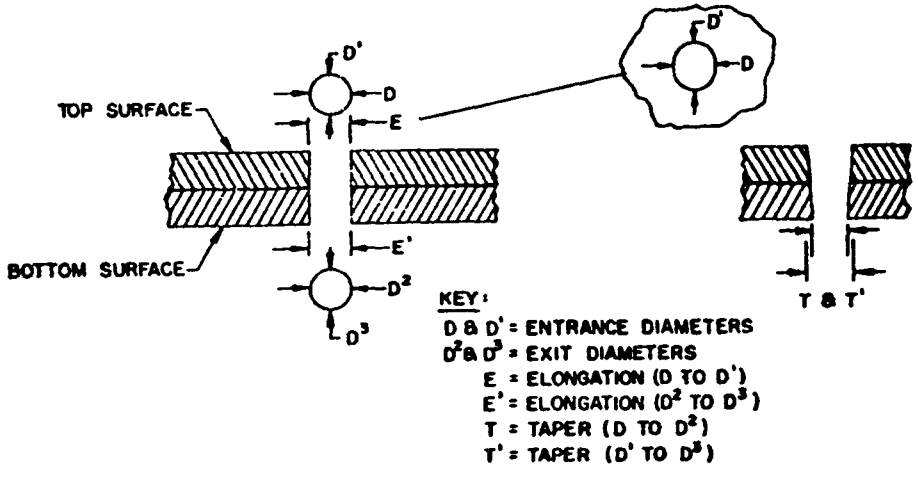


TABLE 58

CONTROLLED FEED AND SPEED PREDRILL AND 450 RPM REAM HOLE GENERATION DATA
*(.2344" Predrill and .2450" Ream at 450 rpm In .087"/.088" Bc Sheet)

SPEC. NO.	PRE-DRILL SIZE	SPEED rpm	FEED ipr	LUBRICANT	HOLE NO.	HOLE GENERATION DATA POINTS (INCHES) D	D'	E	D^2	D^3	E^1	T	T^1	ROINCH HOLE FINISH	EXIT BURR HEIGHT	FLUORESCENT PENETRATION
S-3	*2344	400	.002	Type A	1st	.2450	.2456	.0006	.2450	.2447	.0003	None	.0009	16-24	.005/.010"	None
					10th	.2454	.2452	.0002	.2454	.2453	.0001	None	.0001			
					20th	.2451	.2457	.0006	.2453	.2451	.0002	.0002	.0006			
S-6	*2344	400	.006	Type A	1	.2449	.2455	.0006	.2450	.2452	.0002	.0001	.0003	16-24	.005/.010"	None
					10	.2451	.2454	.0003	.2450	.2456	.0006	.0001	.0002			
					20	.2450	.2450	None	.2454	.2455	.0001	.0004	.0005			
S-9	*2344	1400	.002	Type A	1	.2450	.2450	None	.2453	.2457	.0004	.0003	.0007	16-24	.005/.010"	None
					10	.2457	.2450	.0007	.2454	.2456	.0002	.0003	.0006			
					20	.2452	.2453	.0001	.2451	.2452	.0001	.0001	.0001			
S-12	*2344	1400	.006	Type A	1	.2452	.2450	.0002	.2449	.2450	.0001	.0003	None	16-24	.005/.010"	None
					10	.2450	.2452	.0002	.2453	.2457	.0004	.0003	.0005			
					20	.2450	.2451	.0001	.2456	.2450	.0006	.0006	.0001			
S-18	*2344	3000	.002	Type A	1	.2455	.2452	.0003	.2447	.2450	.0003	.0008	.0002	16-24	.005/.010"	None
					10	.2450	.2457	.0007	.2450	.2457	.0007	None	None			
					20	.2450	.2457	.0007	.2450	.2457	.0007	None	None			
S-15	*2344	3000	.002	Type A	1	.2450	.2458	.0008	.2451	.2454	.0003	.0001	.0004	16-24	.005/.010"	None
					10	.2450	.2451	.0001	.2451	.2449	.0002	.0001	.0002			
					20	.2452	.2452	None	.2450	.2450	None	.0002	.0002			

Specimen material - 7075-T6 X .040" bonded to .040"
Bond line thickness .007"/.008"
Equipment - QOA-10 Quackenbush and 450 rpm hand motor
Drills - DAC No. C652-75556-TDSI-.2344"
Reamer - piloted (.234") machine .2450" body

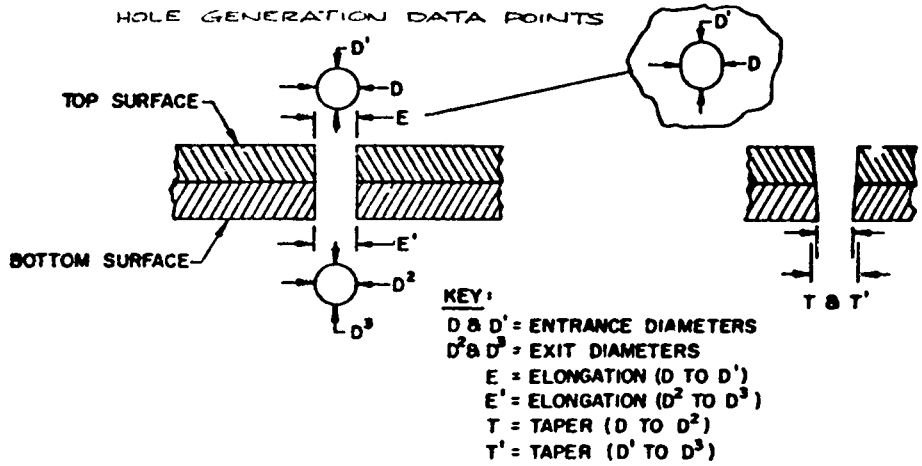
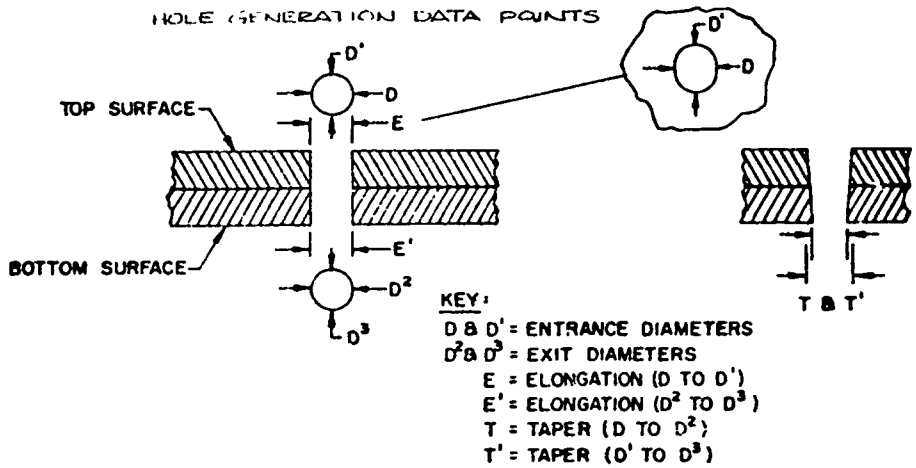


TABLE 58. (CONTINUED)

CONTROLLED FEED AND SPEED PREDRILL AND 450 RPM REAM HOLE GENERATION DATA
*(.2344" Predrill and .2450" Ream at 450 rpm in .1855"/.1875" Bonded Sheet)

SPEC. NO.	PRE-DRILL SIZE	SPEED rpm	FEED ipr	LUBRICANT	HOLE NO.	HOLE GENERATION DATA POINTS (INCHES) D	D^1	E	D^2	D^3	E^1	T	T^1	MICROINCH HOLE FINISH	EXIT BURR HEIGHT	FLUORESCENT PENETRATION
S-80	*2344	400	.002	Type A	1st	.2452	.2454	.0002	.2450	.2452	.0002	.0002	.0002	12-20	.010/.015"	None
					10th	.2450	.2450	.0010	.2451	.2460	.0009	.0001	None			
					20th	.2450	.2460	.0010	.2452	.2456	.0004	.0002	.0004			
S-82	*2344	400	.006	Type A	1	.2453	.2454	.0001	.2450	.2453	.0003	.0003	.0001	16-24	.010/.015"	None
					10	.2454	.2455	.0001	.2451	.2450	.0001	.0003	.0005			
					20	.2460	.2471	.0011	.2460	.2468	.0008	None	.0003			
S-84	*2344	1400	.002	Type A	1	.2450	.2456	.0006	.2455	.2457	.0002	.0005	.0001	16-32	.010/.015"	None
					10	.2455	.2455	None	.2457	.2458	.0001	.0002	.0003			
					20	.2450	.2451	.0001	.2453	.2459	.0006	.0003	.0008			
S-86	*2344	1400	.006	Type A	1	.2457	.2451	.0006	.2449	.2448	.0001	.0008	.0003	16-32	.010/.015"	None
					10	.2451	.2458	.0007	.2452	.2461	.0009	.0001	.0003			
					20	.2449	.2450	.0001	.2450	.2458	.0008	.0001	.0008			
S-90	*2344	3000	.002	Type A	1	.2452	.2456	.0004	.2452	.2454	.0002	None	.0002	16-24	.005/.010"	None
					10	.2450	.2454	.0004	.2454	.2458	.0004	.0004	.0004			
					20	.2450	.2455	.0005	.2449	.2451	.0002	.0001	.0004			
S-88	*2344	3000	.006	Type A	1	.2453	.2452	.0001	.2451	.2452	.0001	.0002	None	16-24	.005/.010"	None
					10	.2454	.2460	.0006	.2450	.2457	.0007	.0004	.0003			
					20	.2451	.2454	.0003	.2451	.2458	.0007	None	.0004			

Specimen material - 7075-T6 X .090" bonded to .090"
Bond line thickness .0055"/.0075"
Equipment - QDA-10 Quackenbush and 450 rpm hand motor
Drills - DAC No. C652-75556-TDSI-.2344"
Reamer - piloted (.2344) machine .2450" body



reported.

The drill fixture was used with slip-fit bushings inserted for centering of drills. A pneumatic power hand motor was used with #20 and 3/16" extension jobbers drills (see Figure 143) to generate the holes. Specimens were drilled dry (without lubricant) and with drills dipped in Type A lubricant.

Hole generation data results for hand drilled specimens are recorded in Tables 59 and 60. Bond delamination was not detected by either ultrasonic C-scan or by examination of bond interface. Inspection under ultraviolet black light showed some fluorescent penetrant around the holes as recorded.

Detail specimens were clamped between drill plates for high speed hole generation. A DAC design drill motor (C652-74859-TDS1) with 20,000 rpm rated spindle speed was used with high spiral/high speed drills for full size (one-shot) drilling and for predrilling. 0.2344" holes which were reamed at 450 rpm with a hand motor and a piloted machine reamer (.2340" pilot x .2450 body). DAC drill lubricants (Type A and Type B) were applied to drills in a mist. Test set-up for high speed drilling is shown in Figure 145.

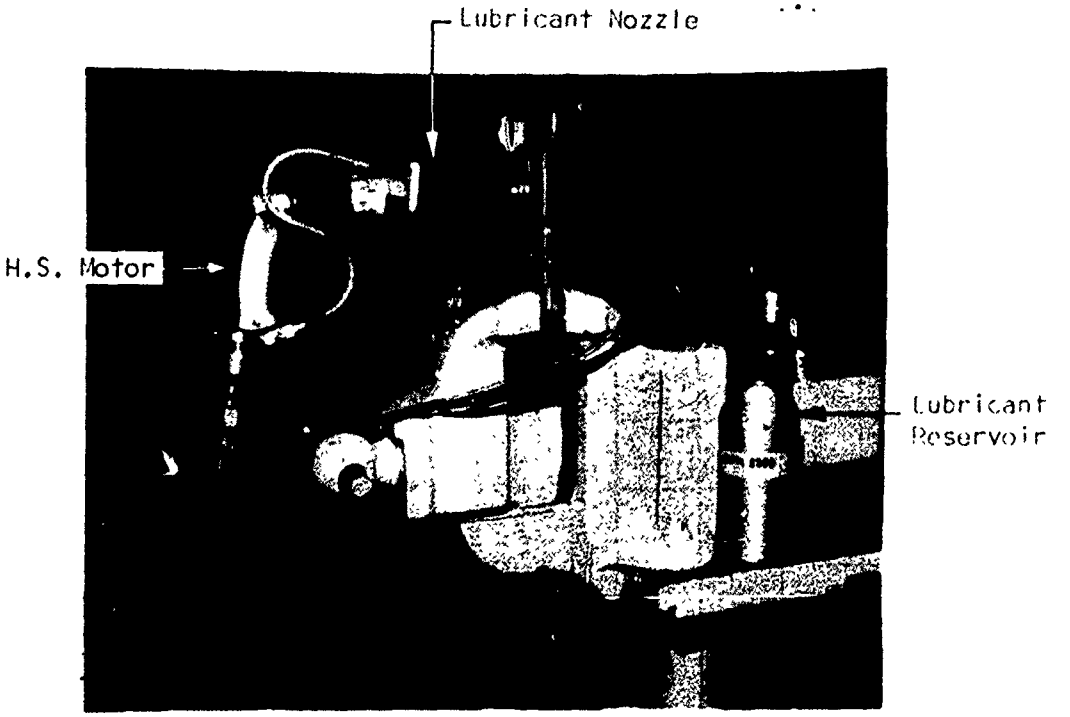


FIGURE 145. HIGH SPEED DRILLING TEST SETUP

TABLE 59

HAND DRILLING HOLE GENERATION DATA IN .087"/.088" BONDED SHEET

SPEC. NO.	DRILL SIZE	SPEED rpm	FEED ipr	LUBRICANT	HOLE NO.	HOLE GENERATION DATA POINTS (INCHES)								MICROINCH HOLE FINISH	EXIT BURR HEIGHT	FLUORESCENT PENETRATION
						D	D'	E	D^2	D^3	E'	T	T'			
S-25	#20	2700	Hand	None	1st	.1643	.1670	.0027	.1637	.1681	.0044	.0006	.0011	63-125	.005/.010"	None
					10th	.1630	.1629	.0001	.1623	.1628	.0005	.0007	.0001			
					20th	.1630	.1629	.0001	.1620	.1620	None	.0010	.0009			
S-26	#20	2700	Hand	Type A	1	.1618	.1629	.0011	.1616	.1619	.0003	.0002	.0010	63-125	.005/.010"	None
					10	.1634	.1639	.0005	.1622	.1627	.0005	.0012	.0012			
					20	.1622	.1630	.0008	.1612	.1617	.0005	.0010	.0013			
S-27	3/16	2700	Hand	Dry	1	.1895	.1869	.0006	.1889	.1880	.0009	.0006	.0009	63-125	.005/.010"	None
					10	.1888	.1883	.0005	.1887	.1880	.0007	.0001	.0003			
					20	.1888	.1898	.0010	.1883	.1883	None	.0005	.0015			
S-28	3/16	2700	Hand	Type A	1	.1886	.1888	.0002	.1877	.1877	None	.0009	.0011	63-125	.005/.010"	Trace at 1 hole
					10	.1889	.1897	.0008	.1887	.1885	.0002	.0002	.0012			
					20	.1890	.1890	None	.1887	.1882	.0005	.0003	0008			

Specimen material - 7075-T6 X .040" bonded to .040"
Bond line thickness - .007"/.008"
Equipment - Ingersoll Rand (2700 rpm) air motor
Drills - DAC No. 04520-206-020 (#20)
DAC No. 04520-206-137 (3/16)

HOLE GENERATION DATA POINTS

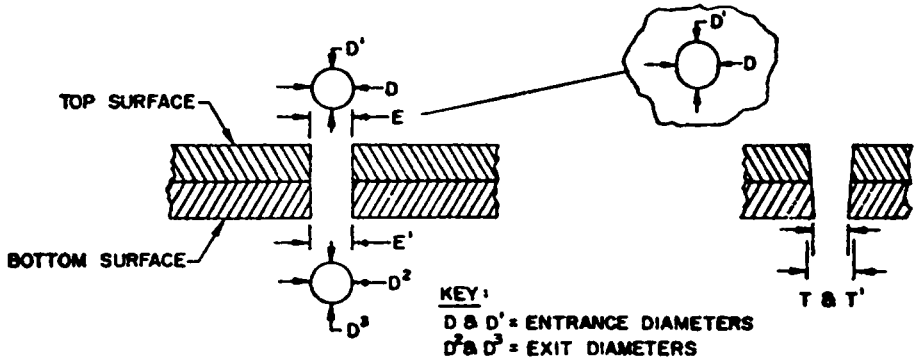


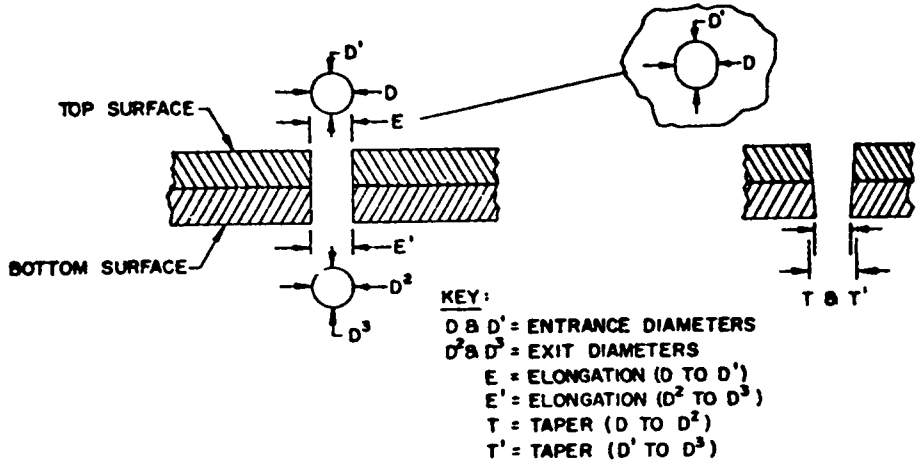
TABLE 60

HAND DRILLING HOLE GENERATION DATA IN .1855"/.1875" BONDED SHEET

SPEC. NO.	DRILL SIZE	SPEED rpm	FEED ipr	LUBRICANT	HOLE NO.	HOLE GENERATION DATA POINTS (INCHES) D	D'	E	D²	D³	E'	T	T'	MICROINCH HOLE FINISH	EXIT BURR HEIGHT	FLUORESCENT PENETRANT
S-97	#20	2700	Hand	None	1	.1622	.1630	.0008	.1610	.1612	.0002	.0012	.0018	40-63	.005/.010"	None
					10	.1624	.1624	None	.1618	.1613	.0005	.0006	.0011			
					20	.1633	.1632	.0001	.1620	.1612	.0008	.0013	.0020			
S-98	#20	2700	Hand	Type A	1	.1626	.1635	.0009	.1617	.1614	.0003	.0009	.0021	63-90	.005/.010"	.032" at hole #4
					10	.1612	.1611	.0001	.1622	.1615	.0007	.0010	.0004			
					20	.1627	.1634	.0007	.1627	.1629	.0002	None	.0005			
S-99	3/16	2700	Hand	None	1	.1906	.1910	.0004	.1909	.1902	.0007	.0003	.0008	63-125	.005/.010"	Trace at 6 holes
					10	.1909	.1912	.0003	.1918	.1923	.0005	.0009	.0011			
					20	.1910	.1923	.0013	.1918	.1911	.0007	.0008	.0012			
S-100	3/16	2700	Hand	Type A	1	.1890	.1883	.0007	.1874	.1875	.0001	.0016	.0008	40-63	.007/.010"	None
					10	.1878	.1886	.0008	.1881	.1882	.0001	.0003	.0004			
					20	.1882	.1880	.0002	.1876	.1878	.0002	.0006	.0002			

Specimen material - 7075-T6 X .090 bonded to .090
Bond line thickness .0055"/.0075"
Equipment - Ingersoll Rand (2700 rpm) air motor
Drills - DAC No. 04520-206-020 (#20)
DAC No. 04520-206-137 (3/16)

HOLE GENERATION DATA POINTS



KEY:
D & D' = ENTRANCE DIAMETERS
D² & D³ = EXIT DIAMETERS
E = ELONGATION (D TO D')
E' = ELONGATION (D² TO D³)
T = TAPER (D TO D²)
T' = TAPER (D' TO D³)

The measured hole data results are recorded in Table 61. Adhesive failures at 90 percent of the holes were observed on speciment S-21 and at one hole on specimen S-92. All other specimens of this variable were free of bond delamination. See Figures 146 and 147 for bond interface adhesive failure and C-scan record of speciment S-21 and figures 138 and 139 for speciment S-92.

Bonded specimens (S-29 through S-32) were subjected to 100 pound and 200 pound applied loads from the points of 3" No. 10 and No. 20 standard jobber drills. The drills were installed in a drill press and the selected load applied with the drill stopped as shown in Figure 148. The drill was started and the applied force at drill break through was recorded. The specimen was allowed to deflect as each hold was unsupported for 3/4". Specimens were inspected for bondline inspection and examination.

The following preliminary work was conducted prior to the applied force test.

- The accuracy of the scale was checked and found to be $\pm$ 2 pounds of the indicated reading.
- Hand drilling tests were run with three mechanics. The applied force ranged from 25 to 33 pounds with a No. 20 drill and from 28 to 52 pounds with a No. 10 drill.
- The applied force ranged from 50 to 55 pounds when drilling with a QDA-10 Quackenbush and a No. 10 drill.

TABLE 61

HIGH SPEED DRILLING (20,000 RPM) AND HIGH SPEED PREDRILL AND REAM HOLE GENERATION DATA
*(.2344" Predrill and Ream at 450 rpm in .087"/.088" Bonded Sheet)

SPEC. NO.	DRILL SIZE	SPEED rpm	FEED ipr	LUBRICANT	HOLE NO.	HOLE GENERATION DATA POINTS (INCHES)								MICROINCH HOLE FINISH	EXIT BURR HEIGHT	FLUORESCENT PENETRATION
						D	D^1	E	D^2	D^3	E^1	T	T^1			
S-19	#20	20000	Hand	Type A	1st	.1623	.1612	.0011	.1616	.1616	None	.0007	.0004	32-63	Zero	.010" at hole #12
					10th	.1618	.1620	.0002	.1615	.1611	.0004	.0003	.0009			
					20th	.1619	.1620	.0001	.1613	.1615	.0002	.000	.0005			
S-22	#20	20000	Hand	Type B	1	.1623	.1613	.0010	.1614	.1610	.0004	.0009	.0003	32-63	Zero	None
					10	.1617	.1618	.0001	.1612	.1612	None	.0005	.0006			
					20	.1623	.1620	.0003	.1628	.1637	.0009	.0005	.0017			
S-20	.1851	20000	Hand	Type A	1	.1901	.1910	.0009	.1891	.1905	.0014	.0010	.0005	63-90	Zero	None
					10	.1865	.1863	.0002	.1878	.1887	.0009	.0013	.0024			
					20	.1860	.1872	.0012	.1861	.1873	.0012	.0001	.0001			
S-23	.1851	20000	Hand	Type B	1	.1891	.1883	.0008	.1855	.1860	.0005	.0036	.0023	63-125	Zero	None
					10	.1892	.1894	.0002	.1860	.1866	.0006	.0032	.0028			
					20	.1877	.1889	.0012	.1870	.1884	.0014	.0007	.0005			
S-21	*2344	20000	Hand	Type A	1	.2452	.2460	.0008	.2450	.2460	.0010	.0002	None	16-32	.025/.032"	None
					10	.2450	.2454	.0004	.2455	.2450	.0005	.0005	.0004			
					20	.2457	.2449	.0008	.2454	.2449	.0005	.0003	None			
S-24	*2344	20000	Hand	Type B	1	.2457	.2474	.0017	.2455	.2451	.0004	.0002	.0023	16-32	.005/.012"	None
					10	.2454	.2456	.0002	.2456	.2458	.0002	.0002	.0002			
					20	.2450	.2450	None	.2450	.2451	.0001	None	.0001			

Specimen material - 7075-T6 X .040" bonded to .040"
Bond line thickness .007"/.008"
Equipment - DAC design drillmotor 20,000 rpm (C652-74589-TDS1)
Drills - DAC No. C652-75556-TDS1-( )
Reamer - piloted (.234) machine .2450" body

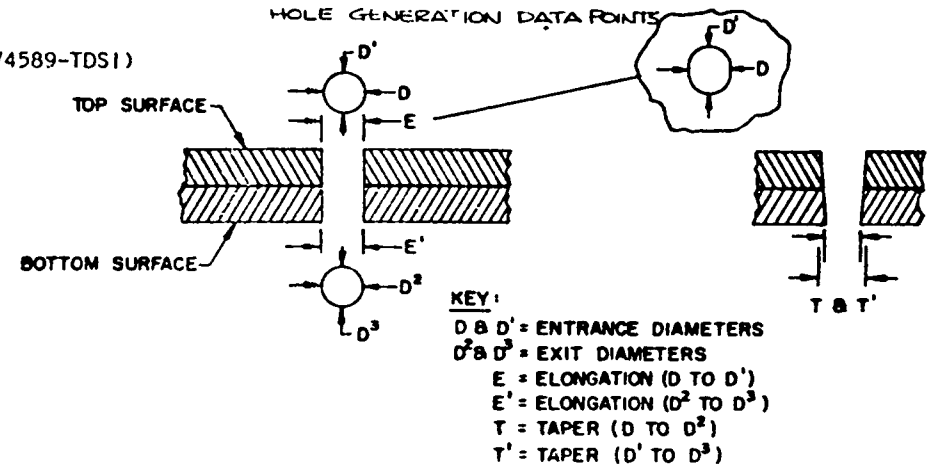


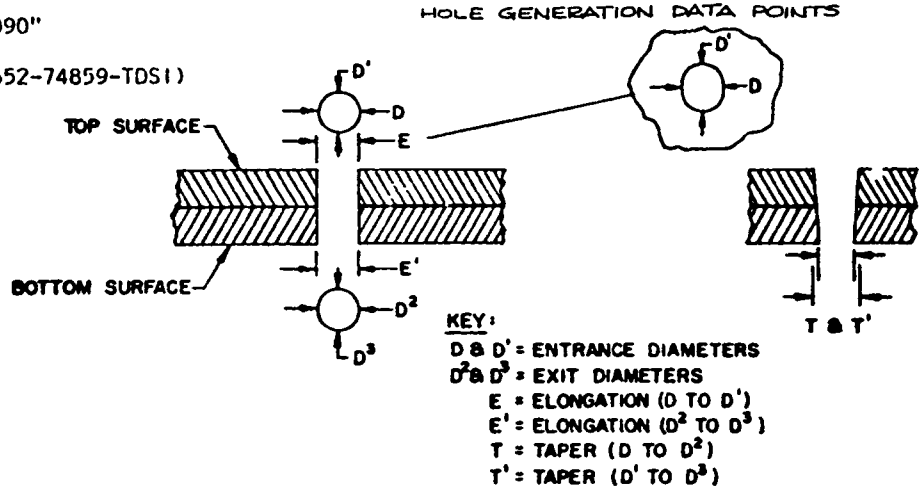
TABLE 61. (CONTINUED)

HIGH SPEED DRILLING (20,000 RPM) AND HIGH SPEED PREDRILL AND REAM HOLE GENERATION DATA

*(.2344 Predrill and Ream at 450 rpm in .1855"/.1875" Bonded Sheet)

SPEC. NO.	DRILL SIZE	SPEED rpm	FEED ipr	LUBRICANT	HOLE NO.	HOLE GENERATION DATA POINTS (INCHES) D	D'	E	D²	D³	E'	T	T'	MICROINCH HOLE FINISH	EXIT BURR HEIGHT	FLUORESCENT PENETRATION
S-91	#20	20000	Hand	Type A	1st	.1613	.1616	.0003	.1616	.1620	.0004	.0003	.0004	40-63	.005/.009"	Trace at 2 holes
					10th	.1625	.1624	.0001	.1623	.1635	.0012	.0002	.0011			
					20th	.1625	.1629	.0004	.1643	.1645	.0002	.0018	.0016			
S-94	#20	20000	Hand	Type B	1	.1626	.1617	.0009	.1613	.1618	.0005	.0013	.0001	40-63	.032/.040" 20% holes	None
					10	.1623	.1615	.0008	.1624	.1626	.0002	.0001	.0011			
					20	.1628	.1629	.0001	.1617	.1624	.0007	.0011	.0005			
S-92	.1851	20000	Hand	Type A	1	.1875	.1877	.0002	.1858	.1857	.0001	.0017	.0020	40-63	.005/.010"	Trace at 3 holes
					10	.1870	.1868	.0002	.1873	.1873	None	.0003	.0005			
					20	.1870	.1865	.0005	.1864	.1864	None	.0006	.0001			
S-95	.1851	20000	Hand	Type B	1	.1886	.1886	None	.1862	.1870	.0008	.0024	.0016	32-63	.000/.005"	.032" at holes #10, 13,18,19&20
					10	.1879	.1882	.0003	.1862	.1865	.0003	.0017	.0017			
					20	.1875	.1878	.0003	.1867	.1871	.0004	.0008	.0007			
S-93	* 15/64	20000	Hand	Type A	1	.2450	.2453	.0003	.2450	.2449	.0001	None	.0004	16-32	.010/.015"	None
					10	.2450	.2450	None	.2453	.2450	.0003	.0003	None			
					20	.2454	.2455	.0001	.2453	.2456	.0003	.0001	.0001			
S-96	* 15/64	20000	Hand	Type B	1	.2449	.2450	.0001	.2450	.2455	.0005	.0001	.0005	32-63	.025/.032"	None
					10	.2454	.2454	None	.2453	.2450	.0003	.0001	.0004			
					20	.2452	.2452	None	.2446	.2451	.0005	.0006	.0001			

Specimen material - 7075-T6 X .090" bonded to .090"
Bond line thickness .0055"/.0075"
Equipment - DAC design drillmotor 20,000 rpm (C652-74859-TDS1)
Drills - DAC No. C652-75556-TDS1-( )
Reamer - piloted (.234) machine .2450 body



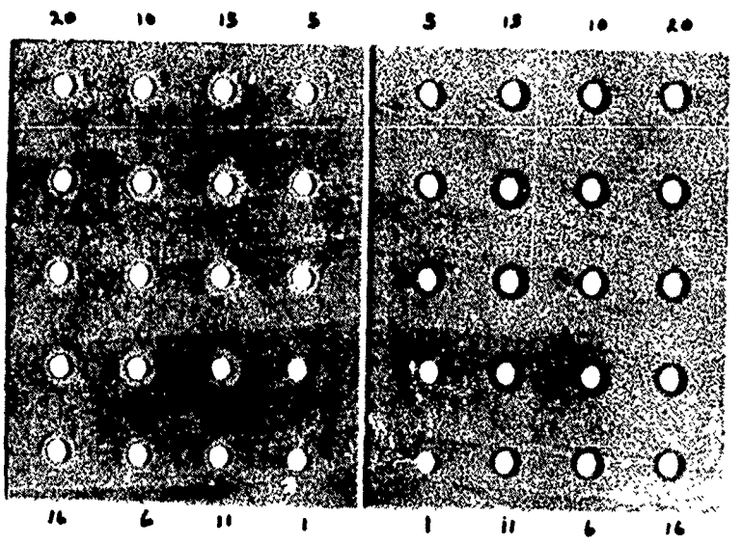


FIGURE 146. BOND INTERFACE ADHESIVE FAILURE

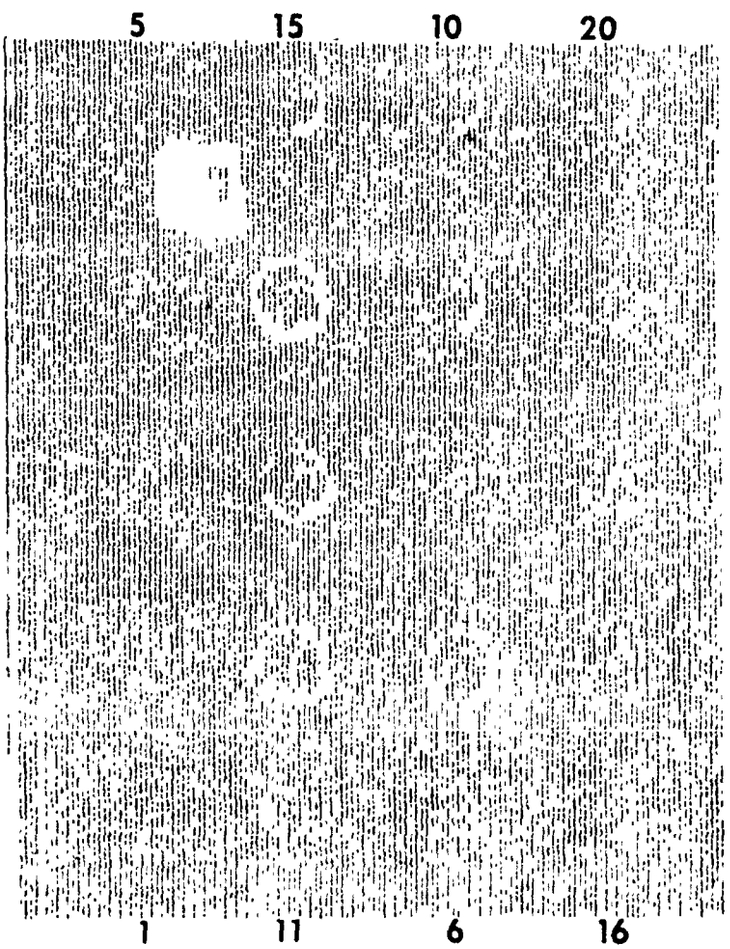


FIGURE 147. BOND DELAMINATION ULTRASONIC C-SCAN RECORD

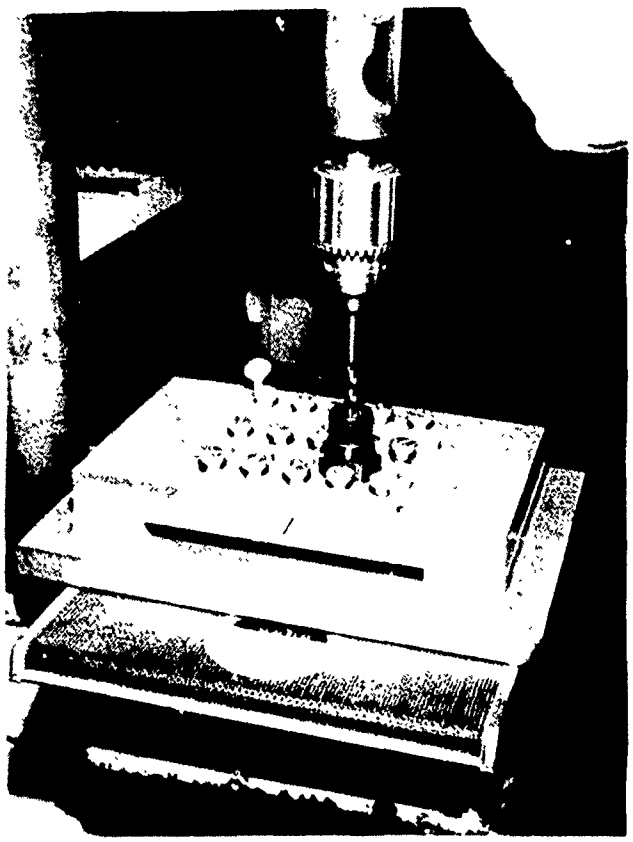


FIGURE 148. DRILL POINT FORCE TEST SET-UP

Specimens subjected to drill point force evaluation were not examined or measured for hole generation data. Ultrasonic inspection of drilled specimens showed no delamination. Visual inspection of bond interface revealed no adhesive failures. Fluorescent penetrant was undetected in the bond interface when viewed with ultraviolet black light. The applied force of 100 and 200 pounds as shown in Table 62 includes the dead weight (18 pounds) on the scale. The net applied force is 3 to 8 times in excess of hand and power equipment drilling.

TABLE 62

DRILL POINT FORCE IN POUNDS

SPEC. NO.	DRILL SIZE	APPLIED FORCE IN POUNDS	BREAK THROUGH FORCE IN POUNDS	NET APPLIED FORCE IN POUNDS	NET BREAK THROUGH FORCE IN POUNDS
S-29	#20	100	80-90	82	62-72
S-30	#20	200	150-190	182	132-172
S-31	#10	200	180-195	182	162-177
S-32	#10	100	90-110	82	72-92

Test specimens were primed with MIL-P-23377 epoxy polyamide primer on the exterior surfaces to determine if primer discoloration would occur, thereby proving a visible means of heat detection. Undersized holes were predrilled and then Tempilaq (Temperature Indicating Liquid) of various temperature melting points was applied to both specimens surfaces at each hole.

Each hole was then opened up to full size with flame torch heated cobalt drills. The drill point was flame heated to temperature of 1400°F to 1500°F while being rotated in a drill press, when the point turned a cherry-red the flame was removed and the speciman was immediately drilled. The specimen surface temperatures as indicated by the melted Tempilaq are recorded with the results in Table 63 . Specimens were subjected to bond line inspection and examination.

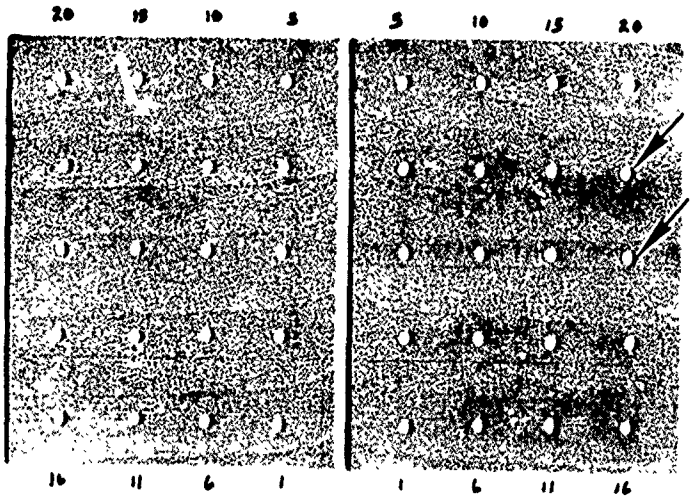
Primed surfaces showed no discoloration after Tempilaq was removed. Specimens were not examined or measured for hole generation data. The ultra sonic C-scan reflector technique was acceptable for these specimens. Visual examination revealed adhesive failures as specified in Table 63 , the adhesive failure at the hole periphery ranged from .005" to .020" with the majority.005" to .010." Inspection of bond interface with an ultraviolet black light showed some fluorescent penetration.
See Figure 149 for adhesive failures on specimen interface. See Figure 150 for photomicrograph of adhesive failure. See Figure 151 for C-scan record of adhesive failures.

TABLE 63

SPECIMEN SURFACE TEMPERATURE DATA

SPECIMEN		DRILL SIZE		SHEET TEMPERATURE °F						VISUAL ADHESIVE FAILURES	FLUORESCENT PENETRATION
NO.	THICKNESS	PREDRILL	FINAL	ENTRANCE			EXIT				
				250	350	450	250	350	450		
S-45	.087"/.088"	#20	#10	M	M	-	M	M	-	17 of 20 holes	Trace at 5 holes
S-46	.087"/.088"	#30	#20	M	M	-	M	-	-	2 of 20 holes	Trace at 10 holes
S-113	.1855"/.1875"	#20	#10	M	M	-	-	-	-	None	.010" at hole 11
S-114	.1855"/.1875"	#30	#20	M	M	-	-	-	-	1 of 20 holes	Trace at 8 holes

"M" indicates that the Tempilaq melted.



S-46

FIGURE 149. EXCESSIVE HEAT ADHESIVE FAILURE
Arrows indicate holes with adhesive failure

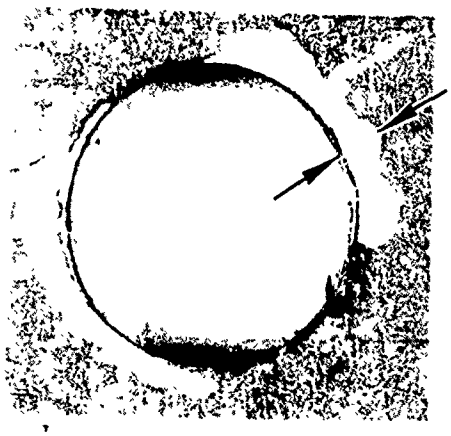


FIGURE 150. PHOTOMICROGRAPH
HOLE NO. 18 ADHESIVE FAILURE

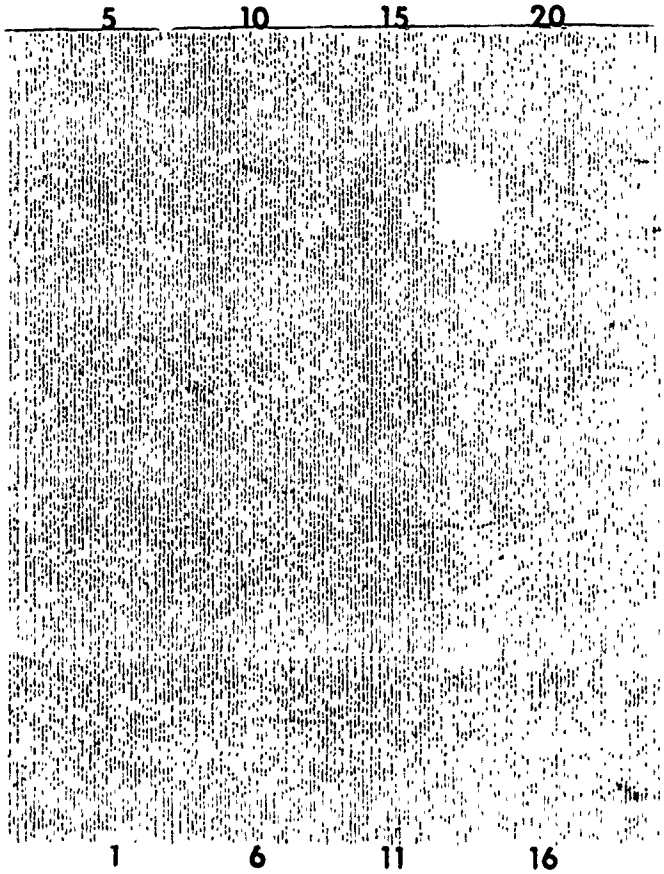


FIGURE 151. BOND DELAMINATION ULTRASONIC C-SCAN RECORD

Riveting Method Procedures: - A total of 16 riveted specimens were prepared to the configurations listed in Table 64 . Universal head MS20470AD5 and MS20470AD6 rivets (2117-T4 aluminum alloy) were upset to maximum diameter and to minimum height to induce maximum rivet expansion. The upset diameter (D.) and height (H.) was .265" D. x .047"H for 5/32" diameter and .312"D x .063"H for 3/16" diameter rivets.

TABLE 64

Riveted Specimen Configurations

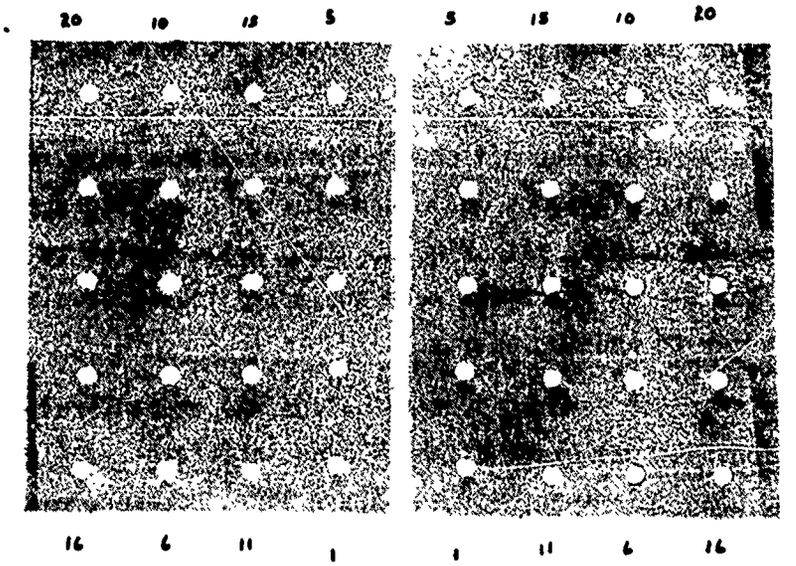
Spec. No.	Bonded Sheet Nom. Thick.	Bond Ply	Rivet Dia.	Hole Dia	Installation Method
S-37	.0875"	1	5/32"	.161/.1635"	Vibrate
S-38	.0875"	1	5/32"	.161/.1635"	Compression Squeeze
S-39	.0875"	1	3/16"	.192/.195"	Vibrate
S-40	.0875"	1	3/16"	.192/.195"	Compression Squeeze
S-109	.1865"	1	5/32"	.161/.1635"	Vibrate
S-110	.1865"	1	5/32"	.161/.1635"	Compression Squeeze
S-111	.1865"	1	3/16"	.192/.195"	Vibrate
S-112	.1865"	1	3/16"	.192/.195"	Compression Squeeze
S-147	.0930"	2	5/32"	.161/.1635"	Vibrate
S-148	.0930"	2	5/32"	.161/.1635"	Compression Squeeze
S-149	.0930"	2	3/16"	.192/.195"	Vibrate
S-150	.0930"	2	3/16"	.192/.195"	Compression Squeeze
S-185	.1930"	2	5/32"	.161/.1635"	Vibrate
S-186	.1930"	2	5/32"	.161/.1635"	Compression Squeeze
S-187	.1930"	2	3/16"	.192/.195"	Vibrate
S-188	.1930"	2	3/16"	.192/.195"	Compression Squeeze

Initially rivet heads and butts were removed because they would mask the ultrasonic beam adjacent to the hole in the area where possible delamination may exist. In the process of rivet head and butt removal, the micro-shaver blade would in some cases penetrate the surface primer and anodize. The bare shiny surfaces (7/16" diameter) adversely affected ultrasonic transmission. An investigation conducted by NDT laboratory personnel revealed that a uniform primed surface was paramount for optimum transmitted signal amplitude. The

following procedure was adopted for all riveted specimens subjected to C-scan inspection:

Rivet heads were drilled off and then rivet shanks were removed from specimens with a drive pin punch and a hammer with a back-up support. Each specimen surface was painted with zinc chromate primer prior to C-scan inspection. After C-scan specimens were subjected to Sandoz aluminum blue dye penetrant prior to wedging apart.

Riveting Method Results: - No bond delamination was encountered by ultrasonic C-scan inspection. Visual examination of bond interface revealed neither dye penetration nor bond delamination (See Figure 152). However, examination with a 10X magnifying glass showed crescent shaped metal slivers in some holes as shown in Figure 153. Spectrographic analysis confirmed that slivers were of the same material (7075) as the specimen sheet. A riveted specimen was cross-sectioned for metallurgical examination. The photomicrograph in Figure 154 shows displacement of the sheet material into the bond interface. It is concluded that the sliver breaks from the parent sheet when it is wedged apart, which may be related to the bond fracture on 50 percent of the holes in thin material of .040" bonded to .040". See Figure 155 for bond fractures at holes. The extent and amount of fractures diminishes in thicker material of .090" bonded to .090".



S-39

FIGURE 152. TYPICAL BOND INTERFACE OF SEPARATED RIVETED SPECIMENS

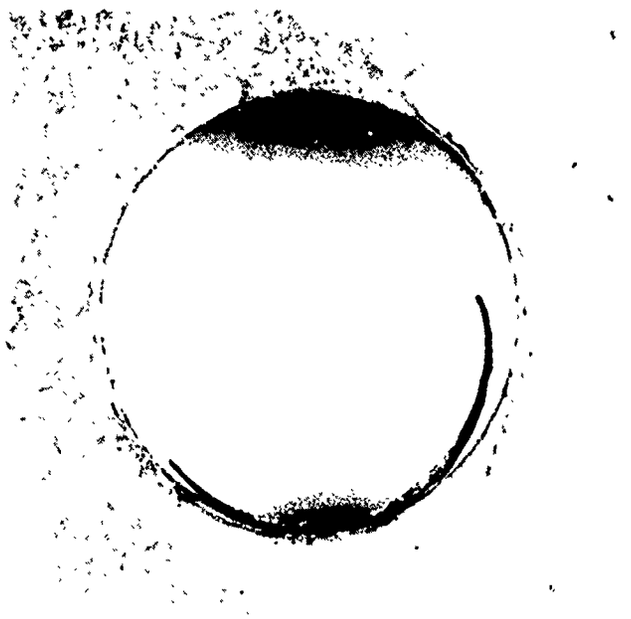


FIGURE 153. PHOTOMICROGRAPH OF HOLE NO. 18 SHOWING CRESENT SHAPED METAL SLIVER

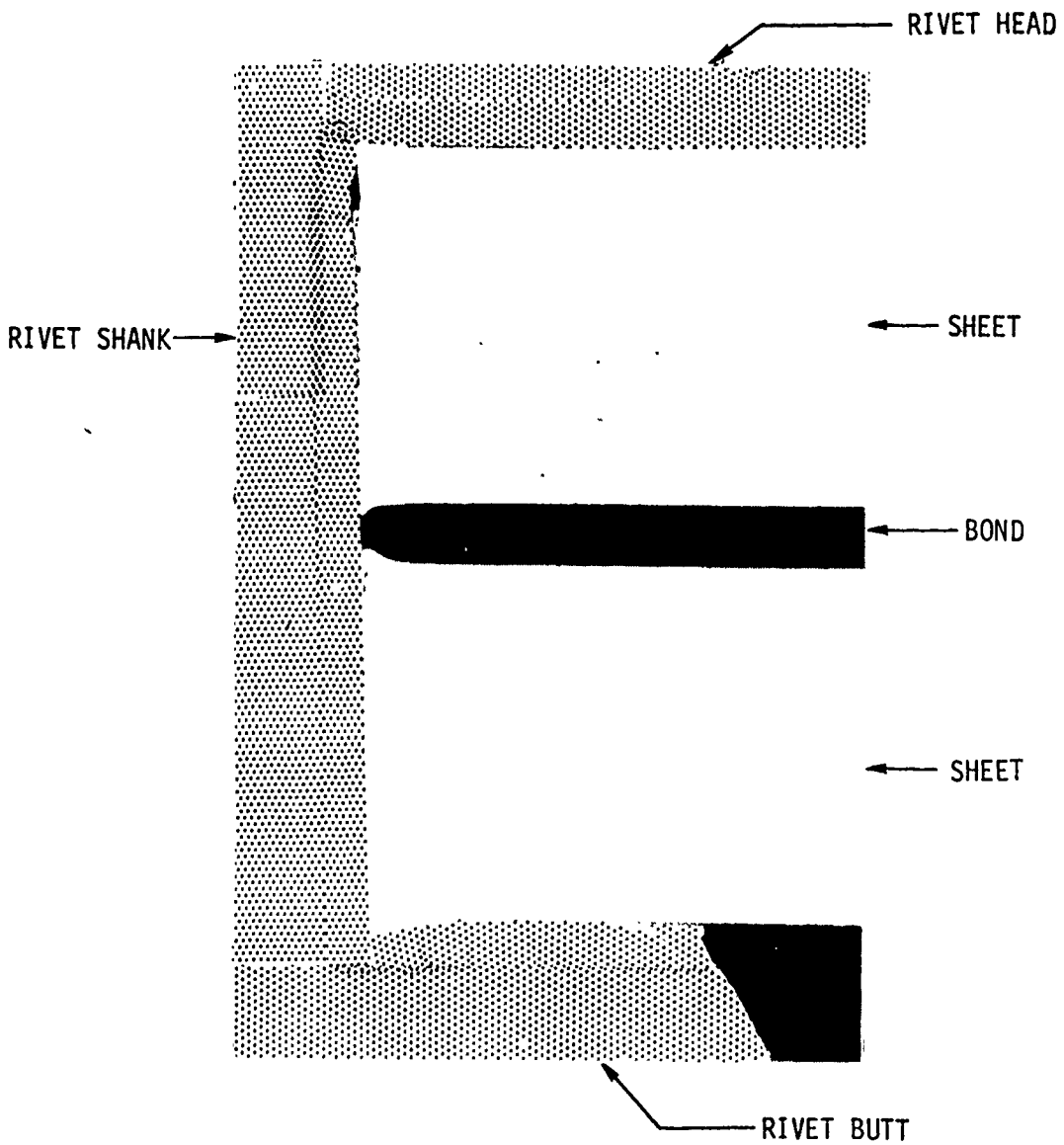


FIGURE 154. PHOTOMICROGRAPH OF CROSS SECTIONED RIVET IN BONDED SPECIMEN MS20470AD6 RIVET

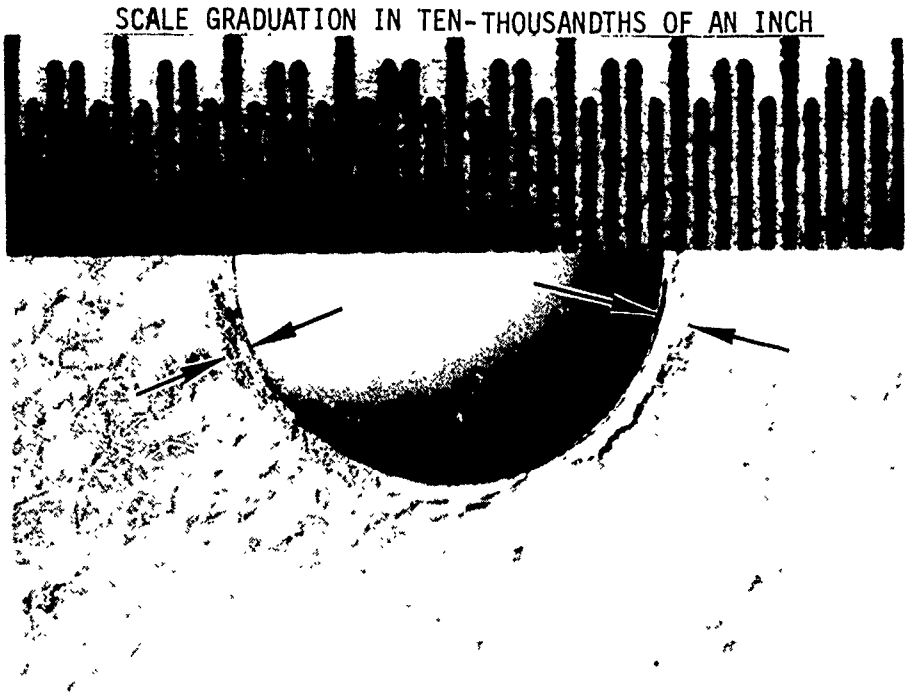


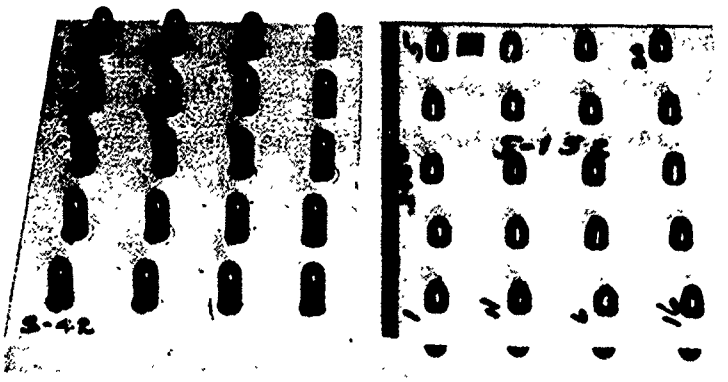
FIGURE 155. PHOTOMICROGRAPH SHOWING BOND FRACTURE AT HOLE PERIPHERY

Interference-fit Fastener Installation: - Specimens with varied amounts of interference-fit were predrilled and reamed to final size to provide the desired interference between the hole and the fastener. Specimens were prepared and evaluated in three phases to determine if bond delamination would occur as the interference was increased. Interference fit of .0045" was evaluated in Phase I interference fits of .0055" and .0065" were evaluated in Phase II and interferences of .0075" and .0085" in Phase III. Each specimen was ultrasonic C-scan inspected after holes were drilled to ensure that specimens were free of bond delamination prior to fastener installation.

The heads of 3/16" and 1/4" diameter, 6AL-4V titanium, close tolerance, straight shank pins were removed for installation. The procedure to install headless pins evolved from initial testing that revealed adverse affects on ultrasonic transmission immediately adjacent to the holes from fastener heads.

Headless pins were vibrated into holes with a rivet gun and a rivet set applied to the shank end. See Figure 156 for typical fastener installation.

The procedure to ultrasonic C-scan specimens with fasteners removed was adopted because installed pin-ends caused reflections that affected ultrasonic transmission. Pins were removed in the same manner as installed. Interference fit test variables and penetrant materials used are listed in Table 65 .



S-42 Thread End S-152 Shank End

FIGURE 156. TYPICAL INTERFERENCE FIT FASTENER INSTALLATION SPECIMENS

TABLE 65

Interference Fit Test Variables

Phase No.	Specimen No.	Spec Thickness Nom.	FM 73 Bond Film	Fastener Nom Dia	Interference F.T. (inches)	Penetrant Material
I	S-41	.0875"	1 Ply	3/16"	.0045	HyRez Type Dye
	S-42	.0875"	1 Ply	1/4"		
	S-151	.0930"	2 Ply	3/16"		
	S-152	.0930	2 Ply	1/4"		
II	S-43	.0875"	1 Ply	3/16"	.0055 & .0065	SANDOZ Aluminum Blue "A" Dye
	S-44	.0875"	1 Ply	1/4"		
	S-153	.0930"	2 Ply	3/16"		
	S-154	.0930"	2 Ply	1/4"		
III	S-47	.0875"	1 Ply	3/16"	.0075 & .0085	ZL60 High Sensitivity Fluorescent Penetrant
	S-48	.0875"	1 Ply	1/4"		

Effect of Interference on Bond-Line/Results: - No unacceptable delamination was discovered by ultrasonic C-scan transmission. Examination of bond interface revealed an absence of delamination and of penetrants. However, it was observed that stress rings were present at each hole and that as the amount of interference increased the diameter of the stress ring increased. See Figures 157 through 159 for bond interface of the various interference-fits and Figure 160 through 164 for stress ring comparisons.

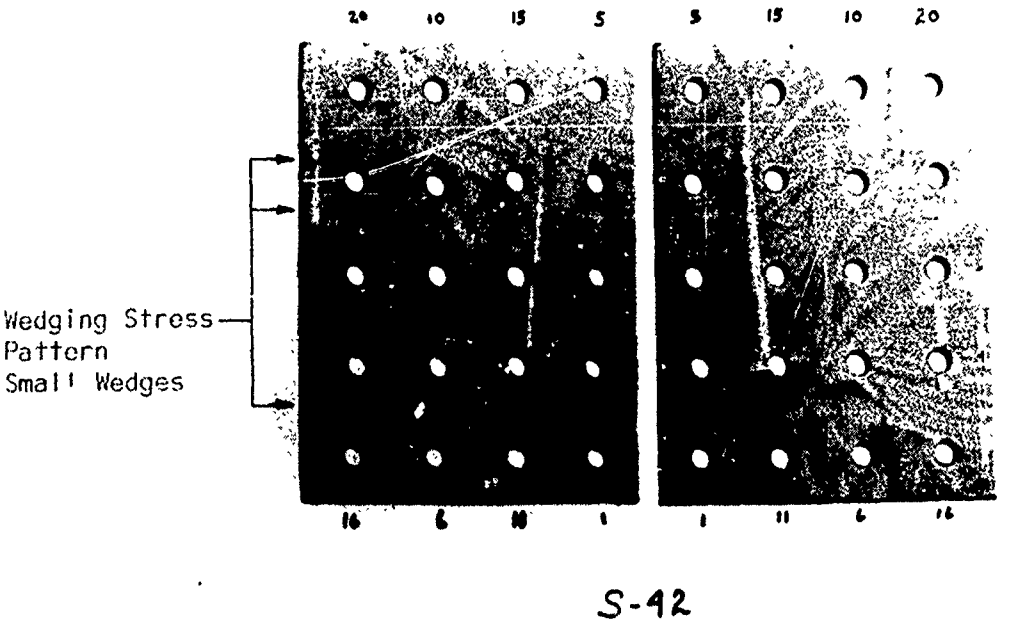


FIGURE 157. BOND INTERFACE FOR 0.0045" INTERFERENCE FIT

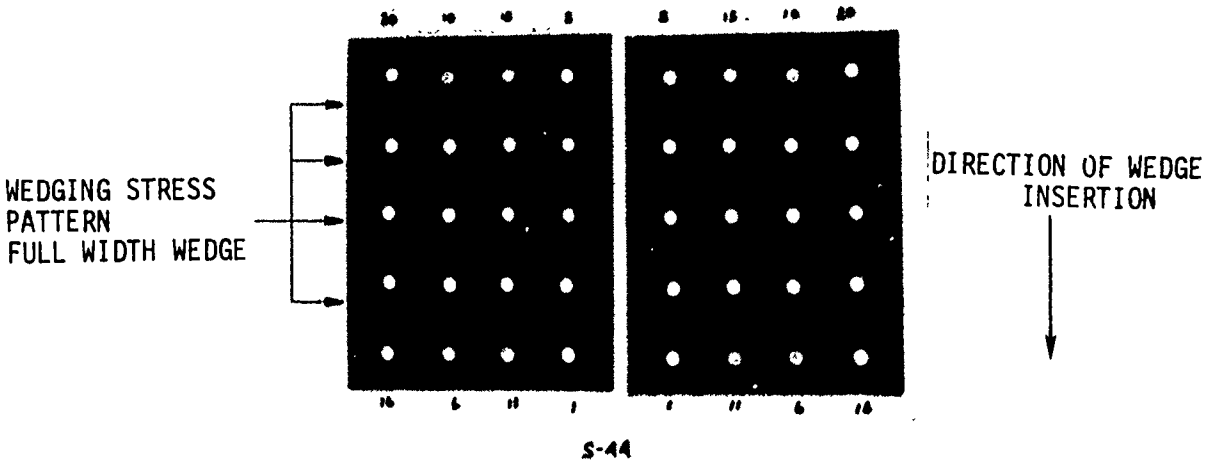


FIGURE 158. BOND INTERFACE FOR .0055" AND .0065" INTERFERENCE FIT

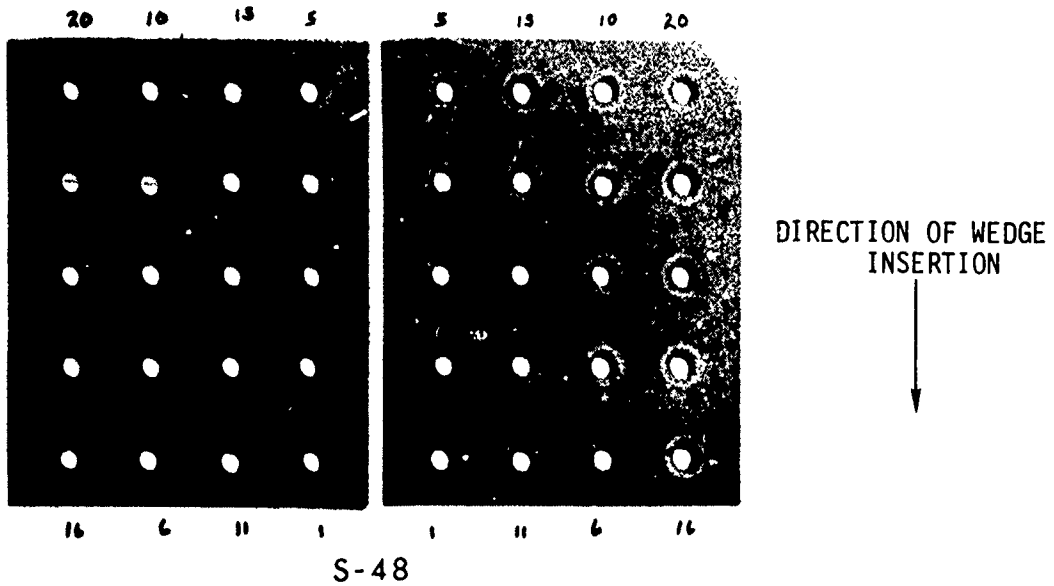
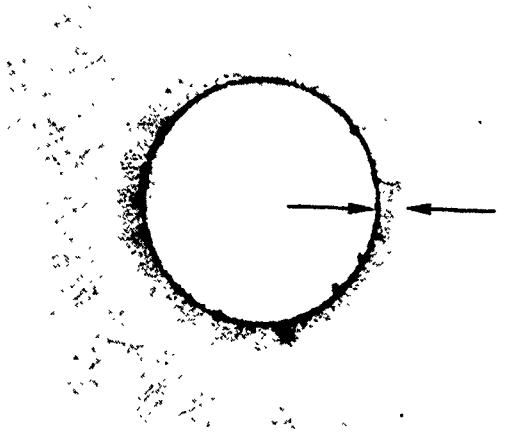
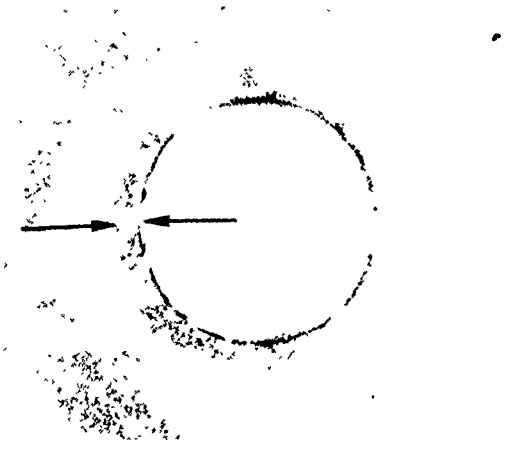


FIGURE 159. BOND INTERFACE FOR .0075" AND .0085" INTERFERENCE FIT



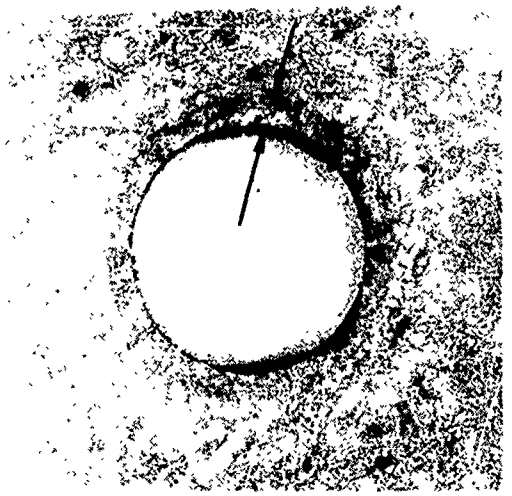
Arrows indicate stress ring

FIGURE 160. STRESS RING - 0.0045" INTERFERENCE FIT



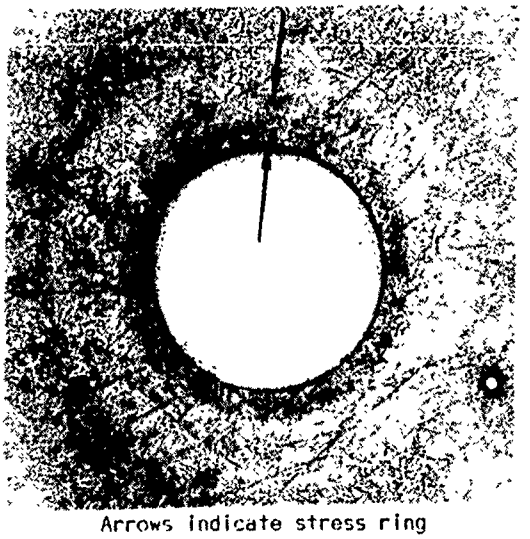
Arrows indicate stress ring

FIGURE 161. STRESS RING - 0.0055" INTERFERENCE FI



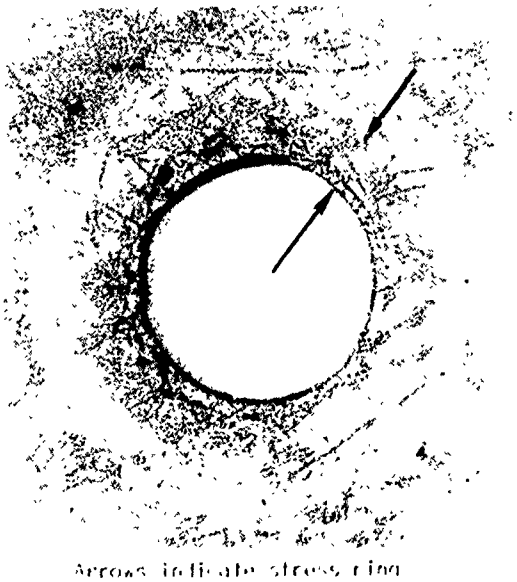
Arrows indicate stress ring

FIGURE 162. STRESS RING - 0.0065" INTERFERENCE FIT



Arrows indicate stress ring

FIGURE 163. STRESS RING - 0.0075" INTERFERENCE FIT



Arrows indicate stress ring

FIGURE 164. STRESS RING - 0.0085" INTERFERENCE FIT

Specimens were prepared for installation of HLT 335-6 HI-LOK pins with .0065" interference-fit and S4931919-8 MD pins with .0045" interference-fit. Pins were driven into holes using the vibratory method. Self-locking type nuts were tightened and torqued to induce joint preloads equivalent to 40 percent and to 80 percent of the titanium alloy pin yield strength. Nuts were torque striped.

Specimen thicknesses were measured and recorded prior to fastener installation, after preload by torquing, and after exposure to test temperature. Test temperatures were ambient and 180°F for a period of 91 hours. After completion of the measurement check, nuts were rotated counter clockwise 180° and then retightened to the original torque values.

Fasteners were removed, specimens were subjected to fluorescent penetrant check. Ultrasonic inspection was by-passed because transmission would be affected by the shiny countersunk cavities. Specimens were separated for visual examination at bond interface. Photographs of typical specimens are shown in Figures 165 and 166 . Test variables and fastener hardware are listed in Table 66 .

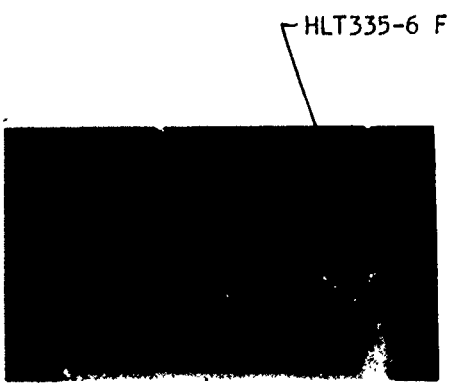


FIGURE 165. JOINT CLAMP-UP 3/16" NOMINAL DIAMETER PIN

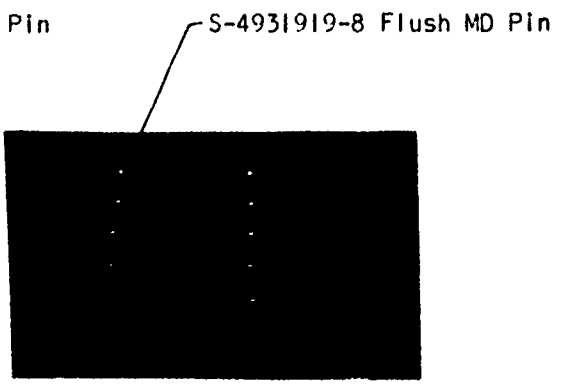


FIGURE 166. JOINT CLAMP-UP 1/4" NOMINAL DIAMETER PIN

TABLE 66

JOINT CLAMP-UP TEST VARIABLES

7075-T6 X .040" bonded to .040"

SPECIMEN NO.	BOND THICKNESS	FLUSH PIN P/N	NOMINAL PIN DIA.	NUT P/N		TORQUE INCH POUNDS	SOAK TEMPERATURE
				HOLES 1-10	HOLES 11-20		
S-50	.007/.008"	HLT335-6	3/16	S4932389-3	MS21042-3	x 25	Ambient
S-51		HLT335-6	3/16	S4932389-3	MS21042-3	x 25	180°F
S-52		HLT335-6	3/16	S4932389-3	MS21042-3	xx 45	Ambient
S-53		HLT335-6	3/16	S4932389-3	MS21042-3	xx 45	180°F
S-56		S4931919-8	1/4	MS21042-4	-	x 68	Ambient
S-57		S4931919-8	1/4	MS21042-4	-	x 68	180°F
S-58		S4931919-8	1/4	MS21042-4	-	xx 110	Ambient
S-59	.007/.008"	S4931919-8	1/4	MS21042-4	-	xx 110	180°F
S-156	.0125/.0130"	HLT335-6	3/16	S4932389-3	MS21042-3	x 25	Ambient
S-157		HLT335-6	3/16	S4932389-3	MS21042-3	x 25	180°F
S-158		HLT335-6	3/16	S4932389-3	MS21042-3	xx 45	Ambient
S-159		HLT335-6	3/16	S4932389-3	MS21042-3	xx 45	180°F
S-160		S4931919-8	1/4	MS21042-4	-	x 68	Ambient
S-161		S4931919-8	1/4	MS21042-4	-	x 68	180°F
S-162		S4931919-8	1/4	MS21042-4	-	xx 110	Ambient
S-163	.0125/.0130"	S4931919-8	1/4	MS21042-4	-	xx 110	180°F

x = 40 Percent Bolt Yield Strength
xx = 80 Percent Bolt Yield Strength

The measured joint thickness remained constant from the initial to the final measurement. Therefore, cold-flow of adhesive did not occur under these test conditions. The torque stripe was realigned on all loosened and retorqued nuts to further substantiate that cold-flow had not occurred. Visual examination of separated specimens revealed no delamination. Adhesive failure was observed at 2 of 120 holes in specimens with .0125"/.0130" bond thickness. No adhesive failures were observed out of 120 holes in specimens with .007"/.008" bond thickness.

Penetrant was not visible between the specimen mating surfaces when inspected with an ultraviolet black light. However, where the 100° countersink cavity extended through the bond line and into the bottom sheet, a ring of penetrant was visible around each hole. These rings were measured with a scale and varied from a trace to .010" for holes in which 3/16" nominal diameter pins were installed, and from .010" to .020" for holes in which 1/4" nominal diameter pins were installed. Figure 167 photograph shows fluorescent penetrant around the hole. Figure 168 photograph shows a cross-section of an installation typical to specimen S-58.

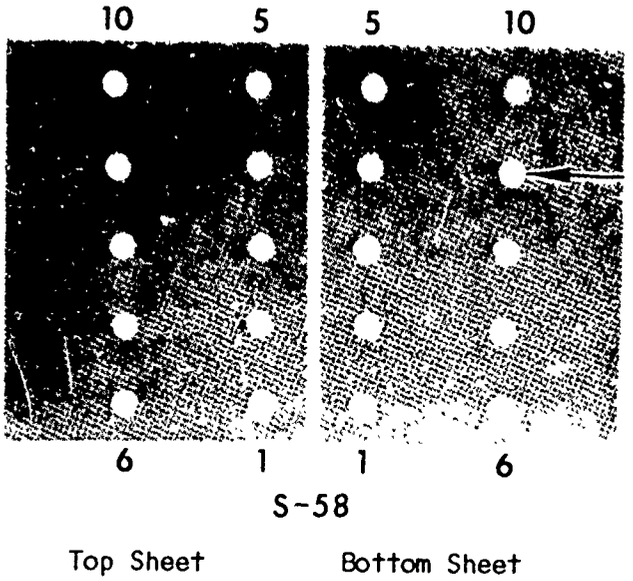


FIGURE 167. FLOURESCENT PENETRANT AROUND HOLES IN BOTTOM SHEET

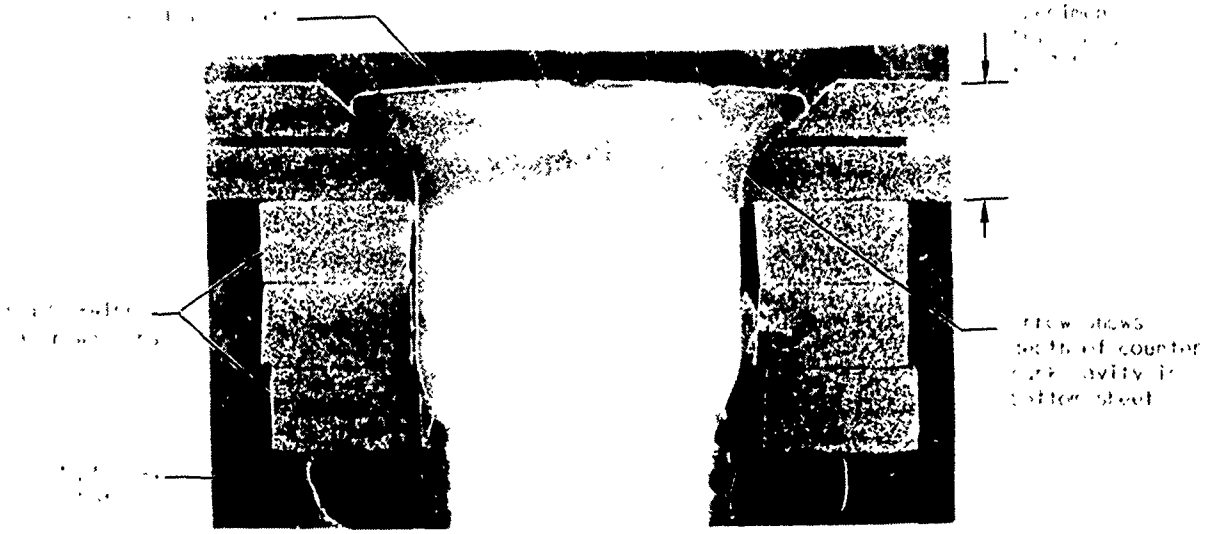


FIGURE 168. CROSS SECTION TO SHOW FASTENER INSTALLATION AND DEPTH OF COUNTERSUNK CAVITY
Typical to specimen S-58

Metallic Materials

The following tests were considered essential for testing metallic materials to PABST design requirements: (1) fatigue, (2) fracture toughness, and (3) crack growth. In Phase Ib most of the testing was directed towards 7475-T761 sheet since it represented a newer aluminum alloy for primary structure.

Smooth fatigue, $K_t = 1$ have been measured at R = +0.05 and R = +0.5 at a maximum stress of 50 ksi and 60 ksi respectively in the longitudinal and transverse direction for 7475-T761 sheet having .090 inch thickness. The effects of phosphoric anodizing and chromic anodizing on fatigue properties were compared to bare condition. Three specimens were tested at each stress level and stress ratio. The log averages are shown in Table 67.

The reduction in smooth fatigue life by chromic and phosphoric anodizing appears to be approximately the same compared to the bare condition.

Four fracture toughness panels of 7475-T761 have been tested in the longitudinal and transverse direction for fracture toughness. The fracture toughness is shown in Table 68. In the longitudinal direction the fracture toughness is approximately equivalent to 2024-T3 sheet; however, in the transverse direction the fracture toughness of 7475-T761 is slightly lower than 2024-T3.

Fatigue crack growth measurements of 7475-T761 were made from $\Delta K = 5$ to $\Delta K = 20$ in longitudinal and transverse directions in laboratory air. The results are shown in Figure 169. Fatigue crack growth in 7475-T761 sheet is higher than literature values of fatigue crack growth in 2024-T3 sheet (reference 6).

Crack growth data at -50°C from (reference 7) was compared to room temperature data for 2024-T3 and 7075-T6. The crack growth at the lower ΔK's, less than 20 ksi $\sqrt{in}$, was always less than at room temperature. At higher ΔK's the crack growth tended to be equivalent.

Crack growth data at elevated temperature from (reference 8) were made in laboratory air from ambient temperature to 572°F for 2024-T3. Crack growth at 212°F is about double compared to laboratory air.

TABLE 67

SMOOTH FATIGUE 7475-T761 SHEET

	GRAIN DIR	STRESS KSI	CYCLES	R
BARE	L	50	55,000	0.05
PHOSPHORIC ANODIZED	L	50	26,200	0.05
CHROMIC ANODIZED	L	50	33,000	0.05
BARE	T	50	41,800	0.05
PHOSPHORIC ANODIZED	T	50	26,600	0.05
CHROMIC ANODIZED	T	50	29,600	0.05
BARE	L	60	370,000	0.5
PHOSPHORIC ANODIZED	L	60	122,000	0.5
CHROMIC ANODIZED	L	60	77,700	0.5
BARE	T	60	122,300	0.5
PHOSPHORIC ANODIZED	T	60	75,200	0.5
CHROMIC ANODIZED	T	60	68,500	0.5

TABLE 68

FRACTURE TOUGHNESS 7475-T761 SHEET

DIRECTION	PLANE STRESS INTENSITY FACTOR, K_c
LONGITUDINAL	155
LONGITUDINAL	163
TRANSVERSE	124
TRANSVERSE	125

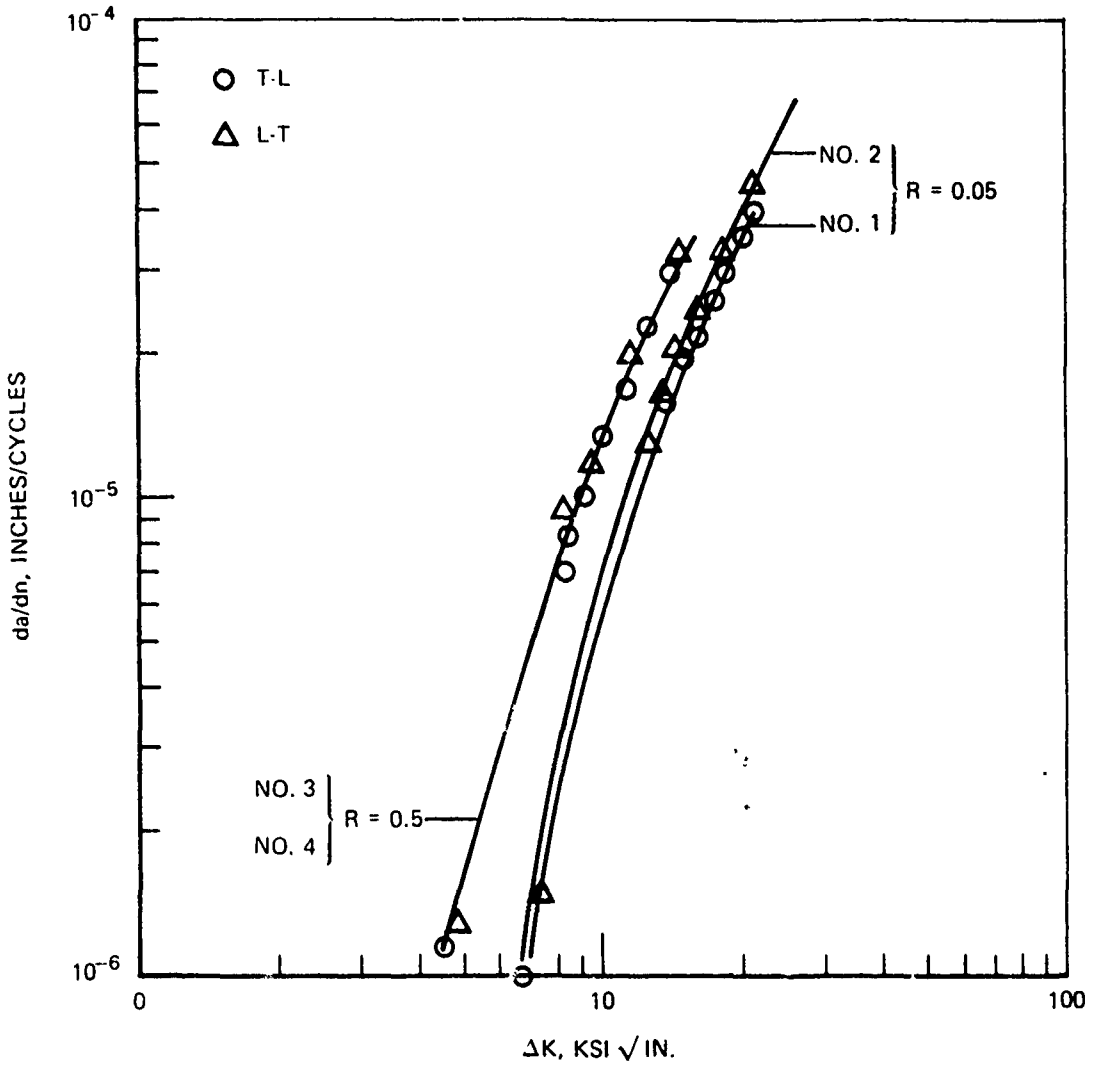


FIGURE 169. FATIGUE CRACK-GROWTH DATA FOR 0.090-INCH 7475-T761 SHEET (36-INCH)

Adhesive Material Properties Obtained from Cast Adhesive Film (Neat) Test Specimen

Early in the PABST program a need to evaluate a number of similar adhesive systems suggested that cast adhesive film (Neat) tension specimens may be used to obtain comparative mechanical property data including the effects of temperature and water absorption. An exploratory test program was initiated to study the use of Neat tension specimens to evaluate adhesive mechanical properties.

Test Method. - A simple Neat adhesive test specimen, consisting of a cured film of adhesive approaching .040 inch thick and cut into a dumbbell shape with a 0.50 inch wide test area approximately 4 inches long, was chosen for all tests in order to take advantage of an alignment jig developed by Douglas Aircraft Company. This jig was designed especially for testing of composite material specimens where accurate alignment of the test specimen was required. Not only is the specimen aligned to minimize eccentricity, but the loading fixture is controlled to clamp the specimen at the same gage length for all tests. This added feature allowed tests to be performed using cross head travel as a strain control. Strain can then be recorded to failure without any problems of extensometer range.

In order to establish a relationship between cross head travel and equivalent gage length, an experiment was set up. A two-inch extensometer was attached to the specimen and set up to drive the test machine recorder at a rate of .004" per inch. Timing marks were scribed on the recorder trace at regular intervals. The equivalent gage length, G, could then be calculated from the equation

$$G = \frac{2T\ (\text{Cross Head Velocity})}{\text{Extensometer Deflection}}$$

where T is the total time for the chosen extensometer deflection. Note that the linearity of the stress strain curve does not enter the relationship. Tests were performed to the displacement limit of the extensometer. The results of four tests were an equivalent gage length G of 4.265 inches with a coefficient of variation of 1.5 percent.

Strain data for large strains accompanied by local neck down will be biased by the use of the 4.265-inch gage length compared with the more customary 2-inch gage. This bias should be recognized when comparing strain to failure data with that obtained with a shorter gage length extensometer.

Stress-Strain Data. - Load deflection curves were generated for three adhesive systems, FM73, AF55, and PL-729-3. Secant modulus curves can be converted to stress by the simple transformation

$$\sigma = \text{Strain Rate} \times \text{Time} \times \text{Secant Modulus}$$

Constant strain rate load deflection curves were generated for FM73, AF55, PL-729-3, M1133, and EA9628. Dry test specimens had been stored in laboratory air prior to testing, while wet specimens were conditioned at 140°F, 100 RH, for at least 48 hours and stored in the humidity chamber until tested. The test chamber was stabilized at temperature prior to testing but did not have humidity control. No anomalies were apparent to indicate that much water was driven off during the test. Data obtained from these tests provides a means for judging effects of strain rate, temperature and water absorption on adhesive mechanical properties.

Stress Relaxation. - In order to obtain additional insight into the time dependent properties of the FM73 adhesive system chosen for the continuation of the PABST program, a number of stress-relaxation experiments were performed. Specimens were loaded at a 2 inches per minute cross head travel rate to a fixed total strain and stress relaxation observed. FM73 adhesive exhibits a very consistent stress relaxation described currently as linear plotted log-log; i.e., $\text{Log } E(t) = m \text{ Log } t + E$.

NONDESTRUCTIVE INSPECTION

The objectives of Nondestructive Inspection, NDI, for Phase Ib were to:

1. Detect defects in adhesive bonded assemblies,
2. Evaluate applications and limitations of NDI methods,
3. Measure cohesive bond strength,
4. Correlate effects of defects on bond strength and fatigue life,
5. Design an evaluation method for production and in-service inspectability,
6. Select NDI methods for in-service inspection,
7. Identify "non-state-of-the-art" NDI concerns.

Evaluation of Built-in Defect Specimens

Various built-in defects were produced in typical laminate and honeycomb specimens. These panels were evaluated by various NDI methods to determine which methods reliably detected the different defects. These methods included:

- Low energy X-ray (5 to 50 Kv)
- Fokker Bondtester
- Sondicator (Automation Industries) Figure 170
- Harmonic Bondtester (Shurtronics) Figure 170
- 210 Sonic Bondtester (NDI instruments) Figure 170
- Ultrasonic Contact Tests (Reflectoscope) Figure 170
  - Pulse-echo ringing
  - Thru-transmission
  - Surface wave
  - Shearwave (Honeycomb only)
- Ultrasonic Immersion Tests (C-scan) Figure 171
  - Thru-transmission
  - Reflector Plate
  - Pulse-echo ringing
- Acoustic Emission (Thermal scanning of defect side or water intrusion side of honeycomb panels)
- Tap Test (coin)
- Neutron Radiography

The results of this investigation for the built-in defect laminate panels and for the build-in defect honeycomb panels are shown in Tables 69 and 70 respectively. Typical comparative results obtained by X-ray radiography, neutron radiography, ultrasonic C-scan, and split-open visual comparison are shown in Figure 172.

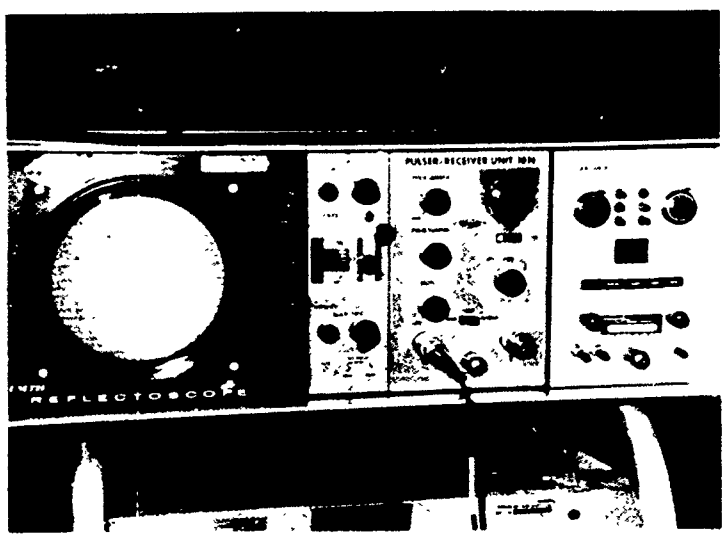
PRECEDING PAGE BLANK-NOT FILMED



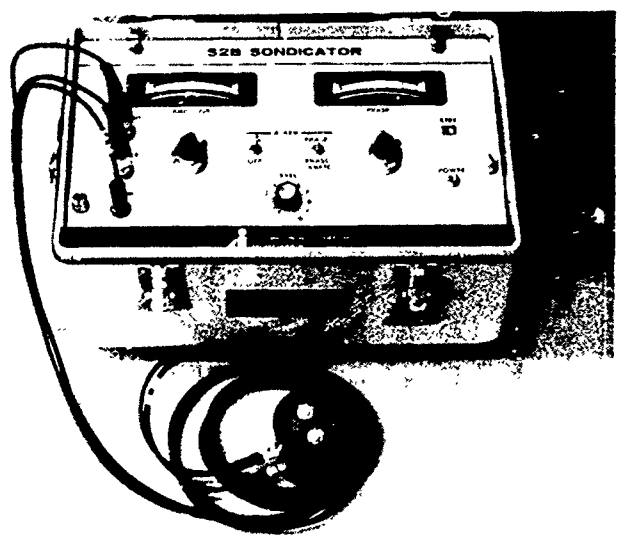
210 BONDTESTER



HARMONIC BONDTESTER



REFLECTOSCOPE



SONDICATOR

FIGURE 170. BONDTESTING INSTRUMENTS



FIGURE 171. ULTRASONIC C SCAN SYSTEM AND DRY PAPER RECORDER

TABLE 69

CORRELATION OF NDT RESULTS FOR BUILT-IN DEFECTS IN LAMINATE PANELS

LAMINATE DEFECTS	NDE METHODS: LOW KV X-RAY	FOKKER BONDTESTER	SONDICATOR	HARMONIC BONDTESTER	210 SONIC BONDTESTER	ULTRASONIC (5): CONTACT PULSE-ECHO	CONTACT THROUGH-TRANSMISSION	IMMERSION C-SCAN PULSE-ECHO	IMMERSION C-SCAN THROUGH-TRANSMISSION	IMMERSION C-SCAN REFLECTOR PLATE	COIN TAP TEST	NEUTRON RADIOGRAPHY	REMARKS
1. VOID	(1)	D	D	D	D	D	D	D[2]	D	D	PD[4]	D	1, 2, 4, 6
2. VOID (C-14 REPAIR)	(1)	D	D	D	D	D	D	D[2]	D	D	PD[4]	D	2, 4
3. VOID (9309 REPAIR)	(1)	D	D	D	D	D	D	D[2]	D	D	PD[4]	D	2, 4
4. LACK OF BOND (SKIN TO ADHESIVE)	(1)	D	D	D	D	D	D	D[2]	D	D	PD[4]	ND	2, 4
5. MFGR'S SEPARATOR SHEET (FM123-41)	(1)	D	D	ND	PD	ND	PD	D[2]	D[3]	D[3]	ND	PD[3]	2, 3
6. THICK ADHESIVE (1, 2, 3 PLY)	(1)	D	ND	ND	D	ND	ND	ND[4]	PD[2]	D[2]	ND	ND	2, 4
7. POROUS ADHESIVE	(1)	D	ND	ND	D	D	D	D	D	D	ND	D	1

ND — NOT DETECTED PD — PARTIAL DETECTION D — DETECTED

1. PANELS WERE MADE USING FM-73 WHICH IS NOT X-RAY OPAQUE.
2. METHOD SUFFERS FROM ULTRASONIC WAVE INTERFERENCE EFFECTS CAUSED BY TAPERED METAL DOUBLERS OR VARIATIONS IN ADHESIVE THICKNESS.
3. MANUFACTURER'S SEPARATOR SHEET NOT DETECTABLE BUT DEVELOPED POROSITY AND AN EDGE UNBOND DURING CURE CYCLE WHICH WAS DETECTABLE.
4. MIL-C-83286 (WHITE) EXTERNAL TOPCOAT AND PR1432G (GREEN) PLUS MIL-C-83019 (CLEAR) BILGE TOPCOAT DAMPENED THE PULSE-ECHO RESPONSE.
5. CONTACT SURFACE WAVE WAS TRIED BUT DID NOT DETECT ANY BUILT-IN DEFECTS.
6. MINIMUM DETECTABLE SIZE APPROXIMATELY EQUAL TO SIZE OF PROBE BEING USED.

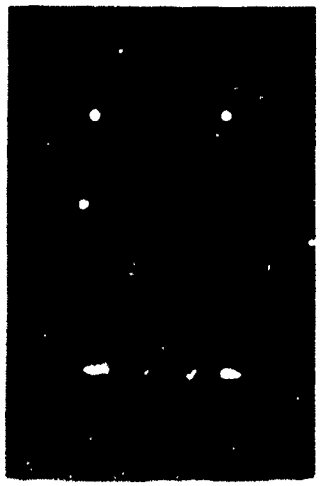
TABLE 70

CORRELATION OF NDT RESULTS FOR BUILT-IN DEFECTS IN HONEYCOMB

	HONEYCOMB DEFECTS	NDE METHODS: LOW Ku X-RAY	FOKKER BONDTESTER	SONDICATOR	HARMONIC BONDTESTER	210 BONDTESTER	ULTRASONIC: CONTACT PULSE-ECHO	ULTRASONIC: CONTACT THROUGH-TRANSMISSION	ULTRASONIC: CONTACT SHEAR WAVE	ULTRASONIC: IMMERSION C-SCAN PULSE ECHO	ULTRASONIC: IMMERSION C-SCAN THROUGH-TRANSMISSION	COIN TAP TEST	NEUTRON RADIOGRAPHY	REMARKS
11	VOID (ADHESIVE TO SKIN)	ND[1]	D	D	D	D	D	D	ND	D	D	D	D	REPLACEMENT 1 STANDARD
12.	VOID (ADHESIVE TO SKIN) REPAIR WITH C-14													NO VOID IMPROPERLY MADE
13	VOID (ADHESIVE TO SKIN) REPAIR WITH 9309													NO VOID IMPROPERLY MADE
14 *	VOID (ADHESIVE TO CORE)	ND	D	–	D	D	ND	D	ND	D	D	D	D	REPLACEMENT STANDARD
15.	WATER INTRUSION	D	ND	ND	ND	ND	ND	D	ND	ND	D	D	D	
16	CRUSHED CORE (AFTER BONDING)	D[2]	PD[4]	ND	PD[4]	ND	ND	PD[4]	ND	PD[4]	PD[4]	D	PD	2, 4
17.	MFGRS SEPARATOR SHEET (SKIN TO ADHESIVE)	ND[3]	ND	ND	PD	ND	PD	D	ND	D	D	PD	D	3
18	MFGRS SEPARATOR SHEET (ADHESIVE TO CORE)	ND[3]	ND	ND	ND	ND	D	ND	ND	D	PD	D	D	3
19	VOID (FOAM TO CLOSURE)	D	D	D	D	D	D	D	ND	D	D	D	D	
20	INADEQUATE TIE-IN OF FOAM TO CORE	D	D	D	D	D	ND	D	ND	D	ND	D	D	
21	INADEQUATE DEPTH OF FOAM AT CLOSURE	D	D	D	ND	PD[5]	ND	ND	ND	ND	ND	PD	D	
22	CHEM-MILL STEP VOID	ND[3]	ND	ND	ND	ND	ND	ND	ND	ND	ND	ND	D	3

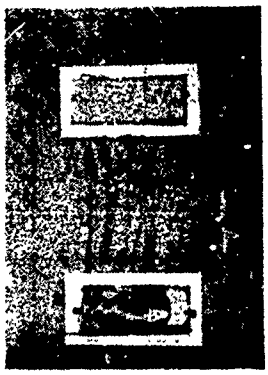
ND – NOT DETECTED PD – PARTIAL DETECTION D – DETECTED

1. PANELS WERE MADE USING FM-73 WHICH IS NOT X-RAY OPAQUE.
2. THE 0.005-AND 0.010-INCH CRUSHED CORE DETECTED BY STRAIGHT AND BETTER BY ANGLE SHOT
3. HAS BEEN DETECTED BY X RAY WHEN ADHESIVE WAS X-RAY OPAQUE (FM-400).
4. DETECTS 0.010 CRUSH CORE.
5. DISCLOSES DEFECT AT A VERY HIGH SENSITIVITY.



X-RAY

NEUTRON



ULTRASONIC

VISUAL

FIGURE 172. COMPARISON OF BUILT-IN DEFECT SPECIMEN

State-Of-The-Art Methods Evaluations

Based on the results of the tests of the build-in defect panels (Tabels 69 and 70) and of the numerous bonded test panels of various sizes and configurations, the following conclusions were obtained:

Low Kv X-Ray. - AF55 and FM400 are X-ray opaque and enable voids and porosity to be detected in metal-to-metal areas. Although attempts have been made by adhesive manufacturers to make adhesives X-ray opaque, Figure 173, it is not anticipated that the FM73, used for the ADP component, will be X-ray opaque. X-ray is required for detecting honeycomb core and fitup defects and water intrusion.

Fokker Bondtester. - This tester is excellent for detecting voids, porosity, and thick glueline in bonded laminates. However, the honeycomb close-out zones are more difficult to inspect using the Fokker than metal-to-metal joints. Correlations of Fokker readings and cohesive bond strength will be made for FM73 during Phase II after joint configurations and thickness of aluminum have been determined. The DAC Fokker Model 67, Figure 174, will be replaced by the more versatile Model 70, Figure 175, purchased to obtain optimum results with this method.

Sondicator. - Various models have been evaluated. Since the repeatability of results and sensitivity has been poor, this method has been dropped from further use on the program.

Harmonic Bondtester. - This tester has limited application. However, it is useful for detecting large voids (1/2-inch dia.) in skin-to-core or single laminate joints where the face sheet is less than .090 inch. In very large disbonds, the instrument may not indicate the disbond when the probe is at its center.

210 Sonic Bondtester. - This tester is excellent for detecting voids in laminates and honeycomb. It is used primarily to inspect all large panels. There are some stability problems with instrument and probes which are being worked out with the vendor.

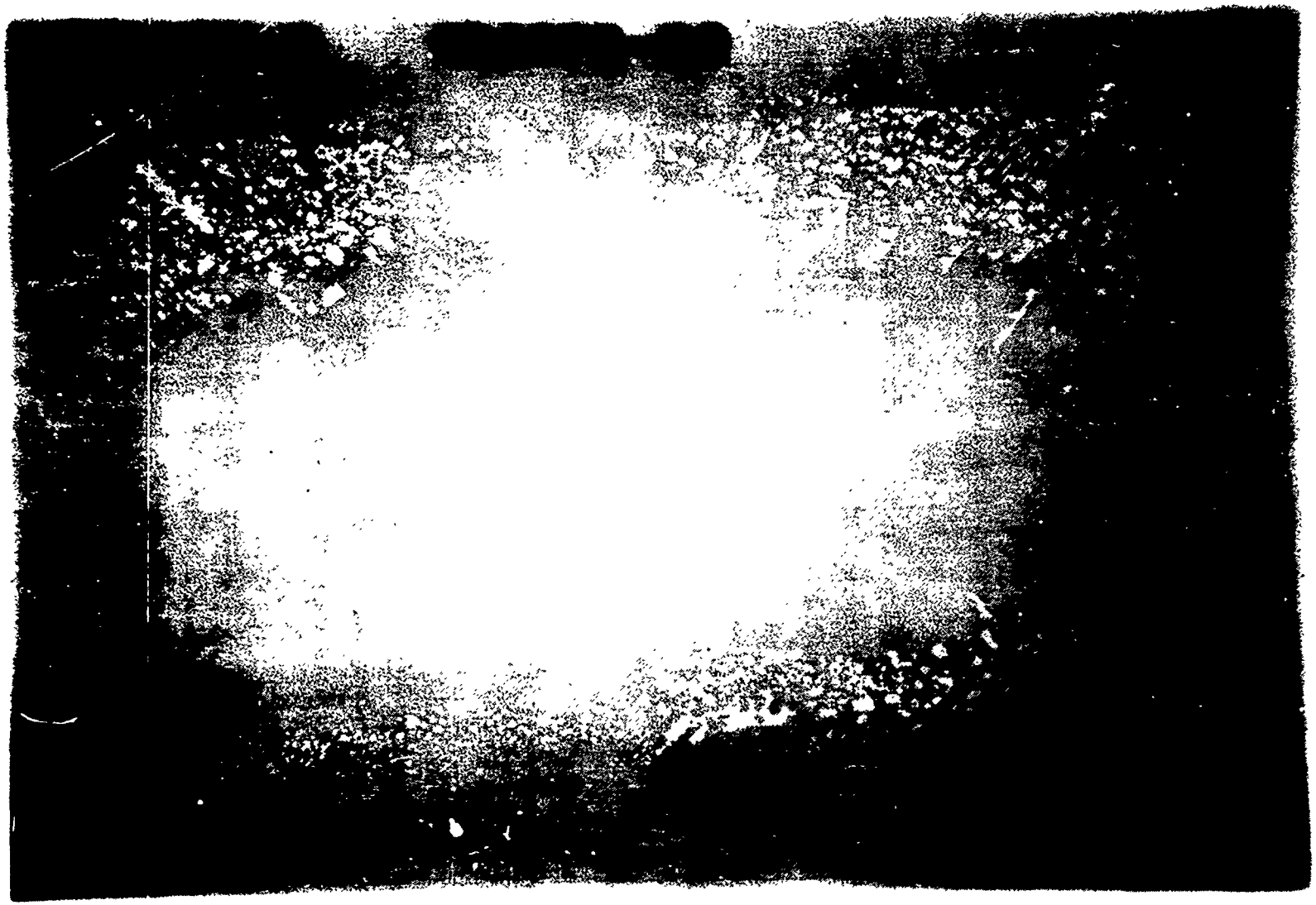


FIGURE 173. RADIOGRAPH OF HYSOL EA9628 ADHESIVE WITH X-RAY OPAQUE ADDITIVE

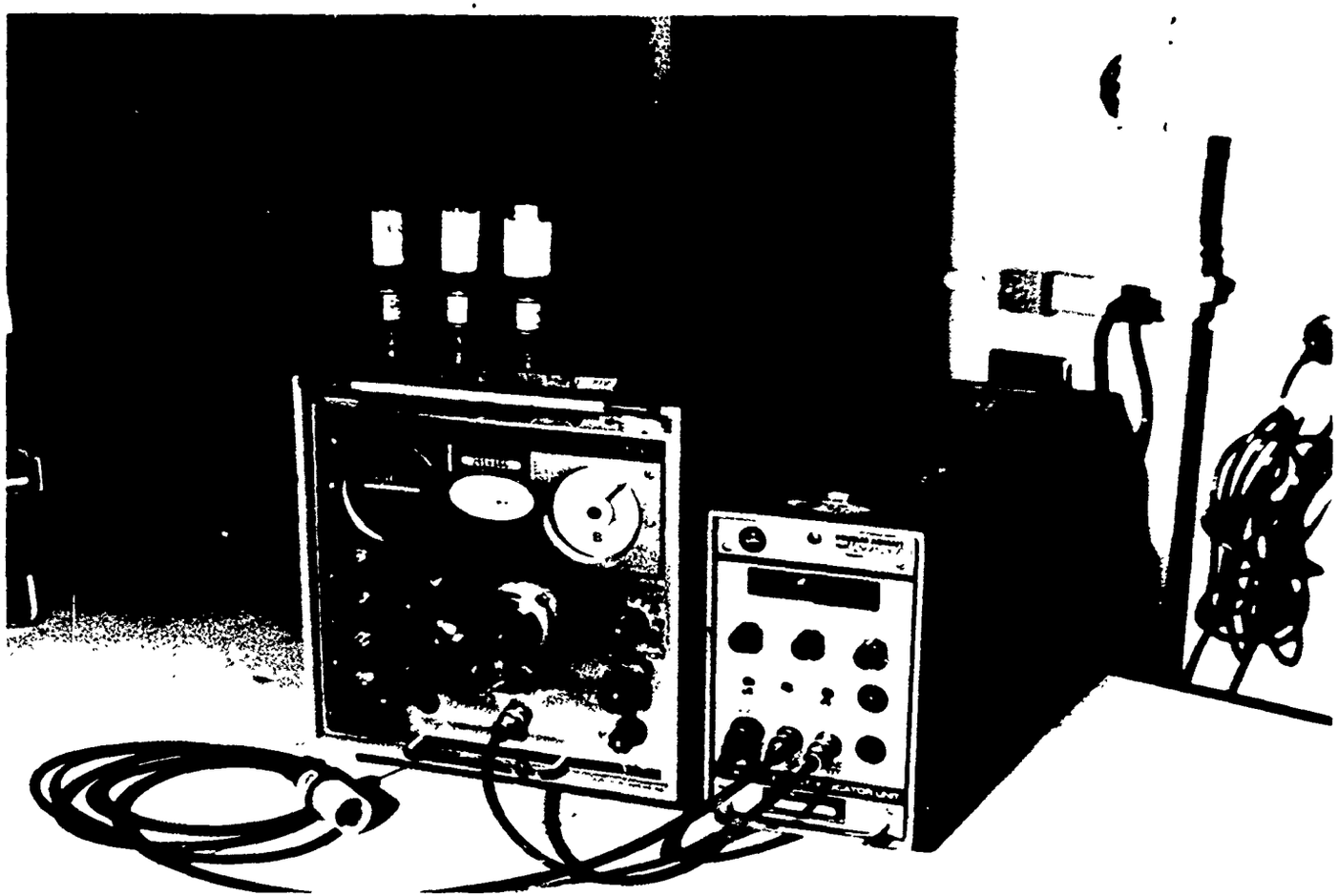


FIGURE 174. FOKKER MODEL 67 BONDTESTER

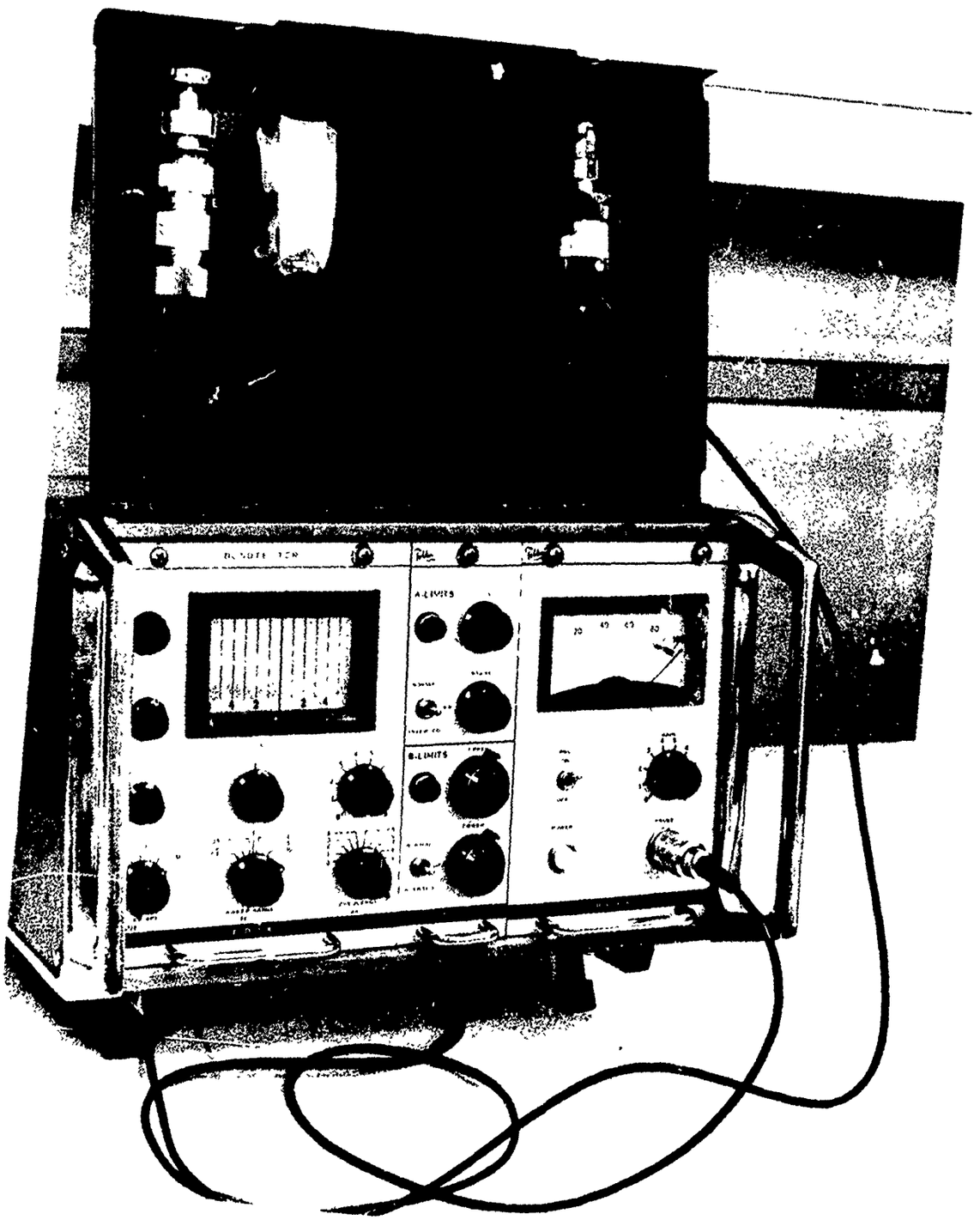


FIGURE 175. FOKKER MODEL 70 BONDTESTER

Contact Pulse Echo Ultrasonic. - This method has limited application, and is used as a back up to the Fokker and the 210 Bondtester. It suffers from destructive wave interference at certain adhesive and metal thicknesses.

Contact Thru-Transmission Ultrasonic. - This method is useful for detecting voids and gross porosity in metal-to-metal close-outs on honeycomb panels and edge doublers on laminates. However, it also suffers from destructive wave interference but less than for the contact pulse echo ultrasonic method.

Immersion Pulse-Echo C-Scan. - This method has limited use. It suffers from destructive wave interference for certain adhesive and metal thickness. It is difficult to use on contoured panels. The maximum specimen size is limited by the immersion tank size.

Immersion Thru-Transmission C-Scan. - This method is excellent for detecting voids and porosity in laminates and honeycomb. However, it requires special equipment for large panels, squirters for honeycomb panels which cannot be immersed, and contour followers for contoured parts. It is easy for an inspector to interpret signals on the CRT. This method is excellent for permanent plan view recording of results for repeat inspections during fatigue tests although it suffers slightly from destructive wave interference.

Immersion Reflector Plate C-Scan. - This method is used extensively for the inspection of flat panels and specimens. It suffers from destructive wave interference. Other concerns are similar to those for the thru-transmission devices described above.

Coin Tap. - This method is useful for large area skin-to-core and upper face-sheet laminate unbond.

Neutron Radiography. - This method is excellent for detecting defects such as voids and porosity in laminates and honeycomb. It is useful for detecting water intrusion in honeycomb. Reactor produced neutron studies were performed at Atomics International at a reasonable cost. This would be an excellent inspection method if costs could be further reduced and an in-plant neutron source was available. It should be noted that the Californium 252 technique was not investigated because of costly quotations for services.

Acoustical Holography. - This technique appears to offer excellent promise for inspecting bonded structures but quotations for services were too costly to pursue.

Holographic Interferometry. - This method has limited use. It is not very useful for inspecting complex laminates because of the inability to stress the void areas; thermal stressing does not work well on aluminum. It is better for inspecting honeycomb but few voids exist at the skin-to-core area. It does not work well on locating voids at honeycomb closures or multi-laminate (honeycomb) metal-to-metal areas. Flaws located by ultrasonic and X-Ray methods are not detectable by holographic interferometry.

Acoustic Emission. - This method appears useful for failure analysis studies especially during fatigue tests but it is not considered to be a state-of-the-art method for PABST. It is capable of detecting cohesive failure but requires correlation studies. Feasibility studies indicate it can detect water entrapment in honeycomb and corrosion in bonded laminates when the part is heated. Further studies are needed before it becomes a state-of-the-art method.

Bonded Reference Standards

Before NDI can be performed, it is desirable to have reference standards with built-in voids at skin-to-adhesive and adhesive-to-second-laminate or honeycomb core. Various methods for making reference standards were investigated. The two most promising methods are illustrated in Figure 176. Standards of this type will be made, for each joint configuration, for Phase III fabrication inspection.

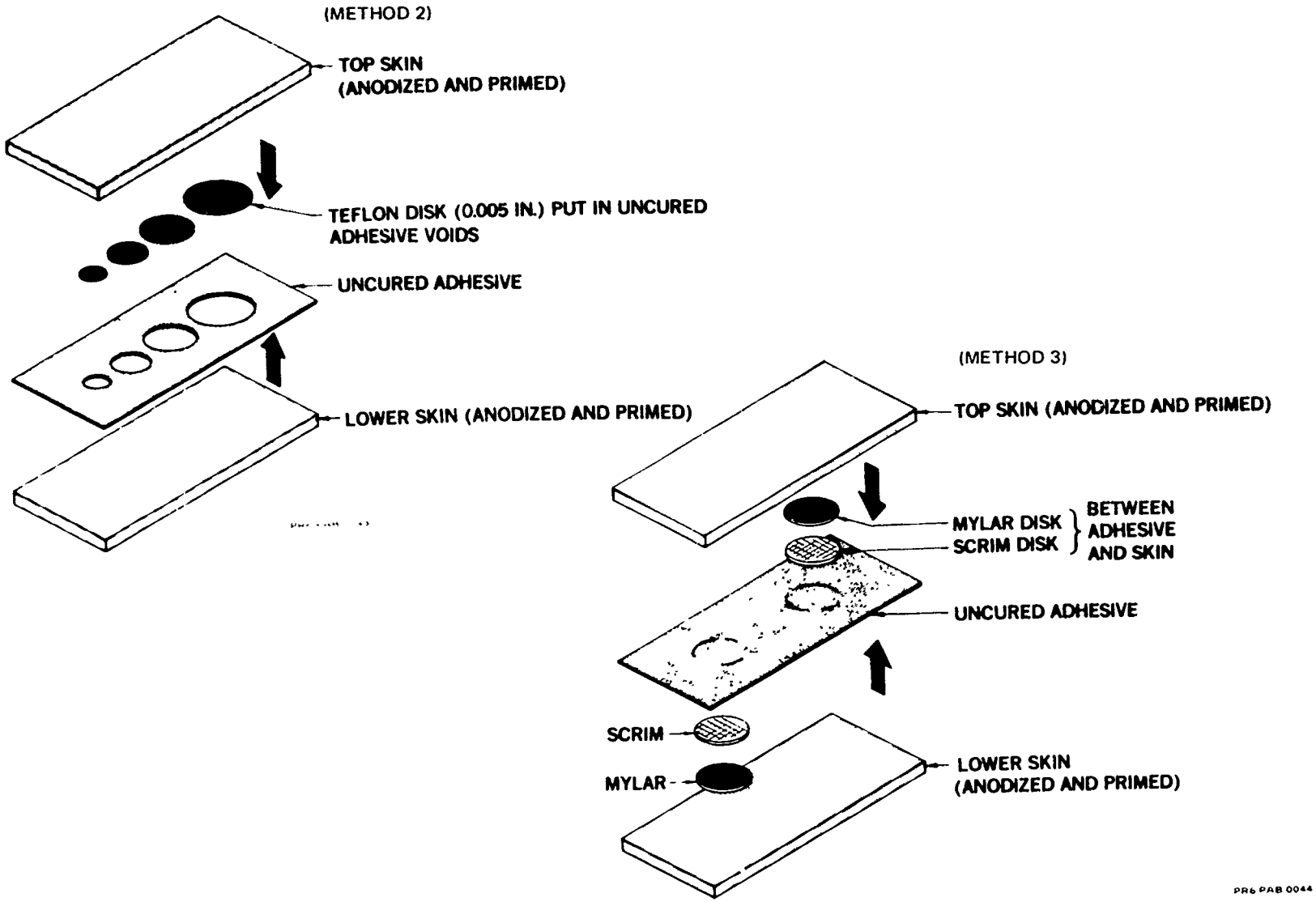


FIGURE 176. METHODS FOR FABRICATING REFERENCE STANDARDS

Correlation of Nondestructive Testing, NDT, Results

Numerous test specimens and bonded assemblies were evaluated by a combination of X-ray or neutron radiography, ultrasonic C-scan, and Fokker, Harmonic, or 210 bondtesters. Results were obtained in the form of ultrasonic C-scans; radiographs; by marking the part surface and photographing; or by making a sketch of the part and denoting the size, type, and location of the discontinuity on the sketch. Certain specimens or parts were selected for defect verification by cutting or separating the joint for visual examination.

X-ray radiography was used to detect voids and porosity in opaque adhesives such as AF55. It has also been used to detect crushed or condensed core and foaming adhesives (not X-ray opaque) tie-in at core splices or closures. Figure 177 is a typical example of porous foaming adhesive at a core splice. Rejectable splice No. 1 was almost completely void of foaming adhesive.

Figure 178 is a composite photograph of NDT results for the front face cold-bonded doublers, of a test panel. The original photographs were in color to define the red (Harmonic) marks from the black (210 Bondtester) marks. The part was photographed before removing the rejected doubler (not shown) and rephotographed again on the face side and adhesive side (Figure 178) for correlation. The best correlation was obtained by the 210 Bondtester. Also see Figure 172 for additional correlations for X-ray, neutron, C-scan, and visual of one of the built-in defect panels. See the section entitled, "Mechanical Attachments", for verification of bond separation, due to overheating, by ultrasonic C-scan. Numerous other examples could be given. Basically, the visual verification of NDT results has been very good.

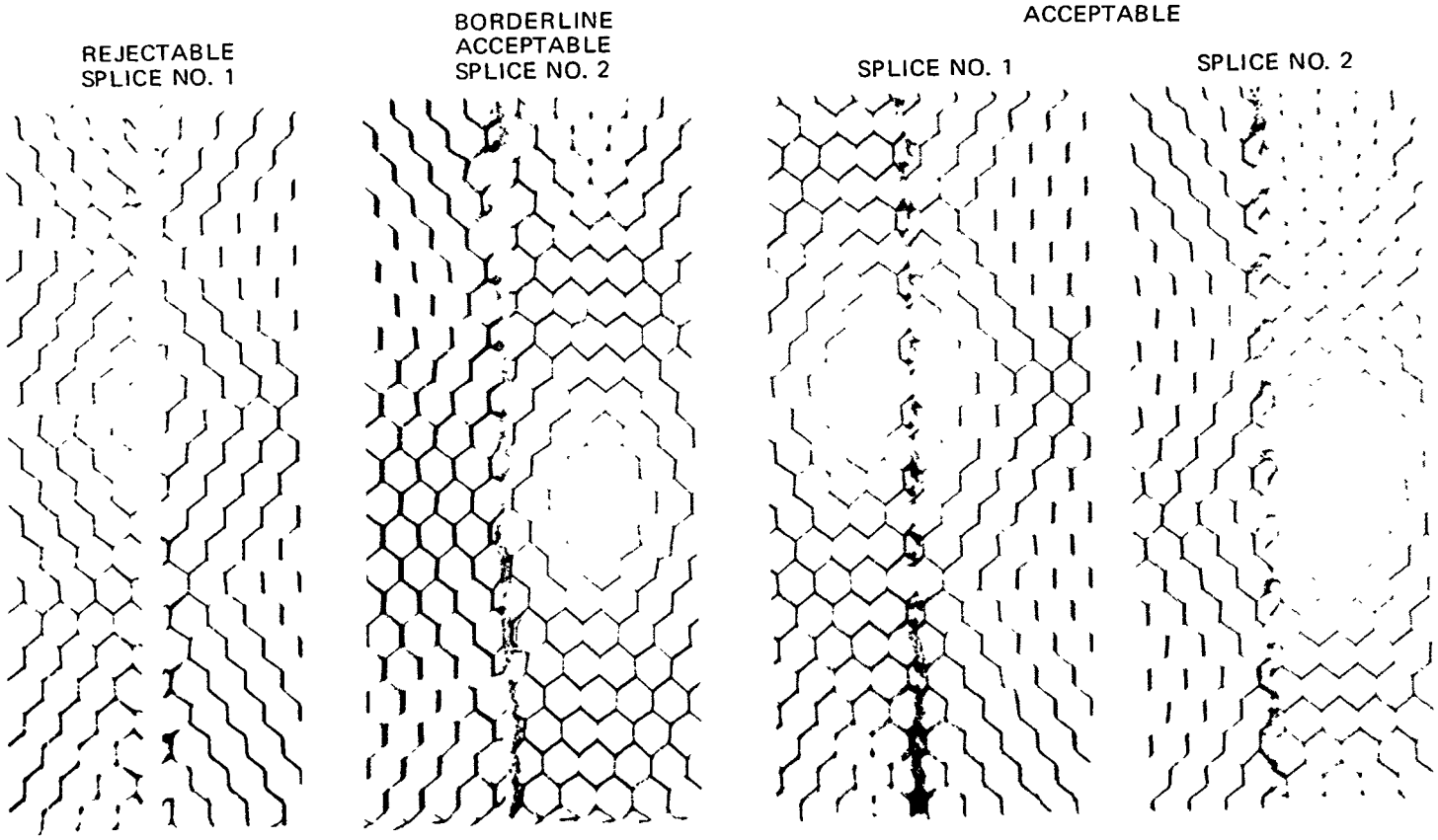


FIGURE 177. RADIOGRAPHS OF BONDED CORE SPLICES

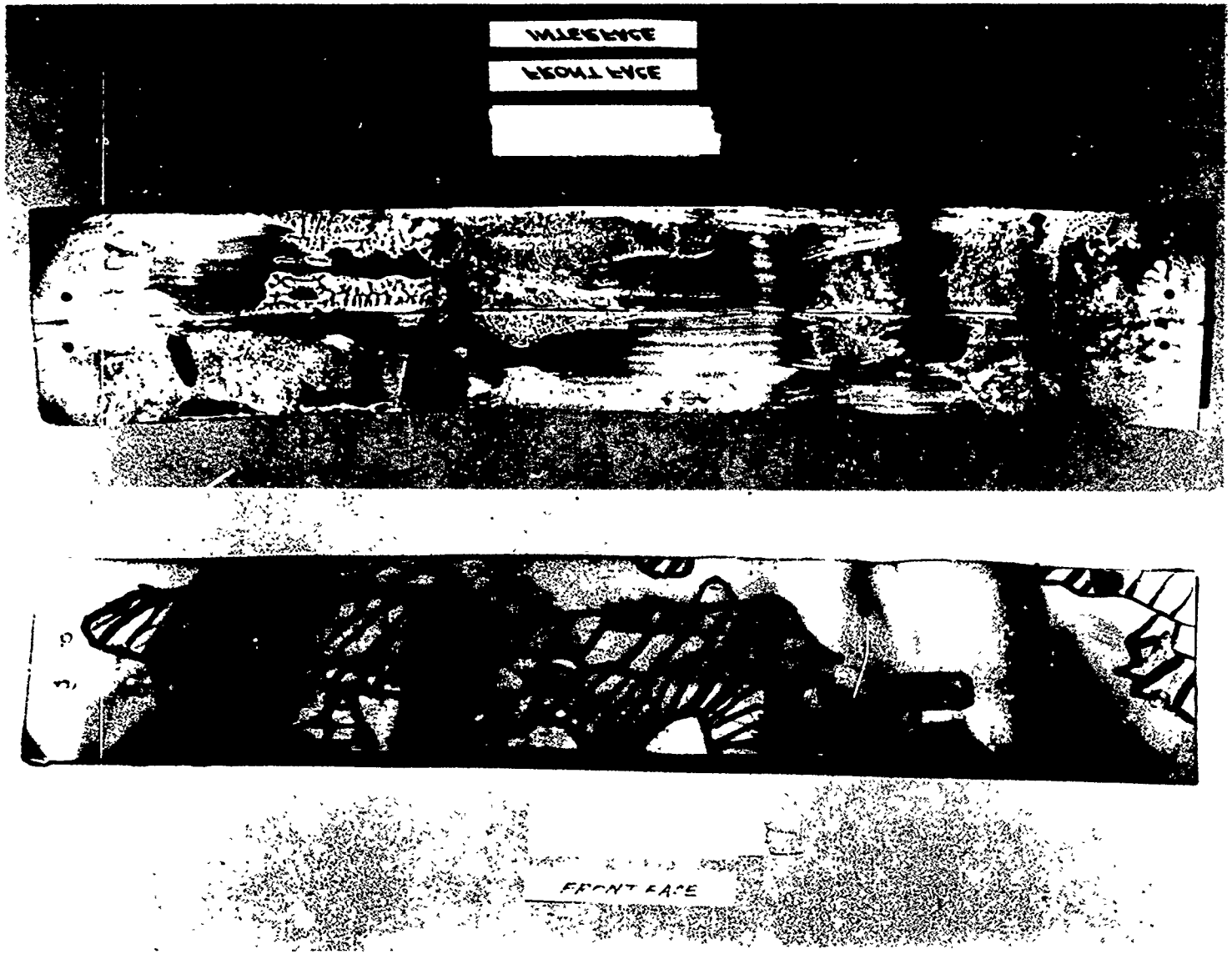


FIGURE 178. CORRELATION OF NDT RESULTS

Cohesive Bond Strength Determination

The Fokker bondtester (Figure 175) is the only state-of-the-art instrument used for measuring cohesive bond strength according to a literature search. MIL-STD-860, "Fokker Ultrasonic Adhesive Bond Test," specifies the test procedure for using the bondtester. It should be noted that MIL-STD-860 needs to be revised based on recent knowledge.

In June, 1976, Fokker-VFW B.V., Reference 9, establishing FM73 correlation curves for shear strength to glueline thickness, to glueline porosity, and to bondtester indication. The adhesive was FM73 with a woven carrier. The sheet material was dural 2024-T3 alclad, thickness 1.6 mm (.063 in.). Surface treatment was carried out in accordance with the Fokker VFW specification TH6.7512 chromic acid anodizing (TH6.7851) included. The anodized surface was sealed with BR127 primer prior to bonding. Similar tests will be run at Douglas but with 2024-T3 bare material, FM73 with mat carrier, and phosphoric acid anodize surface treatment.

Panels are made approximately 12 inches square. The glueline is 1.25 in. wide by 12 inches long running down the center of the panel. On either side of the glueline are 12 inch long shims. The shims are varied in thickness in each panel from .002 in. to .020 in. This causes a controlled thickness change in the adhesive. Also, as the adhesive thickness increases so does the porosity. Neutron radiographs are made of each panel to determine the degree of porosity in the adhesive layer. After Fokker bondtest, 11 shear test specimens are cut out of each panel with each specimen having a width of 1 inch and overlap length of 1/2 inch. The specimens are then destructively tested, the load at failure recorded, and the shear strength calculated. Figure 179 illustrates a typical Fokker bondtester quality diagram for bonded laminates. For quick Fokker evaluation, a tapered adhesive standard, illustrated in Figure 180, may be used. Continuing evaluations of Fokker cohesive bond strength correlations will be made in Phase II.

PRECEDING PAGE BLANK-NOT FILMED

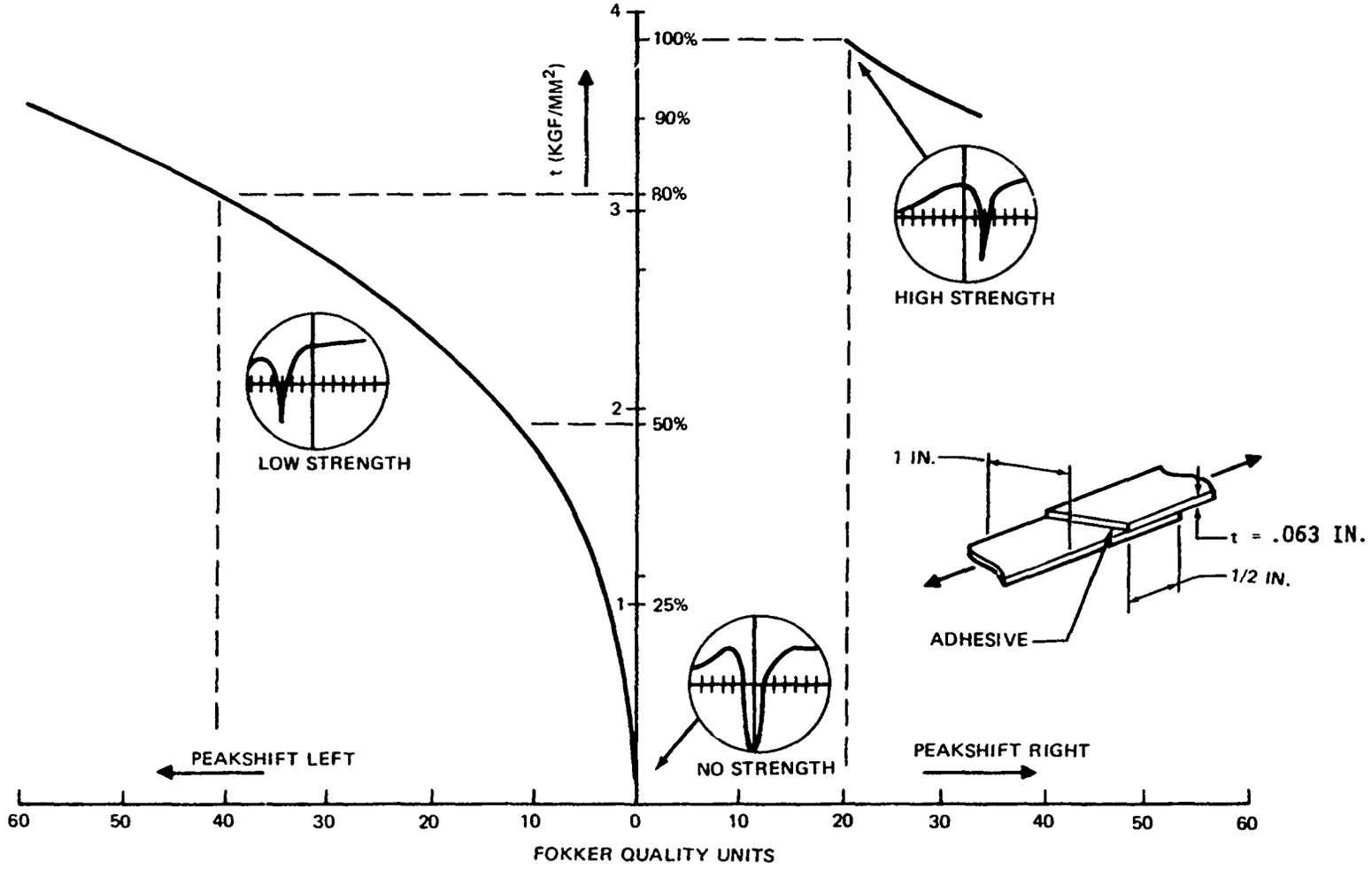


FIGURE 179. TYPICAL FOKKER BONDTESTER QUALITY DIAGRAM

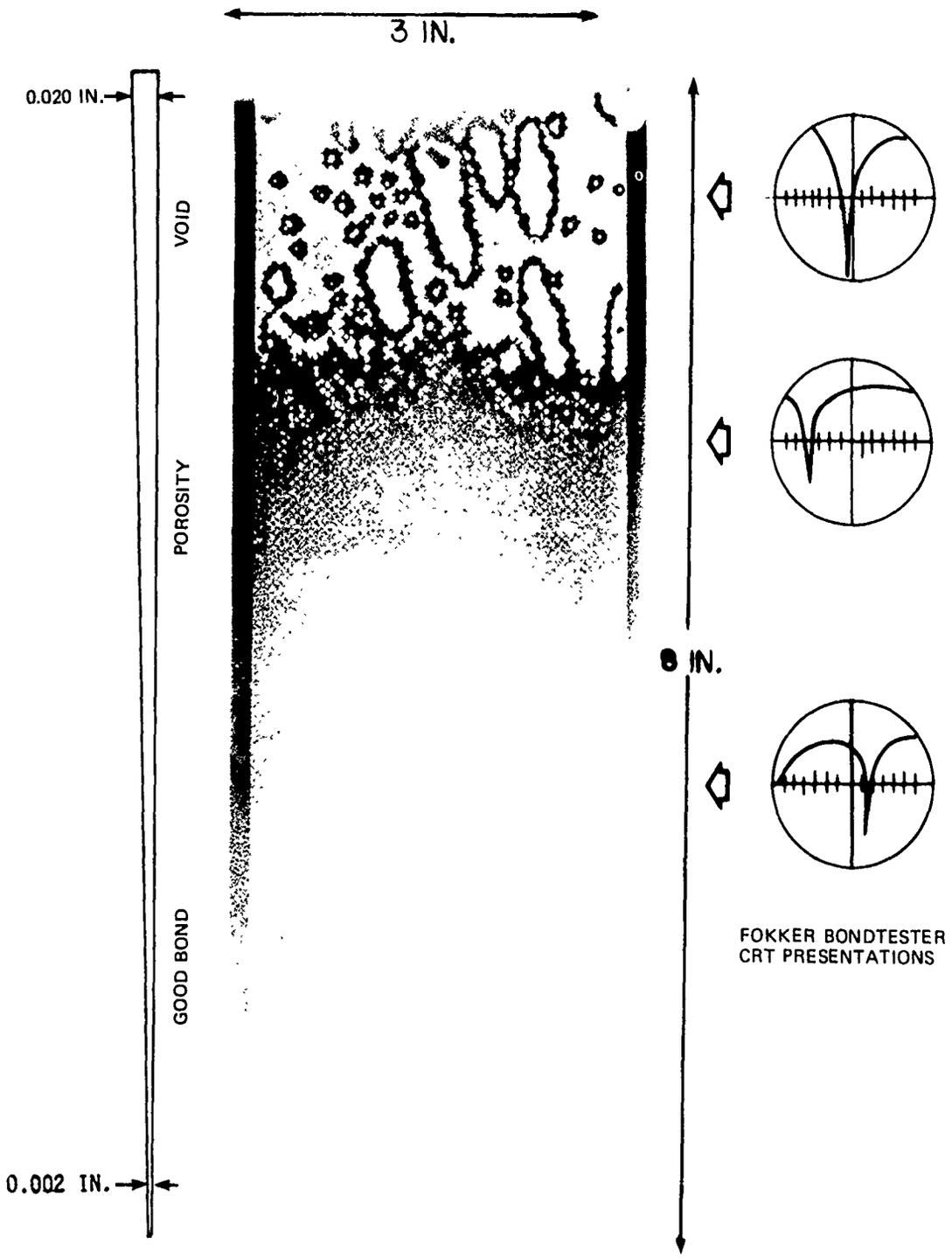


FIGURE 180. POSITIVE REPRODUCTION FROM X-RAY NEGATIVE OF AF-55 TAPERED SHIM STANDARD

Effect of Bond Flaws

During Phase Ib, many design development specimens were fabricated with built-in flaws. All specimens were initially checked by NDI to determine the size of the initial flaw. In some cases, the intended flaws were not generated because FM73 is such a free flowing adhesive that it filled in intended voids. Elox notches were made in some metal members prior to bonding. The growth of cracks, from the notches, were visually monitored if the crack was at an accessible surface; if not, the crack growth rate was followed by periodic X-ray radiography during the fatigue test. Voids or fractured bondlines were periodically checked for growth by Fokker or 210 Bondtesters during fatigue testing. In a few cases, voids were detected during initial inspection and small holes were drilled into the voids and filled with room temperature curing adhesives using hypodermic needles. The void repair was subsequently rechecked by NDI and the parts then fatigue tested. Upon completion of destructive testing, parts which had been rejected by NDI are returned for post test inspection and bondline separation and evaluation.

Figure 181 shows the ultrasonic C-scan of a tapered bonded splice after fatigue test. This C-scan, when compared to initial C-scan, indicated that damage had occured at the bondline. Dye penetrant was brushed along the edge of the bondline and dried with a hot air gun prior to separating the joint. Figure 181 shows that the dye penetrant intrusion was minimal as compared to the ultrasonic extent of damage. Failure analyses was conducted by engineering.

Special effect of bond flaw specimens were fabricated with built-in flaws at specific locations. Flaws included porosity, voids, fractured bondlines, and contaminated surfaces. All specimens were ultrasonically C-scanned, Fokker or 210 Bondtester checked. The AF55 specimens were X-rayed. Void or porosity specimens containing non-X-ray opaque adhesives were neutron radiographed. All NDI test results were recorded. Figure 182 shows typical neutron radiographic results obtained from two bonded laminate defect panels. Wires were inserted into the bond joint to create porosity. In some cases, the intended defects were not generated and the parts were rejected and remade.

PRECEDING PAGE BLANK-NOT FILMED

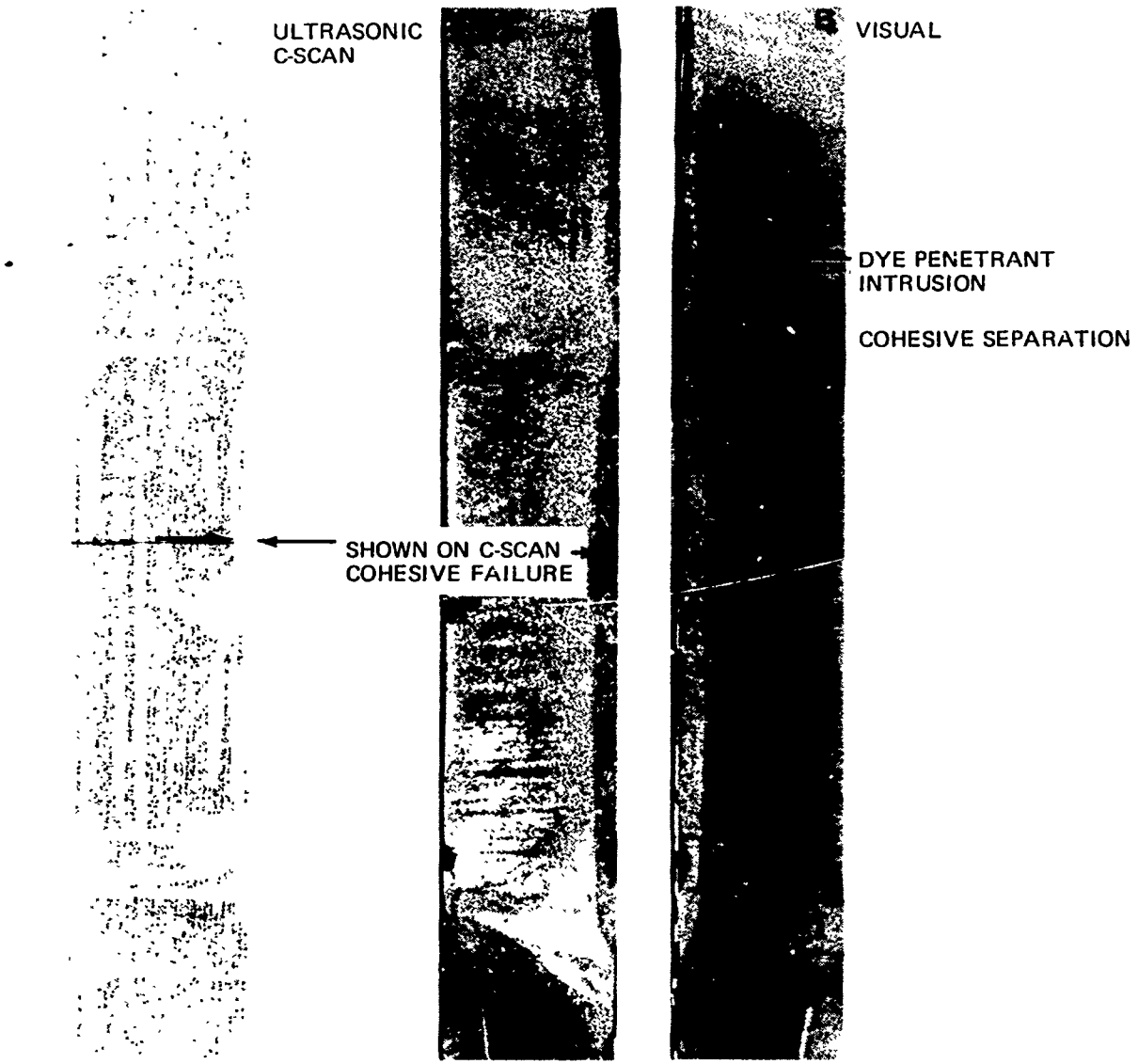


FIGURE 181. CORRELATION OF NDI TEST RESULTS WITH MODE OF FAILURE FOR TAPERED BONDED SPLICE

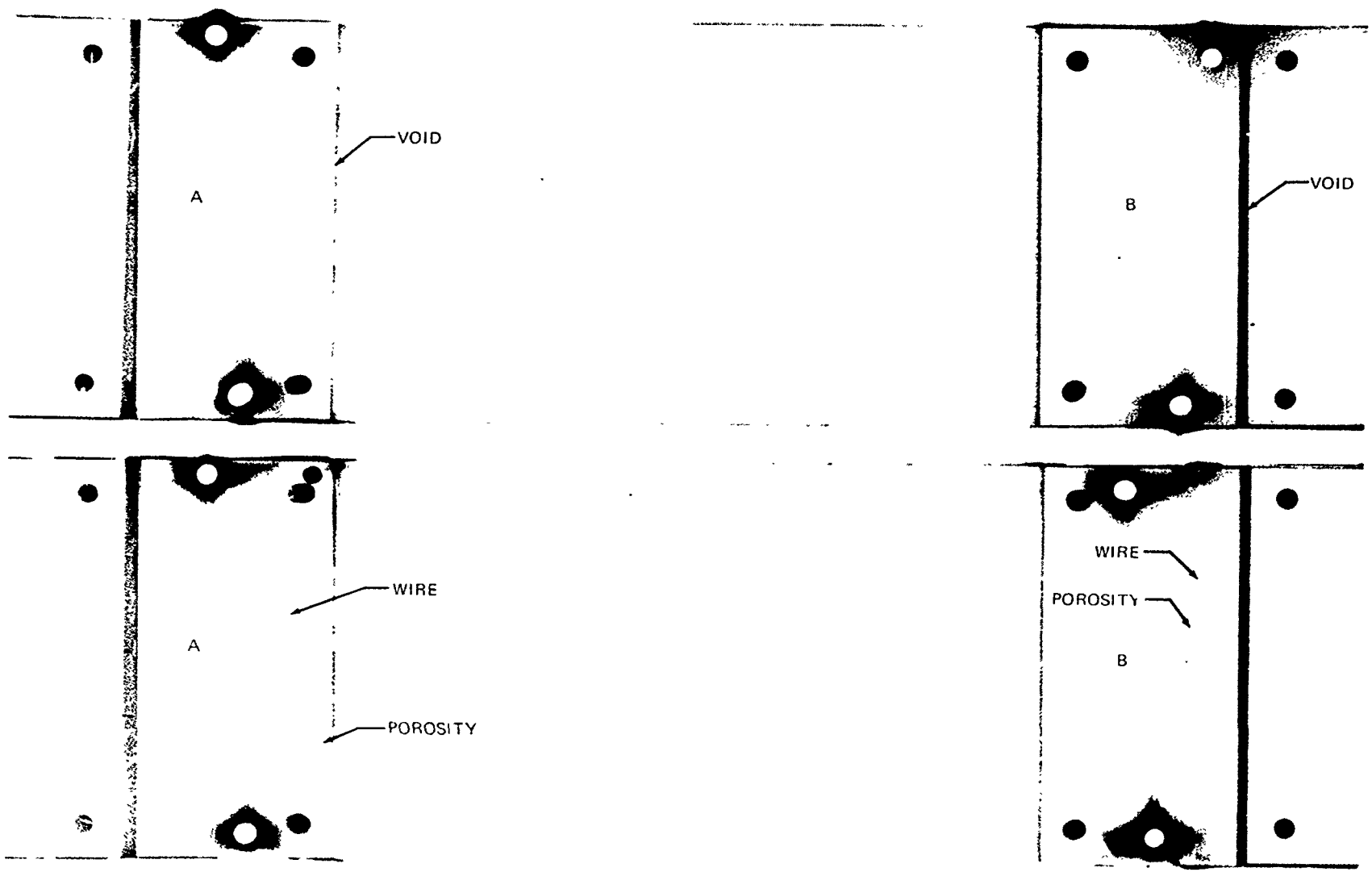


FIGURE 182. NEUTRON RADIOGRAPHS OF DEFECT SPECIMENS

Correlations will be made between defect type, size and damage tolerance criteria to: (1) Improve materials and process controls selection, (2) Improve the design of bonded joints, (3) Establish NDI acceptance criteria for production and in-service inspection, and (4) update the damage tolerance criteria.

Design Review for Production and In-Service Inspectability

Continuous design review is performed to determine the ease or difficulty of inspecting bonded joints. Figure 183 illustrates the basic design concepts vs NDI. Tapered parts are more difficult to inspect than flat parts. Thin parts are easier to inspect than thick parts. "J" or "T" frames cause difficulty in placing the Fokker probe over the bonded joint but a short right-angle connector probe was manufactured for the 210 Bondtester to solve the problem. Because fractured bondlines usually occur at joint edges, it was recommended that multiple bondlines be staggered so a probe can be run along the edge of the joint over a single thickness of material.

The Phase Ib objective was to evaluate the honeycomb, external and internal longeron design concepts for in-service NDI and for: (1) complexity of joint designs, (2) types of defects anticipated in-service, and (3) accessibility for inspection.

The approach was to:

1. Prepare built-in defect specimens and evaluate them by state-of-the-art NDI methods or techniques.
2. Correlate the results of the NDI tests with destructive tests of specimens from production parts and specimens fabricated with built-in defects (Effects of Defects Program).
3. Prepare a rating system.

   NOTE: This evaluation of the concepts was highly qualitative. Based on ALC/PABST/Commercial experience, more detailed evaluation will be conducted on the ADP design in Phase III.

An example of a design review scheme for rating the three concepts is shown in Table 71. General comments concerning in-service accessibility for all concepts is shown in Table 72.

PABST In-Service Insectability Design Rating. - After reviewing the three design concepts, they were numerically rated for inspectability. Table 71 shows that the External Longeron Concept (without external fairing) has the lowest numerical rating and, hence, is more easily inspectable. The ratings

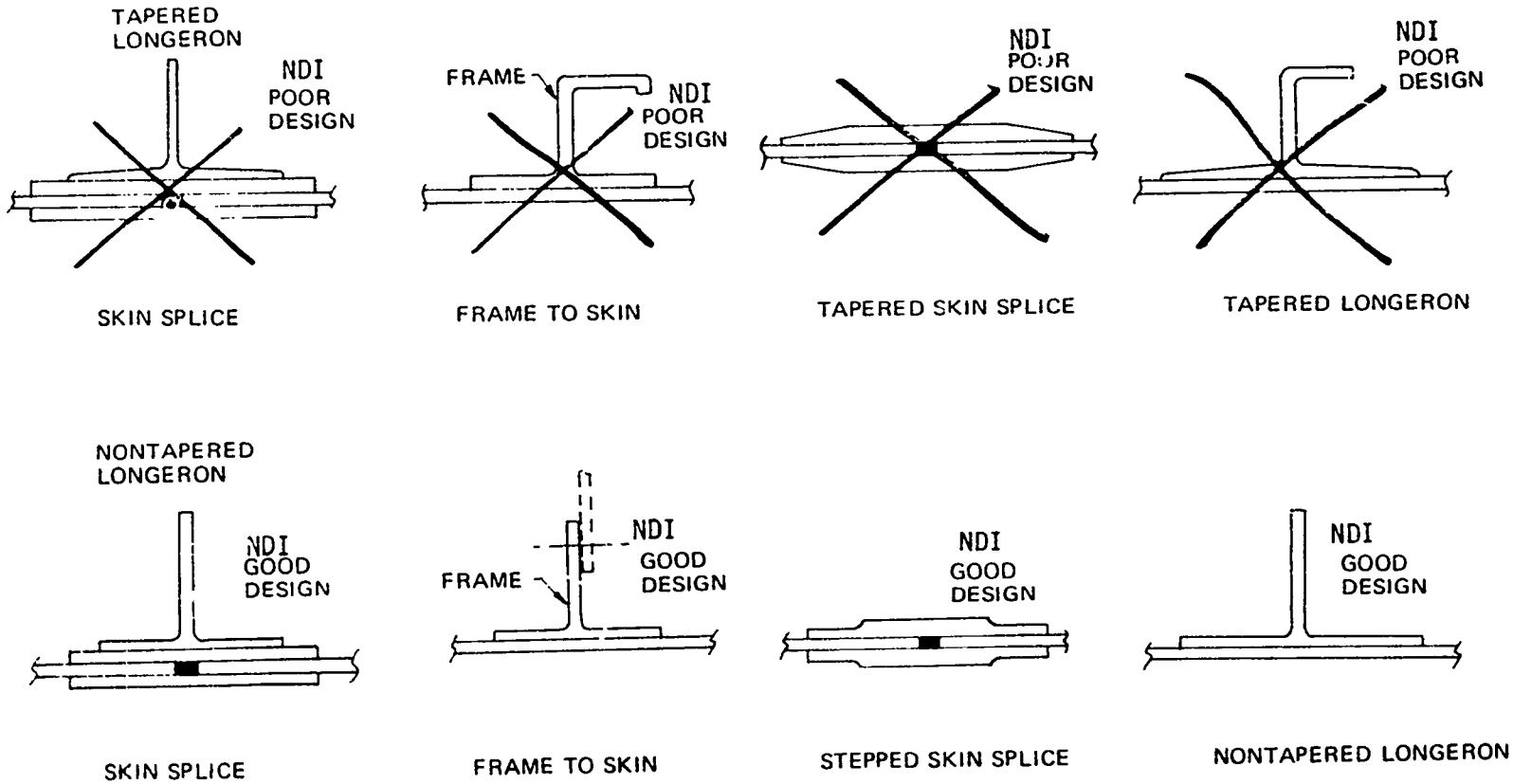


FIGURE 183. DESIGN CONCEPTS VERSUS NONDESTRUCTIVE INSPECTABILITY

TABLE 71
PABST IN-SERVICE INSPECTABILITY
(DESIGN CONCEPTS)

INSPECTABILITY CODE NA – NOT APPLICABLE, 1 – GOOD, 3 – MEDIUM, 5 – POOR, 7 – VERY POOR

	BOND QUALITY DETERMINATION TYPES OF DEFECTS ANTICIPATED IN-SERVICE	INTERNAL LONGERON	EXTERNAL LONGERON		HONEYCOMB	NOTES
			EXTERNAL FAIRING	NO FAIRING		
1	LONGERON TO SKIN DEBOND (UPPER FUSELAGE)	3 A, B	7 D	1 E	NA	A, B, C, D, E
2	LONGERON TO SKIN DEBOND (MID FUSELAGE)	3 A, B	7 D	1 E	NA	A, B, D, E
3	LONGERON TO SKIN DEBOND (BELOW FLOOR)	5 A, B, C	7 D	1 E	NA	A, B, C, D, E
4	FRAME TO SKIN DEBOND (UPPER FUSELAGE) INTERNAL	3 A, B	3 A, E	3 A, E	SHEAR-TEE 3 A	A, B, E
5	FRAME TO SKIN DEBOND (MID FUSELAGE) INTERNAL	3 A, B	3 A, E	3 A, E	SHEAR-TEE 3 A	A, B, E
6	FRAME TO SKIN DEBOND (BELOW FLOOR) INTERNAL	5 A, B, C	5 A, C, E	5 A, C, E	SHEAR-TEE 5 A, C	A, B, C, E
7	INTERNAL SKIN SPLICE DEBOND (UPPER FUSELAGE)	5 A, B, F	3 A, F	3 A, F	7 A, F	A, B, F
8	INTERNAL SKIN SPLICE DEBOND (MID FUSELAGE)	5 A, B, F	3 A, F	3 A, F	7 A, F	A, B, F
9	INTERNAL SKIN SPLICE DEBOND (BELOW FLOOR)	5 A, B, C	5 A, C, F	5 A, C, F	7 A, F	A, B, C, F
10	EXTERNAL SKIN SPLICE DEBOND (UPPER FUSELAGE)	5 B, F	5 D, F	3 F	7 F	B, D, F
11	EXTERNAL SKIN SPLICE DEBOND (MID FUSELAGE)	5 B, F	5 D, F	3 F	7 F	B, D, F
12	EXTERNAL SKIN SPLICE DEBOND (BELOW FLOOR)	5 B, F	5 D, F	3 F	7 F	B, D, F
13	CORRODED BOND JOINT					G
14	CORRODED CORE	NA	NA	NA	5	H
15	WATER INTRUSION INTO HONEYCOMB OR CRUSHED CORE (X-RAY)	NA	NA	NA	5	H
16	SKIN TO CORE UNBOND – EXTERNAL	NA	NA	NA	3	I
17	SKIN TO CORE UNBOND – INTERNAL	NA	NA	NA	5	A, I
	TOTAL	54	59	34	71	

NOTES

- A INTERNAL INSULATION BLANKETS REQUIRE REMOVAL TO PERFORM BOND TEST.
- B TAPERED THICKNESS GEOMETRY MAKES BOND INSPECTION MORE DIFFICULT
- C ACCESS BELOW FLOOR IS NOT GOOD CORROSION-INHIBITING PAINTS REDUCE SENSITIVITY OF INSPECTION. DIRT AND FOUL SMELLING MATERIALS DETRACT FROM INSPECTION
- D EXTERNAL FAIRING MUST BE REMOVED FOR INSPECTION
- E SIMPLE GEOMETRY JOINTS EASY TO INSPECT
- F MULTIPLE-PLY BONDED SPLICES ARE MORE DIFFICULT TO CHECK THAN LONGERON OR FRAME TO SKIN BONDS
- G NO METHODS FOR DETECTING CORRODED JOINTS NEED TO BE DETERMINED.
- H DETECTED BY X RAY COSTLY TIME CONSUMING ACCESS REQUIRED TO INTERNAL AND EXTERNAL SURFACES RADIATION HAZARD
- I LARGE AREA INSPECTION

TABLE 72

PABST IN-SERVICE ACCESSIBILITY - GENERAL ALL CONCEPTS

BONDED JOINTS	REMARKS
1. Internal inspections at upper fuselage.	1. Internal insulation panels must be removed and work stands must be set-up inside fuselage to reach joints. Ducting, control cables, and hydraulic lines will make inspection difficult.
2. Internal inspections floor and upper fuselage.	2. Internal insulation panels must be removed. Remainder of inspection fairly easy to perform.
3. Internal inspections below floor.	3. Difficult access thru crawl-way. Moisture, dirt, etc. must be cleaned up before inspection. Bildge paint reduces sensitivity of inspection.
4. External inspections at upper fuselage.	4. Dirt must be removed from test surface. Special docking facility with cat-walks and stands must be available to reach joints.
5. External inspections at mid fuselage.	5. Easy access. Dirt must be removed.
6. External inspections at lower fuselage.	6. Easy access. Grime must be removed from aircraft surface.
7. External inspections near wheel pod fairings and wing to fuselage fairings.	7. Access to external surface of fuselage appears to be limited in these areas. Needs further study.

are as follows:

(1) External longeron - without external aerodynamic fairings

(2) Internal longeron

(3) External longeron - with external aerodynamic fairings

(4) Honeycomb

and include consideration of the following:

(a) External longeron with external aerodynamic fairings will require removal of fairing to gain access for longeron bond inspection.

(b) External longeron without external aerodynamic fairing allows for easy access to longerons for bond inspection. Internal frames will require bond inspection from inside fuselage.

(c) Internal longeron concept will require inspections be performed from inside fuselage.

(d) Honeycomb will require bond inspections from external and internal surfaces. Splices and edge close out areas are more difficult to NDI than similar areas in metal-to-metal bond joints. Radiography required for determination of core damage, corrosion, or cracked skins due to dents.

In-Service Inspectability Concerns. - In-service inspection of bonded structure will become practical only if:

(1) Joint designs are inspectable,

(2) The number of joints requiring inspection are reduced to a minimum to reduce time and cost of inspection while meeting strength requirements,

(3) NDI methods are capable of reliably detecting service induced defects,

(4) NDI equipment is portable, light weight, easy to operate, repeatable in response, and reliable,

(5) Built-in defect reference standards, of typical joints, are available to NDI personnel for calibrating instruments,

(6) NDI personnel are adequately trained in bond inspection techniques,

(7) Acceptance criteria are established before inspections are conducted,

(8) Repair procedures are established and available to prevent long down time of an aircraft when defects are detected,

(9) NDI procedures and reference standards are established and available to evaluate the quality of the repairs,

(10) The effect of moisture or corrosion (in joint) on debond detection capability is determined, and

(11) The inspection of large wide body aircraft, which is difficult in the "Field" because of lack of access to interior surfaces, availability of work platforms, etc., can be accomplished at the "Depot" with the better equipment and increased personnel.

Selection of NDI Methods for In-Service Inspection. - The PABST ADP article will be fatigue tested during Phase IV. As part of this test, periodic NDI checks will be required on critical areas selected during Phase II and III, along with applicable NDI methods. Both the NDI methods and acceptance criteria will be available in written form for fabrication inspection, Phase III, and for periodic inspection of the ADP article, Phase IV. The manhour costs and ease or difficulty of NDI checks will be determined.

At the present time, the principle debond or fractured bondline detection methods are the Fokker, Harmonic, and 210 Bondtesters. The reports that separated joints filled with moisture may not be detectable by Fokker or 210 Bondtester is presently being investigated at Douglas. A bonded laminate, returned from service with partial corrosion separation at the bondline, has been obtained. The laminate will be evaluated by Fokker Bondtester, Harmonic Bondtester, 210 Bondtester, ultrasonic, X-ray and neutron radiography, and acoustic emission in the dry state. After all test results are recorded, a section of the panel will be placed in a humidity cabinet (to wet the separated areas) and tests repeated to see if moisture alters the test results or detection capability.

Generally, honeycomb assemblies are X-rayed to detect moisture intrusion and corroded core as illustrated in Figure 184. Recently, acoustic emission

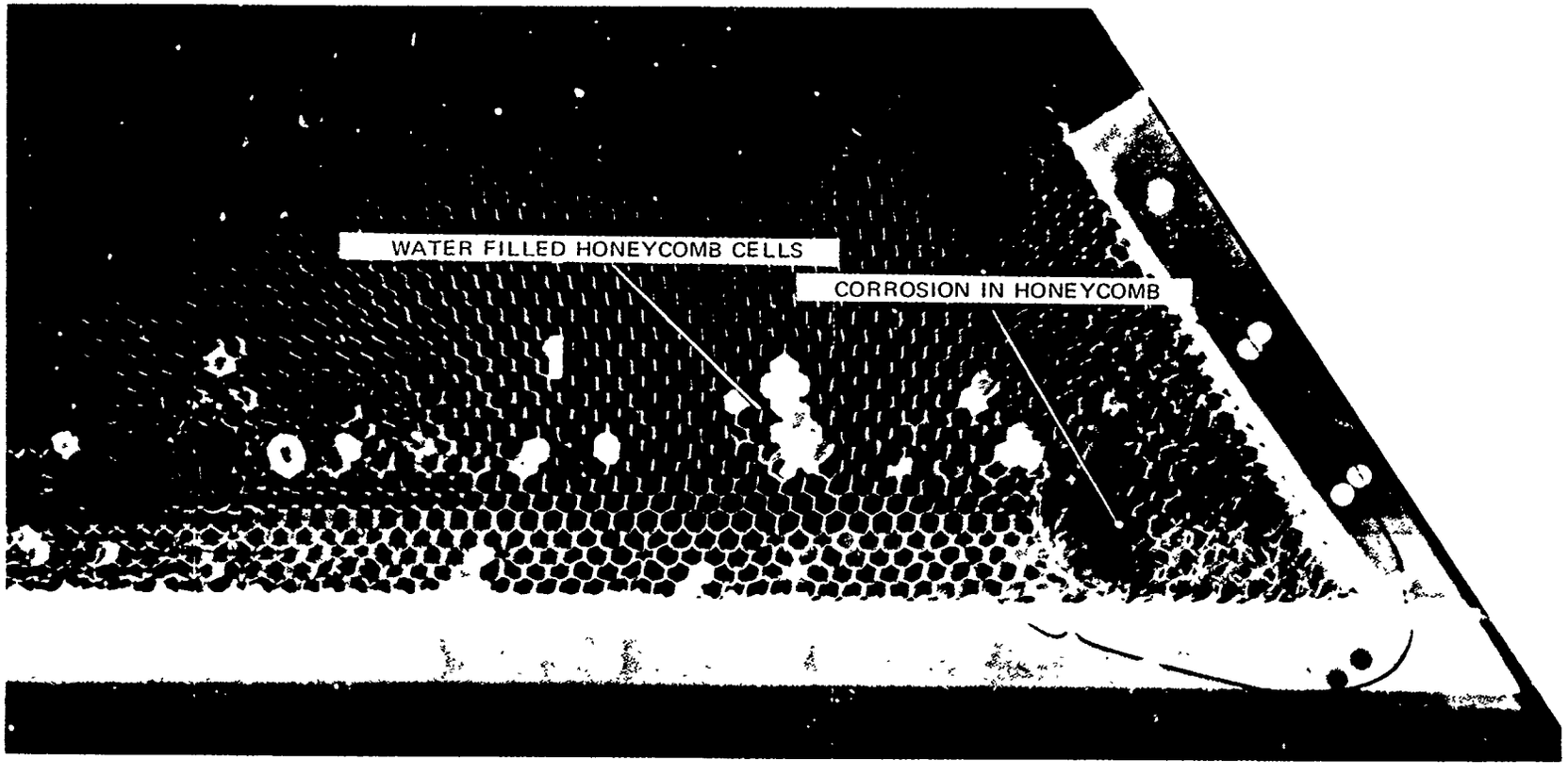


FIGURE 184. RADIOGRAPHIC (X-RAY) OF HONEYCOMB PANELS

has been investigated as a means of detecting moisture and/or corrosion in adhesive bonded laminates or honeycomb. Feasibility studies were conducted using a Dunegan acoustic emission monitor and heating the test specimen, see Figure 185. A corroded laminate (dry) was obtained. The search unit, 100-300 KHz, was placed on one side and the opposite side was scanned with a hot-air gun. At about 1 minute heating time, slight emissions were obtained, Figure 186A. The panel was then soaked in water for 30 minutes and the test repeated. A significant increase in counts was detected, Figure 186A. A new (uncorroded) dry honeycomb panel was obtained. The search unit, 100-300 KHz, was placed on one side of the panel while the opposite side was scanned with a hot-air gun. No acoustic emission response was obtained, Figure 186B. A hole was drilled into one face and into the core and water was added through the drill hole. The panel was retested and yielded a significant increase in acoustic emission response, Figure 186B. These feasibility studies are encouraging and further studies will be performed during Phase II.

NDI Limitations. - During the performance of the program, it was determined that no state-of-the-art NDI methods are available for the following measurements:

(1) Phosphoric acid anodize thickness (2000A),
(2) Adhesive primer thickness (0.1 to 0.3 mils) with accuracy,
(3) Adhesive thickness after bonding (3-12 mils),
(4) Adhesion quality after bonding,
(5) Cohesive bond strength for multilaminate bond joints, and
(6) Moisture intrusion into adhesive after laminate is bonded.

Significant NDI Accomplishments. -

(1) First good study of NDI for adhesive bonds made. Previous studies were cursory because parts were not primary structure.
(2) A thorough classification developed of defect types and major order of occurrence.
(3) First good evaluation of applications and limitations of state-of-the-art NDI methods.
(4) Industry (management) awareness obtained of need for NDI studies during a preliminary design phase.
(5) Unified body of knowledge obtained for NDI of adhesively bonded primary structure.

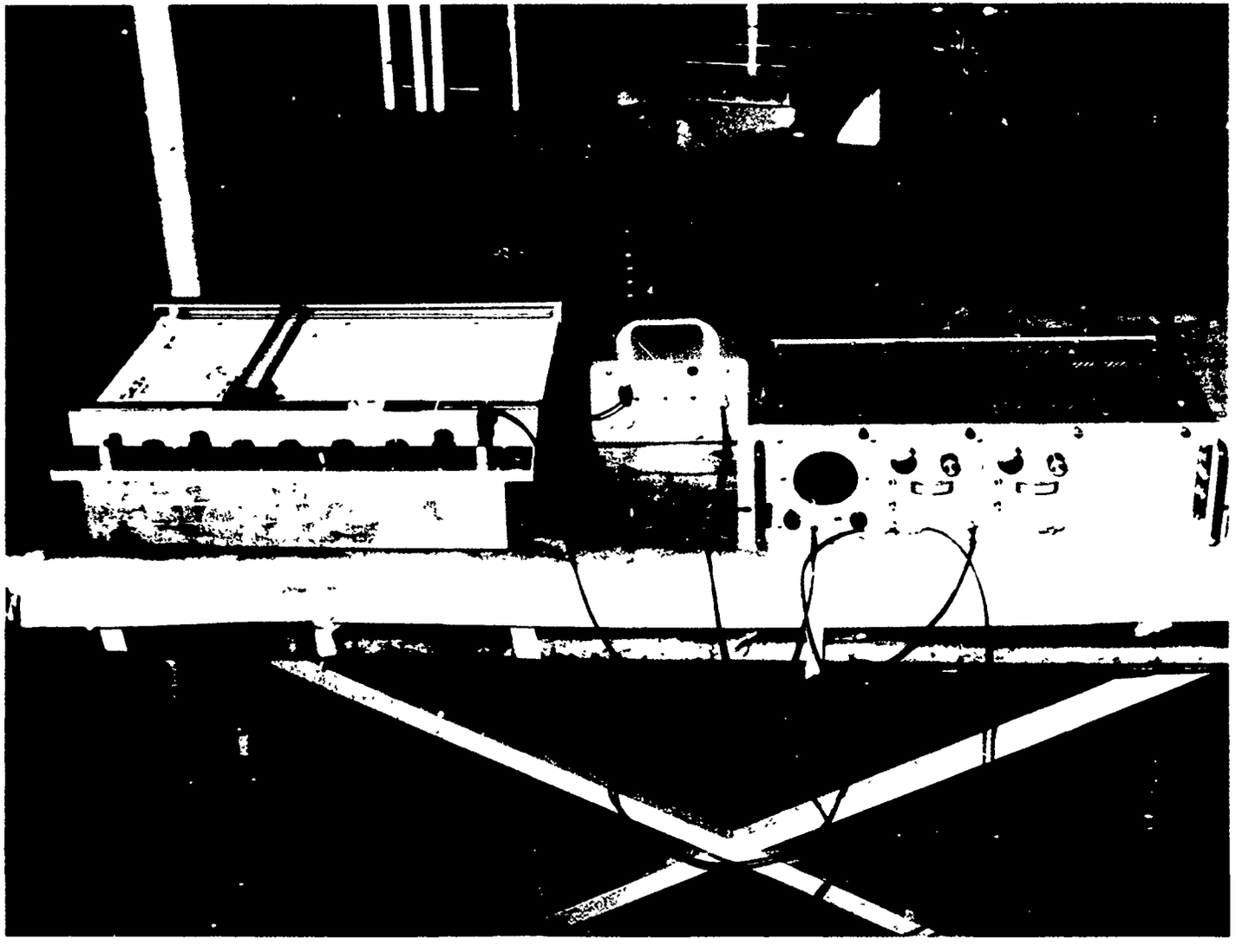
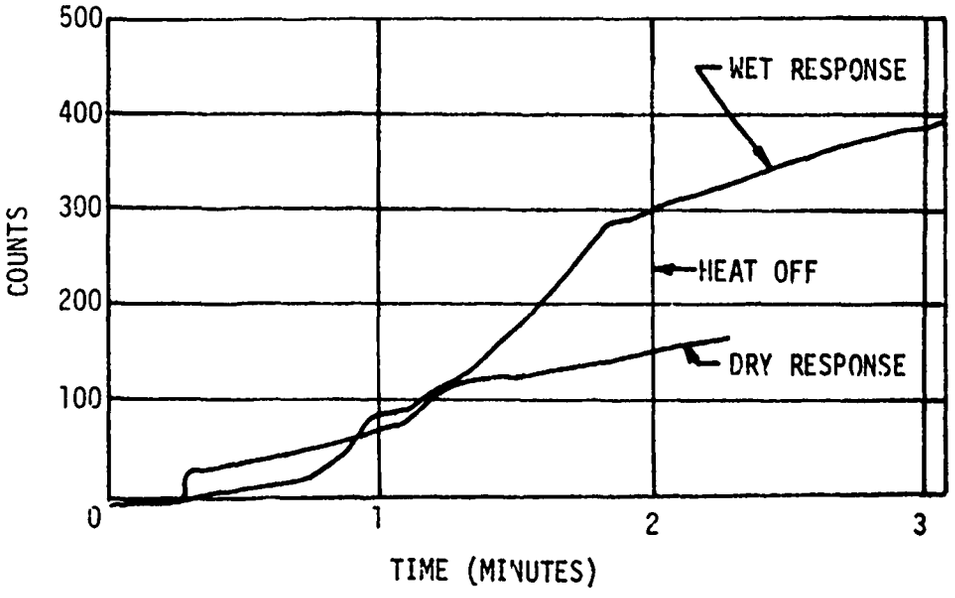
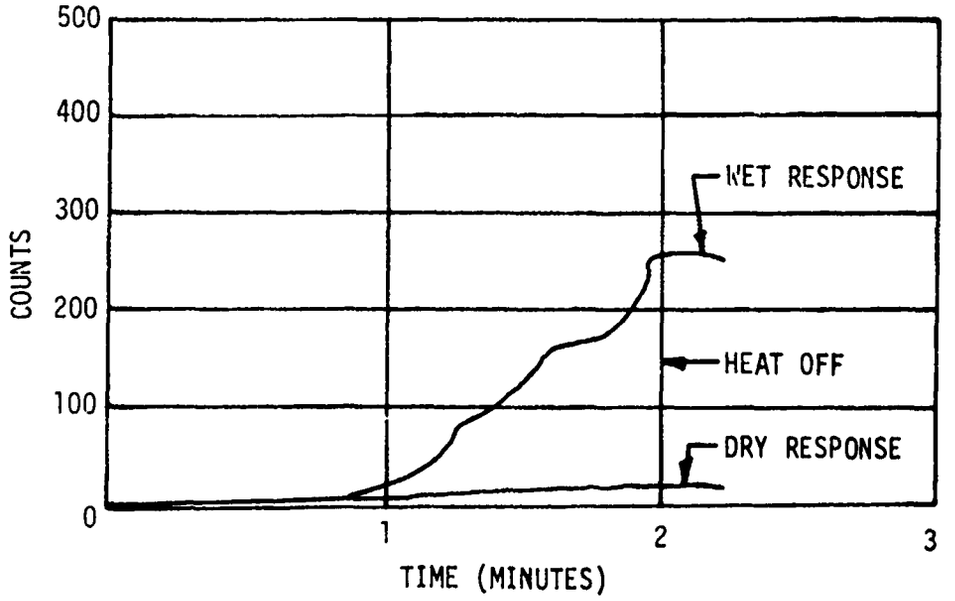


FIGURE 185. DUNEGAN ACOUSTIC EMISSION MONITOR



GAIN 95db
NO FILTER

A. CORRODED ADHESIVE BONDED LAMINATE



GAIN 95db

NO FILTER

B. UNCORRODED ADHESIVE BONDED HONEYCOMB

FIGURE 186. ACCOUSTIC EMISSION RESPONSE FROM HEATED ADHESIVE BONDED PARTS

MANUFACTURING

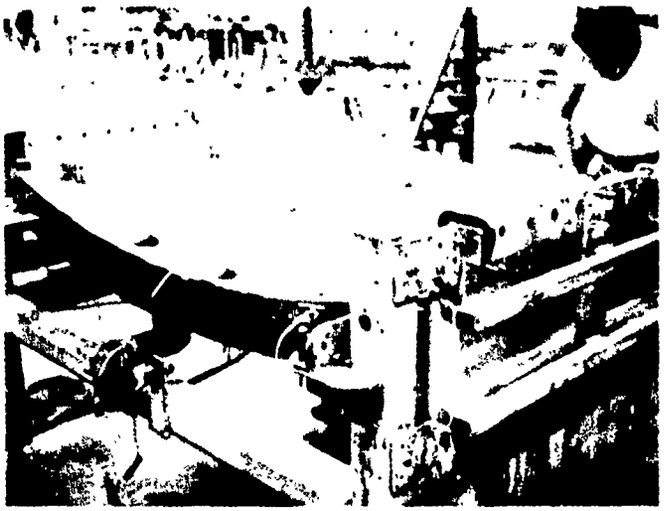
During Phase Ib, manufacturing bonding technology was increased through support of the development test program. Specimens were fabricated ranging in size from small coupons used for materials and process investigation to large panels, used for structural integrity testing. A total of 593 bonded test panels and 94 mechanical assemblies were fabricated during Phase Ib. Fabrication of these specimens aided in the development of the manufacturing capability toward a full scale component for the PABST program. This section describes the tools, prefit, verifilm, anodize, prime, and bonding methods used in Phase Ib.

Tooling.- Bonding fixtures were required to manufacture the large structural integrity test panels used to verify the concept capabilities to resist shear, axial, and pressure loads and to demonstrate damage tolerance. The fabricated test panels, shown in Figure 187 ranged in size from about 4 x 5 feet for the shear panels to 9 x 14 feet for the large curved pressure panels.

A constant section bonding tool was designed to accommodate any size or design concept bonded assembly that would be used for panel testing in Phase Ib or used in fabrication of the full scale demonstration component. (Figure 188) The 10 foot wide by 30 foot long bonding tool was made of a one piece 1/4 inch aluminum skin formed to a 108.25 inch radius and attached to a base structure. The base structure is an aluminum egg crate construction with large holes through the longitudinal and cross members. The holes permit the circulation of autoclave air around the bonding tool to ensure a fast heat up or cool down during the bonding cycle.

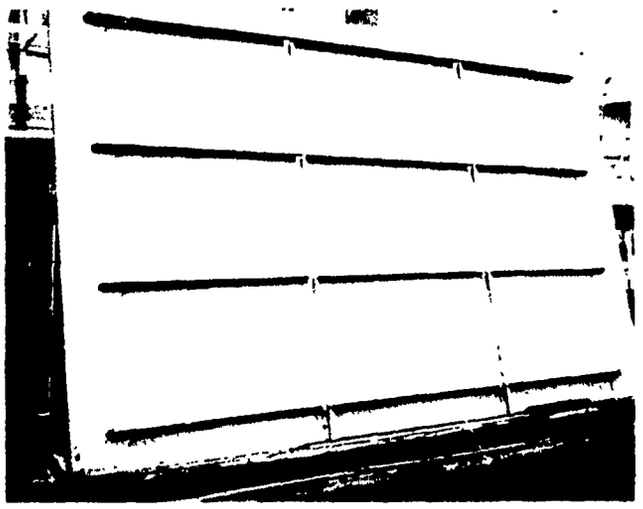
The face sheet is attached to the egg crate by means of studs, spot welded to the outer surface. The studs permit adjustment of the face sheet to the 108.25 radius.

Various thickness and taper doublers used on the large pressure panels required the use of a shim between panel and jig face plate. A rubber blanket was fabricated from multiple layers of uncured thermal conductive



(a) SHEAR AND AXIAL LOAD PANEL

(b) FLAT DAMAGE TOLERANCE PANEL



(c) CURVED FUSELAGE PRESSURE PANEL

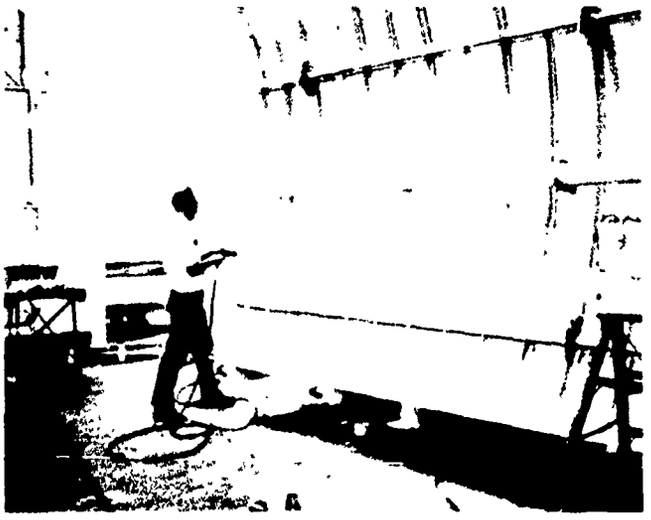


FIGURE 187. TYPICAL STRUCTURAL INTEGRITY PANELS

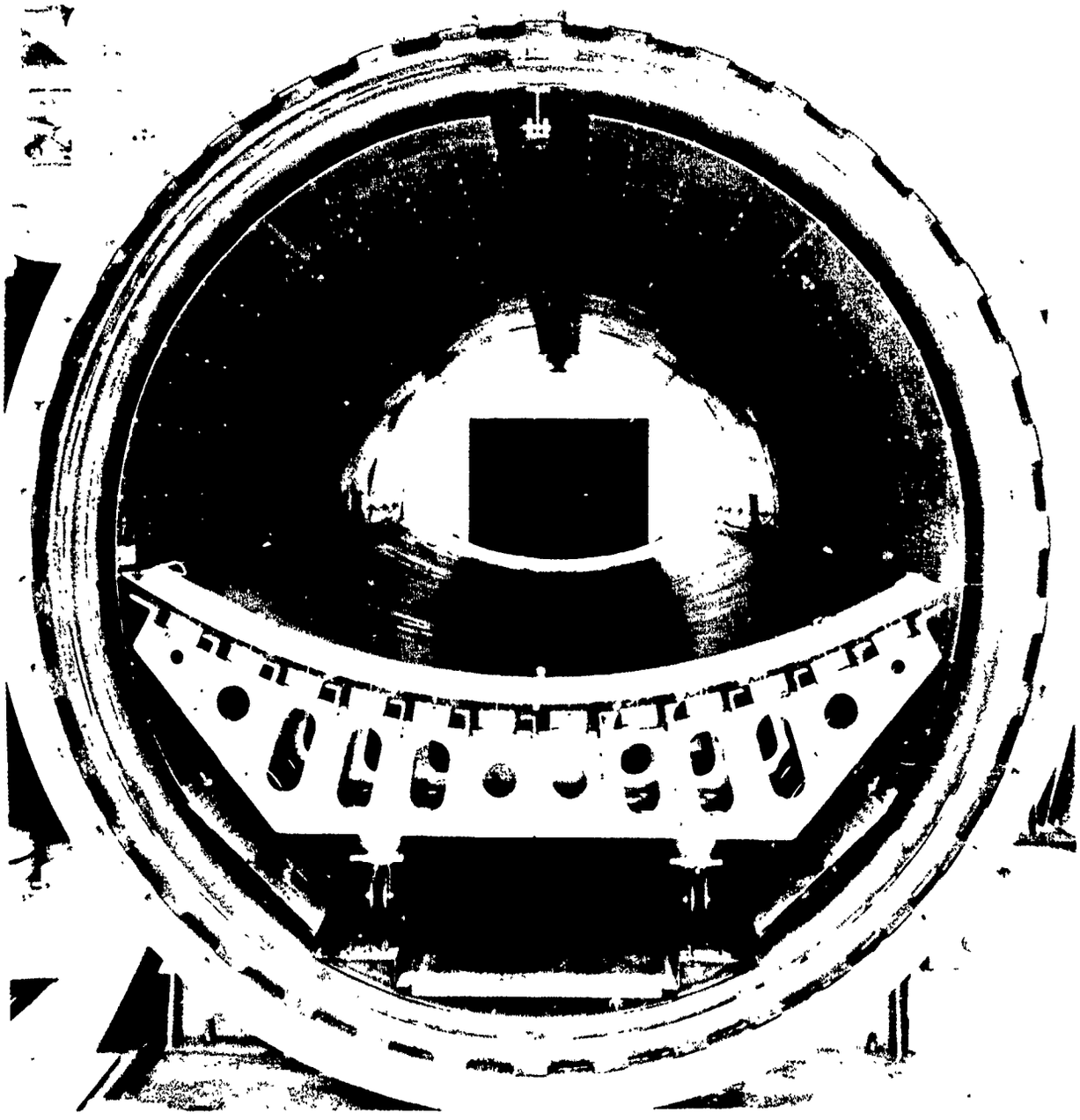


FIGURE 188. CURVED PANEL BONDING FIXTURE IN AUTOCLAVE

silicone rubber. The uncured rubber was placed on the face of the bonding tool with release film placed over the rubber to protect the metal details from coming in contact with the uncured rubber. The assembly was then placed on top of the rubber, bagged and placed in the autoclave. After cure the assembly was removed and the rubber blanket sent through a post-cure cycle.

External longerons required a modification to the existing female bonding tools. Honeycomb core 1-1/2 inches thick and slotted to receive the longeron was placed on surface of bond tool. A sheet of .020 aluminum, slotted to match the core was placed on top of the core. A buildup of thermal conductive silicone rubber approximately 3/16 inch thick was applied over the aluminum sheet. (Figure 189) The longerons were inserted into the slots and an .090 aluminum sheet placed over the entire surface. This assembly was vacuum bagged autoclave cured at 350° at 100 PSI for one hour. The rubber sheet was used to compensate for tapered surface of the longeron leg.

Since surface variances of the detail parts being bonded is a very critical problem, a rubber face bond tool was built to evaluate the ability of the tool to compensate for these minor surface variations. (Figure 190) A 4 x 5 foot, 1/2 inch-thick aluminum plate was rolled to 108.25 inch radius with aluminum studs welded to the back side and mounted to an aluminum egg crate structure to maintain the desired shape. A male plaster cast was constructed having the final desired contour of the bonding tool. The metal surface was cleaned and sprayed with a silicone primer. A layer of 1-mil release film was applied to the surface and held in place with teflon tape. The cast was lowered into the bonding tool and held off the surface with 3/8 inch thick aluminum blocks placed around the outer periphery of the tool. DACPO-50(RTV) was mixed and de-aired, and poured into the space between the plaster cast and the aluminum tool. The rubber was cured at room temperature for 24 hours and oven cured at 140°F for 2 hours. The plaster cast was removed after the 140°F cure and further cured for two hours at 250°F and followed with a post-cure at 350°F for two hours. The rubber face bond tool was used to bond several test assemblies in Phase Ib. The tool was evaluated

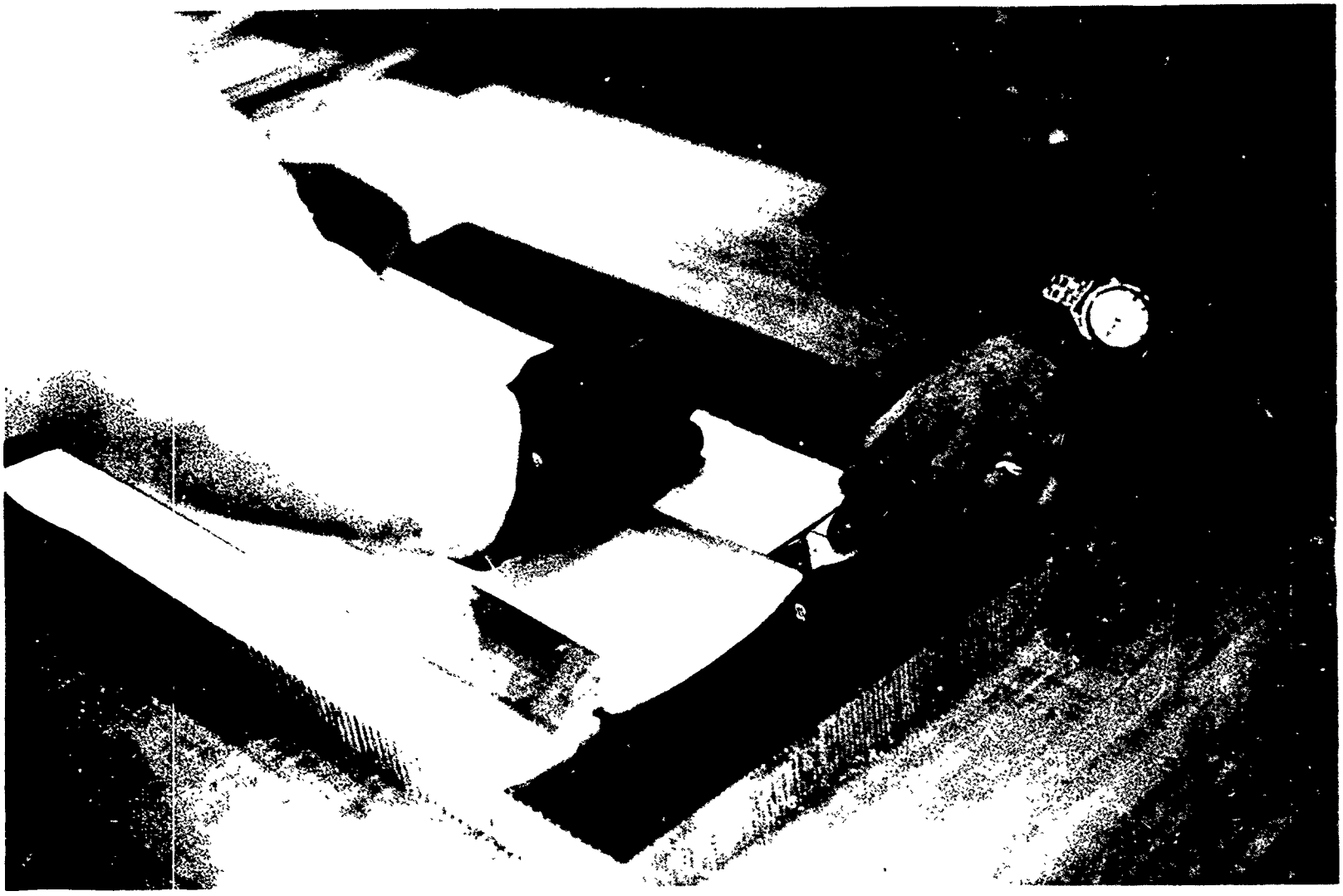


FIGURE 189 MODIFIED BOND TOOL FOR EXTERNAL LONGERONS

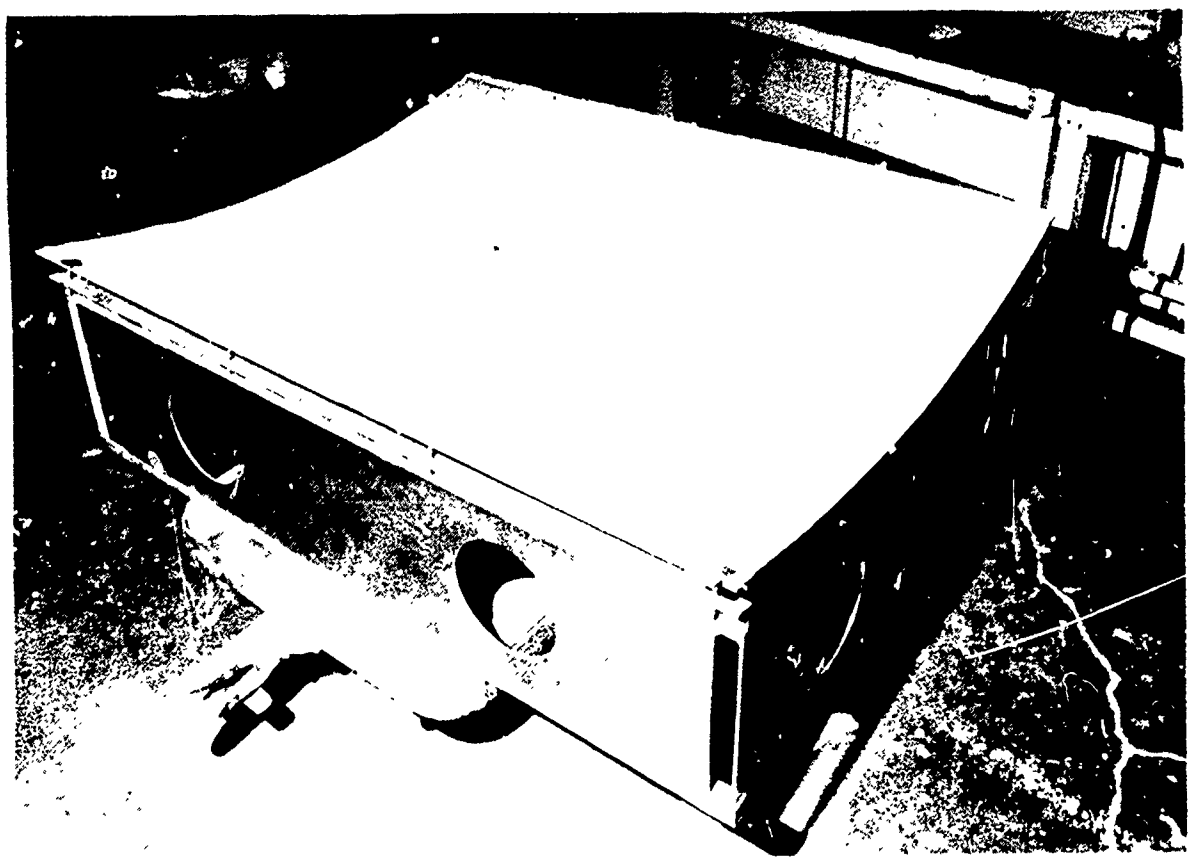


FIGURE 190. RUBBER-FACED BONDING TOOL

for compression properties and thermal conductivity. The tool demonstrated it had sufficient flexibility for parts being bonded with surface variances of not more than 0.020 inch. After several cure cycles the rubber surface took on a permanent waviness. Small detail specimens were also made with a different type of RTV rubber to evaluate the heat transfer and waviness associated with rubber thickness. See Figure 191.

The bonding tool for the non constant section was similar to the design of constant section tool. The face sheet, sourced from large plaster shape, was an autoclave cured epoxy laminate. 1/4 aluminum plates were laminated into the face laminate sheet to receive the stud welded bolts for attachment to the base structure.

The detail part fabrication tooling used for Phase Ib was minimal. The forming tools were fabricated using sheet plywood. The use of plywood caused hard and soft spots in the forming surfaces with these spots creating irregularities in the bonding surfaces of the detail parts. The surface irregularities exceeded the established $\pm$ 0.005 tolerances. This condition has been corrected through the use of masonite, a harder and more durable material for the fabrication of forming tools.

Prefit and Verifilm.- Detail parts for all assemblies were prefit and held to a tolerance of 0.005 inch or less using light finger pressure (approximately 5 psi). When tack rivets were used for locating the detail parts, the rivet hole was made larger than the rivet diameter so that the details would float and seat themselves under pressure and temperature. In order to ensure proper fit, a verifilm operation was used prior to any processing or bonding to prove if the assembly was qualified for bonding. To perform a verifilm test, a complete panel was assembled. Verifilm was placed on all faying surfaces instead of the adhesive, Figure 192. The panel was processed through the autoclave in the same manner as a bonded assembly, except the cure cycle was changed from 90 minutes at temperature to 20 minutes at temperature. It was discovered that verifilm was of little value on flat panels since discrepancies could be visually checked during prefit. Verifilm discrepancies (excessive thickness)are noted on Failure and Rejection Reports.

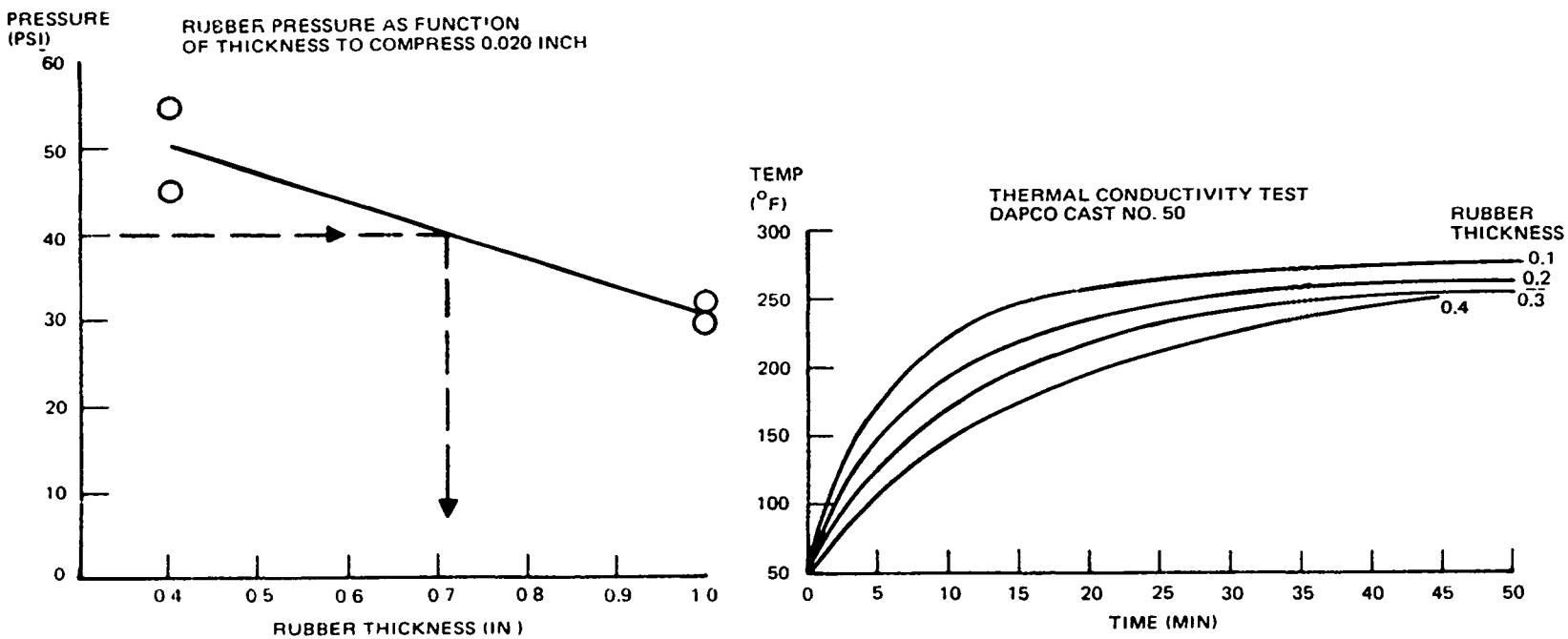


FIGURE 191. DAPCO CAST NO. 50 EVALUATION

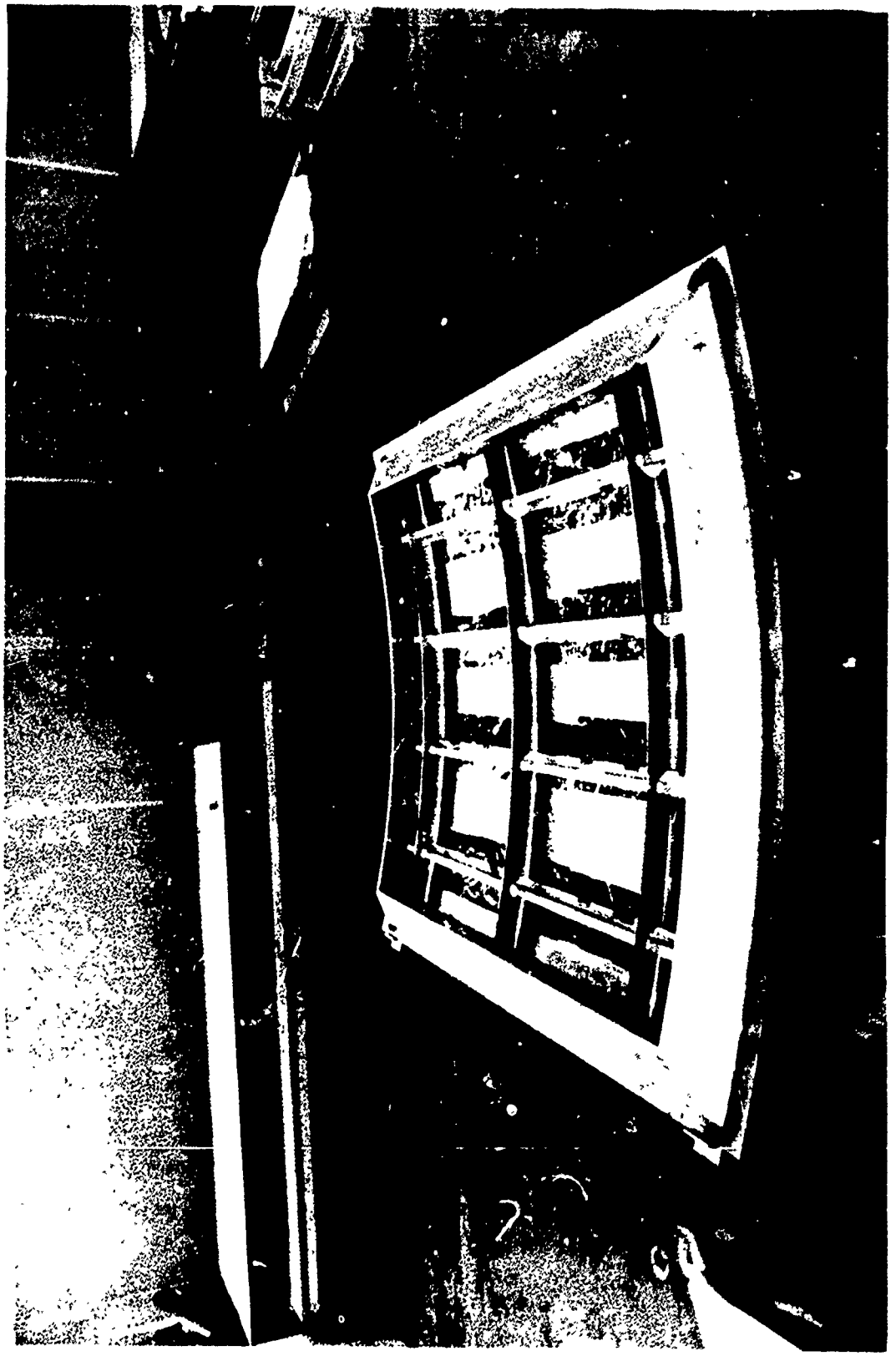


FIGURE 192. SHEAR PANEL ASSEMBLED WITH VERIFILM

Anodize and Prime. - This operation is shown schematically in Figure 193. Parts were received from the metal bond staging area and installed on a picture frame fixture. This fixture, with installed parts, was processed in the anodize tank and then removed to an area where all parts were inspected for anodize and then primed and oven cured. Following this operation parts were inspected and if acceptable, dismantled from the picture frame, protective wrapped, and shipped back to the metal bond area.

Fixture: - A picture frame fixture was fabricated specifically for the PABST program. This frame was adjustable to the different detail part sizes and shapes. The parts were held in the fixture, as shown in Figure 194, with titanium coil springs and titanium spring clips. The spring clips,shown in Figure 195, were "C" shaped with a "V" shaped bend on each end in order to expedite the racking and unracking of the detailed parts of various sizes and shapes. Three different sizes of spring clips were designed and fabricated. With this system, the proper tension could be maintained on the strings of detail parts. The string tension was checked just prior to processing and clips were added as required to produce the desired tension. These springs proved to be successful in providing electrical continuity in the anodizing tank with the picture frame fixture. They saved approximately 65 percent in racking time before anodizing and 75 percent in unracking time after anodizing over the old system that utilized aluminum wire for tying the parts together. No electrical contact was lost while using Ti springs but was lost with the aluminum wire. One wedge crack plate is placed in each electrical path.

Anodize: - The anodize sequence is shown in Figure 196. Out of the 12 tanks located as shown, only eight were used for the PABST program. Seven of these tanks were used for various wash and rinse cycles. The eighth tank (number 537), shown in Figure 197 is a chromic acid anodize tank converted into a phosphoric acid anodize tank by lining the existing tank with 0.50 inch thick, eight percent antimony, lead plate. A PVC liner was mounted over the lead lining to prevent accidental arcing from occurring if a detail part came in contact with the space leadlining.

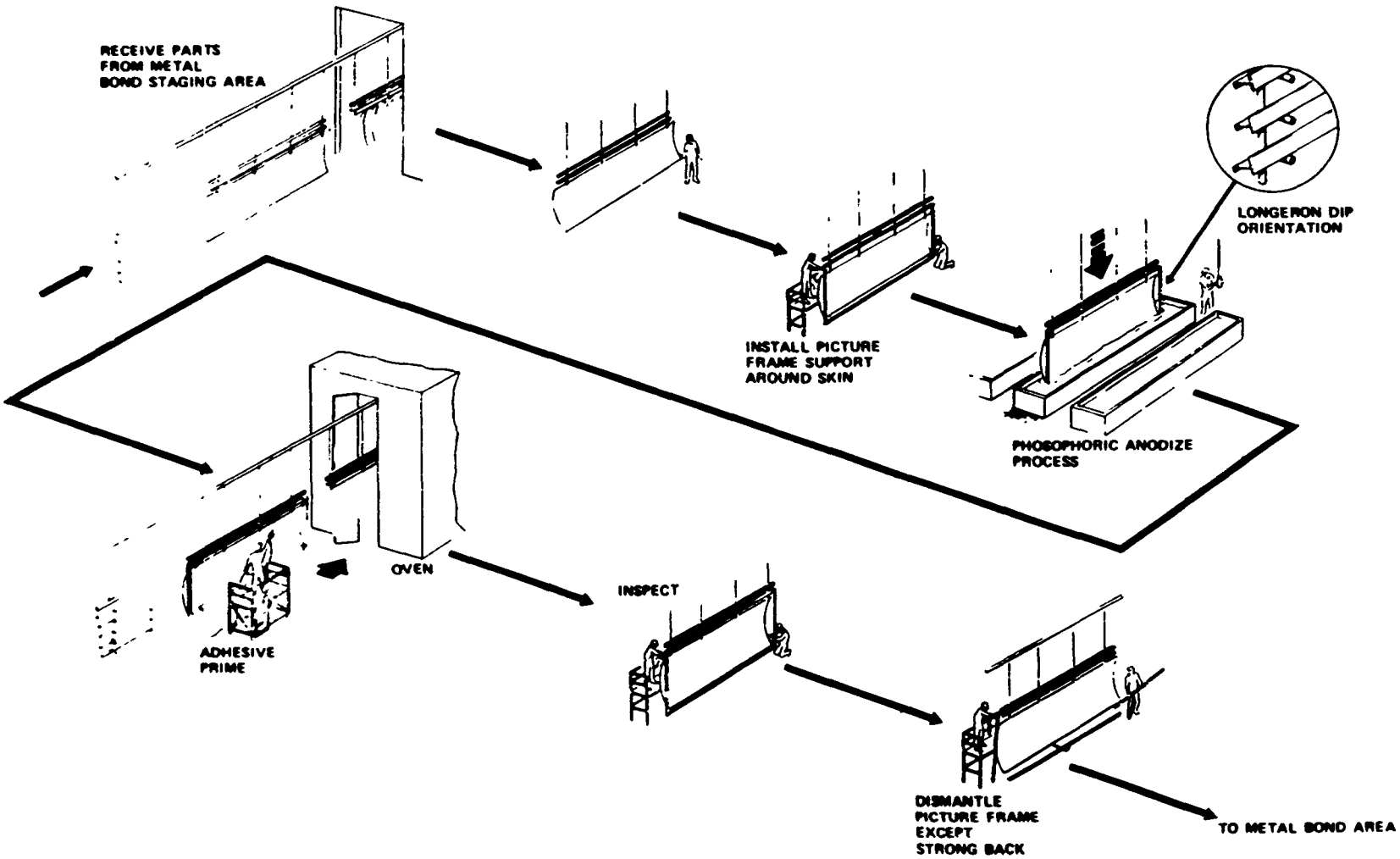


FIGURE 193. SCHEMATIC OF PHOSPHORIC ANODIZE AND ADHESIVE PRIME OPERATION



FIGURE 194. PICTURE-FRAME FIXTURE USED FOR ANODIZING DETAIL PARTS

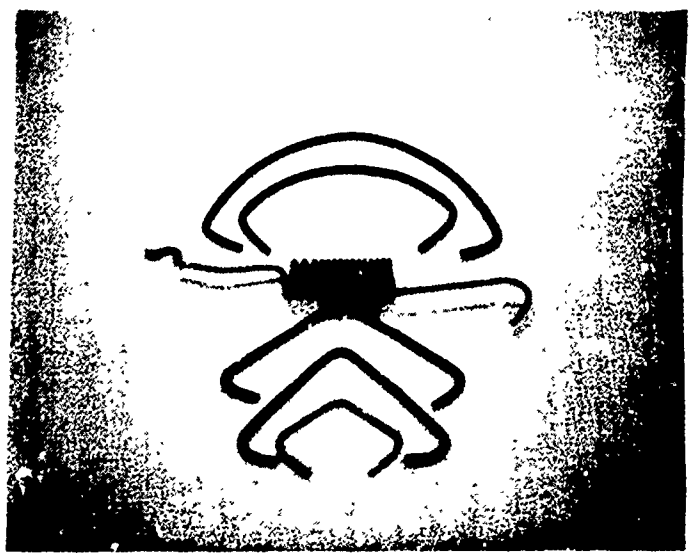


FIGURE 195. TITANIUM SPRINGS AND CLIPS

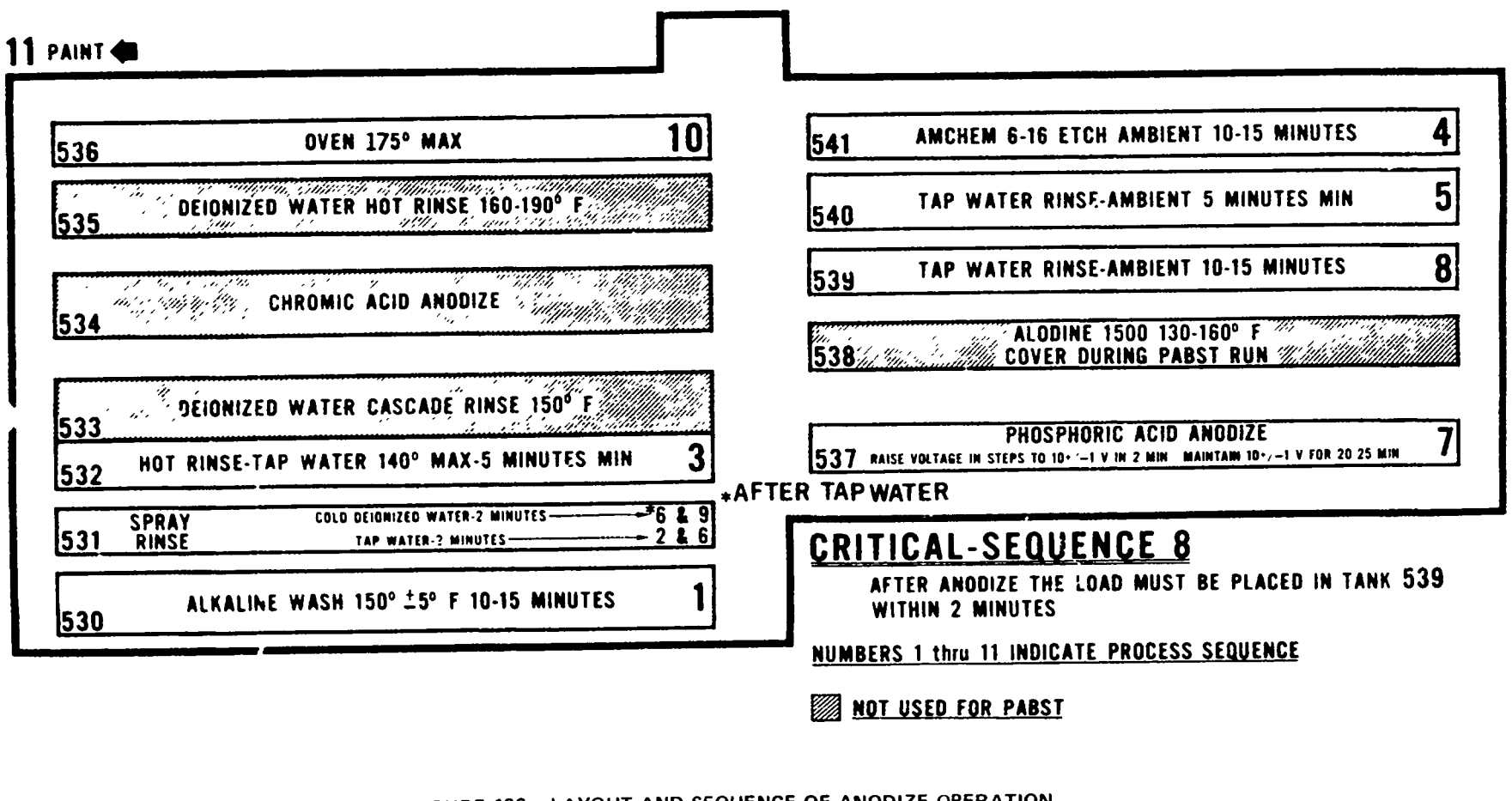


FIGURE 196. LAYOUT AND SEQUENCE OF ANODIZE OPERATION

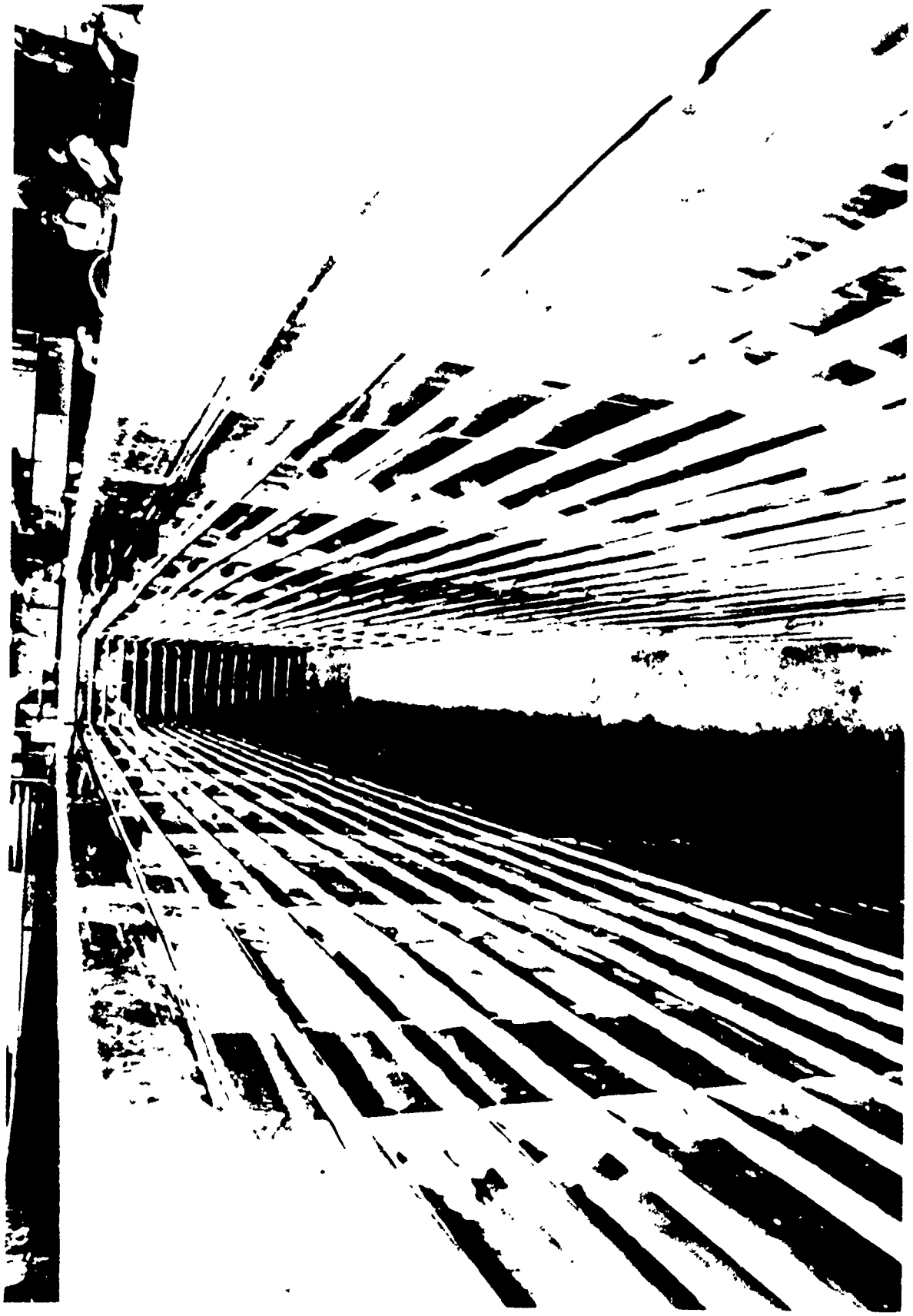


FIGURE 197. ANODIZE TANK

After a period of time (use plus non use), the phosphoric acid anodize solution became contaminated. The anodize solution was found to contain an aerobic mold similar to "mother" as found in vinegar. A filtration system was installed to filter aerobic mold and other contaminants, such as lead phosphates from the tank. The new filtering system was designed to handle 10,000 gallons per hour in order to ensure total filtration. This sytem was installed by first draining and cleaning the tank. While the tank was empty, an additional fluid return line was added to the filtration system. Fluid piping was run full length along the bottom of the tank to provide agitation and circulation of the solution during anodize. Air agitation lines were cleaned and fitted with one way air valves to prevent siphoning of the solution into the air filter. The tank was refilled and recertified.

A system was devised for adding wedge crack coupons to every string of details racked for anodizing. A log, in numerical sequence, is kept for every wedge crack coupon. In addition, the fabrication outline contains a sheet showing the exact position of each detail and coupon in each string of parts and the wedge crack number entered on the fabrication outline. In the event parts are defective and reprocessed,the assembly will retain the original wedge crack numbers.

Prime: - Different methods of applying primer were studied to ensure the proper primer thickness. Primer is presently being applied with a conventional spray gun which must be agitated. Some of the methods studied were automation and the airless spray system. The automation method was ruled out because of the many design concept configurations. Most of the details cannot be racked in the exact attitude and held rigid for automatic spraying. Manual application with conventional spray equipment during Phase Ib was a short term solution. A recirculating spray system will be incorporated for use in Phase II and III.

Several non-destructive techniques were evaluated for measuring film thickness on aluminum substrate. Test specimens were prepared with phosphoric acid anodize and different film thickness ranging from 0.045 mils to 0.32 mils. The film thickness was calculated from the change in weight before and after the adhesive primer was applied. Subsequently, the results were compared using the isometer, an eddy current measuring instrument, the C-Gage, a capacitance measuring instrument, and the betascope making use of beta ray back scattering. Using calculated values as a basis of comparison, it was concluded that for film thickness range considered, the isometer and the C-Gage are somewhat more accurate than the betascope, especially for thin films. The isometer and the C-Gage are more or less comparable in accuracy, however, none of the instruments are accurate enough for film thicknesses less than the 0.1 mils required for production inspection of PABST panels. Further evaluations will be conducted regarding noted instruments for measuring thin coatings.

Bonding. - After the detail parts were anodized and primed, they were shipped to the metal bond area. The bonding operation is schematically shown in Figure 198 for a curved skin panel.The skins were assembled in the bonding tool. Details were reassembled with the adhesive. Separator films, bleeder cloth, flash breaker tape, thermocouple, and vacuum bag were installed The bonding tool and assembled panel were loaded in the autoclave where the bonding took place under temperature and pressure. After bonding, the bonding tool and bonded panel were removed from the autoclave. The bonded panel was inspected and then shipped to the assembly area for further mechanical work.

A typical bonding setup for the internal longeron concept is shown in Figure 199. After prefit, phosphoric acid anodize and prime, the detail parts were assembled, with the adhesive, on the bonding fixture. A layer of release film (E-3760) was placed over the assembled part and tool, followed by a silicone rubber blanket and a layer of bleeder fabric. Aluminum 0.250 inch diameter hollow spheres were used to fill in the areas between frames, longeron and shear tees. The aluminum spheres covered the assembly approximately two inches over the highest point of the assembly. Two layers of

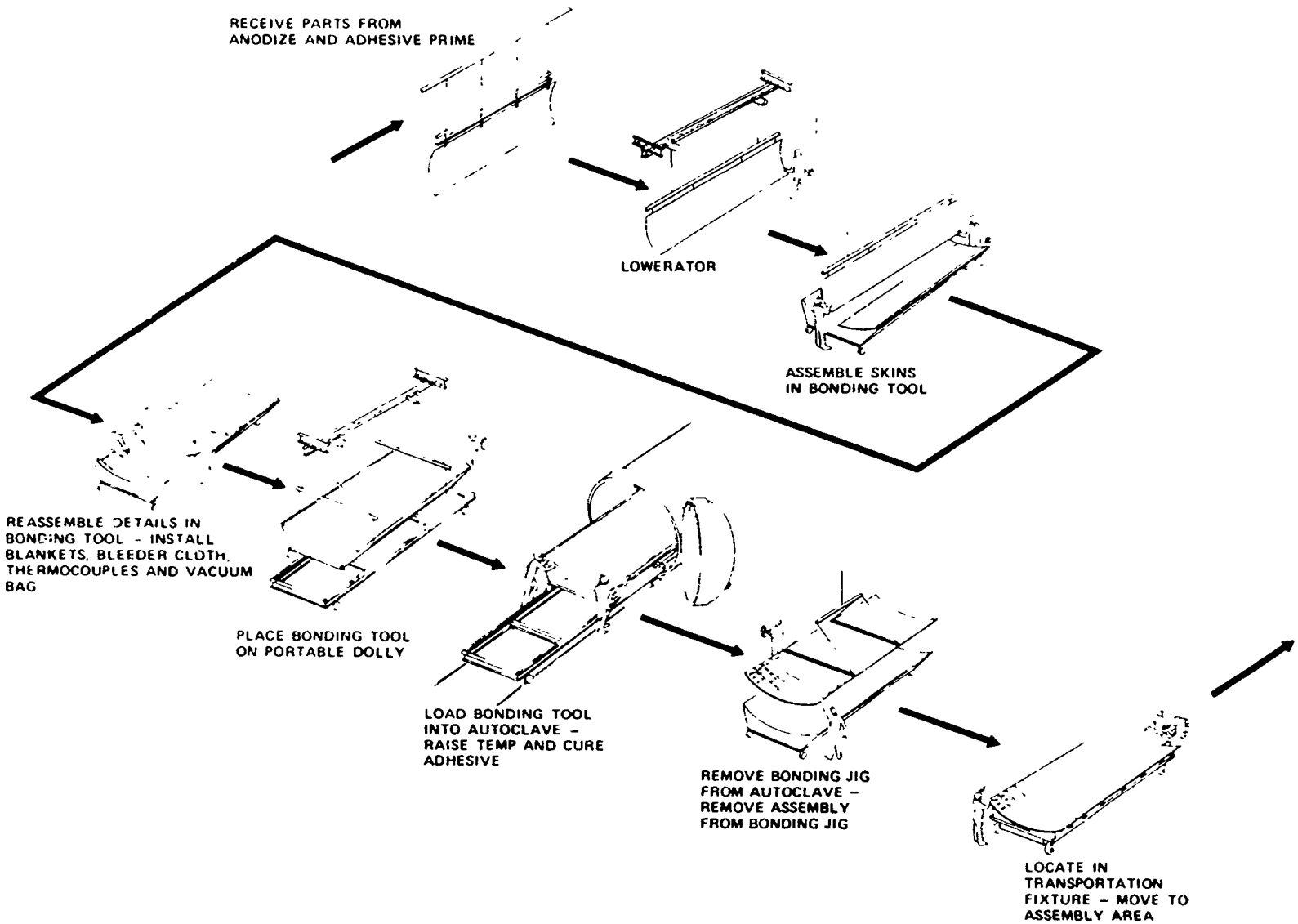


FIGURE 198. SCHEMATIC OF METAL BOND OPERATION

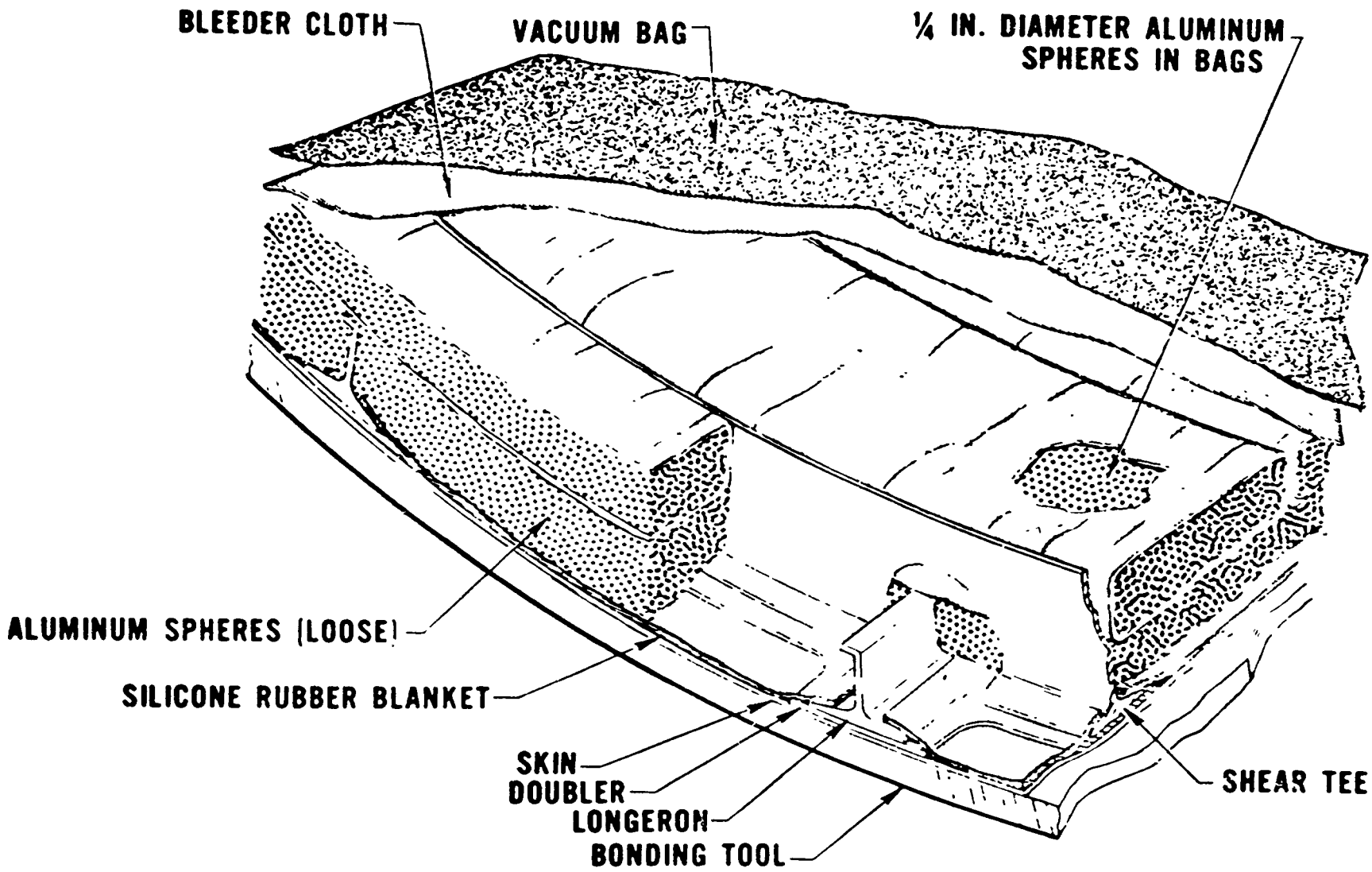


FIGURE 199. TYPICAL BONDING SETUP FOR INTERNAL LONGERON CONCEPT

bleeder fabric were ther placed over the spheres. A vacuum bag was installed and sealed. A vacuum was applied slowly to spread the spheres evenly over the assembly, and checked for leaks. The spheres acted similar to a fluid by applying pressure to the faying surface and holding the details in their proper location. The entire assembly and fixture were placed in the autoclave. After the assembly was cured the aluminum spheres were removed along with the vacuum system.

Excessive adhesive expulsion initially was a major problem since the expulsion interferes with ultrasonic inspection of the assembly. The high flow adhesive system, particularly FM-73, flows readily at 250°F under a pressure of 40 PSI. To better control this adhesive flash for inspection several methods were tried. Mylar tape was applied approximately 1/8 inch from the edges of the details being bonded and also on the detail flanges. During the cure the adhesive flash would migrate under and over the tape. The tape, being only one mil thick, was difficult to remove. Plastic scrapers were used to remove adhesive flash that flowed over this tape. Other methods were tried, such as Teflon Tape and Peel Ply Fabrics. The method developed for PABST was the use of flash breaker # "5" tape. The tape is applied along the faying edge of the assemblies so adhesive has to flow over it, preventing adhesive from bonding to the panel. Next, a layer of perforated armalon cloth is placed between the panel and fiberglass bleeder cloth allowing the bleeder cloth to absorb the excess resin without bonding to the panel. The flashing tape was peeled off the assembly at end of bond cycle. This method reduced cleanup time to a minimum.

Vacuum leak problems were located by using air tech leak detector bleeder fabric. This bleeder fabric is the last layer bleeder to be applied under the vacuum bag. The assembly was pulled down under vacuum and vacuum check performed. The vacuum should not drop over two inches of mercury in five minutes. If this condition occurred, it would be checked by spraying air tech leak detector fluid around the vacuum sealing compound and vacuum valve. The discrepant area would show up immediately by turning the bleeder fabric to a bright red in color. This system was also used

for checking vacuum leaks in high temperature epoxy tooling.

Several vacuum sealing compounds were evaluated to determine which compound held up the best during the cure cycle. Early leak problems occurred during the cure cycle where the compound would become soft or bubbly and peel away from the bond tool. General sealant GS-43 MR was finally selected. At room temperature, this sealant was hard to seal but would not pull away from the bond tool or vacuum bag. After cure, it could be removed from the tool with ease and no cleanup was required.

QUALITY ASSURANCE

This section deliniates the manner in which Quality Assurance is integrated into the design, manufacturing and test cycle. The goal of total quality involvement is to improve the integrity and durability of primary fuselage structure through adhesive bonding in a production environment.

Quality Assurance Plan. - This Quality Assurance plan in Figure 200 encompassed the elements of (1) Engineering & Release, (2) Procurement, (3) Manufacturing, Planning, (4) Tooling, (5) Fabrication, (6) Receiving Inspection, and (7) Engineering test. The Engineering designs were reviewed, verifying that the quality requirements were included and that NDI (Non-Destructive Inspection) would be effectively applied. All Procurement orders were placed with approved DAC supplier sources. The purchase orders were reviewed and quality clauses and inspection characteristics added. Fabrication outlines are reviewed to determine and indicate in the required inspection characteristics. Tooling used to build the test articles are inspected and "bought off" to tool drawing requirements.

The fabricated test articles were inspected with acceptance indicated by a stamp on the test article and the accompanying Fabrication and/or Assembly Outlines.

Materials being received are inspected to determine if they have been tested and meet DAC requirements. The materials are tested to the Quality clauses and characteristics that had been previously added to the Procurement order.

The test articles are checked to the work instructions with pre and post evaluation of the completed test.

Fabrication Inspection. - Ten primary inspection stations were provided within Fabrication as shown in Figure 201 to assure product conformity. The detail parts were inspected to the drawing requirements. The detail parts used for a specific assembly were reviewed to verify that all details were available. The detail parts are assembled (pre-fit) to assure proper fit-up of the

PRECEDING PAGE BLANK-NOT FILMED

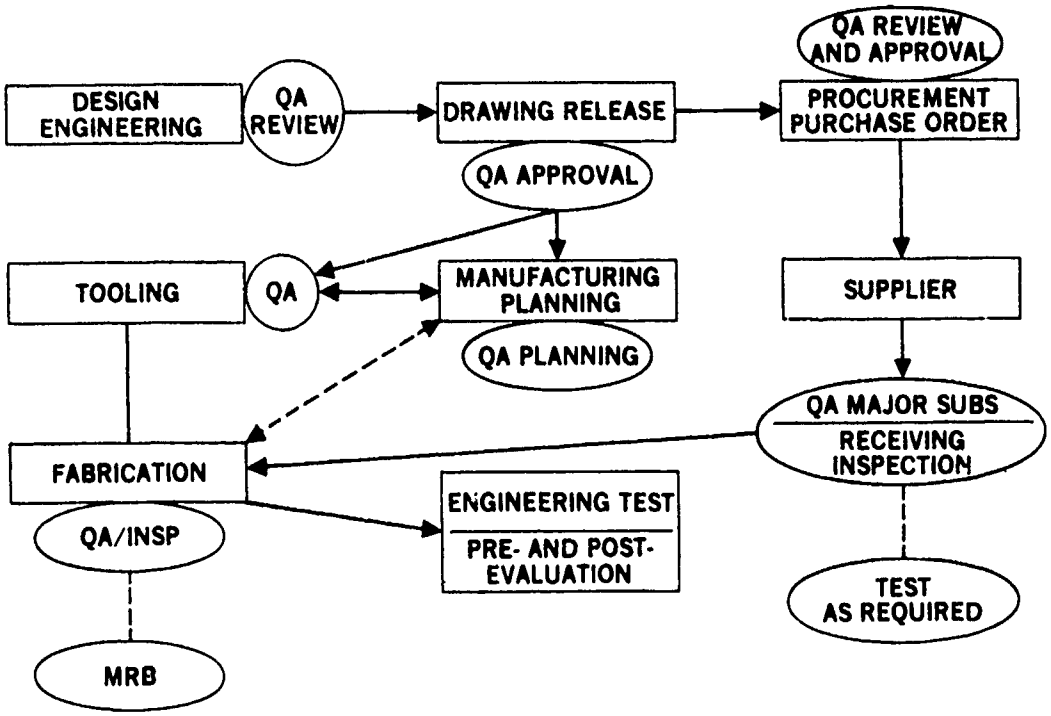


FIGURE 200. FLOW CHART FOR OVERALL QUALITY ASSURANCE PLAN

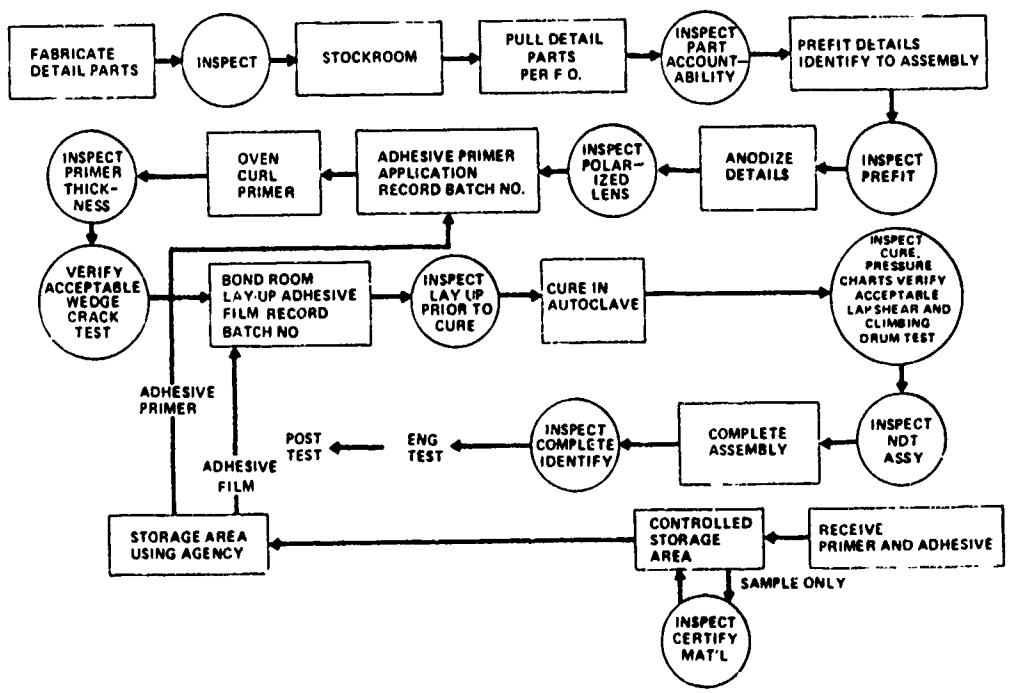


FIGURE 201. FLOW CHART FOR FABRICATION QUALITY ASSURANCE PLAN

details. The pre-fit was inspected and acceptance verified by "buy-off" on the fabrication outline. The details used during this operation were marked with a vibratory pen to maintain identity through anodize and bond. Verifilm as required was performed.

Anodize and Prime Inspection. - Inspection of the anodized surface was accomplished by use of the polarizing filter. The angle of the polarizing lens to the surface of the part to be tested was maintained at 0-10°. The detail surface was observed for the appearance of "interference" colors. While viewing the surface the filter was rotated 90°. An acceptable anodic coating is verified by an observed change to the "complimentary" color (e.g., purple to a yellow green).

The adhesive primer was applied (0.0001-0.0003 inch thickness), oven cured, and the primer thickness verified. The primer had been previously certified as acceptable by DAC. A minimum of five specimens were exposed for one hour at 140°F and 95-100% relative humidity. Authority to continue fabrication was given when acceptable wedge crack specimens met quality requirements.

Assembly Inspection. - The primed details were assembled using adhesive film that had been previously certified by DAC. Acceptance of the "lay up" was indicated on the Fabrication Outline. The assembly was cured with cure and pressure recordings inspected. Lap shear and climbing drum specimens were bonded with the assembly and tested. The assembly was NDI (Non-Destructive Inspection) and acceptance indicated on the Fabrication Outline. The assembly was completed by attaching mechanical hardware as required for test. The complete assembly was then inspected and acceptance verified on the Fabrication Outline and the assembly.

Control Tests and Recorder. - The status of the control tests conducted during this phase are shown in Figure 202. The wedge crack specimens are used to demonstrate the acceptability of the adhesive primers and surface preparation. The climbing drum and lap shear specimens are tested to demonstrate the acceptability of the adhesive film,cure cycle, and pressure cycle.

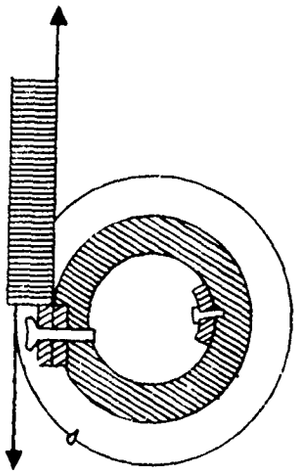
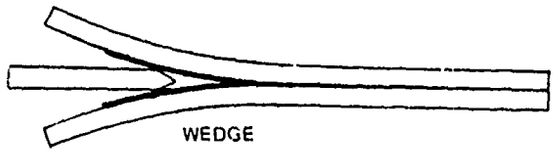
TEST	TEMP	NUMBER SPECIMENS	FAILURE	REJECTION
 CLIMBING DRUM	RT	35	0	0
 LAP SHEAR	RT	667	47	18
 WEDGE	RT	1023	31	14

FIGURE 202. CONTROL TESTS

Aluminum alloys 7049 and 7475, and all structural adhesive primers and adhesive films used during this phase were traceable by lot and/or batch number provided by the supplier to its end use on the assembly. The traceable identifier was recorded in the Fabrication Outline.

PABST non-conforming products are identified and controlled to ensure correction or disposition. Items which can be completed to comply with design and specification requirements are identified and returned for completion. All non-conformances are recorded per FRR. These failure and rejection reports document the reason for the rejection with disposition instructions. The FRR's were used to qualitatively, rather than quantitatively, isolate and identify the problem areas for corrective action. Problem areas identified and solutions are shown in Figure 203.

Contamination Studies. - Production load test failures of two sets of anodized wedge crack test specimens initiated an investigation of materials commonly used in handling metal bond details. Adhesive failure was observed for the first time on phosphoric acid anodized parts. Since these parts were removed from the racks before priming, contamination was suspected.

Abrasion-Compression. - The effect of abrasion and compression, created by drawing a glass rod across aluminum foil over a phosphoric anodized surface, was investigated by Scanning Electron Microscope (SEM). The test was devised to cause compression damage of phosphoric acid anodize to segregate physical damage from the effects of contamination which may incur some physical damage.

Contamination Test. - A program was conducted to determine the effects of the same types of contamination on panels treated with (1) FPL etch and (2) potassium dichromate sealed chromic acid anodize and (3) phosphoric acid anodize. Uncontaminated panels and panels damaged by a hard plastic roller over aluminum foil were made into control specimens. Others were contaminated by white cotton gloves, clean kraft paper, or bare hands. The wedge crack test specimens used were 0.125- by 6-inch plates of 7075-T6 nonclad aluminum. The panels were surface treated, contaminated by lightly rubbing

PROBLEM	SOLUTION
• LAP SHEAR FAILURES ATTRIBUTED TO TAPERED GLUE-LINES	TOOLS FABRICATED TO CONTROL GLUE-LINE
• CONTROL OF PRIMER APPLICATION	PRODUCTION TRAINED AND QUALIFIED BY M&PE
• VERIFICATION OF ADHESIVE PRIMER THICKNESS	PERFORMED IN M&PE LABORATORY ON WEDGE CRACK SPECIMENS
• GLUE-LINE THICKNESS REQUIRED BY ENGINEERING DRAWING NOT CONTROLLED	SHIM PANELS AND USE HEAVY CAUL PLATES DURING BOND
• ADHESIVE PRIMER FAILURE TO SUBSTRATE	ADD WEDGE CRACK SPECIMENS TO EACH CHAIN OF PARTS
• EXCESSIVE FLASH HINDERS NDI AND ASSEMBLY	CONTROLLED WITH FLASHING TAPE
• MEK REMOVES ADHESIVE PRIMER	INVESTIGATION

FIGURE 203. DISPOSITION OF MAJOR QA PROBLEMS AND SOLUTIONS

the bonded surface of the No. 1 panel with the specified contaminates, except for the uncontaminated and the aluminum foil compression specimens. These panels were primed within 2 hours with American Cyanamid BR127, air dried for 30 minutes, and then baked for 1 hour at 250°F. All the panels were bonded using NARMCO M1133 adhesive and cured for 90 minutes at 245°F and 40 psi. SEM micrographs of the surface before priming and after failure were taken to characterize the physical appearance of the surface due to contamination. Auger spectras and the carbon depth profiles of the surfaces were taken.

Results showed the following: (1) There were no wedge crack failures in the phosphori - or the sealed chromic acid anodized surface control specimens on in the a num foil compressed surface specimens. The FPL etch had very slight edge failure in the uncontaminated control and the aluminum foil compressed specimens. This type of failure is typical of FPL etched wedge crack specimens. The white cotton glove, kraft paper, and bare hand contaminated specimens showed gross adhesive failure with FPL etch and phosphoric acid anodize. Chromic acid anodize showed adhesive failure in the wedge crack stress area only. Compression of phosphoric acid anodize in a hydraulic press using aluminum foil and kraft paper even at 100,000 psi, which caused great deformation of the anodized film, did not result in any wedge crack failure. (2) The Auger spectra of the surface before priming, Figures 204, 206 and 208 and the carbon depth profile, Figures 205, 207 and 209, show an increase in carbon from any of the contamination methods for all surface treatments. (3) SEM micrographs of the failed wedge crack specimens showed the replication of the grain boundaries, pits,micropitting and the surface treatment itself.

Controlled Abraasion-Contamination. - A Balance Beam Scrape Adhesion Tester was modified to provide a known wiping load on the rest surface. The surface of the cylinder was covered by clean etched aluminum foil or kraft paper and drawn across the surface of phosphoric acid anodized wedge crack panels under a load of 1 kilogram. Three adjacent 1/2-inch-wide strips were wiped on each of the test panels in the area to be exposed in the wedge crack test after bonding. Cohesive failure was exhibited by the wedge crack test specimens when wiped with etched aluminum foil while adhesive failure was observed on the specimens wiped with kraft paper.

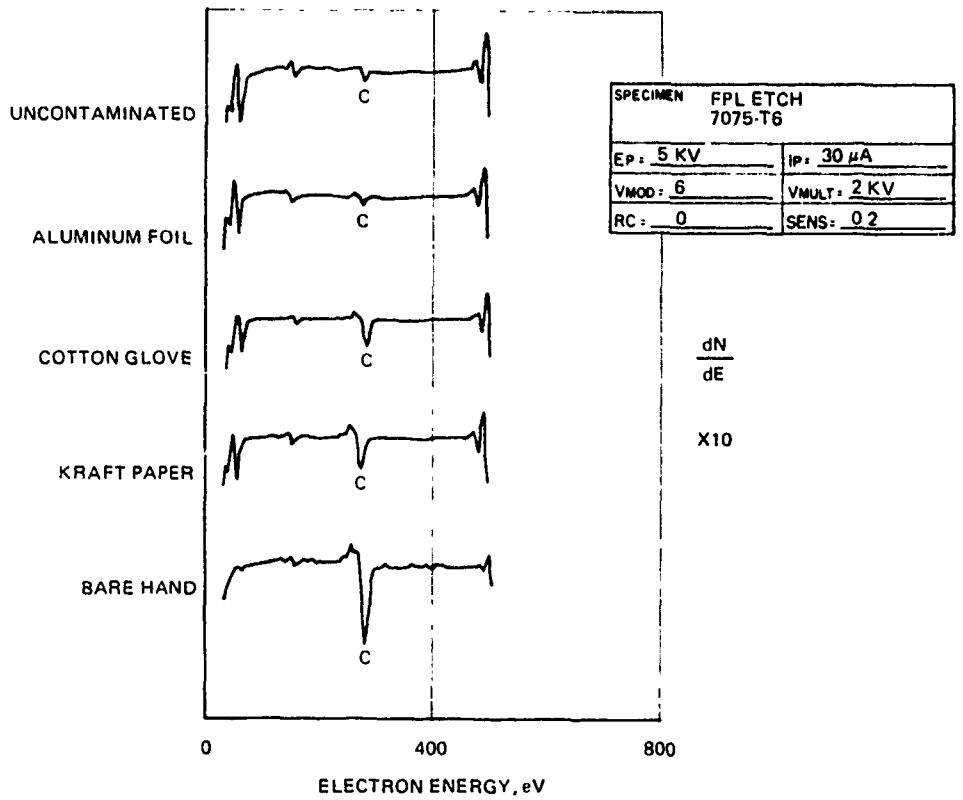


FIGURE 204. FPL - AUGER SPECTRA

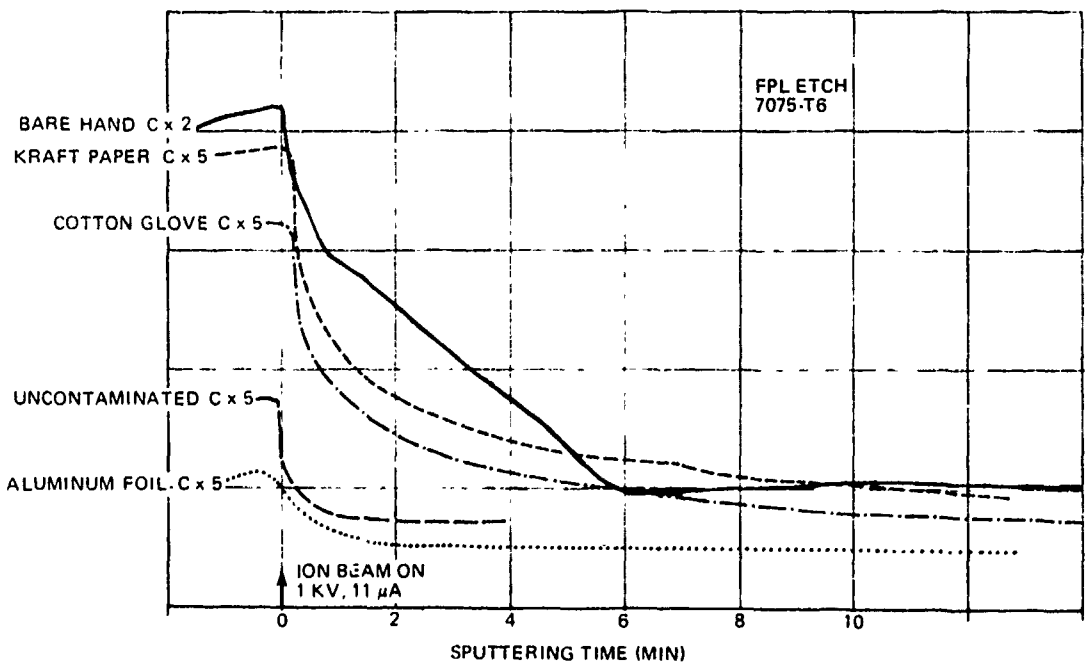


FIGURE 205. FPL - CARBON DEPTH PROFILE

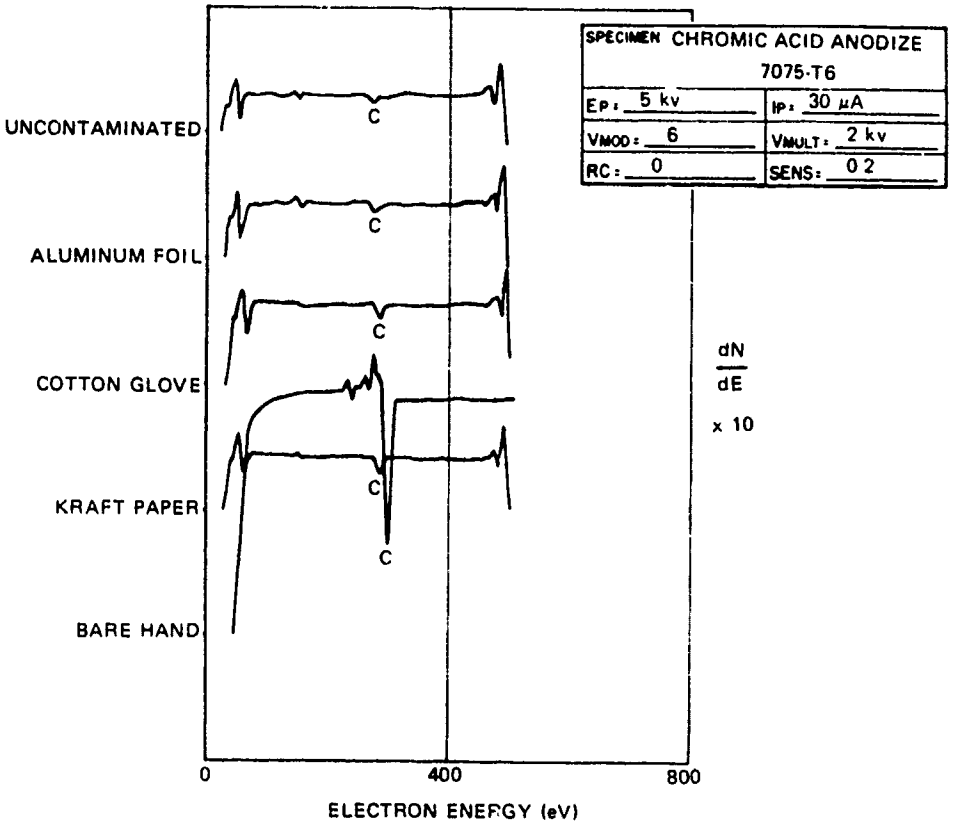


FIGURE 206. CHROMIC ACID ANODIZE - AUGER SPECTRA

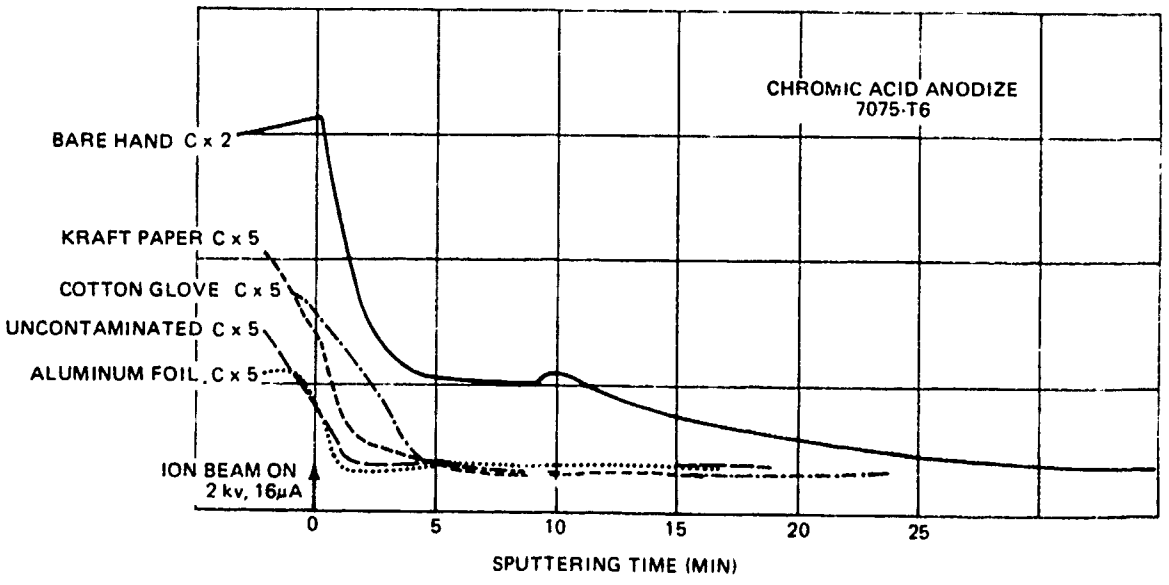


FIGURE 207. CHROMIC ACID ANODIZE - CARBON DEPTH PROFILE

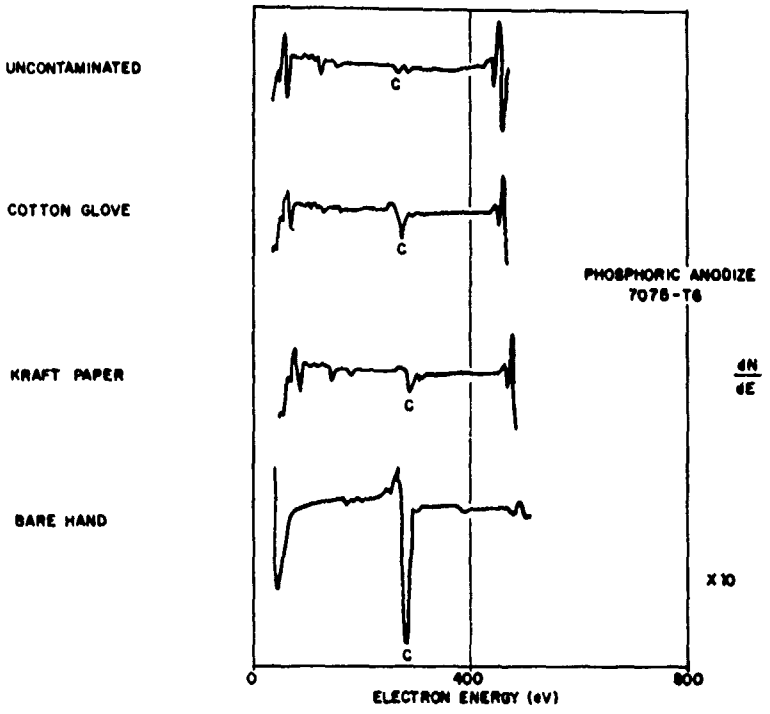


FIGURE 208. PHOSPHORIC ACID ANODIZE - AUGER SPECTRA

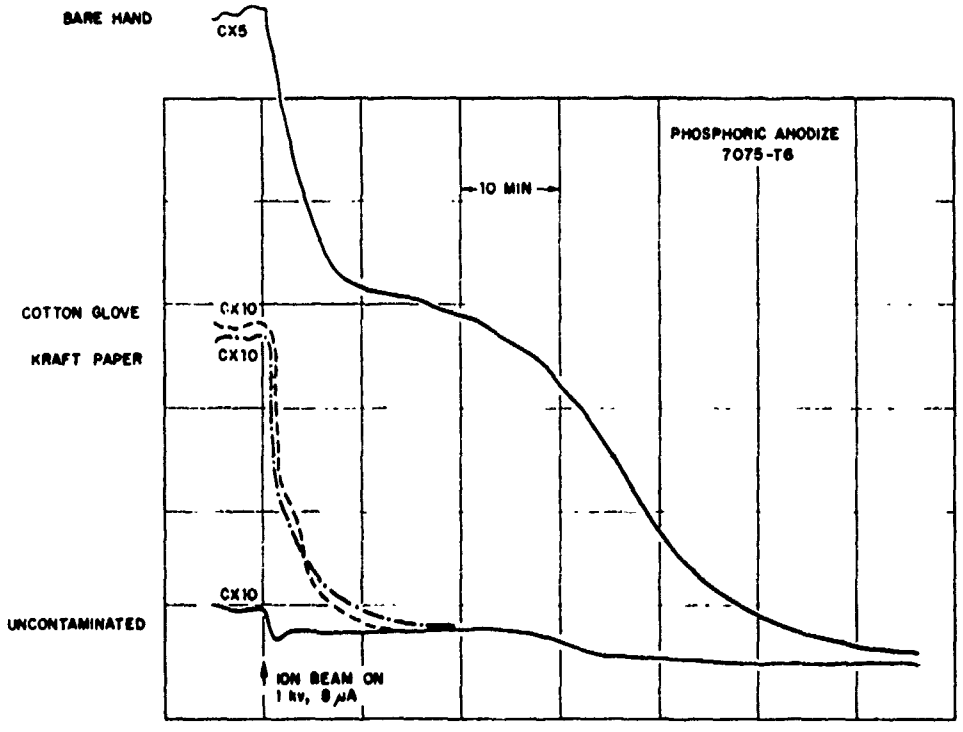


FIGURE 209. PHOSPHORIC ACID ANODIZE - CARBON DEPTH PROFILE

Fokker Contamination Tester. - The Fokker Contamination Tester was used to monitor an uncontaminated phosphoric acid anodized surface and a kraft paper rubbed anodized surface. The Fokker potential of the specimens stabilized after a 48-hour conditioning period. The wedge crack failures of the kraft paper contaminated specimens were grossly adhesive just as the surfaces bonded immediately after contamination.

Physical and Chemical Analysis of Contamination - Abrasion. - Examination of contaminated samples with ellipsometry, PEE, SPD, and water contact angle, concluded that the changes noted were consistent with a physical disturbance of the anodic film. Phosphoric acid anodized surfaces of 7075 have been analyzed by Auger electron spectroscopy, X-ray photoelectron spectroscopy (XPS), ion scattering spectroscopy, and by both positive and negative secondary ion mass spectroscopy (SIMS). Three surfaces were used in this study: a fresh, untouched anodized surface, an anodized surface which had been lightly rubbed with a cotton glove, and an anodized surface which had been rubbed with kraft paper. The oxide formed by phosphoric acid anodizing had a spongy appearance at high magnification. It had been observed that by rubbing this surface, the top of the spongy layer was crushed and smeared out. It had also been found that an oxide which had been rubbed with either a cotton glove or kraft paper was a poor surface for adhesive bonding. To determine whether the poor bonding was due to the deformation of the surface or to contamination transferred during the rubbing, the surfaces were examined by the techniques stated above and the surface features were photographed in a scanning electron microscope. All methods except SIMS showed that there was an increased level of carbon on the glove and kraft paper contaminated phosphoric anodize as compared to the uncontaminated control. When contaminated, the carbon level persisted through the anodize layer. Of the techniques studied, the XPS of the individual carbon lines was perhaps the most powerful method of studying this form of contamination.

The action taken to ensure that the primer is applied prior to the surface being touched in any manner appears justified since the application is load carrying primary structure. Failure, either abrasion or contamination, is prevented by the early application of primer. No wedge crack failures have been observed where the primer was applied before surfaces were handled.

COST EVALUATION

This section contains the cost analysis effort of Phase Ib. A detail effort was made to determine the cost of bonded structure and provide a basis for assessing economic viability. The analysis provided the quantitative cost measures of acquisition and maintenance by which technical, manufacturing and economic decisions were made in the overall process of evaluating and selecting the design approaches and concepts. In developing the cost measures, techniques similar to those used for a production aircraft were used in the estimating process. Credibility for costing was achieved by providing in-depth visibility and traceability of all estimates and in a consistent manner for all concepts and the baseline. The estimating process was integrated into the system development process early in the program to obtain realistic evaluation of the concepts to avoid abstract and speculative judgments.

The results of the cost evaluation in Phase Ib indicates bonding of primary structural components offers significant savings over conventional construction. As bonding requirements and bonding area increased, parts and complexity are reduced. The cost experienced for assembly labor compared with conventional construction were dramatically lowered. However, the acquisition cost is not the only element in the economic assessment. Long term maintenance cost must also be investigated. Results of this study indicate that the concept with the lowest acquisition cost could exhibit the highest maintenance costs and ultimately the highest total overall cost.

PRECEDING PAGE BLANK-NOT FILMED

Acquisition Cost

Acquisition cost is one of two measures that was used as a quantitative basis for evaluating and ranking candidate concepts with respect to a baseline configuration. This measure was also used for the same purpose in the accomplishment of trade studies. Acquisition includes only the labor and material elements required and associated with the manufacture of an assumed production buy of 300 aircraft. This includes the direct production labor for fabrication, assembly, metal bond, initial and sustaining tooling, planning and inspection. This means that all non-recurring and recurring development costs were excluded as well as sustaining engineering. The material element of the acquisition cost is comprised of the raw materials required for fabrication and assembly as well as the raw materials required for tool fabrication.

Approach. - Costs were generated using industrial engineering type procedures and based upon techniques similar to those used on production aircraft that have proven by extensive experience to be accurate and dependable. For Phase Ib these procedures were somewhat modified to exclude, to the maximum extent possible, the use of functional estimating factors. The fundamental premise was to consider the direct estimating approach as the predominant technique.

Since cost was emphasized as a significant determinant in the selection process, a systematic and organized approach was formulated and implemented. This approach is exhibited in Figure 210 which essentially documents the manner in which cost was integrated into the system development process. It also provides the interaction between cost analysis and design/development at all stages of analysis and synthesis.

Estimating Process: - The estimating process, in general terms, consisted of determining (a) the total quantity of parts to be manufactured and by type, (b) the number of assemblies per release, and (c) the number of releases.

Material Costs: - Costs were determined for raw materials and purchased parts by alloy, form and weight. Material utilization factors were assigned based on the method of fabrication to arrive at the amount of procured material required versus design weight. Material cost factors were then applied to quantity requirements and/or utilized vendor quotes.

PRECEDING PAGE BLANK-NOT FILMED

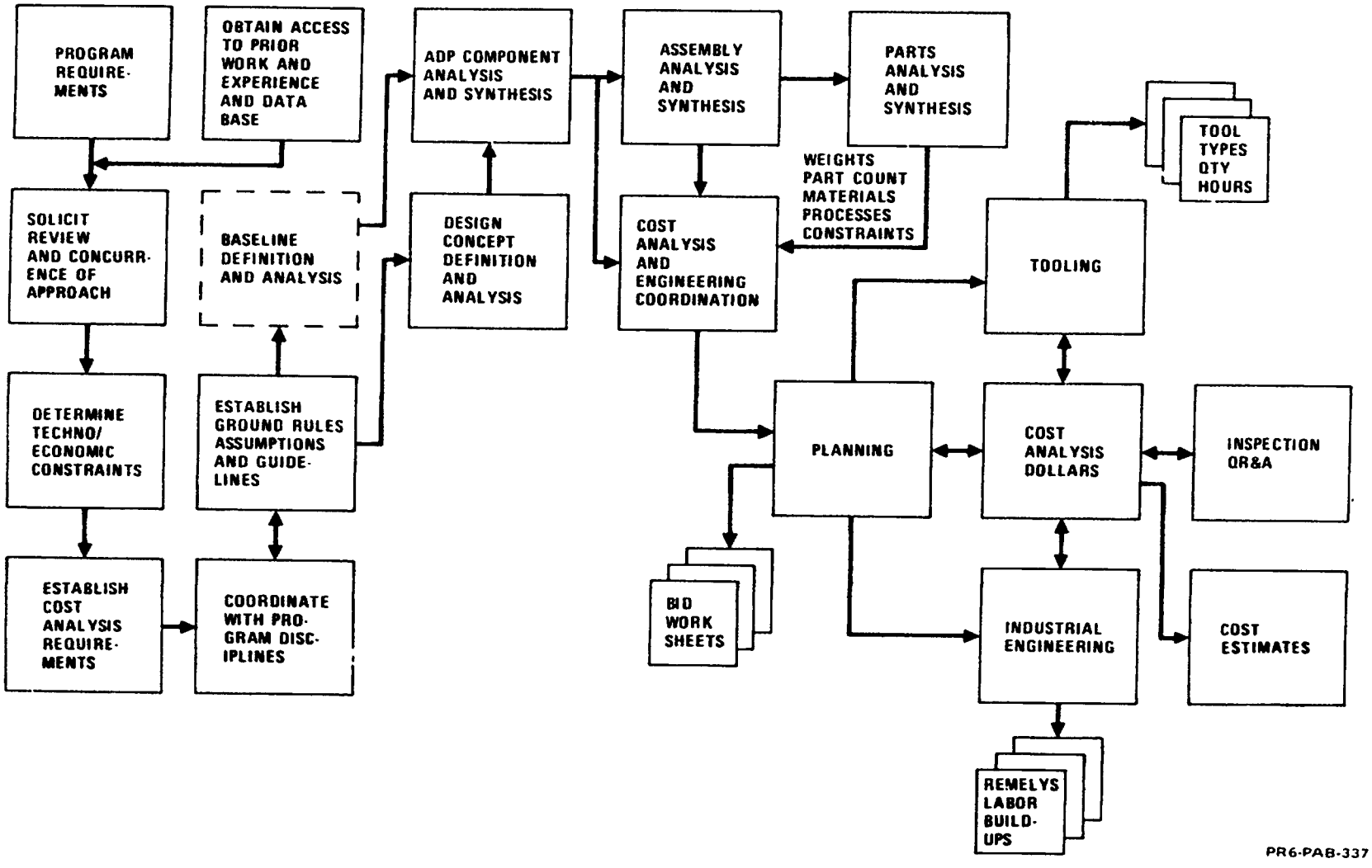


FIGURE 210. COST ANALYSIS ESTIMATING PROCESS

Direct Production Labor Elements: - Operational sequence planning on Bid Worksheets were developed to identify fabrication of detail parts or components by type and quantity and to identify the assembly of detail parts to provide end item or component of end item.

The type, quantity, design and fabrication of tooling were determined for use with the specified manufacturing method. Base standard hours for operational sequence were developed to include set-up time and run time at unit T_{100}. Base standard hours were then converted to estimated actual hours which provided the amount of hours necessary to manufacture the item, including all tangible and intangible operations. Estimated actual hours to quantity requirements were projected using progress curve application. Manufacturing estimated actual hours to direct labor dollars were then converted for a base period year.

Planning hours as well as the inspection hours for fabrication, assembly, metal bond, and tooling were determined separately. Inspection and tooling hours were converted to labor dollars for a base period year.

All production labor elements were summed. The factors for functional estimating, direct estimating and conversion to base year dollars are shown in Table 73 .

Ground Rules, Assumptions and Guidelines. - One of the purposes of Phase Ib was to produce a realistic base of technical and engineering data as inputs to other disciplines that would permit the selection of a specific concept in a systematic manner. A prerequisite to implementing the costing approach was a thorough understanding of the economic, technical/engineering and manufacturing ground rules, assumptions and guidelines in order to derive meaningful results.

Economic Assumptions and Ground Rules: - All costs are expressed in constant 1975 dollars and the labor rates include overhead and G&A, but exclude profit. RDT&E non-recurring and recurring elements are excluded from the estimates. The costs are based on a production buy of 300 aircraft. All raw materials are flat priced and based on a combination of historical data and vendor quotes. Material costs are based on procured weights and utilization. Sustaining engineering is excluded from production.

TABLE 73

COST ESTIMATING FACTORS

- MFG LABOR RATE $21.15/HR
- INSPECTION LABOR RATE $24.23/HR
- TOOLING LABOR RATE $24.54/HR
- PLANNING LABOR RATE $21.15/HR
- FABRICATION PROGRESS SLOPE 90%
- ASSEMBLY PROGRESS SLOPE 80%
- METAL BOND PROGRESS SLOPE 80%
- TOOLING PROGRESS SLOPE 53.7%
- NON RECURRING PLANNING . . . . . 24% (FUNCTION OF NON-RECURRING TOOLING HOURS)
- RECURRING PLANNING . . . . . 6% (FUNCTION OF FABRICATION AND ASSEMBLY HOURS)
- FABRICATION LABOR INSPECTION 4.5%
- ASSEMBLY LABOR INSPECTION 6.5%
- METAL BOND LABOR INSPECTION 6.72%
- NDT INSPECTION . . . . . DIRECT
- QR&A LEVEL OF EFFORT . . . . . 4.0% (FUNCTION OF TOTAL MFG LABOR HOURS)
- TOOLING LABOR INSPECTION 4.5%
- ULTRASONIC INSPECTION, TIME/UNIT OF AREA . . . . . .10 MIN/SQ FT
- ULTRASONIC INSPECTION, TIME/LENGTH . . . . . 5 MIN/FT
- RADIOGRAPHIC INSPECTION, TIME/UNIT OF AREA . . . . . .10 MIN/SQ FT

PR6-PAB-335

Technical/Engineering Ground Rules and Assumptions: - Each design concept reflects a bonded shell with the baseline a riveted shell. Tear straps were included only in the honeycomb concepts. All configurations contain the hell hole supporting structure. The window support structure is included in all configurations. Emergency exit structure is excluded from all configurations; however, the hatch support structure is included in all configurations.

Items excluded from the estimates were floors, joining fittings forward of 330 and aft of 992.5, forward pressure bulkhead barrier, wing box, nose gear provisions, bulkhead panels and keel members, doors, hatches and plugs, provisions for systems, landing gear pod attachments, the support structure for landing gear except main landing gear forgings, and sustaining engineering.

Floor tees were bonded on the external and honeycomb concepts to replace a floor tie-in longeron; however, it was an integral part of the internal concept. Fairing from wing box to fuselage is included in all configurations.

Manufacturing Ground Rules and Assumptions: - Acquisition cost was a primary quantitative measure for assessing economic viability and the one by which technical,manufacturing and economic decisions were made in the overall process of evaluating and selecting design approaches and concepts. Therefore, the costing framework was structured to focus only on the resource elements of the production function. Within this framework, emphasis was placed on the recurring elements associated with the production function and this provided the basis for the manufacturing ground rules and assumptions.

Estimates for the direct labor elements and the material requirements were based on an average type program of 18 production releases with approximately 17 aircraft per release. The conceptual production plan and schedule associated with such a program considered that plant facilities and all capital equipment were in place at the outset. It was also felt that any new aircraft program in which adhesive bonding of both primary and secondary structure became a major element of the manufacturing process would incorporate new fabrication/assembly flow procedures and also maximize manufacturing efficiency. These procedures, of necessity, must account for the element of time as a key

item of certain aspects of the manufacturing process. It was therefore assumed that an integrated and self contained manufacturing facility produced the product with appropriate and selective automation. For example, surface preparations and treatments were assumed to be integrated into the facility and automated. Also, adhesive bonding of structural components involves more stringent and time consuming NDI requirements compared to those associated with conventional manufacturing. Automation of NDI was assumed in which a test fixture with multiple heads traversed the structure or the structure was conveyed past the test fixture incorporating the multiple heads.

In deriving the tooling estimates, consideration was given to the ground rules and assumptions that governed the manufacturing labor. Therefore, the tooling costs reflects the basic production plan and assumptions regarding lot sizes and releases. In addition, part type, quantity and commonality were significant elements in developing the estimates.

Supporting functions to manufacturing (e.g., inspection and planning) were estimated in two ways. It was assumed that conventional manufacturing for all configurations induced no changes to the process of making estimates as a function of the direct manufacturing labor. However, NDI presented a different problem. Experience showed that this element required a direct estimate based on area and length in order to avoid a bias to the estimates.

Description of Concepts

The basic fuselage used in this study is a segment 662.5 inches long (station 330 to 992.5) with provisions for three windows, two top hatches, one hell hole, one crew entrance, dummy wing box attachments and keel and bulkhead attachments.

Baseline. - The baseline is a conventional internal longeron stiffened semi-monocoque fuselage structure with a constant cylindrically shaped section approximately 55 feet in length and 18 feet in diameter. The fuselage has a constant cross section of 108-inch radius aft of station 516 with provisions for attaching a simulated wing box between station 703 and station 847. Conventional aircraft construction was used and comprised of aluminum skins; longerons 13-16 inches on center for top and bottom quadrants and 70 to 80 inches on center for side quadrants; frames 24 inches apart; floor concept 76 inches below FRP although not costed; and two longitudinal keels not costed 20 inches each side of fuselage centerline. Floor bulkheads would have been located 48 inches apart an' spliced to the basic frame sections above the floor. The basic frame section corsisted of a formed 'Z' with return flanges joined to the longeron by butterfly clips.

Internal Longeron. - This concept is essentially identical to the baseline except that the longerons and frame shear tees are bonded to the skins instead of being mechanically fastened. The frame clips are tee sections for bond strength to the skin in contrast with angles in the baseline. The longerons are J sections versus Z sections for the baseline.

External Longeron. - This concept is a stiffened shell similar to the internal longeron concept except that the longerons are bonded to the outer surface of the skins. The longerons are tee shaped to reduce the effect of aerodynamic crossflow. This concept uses unnotched shear clips bonded to the internal surface. Frame spacing is identical to the internal longeron concept where required crown head rivets are used.

Honeycomb. - This concept is a full depth honeycomb sandwich with no longerons for the pressure shell. Frame spacing is increased from 24 inches to 48 inches except under the wing on the side panels. The majority of the shell splices are hot bonded with the remainder cold bonded and mechanically fastened.

Frames consist of a cap tee bonded directly to the shell. The inner element of the frame is either a formed 'J' or machined 'L' mechanically joined to the tee. Treatment of bulkhead and keels is identical to the other bonded concepts. In all other areas where mechanical attachments are used to join other structure to honeycomb sandwich, solid aluminum edge members are used for local reinforcement.

MAINTENANCE

It was recognized that measuring and assessing quantitatively the impact of maintenance on cost was an involved and complex procedure. This was reinforced by the unavailability of a firm and audited data base that was representative of operational bases and depots. Therefore, cursory analyses were conducted to obtain a gross categorization or ranking of concepts with respect to maintenance. The primary objective was to establish a ranking of repairs for specific concepts and in a general manner determine if acquisition savings were offset. In this regard, assessments were made of the repair actions for assumed physical damages in specific locations on each concept. The repair concept assumed single repair actions (no production line type repairs) and followed the production procedures outlined earlier but utilized shop aid tooling. The results show that the most expensive repair cost were attributable to the honeycomb concept. Of the total of five types of damages assumed, corner repairs incur the greatest cost regardless of concept. The external and internal concepts were relatively close for all repairs and have a slight edge over the baseline - not as commanding a reduction as the acquisition cost comparison. The results should be considered at this time as preliminary and not applicable as a decision-making tool similar to the acquisition cost results. During Phase II the maintenance aspect is to be investigated more thoroughly and an attempt will be made to obtain a usable data base from which to measure and derive maintenance costs.

Results

Part Quantity Comparison. - The bid worksheets were developed and the detailed part count made with the parts grouped or classified by type. The part count was representative of the concepts and baseline based on the costing ground rules and assumptions. Table 74 is a compilation of part type and part quantity and shows a comparison of all concepts with the baseline configuration.

The part count for the baseline and the internal longeron concept are the same since the baseline is an internal longeron concept assembled with conventional riveted and mechanical construction. A feature of the three concepts evaluated was that as the amount of bonding increased the part count decreased.

Within the part count of the external longeron concept there is a redundancy of 199 parts for floor and keel attach tees to fuselage skin. These were included at the cost analysis design freeze but should be removed and the external longeron concept part count reduced from 3116 to 2917 and the grand total from 82,908 to 82,709. This change would also impact the tool quantity requirement for the external concept and would reduce the overall cost of the external concept. Based on the parts count shown in Table 74 and the assumption that parts count is a good indicator of complexity, a preliminary projection was made of ranking of the concepts with respect to acquisition cost - honeycomb concept lowest, external second and internal third.

Tooling Comparison. - The detailed information with respect to part type, tool type, quantities and method of manufacture was directly coordinated with the tooling estimator. While this information provided the tooling estimator with the basic data, it was necessary to conduct a thorough review of the drawings and coordinate his efforts with the experiences gained with the tooling constructed for the large test panels. Tool concepts were derived and specifically sized for the parts identified on both the planning documents and the drawings. As noted earlier, the 199 redundant parts in the external longeron concept would impact the tooling toward reduced requirements and reduced costs. A comparison of tool type and quantity is contained in Table 75 and a glossary of types of tools delineated in that table is shown in Table 76 .

TABLE 74

PARTS BREAKDOWN AND QUANTITY COMPARISON

PARTS IDENTIFICATION AND GROUPING	BASELINE	INTERNAL LONGERON	EXTERNAL LONGERON	HONEYCOMB
SKINS	41	41	41	130
SKIN SPLICES	322	322	437	158
FRAMES	259	259	237	95
FRAME SPLICES AND SHEAR TEE SPLICES	216	216	371	230
CLIPS	239	239	149	198
BUTTERFLY CIPS	735	735	–	–
DOUBLERS	26	26	23	167
SHEAR TEES	172	172	213	120
INTERCOSTALS AND OTHER (GUSSETS, SHIMS, ANGLES, CAPS)	352	352	431	435
LONGERONS	151	151	151	–
LONGERON SPLICES	361	361	414	–
HATCHES, DOORS, WINDOWS, ATTACHMENTS	445	445	450	113
EDGE MEMBERS	–	–	–	399
HONEYCOMB CORE	–	–	–	300
FLOOR AND KEEL ATTACH TEE TO FUSELAGE SKIN	–	–	199	78
TOTAL (LESS FASTENERS)	3,319	3,319	3,116	2,423
FASTENERS	132,234	86,521	79,792	11,500
GRAND TOTAL	135,553	89,840	82,908	13,923

PR6-PAB-327A

TABLE 75

TOOL TYPE AND QUANTITY COMPARISON

TOOL TYPE	BASELINE	INTERNAL LONGERON	EXTERNAL LONGERON	HONEY-COMB	TOOL TYPE	BASELINE	INTERNAL LONGERON	EXTERNAL LONGERON	HONEY-COMB
AJ	17	6	6	6	MC	342	342	342	125
AT	472	472	543	265	MCM	24	24	24	50
ATP	35	35	35	42	MET	7	7	7	2
BF	6	6	6	3	MF	71	71	71	35
BJ	–	11	11	8	MLD	471	471	540	605
CKF	120	120	148	103	NC	13	13	13	134
CT	31	31	35	190	PB	11	11	11	–
DD	3	3	3	–	PBT	133	133	163	156
DFT	1	1	1	–	PBD	1	1	1	–
DJ	21	21	21	26	PDS	2	2	2	–
DLT	–	–	–	28	PT	50	50	50	6
FB	248	248	274	179	RB	153	153	151	101
FDP	9	9	9	–	RLT	16	16	16	–
FR	1	1	1	1	SCJ	7	7	7	7
HFLD	2	2	2	–	SF	15	15	15	89
HRT	3	3	3	–	SFB	2	2	2	–
IF	1	1	1	–	SST	4	4	4	–
IGP	8	8	8	4	STB	154	154	182	160
JD	6	6	6	–	STT	2	2	2	2
LT	262	262	301	529	TMCM	14	14	14	5
LTU	1	1	1	–	WS	2	2	2	2
MAM	4	4	4	8					
SUBTOTAL	1251	1251	1419	1392	SUBTOTAL	1494	1494	1619	1479
TOTAL	–	–	–	–	TOTAL	2745	2745	3038	2871

PR6-PAB-343

TABLE 76

TYPES OF TOOLS ESTIMATED

AJ	– ASSEMBLY JIG
AT	– APPLY TEMPLATE
ATP	– AUXILIARY TOOL, PRODUCTION
BF	– BORING FIXTURE
CKF	– CHECK FIXTURE
CT	– CHECK TEMPLATE
DD	– DRAW DIE
DFT	– DRAW FORM TOOL
DJ	– DRILL JIG
DLT	– DEVELOPMENT LAYOUT TEMPLATE
FB	– FORM BLOCK
FDP	– FORM DIE PRESS
FR	– FORM ROLL
HFLD	– HOLDING FIXTURE LINE DOLLY
HRT	– HAND ROUTING TEMPLATE
IF	– INSTALLATION FIXTURE
IGP	– INSPECTION GAGE – PRODUCTION
JD	– JOGGLE DIE
LT	– LAYOUT TEMPLATE
LTU	– LAYOUT TEMPLATE UNCUT
MAM	– MASTER MODEL
MC	– MILL CUTTER
MCM	– MACHINE CONTROL MEDIUM
MET	– MINOR EXPENDABLE TOOL
MF	– MILL FIXTURE
MLO	– MASTER LAYOUT
PB	– PROFILE BLOCK
PBT	– PIERCE BLANKING TOOL
PBD	– PIERCE BLANK DIE
PDS	– PRODUCTION DATA SHEET
PT	– PROFILE TEMPLATE
RB	– ROUTER BLOCK
RLT	– ROUTER LAYOUT TEMPLATE
SCJ	– STRETCH CHUCK JAWS
SF	– SPECIAL FIXTURE
SFB	– SPIN FORM BLOCK
SST	– STOCK SIZE TEMPLATE
STT	– STRETCH BLOCK
TMCM	– TOOL MACHINE – CONTROL
WS	– WORK STAND

Cost Summary by Major Resource Element. - A cost summary by major resource element of the acquisition cost is shown in Table 77 . These costs are in constant 1975 dollars and are the cumulative average of the 300 production units. The manufacturing labor elements of fabrication, assembly and metal bond have been segmented in order to clarify the changes that occurred in each element as the amount of bonding increased and the area bonded increased. As the quantity of parts bonded and area increased (internal to external to honeycomb) the metal bond labor and inspection costs increased; but, the overall fabrication and assembly and metal bond labor was dramatically reduced. The highest cost for inspection was experienced with the honeycomb due to the large amount of NDT requirements. Overall significant cost savings were demonstrated for each of the concepts compared to the baseline. The honeycomb ranked number one, external longeron number two and the internal longeron concept third. However, the results indicate that the internal and external concepts are very close.

Manufacturing Labor Hours Reduction. - One of the most encouraging aspects of the results is that large savings in direct manufacturing labor can be achieved with adhesive bonding. As examples, the percentage reduction in labor hours compared to the baseline was estimated at 25% for the internal concept, 27% for the external concept and 43% for the honeycomb concept. This reflects directly into productivity improvements for the manufacturing function. From that standpoint, the improvement in pounds produced per dollar of input over the baseline ranged from a +27% to +62% for the concepts studied.

Damage Repair Cost Summary. - Table 78 contains a comparison of the costs to make a single repair of the types given on a single aircraft and would not be typical with a production line type of operation. In effect it is a T_1 type value built up the same as that explained for the acquisition cost but not reduced to cumulative average value of 300. The tooling is primarily a shop aid classification.

The results show that the most expensive repair costs are experienced with the honeycomb. Of the five repair examples door corner repairs incur the greatest cost regardless of concept. The external and internal concepts are relatively close for all repairs and exhibit a slight edge over the baseline - not as commanding a reduction as the acquisition cost comparison.

TABLE 77

COST SUMMARY BY MAJOR RESOURCE ELEMENT

CONSTANT 1975 DOLLARS

RESOURCE ELEMENT	BASELINE	INTERNAL LONGERON	EXTERNAL LONGERON	HONEYCOMB
MANUFACTURING LABOR				
FABRICATION	82,151	82,256	89,576	50,779
ASSEMBLY	347,701	174,279	150,514	77,499
METAL BOND	–	47,882	51,381	71,648
SUBTOTAL	429,852	304,417	291,471	199,926
INSPECTION	53,591	47,853	45,706	61,700
TOOLING	47,122	47,122	53, 799	50,604
PLANNING	31,423	23,930	24,038	18,449
RAW MATERIALS	49,347	49,505	53,153	58,567
TOTAL	611,335	472,827	468,167	389,246
COST RATIO	1.00	0.773	0.766	0.637
		–22.7%	–23.4%	–36.3%

PR6-PAB-332A

TABLE 78

DAMAGE REPAIR COST SUMMARY

CONSTANT 1975 DOLLARS

DAMAGE TYPE	COST PER REPAIR FOR GIVEN CONCEPT – T_1 DOLLARS			
	BASELINE	INTERNAL LONGERON	EXTERNAL LONGERON	HONEYCOMB
A. SKIN				
TOTAL COST	5,523	5,684	5,020	11,794
COST RATIO	1.0	1.029	0.909	2.135
B. SKIN AND LONGERON				
TOTAL COST	9,354	8,461	8,962	
COST RATIO	1.0	0.905	0.958	
C. SKIN AND FRAME				
TOTAL COST	11,323	10,705	10,340	14,821
COST RATIO	1.0	0.945	0.913	1.309
D. AFT DOOR CORNER CRACK				
TOTAL COST	15,138	14,633	14,453	21,866
COST RATIO	1.0	0.967	0.955	1.444
E. AFT DOOR CORNER DISBOND				
TOTAL COST		14,633	14,453	26,257
COST RATIO		–	–	–

PR6 PAB-311A

Integrated Cost Measure. - This overall cost includes the acquisition costs plus the long term maintenance cost represented by the repairs described earlier but continuing over a life period of 20-years. This should not be considered as the life cycle cost since many elements of cost have been excluded.

The ground rules and assumptions used as guidelines for implements to the cost measure were:

(a) A fleet of 300 aircraft was assumed for acquisition and operations.

(b) Aircraft utilization was based on 5 days per week and 260 days per year.

(c) It was assumed that the fleet would incur a minimum of one physical damage per operating day.

(d) The only maintenance considered is that associated with the physical damage or hypothetical repair.

(e) All part details and expendable tools and shop aids were fabricated at the base where repair occurred.

(f) Estimates are based on the hypothetical repairs depicted in engineering drawings and could or could not be typical of other areas.

(g) Labor estimates include initial inspection, disassembly, tooling fabrication, part fabrication, damage repair, reassembly and final inspection.

(h) All labor expended on the aircraft assumes two men working.

(i) The damage was repaired because it was known to exist. Inspection to disclose damage was not considered.

(j) Three separate cases were evaluated based on number of repairs incurred.

1. Fixed Case - All concepts and the baseline incur the same number of repairs.
2. Variable Case - Assumed a fixed quantity of repairs for both the baseline and internal concept (260); a ten per cent increase (or 286) in repairs for the external concept due to exposure to physical elements for damage; and a 50% increase in repairs for the honeycomb due to skin thickness and greater susceptibility to a variety of causes for physical damage.
3. Sensitivity - All concepts and baseline estimated for a series of damages at 50, 100, 200 and 300.

The basic data for implementing and ranking the concepts by the integrated measure is shown in Table 79 . In the first horizontal column the unit acquisition cost and the unit repair cost is given for each configuration.

TABLE 79

BASIC COST MEASURE DATA

ITEM	BASELINE	INTERNAL LONGERON	EXTERNAL LONGERON	HONEYCOMB
COST BASIS				
ACQUISITION COST/UNIT	$611,335	$472,827	$468,167	$389,246
REPAIR COST/UNIT	$ 10,335	$ 10,823	$ 10,646	$ 18,685
VARIABLE CASE				
NUMBER OF REPAIRS	260	260	286	390
TOTAL COST	$237M	$198M	$200M	$263M
FIXED CASE				
NUMBER OF REPAIRS	260	260	260	260
TOTAL COST	$237M	$198M	$195M	$214M
SENSITIVITY CASE				
NUMBER OF REPAIRS				
50	$194M	$153M	$150M	$136M
100	$204M	$164M	$161M	$154M
200	$225M	$185M	$182M	$192M
300	$245M	$207M	$203M	$229M

PR6-PAB-312A

The remaining three horizontal columns contain the information with respect to the number of repairs incurred per year for the total fleet and the total dollars incurred for acquisition plus 20 years of maintenance repairs. As an example, in the variable case or second horizontal column 260 repairs are shown for the baseline and a cost of $237M. To arrive at the $237M the following calculations are made.

1. The average unit acquisition cost (first column) of $611,335 is multiplied by the 300 production aircraft which yields a value of $183.4M. This is a one-time cost.
2. The average unit repair cost (first horizontal column) of $10,335 is multiplied by the number of repairs per year (in horizontal column) and then by 20 years for a value of $53.5M.
3. The two costs (acquisition and maintenance) are summed for a total of $237M (rounded).

The same procedure is used for all cases except in the sensitivity case the number of repairs are shown in the left hand column. The repair cost per unit is the average of the values given in Table 78.

The data contained in Table 79 were used to develop the graph of the integrated measure of the acquisition cost and the maintenance cost shown in Figure 211. The points plotted on the various curves for the configurations is for the variable case contained in Table 79 and was only as an example. In that example the internal longeron concept (N) and the external longeron concept (X) exhibited the lowest total costs - respectively $198M and $200M. These plots in Figure 211 clearly show that the baseline (B_L) is not competitive with the internal and external concepts regardless of the number of repairs due to its higher front end costs (acquisition). The baseline becomes competitive with the honeycomb only at the larger quantities of repair due to the significantly higher repair costs for the honeycomb concept. For fixed case assumptions, the honeycomb concept is competitive with the internal and external concepts respectively up to repair quantities of approximately 160 and 140. However, since it is more likely that the honeycomb concept would incur more damages the fixed case consideration should not be emphasized.

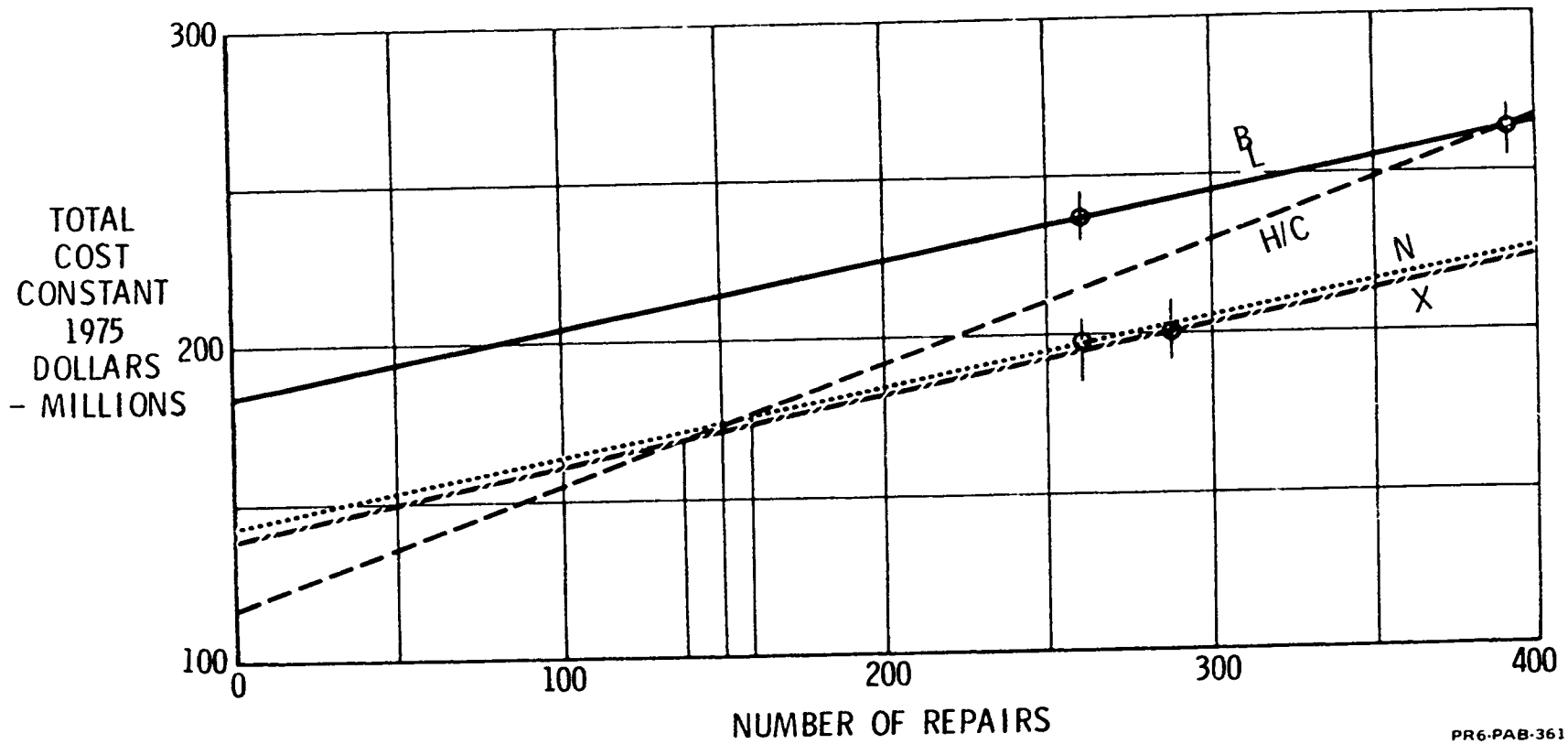


FIGURE 211. INTEGRATED MEASURE OF ACQUISITION AND MAINTENANCE

Cost Conclusions

From the knowledge and understanding coupled to the technical and manufacturing results over an 18-month Phase Ib period, sufficient economic and cost data have been derived to conclude the following: (a) all concepts evaluated offer decisive acquisition cost advantages over conventional construction, (b) front end exposure costs (production) are significantly reduced, (c) lower total long-term costs (acquisition plus maintenance) for both producer and user, (d) the honeycomb concept offers the least exposure to front end manufacturing costs, (e) the external concept provides acquisition cost advantages over the internal longeron concept; but on the basis of total long term costs (maintenance included) these two concepts are very close, (f) honeycomb repair costs rank highest (most costly) while the internal and external are similar.

Additional maintenance analyses are needed to establish type of inspection problems, scheduled and unscheduled maintenance requirements and their frequency.

APPENDIX A

This section contains trade studies which were used to determine the merits of various combinations of structural arrangements, materials, manufacturing and joining methods as they affect the selected and approved structural design concepts. The following trade studies are included in this section:

- Honeycomb Stiffened Skin Panel Impact Resistance Tests
- Foreign Object Damage
- Honeycomb Core Thickness Study
- Honeycomb Edge Member Study
- External Longeron Evaluation
- Internal Longeron Shape Study
- Maintenance Repair Designs For Production Concepts

PRECEDING PAGE BLANK-NOT FILMED

Honeycomb Stiffened Skin Panel Impact Resistance Tests

Summary. - Impact tests on metal honeycomb stiffened skin panels have shown that impact resistance can be improved by increasing the skin thickness or by decreasing the honeycomb cell size. Skin rupture energy can be increased by increasing the honeycomb core density at constant cell size. From an overall appearance point of view, all of the honeycomb stiffened skin panels were dented to an extent that repair would probably be required.

Purpose. - These tests were conducted to: (1) determine the impact resistances of honeycomb stiffened fuselage skin panels made from different face sheets, honeycomb core densities, and honeycomb cell sizes, and (2) compare these impact resistances with the impact resistance of a conventional longeron/frame stiffened fuselage skin panel.

Test Specimens. - Eleven honeycomb stiffened skin panels and one longeron/frame stiffened skin panel, shown in Figure A1 , were tested for impact resistance. The longeron/frame stiffened skin panel was a broken piece from a previously tested shear panel. This panel was cylindrically shaped with a 108.0 inch radius identical to the fuselage constant section. The skin was 0.040 inch thick, 7075-T6 bare aluminum material. Longerons and frames stiffened the skin at twelve and twenty-four inch spacing, respectively. The honeycomb stiffened skin panels were also cylindrically shaped with a 108.0 inch radius. Panel width and length was twelve inches. The face sheets were 2024-T3 bare aluminum material of 0.020, 0.032, and 0.040 inch thickness. These face sheets were stiffened by 0.80 inch thick 5056 aluminum hexagonal non perforated honeycomb core having densities of 3.1, 3.4, 4.3, and 5.2 pounds per cubic foot. Corresponding cell sizes were 0.188 inch for the 3.1 pcf honeycomb core and 0.250 inch for the other honeycomb cores. Corresponding cell wall thicknesses were 0.001, 0.0015, 0.002, and 0.0025 inch.

Test Setup. - All panels were tested using the Gardner impact test machine as illustrated in Figures A2 and A3. The honeycomb stiffened skin panels were supported along their straight edges. The longeron/frame stiffened skin

PRECEDING PAGE BLANK-NOT FILMED

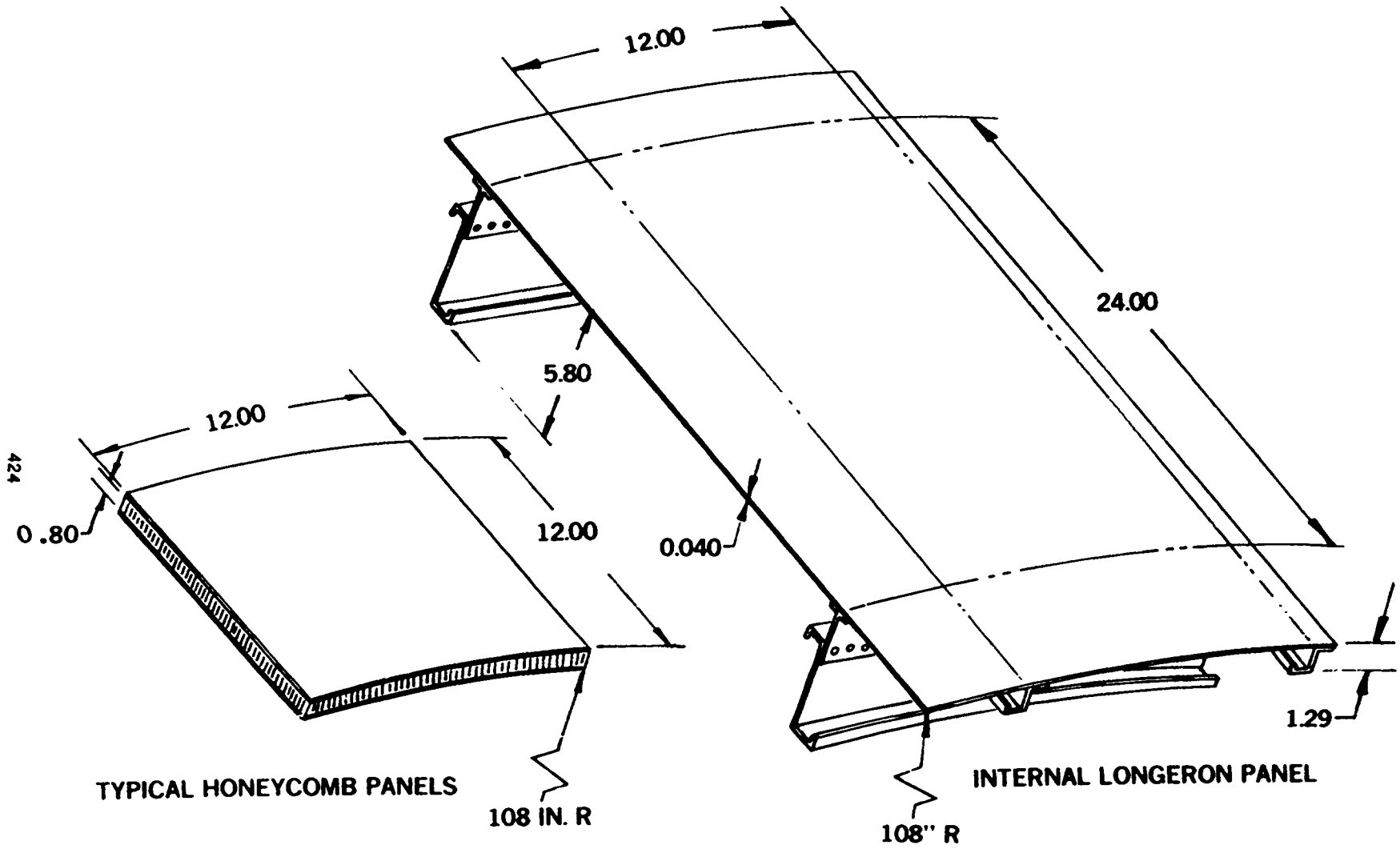


FIGURE A1. IMPACT RESISTANCE TEST PANELS

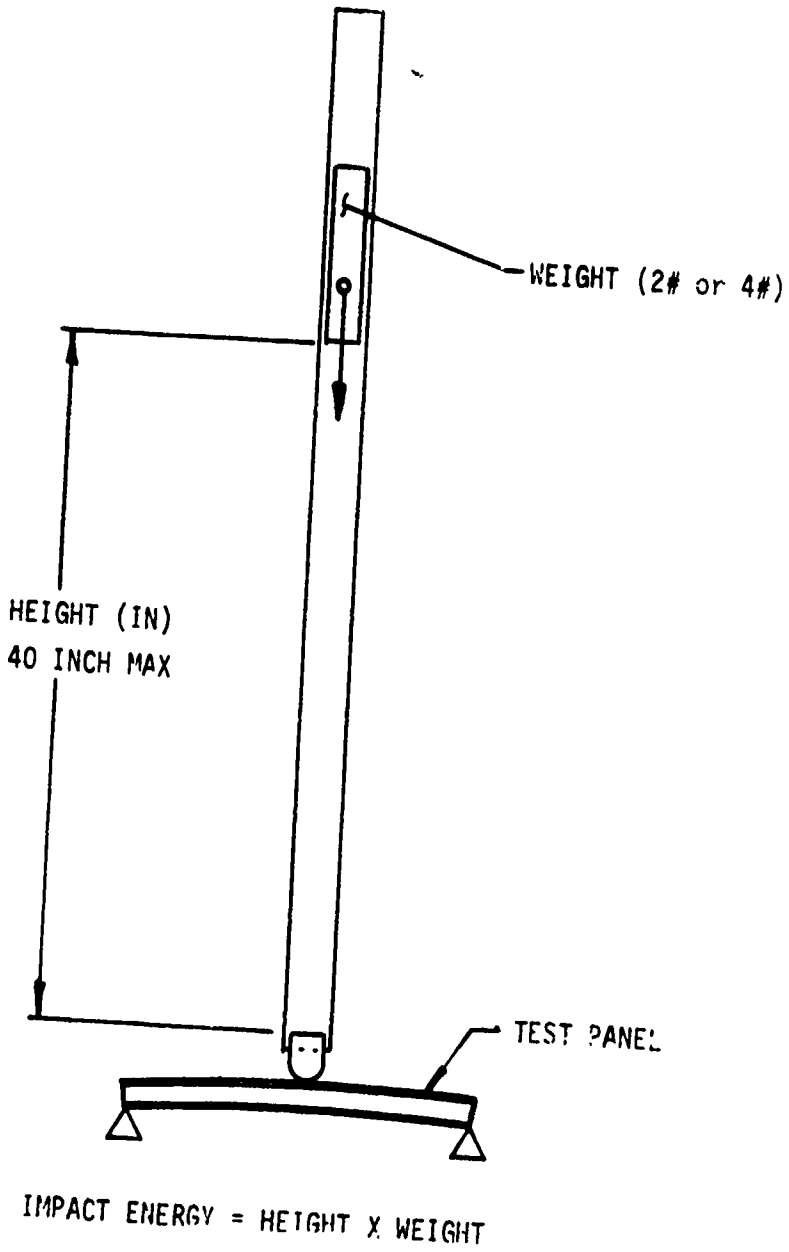


FIGURE A2. GARDNER IMPACT MACHINE TEST SETUP

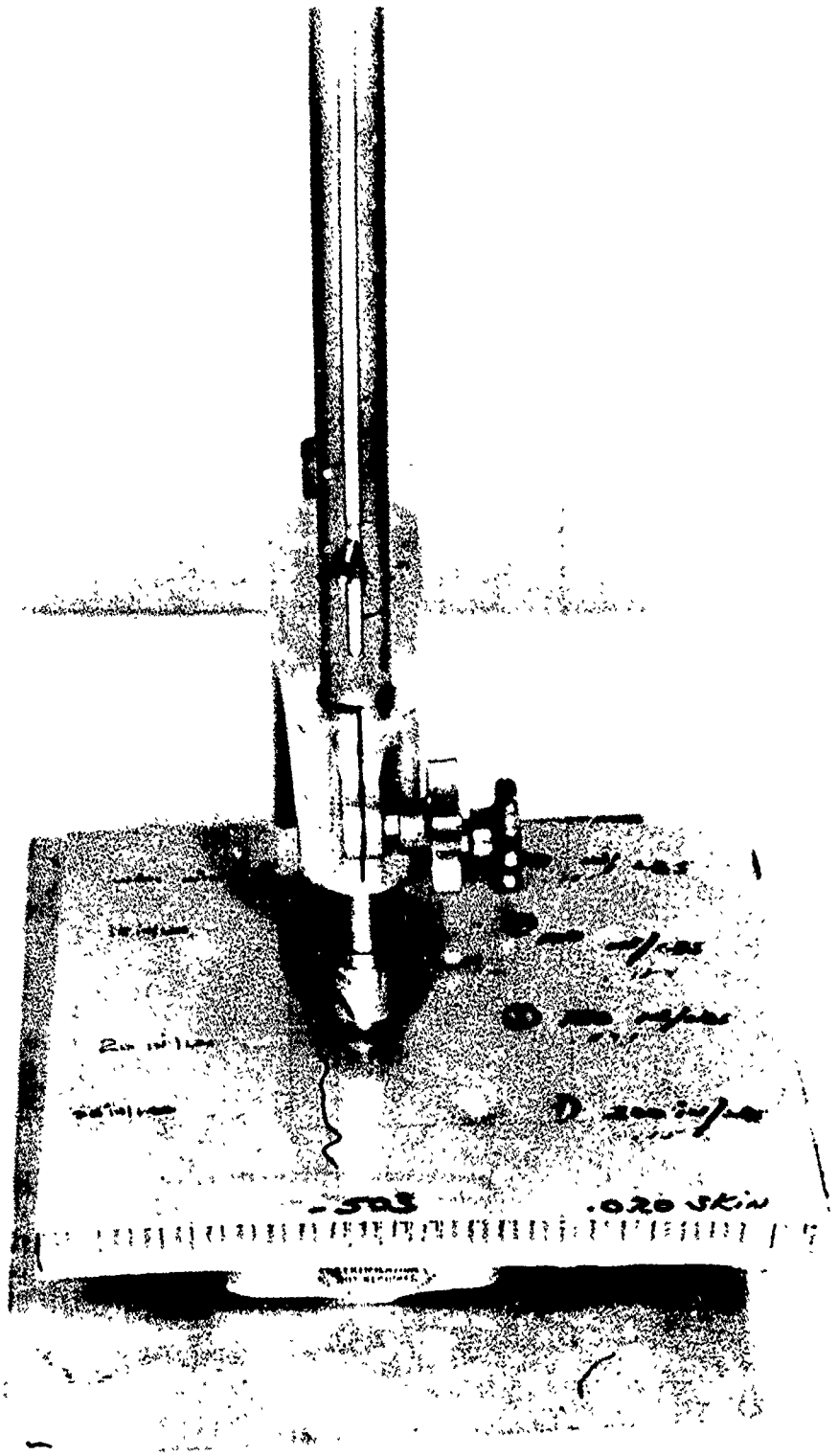


FIGURE A3. PHOTOGRAPH OF GARDNER IMPACT MACHINE TEST SETUP

panel was supported by its frames. Testing was accomplished by raising the weight inside the impact machine to a predetermined height and releasing it. The weight drops and strikes a mandrel with a spherical nose (0.50 inch diameter) which impacts the specimens. Impact energy (in-lbs) is the product of the weight multiplied by the height from which the weight is dropped.

Test Results. - Impact energies of 50, 100, and 150 inch pounds were applied to all panels. The depth of indentation was recorded for the honeycomb stiffened skin panels, see Table A1. Depth of indentation ranged from 0.058 to 0.189 inch. For the longeron/frame stiffened panel, impact energies were applied to the skin in an area centered between the longerons and frames and also along the longeron attaching flange. Depths of indentation were less than 0.010 inch along the longeron attaching flange for all applied impact energies. In the centered area, between longerons and frames, indentations were 0.038, 0.045 and 0.050 inch corresponding to impact energies of 50, 100 and 150 inch pounds. Figures A4 and A5 show a honeycomb stiffened skin panel and the longeron/frame stiffened skin panel after testing.

None of the skins were ruptured at impact energies of 50, 100, or 150 inch pounds. In an attempt to obtain skin rupture, the two weights (2# and 4#) of the Gardner impact machine were combined and dropped from 33 inches to obtain an impact energy of 200 inch pounds. The two weights separated during the fall and impact energy was actually less than the combined weight times height. This can be seen in Figure A4 for the -503 panel where the depth of indentation for 200 inch pounds is 0.158 inch which is less than the depth of indentation at 150 inch pounds of 0.171 inch. Thus, with the present setup for the Gardner impact machine, 160 inch pounds is the maximum possible impact energy (4# from 40 inches).

Rupture of the honeycomb face sheets was obtained by placing a 0.063 inch diameter wire on the skin, under the spherical nosed mandrel and applying an impact energy. Impact energy required for face sheet rupture is shown in Table A2 for the honeycomb stiffened skin panels. The skin of the longeron/frame stiffened skin panel could not be ruptured with the 0.063 inch diameter wire at an impact energy of 160 inch pounds. In fact this impact energy did not significantly mark the panel.

TABLE A1

DEPTH OF INDENTATION FOR HONEYCOMB PANELS

CONFIGURATION	-1	-501	-503	-505	-509	-511	-513	-515	-517	-519	-521
FACE THICKNESS (IN.)	020	←	←	.020	032	←	0 32	.040	←	←	.040
CORE DENSITY (PCF)	3.1	3.4	4.3	5.2	3.4	4.3	5.2	3.1	3.4	4.3	5.2
CELL DIAMETER (IN.)	.188	.250	←	←	←	←	.250	.188	.250	←	250
ENERGY (IN LB)	INDENTATION (INCHES)										
50	.094	.099	105	088	.073	.072	.079	.060	.065	058	.061
100	.138	.145	.154	.121	.113	.101	.117	.091	.100	.097	.099
150	.174	.189	.171	.147	110	.123	.147	.115	.129	.120	.118

TABLE A2

IMPACT ENERGY REQUIRED FOR HONEYCOMB FACE SHEET RUPTURE

CONFIGURATION	SKIN THICKNESS INCHES	CORE DENSITY PCF	IMPACT ENERGY IN. LB
-1	.020	3.1	25
-501	↓	3 4	25
-503	↓	4.3	25
-505	020	5 2	30
-509	032	3 4	40
-511	↓	4 3	35
-513	032	5 2	48
-515	040	3 1	56
-517	↓	3 4	56
519	↓	4 3	56
521	040	5 2	68

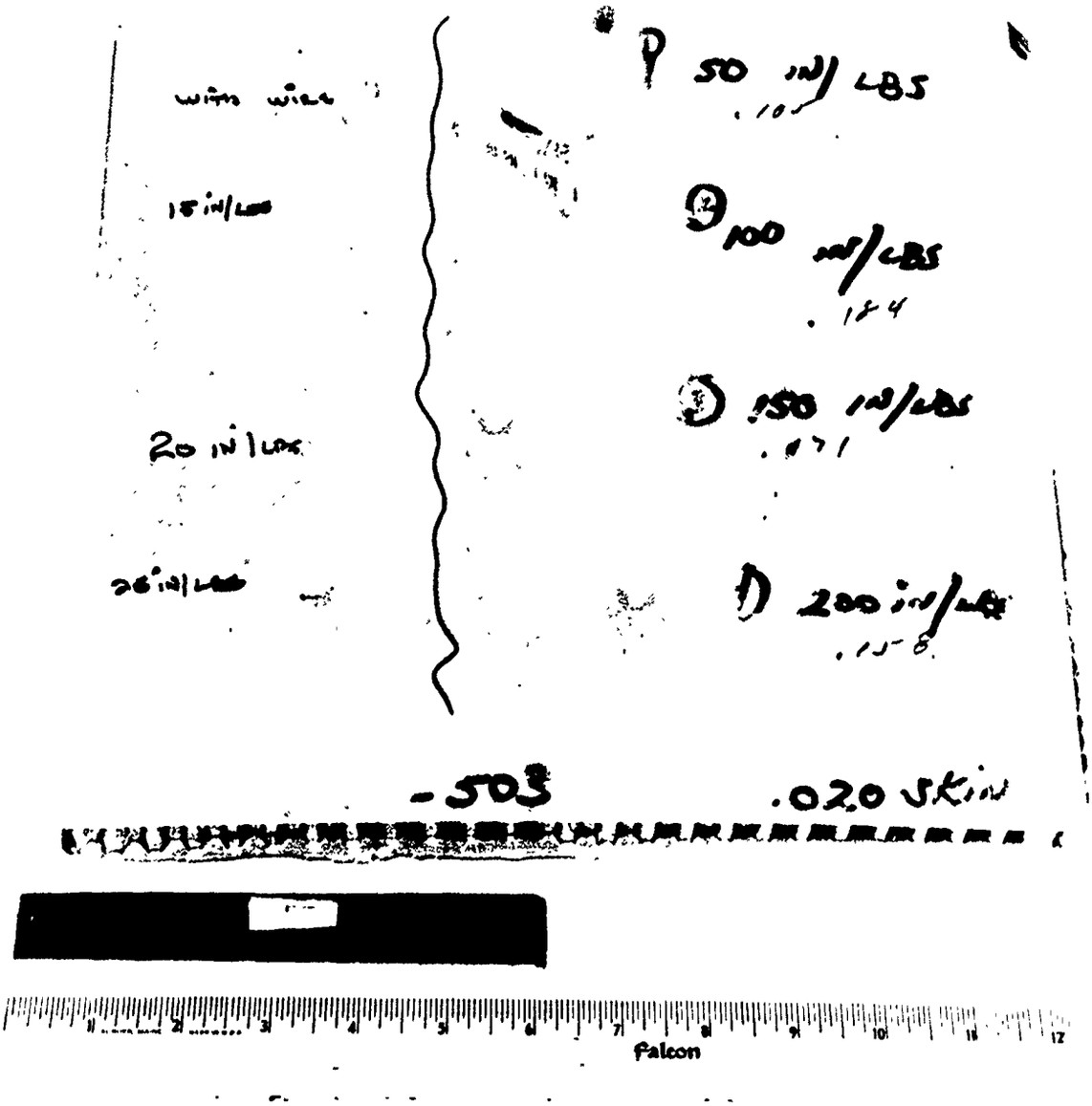


FIGURE A4. HONEYCOMB STIFFENED SKIN PANEL AFTER TESTING

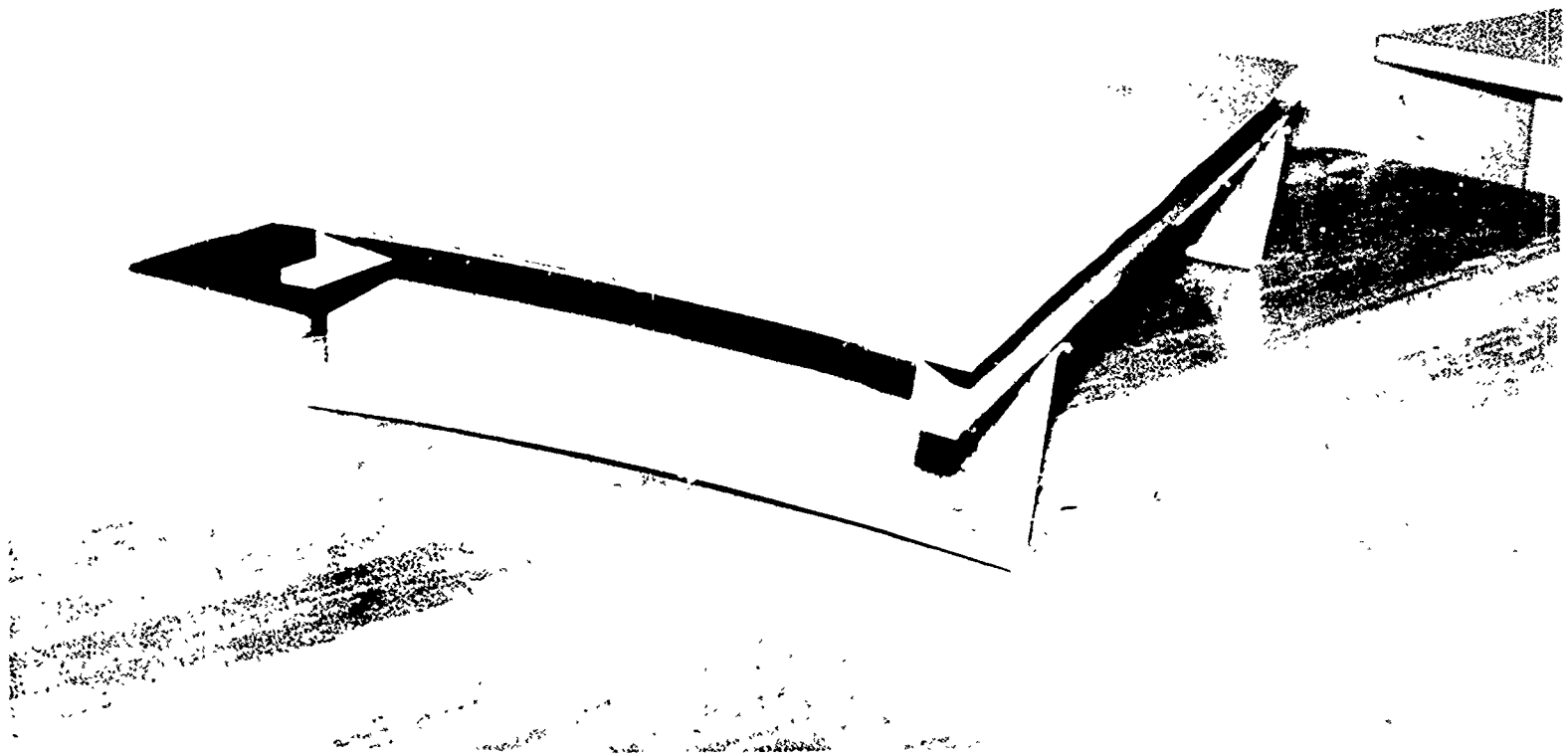


FIGURE A5. LONGERON/FRAME STIFFENED SKIN PANEL AFTER TESTING

Data from Table A1 for the honeycomb stiffened skin panels are graphically shown in Figure A6 along with the data for the longeron/frame stiffened skin panel. These data show that depth of indentation (1) increases as impact energy is increased, (2) decreases as honeycomb cell size is decreased, and (3) is not significantly affected with changes in core density at constant cell size. The ratio of depth of indentation between the highest and lowest impact energies was 1.32 for the longeron/frame stiffened skin panel. This ratio averaged 1.82 for the honeycomb stiffened skin panels with a high of 2.07 and a low of 1.63. A decrease in the honeycomb cell size from 0.25 to 0.188 inch at core densities of 3.4 and 3.1 pcf produced less depth of penetration than an increase in the core density at constant 0.25 inch cell size to 4.3 pcf or 5.2 pcf for the 0.02 and 0.04 face sheets, respectively. Core density change at constant cell size appears to have a significant effect in reducing depth of indentation for the 0.020 inch face sheets but this trend reverses for the 0.032 inch face sheets and is negligible for the 0.040 inch face sheets, at the maximum applied impact energy.

Figure A7 shows the effect of face sheet thickness on depth of indentation for parametric variation in impact energy. Data relevant to honeycomb core are scattered within the bandwidths of impact energy for the honeycomb stiffened skin panels. Therefore, parametric changes in core do not appear to be as significant in reducing depth of indentation as changes in face sheet thickness. The longeron/frame stiffened skin panel data fell well below the honeycomb stiffened skin panel data.

Data from Table A2 are plotted in Figure A8 which shows honeycomb face sheet thickness as a function of impact energy required for skin rupture. At honeycomb core densities of 3.1 to 4.3 pcf, there is little distinction between impact energies required to rupture the skin. These data are shown by a bandwidth. However, an increase in the core density to 5.2 pcf produced a noticeable increase in impact energy required to rupture the skin.

In general, over the range of impact energies applied, honeycomb stiffened skin panels, regardless of the face sheet thickness, core density, or cell size, were dented to an extent that repair would probably be desired from

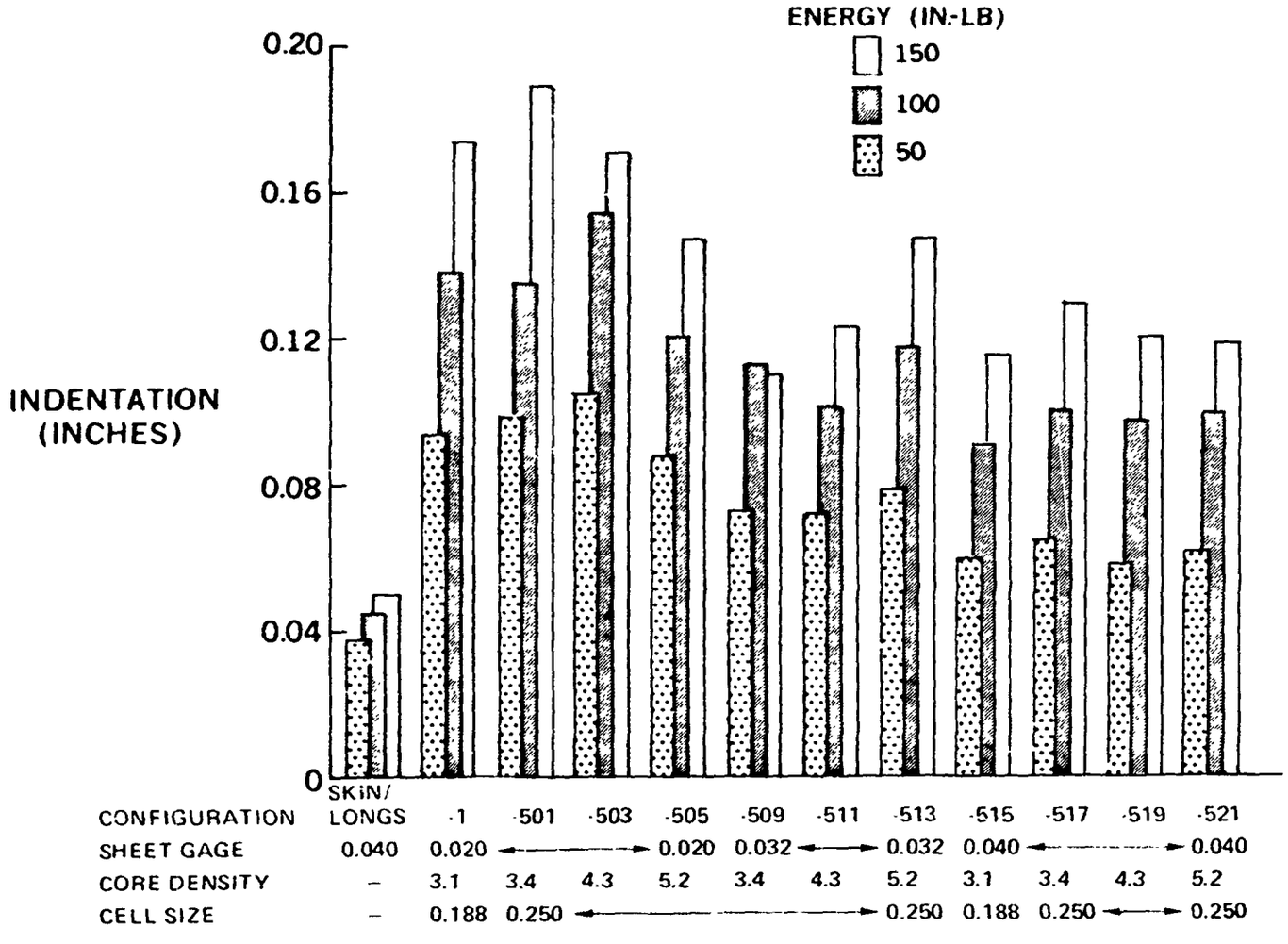


FIGURE A6. EFFECT OF SKIN THICKNESS, CELL SIZE, AND CORE DENSITY ON INDENTATION OF A HONEYCOMB PANEL

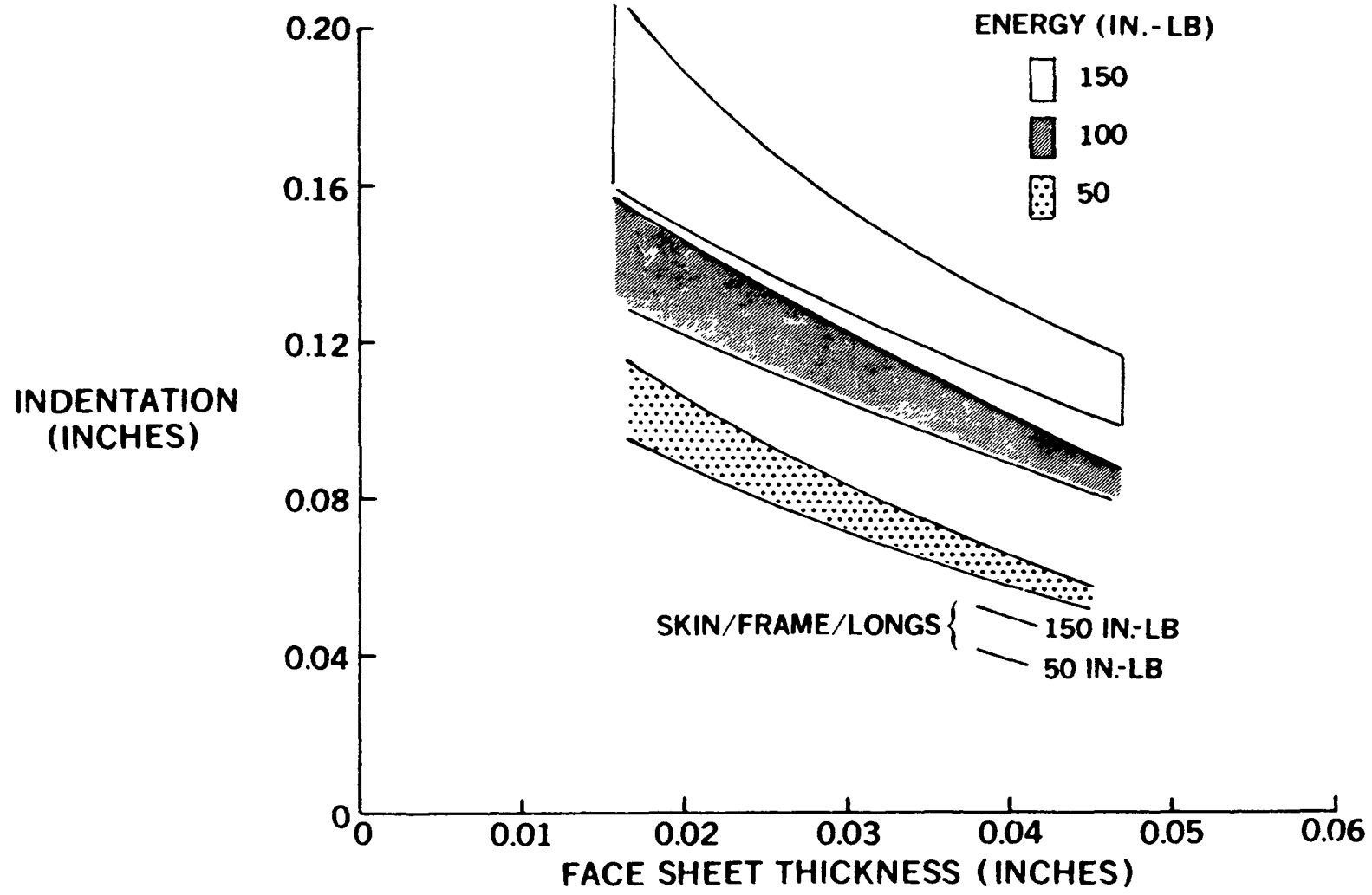


FIGURE A7. EFFECT OF FACE SHEET THICKNESS ON INDENTATION OF A HONEYCOMB PANEL

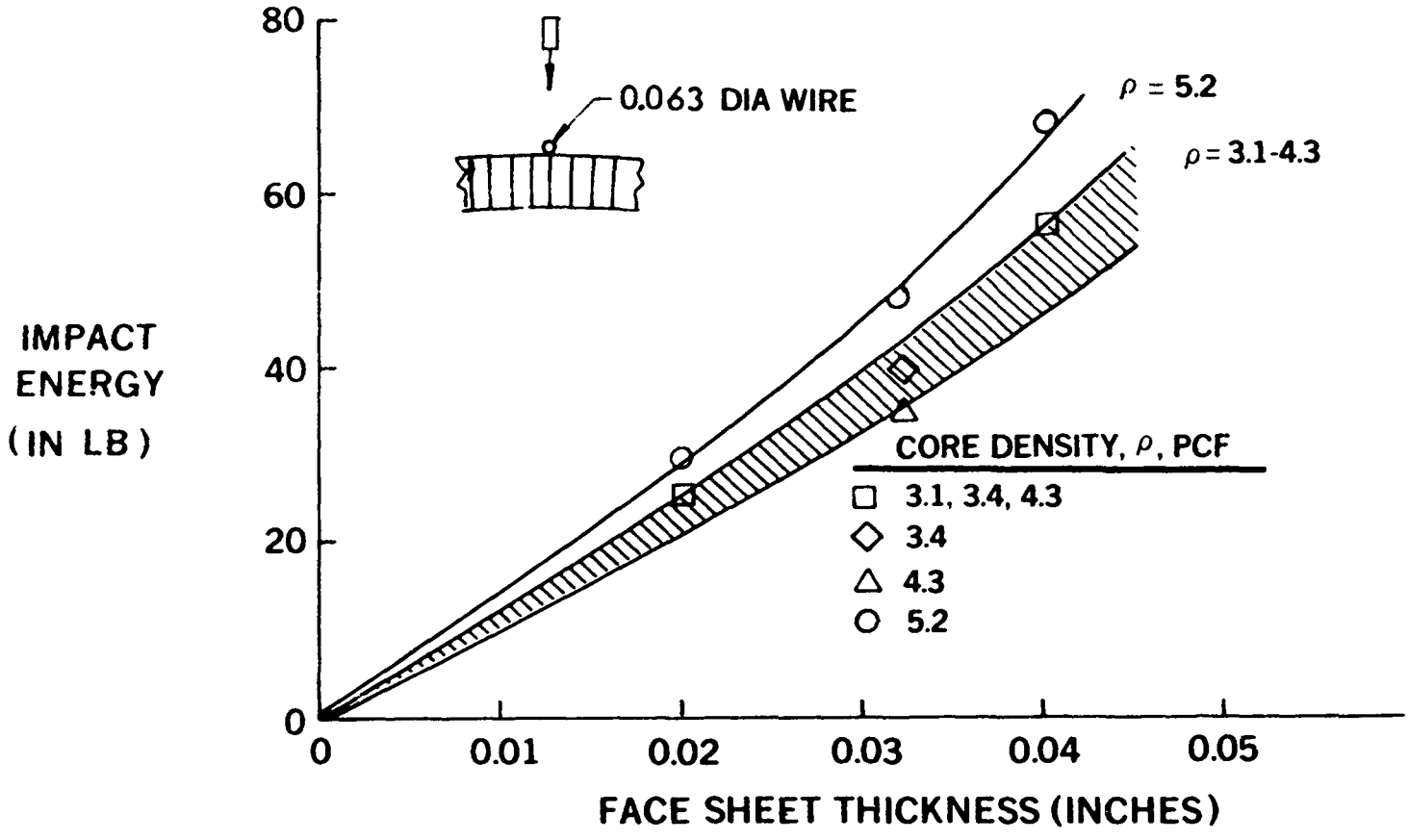


FIGURE A8. IMPACT ENERGY REQUIRED TO RUPTURE HONEYCOMB FACE SHEET

an appearance point of view. Whereas, the longeron/frame stiffened skin panel did not appear to be damaged to an extent that would require repair. This is attributed to the fact that the bending stiffness of the honeycomb stiffened skin panels supplied much more resistance to impact than the thin 0.040 inch thick skin supported by frames and longerons at 24.0 and 12.0 inches, respectively. Therefore, when deciding on the usage of honeycomb stiffened skin panels in primary structure, close attention will have to be given to the cost of repair due to foreign object damage in both manufacture and service. This could be an overriding factor to the apparent weight savings afforded by the honeycomb design concept. A typical type of impact damage is shown in Figures A9 and A10. The honeycomb panel was clamped to a fixture as shown in Figure A9. When the C clamp was loosened, a bearing plate free fell the length of the panel and impacted the 0.020 inch thick inner face sheet with about 50 inch lbs (0.50 pounds from 100 inches). The resultant face sheet rupture is shown in Figure A10.

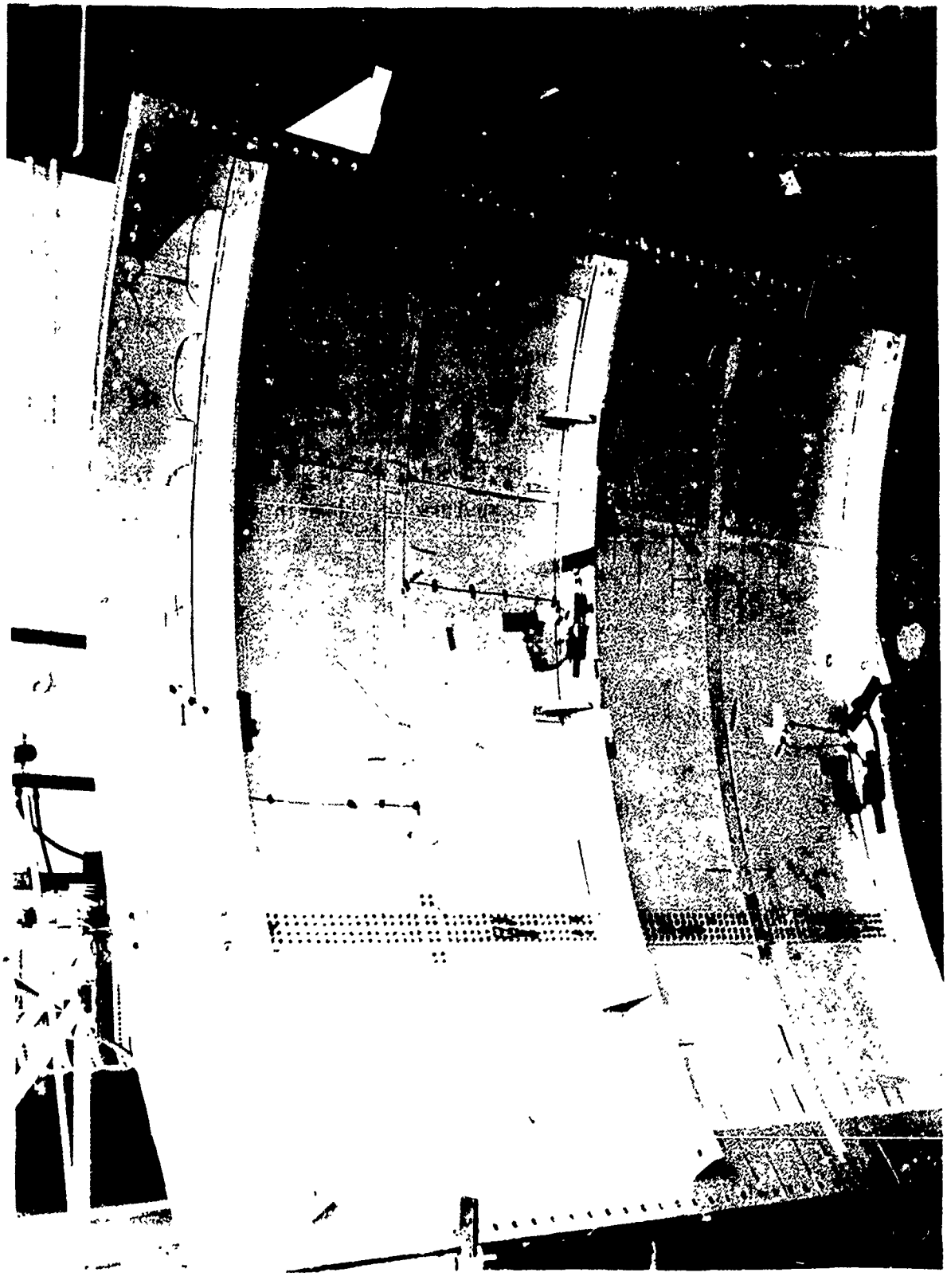


FIGURE A9. HONEYCOMB STIFFENED SKIN PANEL IN SUPPORT FIXTURE

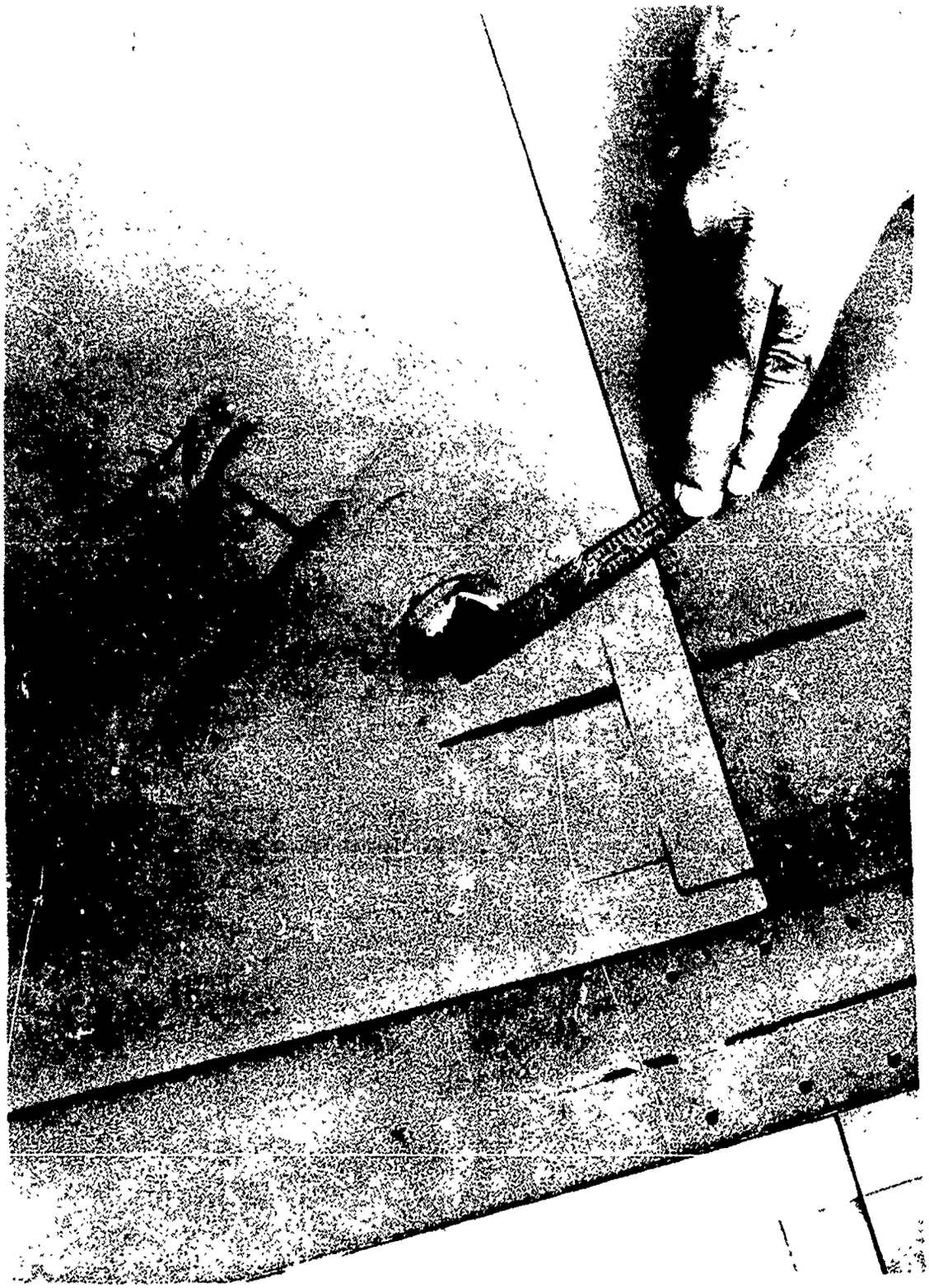


FIGURE A10. CLOSE-UP OF FACE SHEET RUPTURE

Foreign Object Damage

Introduction. - Minimum PABST fuselage skin gages may be required to prevent damage from foreign objects. As an aid toward establishing foreign object damage criteria, a survey was made of the C-130, C-141, Atlantique, DC-8, DC-9 and DC-10 aircraft to determine what skin problems, if any, were encountered in service due to foreign object damage. This survey was used as a guide toward establishing the minimum skin gage requirements for the PABST conceptual studies.

Aircraft Service Data.

C-130: - The C-130 fuselage skin materials are 2024-T3 and 7075-T6 aluminum alloy. The overall minimum skin gage used on the C-130 fuselage is 0.025 inch 7075-T6 aluminum alloy. Minimum skin gage for the fuselage lower belly is 0.040 inch although this was later modified to 0.080 inch.

Data obtained at Warner-Robbins concerning foreign object damage on the C-130 showed that some of the top fuselage skin gages were increased and intercostals were added because of damage experienced by people walking on the top of the aircraft fuselage. The escape hatch forward of the wing was honeycomb at one time but was changed to conventional sheet metal construction because of damage sustained by people walking on the escape hatch.

C-141: - The main landing gear doors and petal doors of the C-141 are aluminum honeycomb construction. These consist of an inboard and outboard door stiffened by two to three inch deep honeycomb and aluminum face sheets. The inboard door face sheet thikcness is 0.032 inch. The outboard door face sheet thickness is 0.020 inch. During landing, the inside surface (.032 inch thick face sheet) of the inboard door is under the belly of the aircraft and exposed to foreign object damage. The petal doors are a box construction consisting of an external and internal sandwich structure. Each of these structures consists of about a half inch thick honeycomb core sandwiched between 0.032 inch thick face sheets.

PRECEDING PAGE BLANK-NOT FILMED

Warner Robbins data on the C-141 with respect to the main landing gear doors and petal doors showed that damage was experienced on the external skin of the petal doors from work stands, ladders, etc. The external skin thickness was increased from 0.020 to 0.032 inch because of this damage. However, the predominant problem on these doors was water entrapment and the resulting corrosion. There was more trouble with the external sandwich structure than the internal sandwich structure of these doors. There may also be a stress problem with them. Some problems were experienced with the inner skins becoming delaminated due to people walking on them when checking the latches. There has been little trouble with the inboard main landing gear door because of foreign object damage during landing. This door is about 14 - 16 inches from the ground during landing and has 0.032 inch thick sheets. The outboard main landing gear door experienced delaminations from people walking on it. However, dings are not usually made from people walking on the 0.020 inch thick outboard main landing gear door face sheets. In addition to door damage, wing damage was experienced on the leading edge that is fabricated using sandwich construction with an 0.040 inch thick outer skin, that is chem-milled to a minimum thickness of 0.020 inch. The primary cause of damage has been from ladders and work stands. The skin gage was increased to a constant 0.040 inch which apparently was still insufficient.

Atlantique: - The following data was obtained from FOKKER concerning the sandwich structure of the Atlantique aircraft fuselage:

> The greater part of Atlantique aircraft fuselage is sandwich-structure with 0.5 mm (.0197 inch) face sheets, 1/4 inch cell size, and 0.0015 inch cell wall thickness. Same configuration is used on main undercarriage doors and bomb doors. Small hatch doors have 0.4 mm (.016 inch) faces.
>
> All mentioned components suffered considerable damage from ground handling by contact with steps, scaffolding, etc., during usage and maintenance. Also, walking on fuselage caused damage. Aircraft are used on well paved and clean runways, so stone damage only is very limited. Experience with FOKKER aircraft operating from unpaved runways

indicates that honeycomb structures suffer store damage in areas behind and adjacent to undercarriage. As far as satisfactory configurations are concerned, it is only known that the damage to the parts with thicker faces 0.8 mm (0.0314 inch) and up has been less. However, these components, such as stabilizers and wing panels, are on much less vulnerable locations.

DAC Commercials: - The DC-8, DC-9 and DC-10 wing trailing edge panels are honeycomb assemblies having face sheet thicknesses of 0.012, 0.016 and 0.020 inch. The flap vane is a honeycomb assembly with 0.016 inch thick face sheets and 0.188 inch cell size honeycomb. The DC-10 horizontal stabilizer trailing edge has .020 inch face sheet stiffened by honeycomb. In regards to the DC-8, DC-9 and DC-10 wing trailing edge panels, Douglas has had no foreign object damage reported from the airlines.

Douglas Customer Service data, with regard to foreign object damage on the DC-8, DC-9 and DC-10 showed that the flap vane receives damage from foreign objects that are propelled by the wheels, but this damage is repairable. The trailing edge of the DC-10 horizontal stabilizer has experienced no problems. Spoiler tabs and flap vanes of the DC-9 have no reported history of foreign object damage.

The DC-10 floors are made from thin face sheets (0.004-0.020 inch) bonded to nomex and balsa wood core having densities of 3 to 8 pcf. An extensive development test program was performed in selection of these floors that covered a wide spectrum of service life requirements (Cart Roller, Static Bending and Shear, Concentrated load, Peel, Impact resistance, damage tolerance, etc.). To date, no major service problems have been found on the DC-10 floors because of foreign object damage.

Minimum Honeycomb Face Sheet Thickness: - Based solely on strength requirements, the honeycomb sandwich concept for the PABST ADP Component requires face sheet thicknesses that are much less than those required for the longitudinally stiffened skin ADP Component. Considerable service experience has demonstrated that the longitudinally stiffened skin thicknesses are adequate, if not more than adequate, to resist foreign object damage. However,

some concern has been expressed over the resistance of the thin faced honeycomb sandwich panel skins to foreign object damage. With reference to the preceding aircraft service data, proposed minimum face sheet thicknesses for the honeycomb sandwich concept are 0.020 inch for the interior surface and 0.032 inch for the exterior surface.

An 0.020 inch face sheet was selected as minimum for the interior skin because in the C-15 it will be protected, for insulation purposes, by a blanket material that consists of 4 inch thick batting (0.6 pcf) covered with a tedlar aluminum and nylon material (0.0083 psf/side). The under floor internal area of the fuselage may be vulnerable to damage from dropped objects. However, maximum drop distance from the lower surface of the floor to the interior skin is 29.5 inches. At this distance, the 4 inch blanket will provide sufficient energy absorption to protect an 0.020 inch thick face sheet against reasonable sized maintenance tools or foreign objects (about a pound or less) that are dropped. The interior skin and side skin surfaces above the floor are also protected by the blanket. Their physical position relative to the floor minimizes the probability of foreign object damage.

The exterior minimum skin thickness was set at 0.032 inch in order to minimize the damage that may occur when workmen are doing maintenance and repair work. It is believed that 0.016 inch thick face sheet thickness is adequate for walking on sandwich surfaces. This conclusion is based on the fact that the DC-10 floors have 0.016 inch thick face sheets. Numerous tests have been conducted to establish that this thickness is adequate for flooring of an aircraft with respect to human foot traffic. However, the probability of dropped tools, ladders, and workstands impacting the exterior surface is very high. Most exterior surfaces on the surveyed aircraft are 0.032 inch or better in areas where maintenance and repair traffic are heavy. For this reason, 0.032 inch thick exterior face sheets was proposed for the majority of the fuselage. The fuselage belly outer surface is most vulnerable to damage from foreign objects. This is especially so just aft of the nose gear wheels. An exterior face thickness of 0.040 inch is proposed in this area because of experience at FOKKER on landings on unimproved landing fields.

Honeycomb Core Thickness Study

Summary. - Weighted average honeycomb core thickness for the PABST honeycomb concept was determined to be 0.80 inch based on compression-shear interaction. Minimum core thickness was determined to be 0.30 inch based on pressurization requirements.

Purpose. - This study was conducted to determine the honeycomb core thickness to be used for the PABST honeycomb concept.

Procedure. - Honeycomb core thickness is influenced by compression and shear interaction on the surface of the fuselage shell and by pressure loads normal to the fuselage shell. Structurally, it is advantageous to have constant core thickness over the entire shell in order to minimize eccentricities and simplify splices. In order to obtain this structural advantage without introducing a weight penalty, honeycomb core thickness selection was based on consideration of the average load spectrum over the entire fuselage shell. Evaluations were made to establish a representative core thickness which would (1) resist pressure loads and (2) meet compression and shear interaction requirements.

In order to quantify compression and shear interaction, nine check points were selected along the fuselage length at fuselage stations 463, 655, and 887. Compression and shear loads that produced maximum interaction were obtained for these check points from the YC-15 internal loads analysis. Ultimate pressure load normal to the fuselage shell surface was 14.3 psi (2p) based on the YC-15 criteria. With these loads for pressure, compression and shear, core thickness was determined such that panel weight was minimum subject to the constraints that minimum face sheet thickness was 0.016 inch corresponding to a 24,000 psi hoop tension stress at limit pressure (1p) and that core density was 3.4 pcf which is adequate for face wrinkling, intercell buckling, and flexural shear.

Pressure Loads: - Bending moments and flexural shears are introduced in the fuselage shell around the circumference because of frame interaction with the shell under applied normal loads. These loads are maximum at the frames.

Axial loads are introduced in the shell due to pressure at the ends of the shell. The honeycomb core resists the flexural shear loads. The face sheets resist the circumferential bending moments and the axial loads. Interaction between these loads for the overall honeycomb panel is approximated by the equation $(R_a + R_b)^2 + R_s^2 = 1.0$ where R_a, R_b, and R_s are the stress ratios (applied stress-to-allowable stress) for axial load, bending moment, and flexural shear.

Applied loads of shear and bending moment were computed based on the classical solution for a long cylinder subject to internal pressure. This solution expresses the continuity between frame and shell. Thus, the circumferential moment in the shell at the frames is

$$M_o = \frac{PR^2 (1 - 0.5\nu)}{Et\left[\frac{1}{2\beta^2 D} + \frac{4\beta R^2}{EA}\right]}$$

where for honeycomb skin panels

$$\beta = \left[\frac{1 - \nu^2}{R^2 h^2}\right]^{1/4}$$

$$D = \frac{Et_f h^2}{12\,(1-\nu^2)}$$

$$t = 2t_f$$

t_f = Face Sheet thickness, in

and
- A = Area of Frame, in^2
- E = Face sheet modulus of elasticity, in^2
- h = Distance between face sheet centroids, in
- p = Internal pressure, psi
- R = Mean shell radius of curvature, in
- ν = Poissons ratio

The circumferential shear in the shell at the frames is

$$Q_o = 2\beta M_o$$

Applied axial stress is given by the boiler formula.

$$\sigma = .5pR/t$$

Allowable face sheet stress was taken as F_{tu} = 66,000 psi ("B" value) from MIL-HDBK-5a for bare 2024-T3 aluminum material. Allowable shear stress was taken as 230 psi from American Cyanamid data for 5056 aluminum core with 3.4 pcf density and 0.25 inch cell size.

Based on the interaction equation and the relationship for applied shear, moment, and axial stress, applied shear stress was calculated to produce zero margin of safety for variations in core thickness. Figure A11 shows a plot of these data along with a plot of applied shear stress. The intersection of the two curves gives the minimum core thickness for zero margin of safety. This value is about 0.3 inch.

Compression and Shear Interaction: - For honeycomb panels, interaction is given in MIL-HDBK-23a as $R_c + R_s = 1.0$ where R_c and R_s are the stress ratios for compression and shear. Applied compression and shear loads are given in Table A3 for the nine fuselage check points along with the core thickness and face sheet thickness combination which produced minimum panel weight with zero margin of safety in the interaction equation. These values of core thickness and face sheet thickness were obtained by an iteration procedure which made use of the allowable loads shown in Figures A12 and A13 for compression and shear. Generally, minimum weight was obtained for the smallest face sheet thickness which would meet the compression load requirements.

Figure A14 shows honeycomb panel weight plotted as a function of core thickness for parametric variations in face sheet thickness. The relative flatness of the weight curve for constant face sheet thickness is an indication that smallest face sheet thickness will give least weight. Weight values for the nine check points are superimposed on the honeycomb panel weight plot. Loads interaction criteria for most of the check points was

satisfied with minimum face sheet thickness. Core thicknesses ranged from 0.3 to 0.8 inch. The two highest load conditions required 0.032 and 0.040 inch face sheets, respectively with 0.78 and 1.20 inch core thickness.

Based on the weight values and core thicknesses required for the nine check points, a weighted core thickness for the fuselage shell was determined as

$$h_{av} = \Sigma_1^9 W_i h_i / \Sigma_1^9 W_i$$

Where W_i is the panel weight and h_i is the core thickness for each of the check points. Figure A15 shows the core thickness for the nine check points along with the weighted average core thickness which was 0.74 inch. For the honeycomb concept study, the core thickness was taken at a constant 0.80 inch for the entire fuselage shell.

TABLE A3. HONEYCOMB PANEL REQUIRED FOR MINIMUM WEIGHT

FUSELAGE STATION	← 463 →			← 655 →			← 887 →		
CHECK POINT	1	2	3	4	5	6	7	8	9
COMPRESSION LOAD, #/IN	277	300	126	559	570	458	267	659	1095
SHEAR LOAD, #/IN	195	378	13	91	266	339	15	2163	639
MINIMUM CORE THICKNESS FOR ZERO M.S., IN	.49	.72	.30	.50	.75	.77	.30	1.21	.78
FACE SHEET THICKNESS, IN	.016	.016	.016	.016	.016	.016	.016	.040	.032
PANEL WEIGHT PSF	.604	.670	.550	.607	.670	.683	.550	1.506	1.152

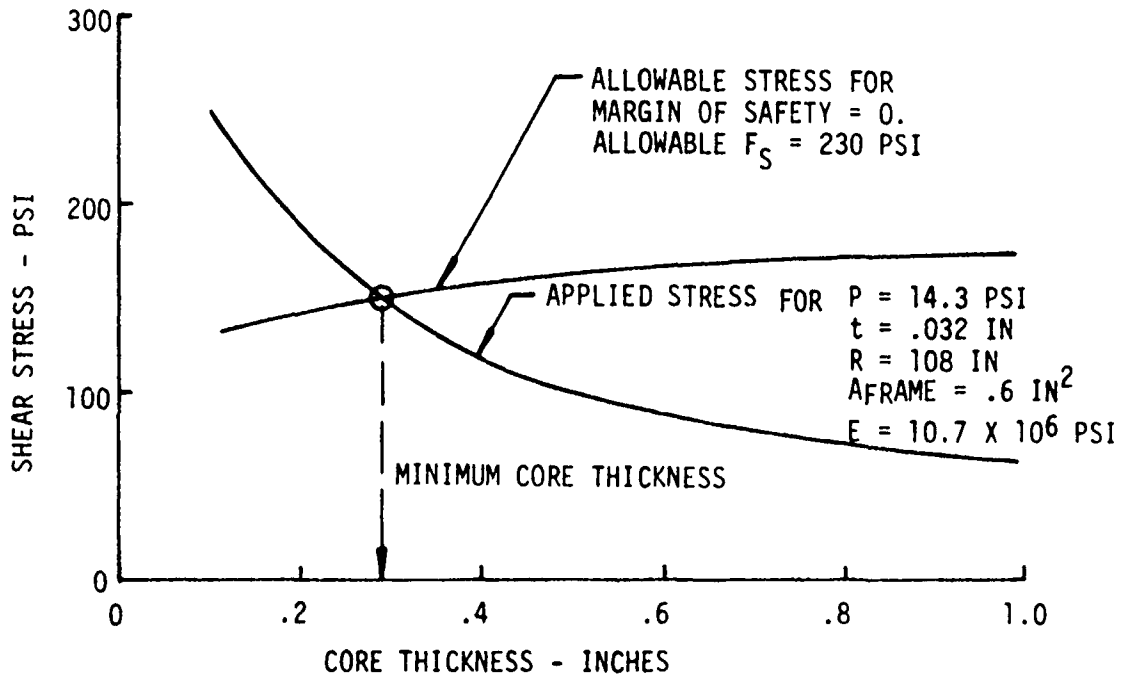


FIGURE A11. MINIMUM CORE THICKNESS REQUIRED FOR FUSELAGE PRESSURE

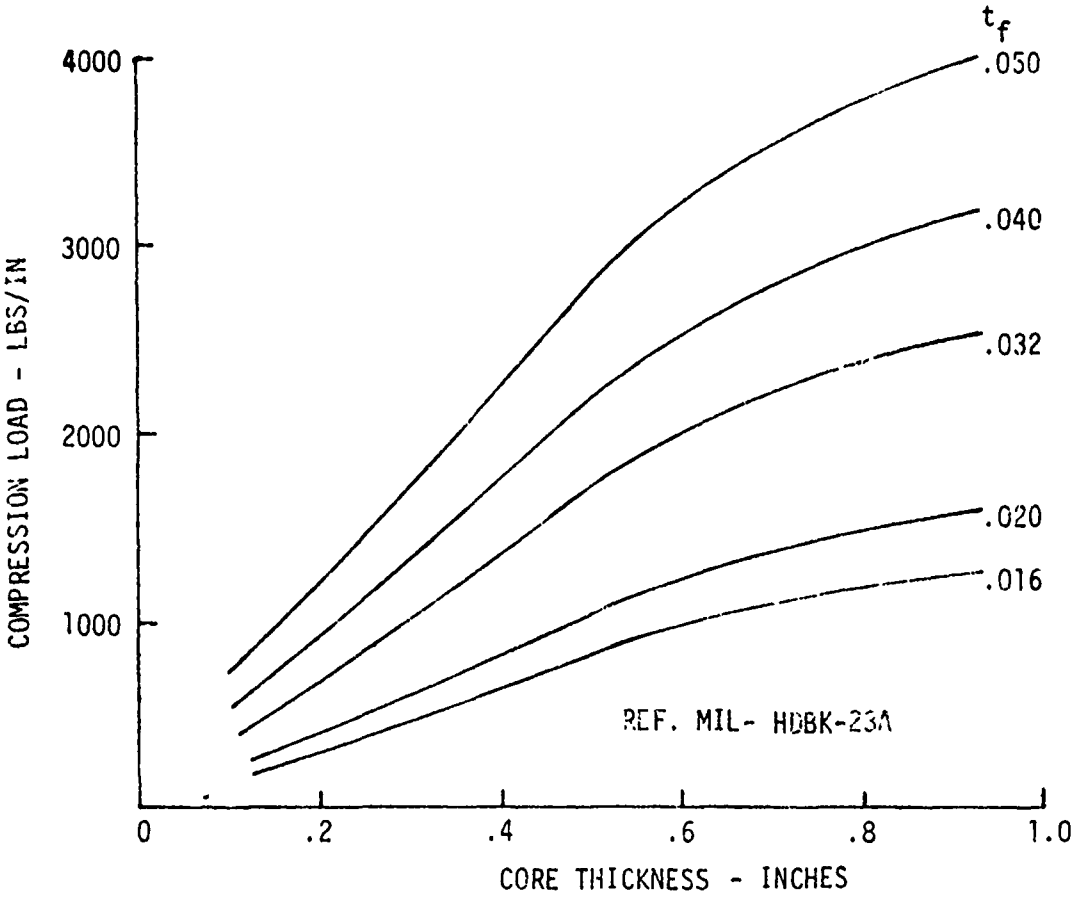


FIGURE A12. HONEYCOMB PANEL COMPRESSION LOAD CAPABILITY

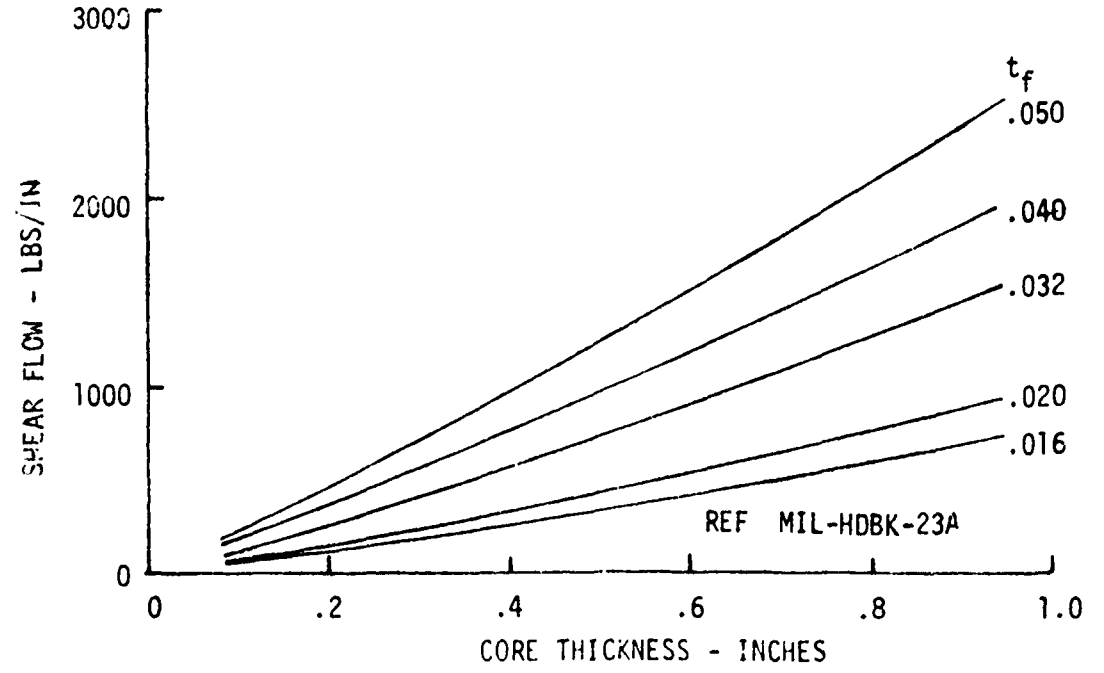


FIGURE A13. HONEYCOMB PANEL SHEAR LOAD CAPABILITY

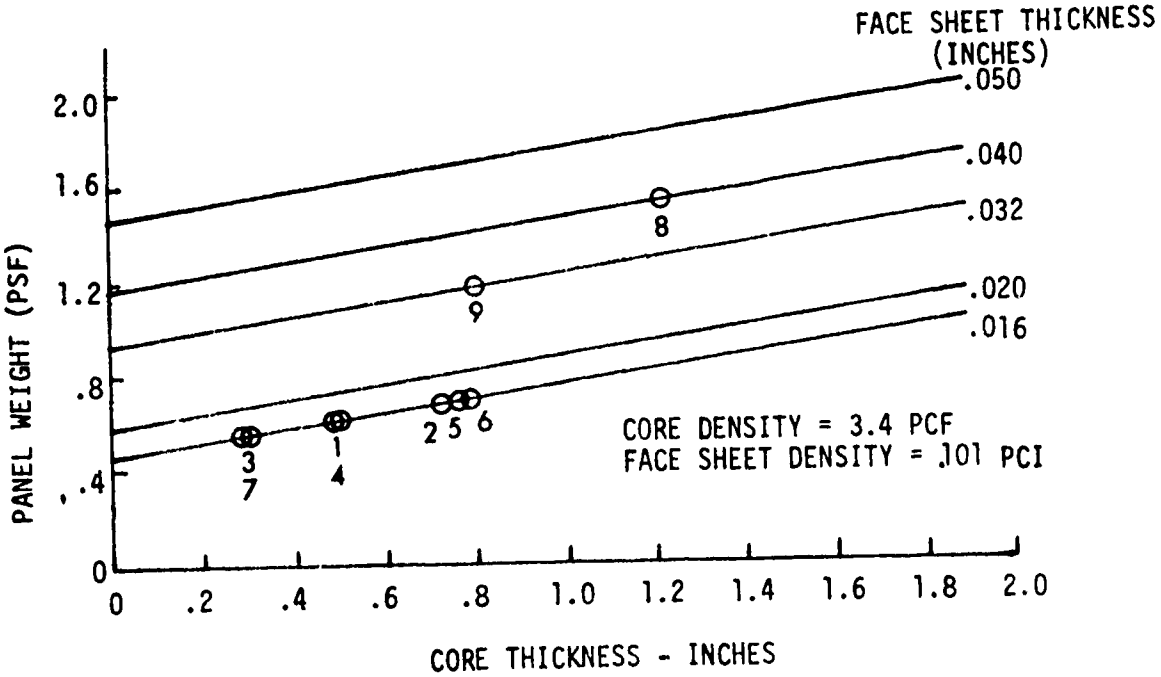


FIGURE A14. HONEYCOMB PANEL WEIGHT FOR VARIATIONS IN CORE THICKNESS AND FACESHEET THICKNESS

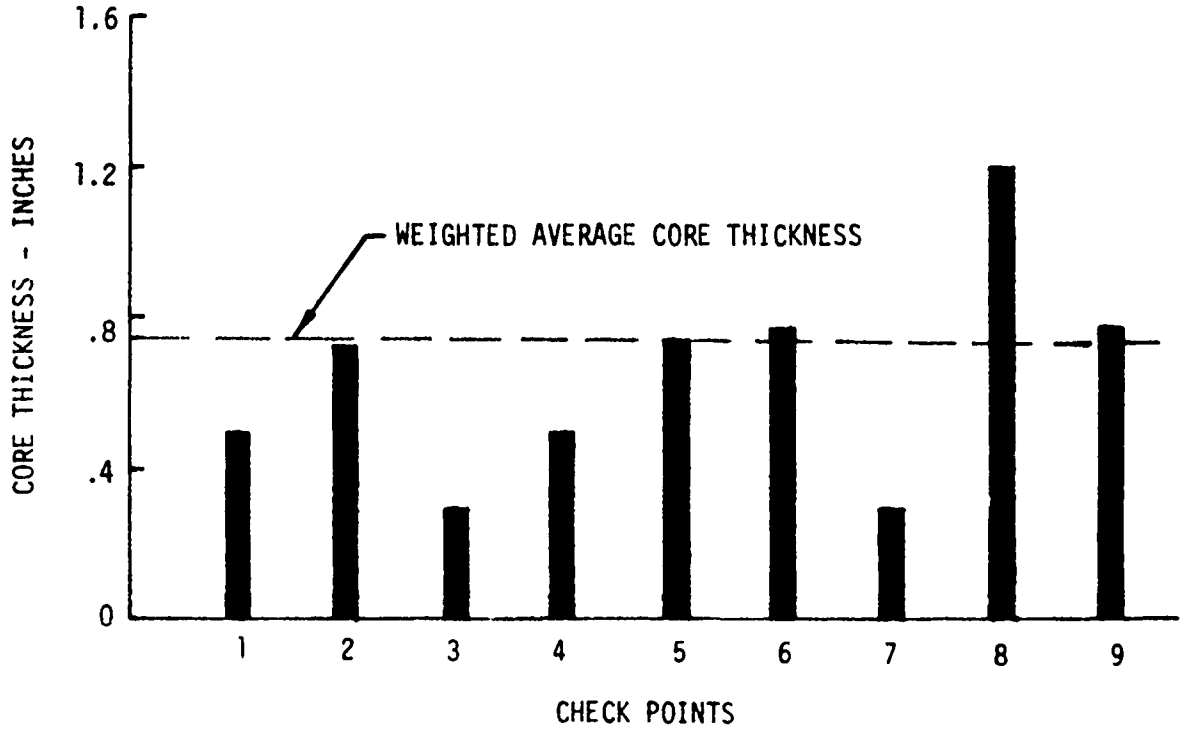


FIGURE A15. CORE THICKNESS REQUIRED FOR COMPRESSION/SHEAR INTERACTION

Honeycomb Edge Member Trade Study

Summary. - Four edge member concepts; high density core, potted edge, solid bar, and channel section were evaluated based on weight, reliability and cost. The solid bar concept was selected as the design concept because of its reliability and low cost.

Purpose. - This trade study was conducted to determine the most efficient edge member design for honeycomb skin panels with respect to weight, reliability, and cost. The concepts evaluated are shown in Figure A16. They are (1) high density, 55 pounds per cubic foot, honeycomb core, (2) potted edge, (3) solid bar, and (4) channel section. Two potted edge member designs were considered; (a) solid potting compound and (b) low density core filled with potting compound. For the solid bar edge member, alternate concepts were considered with extruded and machined slots to reduce the weight. Both extruded and sheet metal channel sections were evaluated. For cost purposes, the edge member concepts were assumed to tie to the face sheets through a two layered stepped doubler arrangement. Three doubler concepts, shown in Figure A17were cost evaluated; chem milled doublers integral with the skin, separate chem milled doubler bonded to the skin, and two doublers separately bonded to the skin.

Fastener Selection. - Qualitative evaluations were made of the honeycomb edge concepts (high density and potted edge) to determine fastener installation problems. Specimens were manufactured from 0.80 inch thick high density honeycomb core sandwiched between face sheets having thicknesses ranging from 0.020 to 0.050 inch with corresponding edge doubler thickness. Lockbolts, Hi-Loks, and AD rivets were installed in these specimens to simulate actual production fastener installations. The lockbolts were installed with and without washers under the heads and collars. Table A4 shows the results of these tests. Of the three fasteners, Hi-Loks were determined to be the only acceptable fastener. The rivets expanded in the core and had small upset heads. Lockbolt installation produced dimpling of the thin face sheets. Specimens were made with potted edges in place of the high density core which produced similar results. Hi-Loks proved to be the acceptable fastener for the potted edge concepts.

PRECEDING PAGE BLANK-NOT FILMED

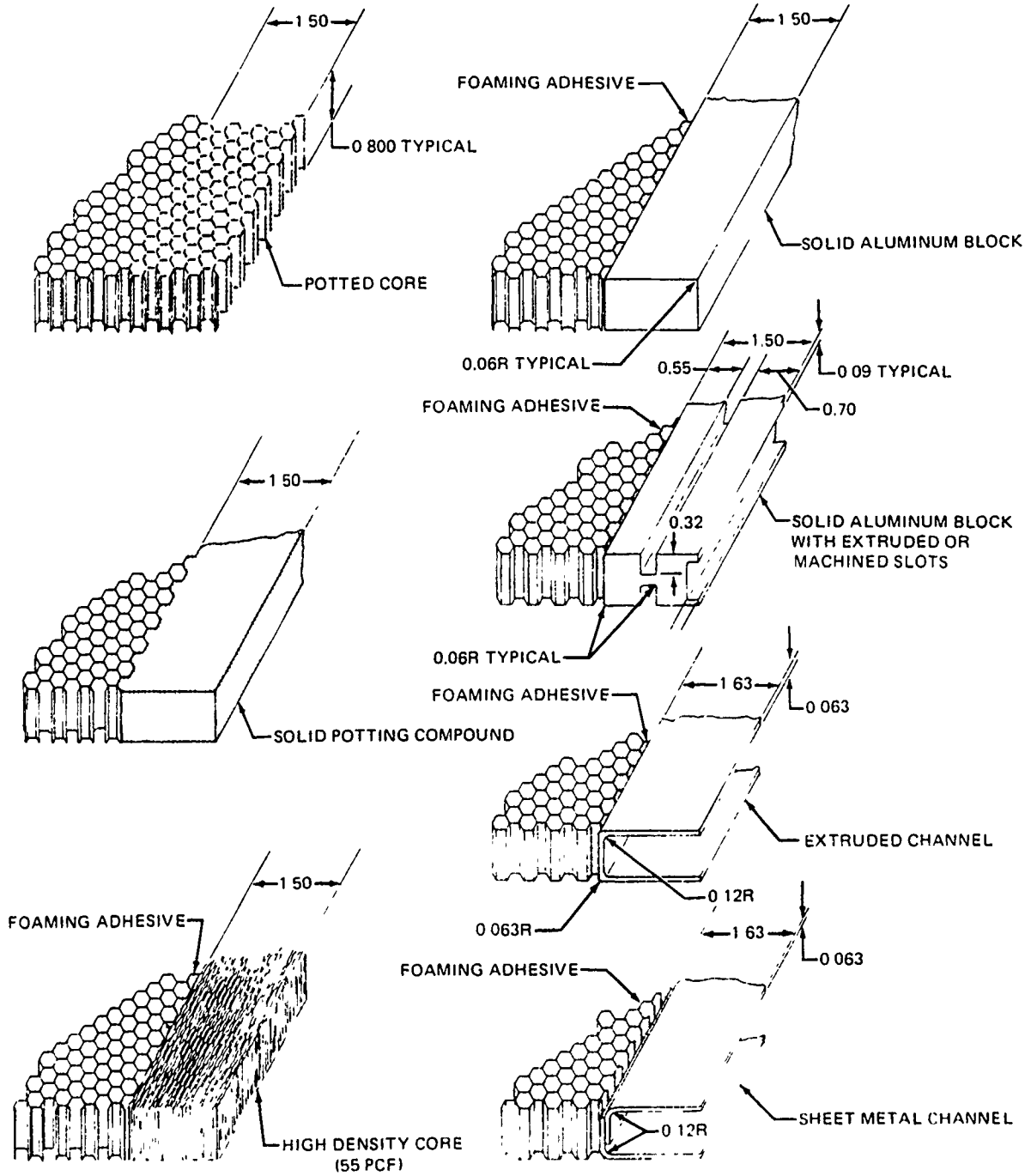
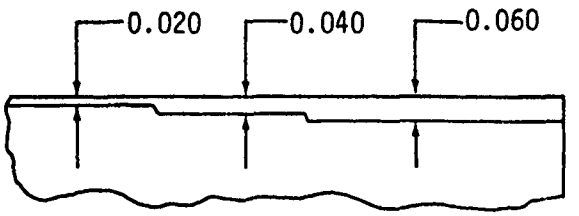


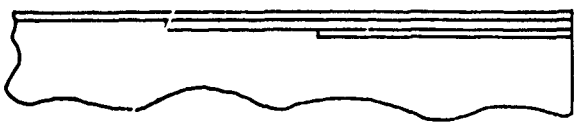
FIGURE A16. HONEYCOMB PANEL EDGE MEMBERS



CHEM MILLED SKIN/DOUBLER
(ONE PIECE)



SKIN AND CHEM MILLED DOUBLER
(TWO PIECES)



SKIN AND LAMINATED DOUBLER
(THREE PIECES)

FIGURE A17. EVALUATED SKIN AND DOUBLER CONFIGURATIONS

TABLE A4. FASTENER INSTALLATION IN HIGH DENSITY HONEYCOMB CORE (0.80 INCH THICK)

ITEM	DESCRIPTION		FASTENERS	WASHERS	COMMENTS	RATING
	FACE SHEET	DOUBLERS	0.188" DIA			(1)
1	.020	.020	AD Rivet	None	Rivets expanded in core which resulted in small upset head	U
2			Lockbolt	None	Dimpled face sheets	U
3	.020	.020	Hi-Lok	None	No Dimpling	A
4	.025	.025	Lockbolt	None	Dimpled face sheets	U
5			Lockbolt	.032	Dimpled face sheets	U
6			Lockbolt	.063	Dimpled face sheets	U
7	.025	.025	Hi-Lok	None	No dimpling	A
8	.032	.032	Lockbolt	None	Slightly dimpled face sheets	U
9			Lockbolt	.032	Slightly dimpled face sheets	U
10			Lockbolt	.063	Slightly dimpled face sheets	U
11	.032	.032	Hi-Lok	None	No dimpling	A
12	.040 inner .050 outer	.040 inner .050 outer	Lockbolt	None	Slightly dimpled face sheets	U
13			Lockbolt	.032	Slightly dimpled face sheets	U
14			Lockbolt	.063	Slightly dimpled face sheets	U
15	.040 inner .050 outer	.040 inner .050 outer	Hi-Lok	None	No dimpling	A

(1) A Acceptable
U Unacceptable

TABLE A5. WEIGHT COMPARISON BETWEEN EDGE MEMBER CONCEPTS

CONCEPT	WEIGHT PPF	WEIGHT RATIO Wi/Wb	PANEL WEIGHT PSF	RELATIVE PANEL WEIGHT Pi/Pb
SOLID BAR	1.45	1.27	1.26	1.07
SOLID BAR/SLOTS	1.14	1.00	1.18	1.00
HIGH DENSITY CORE	0.46	0.40	1.01	0.86
POTTED EDGE	0.42	0.37	1.00	0.85
CHANNEL SECTION	0.30	0.26	0.96	0.81

Wi = Concept Weight
Wb = Base Weight (Solid bar with slots)
Pi = Panel Weight
Pb = Base Panel Weight (Solid bar with slots)
PPF = Pounds per foot
PSF = Pounds per square foot

Weight. - Edge member concepts were evaluated for weight potential with respect to each other and with respect to impact on the total honeycomb panel weight. Results of this comparison are shown in Table A5. The concept ratings from least weight to most weight are channel section, potted edge, high density core, solid bar with slots, and solid bar. The least weight edge member concept, the channel section, is 74 percent lighter than the extruded solid block with slots, based solely on edge member weight. With respect to overall honeycomb panel weight for the entire study fuselage, this weight difference is 19 percent.

Reliability. - In regard to reliability of the edge member concepts, the concepts in order of preference were rated solid bar, potted core, high density core, and channel section. Solid bar was preferred because fastener installation was similar to conventional structure which has performed well in the past. Potted core has been used successfully, but care must be taken to provide proper proportioning, mixing, and application of the potting compound. Too high fastener torque can produce cracking of the potting compound which is uninspectable. There was a high degree of reluctance to install fasteners in honeycomb with low or high density core because this provides an entry point for moisture. The moisture freezes at reduced temperatures and gradually opens additional entry points for moisture. The final result, caused by repeated aircraft climb and decent is delamination of the bond and in some instance corrosion of the core or face material. The channel section concept required blind lockbolt fasteners which are always suspect from a reliability point of view since they cannot be inspected.

Cost. - Cost analyses were performed for the three solid bar concepts, the two channel section concepts, and the two potted edge concepts. All concepts were evaluated with the three skin/doubler approaches. These costs are shown in Table A6 expressed in 1976 dollars for both labor and material. Labor costs are broken down into four categories; fabrication, bond assembly, mechanical assembly, and tooling. Material costs are shown for the edge member, skin/doubler, and fasteners. Quality assurance was evaluated for each configuration. No significant quantitative cost difference existed among the configurations so this cost was omitted.

TABLE A6.

LABOR AND MATERIAL COSTS FOR GIVEN CONFIGURATIONS OF HONEYCOMB PANEL EDGES

JANUARY 1976 DOLLARS
CUMULATIVE AVERAGE 300 UNITS

CASE NO	DESIGN CONFIGURATION	LABOR					MATERIAL				GRAND TOTAL
		FABRICATION	ASSEMBLY BOND	ASSEMBLY MECHANICAL	TOOLING	TOTAL	EDGE MEMBER OR POTTING	SKIN & DOUBLER	FASTENER	TOTAL	
1	POTTED HONEYCOMB WITH CHEM MILL SKIN/DOUBLER	121	1577	5077	88	10,700	34	182	14	230	7,093
2	POTTED HONEYCOMB WITH CHEM MILL DOUBLER	115	1822	5077	39	10,890	34	57	14	105	7,158
3	POTTED HONEYCOMB WITH LAMINATED DOUBLER	91	2020	5077	38	11,065	34	56	14	104	7,332
4	POTTED EDGE HONEYCOMB WITH CHEM MILL SKIN DOUBLER	121	1640	5077	88	10,763	34	182	14	230	7,156
5	POTTED EDGE HONEYCOMB WITH CHEM MILL DOUBLER	115	1885	5077	39	10,953	34	57	14	105	7,221
6	POTTED EDGE HONEYCOMB WITH LAMINATED DOUBLER	91	2020	5077	38	11,063	34	56	14	104	7,330
7	SOLID BAR WITH CHEM MILL SKIN/DOUBLER	1219	1413	2816	200	5,648	84	182	14	280	5,928
8	SOLID BAR WITH CHEM MILL DOUBLER	1213	1658	2816	150	5,837	84	57	14	155	5,992
9	SOLID BAR WITH LAMINATED DOUBLER	1189	1856	2816	149	6,010	84	56	14	154	6,164
10	SOLID BAR MACHINED SLOTS WITH CHEM MILL SKIN/DOUBLER	1281	1413	2816	200	5,710	84	182	14	280	5,990
11	SOLID BAR MACHINED SLOTS WITH CHEM MILL DOUBLER	1275	1658	2816	150	5,899	84	57	14	155	6,054
12	SOLID BAR MACHINED SLOTS WITH LAMINATED DOUBLER	1251	1856	2816	149	6,072	84	56	14	154	6,226
13	SOLID BAR EXTRUDED SLOTS WITH CHEM MILL SKIN/DOUBLER	1219	1413	2816	200	5,648	65	182	14	261	5,909
14	SOLID BAR EXTRUDED SLOTS WITH CHEM MILL DOUBLER	1213	1658	2816	150	5,837	65	57	14	136	5,973
15	SOLID BAR EXTRUDED SLOTS WITH LAMINATED DOUBLER	1189	1856	2816	149	6,010	65	56	14	135	6,145
16	CHANNEL EXTRUSION WITH CHEM MILL SKIN/DOUBLER	1456	1413	7311	204	10,384	17	182	152	351	10,735
17	CHANNEL EXTRUSION WITH CHEM MILL DOUBLER	1450	1658	7311	155	10,574	17	57	152	226	10,800
18	CHANNEL EXTRUSION WITH LAMINATED DOUBLER	1426	1856	7311	154	10,751	17	56	152	225	10,976
19	SHEET METAL CHANNEL WITH CHEM MILL SKIN DOUBLER	259	1471	7311	142	9,183	11	182	152	343	9,526
20	SHEET METAL CHANNEL WITH CHEM MILL DOUBLER	253	1715	7311	92	9,371	11	57	152	220	9,591
21	SHEET METAL CHANNEL WITH LAMINATED DOUBLER	229	1937	7311	88	9,565	11	56	152	219	9,784

Fabrication costs included a single edge member 196 inches long located in the non-constant section of the fuselage. Only the outside skin of the honeycomb panel and the two adjacent doublers were considered for fabrication. All the necessary heat treatment, cutting, machining, forming, and checking operations are included in the fabrication estimate.

Bond assembly includes the edge member, inside and outside skin and doublers, and honeycomb core. Mechanical assembly includes drilling, fitting and installation of fasteners for two panels with a joint 196 inches in the longitudinal direction of the non-constant section of the fuselage. Two rows of fasteners 1.0 inch on center were considered. Fasteners were installed dry.

Tooling costs include design and fabrication necessary for one ship-set of tools to support fabrication, bond assembly and mechanical assembly.

Material costs include edge members, outside skin and two adjacent doublers, and fasteners used to join two panels 196 inches long. It does not include the honeycomb core, inside skin and doubler, interior or exterior splice doublers, and the adhesives for hot or cold bond.

Results of the cost analyses show with regard to skin and doubler arrangement that the integrally chem milled doubler is the lowest cost of the three arrangements. With regard to edge concepts, the potted core concept is more costly than the solid bar concept because of the high cost of mechanical assembly for Hi-Lok fasteners (about 70 percent of the total cost). In addition, it is concluded that the high density core concept cost would be almost as high as the potted core concept because it also requires Hi-Loks. Differences in costs between potted edges and high density core are primarily in fabrication and bond assembly operations. The channel section edge member was the most costly primarily because blind lockbolts were considered for joining the panels. These fasteners are harder to install than lockbolts. Also, the channel section concept requires twice as many fasteners.

Conclusions. - Based on the results of the weight, reliability, and cost analyses, a methodology was established to rank the four edge member concepts. A merit factor was assigned to each analysis which expressed its relative importance in percent to the program. These merit factors were 10 percent for weight, 45 percent for reliability, and 45 percent for cost. The four edge member concepts were assigned a value of 1 to 4, with the lowest value assigned to the best in each category. The product of this assigned value and the merit factor gave weight, reliability, and cost factors which were summed to obtain a cumulative factor. The lowest sum was the best overall edge member concept. In Table A7, the best edge member concept is shown to be the solid edge member with slots.

TABLE A7. CONCEPT EVALUATION AND RANKING

CONCEPT	WEIGHT RATING	RELIABILITY RATING	COST RATING	WEIGHT FACTOR	RELIABILITY FACTOR	COST FACTOR	CUMMULATIVE RANKING
Solid Edge/Slots	4	1	1	.4	.45	.45	1.30
Potted Core	2	2	3	.2	.90	1.35	2.45
High Density Core	3	3	2	.3	1.35	.90	2.55
Channel Section	1	4	4	.1	1.80	1.80	3.70

External Longeron Evaluation

Summary. - Six different cross sectional longeron shapes were evaluated with respect to manufacture, assembly, inspection, repair and fail-safe considerations for the external longeron fuselage concept. From this group, three were selected for aerodynamic study: plain tee, bulb tee and faired longerons. This study indicated a lower cruise drag penalty would be incurred by the faired longeron for the external longeron fuselage concept. However, the plain tee and bulb tee longerons still had an overall advantage with respect to ease of manufacture, assembly, inspection and repair and were chosen for further strength evaluation. From this analytical investigation, the bulb tee longeron was selected for the external longeron fuselage concept.

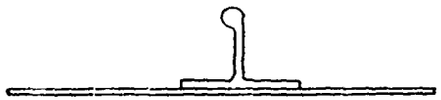
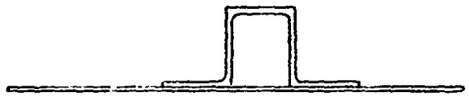
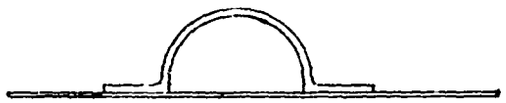
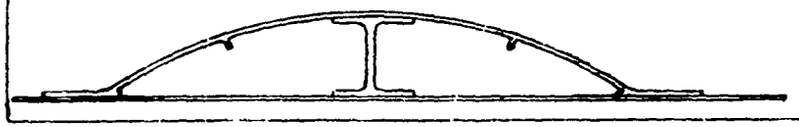
Purpose. - Various longerons were evaluated to determine the preferred cross-sectional shape for the external longeron fuselage concept.

Shape Selection. - Six different longeron cross-sectional shapes were evaluated with respect to manufacture, assembly, inspection, and fail-safe conditions. These evaluations are summarized in Table A8. Based on these evaluations, two candidates were selected as most promising for aerodynamic investigation: A plain tee section and a faired I-section.

Aerodynamic Study: - The aerodynamic effects of the external longerons on low-speed stability and performance (lift) characteristics were evaluated using the .06-scale YC-15 powered Model LB-368C in the NRC 30-foot V/STOL wind tunnel. The longerons consisted of T-shaped plastic extrusions located on the exterior surface of the model as shown in Figure A18. Adjustment of longeron height for the difference in boundary layer thickness between wind tunnel and flight conditions (tunnel Reynolds number is lower than flight) was also made. The equivalent full-scale heights of the two longeron sizes thus selected were 1.0 and 1.67 inches. Regardless of thrust level or flap deflection, the longerons had no measurable effect on the aircraft lift characteristics. They also had little or no effect on longitudinal stability. The effect of the longerons on the wing dihedral was insignificant.

The effect of the longerons on directional stability characteristics was

TABLE A8. LONGERON CROSS SECTIONAL SHAPE EVALUATION

LONGERON CROSS SECTIONAL SHAPE	SIMPLICITY OF MANUFACTURING	SIMPLICITY OF ASSEMBLY	EASE OF INSPECTION	EASE OF REPAIR	FAIL-SAFE DESIGN
	EXCELLENT	EXCELLENT	EXCELLENT	EXCELLENT	EXCELLENT
	EXCELLENT	GOOD TO EXCELLENT	EXCELLENT	GOOD TO EXCELLENT	EXCELLENT
	GOOD	GOOD TO POOR	POOR	GOOD TO POOR	EXCELLENT
	GOOD	GOOD TO POOR	POOR	GOOD TO POOR	EXCELLENT
	GOOD	POOR	POOR	POOR	EXCELLENT
	POOR	POOR	POOR	POOR	EXCELLENT

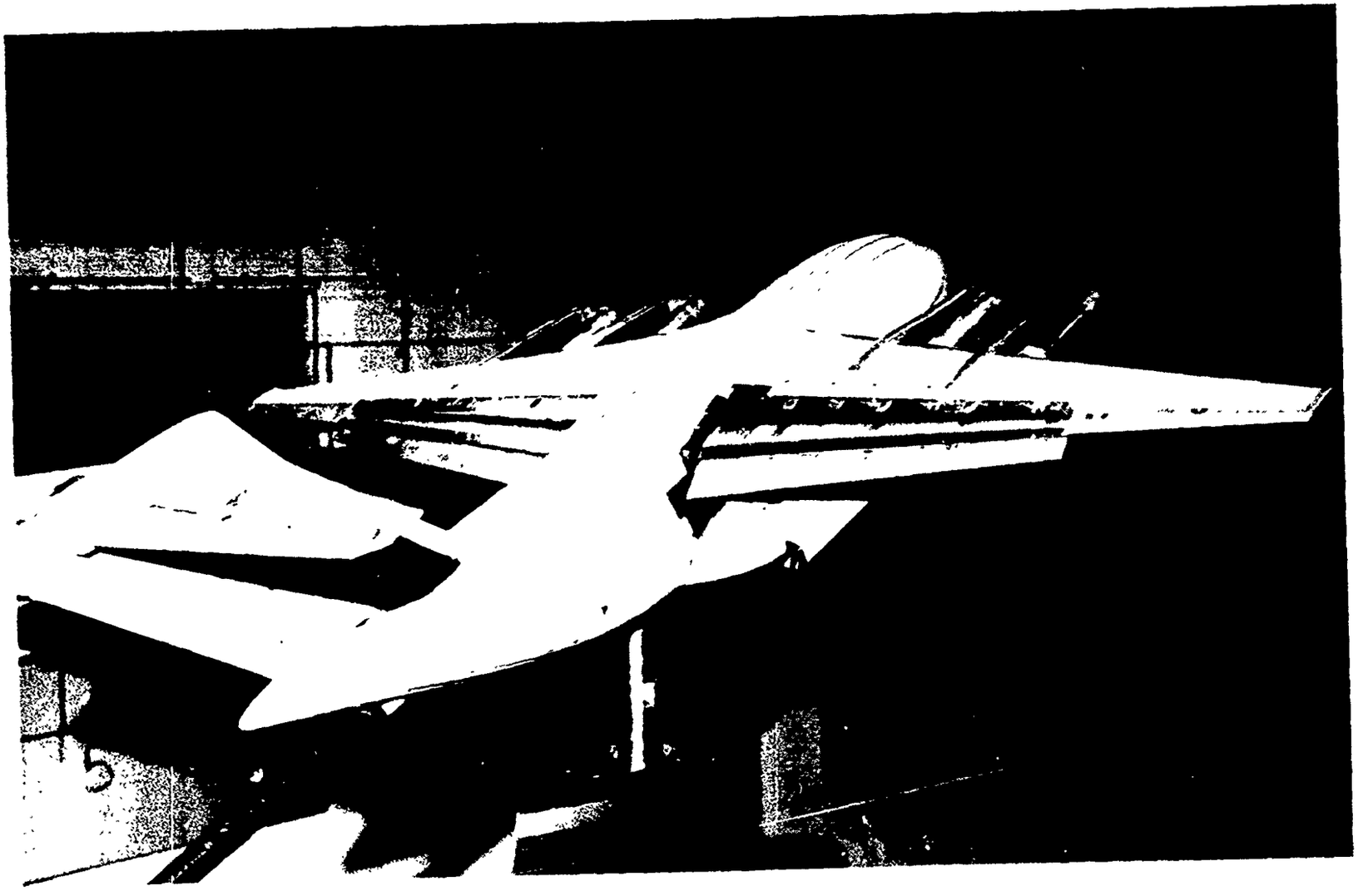


FIGURE A18. WIND TUNNEL MODEL OF YC-15 WITH EXTERNAL LONGERONS

evaluated. A slight difference with and without the longerons was noted. The directional stability level is generally reduced by the addition of the longerons, but the reduction is not considered to be significant.

The NRC 30-foot tunnel force balance system is designed to withstand the large axial (drag) forces associated with powered high-lift models. Cruise-configuration drag levels at high thrust settings exceed normal operating cruise drag levels by a factor of nearly 30; thus, the sensitivity level of this force balance precluded any meaningful measurement of the cruise drag penalty associated with the external longerons. Consequently, the cruise drag penalty has been estimated by the conventional Douglas analysis method. for the plain tee section longeron as follows: First, the basic parasite drag of the longerons is accounted for as flat-plate skin friction drag, based on the additional exposed wetted area and Reynolds number at cruise conditions. Second, the longeron splices (series of protruding bolt and nut heads) are accounted for separately by applying frontal-area drag coefficients and shielding factors from Hoerner. Dynamic-pressure variations due to the fuselage boundary layer have been included also. Third, crossflow effects (drag increase caused by the local flow passing over the longerons at an angle) were estimated by applying correlations of experimental data on plates inclined to the local flow (Hoerner), together with corrections for variations in local dynamic pressure. The flow field over the fuselage was calculated by the Douglas three-dimensional lifting potential flow program, and streamlines approximately one inch off the fuselage surface were computed to determine the local flow angularity along each longeron. Inasmuch as the drag associated with crossflow is quite sensitive to small changes in local flow angularity and since the effective longeron aspect ratios are small (normally characterized by a marked decrease in lift curve slope), a range of values for this component of the drag has been estimated.

The resulting total parasite drag area at cruise conditions for the external longerons ranges from a minimum of 1.57 sq. ft. to 3.23 sq. ft., the difference being a measure of the sensitivity of the crossflow term. This represents a penalty of about 2.1 percent to 4.4 percent of the total aircraft cruise drag.

The impact of a drag penalty of this magnitude on aircraft performance is readily apparent when presented in terms of an equivalent weight penalty. Such penalties are mission-dependent. Based on YC-15 performance ground rules, the equivalent weight penalty (weight savings required to offset the drag of the external longerons and maintain equivalent performance) for the basic STOL design mission (27,000 pound payload, 400 N.Mi. radius, 2000-foot field length) ranges from 283 pounds to 582 pounds. In terms of ferry range, this penalty increases by an order of magnitude. The ferry range equivalent range) ranges from 3000 pounds to 6140 pounds.

Similarly, the cruise drag penalty was estimated for the faired longeron configuration based on YC-15 performance ground rules. The equivalent weight penalty for the basic STOL mission was 54 pounds to 172 pounds at 400 n.m. range. The ferry range equivalent weight penalty was 570 pounds to 1810 pounds. Added to these penalties would be the weight of the fairings.

From these evaluations of the external fuselage longeron concept, a summary of results are as follows: The longerons had little or no measurable effect on airplane lift characteristics or longitudinal stability. Likewise, the longerons had no significant effect on static directional stability or dihedral effect. The estimated total cruise drag penalty is shown in Table A9. The expected nominal operational life was calculated in order to apply the fairing weight penalty. The fairing weight penalty was determined over the operational life of the YC-15 airplane. Thus the total weight penalty for the longeron configuration was determined.

Strength Evaluation: - The plain tee and bulb tee section longerons were selected over the faired longeron due to the complexity of manufacturing, assembly installation, inspection, and repair of the faired longeron. These complexities outweighed the aerodynamic drag considerations. The plain tee and bulb tee were analyzed for compression strength-to-weight ratio, based on a computerized solution of the Euler-Engesser column stability equation. Figure A19 shows these results along with the results for a J-section longeron used on the internal longeron fuselage concept.

TABLE A9. CRUISE DRAG AND CONFIGURATION PENALTY

CONFIGURATION	CRUISE DRAG PENALTY			NOMINAL OPERATIONAL LIFE(POUNDS) 400 N. MI RANGE (.7) + FERRY MISSION (.3)	FAIRING WEIGHT PENALTY (POUNDS)	TOTAL WEIGHT PENALTY (POUNDS)
	PERCENT	400 N.MI RANGE (POUNDS)	FERRY MISSION (POUNDS)			
TEE	2.10-4.40	283-582	3000-6140	1098 - 2250 1674 (AV.)	0	1674 (AV.)
FAIRED LONGERON	.40 - 1.30	54 - 172	570-1810	208.8 - 663.4 436 (AV.)	600	1036 (AV.)

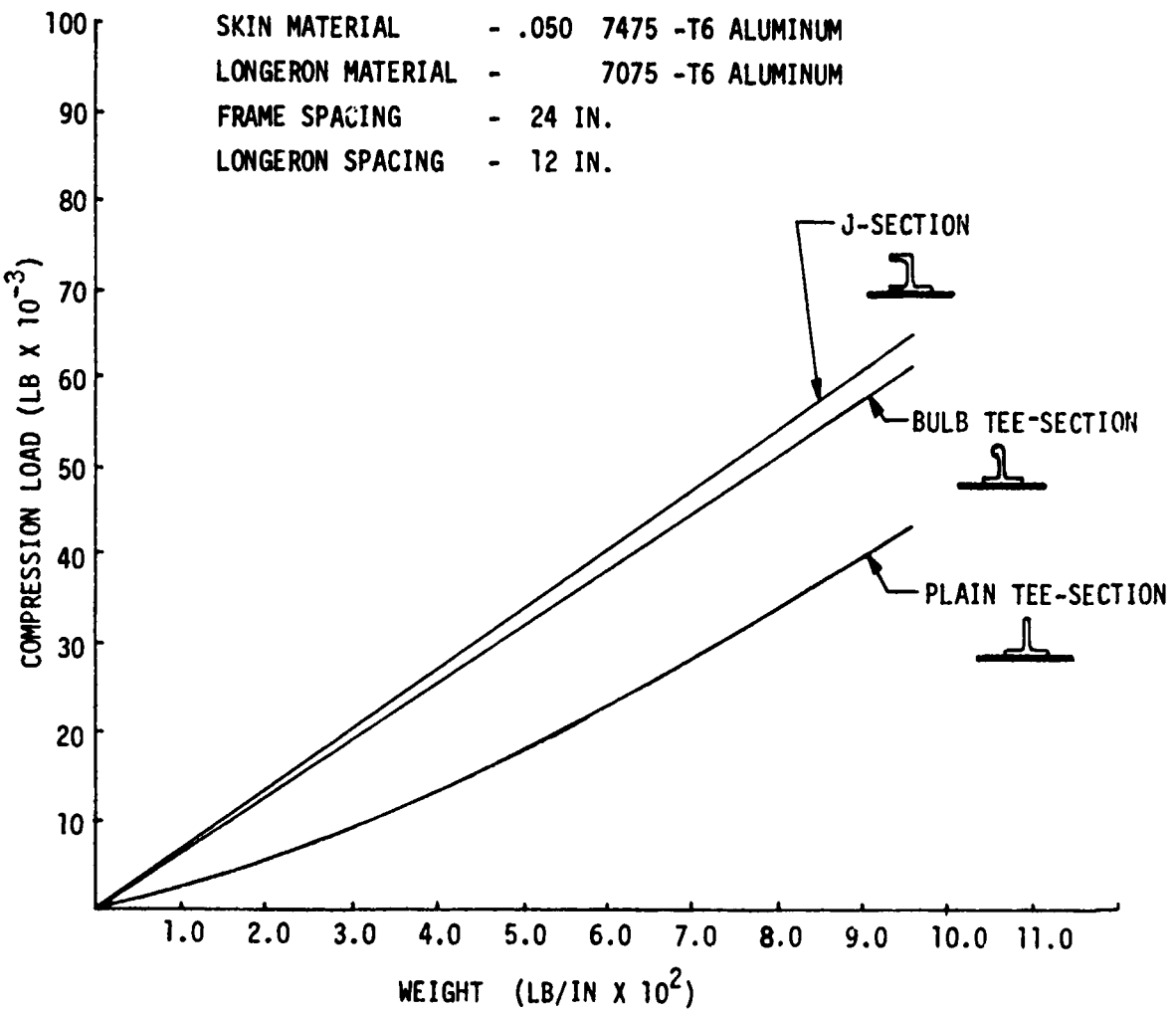


FIGURE A19. LONGERON COMPRESSION STRENGTH

Conclusion. - From the evaluation of the six different longeron cross sectional shapes, the bulb tee angle was chosen for the external longeron fuselage concept. This cross sectional shape had advantages equal to or greater than the other proposed shapes when evaluated for ease of manufacture, assembly, repair, inspection and simplicity of fail-safe design. Aerodynamic weight penalty was incurred for the bulbed tee section, but the other advantages outweighed this disadvantage. The strength of the bulb tee section shape was higher than the strength of plain tee section shape. It approached the strength allowables of the J-section shape (internal longeron concept).

Internal Longeron Shape Study

Two groups of longeron sections (Z's and J's) were evaluated for application to the PABST bonded fuselage. The Z-section was considered first (baseline case) with proven advantages of adequate strength with minimum installed cost, i.e., a single row of mechanical fasteners joining the longeron to the skin.

The J-section longeron was selected for the bonded new design concept for several reasons:

° The symmetrical flange on the J-section minimizes peel action and loads on the bonded interface. The Z-section causes high unacceptable peel loads at the junction of the vertical leg and the bonded flange when shear wrinkles are present or compression buckling occurs.

° The symmetrical flange on the J-section permits balanced tapered flanges to provide a relatively flexible flange in the transverse direction which minimizes peel loads on the adhesive bond line.

° The J-section with summetrical flanges has been successfully bonded in the autoclave with minimum variations in bond line thickness. The Z-section exhibited a tendency to rotate during the bonding cycle resulting in greater variations in bond line thickness.

The height for the longeron was bounded on the lower side by the minimum required for longeron splices and for attaching the frame shear clip (1.25 in.). Generally, increased height is desireable for improving the section properties which directly influence compressive stability allowables. However, since the AMST fuselage is relatively short and large diameter, the required longeron area for most of the fuselage is low and further constrained by minimum thickness, i.e., increased height results in a weight penalty except for three highly loaded longerons (1-9, L-10, & L-15).

Additionally, deeper shear clips (tees) are required resulting in even greater weight penalties.

The selected longeron height for the internal longeron bonded concept is 1.25 inch.

CONCLUSIONS

During Phase Ib, varieties of design concepts were investigated to arrive at a configuration for the large forward fuselage component that would be designed in Phase II, fabricated in Phase III and tested in Phase IV. Based on these investigations, a concept was selected consisting of internal longerons in the upper fuselage and external longerons below the floor. On a manufacturing cost basis, the internal and external longeron concepts are approximately equal. Although the external longeron presently has a drag penalty due to crossflow, the lack of entrapment of bilge fluids below the floor, justifies its use in that area. Honeycomb was not considered for the large component due to the high costs associated with repair and the cost of non-destructive inspection.

Phase Ib also identified a new series of environmental and cycle evaluation tests. A large number of coupon, specimen and large panel tests were conducted in Phase Ib to provide test data for the detail design of the concepts.

During Phase II, a series of tests will be made to determine the preconditioning, test environment, load rates and cycle that will simulate "real life" conditions. These tests will include more wedge crack, lap shear, peel, thick adherend, double cantilever, neat adhesive and RAAB specimens. Testing similar to Phase Ib will be accomplished to provide additional design data of the design concept and evaluate design refinements.

A non-circular pressurized shell structure with a door opening representative of the forward fuselage will be fatigue tested. In addition, shear plus compression panels will be cycled with and without representative real live cyclic environment.

PRECEDING PAGE BLANK-NOT FILMED

REFERENCES

1. Wilhem, D.P., "Fracture Mechanics Guidelines for Aircraft Applications". Air Force Report AFFDL-TR-69-111. February 1970.

2. Liu, A.F., "Stress Intensity Factor for a Corner Flaw". Engineering Fracture Mechanics. Pergaman Press. 1972. Vol. 4, P. 176.

3. Engle, Robert M.,Jr., "CRACKS, A FORTRAN IV Digital Computer Program for Crack Propagation Analysis". Air Force Report AFFDL TR-70-107,, October 1970. Page 7.

4. Swift, T., "The Effects of Fastener Flexibility and Stiffener Geometry on the Stress Intensity in Stiffened Cracked Sheet." Prospects of Fracture Mechanics, Noordhoff International Publishing Co., Leyden, Netherlands, 1975.

5. Kuhn, P., "Notch Effects on Fatigue and Static Strength." Current Aeronautical Fatigue Problems (Proceedings of a Symposium held in Rome). 1963.

6. "Damage Tolerant Design Handbook", Air Force Materials Laboratory and Air Force Flight Dynamics Laboratory, MCIC-HB-01, December 1972.

7. Broek, D., "Fatigue Crack Growth and Residual Strength of Aluminum Alloy Sheet at Temperatures Down to -75°C." NLR TR 72096U.

8. "The Influence of Temperature and Stress Intensity Factor upon Striation Spacing and Fatigue Crack Propagation of Aluminum Alloy", Journal of the Institute of Metals, Japan, 38, 720-724 (1974).

9. Schliekelmann, Ir. R. J., "Establishment of the Influence of Glueline Thickness on the Fokker Bond Tester Indication and the Shear Strength of FM-73 Etc.". Fokker-VFW, Report No. R-1988, June 1976.

PRECEDING PAGE BLANK-NOT FILMED